THE MODIFICATION OF POLYMERIC MATERIALS
WITH PLASTICIZERS OR ELASTOMERS

by

ELAINE MARIE YORKGITIS

Dissertation submitted to the Faculty of the
Virginia Polytechnic Institute and State University
in partial fulfillment of the requirements for the degree of

DOCTOR OF PHILOSOPHY

in

Materials Engineering Science

APPROVED:

_____
G. L. Wilkes
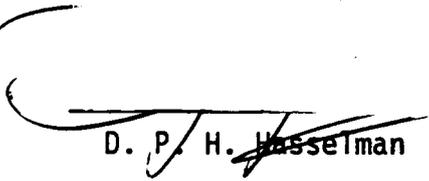
_____   _____
D. P. H. Hasselman   T. C. Ward
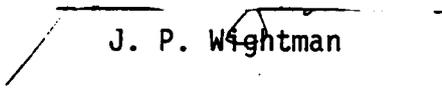
_____   _____
J. E. McGrath   J. P. Wightman

April, 1985
Blacksburg, Virginia

THE MODIFICATION OF POLYMERIC MATERIALS WITH PLASTICIZERS OR ELASTOMERS

by

Elaine Marie Yorkgitis

Committee Chairman: Garth L. Wilkes

Materials Engineering Science

(ABSTRACT)

The modification of polymeric materials using plasticizers or elastomers has been investigated in three research programs. The first describes epoxy resins modified with dimethylsiloxane, dimethyl-co-methyltrifluoropropyl siloxane, and dimethyl-co-diphenyl siloxane. The apparent compatibility between the epoxy and the siloxanes was enhanced by increasing methyltrifluoropropyl or diphenyl siloxane content or lowering molecular weight, resulting in profound changes in morphology and the resultant mechanical properties of the modified resins. Fracture toughness was most significantly improved using siloxanes containing at least 40% methyltrifluoropropyl siloxane or 20 and 40% diphenyl siloxane. Comparison of siloxane modifiers with butadiene acrylonitrile modifiers was valuable with regard to both property and morphological effects. The second research project considers the structure-property behavior of polyvinyl chloride (PVC) plasticized with low molecular weight diesters with emphasis on the contrasting effects of different plasticizers on the breadth of PVC's dynamic mechanical spectrum. It was clearly demonstrated that a less soluble plasticizer promoted a greater broadening at intermediate concentrations. Crystallization phenomena and static mechanical properties reflected the greater diluent effect of a more

soluble plasticizer. The dynamic mechanical behavior as well as other critical experimental observations were explained using a model which postulates that the network junctions of plasticized PVC consist of "pockets" containing several small crystallites. These pockets are randomly dispersed in a matrix whose homogeneity is governed by the plasticizer's solubility and molar volume. The third research project describes the modification of high 1,4 polybutadiene (PB) with isopropyl azodicarboxylate (IAD) for potential use as impact modifiers for polar polymers. A method for finding the extent of IAD modification of the PB has been developed using ^{13}C nmr and UV spectroscopy. Solution blends of PVC with PB modified with up to 11 mol% IAD were found to be immiscible. Stress-strain testing suggested that IAD modification (11%) enhanced the apparent compatibility between PB and PVC at 25% rubber content. The relatively poor mechanical response of the blends was believed to be related to their somewhat porous morphology.

DEDICATION

This dissertation is dedicated to the memory of

Aćiū Labai, Grandma.

ACKNOWLEDGEMENTS

When will I get out of here?
Let me count the days.
How will I get out of here?
Let me count the ways.

apologies to E. B. Browning

I have learned much from Garth Wilkes and his interesting way of being my boss the last few years; from the present results, one might tentatively suggest that it may perhaps have worked somewhat. I am grateful to J. E. McGrath, T. C. Ward, J. P. Wightman, and D. P. H. Hasselman for serving on my advisory committee.

I would like to thank Billy Williams and Wendell Brown for their skill and inventiveness in the Chemical Engineering Shop; Chi Tran and Norm Eiss for an enjoyable collaboration on siloxane-modified epoxies; Pat Sormani for several translations of German articles from the literature; and the office staff of the Chemical Engineering Dept.: Sandy Simpkins, Diane Haden, Mary Robinson, Diane Cannaday, and Jan Chance, for many small favors that have made a very big difference.

A parting nod to the present inhabitants and ghosts of 151 and 149 Randolph Hall; many memories will I carry with me: the Orler Shuffle, the Rocks and Hard Places, the Ceremonial Ionomer Beatings, the Allen Court, the Honorable Hertzler, the Slammed Door, Tennis Whites, Cat Stevens sung in "Hindi," the Partitioning Brooms, the Nesh and Nightshift. Thanks also to the Davidson Hall Division of the PMIL for

technical assistance and occasional refuge from the Randolph Hall Division of the PMIL.

A fond thanks to my parents and my brothers and sisters -- Susan, David, Mimi, Chip, and Lisa -- for their support and encouragement throughout my schooling. A special thank you to Tracy Browne for giving me a new perspective. I thank Carol Roberts Wright for her continual confidence in me and the privilege of her friendship; these gifts have sustained me on many occasions.

My research would not have been possible without the financial support of the Office of Naval Research, the National Aeronautics and Space Administration, the Army Research Office, and Phillips Petroleum Co. I am grateful to the following individuals and companies for providing specialized materials for various projects: Linda Sharkus and Ken Ruzkuszka of Rohm and Haas for ample amounts of Diamond Shamrock 450 and Geon 86; Wickhen Products, Inc., for a generous supply of diethylhexyl succinate; and Wayne Wang, formerly of Phillips Petroleum Co., for several batches of polybutadiene elastomers.

In the words of a not-so-famous oldie, "Thank the Lord for the nighttime, forget the day."

TABLE OF CONTENTS

Chemical Modification of Polybutadiene with
Isopropyl Azodicarboxylate for Use as a Potential Impact Modifier

CHAPTER ONE

A GENERAL INTRODUCTION TO

THE MODIFICATION OF POLYMERIC MATERIALS

WITH PLASTICIZERS AND ELASTOMERS

1.1. INTRODUCTION

Virtually every polymeric material marketed today contains additives which control or alter any number of its properties. It is convenient to divide these additives into two groups (1), anti-aging agents and modifiers. The first group includes heat stabilizers, flame retardants, anti-oxidants, and other substances which prevent chemical changes in the polymer so as to maintain its desired properties. The second group, modifiers, is the subject of this chapter.

A modifier may be considered to be a resin, elastomer, or low molecular weight material which alters the processing characteristics or physical properties of the basic resin. In a broad sense, this category of modifiers would include plasticizers, lubricants, mold-release agents, macromolecular modifiers (elastomers or thermoplastics), reinforcing agents, colorants and brightening agents, blowing agents, and anti-static agents (1). This chapter will consider primarily plasticizers and elastomeric modifiers. This focus on two types of modifiers should not blind one to the importance and interdependence of each kind of modifier. The final properties of a polymeric material are the product of its total composition.

Plasticizers are generally added to a polymer to make it more flexible and impart to it some degree of elasticity. The plasticizers chosen are intended to produce a flexibility that will remain over a specific temperature span. It is usually assumed that the plasticizer will be soluble with the resin.

Elastomers are added to a thermoplastic or thermoset to improve impact and fracture resistance while maintaining the strength and modulus of the host polymer as fully as possible. It is important that the elastomer and the resin be immiscible with each other because the elastomer is usually intended to be a dispersed phase. However, it is highly desirable for the elastomeric phase to wet and adhere well to the matrix.

In this chapter, *miscibility* and *compatibility* will have distinctly different meanings and be applied exclusively to mixtures of high molecular weight components. Use of the term *miscibility* does not necessarily imply that mixing has occurred on a molecular level. Rather it suggests, in the words of Olabisi, Robeson, and Shaw (2), that "the level of molecular mixing is adequate to yield macroscopic properties expected of a single phase material." Miscibility is frequently given a thermodynamic basis: two substances which are miscible have a free energy of mixing, ΔG_m, which is less than zero. It is perhaps more often cited that the second derivative of ΔG_m must be less than zero for miscibility to occur (2). The quantity ΔG_m is determined by the magnitudes of enthalpy (H) and entropy (S), as defined by the relationship $\Delta G_m = \Delta H_m - T\Delta S_m$.

When ΔG_m is positive, a system is not considered to be thermodynamically miscible. The term *compatibility* then becomes convenient for describing the extent of phase mixing. By the definition that will be used here, compatibility (2) describes the situation where

mixing is not intimate but the separate phases adhere well and the material properties generally reflect the modification of the matrix by a dispersed phase. A fine line can exist between miscibility and compatibility, particularly in the realm of very small but separate phases measuring less than 50 A.

Whatever the degree of mixing, it will strongly dictate the properties of a two-component material. The concepts of mixing are thus central to both plasticization and rubber modification. From this common point, however, the uses of plasticizers and elastomers as modifiers diverge considerably. The properties that are most important in one case may be secondary in another. However, both plasticized and rubber-modified materials are two-component systems, and the same experimental techniques are often applied to both.

This chapter will begin with a discussion of solubility, miscibility, and compatibility from a primarily theoretical standpoint. Plasticization, rubber modification of thermoplastics, and rubber modification of thermosets will then be dealt with in turn. Rubber modification of thermoplastics and thermosets will initially be discussed jointly as they have many common aspects.

This chapter will serve as a *general* introduction to the plasticization and rubber modification of polymeric materials. It is not meant to be a detailed review of these areas, particularly in view of the fact that several books and chapters already published do them excellent justice (3-7). Emphasis is given here to topics which although important

to the topics of the next three chapters, are not covered there in detail. Points that are discussed at length in the following chapters are therefore covered in this chapter only to the extent that they will facilitate continued discussion.

1.2. SOLUBILITY, MISCIBILITY, AND COMPATIBILITY

1.2.1. Thermodynamics of Mixing

Plasticization may generally be approached by way of solution thermodynamics, that is, the thermodynamics of mixing a polymer and a low molecular weight solvent. In describing rubber modification, however, one must go one step further and consider the thermodynamics of a polymer-polymer solution. But before beginning to discuss either case, it is necessary to introduce appropriate terms.

The thermodynamic state of a mixed two-component system can be described by its free energy, $\Delta Gm = \Delta Hm - T\Delta Sm$. For the ideal solution,

$$\Delta Sm = -kN(X1\ln X1 + X2\ln X2) \qquad (1)$$

where X1 and X2 are the respective mole fractions of the two components and N is the total number of molecules. Equation (1) describes the entropy gained by literally combining two components of similar molecular size, hence is called the *combinatorial entropy*. This entropy alone describes the free energy of the ideal solution because the change in enthalpy upon mixing, ΔHm, is zero.

For the regular solution, ΔHm is finite (solute and solvent interact) and may be expressed by Equation (2)

$$\Delta Hm = z\Delta W12N1X2 \tag{2}$$

where $\Delta W12$ is the energy change associated with the formation of a solvent-solute contact, z is a coordination number, and X2 is the mole fraction of the solute. The entropy expression remains unchanged from that of the ideal solution, so ΔGm for the regular solution is found by combining Equations (1) and (2) with the appropriate coefficient of temperature.

The expressions for the ideal and regular solutions may be derived by considering the arrangement of molecules of similar size on a lattice as the one in Figure 1.1a. The dissolution of a *polymer* in a solvent requires that the segments of the polymer chain be adjacent to and bound to two similar segments as pictured in Figure 1.1b. Considering the constraints that this places on the entropy, Flory (8) has made the *combinatorial entropy* of Equation (1) a *configurational entropy* through Equation (3)

$$\Delta Sm = -k(N1\ln\phi1 + N2\ln\phi2) \tag{3}$$

where ϕ represents the volume fraction of a component and N denotes the individual number of lattice units of that component. Flory (8) has pointed out that Hildebrand (9) was able to arrive at Equation (3) without resorting to the lattice concept by viewing the *greater free volume* available to solvent and polymer upon mixing.

The enthalpy of this polymer solution requires revision of ΔH_m as given in Equation (2). Specifically, the situation is generalized to include a total number of solvent segment units N_1X_1, thus converting Equation (2) to

$$\Delta H_m = z\Delta W_{12}N_1X_1\phi_2 \qquad (4)$$

Equation (4) may be restated as

$$\Delta H_m = kTxN_1\phi_2 \qquad (5)$$

where the "chi" parameter, also known as the Flory-Huggins interaction parameter, is

$$x = z\Delta W_{12}X_1/kT \qquad (6)$$

Equation (6) implies that x is dependent only on T, however the interaction energy, ΔW, is intrinsically a function of G, the free energy. In addition to its enthalpic contributions, the parameter x thus contains an entropy contribution which reflects its dependence on concentration as well as temperature (10).

It is common to consider the critical x value, above which solubility is not expected, to be that given by Equation (7)

$$x_c = \frac{(1 + x^{1/2})^2}{2x} \qquad (7)$$

where x is the degree of polymerization of the polymeric species. It can be shown that the critical polymer concentration is

$$\phi_{2c} = \frac{1}{1 + x^{1/2}} \qquad (8)$$

For a polymer of any appreciable molecular weight, $x_c = 0.5$ and ϕ_{2c} is zero (11).

Returning to the lattice concept first shown in Figure 1.1, consider the situation where two different polymers are placed on the same lattice. Figure 1.2 shows that placing chains of two different polymers on a lattice severely restricts the total number of possible arrangements. Because the change in entropy upon mixing two polymers is so small, the enthalpy of mixing must be made as small as possible, and preferably as negative as possible, for two polymers to be miscible. This is possible if two dissimilar polymers are capable of specific interactions.

Polymers may experience several types of intermolecular attractions including dipole-induced dipole, random dipole-induced dipole, dipole-dipole, ion-dipole, hydrogen bonding, acid-base, and charge transfer (2). The first of these is the source of the well known London dispersion forces which may occur between any two compounds. Any of these forces or attractions may also, of course, promote miscibility between

any two chemical species, regardless of their molecular weights. Hydrogen bonding is the most common driving force of many miscible polymer pairs (2).

Critical phenomena in polymer-polymer mixtures are functions of composition and temperature and a strong function of molecular weight. Consider, for example, Scott's expression (12) for ΔGm as per Krause (13)

$$\Delta Gm = \frac{RTV}{Vr} \left[\frac{\phi 1}{x1} \ln\phi 1 + \frac{\phi 2}{x2} \ln\phi 2 + \chi 12\phi 1\phi 2 \right] \qquad (9)$$

where Vr is a reference volume as close as possible to the molar volume of the smallest possible polymer repeat unit of the given polymer pair, $x1$ and $x2$ are the respective degrees of polymerization of the two polymers, and V is the total volume of the system. Knowing that the second and third derivatives of ΔGm with respect to $\phi 1$ are zero at the critical point, Scott derived the critical quantities in Equations 10a-c

$$\chi 12c = \frac{1}{2} \left(\left(\frac{1}{x1}\right)^{1/2} + \left(\frac{1}{x2}\right)^{1/2} \right) \qquad (10a)$$

$$\phi 1c = \frac{x2^{1/2}}{x1^{1/2} + x2^{1/2}} \qquad (10b)$$

$$\phi 2c = \frac{x1^{1/2}}{x1^{1/2} + x2^{1/2}} \qquad (10c)$$

One sees immediately that the critical χ value would indeed be very small for polymers of typical molecular weights.

1.2.2. *Phase Equilibria*

The thermodynamic state of any two-component mixture will be either stable, unstable, or metastable. The standard diagrams showing energy wells and peaks are sufficient to describe stable and unstable states. The metastable state is equivalent to superimposing an energy well on an energy peak, implying that the metastable state possesses a narrow but measurable range of stability.

Temperature-composition diagrams such as those in Figure 1.3 are convenient for showing the equilibrium between miscibility and separation for two-component mixtures. Figures 1.3a and 1.3b are particularly suitable for polymer mixtures. Both binodals and spinodals are given for these two figures. The binodal marks the boundary between stable and metastable compositions while the spinodal separates metastable and unstable compositions. The spinodal can be calculated from the assumption that the second derivative of ΔGm is 0, but the binodal is obtained through considerably more complicated measures (13).

1.2.3. *Predictions and Measures of Solubility and Miscibility*

The solubility parameter has become a useful measure of the attraction between both high and low molecular weight species. It is defined as

$$\delta = \left(\frac{\Delta Ev}{V}\right)^{\frac{1}{2}} \left(\frac{cal}{cc}\right)^{\frac{1}{2}} \tag{11}$$

where $\Delta E_v/V$ is the molar energy of vaporization. Units of $(J/cc)^{1/2}$ may also be seen for δ; $(J/cc)^{1/2} = 2.05 \ (cal/cc)^{1/2}$. The quantity δ^2, with units of cal/cc or J/cc, is called the cohesive energy density. The extent of mixing between species "1" and "2" is often related to the heat of mixing through Equation (12)

$$\Delta H_m = V \ (\delta 1 - \delta 2)^2 \ \phi 1 \phi 2 \tag{12}$$

where V is the total volume. This equation interestingly predicts that ΔH_m will always be positive but will approach zero as $\delta 1$ and $\delta 2$ approach each other.

By equating ΔH_m from Equation (5) with that in Equation (12), one will note that $x \propto (\delta 1 - \delta 2)^2$. However, this is strictly an approximation since the $\Delta W12$ term in Equation (5) can render x negative if suitable specific interactions exist. Generally speaking, if x is negative, ΔG_m will be negative as well. If x is greater than zero, ΔG_m may be positive for a polymer-solvent mixture and will most likely be positive for a polymer-polymer mixture. By definition, x describes a "solution" at a fixed temperature and composition. It may be *measured* for a given polymer-solvent pair by several different means including swelling studies of lightly crosslinked polymers (14) and inverse gas chromatography (15).

According to its definition, δ is a "fixed" value for any *compound*. Therefore, the concept of the solubility parameter may be used to *predict* the degree of mixing between COMPONENT A and COMPONENT B strictly on the basis of the value of the quantity $(\delta A - \delta B)^2$. If another

material, COMPONENT C, is mixed with COMPONENT A such that (δA - δC)^2 is less than (δA - δB)^2, then A and C are said to be more soluble or more compatible than A and B. No predictions are made about the effects of composition and temperature. The solubility parameter may be estimated by various means, several of which involve calculation from easily obtained physical properties. Several of these calculations are described in Chapter Three.

The parameters δ and χ are now established as tools of polymer science. For the study of plasticization in particular, it will be seen that they have proven themselves quite useful.

1.2.4. *Summary of Important Concepts*

The solubility of polymers with many low molecular weight species is conveniently predicted using solution thermodynamics as developed by Flory and Huggins. Traditional thermodynamics generally does not predict polymer-polymer miscibility because of a relatively small entropy of mixing and generally positive enthalpy. However, this is not meant to imply that polymers are always immiscible with each other. Many exceptions can be found (2,13).

In general, the degree of mixing varies to some extent with temperature, composition, and molecular weight. To the delight of many polymer scientists, affinity between componets may often be enhanced by specific interactions. By careful attention to these factors, it is possible to realize the degree of mixing needed to produce the optimal physical

properties for a particular application. The upcoming discussions of plasticization and rubber modification will never stray far from these concepts.

1.3. *PLASTICIZATION OF POLYMERIC MATERIALS*

1.3.1. *Background*

Plasticization has been practiced since the beginning of the modern plastics industry. When applied creatively, it can expand the utility of many polymeric materials. This in turn increases the market available to manufacturers of plastic products and has made plasticization indispensable to them. PVC compounds account for approximately three-fourths of the plasticizers produced annually (16). Not surprisingly then, plasticized PVC has received more attention than any other plasticized material.

Unplasticized PVC will not be discussed here in detail as that will be done elsewhere (see Chapter Three), however, any discussion of plasticization requires some understanding of PVC's salient features. Most prominent is its rapid degradation at its processing temperatures, 150° to 185°C. PVC must therefore be processed in the presence of a heat stabilizer. The high cost of these additives has prompted considerable research into the possible mechanisms of PVC's thermal dehydrochlorination as well as the stabilizers' role in controlling it (17-22).

PVC is produced by bulk, suspension, and emulsion processes, all of which result in a particulate structure. These particles are characterized primarily by size, porosity, and ease of fusion, the latter

being a partial function of the surface characteristics of the material. To a large extent, the form of the resin determines its end use.

Though sometimes listed as an amorphous polymer, virgin PVC has a low degree of crystallinity which melts over a broad temperature range from about 100° to over 200°C. This small amount (~ 10%) of crystallinity interferes with the fusion of PVC during processing, particularly since PVC is not often processed beyond a temperature of about 185°C. Plasticization often lowers the melt viscosity of PVC, thus facilitating its processing. In general, those plasticizers which are most efficient at lowering the glass transition temperature (Tg) of PVC also lower its melt viscosity the most.

Topics to be included in the following discussion are the processing of plasticized PVC, general characteristics of plasticizers, practical measures of solubility, and the general effects of plasticization on properties of PVC.

1.3.2. *Processing of Plasticized PVC*

Prior to final fabrication, plasticized PVC will be found in one of three forms. Dry blends, which may contain up to about 30% plasticizer, are prepared in a high speed mixer at elevated temperatures (23). Polymer and additives other than plasticizers are mixed first at ambient temperatures, then the plasticizer is blended in at 60 to 90°C followed by a mixing at 90 to 110°C. The plasticizer is absorbed into the individual PVC particles so that the mixture is actually "wet" at first, but emerges

from the mixer as a dry powder and is removed to a cooling chamber. The polymer used in the dry blending process should absorb plasticizer homogeneously, therefore mass or suspension PVC is usually chosen since these materials have a suitable porosity and grain structure. Marks (24) has compared and contrasted the characteristics of mass and suspension PVC.

Dry blending may be followed directly by melt mixing in Banbury mixers or on compounding mills although single screw extruders are now being used more and more (25). The product is then made into a pelletized feedstock for use later in a final fabrication procedure.

PVC plastisols are a "paste" of resin and plasticizer plus other minor ingredients. Emulsion or microsuspension PVC's are preferred for plastisols since their particles are only 1.0 to 2.0 μm in size and are denser than either suspension or bulk polymerized PVC. The smaller size produces a more homogeneous dispersion of the polymer particles while the higher particle density prevents plasticizer absorption and maintains the plastisol's "pourability." Plastisols are convenient for processes such as rotational molding, slush molding, casting, dip coating, dip molding, spread coating, and spray coating. Following application to a substrate or mold, the paste is fused at temperatures betweeen 160 and 180°C (23).

The initial absorption of plasticizer which produces sufficient coherency to form a solid mass is termed *gelation*. This solid is weak and crumbly but is held together by a small amount of liquid phase. The

individual PVC particles are just touching at this point. Gelation as used in a processing context should not be confused with the formation of gel networks in PVC solutions containing moderate to large amounts of solvents. *Fusion* results from continued heating accompanied by increased interaction between polymer and plasticizer until a homogeneous mass is developed having the desired physical properties.

1.3.3. *Plasticizers*

Plasticized PVC formulations rarely include only one plasticizer but frequently contain often proprietary blends of two or more plasticizers. In this way, one can achieve a balance between the factors of cost, solubility, permanence, and efficiency while fine tuning the properties of the final material. The dialkyl phthalates represent the largest class of *primary* plasticizers, those which are most soluble with PVC and used in the largest proportions in most formulations. Krauskopf (26) has called five particular phthalate plasticizers the "workhorse" plasticizers. These are di-2-ethylhexyl phthalate (DOP), diisononyl phthalate (DINP), diisooctyl phthalate (DIOP), di-2-ethylhexyl terephthalate (DOTP), and diisoheptyl phthalate (DIHP). In addition to the phthalate plasticizers, several phosphates, particularly the triaryl phosphates, are commercially important primary plasticizers.

DOP has become the industry standard for general purpose applications. It is relatively cheap, has good weatherability, and has good solubility with PVC. It is only moderately volatile. Its flex temperature of -38°C at 40 percent concentration in PVC limits its low-

temperature flexibility. DOP accounted for 25% of total U.S. plasticizer consumption in 1982, down from 42% in 1972 (16). Its share of the market is being increasingly taken up by other general purpose plasticizers. Any one of the five "workhorse" plasticizers listed earlier is chosen for one out of three of all flexible PVC applications (26). Table 1.1 lists the properties of these five phthalates.

The solvating ability of a plasticizer is extremely important to the PVC compounder. Although x and δ are commonly determined, several more specific but empirical measures of solvation are used in practice. The *fusion temperature*, which is strictly applicable only to dry blends, is generally taken as the temperature at which maximum torque (or power) is measured in a Brabender Plasti-Corder or Plastograph (27). Time to fusion may also be measured. The *minimum fluxing temperature* is most suitable for measuring plastisol fusion. It may be defined roughly as the temperature at which a plastisol may be lifted from a heated plate in one piece after 20 minutes of contact (28). DOP has a minimum fluxing temperature of 105°C (28), but an initial fusion temperature of 84°C (3). Within the time scale of the measurement, fusion will not be complete at these relatively low temperatures.

Figure 1.4 demonstrates the effect of different plasticizers on the power requirements of a Banbury mixer during mixing and fusion of plasticizer-PVC blends. The arrows indicate the fusion times for each compound; DOA-PVC and DOS-PVC did not fuse before the mixing time of 2.5 minutes. (Solubility parameters (from Ref. 3) have been added by the author.) It is interesting to note that the sharper the peak current,

the lower the time needed for fusion. The time for fusion is lowered as the solubility parameter of the plasticizer approaches that of PVC, about 9.6. These trends indicate the interplay between solubility, plasticizer absorption, and power needed for production of an acceptable material.

The clear point temperature is denoted as that temperature where a mixture of PVC and plasticizer becomes clear (30). It is generally inversely proportional to the solubility of the plasticizer with the PVC and is quite practical since one of PVC's principal qualities is its transparency. DOP and DIOP have clear points of 117 and 116°C, respectively, while DOA and DOS have respective clear points of 138 and 151°C.

Other measures of solubility include the so-called "Ap/Po ratio" which divides the number of *aliphatic* carbon atoms in a plasticizer by the number of ester groups. DOP would thus have a ratio of 8. These ratios correlate well with clear point temperature (30). Compatibility may be judged qualitatively by the loop or roll test in which a strip of a plasticized PVC film is wrapped into a tight roll or bent into a loop for no more than 24 hours and then unwrapped to reveal or not reveal exuded plasticizer. The assessment of solubility by this test is subjective, of course, but is said to provide a reasonable measure of the ease of exudation (30).

An often useful measure of plasticizer solubility is the value of its dielectric constant (ε) (31). Most plasticizers for PVC have ε values between about 4 and 8-10. As Figure 1.5 shows, the χ and ε values for

a variety of hydrocarbons and ester plasticizers correlate well with each other.

In many cases, the solubility of a plasticizer with PVC may be too low to allow it to be used as a primary plasticizer. These *secondary* plasticizers are thus used in smaller quantities to impart special qualities to plasticized PVC such as low-temperature flexibility, flame-retardancy, better electrical resistance, or better migration resistance. Low-temperature flexibility is usually enhanced by adding aliphatic diesters such as the sebacates and azelates. Polymeric or reasonably high molecular weight plasticizers generally improve migration resistance for obvious reasons; candidates include oligomeric polyesters and epoxidized soybean oils.

PVC compounds typically contain additives other than plasticizers. These may include stabilizers, lubricants, fillers, pigments, biocides, and even anti-oxidants for the plasticizers. Foamed plasticized PVC requires blowing agents and foam stabilizers. The reader is referred to Sears and Darby (3), Nass (32), Sarvetnick (33), and Titow (23) for further discussion of plasticizers and other PVC additives.

Resins other than PVC may also include plasticizers in their formulations to meet certain needs in their processing or end-use applications (34). For example, plasticizers are sometimes added to (semi-crystalline) nylon or polyvinylidene fluoride (PVDF) to aid in processing or to improve properties attributed to their amorphous regions such as flexibility, toughness, and adhesion. Plasticizers can function as dye carriers in materials such as polyethylene terephthalate which resist dye diffusion. Various rubbers are also compounded with fairly large amounts of plasticizers. Hertz (35a) recently presented a rather extensive study of the effect of various phthalate plasticizers on the dynamic mechanical properties of nitrile rubber. The cellulosic polymers, particularly cellulose nitrate, are frequently plasticized for use in coating and film applications. Polycarbonate is often given 0.2 to 5.0% of a plasticizer to reduce its high melt viscosity. Various acrylic polymers may be plasticized for coating applications. Polyvinyl butyral, which is typically derived from polyvinyl alcohol, is plasticized with about 30 parts per hundred parts polymer of a low molecular weight ester for use as the interlayer in safety glass laminates (35b).

1.3.4. *Properties of Plasticized PVC*

The properties of plasticized PVC are very sensitive to the plasticizer used. Considerable effort has been made to relate property changes to various plasticizer parameters including molar volume,

molecular weight, and alkyl chain length (of a diester plasticizer). It was recognized in the 1940's that the general properties of solubility, efficiency, and permanence were interrelated (36). Solubility has already been discussed, but the other "general" properties warrant discussion.

Efficiency is usually a function of the ability of plasticizer to lower either Tg or modulus. For example, the efficiency factor has been defined as the phr (parts per hundred resin) of a plasticizer needed to make a plasticized PVC with a modulus of 7.6 MPa at 100% elongation at 23°C *normalized with* the appropriate value for DOP, 62.8 (30). DOP thus has a value of 1.0 while dibutyl phthalate (DBP) and DIOP have efficiency factors of 0.86 and 1.02, respectively. This indicates that DBP is more efficient than DOP and DIOP in lowering modulus.

It is found in general that a smaller plasticizer molecule is more efficient than a larger one. This is demonstrated by Figure 1.6 which shows the increase of efficiency with decreasing solvent molar volume for a copolymer of vinyl chloride and 14% vinyl acetate. In this case, efficiency is defined relative to the ability of the plasticizer to lower Tg. Many years ago, Lawrence and McIntyre (38) showed that efficiency (based on a modulus measurement) generally decreased with increasing

alkyl chain length of several phthalates, sebacates, and phosphate plasticizers. However, the flex temperature, below which plasticized PVC loses its flexibility, *decreases* with increasing alkyl chain length. Thus one must often choose between high modulus and low flex temperature, only one of several trade-offs that might have to be made in choosing the correct plasticizer or combination of plasticizers for a particular application.

A third major area of concern in selecting a plasticizer is *permanence*. Permanence may be evaluated in any of three modes, volatilization (loss into air), extraction (loss into liquid), and migration (loss into a contacting solid surface) (30). Permanence may be assessed through simple weight loss measurements but more sophisticated approaches may be taken. For example, diffusion between bulk liquid alcohols and plasticizers in PVC has been monitored by radiotracer techniques by Park and associates (39). The subject of plasticizer diffusion into alcohol and other liquids has become a commercially important area and is dealt with in several publications (40-43).

PVC is plasticized primarily to change its mechanical properties. Figure 1.7 shows the general trends seen in increasing DOP content in

PVC. The phenomenon of anti-plasticization, which will be discussed later, is responsible for the initial changes in properties. However, beyond 15-20% plasticizer, one finds that as more plasticizer is added, elongation and impact strength go up while tensile strength and modulus go down. Plasticization affects many of PVC's other properties. Dynamic mechanical properties, discussed at length in Chapter Three, change in ways reflecting both the lowered modulus and Tg of plasticized compositions relative to unplasticized PVC. Plasticization may also affect electrical, thermal, and permeability and diffusion properties (3). Plasticizers are known to sometimes complement the effects of non-plasticizer additives, such as stabilizers and flame-retardants (3,21).

The anti-plasticization phenomenon referred to earlier (see Figure 1.7) was first demonstrated in the literature in 1935 (45). Jacobson (46) showed how these effects could be observed with a variety of plasticizers. Several of his results are given in Figure 1.8 from which it is seen that the effects of anti-plasticization persist to higher percentages of plasticizer when the plasticizer is more soluble with the PVC. Ghersa (44) showed through data such as that given in Figure 1.9 that the concentration at which anti-plasticization reverses itself increases with decreasing temperature.

Horsley (47) suggested that the observed increases in tensile strength, decreases in impact strength, etc. were due to increased

amounts of crystallinity at low plasticizer concentration (46,30). Jacobson (46) neither agrees with or refutes this proposal, noting that the maximum crystallinity (as determined by X-ray diffraction methods) passes through a maximum near the same concentrations at which various mechanical property measurements are passing through maxima or mimima. Buszard (30), however, points out that the increases in crystallinity are very small, implying that they cannot be entirely responsible for the phenomenon. Pizzoli, Pezzin, and Ceccorulli (48) quote from unpublished work which shows similar wide- and small-angle X-ray scattering patterns for PVC containing up to 20% plasticizer content.

Small amounts of plasticizer have been noted to suppress the β-peak of PVC which is marked in unplasticized PVC by a low and broad secondary relaxation centered at -50 to -30°C. An example of the noted suppression is shown in Figure 1.10 for data taken from Pizzoli et al (48). Efforts to tie in the β-peak suppression and increased crystallinity with anti-plasticization were weakened when Pezzin et al (49) showed that although PVC with a crystallinity of about 20% had a higher glass transition temperature than a PVC with about 10% crystallinity, the β-peaks of the two materials were essentially identical.

Robeson and Faucher (50) observed that the β-peaks of polysulfone and polycarbonate were also suppressed by low levels of plasticizers.

They showed that the specific volume of the two polymers initially decreased as diluents were added and, in fact, passed through a minimum for one of the polymer-diluent pairs studied. Robeson and Faucher therefore postulated that the anti-plasticizers filled free volume in the polymer, restricting main chain mobility and thereby increasing chain stiffness and suppressing the main chain cooperative motions to which the β-relaxation has been attributed. Robeson (51) later provided more convincing evidence that specific volume passed through a minimum upon addition of small amounts of plasticizer. Water sorption experiments showed that anti-plasticized polysulfone absorbed less water than unplasticized polysulfone. The "free volume" concept is apparently the most satisfactory explanation of anti-plasticization at this time.

1.4. RUBBER MODIFICATION OF THERMOPLASTIC AND THERMOSETTING RESINS

The basic idea of adding a rubber to a brittle plastic material to improve its fracture properties dates back to the 1940's and the invention of high-impact polystyrene (HIPS). The nearly forty years between then and now have witnessed the impact modification of a variety of other materials including epoxy resins, crosslinked polyimides, polymethyl methacrylate, polypropylene, and polyvinyl chloride. The broad range of structure and properties which these materials represent in their unmodified states is maintained as fully as possible upon the addition of a rubber modifier. The methods used to incorporate the rubbers vary from one material to another. Consequently, the principal mechanisms by which the rubber-modified materials dissipate energy during fracture depend on the method of rubber modification as well as the properties of the "host" resin.

This review will first introduce a few of the more common techniques used in evaluating improvements in fracture properties. This will assist discussion of quantitative results for the various rubber-modified resins. The important criteria of these methods and special considerations in applying them to polymeric materials will be among the principal points raised. Several prominent examples of rubber-modified polymeric materials will then be described. Emphasis will be placed on the extents of impact strength or toughness improvement and the toughening mechanisms believed to be active in each material.

1.4.1. *Evaluation of Toughening*

Toughness of a rubber-modified material may be evaluated by either an impact test or a method designated by linear elastic fracture mechanics (LEFM). The more rigorous approach of LEFM will be dealt with first.

LEFM has its roots in the well known work of Griffith (52) who in the 1920's considered the conditions under which a crack such as that shown in Figure 1.11 could remain stable, i. e., would not propagate. Griffith constructed an energy balance between the surface energy of such a crack and the stored elastic energy (plus any external fracture work). Based on this balance, he proposed that the crack would propagate if the critical stress exceeded a value designated by Equation (13)

$$\sigma^* = \left(\frac{2E\gamma}{a}\right)^{1/2} \tag{13}$$

where E is the Young's modulus, γ is the thermodynamic surface energy, and a is half the length of the crack in the thin sheet pictured in Figure 1.11. Griffith's approach holds strictly for a perfectly brittle solid for which surface energy may be considered to be the only form of energy responsible for an increase in crack surface area. A more general approach may be found in Equation (14)

$$\sigma^* = Y \left(\frac{2ET}{a} \right)^{1/2}$$
(14)

where Y is a geometry factor dependent on a test specimen's shape and dimensions and T is the total energy absorbed during the creation of unit area of new fracture surface. Griffith's work laid the basis for later work by Irwin (53) and Orowan (54).

One of the most important parameters in LEFM, the stress intensity factor, K, may be reached by first rewriting Equation (14) as

$$\sigma^{*2} a = const \ E \ T$$
(15)

which may be extended to

$$K^2 = Y' \sigma^2 a$$
(16)

The critical conditions for fracture may then be defined as in Equation (17)

$$Kc^2 = Y' \sigma^{*2} a$$
(17)

where Kc is usually referred to as the critical stress intensity.

Based on loading conditions, crack extension can be placed into one of the three modes illustrated in Figure 1.12. Crack extension is most directly affected by the opening or tensile mode, Mode I. As Figure 1.12

implies, the shear modulus, rather than Young's modulus, is most applicable to Modes II and III. Mode II is very difficult to enact experimentally. Mode III is easily analyzed mathematically, but is used only occasionally in practice (55). It is possible for fracture to occur in mixed modes, particularly in adhesive joints (56,57). The present discussion will be restricted to Mode I.

Hayes (58) has stated the object of fracture mechanics as the prediction of the fracture behavior of one cracked body based on the observed behavior of another cracked body. For this reason, the most important parameter in fracture mechanics is the crack itself. The stress field at the tip of an infinitely sharp crack under crack opening Mode I is schematically represented in Figure 1.13. Note that $\sigma(y)$ is infinite at the very tip of the crack and then decreases as the distance from the crack tip increases along x. One can picture volume elements such as the ones shown which elongate under deformation to a lesser extent as x increases. As these elements stretch along y, they will contract in the x and z directions. The overall volume change of such an element will be less as it is moved further away from the crack tip, which sets up stresses ($\sigma(x)$ and $\sigma(z)$) between a large number of such volume elements. Under these conditions of *triaxial stress*, the crack tip is said to be under *mechanical constraint*.

The depth of the crack and the dimension in the z-direction dictate the degree of triaxiality or mechanical constraint. If the crack is too shallow, the stress field at the crack tip cannot fully develop. If the dimension along the z-axis is too small, $\sigma(z)$ will not exceed the yield

stress needed for contraction of the imaginary volume elements. Figure 1.14 illustrates that KI decreases with sample thickness until it reaches a critical value, KIc. As thickness increases, the material passes from a state of plane stress ($\sigma(z) = 0$) to a state of plane strain. Hence, KIc is often referred to as plane-strain fracture toughness. Only when a material is in a state of plane strain, i. e., mechanical constraint and triaxiality exist, can classical LEFM be applied.

The parameter KIc is by definition a material constant, and so its value does not depend on specimen geometry. This is accounted for by analytical expressions for KIc which have general forms as Equation (18)

$$KIc = \frac{Pc}{BW}\, a^{1/2}\, Y \tag{18}$$

where W is a sample dimension parallel to the crack length a, B is the specimen thickness, Y is a geometry factor, and Pc is the load at break. Figure 1.15 demonstrates the compact tension and three-point bend specimens, two common LEFM sample geometries. Their corresponding expressions for KIc are given. Various guidelines have been established for valid plane-strain fracture toughness testing. ASTM E399 details these, however, the discussion by Knott (60) is also particularly helpful.

LEFM study of polymers often utilizes the parameter G, termed the strain energy release rate (60), which is related to KIc for an *elastic* solid by Equations (19) and (20)

$$GIc = \frac{KIc^2}{E} \qquad \text{(plane stress)} \qquad (19)$$

$$GIc = \frac{(1 - \nu^2)}{E} KIc^2 \qquad \text{(plane strain)} \qquad (20)$$

G is defined as the change in stored elastic energy with crack extension. It is frequently referred to as simply the fracture energy.

Sample geometries are available for which the fracture toughness is independent of crack length (7). One which has found considerable use in polymers is the tapered double cantilever beam (TDCB) (61). Figure 1.16a illustrates use of the TDCB for bulk testing while Figure 1.16b shows how it can be used for adhesive testing. For *any* geometry, the fracture energy may be defined as

$$Gc = \frac{Pc^2}{4B} \left(\frac{dC}{da} \right) \qquad (21)$$

where B is the sample width as before and dC/da is the change in compliance with crack length. For the TDCB

$$GIc = \frac{4Pc^2}{B^2Eb} \left(\frac{3a^2}{h^3} + \frac{1}{h} \right) \qquad (22)$$

where Eb is the bending modulus and h is a sample dimension perpendicular to the crack direction. See Figure 1.16. The taper of the TDCB is such that the bracketed term in Equation (22) is a constant for any crack length as long as it stays within the limits of the taper. The calculation of GIc then only requires knowledge of Pc.

Equation (21) allows one to use compliance measurements to determine GIc or KIc without constant surveillance of crack length. It requires prior establishment of a calibration curve of compliance as a function of crack length for a given material and geometry. The TDCB has a *linear* crack length-compliance curve, but the compact tension geometry has a non-linear curve. Use of a crack-compliance curve makes it possible in practice to determine crack length without viewing the specimen. This may be convenient for routine testing but necessary if the material is opaque or is not able to be viewed as is the case for some environmental testing experiments. One can measure crack velocities with these methods or study crack arrest in certain materials. The publications of Bascom, Hunston, and associates provide extensive data for bulk and adhesive samples obtained with the TDCB (62-5). The compliance method must be used with care; general introductions are given by Knott (60) and Hickerson (55).

It is important to remember that these developments are valid only for an elastic material. When extensive plastic deformation accompanies crack extension, LEFM does not apply. Williams (66) describes four types of fracture according to their adherence to the value of a "size scale for yielding," ι, defined as

$$\iota = \frac{KIc^2}{2 M^2 \Psi^2} \tag{23}$$

where Ψ represents the yield stress and $M = (1-2\nu)^{1/2}$, ν being Poisson's ratio. The four types of fracture which Williams proposes are given in

Figure 1.17. Except for case 1, where LEFM holds, the previous developments are not valid and alternate means must be found to characterize fracture toughness.

Rice (67) proposed the the *J-integral* as a means of determining fracture energies for non-linear elastic solids. It is defined as the rate of change in potential energy upon crack extension. The J-integral is a line integral taken on any curve surrounding the notch tip, as long as that curve begins on one surface and ends on the other. When applied to a linear elastic body containing a sharp crack, J-integral analysis will equate J with G. For the cases presented in Figures 1.17b, c, and d, Williams (66) has derived the appropriate J-integral expressions. To the author's knowledge, J-integral methods have been limited primarily to single component polymeric systems.

Impact testing subjects notched and unnotched materials to loads at high rates. Several different types are employed: flexed beam, falling weight, and high-speed tensile testing. Typical strain rates and impact velocities of the various impact methods are given in Table 1.2. Figure 1.18 illustrates the methods of Charpy and Izod impact testing. In practice, a swinging pendulum is dropped from a known height, thus having a known potential energy, and upon meeting the sample, imparts to it some of its kinetic energy, thereby fracturing it. The pendulum then follows through to a height lower than its original height. From the difference between the first and second heights, one can calculate the loss of energy. As a first approximation, it is assumed that all of the

energy lost by the pendulum is absorbed by the sample *before* it breaks. In actuality, several types of energy dissipation are encountered, for example, some of the energy is converted to mechanical energy as the sample flies from its testing position. Various corrections can be made for these energy differences.

Izod and Charpy tests are prone to various physical errors such as specimen fabrication, specimen placement, and notch sharpness. It is therefore recommended that one perform a battery of tests with the variables of notch radius and temperature. Results for a polyvinyl chloride sample are given in Figure 1.19. One notes, and this is a general observation in all tests involving tensile loading of cracks, that a "blunt" notch gives a higher estimate of a sample's resistance to fracture. This arises from the stress concentration at the tip of the crack (Equation (24))

$$K = 1 + 2 (a/r)^{1/2} \tag{24}$$

which increases with (i) a deeper notch (higher value of a) and (ii) a sharper notch (smaller notch tip radius r) (69).

Until fairly recently, impact tests were more or less empirical and did not represent and could not be related to a material constant. In 1973, Brown (71) and Marshall, Williams, and Turner (72) presented independent work relating impact strength and strain energy release rate, G, for notched impact tests. They assumed that the strain energy absorbed *by the sample* from the pendulum, Uc, is equal to UH-UI,

where UH is the energy lost by the pendulum and UI is the energy lost in accelerating the sample from rest. It may be shown (66) that

$$UH = GIcBWZ - UI \qquad (25)$$

where B and W are sample dimensions and

$$Z = \frac{C}{\partial C / \partial(a/W)}$$

where C is the compliance. One may plot $Uc = UH - UI$ vs. BWZ and obtain GIc from its slope (7). Data from Charpy and Izod tests subjected to this analysis can show good agreement. It is possible to apply J-integral fracture mechanics to the impact test; this is described by Kinloch and Young (7).

Falling weight impact tests cannot be subjected to LEFM analysis because they do not involve the propagation of a pre-formed crack. However, their results are often more useful in evaluating the toughness of materials fabricated into large flat or slightly curved pieces which might be subjected to sudden blows.

The sample is generally a small disk 2-3 inches in diameter and is placed on a supporting hollow steel cylinder. A loaded tup or dart is dropped on the sample from a known height and thus impacts the sample at a known velocity with a known potential energy. Typical output for the test consists of apparent modulus, peak energy, breaking energy, total energy, and maximum load. Results are often plotted as energy or load vs. displacement.

Failure usually occurs in either a brittle or ductile fashion. In the former case, the sample may shatter into several pieces or its center may be broken out and several cracks formed at the edges of the irregular hole. If ductile failure occurs, a hole will be punched in the center of the disk as plastically deformed material is pushed out to the other side of the disk. The mass of a sample which fails in a ductile manner will not change as a result of the test.

A single value of falling weight impact strength is of little merit when one is characterizing the impact strength of a material. Proper falling weight testing should be carried out on a series of sample specimens over a range of impact velocities by raising or lowering either the load or drop height of the falling weight. The energy level at which 50% of the specimens break is often given as the impact strength. Testing is particularly valuable if performed over a wide temperature range because it can permit one to locate the ductile-to-brittle transition of a material, assuming it exists. Thickness can also be an important variable.

Both thickness and temperature effects on impact strength are shown in Figure 1.20 for several unmodified and rubber-modified thermoplastics. Reid and Horsley (73) point out that PVC, which showed a sharp increase in impact strength with thickness (Figure 1.20a) failed in a ductile manner whereas the toughened polystyrene failed in a brittle manner. They did not give the temperature at which the data in Figure 1.20a was obtained but it was probably close to or at room temperature.

One notes from Figure 1.20b the variety of responses to temperature shown by high impact PVC. The first sudden change in impact strength exhibited by the toughened PVC may be attributed to the passing of the Tg of the rubber phase, however, other dramatic changes occur near room temperature and again near the Tg of PVC.

It has been suggested that the 50% method described above provides an unfair measure of the impact resistance of a material. An alternative method described by Morris (74) is the "Probit" method which shows the relationship between impact energy and the percentage of specimens fractured. This method is illustrated in Figure 1.21 for an acrylonitrile-butadiene-styrene (ABS) terpolymer, which consists of a graft of a "random" styrene-acrylonitrile copolymer onto a polybutadiene latex. Of particular note is the fact that the impact energies for the "50%" failure rate are very similar for all the temperatures tested while the impact energies for a "1%" failure rate reveal significant differences between materials.

Fatigue, or cyclic loading, studies have become a valuable aspect of fracture mechanics testing. Like falling weight impact tests, they are often good physical reproductions of field use of plastic materials. In practice, the sample, often a compact tension specimen, is cycled between two K values, both being below the critical stress intensity. The change in crack length with the number of loading cycles (da/dN) is measured using a travelling microscope, a compliance-crack length curve, or, in current state of the art, a glue-on network of tiny wires

across which a resistance is continually monitored. A schematic illustration of a full fatigue curve is given in Figure 1.22a. An important parameter for fatigue crack propagation (FCP) evaluation is the slope of the linear portion of this curve, the so-called stable growth region. It is defined by the Paris equation as described in the figure. An example of FCP for unmodified and rubber-modified PVC is given in Figure 1.22b. Adding a rubber to a thermoplastic generally shifts the FCP curve to the right so that crack propagation is lower for the same ΔK. Fatigue of plastic materials is the subject of a book by Hertzberg and Manson (75).

1.4.2. *Toughening Mechanisms*

This section will define the predominant energy absorption mechanisms in polymer materials. The first of these, shear yielding, may occur in thermoplastics or thermosets, but the second, crazing, is for the most part restricted to thermoplastics.

Shear yielding behavior of polymer materials is time- and temperature-dependent due to their viscoelastic nature. This is demonstrated well by Figure 1.23 where the ratio of yield stress (σy) to temperature is plotted vs. the logarithm of strain rate for polycarbonate. The linear relationship shown for each temperature is predicted by Eyring's theory (see Ref. 77) which gives

$$\frac{|\sigma_y|}{T} = \frac{\Delta E^*}{\nu^* T} + \frac{R}{\nu^*} \ln\left(\frac{\dot{e}}{A\dot{E}}\right) \tag{26}$$

where AE is a constant and v^* and ΔE^* are somewhat arbitrary parameters which empirically represent an energy of activation and an activation volume and are chosen to give a best fit to the data shown. From the data shown in Figure 1.23, Bauwens-Crowet et al (77) determined values of 335 kJ/mol and 2.8 nm³ per molecule for ΔE^* and v^*, respectively. Equation (26) holds adequately over certain temperature ranges, but agreement can be poorer over wide temperature ranges. It is then helpful, at least for polycarbonate, to assume that a different activated-flow process occurs at the upper and lower ends of the temperature scale (7).

The outward sign of shear processes during fracture is often a *shear band,* which can form in any amorphous glassy polymer in regions of intense shear. The two extremes of shear bands are demonstrated in Figure 1.24. The sharp so-called "microshear bands" shown for polystyrene (Figure 1.24a) indicate a higher shear strain than do the diffuse shear bands shown for polymethylmethacrylate (PMMA) in Figure 1.24b (7). The simple technique of viewing a sample between crossed polars is sufficient for observing shear bands in some transparent materials, provided that they yield on a fairly large scale. However, more detailed information about shear bands may also be obtained from SEM and TEM. Shear processes need not involve shear band formation. Shear may occur homogeneously as well. It may also occur in semi-crystalline polymers through interlamellar and intralamellar sliding.

Like shear banding, crazing requires localized plastic deformation and is time- and temperature-dependent. Figure 1.25 presents a

stylized version of the microstructure of a craze. Many microfibril structures span the width of the craze, which is usually less than 1 μm. Crazes are only partially filled with polymer material, thus their densities and refractive indices are less than those of the undeformed polymer. Macroscopically, they appear to be fine cracks.

The main plane of a craze will always be perpendicular to an applied uniaxial tensile load. For more complicated stress fields, the craze will develop perpendicular to the maximum principal stress (80). Crazes will not form under a uniaxial compressive stress. Crazing results from the dilatational terms of a tensile stress field and therefore involves a volume expansion. Shearing processes result from the deviatoric terms of the stress field and do not involve any volume change. Consequently, the extent of volume expansion during a tensile test is a principal means of determining the extent of craze formation and the relative amounts of crazing and shearing in materials which undergo both deformation processes (81). This means of differentiating between crazing and shear yielding has, however, met with some criticism, as will be seen later.

It is generally agreed that both crazes and shear yielding are initiated by defects (5,7). Crazes may start at the surface of a bulk polymer through cracks or scratches. Both crazing and shear yielding may be initiated internally through bubbles, dust, voids, or other flaws.

Rubber modification is effective primarily because it increases the volume over which shear yielding and/or crazing may develop (7). The formation of shear bands and crazes is therefore central to the

enhancement of toughening by the addition of a rubber modifier to a brittle polymer. The interplay between shear yielding and crazing is an important feature of mechanistic studies of toughened plastics (82).

Several rubber-toughened polymers will now be examined in terms of their preparation, properties, and toughening mechanisms. Examples of rubber-toughened thermoplastics will include those based on polystyrene, styrene-acrylonitrile copolymers, polyvinyl chloride, and polypropylene. Rubber-modified epoxy resins will be highlighted as examples of rubber-toughened thermosets.

1.4.3. *Toughened Amorphous Thermoplastics*

High-impact polystyrene (HIPS) was the first commercially important toughened plastic. The original processes patented by Dow Chemical Co. involved dissolving SBR (styrene butadiene rubber) in styrene monomer followed by bulk polymerization of the styrene. Agitating the solution during the early stages of the polymerization is believed to effect complete phase inversion (83). This phase inversion makes the polystyrene (PS) the continuous phase and produces a prepolymer which is further polymerized using mass, suspension, or solution processes (84). The final product is a mixture of polystyrene, SBR, and SBR grafted with polystyrene chains.

The morphology of the dispersed phase in HIPS is generally observed to consist of rubber particles containing PS occlusions, as depicted schematically in Figure 1.26. Other structures include solid

rubber particles and single PS particles surrounded by a thin layer of rubber. While agitation most strongly controls this morphology, contributing factors are the viscosities and molecular weights of the PS and the SBR, the free radical initiator used, the crosslink density of the rubber, and the final grafting level.

Turley (85) compared the properties and morphologies of solution prepared (grafted) HIPS and a rubber-modified PS prepared by mechanically blending the rubber and polystyrene. Phase contrast microscopy showed a smaller particle size for the mechanical blend. The low-temperature mechanical damping peak attributed to the rubber was more pronounced for the solution polymer, which suggested to Turley that the rubber in the solution blend was capable of greater energy absorption. Dart drop impact testing showed remarkable differences in impact energy for the solution polymer as a function of rubber content but virtually no change for the simple blend (see Figure 1.27a). Photomicrographs of the films subjected to the dart drop test are given in Figure 1.27b. The "dart" was a projectile similar in size and shape to a sewing needle (85). The ductile behavior of the HIPS as compared to the PS homopolymer and the mechanical blend is clearly evident.

Although noting the widespread crazing of the HIPS film in Figure 1.27b, Turley (85) frequently referred to the data presented in Figure 1.27 in terms of the energy absorbing capabilities of the rubber. This simplistic interpretation was commonly invoked twenty years ago, however, it has been shown that the energy absorption of a dispersed rubber is only one-tenth of that which is observed to be absorbed by a

toughened plastic (86). Most of the energy absorbed must therefore arise from processes occurring in the matrix.

Bucknall and Smith (87) gave the first decisive evidence of crazing as the predominant energy dissipative mechanism in HIPS. Crazes had earlier been observed in unmodified PS (79), but Bucknall and Smith showed that HIPS developed a large number of short crazes upon loading. Since it is the *formation* of the craze that absorbs the most energy, this observation indicated that extensive crazing could indeed be the source of HIPS's enhanced impact strength.

In a two-part series, Bucknall et al (88,89) followed time-dependent volume changes during creep experiments of HIPS and blends of HIPS and polyphenylene oxide (PPO). A more current label for PPO is poly(xylenol ether) (PXE). Data taken at short (< 2500 sec) and long times (> 30,000 sec) is provided in Figure 1.28. During such experiments, one measures the longitudinal strain ($\varepsilon 3$) and thickness strain ($\varepsilon 1$) from which $\Delta V/V$ is determined using Equation (27)

$$\frac{\Delta V}{V} = [(1 + \varepsilon 3)(1 + \varepsilon 1)^2 - 1] \tag{27}$$

It is noted that the volume strain is more rapid at higher stress levels which correlates with Bucknall and Clayton's (88) statement that HIPS instantaneously deforms under tensile creep conditions and then crazes. In the later stages of crazing, microcracks are believed to develop (79).

In similar experiments with a 50/50 HIPS/PXE blend, Bucknall, Clayton, and Keast (89) found that crazing accounted for only about 30% of the observed time-dependent creep. Shear deformation was estimated to account for 70% of the deformation. The percentages given are determined by the relative increases of longitudinal and volume strains. In HIPS, they increase at the same rate. The offset is illustrated in Figure 1.29.

Kinloch and Young (7) caution against use of volume strain measurements as indicative of anything more than the kinetics of dilatational (changing volume) and deviatoric (constant volume) mechanisms. Although shear yielding is a constant volume process, it can be accompanied by voiding, the latter of which would be measured as a dilatational process. It is therefore necessary to utilize microscopy or other suitable techniques for investigating the toughening processes of rubber-modified polymers, as Bucknall, Clayton, and Keast (89) point out.

One such study by Donald and Kramer (90) utilized optical microscopy (OM) to observe deformation mechanisms during strain of HIPS. The resultant microstructure was observed in the TEM after specific strain levels were reached. The shape of the deformed samples was maintained by a supporting copper grid. Donald and Kramer were able to show that solid rubber particles act as craze initiators but also nucleate voids whose growth leads to premature craze failure. Rubber particles with occluded PS also nucleated crazes but maintained good adhesion to the matrix so that voiding did not lead to craze failure.

Fatigue crack propagation studies of PS/HIPS/PXE blends were conducted by Morelli and Takemori (91). They found that extensive "microcrazing" occurred at the crack tips of blends containing only 3% rubber by weight. The craze zone for these blends was larger than in a comparable PS/PXE blend; PS and PXE are a miscible polymer pair, therefore, their blends contain no dispersed phase to provide stress concentration.

An SEM and TEM study of PXE/HIPS blends undertaken by Rimnac et al (92) showed various features of their fatigue fracture surfaces. The authors found that the HIPS particles failed by rupturing. The matrix failed by multiple crazing at low crack growth rates and predominantly by shear yielding at higher rates.

While HIPS has been commercially successful, its impact strength is improved only seven- to ten-fold over that of PS. Styrene-acrylontrile copolymers toughened with butadiene rubber (ABS) have made further strides towards toughening polystyrene. First a polybutadiene (PB) latex is formed in emulsion polymerization. This latex is mixed with styrene and acrylonitrile (AN) monomer and typically a chain transfer agent and free radical initiator (35b). The styrene and AN polymerize and graft to the surface of the small PB latex particles. Particles can agglomerate so that occluded particles grow, similar to those described earlier for HIPS. The grafting is often accompanied by crosslinking (84). The final product contains PB, PB grafted with AN and styrene, and SAN copolymer. Size of the rubber particles directly affects both impact

strength and gloss, with smaller particles favoring better gloss. In order to optimize both properties, one can introduce two particle sizes through controlled particle agglomeration of the PB latex or other methods (84). It is important that the particles be uniformly distributed throughout the SAN matrix. ABS may also be made by bulk polymerization and mechanical blending processes. Although more expensive, emulsion and bulk/suspension prepared ABS have the most desirable properties due to their occluded rubber particles. ABS usually has a particle size of a few tenths of a micron while the dispersed phase in HIPS ranges from 1 to 5 microns (84).

Substantial improvements in the impact strength of PS have been reported by Durst et al (93) for a blend of polystyrene and a proprietary SBS (styrene-butadiene-styrene) block polymer. A polybutadiene rubber content of 20% produced excellent impact strength as compared to unmodified PS. PS homopolymer has an Izod impact strength of 0.2 to 0.3 ft-lb/in (35b,93). Impact strengths for HIPS, ABS, and the PS/SBS blend are 2.2, 7.0, and 7.5 ft-lb/in, respectively (93). It is presumed that the adhesion between the PS matrix and the rubber phase is strong in the PS/SBS blend due to the anchoring of the styrene blocks in the styrene matrix (5). This blend was not commercialized, however, as it was not competitive in terms of its percent elongation, "dart" impact strength, and other important mechanical properties (94).

Dillon and Bevis (95,96) studied model ABS materials which differed in the molecular weight of the matrix, rubber particle size, rubber

content, and degree of grafting. They found that neither the molecular weight of the SAN matrix nor the rubber content were particularly influential in determining the mechanism of deformation. On the other hand, graft frequency, another variable studied, strongly controlled the adhesion of the particles to the matrix and affected mechanical properties. As graft frequency increased, ABS materials containing solid rubber particles showed somewhat higher yield stresses and elongations to break. ABS containing occluded particles suffered drops in these two properties at the highest grafting frequencies. Dillon and Bevis point out that "grafting frequency" is a somewhat arbitrary measurement as currently practiced (see Dillon and Bevis (96)), but they note that the occluded particles form only at "high" grafting frequency. Dillon and Bevis observed that crazing was the predominant mechanism for all the ABS materials, whether studied as tensile bars or solution cast thin films. However, if crazes were terminated by large rubber particles, then shear banding was observed to proceed to some extent. It is generally recognized (66,97) that crazing and shear yielding usually occur simultaneously in ABS. The detailed interactions of shear bands and crazes are still not entirely understood.

The tendency of a rubber-modified thermoplastic matrix to yield or craze is often controlled by temperature. HIPS and ABS generally show three regions of impact strength as a function of temperature. These are illustrated by Figure 1.30a and b. The transition from Region I to II coincides approximately with the T_g of the rubber; -90°C for PB, for example. At sufficient rubber contents, a second rise in impact strength is observed as the ductility of the matrix increases.

1.4.4. *Toughened Semi-Crystalline Polymers*

Polypropylene (PP) and polyvinyl chloride (PVC) are the two semi-crystalline polymers which have been most successfully modified with rubber tougheners. PVC has a low degree of crystallinity (~ 10%) while isotactic-PP (i-PP) may be 70% crystalline. There have also been reports of rubber-toughened polyamides (98-100). This section will first consider rubber toughening of PVC and follow this with a brief discussion of PP impact modification.

Important aspects of impact-modified PVC that will be covered here include i) the extent of impact reinforcement obtained by rubber modification of PVC, ii) the morphology of impact-modified PVC and proposed structure-property relationships, and iii) the possible mechanisms of energy absorption in rubber-modified PVC. For further discussion of impact modifiers used in PVC, one might consult Manson (101), Ryan and Jalbert (102), and Titow (23).

PVC is actually a fairly tough material as compared to many glassy polymers such as polymethylmethacrylate and polystyrene, however, its sensitivity to flaws makes impact modification necessary for some applications. Figure 1.31 illustrates the temperature dependence of Izod impact strength for a PVC modified with 10 and 20% of a commercial methacrylate-butadiene-styrene (MBS) modifier (103). One notes the sigmoidal nature of the temperature dependence, the inflection point of which is generally referred to as the ductile-to-brittle transition or ductile/brittle transition. This transition temperature is lowered from

about 45°C in PVC to 10-15° and 0°C, respectively, for the two modified materials. The figure indicates that the Izod impact strength at room temperature is increased about 20 times through MBS modification, which is typical for the better impact-modified compositions (23). The amount of an impact modifier usually added to PVC for general purposes is 5 to 20 phr (parts per hundred resin), which translates to about 5 to nearly 17 weight percent modifier.

The most common impact modifiers for PVC are the methacrylate-butadiene-styrenes (MBS), chlorinated polyethylenes (CPE), acrylonitrile-butadiene-styrenes (ABS), nitrile rubbers, ethylene-vinyl acetate (EVA) copolymers, and polyacrylates. The impact and toughness properties of PVC can be influenced by other modifiers not added expressly to improve impact resistance. PVC pipe, although not rubber-modified, contains processing aids which impart a ductility sufficient for adequate impact resistance. The effect of various stabilizers on PVC's toughness has been investigated by Younan et al (105). Manson and co-workers (106) have contributed studies of fatigue crack propagation in plasticized PVC to this general area.

The morphology of PVC in an impact-modified compound and of the material as a whole apparently has a considerable influence on its impact strength. Lutz (104) has accordingly divided PVC impact modifiers into three categories which he names and defines as follows:

1. Predefined elastomer (PDE) particle size: found with MBS, methacrylate-acrylonitrile-butadiene-styrene (MABS), acrylics, and modified arylics.

2. Not predefined elastomer (NPDE) particle size: found

with CPE and EVA.

3. ABS may be classed as a "transition" modifier, as defined below.

According to Lutz, PDE modifiers form the dispersed phase in PVC, a state which is changed little by processing over a range of temperatures and milling times. NDPE elastomers apparently function as a binder for unfused PVC particles, thus forming a network of rubber in which PVC particles are embedded; this morphology has been described as a "honeycomb." (Because it degrades well below its melt temperature, PVC is generally processed under conditions where its primary particles ($\sim$ 1 μm) remain intact (107-9).) The "honeycomb" network of NDPE modifiers in PVC is destroyed by relatively high temperatures and long milling times. From a producer's standpoint, the NDPE modifiers can prohibit strict quality control. Typical responses to increased milling temperatures or milling times are presented in Figure 1.32 for various modifiers. Lutz (104) describes ABS (see Figure 1.32b) as a "transition" modifier because its loss of impact strength under extreme processing conditions is due to loss of its well-defined phase dispersity as well as its thermal degradation.

Breuer, Haaf, and Stabenow (110) present a somewhat different picture of ABS as a PVC modifier. They show using TEM micrographs that a network structure formed by ABS at low milling temperatures (140°C) is most conducive to a high impact strength. Milling at 185°C disperses the ABS, as schematically pictured in Figure 1.33, and impact strength drops from 42 to 8 kJ/m². Dimitrov and Foldes (111) have placed the CPE, EVA, and MBS modifiers in a single group with respect to their dispersion in PVC at commercially useful rubber levels.

Lutz's classification of EVA as an NPDE (104) conflicts with Deanin and Shah's (112) finding from optical microscopy that EVA exists as discrete particles, 1-3 μm across, at the modifier levels (5 to 10%) where impact strength was nearly twenty times that of the unmodified PVC. A continuous phase was formed at EVA contents of 25% and above, but this material suffered severe losses in hardness. It is quite likely that the performance of an EVA copolymer as an impact modifier depends on its vinyl acetate percentage.

Siegmann and Hiltner (113) studied the morphologies of CPE/PVC blends using SEM and TEM and related their features to impact performance. They found that a continuous network of interconnected CPE particles is formed at 12-13 weight percent CPE. Fleischer, Fischer, and Brandrup (114) showed network structures for similar compositions of CPE/PVC blends. Siegmann and Hiltner saw the most marked improvement in impact strength when unfused PVC particles remained. They therefore maintained that the PVC primary particles must not be fused (or the CPE dispersed) by long working times or high milling temperatures. The corresponding trends in impact strength are quantified in Table 1.3.

Jyo, Nozaki, and Matsuo (115) showed through staining techniques that EVA/PVC blends retain PVC primary particles up to at least 50% of the modifier. No mechanical properties of the formulations were provided. The extent of fusion is recommended by Benjamin (116), as reported by Krzewki and Collins (117), to be about 60 to 70 percent for

optimal physical properties in impact-modified PVC. However, the supposition that the PVC should remain unfused to any extent has been challenged by Summers, Isner, and Rabinowitch (118), as referenced by Lutz (104). In spite of the apparent lack of a consistent view of the overall morphology of rubber-modified PVC, it is agreed that the morphology which is established by processing conditions can bear heavily on the final impact properties.

The mechanism whereby elastomeric impact modifiers increase the toughness of PVC remains only partially understood. Petrich (103) found no crazing in MBS-modified PVC and attributed its impact improvement over PVC to enhanced matrix yielding near modifier particles. A study of MBS-modified PVC using transmission electron microscopy, light scattering, and optical microscopy (110) has also indicated that MBS raised the impact strength of PVC by generating shear bands (matrix yielding) rather than crazing. However, Siegmann et al (119) did find crazing to a limited extent in PVC and in lightly modified PVC. However, at 13 weight percent CPE, where impact strength was maximized, cavitation was the predominant microdeformation mechanism. Matsuo (120) clearly showed stress whitening and crazing in PVC with rubber modifiers. His results came from samples with an undefined deformation history, however, as they were prepared simply by bending to an angle at which stress whitening was observed. The question of crazing in rubber-modified PVC would appear to be unresolved at this time.

Polypropylene (PP) is modified primarily to improve its low-temperature impact strength. Most of the modification involves combining PP with ethylene or polyethylene through copolymerization, blending, or both. For example, Speri and Patrick (121) were able to raise the notched Izod impact strength of PP from 0.6 to 11.0 ft-lb/in by adding 20% by weight of a blend of high-density polyethylene (HDPE) and the elastomer EPDM. Ramsteiner et al (122) modified PP with polyethylene (PE) in two ways. One was to blend an ethylene-propylene copolymer with 20% HDPE, and the second was to prepare an ethylene-propylene block polymer. D'Orazio et al (123) presented work on blends of HDPE and isotactic-PP containing ethylene-propylene random copolymers. Marked improvements in Izod impact strength were seen for PE/i-PP blends containing up to 15% copolymer. The strongest rise in impact strength occurred at 25% of either PE or PP. It was postulated that the copolymer acted as a "compatibilizer" between the PE and PP, thus enhancing phase adhesion and allowing fracture behavior to pass from a brittle to ductile mode at room temperature.

The effect of rubber modification on the spherulitic superstructure of semi-crystalline PP was investigated by Karger-Kocsis et al (124) using various techniques. Although blending with several different elastomeric modifiers was found to decrease the average spherulite size, this in itself did not always lead to improved impact strength.

1.4.5. *Rubber-Modified Epoxy Resins*

Several different thermosetting resins have been successfully rubber-modified, that is, their fracture properties have been improved by rubber modification without substantial loss of modulus. Examples include epoxy resins, unsaturated polyesters (125), and polyimides (126). The greatest advances have been made with the epoxy resins through modification with CTBN elastomers (carboxyl-terminated butadiene acrylonitrile).

Chapter Two presents considerable discussion of the properties of epoxy resins modified with the conventional butadiene acrylonitrile elastomers. The present discussion will concentrate on the areas of phase mixing and phase separation in rubber-modified epoxies, specific mechanisms of toughening, the effects of time and temperature on toughening, and toughening effects in rubber-modified epoxy adhesives. The developments described here will become more and more critical as elastomers other than the butadiene acrylonitrile copolymers are used to toughen epoxy resins. This will inevitably happen as there is a need for rubber modifiers with better oxidative stability and low temperature toughness than can be offered by elastomers based on butadiene (127).

Preparation of an *un*modified epoxy resin consists of mixing the resin and hardener, usually at elevated temperatures, and curing for several hours at an appropriate temperature. Rubber-modified epoxies may be made in a similar manner by including the reactive rubber in the mixture, however, a two-step procedure is often used. This requires

mixing the rubber and an excess of epoxy resin at moderate temperatures to chemically cap the rubber with the resin. Then a hardener, usually an amine, is added and mixed in well. The mixture is then poured into a mold and cured at elevated temperatures for a few hours. The two-step process ensures that the rubber will be covalently bound to the epoxy resin network. A general reaction scheme is given in Figure 1.34.

The rubber and the resin should be completely miscible prior to the start of the curing schedule. As curing proceeds, the rubber will separate out in the form of dispersed rubber particles. The extent of initial miscibility and its relationship to compatibility as well as the consequent effects on particle size are discussed at length in the next chapter; it will suffice to say here that the size of the precipitated particles will be inversely proportional to the degree of mixing between the rubber and the resin. The growing molecular weight of the crosslinking epoxy resin forces the rubber out of solution. This is believed to occur well before the gelation of the resin as shown, for example, by a small-angle light scattering study of the curing of a CTBN-modified cycloaliphatic epoxy resin (128).

Volume-fraction:

It is well documented that the elastomeric phase in CTBN-modified ✓ epoxies often contains occluded epoxy resin (129,130), as shown by TEM and suggested by SEM. Consequently, the *effective volume fraction* of the elastomeric phase can be larger than the actual added volume fraction of CTBN. The definitive study in this regard was conducted by Bucknall and Yoshii (130) who utilized the variables of curing

conditions, curing agent, and bisphenol A to vary the volume fraction of the elastomeric phase at constant rubber content. The corresponding resin formulations are given in Table 1.4. Rubber phase volume is typically determined by measuring the percentage of area covered by the elastomeric phase in stained cross-sections using TEM. In doing so, one counts particles of "pure" rubber as well as rubber and occluded epoxy resin. Figure 1.35 shows the effect of rubber phase volume fraction on the size of the mechanical damping peak and GIc. Bucknall and Yoshii (130) found in all cases that the measured rubber phase volume was higher than the nominal rubber volume. The importance of the effective rubber volume fraction has also been recognized in rubber-modified thermoplastics (5).

It seems reasonable to assume that the amount of "trapped" resin would be a function of the completeness of phase separation during cure as well as the degree of miscibility achieved prior to cure. Both sides of this point were studied recently by Wang and Zupko (131) who reported a light scattering study of the phase mixing and phase separation of CTBN-modified epoxies. CTBNs having AN contents of 10 and 17% were investigated; the former materials were shown by cloud point determinations to be less miscible with the epoxy resin, which would be expected based on solubility parameters (132). The construction by Wang and Zupko (131) of skewed phase diagrams suggested to them that the epoxy could coexist with a mixed phase of rubber and resin.

A rather sophisticated thermodynamic model of the phase separation processes of rubber-modified epoxy resins during crosslinking was

recently published (133). Finally, Gillham's TTT (time-temperature-transformation) diagram (134) has recently been applied to these systems, and could perhaps eventually be used to predict the necessary conditions of cure for rubber-modified epoxies of optimum physical properties.

The first progress towards a fundamental understanding of rubber toughening in epoxies came in the late 1960's. At that time, McGarry (135,136) demonstrated that fracture surface work could be improved up to nearly 15 times by incorporating 5 to 15% CTBN in epoxy resins. In this early work, Sultan and McGarry (137) claimed that a small particle size encouraged shear yielding while a larger particle size induced crazing. Riew, Rowe, and Siebert (138) agreed with this view, although they observed in rubber-toughened epoxies no "fibrous" crazes similar to those identified in thermoplastics.

Only a few reports of crazing in epoxies published in the open literature have been supported by microscopic evidence. One is a TEM micrograph of an ultrathin section of rubber-modified epoxy taken from the thesis of one of Bucknall's students, Yoshii; the photo appears in Bucknall's book (5). Lilley and Holloway (139) showed craze-like features in several unmodified epoxy resins which occurred at loaded crack tips much as crazes sometimes occur in polystyrene, but no evidence was given that the epoxy structures had the fibrous nature of the crazes seen in thermoplastics. Perhaps the last prominent mention of crazes in connection with rubber-modified epoxies was a 1978 paper in which Bucknall and Yoshii (130) showed through plots of volume vs.

longitudinal strain that there was some increase in volume upon loading in CTBN-modified resins. (See earlier Figures 1.28 and 1.29 and accompanying discussion.) However, as pointed out earlier, voiding will also cause a volume increase in rubber-modified polymers.

On the whole, it is now accepted that crazing, at least as occurs in thermoplastics, is not active in the failure mechanisms of structural epoxy resins which have high crosslink densities and high glass transition temperatures. Donald and Kramer (82) have suggested that crazing is limited in thermoplastics that have a low molecular weight between chain entanglements. On the basis of Donald and Kramer's proposal, crazing is not to be expected in fully cured epoxy resins which have a low molecular weight between crosslinks (7).

Kinloch, Shaw, Tod, and Hunston (140) recently evaluated the proposed toughening mechanisms in rubber-modified epoxy resins. Finding none of them adequate, they have studied a rubber-modified epoxy over a variety of loading rates and temperatures. As a result of that work, Kinloch and co-authors proposed a mechanism for the onset of unstable crack growth. Intrinsic to this mechanism is the generation of a triaxial stress ahead of the crack tip which provokes void formation either inside the rubber particles or between the particles and the matrix. The stress concentration produced at the equators of the rubber particles is said to nucleate shear deformations in the matrix surrounding each particle. Shear yielding begins at one particle and is suggested to terminate at another one. Kinloch et al (140) found that voiding is more important in the early stages of fracture and is intimately

involved with shear deformations, however, it is the shear yielding that is the main source of energy dissipation.

In a second part of the previous study, Kinloch, Shaw, and Hunston (141) extended their proposal to studies of crack blunting in CTBN-modified epoxies and proposed a unique failure criterion which consists of two parameters, $\sigma(tc)$ and c. The parameter c denotes the critical distance ahead of a *sharp* crack at which the critical stress for crack propagation, $\sigma(tc)$, must be attained for crack propagation. The reader may consult Kinloch et al (141) for a quantitative derivation of this criterion. The basis of their formulation is the ability of shear deformation at the loaded crack tip to blunt the crack tip. A blunted crack tip may be associated with an enlarged plastic zone. Equation (21) given earlier illustrates that KIc (as measured) is proportional to the amount of plastically deformed material at the crack tip.

Kinloch et al (141) found $\sigma(tc)$ and c values of 340 MPa and 1.0 μm, respectively, for an unmodified epoxy. Values of 200 MPa and 10 μm were found for a CTBN-modified epoxy. These parameters suggested to Kinloch et al that the parameter $\sigma(tc)$ may be viewed as a constrained yield stress acting over, for the rubber-modified material, a relatively large plastic zone. The level of constraint is presumably less for the rubber-modified epoxy than the unmodified epoxy. Constraint being partially relieved, it is then easier for shear processes to occur at the tip of the crack in the rubber-modified resin. Kinloch, Shaw, and Hunston (141) conclude that further work is needed to determine the physical significance of the critical distance c as well as $\sigma(tc)$. The

reader might consult Kinloch and Williams (142) for the theoretical development of crack blunting mechanisms in epoxies as well as Yamini and Young's work (143) on plastic deformation mechanisms in unmodified epoxy resins. Also helpful is Knott's discussion of the crack opening displacement method in fracture studies (60).

The proposed toughening mechanism of Kinloch and co-workers (140-1) represents the current level of understanding of the toughening in rubber-modified epoxy resins. The primary strength of the theory is its proposal of a unique failure criterion. Bascom et al (63,64) and Yee and Pearson (144,145) have certainly noted the importance of a large plastic zone in achieving high toughening in rubber-modified epoxies. In fact, Yee and Pearson described the roles of voiding and shear yielding and eventual crack blunting in a manner very similar to that of Kinloch et al, but they provided no quantitative criterion.

The matrix itself is given paramount importance in the theories just described. A rather different approach has been taken by Kunz and co-workers (146-8). They have derived a model for the toughness of rubber-modified epoxies based on the observation that crack propagation in these materials is accompanied by the stretching of rubber particles across the tip of the growing crack. These rubber ligaments are observed in the optical microscope to break at critical strains. The energy stored in the elastic rubber is then dissipated. Kunz, Beaumont, and Ashby (146) proposed that the change in G_{Ic} could be expressed by Equation (28)

$$\Delta GIc = \left(1 - \frac{6}{\lambda^2 + \lambda + 4} \right) 4\Gamma V_p \qquad (28)$$

where Γ is the rubber tear energy and V_p is the volume fraction of rubber. This model, which has found qualitatively good agreement with experiments, predicts that toughness will increase with tear energy and volume fraction of the elastomeric phase. The most recent work dealing with this model involved γ-radiation crosslinking of the rubber phase in the *cured* epoxy resins. Free-induction decay nmr experiments indicated that the mobility of the matrix was negligibly affected by the radiation treatment. The Tg of the rubber rose from -55 to about -30°C over the range of administered radiation dosage. The model predicted that GIc would rise with radiation dosage but instead GIc increased slightly and then decreased at the point where it was expected to rise. Sayre et al (148) attributed the lack of agreement to the slow response of the crosslinked rubbers to the fast moving crack. They collected data at only one loading rate. In summary, although this model seems to have merit, its present inability to corroborate theory with experiment in a straightforward manner hinders its potential contribution to mechanistic studies of the toughening of rubber-modified resins. However, the theory does provide a reasonable quantitative estimate of the contribution of the rubber to the total fracture energy.

Time - Temperature effects

xSeveral researchers have demonstrated the effects of time and temperature on the fracture behavior of rubber-modified epoxies. Kinloch et al (140) found that considerable crack blunting occurred in epoxies at high temperatures and slow testing rates. The value of KIc for a *sharp* crack (KIcs) which was used in evaluating the criterion

discussed above was therefore taken to be the value measured at the lowest testing temperature, about -90°C.

Kunz and Beaumont (147) showed the dependence of GIc, KIc, and ✓ E (Young's modulus) on temperature for CTBN-modified epoxy resins. Figure 1.36 shows that in essentially all cases, CTBN modification increased KIc and GIc relative to the unmodified resin., One will recall that GIc is directly proportional to KIc but inversely proportional to Young's modulus (see Equations (19) and (20)). Therefore, changes in both KIc and E will be reflected in GIc as is indicated by Figure 1.37. This is an important demonstration as the conversion to GIc using KIc is now common. (See also Equation (20)).

The effect of loading rate on fracture toughness testing of epoxy ✓ resins. has been demonstrated by various authors (64,65,149-51). A typical example is given in Figure 1.37. As loading rate increases, the dispersed rubber particles become less and less effective as toughening agents. However, even at high toughening rates (akin to low temperatures), the fracture energy of the rubber-modified materials does not fall to that of the unmodified epoxy. See also Figure 1.36.

The toughness of rubber-modified epoxy adhesives has been extensively studied by Bascom, Hunston, and associates (62-5,149-51). One of their more significant findings is the effect of thickness on the adhesive fracture energy. Results taken from a tapered double cantilever beam specimen are given in Figure 1.38. It is seen that the fracture energy passes through a maximum with increasing bond

thickness; further, the maximum occurs at a lower bond thickness with decreasing temperature. The noted increase in fracture energy with increasing bond thickness has been attributed to the development of a fully developed plastic zone (63), however, to this author's knowledge, there is as yet no satisfactory explanation for the decrease in fracture energy beyond a certain thickness. These thickness effects are of concern not only to users of structural adhesives but to the designers of fiber/epoxy composites.✦↖

Possible ramifications of the above thickness effects were demonstrated several years ago by Scott and Phillips (153) who found that the large increases obtained in GIc of bulk CTBN-modified epoxies were not realized in composite materials based on those same resin systems. Unmodified epoxies did not exhibit this difference between bulk and composite fracture energy values. In addition, the interlaminar shear strengths (between matrix and fiber) did not seem to be significantly lowered by rubber modification. Scott and Philips (153) suggested that the unexpectedly low fracture energies of the composite matrices examined were due to the thin film nature of the matrix between the reinforcing fibers. Bascom et al (154) have made some worthwhile comments relating the type of reinforcement (woven vs. non-woven) to the fracture behavior of rubber-modified composites.

REFERENCES

1. Stepek, J., Doaust, H., *Additives for Plastics*, Springer-Verlag: New York, 1983.

2. Olabisi, O., Robeson, L. M., Shaw, M. T., *Polymer-Polymer Miscibility*, Academic Press: New York, 1979.

3. Sears, J. K., Darby, J. R., *The Technology of Plasticizers*, Wiley: New York, 1982.

4. *Plasticization and Plasticization Processes*, Platzer, N. A., ed., Am. Chem. Soc. Adv. Chem. Ser., *48* (1965).

5. Bucknall, C. B., *Toughened Plastics*, Applied Science: London, 1977.

6. *Rubber-Modified Thermoset Resins*, Riew, C. K., Gillham, J. K., eds., Am. Chem. Soc. Adv. Chem. Ser., *208* (1965).

7. Kinloch, A. J., Young, R. J., *Fracture Behaviour of Polymers*, Applied Science: London, 1983.

8. Flory, P. J., *Principles of Polymer Chemistry*, Cornell Univ. Press: Ithaca, NY, 1953.

9. Hildebrand, J. H., J. Chem. Phys., *15*, 225 (1947).

10. Elias, H.-G., *Macromolecules-1: Structure and Properties*, Plenum Press: New York, 1977.

11. Flory, P. J., J. Chem. Phys., *9*, 660 (1941).

12. Scott, R. L., J. Chem. Phys., *17*, 279 (1949).

13. Krause, S., Chap. 2 in *Polymer Blends*, Vol. 1, Paul, D. R., Newman, S., eds., Academic Press: New York, 1978.

14. Doty, P., Zable, H. S., J. Polym. Sci., *1*, 90 (1946).

15. Su, C. S., Patterson, D., Schreiber, H. P., J. Appl. Polym. Sci., *20*, 1025 (1976).

16. Stinson, S. C., Chem. Eng. News, p. 27 (June 18, 1984).

17. Naqvi, M. K., J. Macromol. Sci. -- Rev. Macromol. Chem. Phys., *C25*, 119 (1985).

18. Danforth, J. D., Spiegel, J., Bloom, J., J. Macromol. Sci. -- Chem., *A17*, 1107 (1982).

19. Tudos, F., Kelen, T., Nagy, T. T., Chap. 7 in *Developments in Polymer Degradation - 2*, Grassie, N., ed., Applied Science: London, 1979.

20. Starnes, W. H., Jr., Schilling, F. C., Plitz, I. M., Cais, R. E., Freed, D. J., Hartless, R. L., Bovey, F. A., Macromolecules, *16*, 790 (1983).

21. Titow, W. V., Chap. 9 in *PVC Technology*, Fourth Edition, Titow, W. V., ed., Elsevier: London, 1984.

22. Nass, L. I., Chaps. 8 and 9 in *Encyclopedia of PVC*, Vol. 1, Nass, L. I., ed., Marcel Dekker: New York, 1976.

23. *PVC Technology*, Titow, W. V., ed., Fourth Edition, Elsevier: London, 1984.

24. Marks, G. C., Chap. 2 in *Developments in PVC Technology*, Henson, J. H. L., Whelan, A., eds., Applied Science: London, 1973.

25. Tester, D. A., Chap. 10 in *Manufacture and Processing of PVC*, Burgess, R. H., ed., Applied Science: London, 1982.

26. Krauskopf, L. G., Plast. Compd. (Jan/Feb 1983).

27. McKinney, P. V., J. Appl. Polym. Sci., *9*, 3359 (1965).

28. Frissell, W. J., Mod. Plast., *38*, 232 (1961).

29. Bargellini, F., Mater. Plast., *28*, 372 (1962), adapted in Ref. 3.

30. Buszard, D. L., Chaps. 5 - 7 in *PVC Technology*, Fourth Edition, Titow, W. V., ed., Elsevier: London, 1984.

31. Darby, J. R., Touchette, N. W., and Sears, J. K., Polym. Eng. Sci., *7*, 295 (1967).

32. *Encyclopedia of PVC*, Vol. 1, Nass, L. I., ed., Marcel Dekker: New York, 1976.

33. Sarvetnick, H. A., Chap. 5 in *Polyvinyl Chloride*, Van Nostrand Reinhold: New York, 1969.

34. Sears, J. K., Touchette, N. W., in *Kirk-Othmer Encyclopedia of Chemical Technology*, Vol. 18, Wiley: New York, 1982, p.111.

35a. Hertz, D. L., Paper presented at the 123rd Meeting, Am. Chem. Soc., Rubber Division, May 11, 1983.

35b. Saunders, K. J., *Organic Polymer Chemistry*, Chapman and Hall: London, 1973.

36. Boyer, R. F., J. Appl. Phys., *20*, 540 (1949).

37. Hansen, C. M., Off. Dig. J. Paint Technol. Eng., *37*, 57 (1965), referenced in Ref. 3.

38. Lawrence, R. R., McIntyre, E. B., Ind. Eng. Chem., *41*, 689 (1949).

39. Park, G. S., Van Hoang, T., Eur. Polym. J., *15*, 817 (1979).

40. Zieminski, K. F., Peppas, N. A., Die Angew. Makromol. Chem., *116*, 77 (1983).

41. Kampouris, E. M., Regas, F., Rokotas, S., Polychronakis, S., Pantazoglou, M., Polymer, *16*, 840 (1975).

42. Zieminski, K. F., Peppas, N. A., J. Appl. Polym. Sci., *28* 1751 (1983).

43. Messadi, D., Vergnaud, J. M., J. Appl. Polym. Sci., *27,* 3945 (1982).

44. Ghersa, P., Mod. Plast. *36,* 135 (1958), referenced in Refs. 3 and 30.

45. Brous, S. L., Semon, W. L., Ind. Eng. Chem., *27,* 667 (1935), referenced in Refs. 3 and 30.

46. Jacobson, U., Brit. Plast., *32,* 152 (1959).

47. Horsley, R. A., in *Plastics Progress 1957,* Iliffe and Sons: London, 1958, pp. 77-88, referenced in Ref. 46.

48. Pizzoli, M., Pezzin, G., Ceccorulli, G., J. Macromol. Sci. -- Phys., *B14,* 241 (1977).

49. Pezzin, G., Ajroldi, G., Casiraghi, T., Garbuglio, C., Vittadini, G., J. Appl. Polym. Sci., *16,* 1839 (1972).

50. Robeson, L. M., Faucher, J. A., J. Polym. Sci.: Polym. Lett., *7,* 35 (1969).

51. Robeson, L. M., Polym. Eng. Sci., *9,* 277 (1969).

52. Griffith, A. A., Phil. Trans. Roy. Soc., *221,* 163 (1920).

53. Irwin, G. R., Trans. ASME, J. Appl. Mech., *24,* 361 (1957); Irwin, G. R., Kies, J. A., Smith, H. L., Proc. ASTM, *58,* 640 (1958); Irwin, G. R., 9th Intern. Congr. Appl. Mech., *VIII,* Paper 101, Univ. Brussels, 245 (1957).

54. Orowan, E., Trans. Inst. Engrs. Shipbuilders Scotland, *89,* 165 (1945).

55. Hickerson, J., Sandia National Labs, unpublished text.

56. Bascom, W. D., Hunston, D. L., Timmons, C. O., Org. Coat. Plast. Chem., *38*, 179 (1978).

57. Bascom, W. D., Timmons, C. O., Jones, R. L., J. Mater. Sci., *10*, 1037 (1975).

58. Hayes, D. J., Chap. 1 in *A General Introduction to Fracture Mechanics*, Mechanical Engineering Publications: London, 1978.

59. Loss, F. J., "Concepts of Fracture Toughness and Structural Integrity," NRL Report 8085, March 31, 1977.

60. Knott, J. F., *Fundamentals of Fracture Mechanics*, Wiley: New York, 1973.

61. Mostovoy, S., Ripling, E. J., J. Appl. Polym. Sci., *10*, 1351 (1966).

62. Bascom, W. D., Cottington, R. L., J. Adhesion, *7*, 333 (1976).

63. Bascom, W. D., Cottington, R. L., Jones, R. L., J. Appl. Polym. Sci., *19*, 2545 (1975).

64. Bascom, W. D., Hunston, D. L., Chap. 14 in *Adhesion - 6*, Allen, K. W., ed., Applied Science: London, 1982.

65. Hunston, D. L., Bitner, J. L., Rushford, J. L., Oroshnik, J., Rose, W. S., J. Elast. Plast., *12*, 133 (1980).

66. Williams, J. G., *Fracture Mechanics of Polymers*, Ellis Harwood: Chichester, Great Britain, 1984.

67. Rice, J. R., Trans. ASME, J. Appl. Mech., 379 (June 1968).

68. Reed, P. E., Chap. 4 in *Developments in Polymer Fracture -1*, Andrews, E. H., ed., Applied Science: London, 1979.

69. Turner, S., *Mechanical Testing of Plastics*, CRC Press: Cleveland, 1973.

70. Vincent, P. I., "Impact Tests and Service Performance of Materials," Plastics Institute, referenced in Ref. 69.

71. Brown, H. R., J. Mater. Sci., *8*, 941 (1973).

72. Marshall, G. P., Williams, J. G., Turner, C. E., J. Mater. Sci., *8*, 949 (1973).

73. Reid, D. R., Horsley, R. A., Brit. Plast., *32*, 156 (1959).

74. Morris, A. C., Plast. Polym., *36*, 433 (1968).

75. Hertzberg, R. W., Manson, J. A., *Fatigue of Engineering Plastics*, Academic Press: New York, 1980.

76. Skibo, M. D., Manson, J. A., Hertzberg, R. W., Collins, E. A., Am. Chem. Soc. Symp. Ser., *95*, 311 (1979).

77. Bauwens-Crowet, C., Bauwens, J. C., Homes, G., J. Polym. Sci.: Part A-2, *7*, 735 (1969).

78. Bowden, P.B., Phil. Mag., *22*, 455 (1970).

79. Kambour, R. P., J. Polym. Sci.: Macromol. Rev., *7*, 1 (1973).

80. Hull, D., in *Deformatiion and Fracture of High Polymers*, Kausch, H. H., Hassell, J. A., Jaffee, R. I., eds., Plenum Press: New York, 1973.

81. Haward, R. N., Bucknall, C. B., Pure Appl. Chem., *46*, 227 (1976).

82. Donald, A. M., Kramer, E. J., J. Mater. Sci., *17*, 1871 (1982).

83. Molau, G. E., Keskkula, H., Appl. Polym. Symp., *7*, 35-40 (1968).

84. Platzer, N., Chemtech, *7*, 634 (1977).

85. Turley, S. G., Appl. Polym. Symp., *7*, 237 (1968).

86. Newman, S., Strella, S., J. Appl. Polym. Sci., *9*, 2297 (1965).

87. Bucknall, C. B., Smith, R. R., Polymer, *6*, 437 (1965).

88. Bucknall, C. B., Clayton, D., J. Mater. Sci., *7*, 202 (1972).

89. Bucknall, C. B., Clayton, D., Keast, W. E., J. Mater. Sci., *7*, 1443 (1972).

90. Donald, A. M., Kramer, E. J., J. Mater. Sci., *17*, 2351 (1982).

91. Morelli, T. A., Takemori, M. T., J. Mater. Sci., *18*, 1836 (1983).

92. Rimnac, C. M., Hertzberg, R. W., Manson, J. A., Polymer, *23*, 1977 (1982).

93. Durst, R. R., Griffith, R. M., Urbanic, A. J., Van Essen, W. J., Am. Chem. Soc. Adv. Chem. Ser., *154*, 239 (1976).

94. McGrath, J. E., personal communication.

95. Dillon, M., Bevis, M., J. Mater. Sci., *17*, 1895 (1982).

96. Dillon, M., Bevis, M., J. Mater. Sci., *17*, 1903 (1982).

97. Bucknall, C. B., Page, C. J., Young, V. O., Am. Chem. Soc. Adv. Chem. Ser., *154*, 179 (1976).

98. Newman, S., Chap. 13 in *Polymer Blends*, Vol. 2, Paul, D. R., Newman, S., eds., Academic Press: New York, 1978.

99. Flexman, E. A., Polym. Eng. Sci., *19*, 564 (1974).

100. Chuang, H.-K., Han, C.-D., J. Appl. Polym. Sci., *30*, 165 (1985).

101. Manson, J. A., Pure Appl. Chem., *53*, 471 (1981).

102. Ryan, C. F., Jalbert, R. L., in Chap. 12, *Encyclopedia of PVC*, Vol. 2, Nass, L. I., ed., Marcel Dekker: New York, 1977.

103. Petrich, R. P., Polym. Eng. Sci., *13*, 248 (1973).

104. Lutz, J. T., Polym.-Plast. Technol. Eng., *21*, 99 (1983).

105. Younan, M. Y. A., El-Rifai, M. A., Hohsen, R., El-Hennaw, I. M., J. Appl. Polym. Sci., *28,* 3247 (1983).

106. Rimnac, C. M., Hertzberg, R. W., Manson, J. A., Pract. Mater. Sci., ASTM STP 733, Gilbertson, L. N., Zipp, R. D., eds., p. 291 (1981); Skibo, M., Manson, J. A., Hertzberg, R. W., Collins, E. A., J. Macromol. Sci. -- Phys., *B14,* 525 (1977).

107. Berens, A. R., Folt, V. L., Trans. Soc. Rheol., *11,* 95 (1967).

108. Singleton, C., Isner, J., Gezovich, D. M., Tsou, P. K. C., Geil, P. H., Collins, E. A., Polym. Eng. Sci., *14,* 371 (1974).

109. *Particulate Nature of PVC,* Butters, G., ed., Applied Science: London, 1982.

110. Breuer, H., Haaf, F., Stabenow, J., J. Macromol. Sci. -- Phys., *B14,* 387 (1977).

111. Dimitrov, M., Foldes, E., Die Angew. Makromol. Chem., *106,* 91 (1982).

112. Deanin, R. D., Shah, N. A., J. Vinyl Technol., *5,* 167 (1983).

113. Siegmann, A., Hiltner, A., Polym. Eng. Sci., *24,* 869 (1984).

114. Fleischer, D., Fischer, E., Brandrup, J., J. Macromol. Sci., *B14,* 17 (1977).

115. Jyo, Y., Nozaki, C., Matsuo, M., Macromolecules, *4,* 517 (1971).

116. Benjamin, P., Proc. Intern. Conf. PVC Process., p. B5, Plastics and Rubber Institute, London (April 1978).

117. Krzewki, R. J., Collins, E. A., J. Vinyl Technol., *3*, 116 (1981).

118. Summers, R. J., Isner, J. D., Rabinovitch, E. B.,
     36th SPE ANTEC, 1978, p. 757.

119. Siegmann, A., English, L. K., Baer, E., Hiltner, A.,
     Polym. Eng. Sci., *24*, 877 (1984).

120. Matsuo, M., Polym. Eng. Sci., *9*, 206 (1969).

121. Speri, W. M., Patrick, G. R., Polym. Eng. Sci., *15*, 668 (1975).

122. Ramsteiner, F., Kanig, G., Heckmann, W., Gruber, W., Polymer,
     24, 365 (1983).

123. D'Orazio, L., Greco, R., Mancarella, C., Martuscelli, E.,
     Ragosta, G., Silvestre, C., Polym. Eng. Sci., *22*, 536 (1982).

124. Karger-Kocsis, J., Kallo, A., Szafner, A., Bodor, G.,
     Senyei, Zs., Polymer, *20*, 37 (1979).

125. Engelhardt, J. T., Nichols, C. S., Am. Chem. Soc. Adv.)
     Chem. Ser., *208*, 335 (1984).

126. Kinloch, A. J., Shaw, S. J., Tod, D. A., Am. Chem. Soc. Adv.
     Chem. Ser., *208*, 101 (1984).*

127. Bucknall, C. B., J. Elast. Plast., *14*, 204 (1982).

128. Visconti, S., Marchessault, R. H., Macromolecules, 7, 913 (1974).

129. Manzione, L. T., Gillham, J. K., McPherson, C. A., J. Appl.
     Polym. Sci., *26*, 889, 907 (1981).

130. Bucknall, C. B., Yoshii, T., Brit. Polym. J., *10*, 53 (1978).

131. Wang, T. T., Zupko, H. M., J. Appl. Polym. Sci., *26*,
     2391 (1981).

132. Rowe, E. H., Siebert, A. R., Drake, R. S., Mod. Plast., *47*, 110 (Aug 1970).

133. Williams, R. J. J., Borrajo, J., Adabbo, H. E., Rojas, A. J., Am. Chem. Soc. Adv. Chem. Ser., *208*, 195 (1984). ✓

134. Chan, L. C., Gillham, J. K., Kinloch, A. J., Shaw, S. J., Am. Chem. Soc. Adv. Chem. Ser., *208*, 235, 261 (1984).

135. McGarry, F. J., Proc. Roy. Soc. Lond., *A319*, 59 (1970).

136. McGarry, F. J., Sultan, J. N., 24th Ann. Tech. Conf. Reinf. Plast./Compos. Div., SPI, Sect. 11-B, (1969).

137. Sultan, J. N., McGarry, F. J., Polym. Eng. Sci., *13*, 29 (1973).

138. Riew, C. K., Rowe, E. H., Siebert, A. R., Am. Chem. Soc. Adv. Chem. Ser., *154*, 326 (1976).

139. Lilley, J., Holloway, D. G., Phil. Mag., *28, Ser. 8*, 215 (1973).

140. Kinloch, A. J., Shaw, S. J., Tod, D. A., Hunston, D. L., Polymer, *24*, 1341 (1983).

141. Kinloch, A. J., Shaw, S. J., Hunston, D. L., Polymer, *24*, 1355 (1983).

142. Kinloch, A. J., Williams, J. G., J. Mater. Sci., *15*, 987 (1980).

143. Yamini, S., Young, R. J., J. Mater. Sci., *15*, 1814, 1823 (1980).

144. Yee, A. F., Pearson, R. A., General Electric Co., NASA Contractor Report 3718, 1983.

145. Yee, A. F., Pearson, R. A., 28th IUPAC Macromol. Symp., 621 (1982).

146. Kunz-Douglass, S. C., Beaumont, P. W. R., Ashby, M. F., J. Mater. Sci., *15*, 1109 (1980).

147. Kunz, S. C., Beaumont, P. W. R., J. Mater. Sci., *16*, 3141 (1981).

148. Sayre, J. A., Kunz, S. C., Assink, R. A., Am. Chem. Soc. Adv. Chem. Ser. *208*, 215 (1984).

149. Ting, R. Y., Cottington, R. L., Polym. Bull., *2*, 211 (1980).

150. Bitner, J. L., Rushford, J. L., Rose, W. L., Hunston, D. L., Riew, C. K., J. Adhesion, *13*, 3 (1981).

151. Kinloch, A. J., Shaw, S. J., J. Adhesion, *12*, 59 (1981).

152. Bascom, W. D., Ting, R. Y., Moulton, R. J., Riew, C. K., Siebert, A. R., J. Mater. Sci., *16*, 2657 (1981).

153. Scott, J. M., Phillips, D. C., J. Mater. Sci., *10*, 551 (1975).

154. Bascom, W. D., Bitner, J. L., Moulton, R. J., Siebert, A. R., Composites, *10*, 9 (1980).

Table 1.1. Typical Properties of General-Purpose Plasticizers (26)

	Diisononyl phthalate	Di(2-ethylhexyl) phthalate	Diisooctyl phthalate	Di(2-ethylhexyl) terephthalate	Diisoheptyl phthalate
Common name	DINP	DOP	DIOP	DOTP	DIHP
Molecular weight	419	391	391	391	362
Color, Pt Co	<25	<25	<25	<25	<25
Specific gravity, 20/20C	0.972	0.986	0.985	0.984	0.995
Refractive index, n_D^{20}	1.486	1.486	1.487	1.489	1.488
Pour point, deg C	-48	-46	-46	-64	-40
Viscosity, cs at					
0C (32F)	500	386	385	415	200
20C (68F)	102	22	21	65	51
37.8C (100F)	37	31	30		22
100C (212F)	6	5	5		4
Vapor pressure, mm Hg at					
100C	0.0018	0.003	0.004	<0.001	0.006
200C	0.50	1.20	1.30	0.40	2.2
300C	40	96	97	50	150
Boiling point at 5 mm Hg, deg C	252	231	235	258	220
Flash point, P-M closed cup, deg C (F)	213(415)	206(403)	204(400)	223(432)	199(390)
Coefficient of expansion, cm³/g/deg C at 20C	0.00076	0.00076	0.00076	0.00076	0.00076
Water content, wt-%	<0.1	<0.1	<0.1	<0.1	<0.1
Wt/vol, lb/gal at 20C	8.09	8.21	8.21	8.19	8.28
DOT hazard class			Nonhazardous		

Table 1.2. Order-of-Magnitude Characteristics
of Various Impact Tests (68)

Method	Order of magnitude of strain rate (s^{-1})	Velocity m s^{-1}
Charpy	(10)	3
Izod	(60)	2·44
Falling ball	10^{-1} 10	1·4
Conventional Instron	10^{-3} 10^{-1}	10^{-5} 10^{-1}
Pneumatic gun	10^2–10^4	20–240
Hydraulic systems	1 10^2	·008 4

Table 1.3.   Impact Strength of
CPE/PVC Blends*

CPE Wt. % in PVC	Mixing temperature and time	Impact Strength+ (ft-lbs/in notch)
0	5 min - 178°C	0.81
2	5 min - 178°C	0.94
7	5 min - 178°C	2.81
13	5 min - 178°C	23.91
17	5 min - 178°C	26.82
13	20 min - 178°C	11.30
13	10 min - 178°C	1.52

* From Siegmann and Hiltner (113)

+ ASTM-D256;   samples compression molded at 193°C for 5 min.

Table 1.4. Resin Formulations (Bucknall and Yoshii (130))

Resin	CTBN (wt. %)	Hardener (phr)	Bisphenol A (phr)	Cure Temperature (°C)	Particle Size (µm)	Rubber Phase Vol. %	GIc (kJ/m²)
A	0	80 HHPA, 1 BDMA	0	120	---	---	0.38
B	0	5 Pip.	0	120	---	---	0.72
C	0	5 K61B	24	130	---	---	0.76
D	8.7	40 HHPA 1 BDMA	0	120	0.9	9.3	3.5
E	8.7	80 HHPA, 1 BDMA	0	120	1.1	9.8	2.5
F	8.7	5 K61B	0	130	1.4	11.2	6.5
G	8.7	5 K61B	12	130	1.3	12.4	6.3
H	8.7	5 Pip.	0	120	1.7	12.7	5.3
J	8.7	5 K61B	40	130	0.5/3.0	18.3	6.1
K	8.7	5 K61B	24	130	1.1	19.0	8.4
L	8.7	5 K61B	24	130	0.1/4.0	19.5	7.8
M	8.7	5 K61B	0	130	1.6	20.5	9.2

Notes from original reference:
(i)   Resins J and L have bimodal distribution of particle sizes.
(ii)   Resin L: bisphenol A was pre-reacted with the epoxy resin
       before rubber andd hardener were added.
(iii) Resin M: prepared from Araldite 6100 (a high molecular weight
       epoxy resin; all others prepared from Epikote 828 epoxy resin.

From author:
(i)   The rubbers were not explicitly capped with the resin prior
       to the addition of the hardener.
(ii)   HHPA = Hexahydrophthalic anhydride
       BDMA = benzyl dimethyl amine (an accelerator)
       Epikure K61B = Tri-(2-ethyl hexanoic acid) salt of
               2,4,6-tri-dimethylaminomethyl phenol
       Pip. = Piperidine
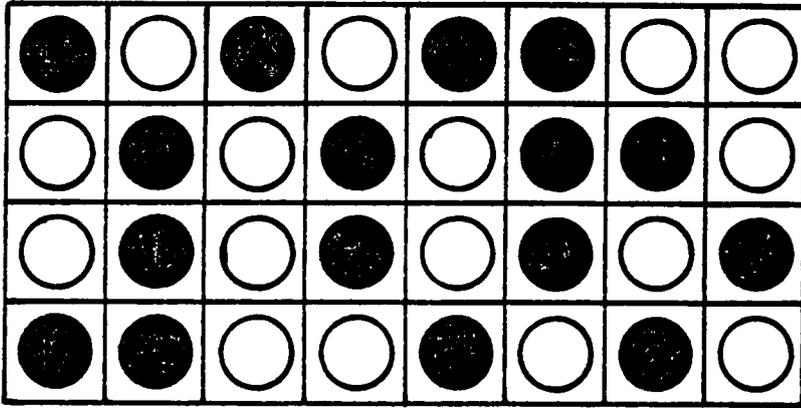
a
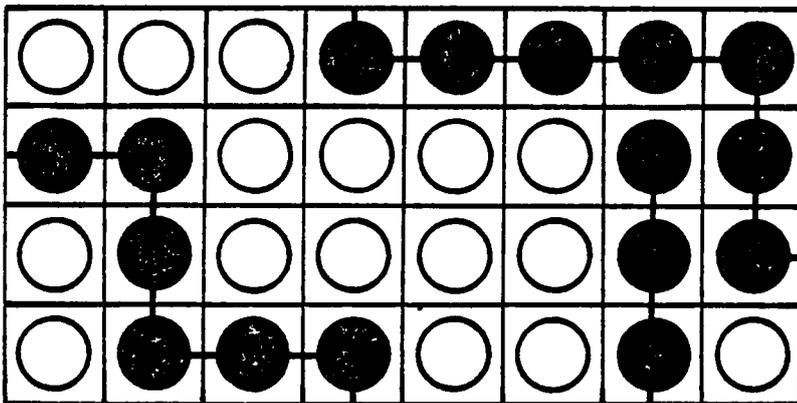
b

Figure 1.1. Lattice representation of a) a mixture of two low molecular
weight species and b) a mixture of low and high molecular
weight species.
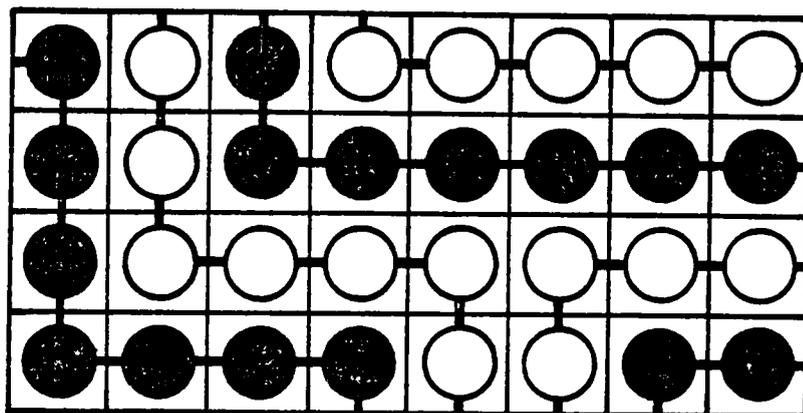
Figure 1.2.   Lattice representation of a polymer-polymer solution.
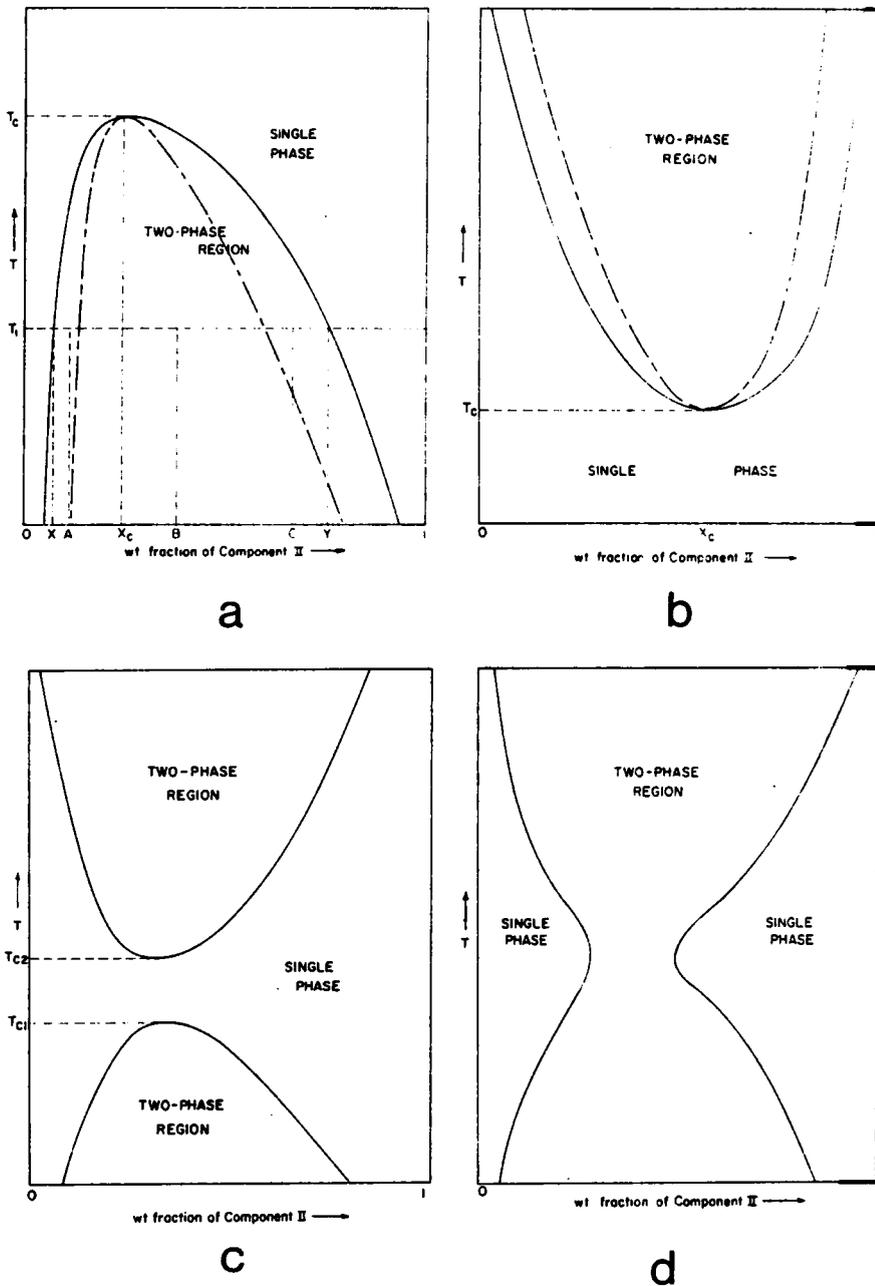
Figure 1.3. Phase diagrams for various two-component mixtures as a function of temperature: a) a mixture with an upper critical solution temperature (UCST): binodal (_____), spinodal (------); b) a mixture with a lower critical solution temperature (LCST): binodal (_____), spinodal (------); c) a mixture with an LCST above a UCST, and d) a mixture with a tendency towards greater solubility at intermediate temperatures. Ref. 13.
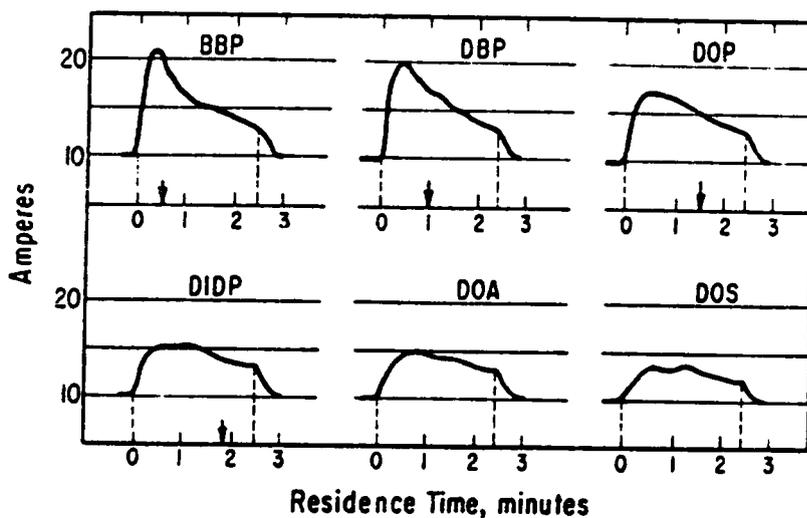
Plasticizer	Solubility Parameter $(cal/cc)^{\frac{1}{2}}$
BBP	9.88
DBP	9.41
DOP	8.83
DIDP	8.56
DOA	8.46
DOS	8.43

Figure 1.4. Profiles of power requirements during fusion and mixing of PVC-plasticizer blends in a Banbury mixer. Ref. 29, taken from Ref. 3. Solubility parameters from Ref. 3, calculated by Small's method.
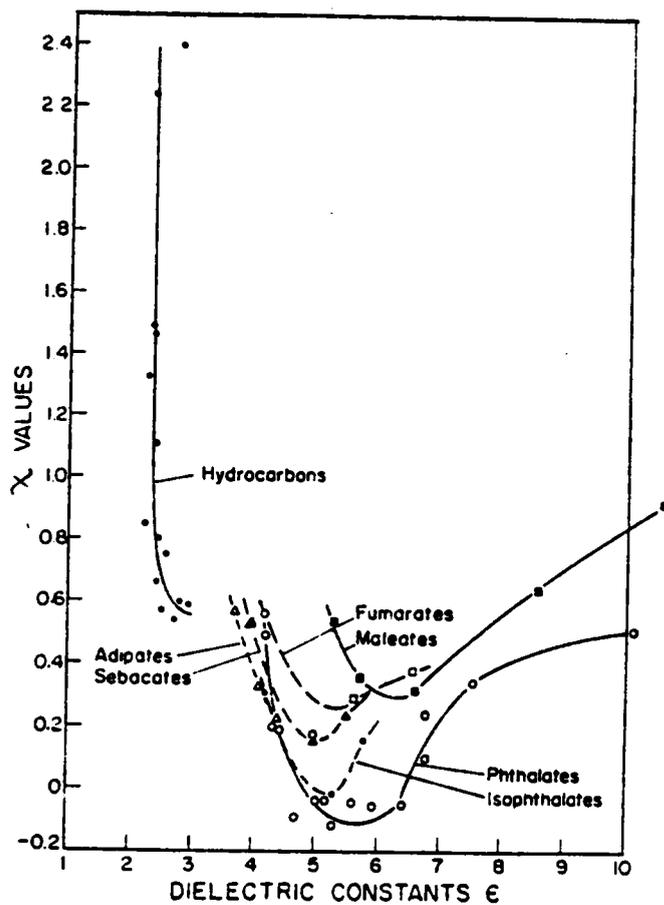
Figure 1.5. Chi parameter (x) vs. dielectric constant (ε) for various homologous series. Ref. 31, taken from Ref. 3.
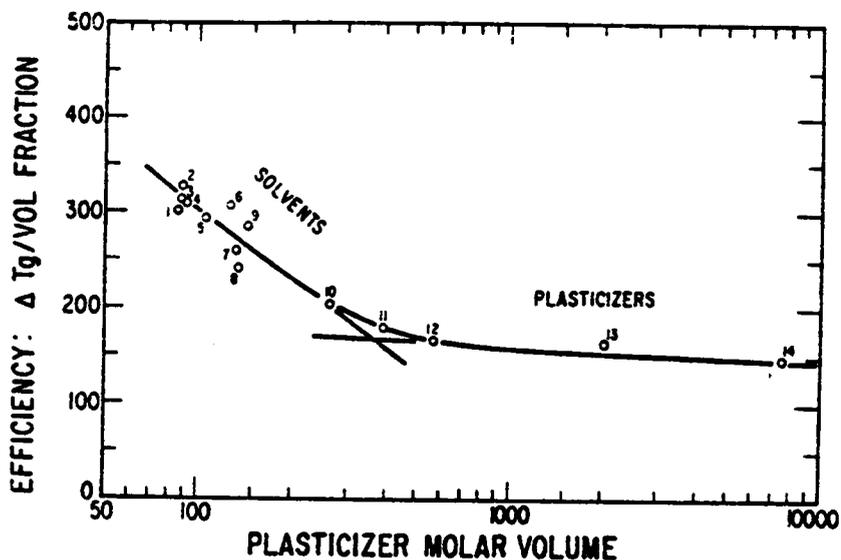
Figure 1.6. Effect of molar volume on plasticizing efficiency as measured by Tg depression of a copolymer of vinyl chloride and 14% vinyl acetate. Data points: 1 = 2-nitropropane, 2 = methyl ethyl ketone, 3 = trichloroethane, 4 = ethyl acetate, 5 = toluene, 6 = methyl isobutyl ketone, 7 = n-butyl acetate, 8 = 2-ethyoxyethyl acetate, 9 = methylisoamyl ketone, 10 = DBP, 11 = DOP, 12 = acetyl tri-2-ethylhexyl citrate, 13/14 = oligomeric polyesters. Ref. 37, taken from Ref. 3.
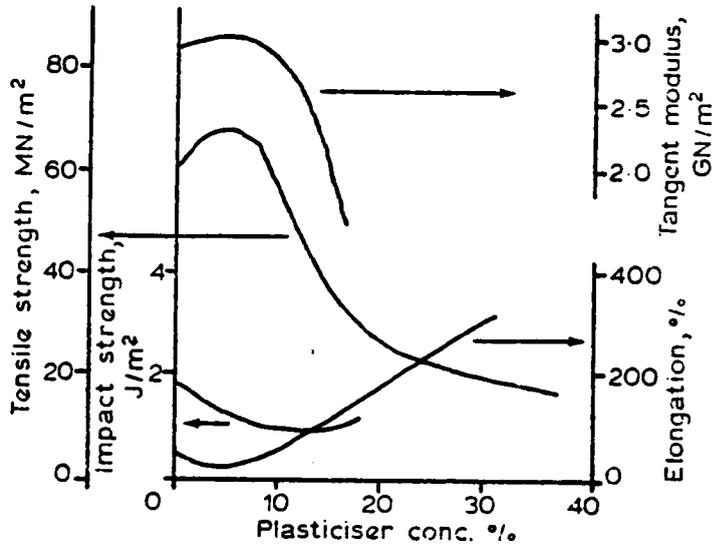
Figure 1.7. Effect of low concentrations of DOP on some mechanical properties of PVC. Ref. 30, after Ref. 44.
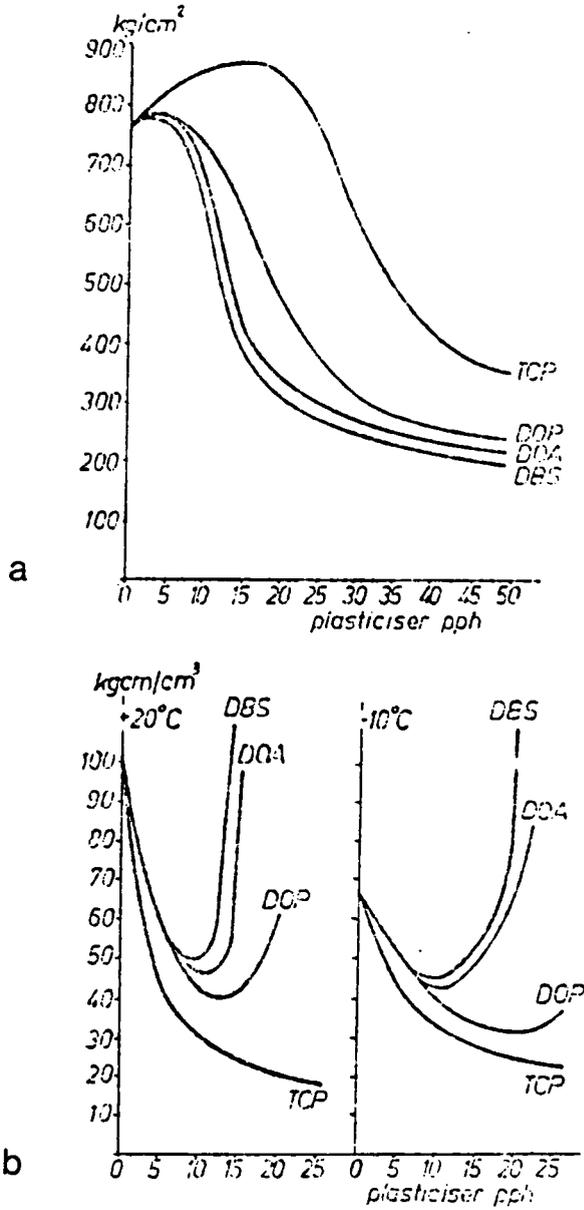
Figure 1.8. Effect of low concentration of plasticizers on PVC's a) impact strength at 20° and -10°C and b) tensile strength. Ref. 46. Solubility parameters: TCP = 9.86, DOP = 8.83, DOA = 8.46, DBS = 8.63, from Ref. 3.
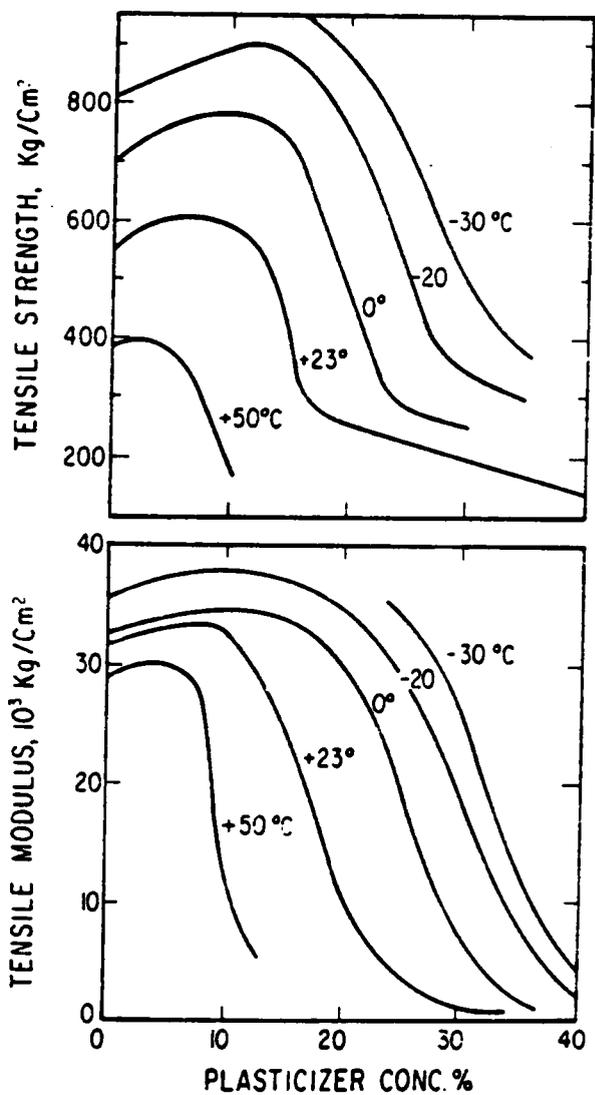
Figure 1.9. Effect of low concentration of DOP on PVC's tensile strength and tensile modulus as a function of temperature.
Ref. 44, taken from Ref. 3.
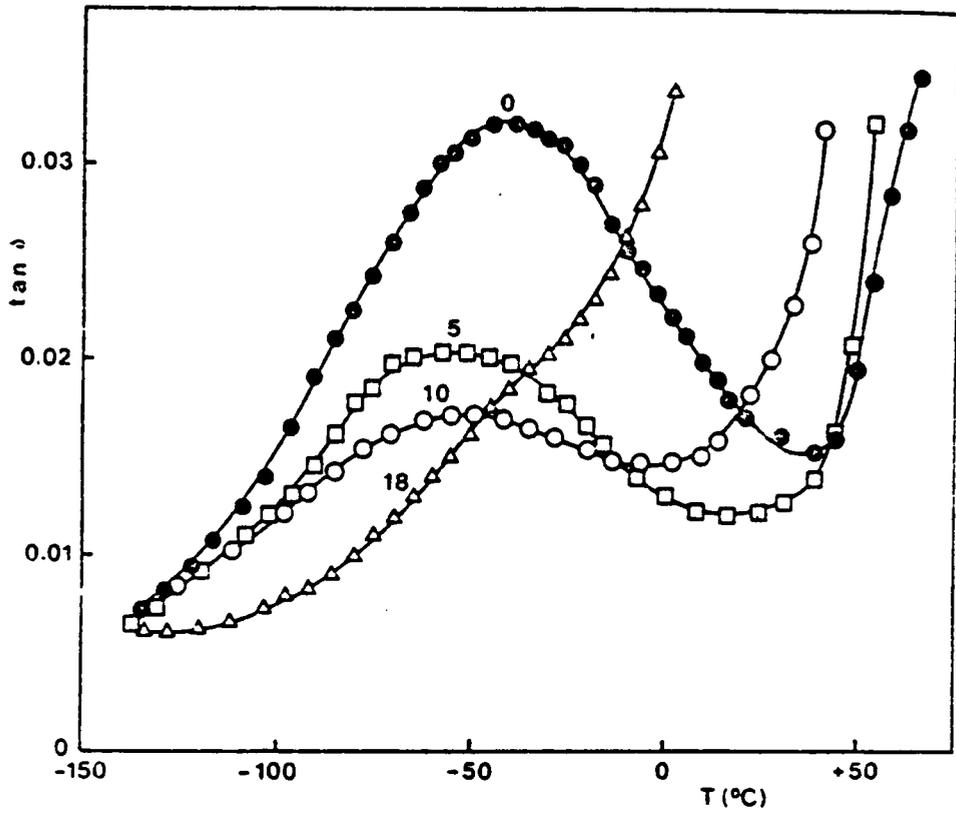
Figure 1.10. Loss tangent as a function of temperature at 11 cps. Numbers indicate weight percent DBP in PVC. Ref. 48.
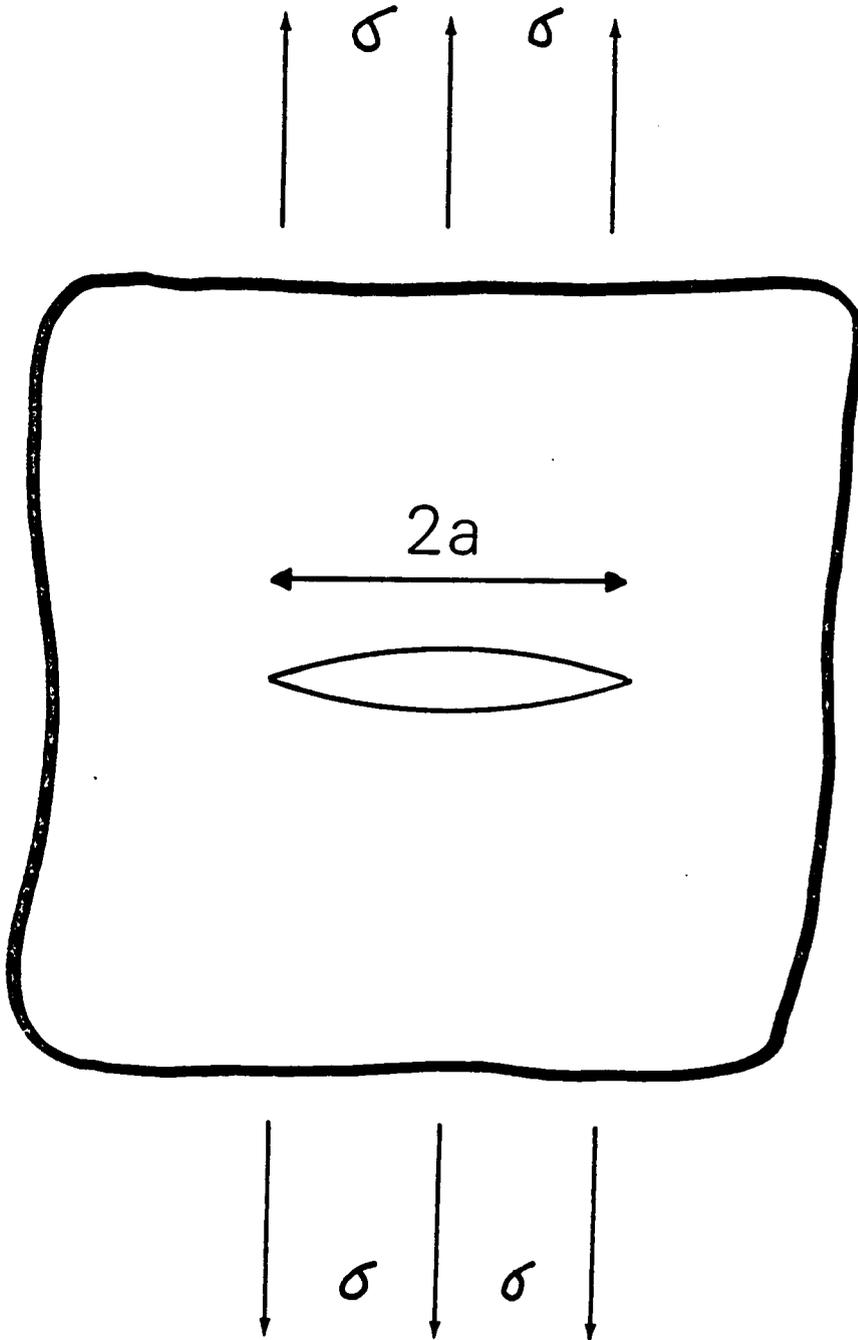
Figure 1.11.   Crack of length 2a in a thin sheet loaded in tension.

MODE I: the opening or tensile mode

MODE II: the sliding or in-plane shear mode

MODE III: the tearing or anti-plane shear mode

MODE I   MODE II   MODE III
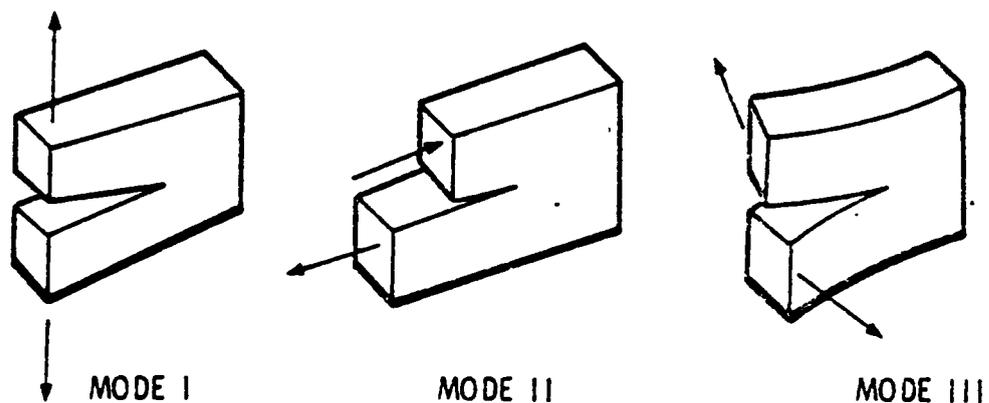
Figure 1.12.   Modes of loading about a crack.   Ref. 55.
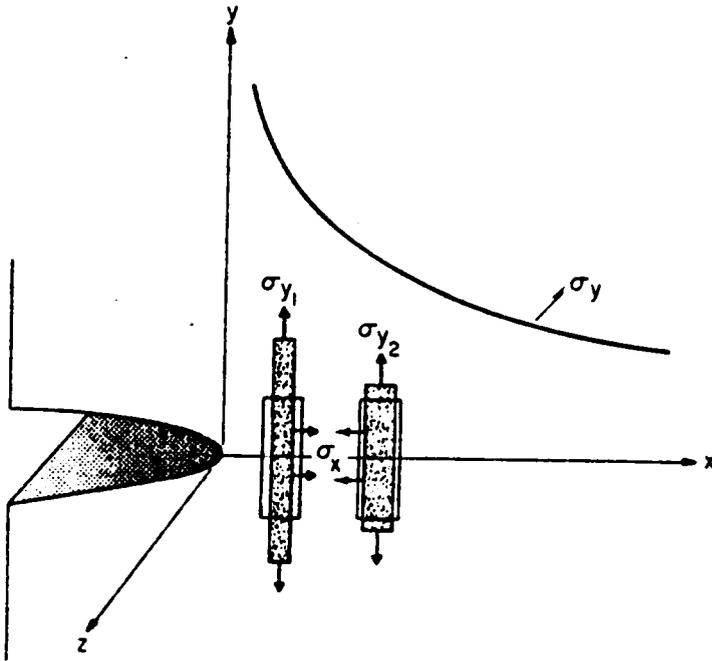
Figure 1.13. Schematic representation of the triaxial stress distribution that produces mechanical constraint at the tip of a crack loaded in tension. Ref. 59.
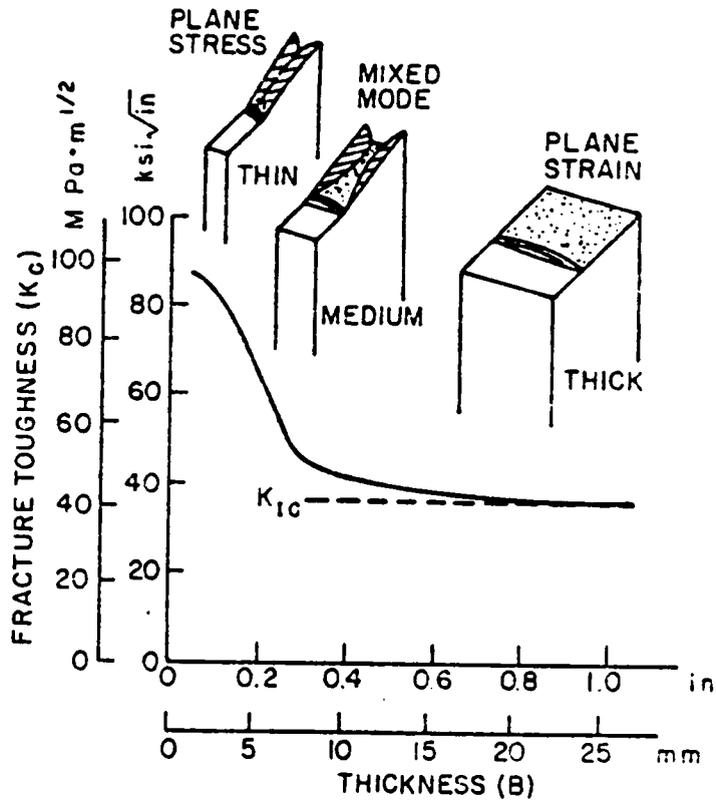
Figure 1.14. Effect of specimen thickness on fracture toughness. Schematic representation of fracture surfaces. Ref. 59.

a
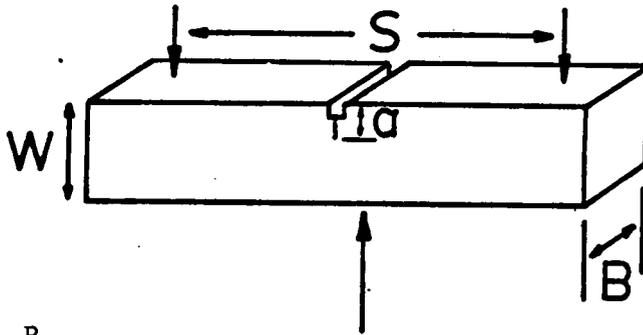
$$K_{Ic} = \frac{P_c}{BW^{\frac{1}{2}}} \, f(a/w) \qquad Y = f(a/w)$$

$$Y = 29.6R^{1/2} - 185.5R^{3/2} + 655.7R^{5/2} - 1017R^{7/2} + 638.9R^{9/2}$$

b
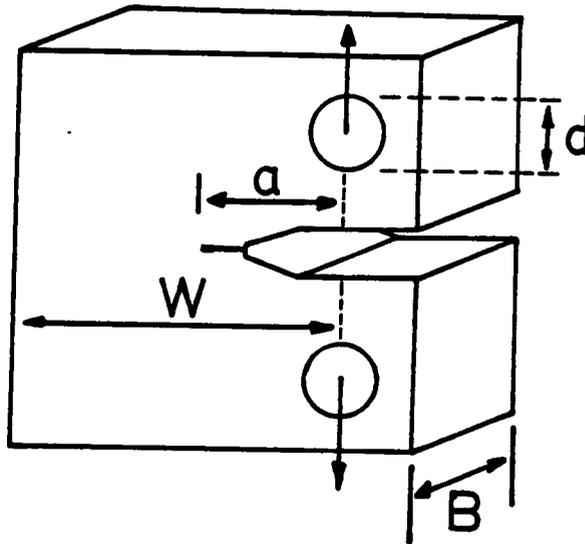
$$K_{Ic} = \frac{6P_c}{BW^{\frac{1}{2}}} \, f(a/w) \qquad Y = f(a/w)$$

$$Y = 1.93R^{1/2} - 3.07R^{3/2} + 14.53R^{5/2} - 25.11R^{7/2} + 25.80R^{9/2}$$

Figure 1.15. Fracture mechanics testing geometries: a) three-point bend and b) compact tension.
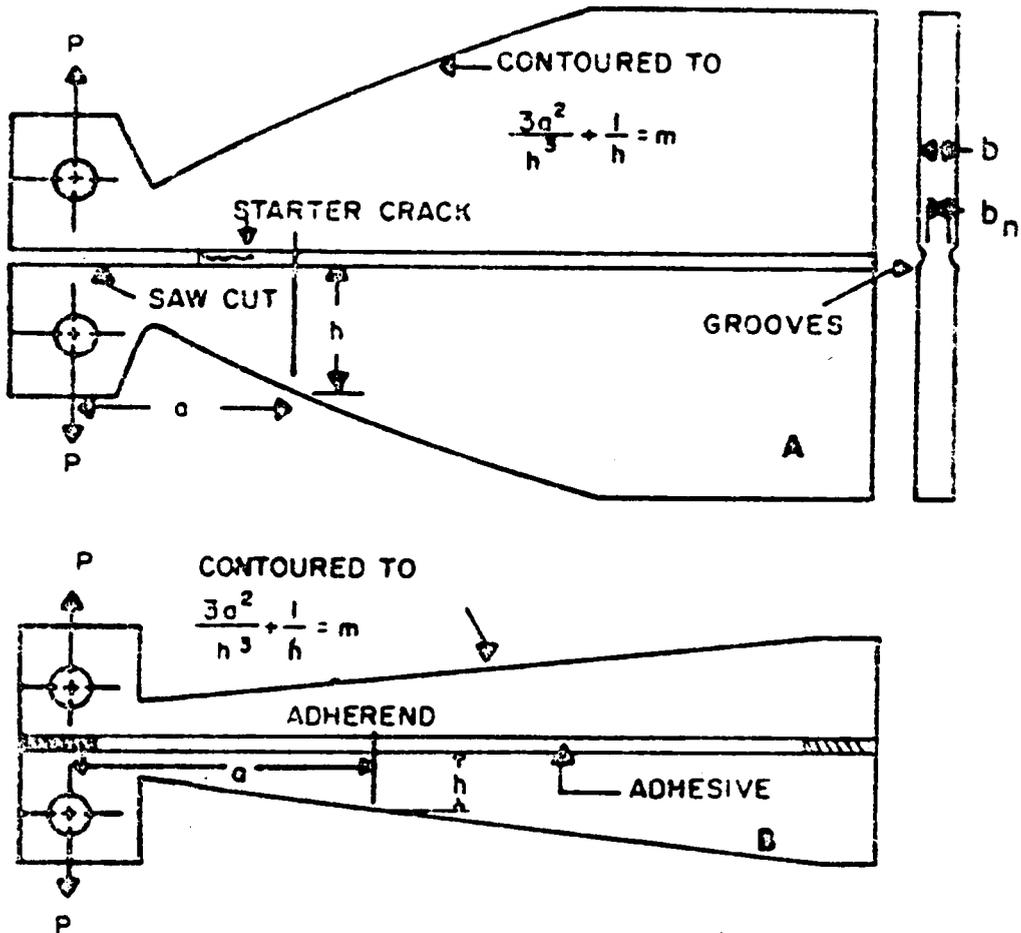
Figure 1.16. Tapered double cantilever beam geometry for A) bulk and B) bonded (adhesive) specimens. Ref. 65.
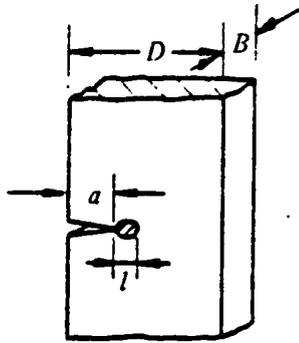
(i) Class 1, $l << a, D, B$.
Elastic fracture
mechanics
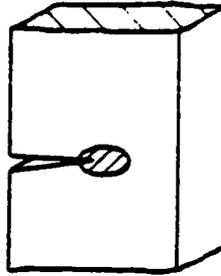
(ii) Class 2, $l < D - a$.
Contained yielding
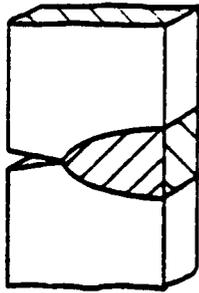
(iii) Class 3, $l > D - a$.
Fully yielded
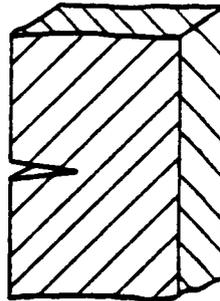
(iv) Class 4. Diffuse
dissipation

Figure 1.17. Types of fracture with reference to the size of the yielding zone. Ref. 66.
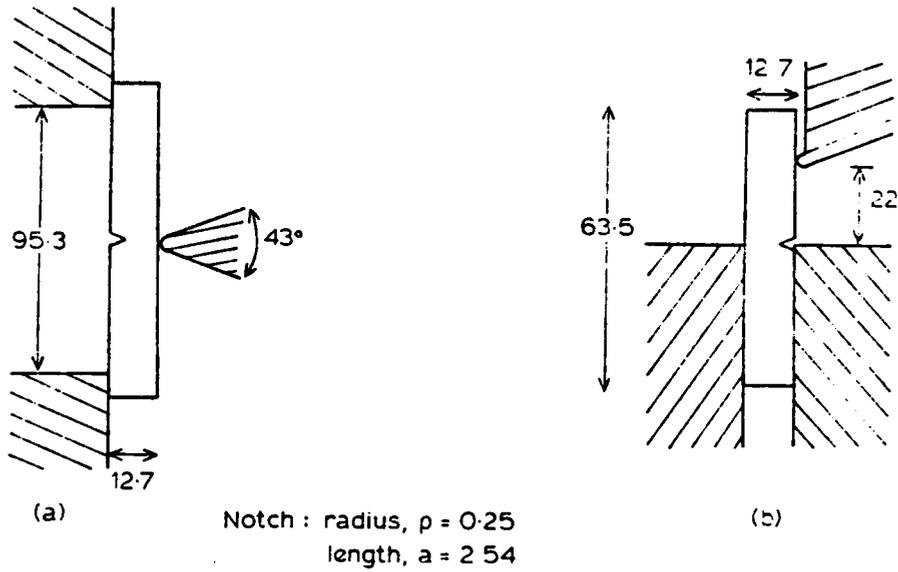
Figure 1.18. Testing and specimen support arrangement for a) Charpy and b) Izod impact tests as given in ASTM-D256. Dimensions are in mm. Charpy specimen is unclamped, Izod is clamped. Ref. 7.
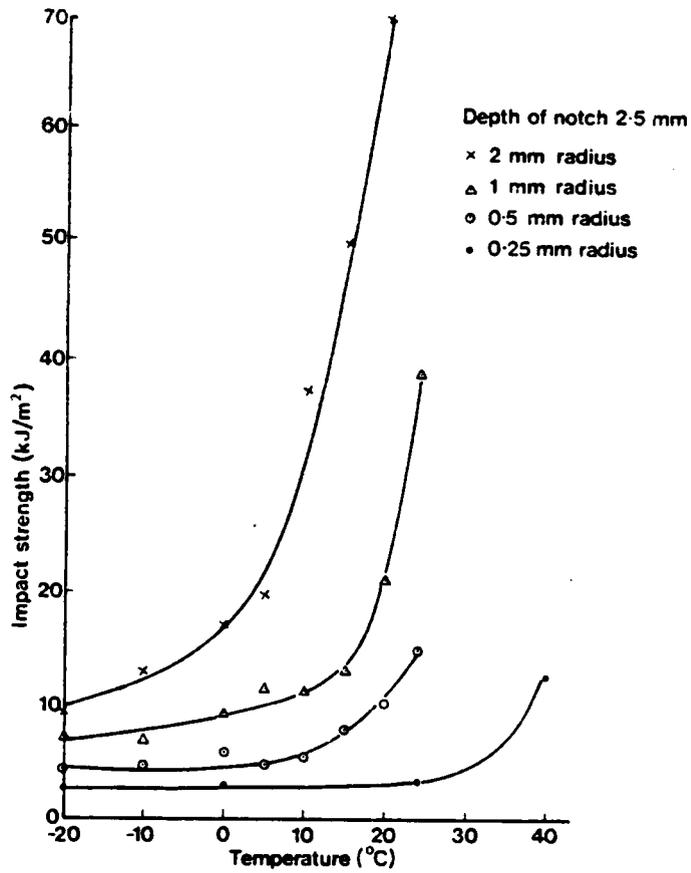
Figure 1.19. Impact strength of PVC as a function of temperature for 4 different notch depths. Ref. 79, after Ref. 70.
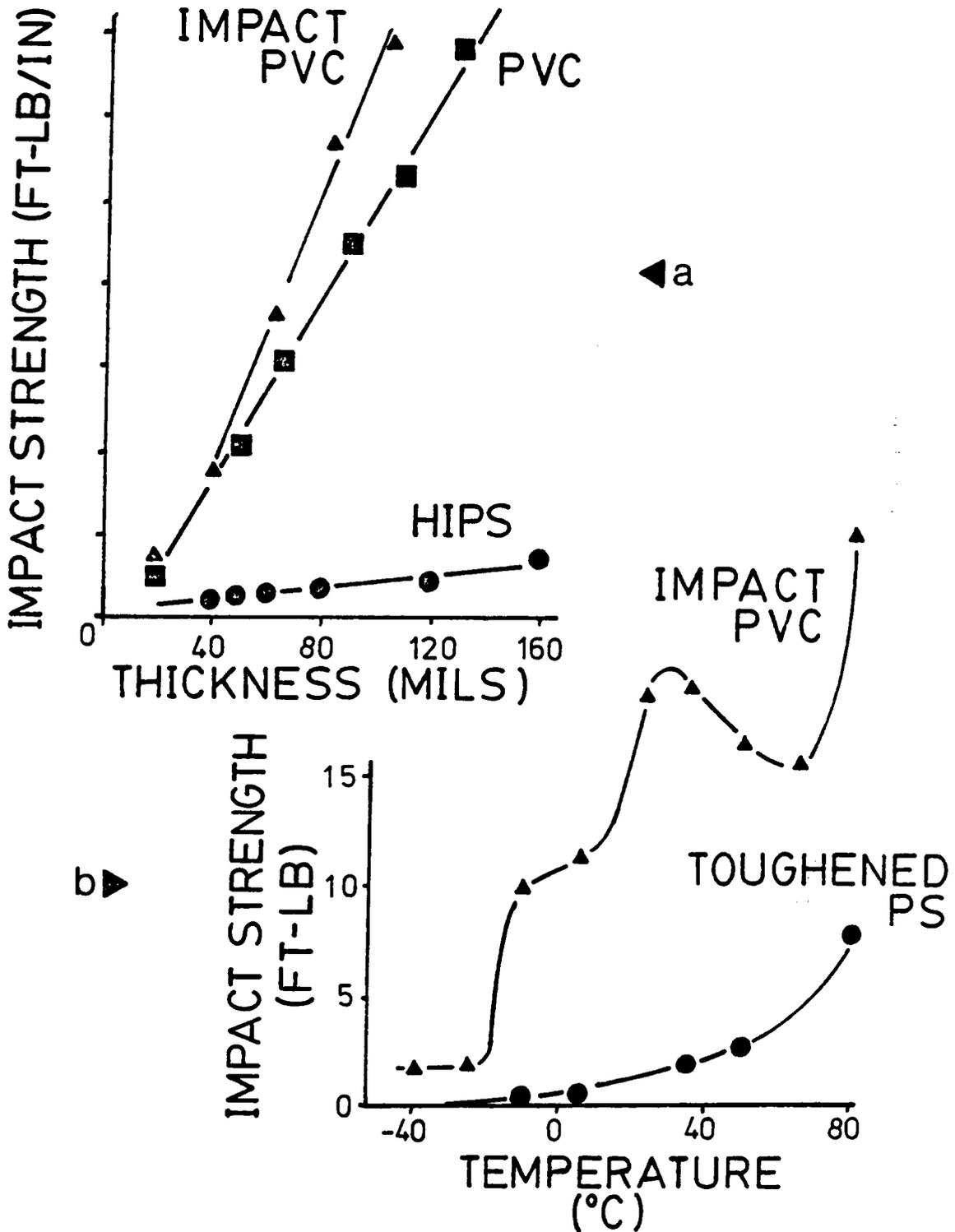
Figure 1.20. Falling weight impact strength of PVC, impact PVC, and toughened polystyrene as a function of a) thickness and b) temperature. Adapted from Ref. 73.
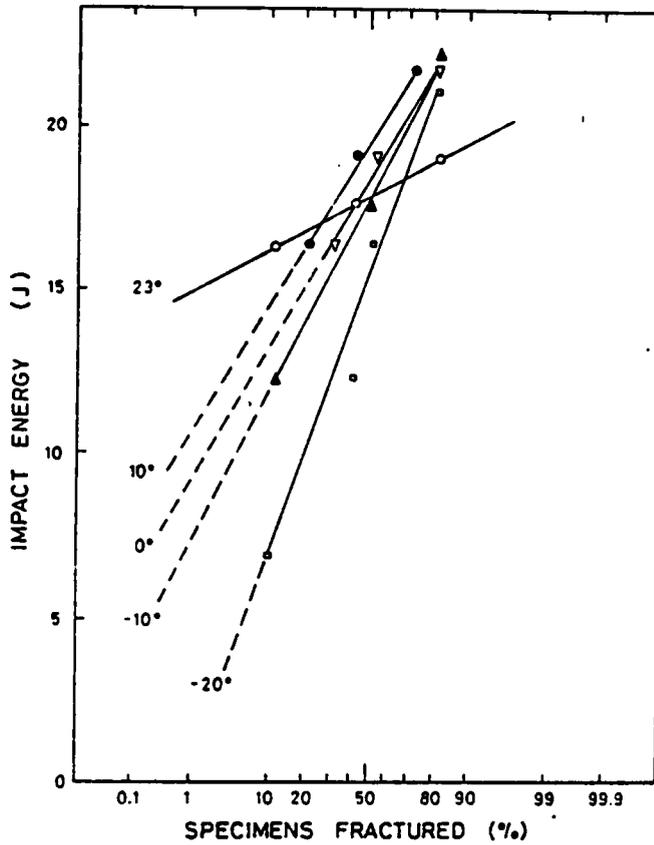
Figure 1.21. "Probit" curves. Falling weight impact tests on ABS as function of temperature. Plate thickness 2 mm. Ref. 74, taken from Ref. 5.
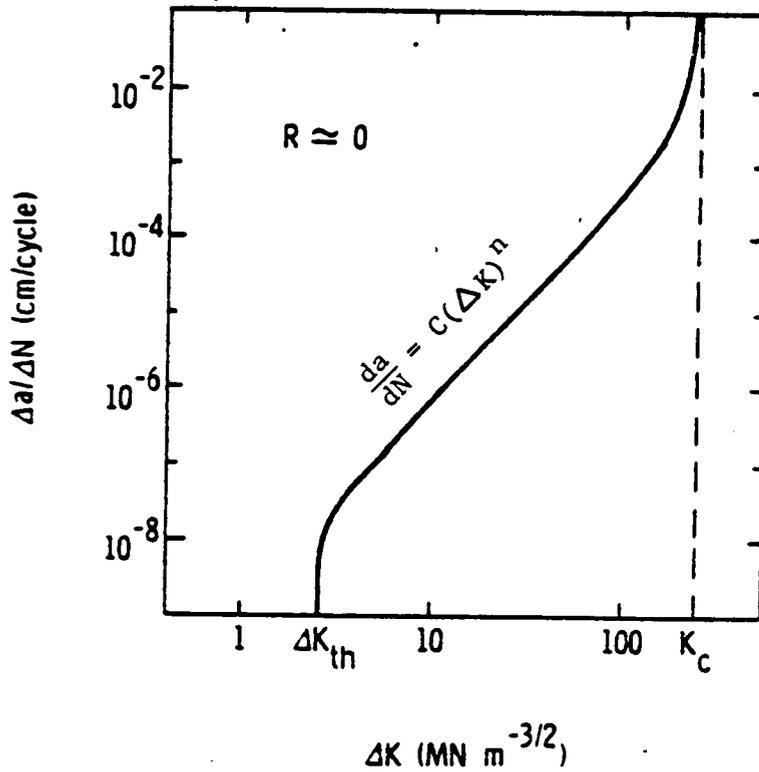
Figure 1.22. a) General fatigue crack propagation curve. KTH = threshold stress intensity below which no crack growth is observed. Kc = critical stress intensity for unstable crack propagation. R is a ratio: Kmin/Kmax, which is usually kept between 0.0 and 0.1. Paris equation given for region of stable crack growth. Ref. 55.
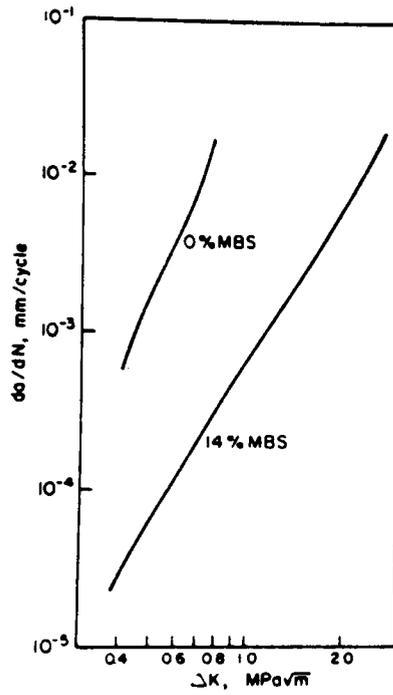
Figure 1.22. b) Effect of a methacrylate-butadiene-styrene (MBS) modifier on the FCP behavior of PVC. Percent represents parts per hundred resin. Ref. 76, taken from Ref. 75.
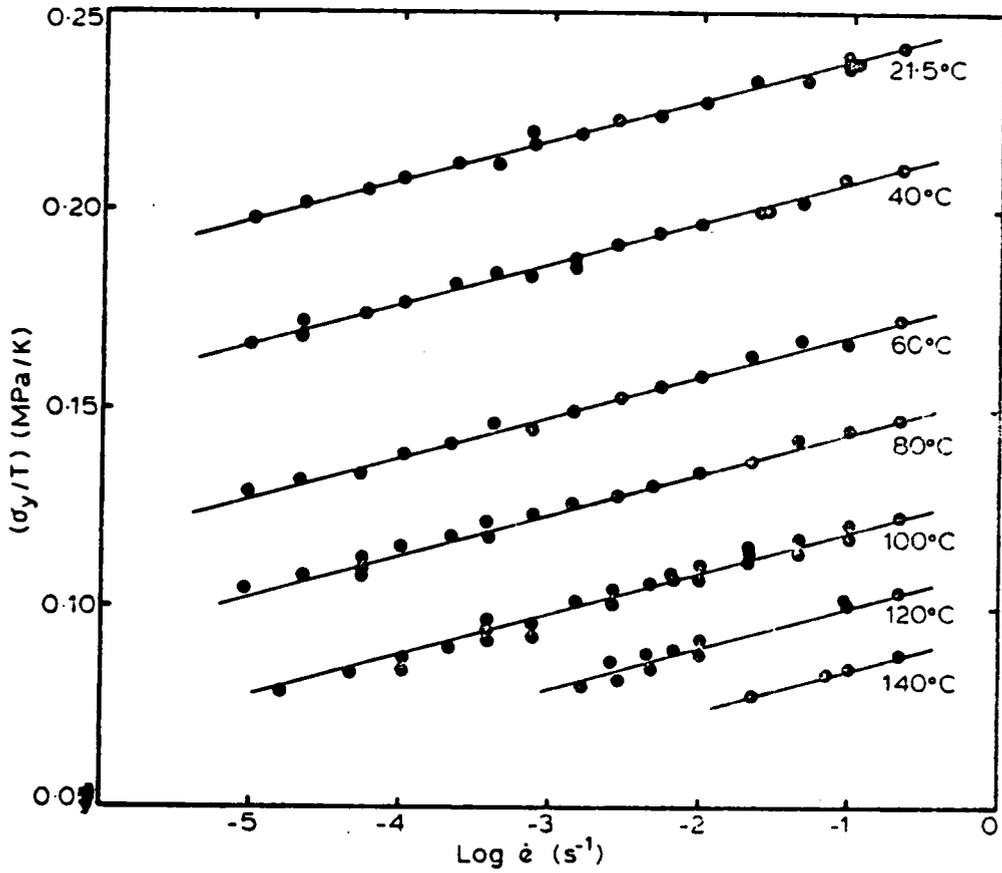
Figure 1.23. Measured ratio of yield stress σ(y) to temperature T as a logarithmic function of strain rate at several temperatures. Material is polycarbonate. Ref. 77, taken from Ref. 7.
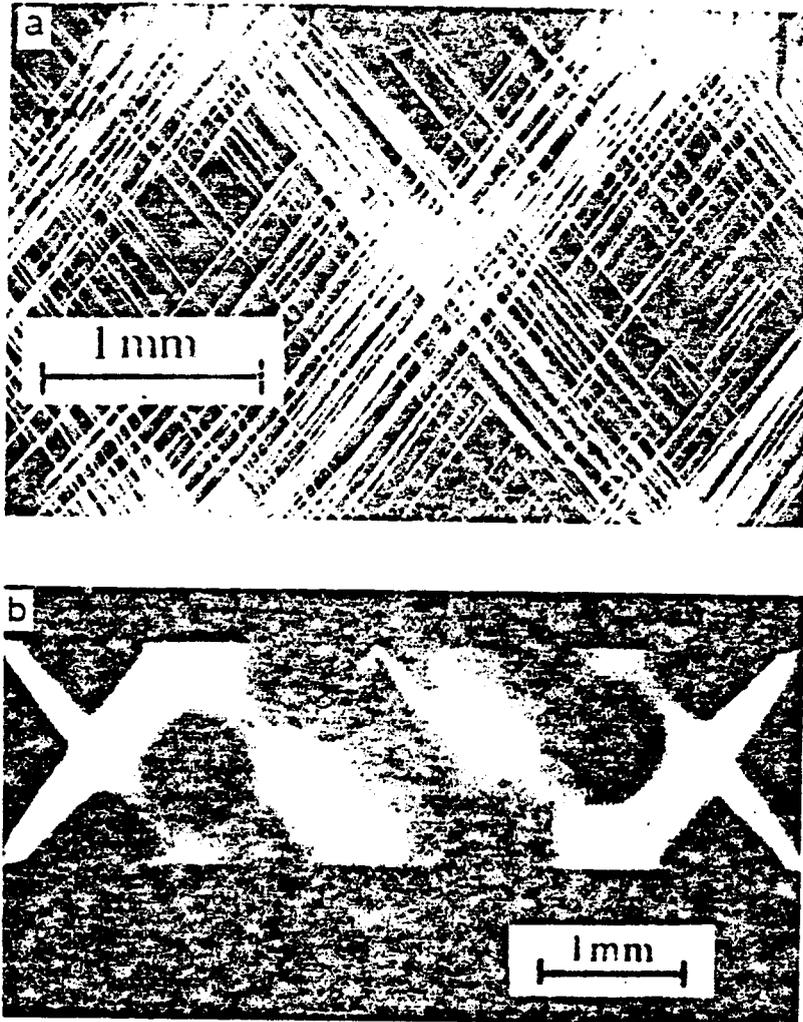
Figure 1.24. Sections cut from specimens that have been deformed until just beyond yield point in a plane-strain compression test at 22°C. Viewed between crossed polars: a) polystyrene and b) polymethylmethacrylate. Ref. 78, taken from Ref. 7.
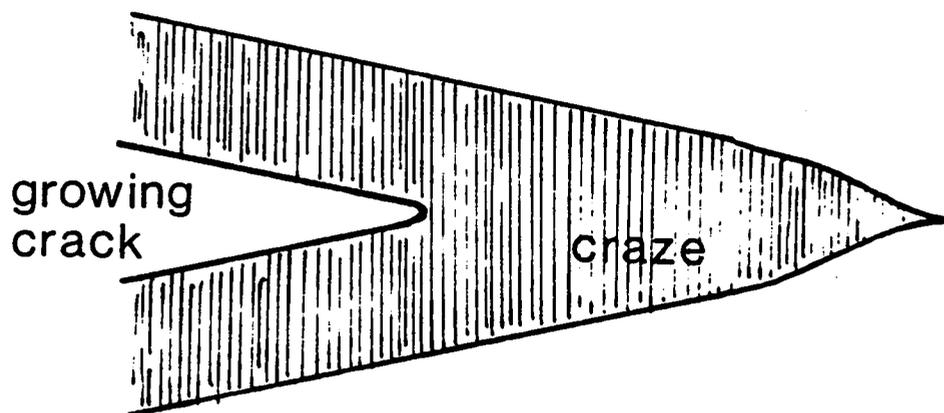
Figure 1.25. Idealized structure of a craze in an amorphous thermoplastic showing tip geometry, fibrous tendrils stretching between craze walls, and the oncoming craze failure in the form of a growing crack. After Ref. 79.

1 μm
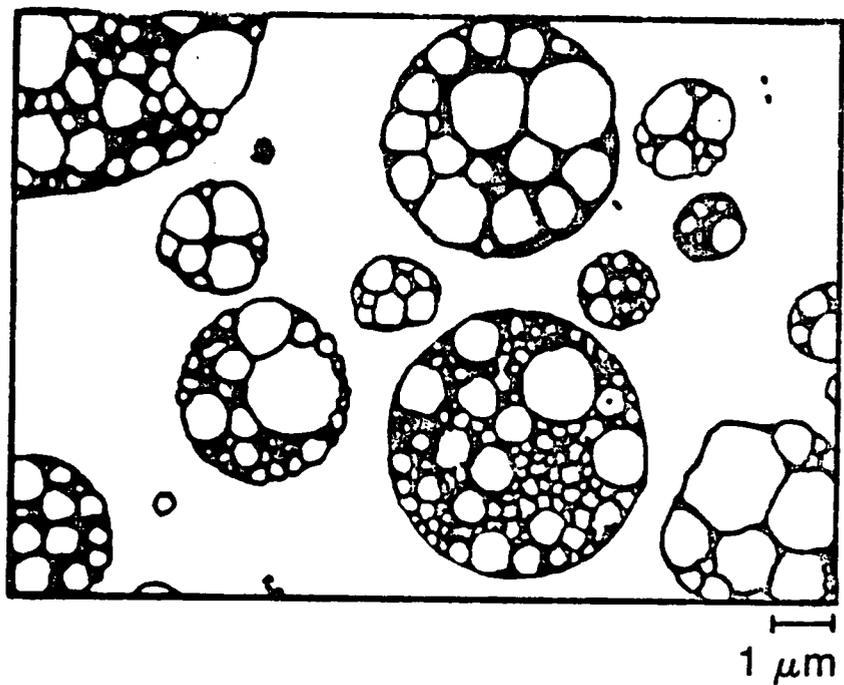
Figure 1.26. Schematic illustration of stained thin section of HIPS as seen in TEM. Types of particles: large occluded PS/rubber, small solid rubber (black), and small solid polystyrene (white). Ref. 84.
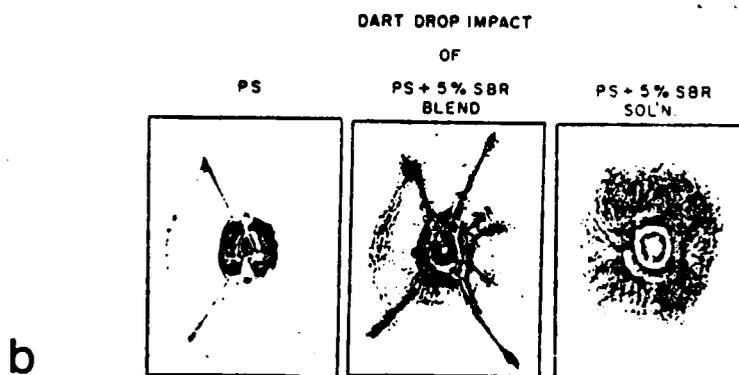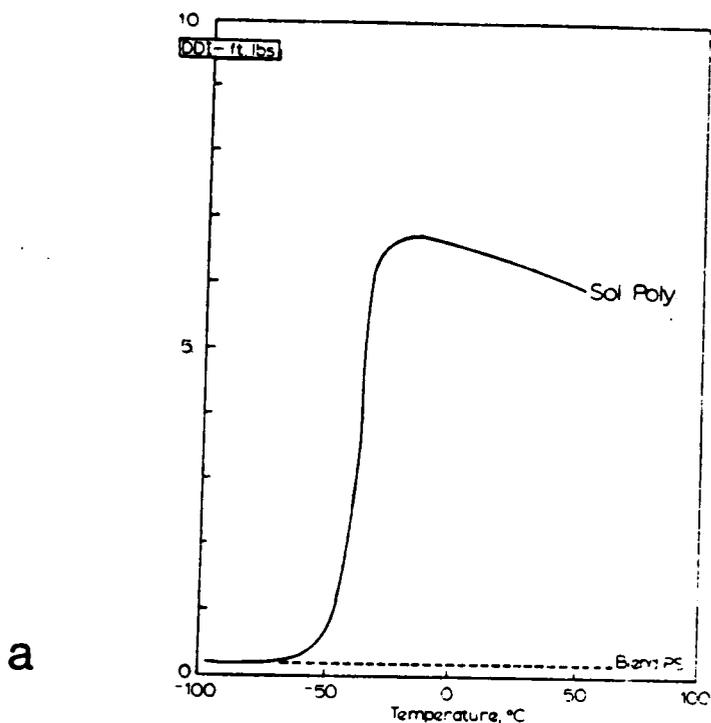
Figure 1.27. a) Dart drop impact as a function of temperature for
mechanical blend of styrene and rubber (------) and
toughened polystyrene prepared by a solution process (_____);
b) micrographs of dart drop impact areas of thin film samples, samples
as labelled. Ref. 85.
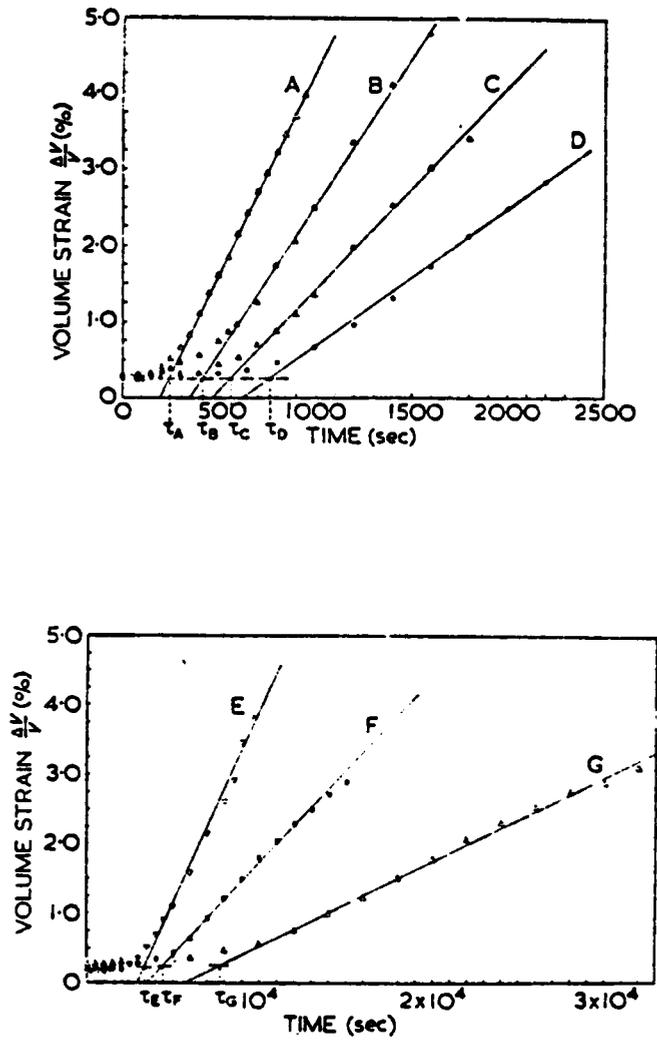
Figure 1.28.   Volume strain during creep of HIPS: a) short times:
stress levels, A = 23.35, B = 23.00, C = 22.67, D = 22.14 MN/m²;
b) long times: stress levels, E = 21.65, F = 20.91, G = 20.25 MN/m².
Ref. 88.
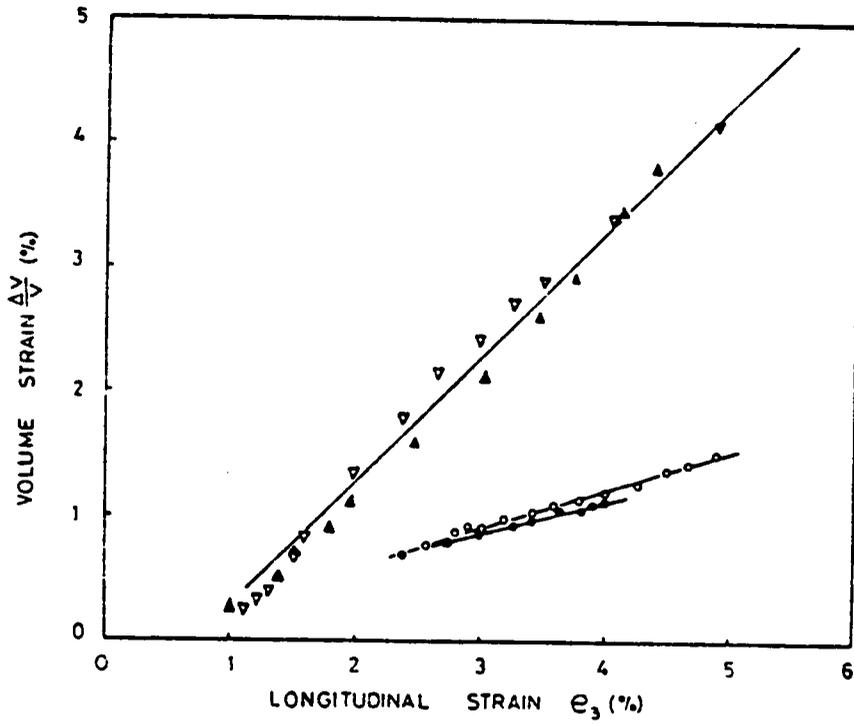
Figure 1.29. Volume strain vs. longitudinal strain for HIPS (∇ ▲) and 50/50 blend (o •), at two different stress levels. Ref. 89.
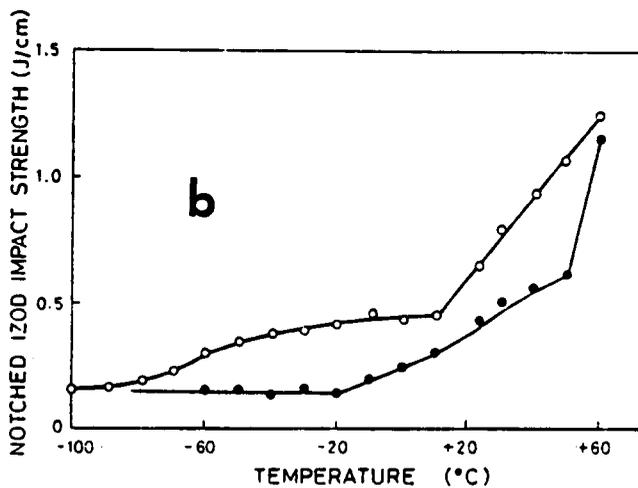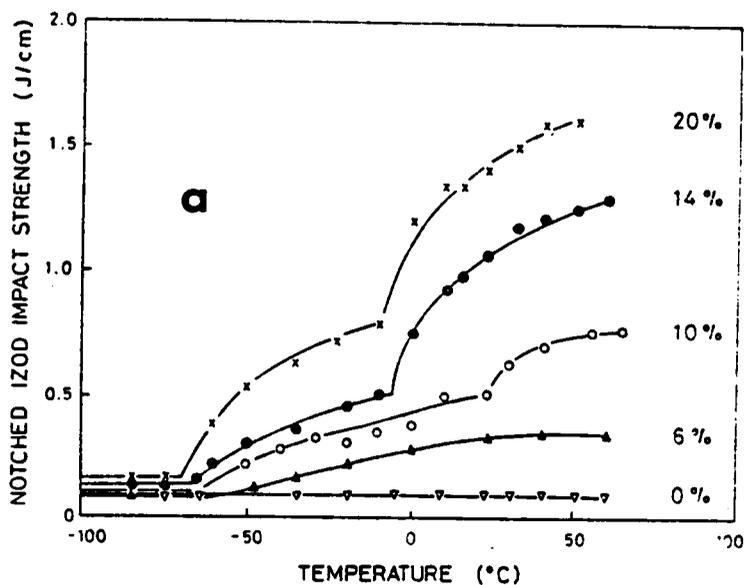
Figure. 1.30.   Notched Izod impact strength vs. temperature for
a) styrene-acrylonitrile copolymer (∇) and ABS
with 6 - 20 % polybutadiene and b) HIPS toughened with polybutadiene
(o) and HIPS toughened with SBR (•).   Ref. 5.
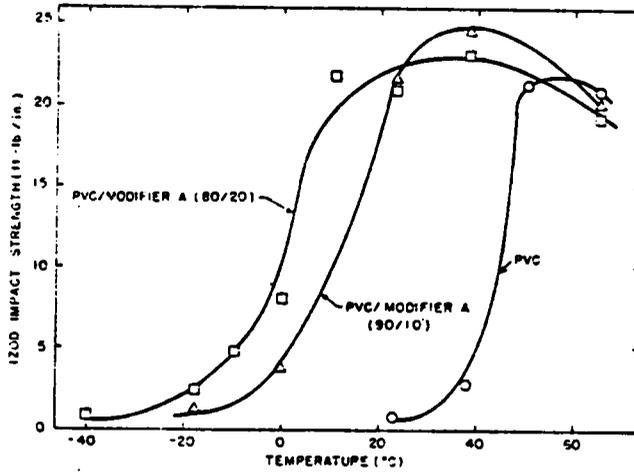
Figure 1.31. Izod impact strength for PVC containing 0, 10, and 20% of an MBS modifier. Ref. 103.
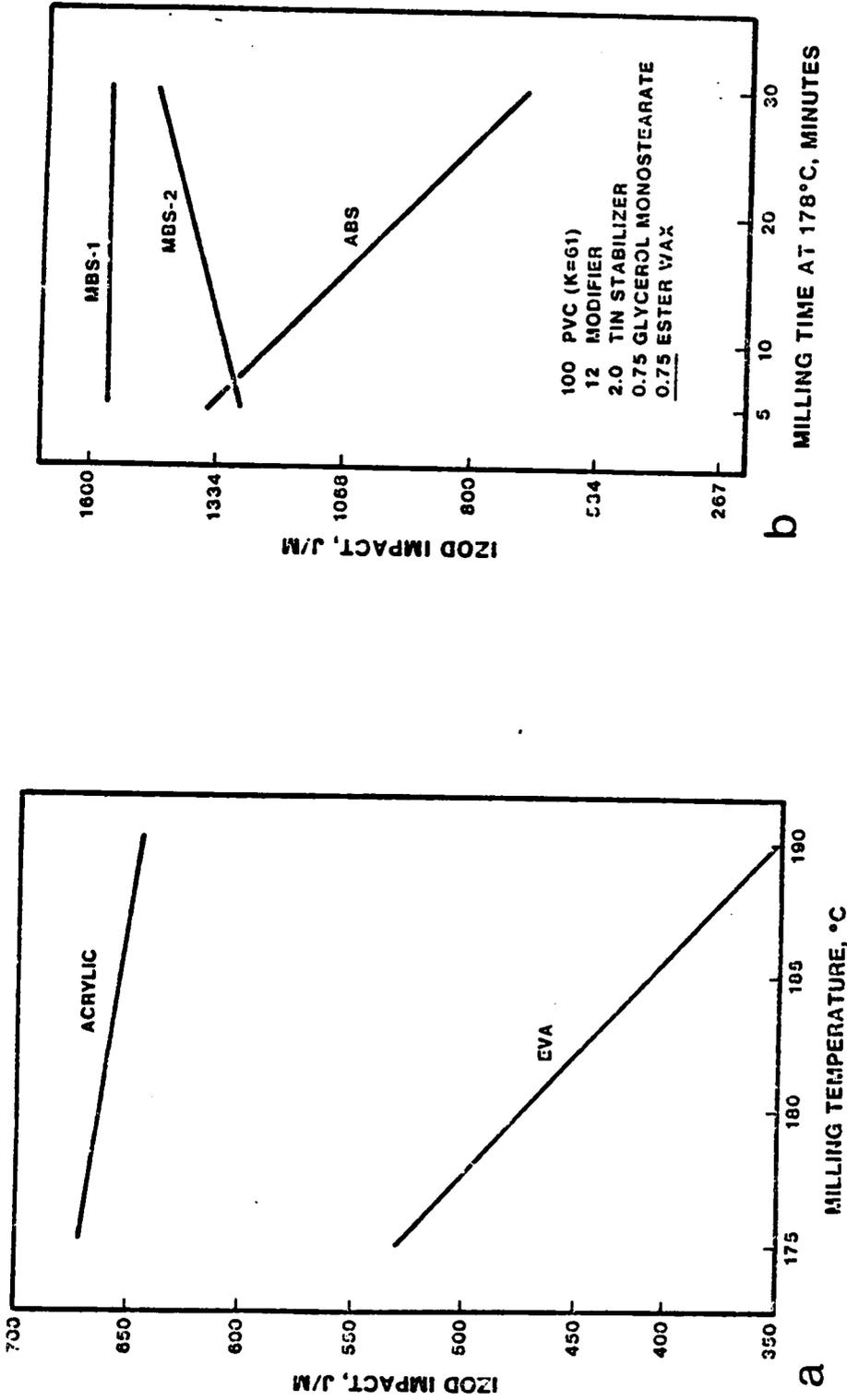
Figure 1.32. Effect of a) milling temperature and b) milling time at 178°C on Izod impact strength of PVC containing various modifiers. Abbreviations given in text. Ref. 104.
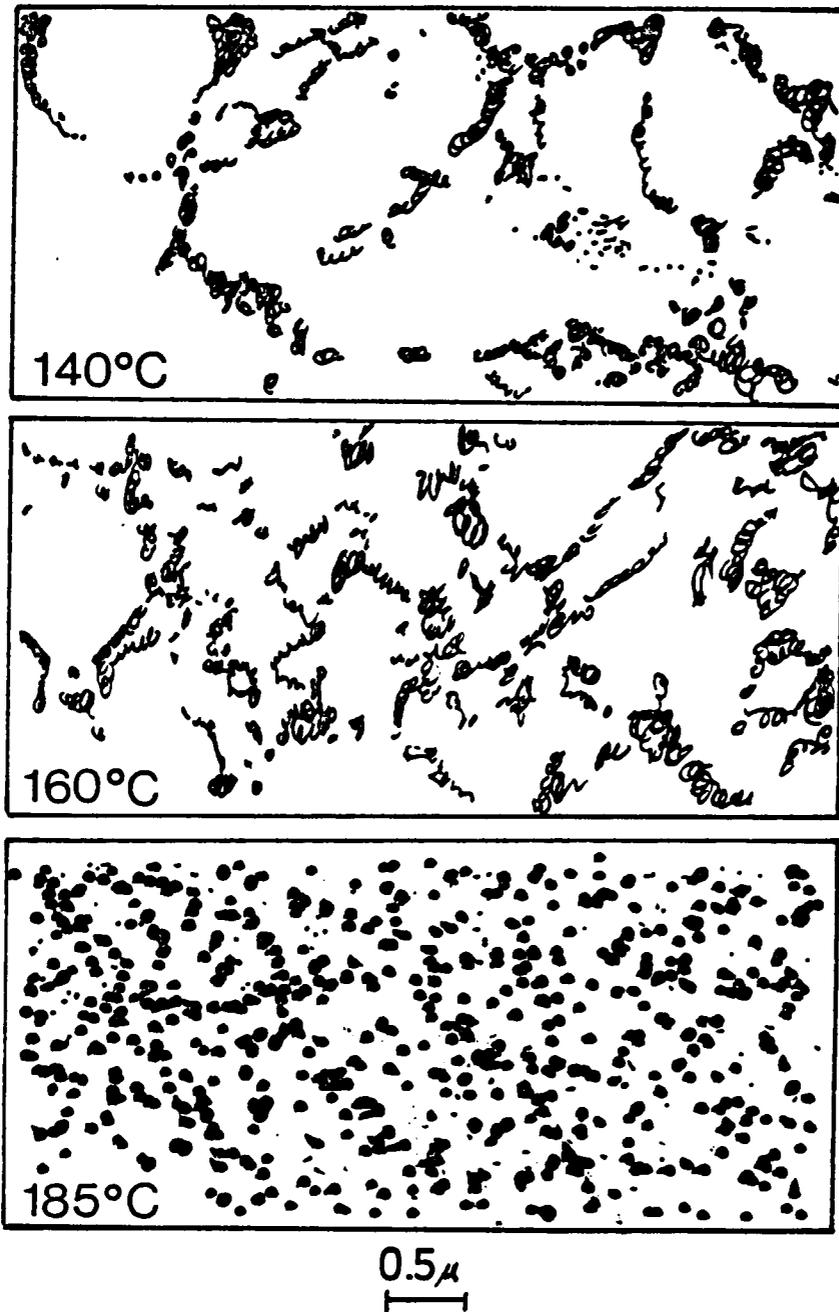
Figure 1.33. Schematic illustration of TEM micrographs for ABS with 25% grafting level. Milling temperatures given. After Ref. 110.
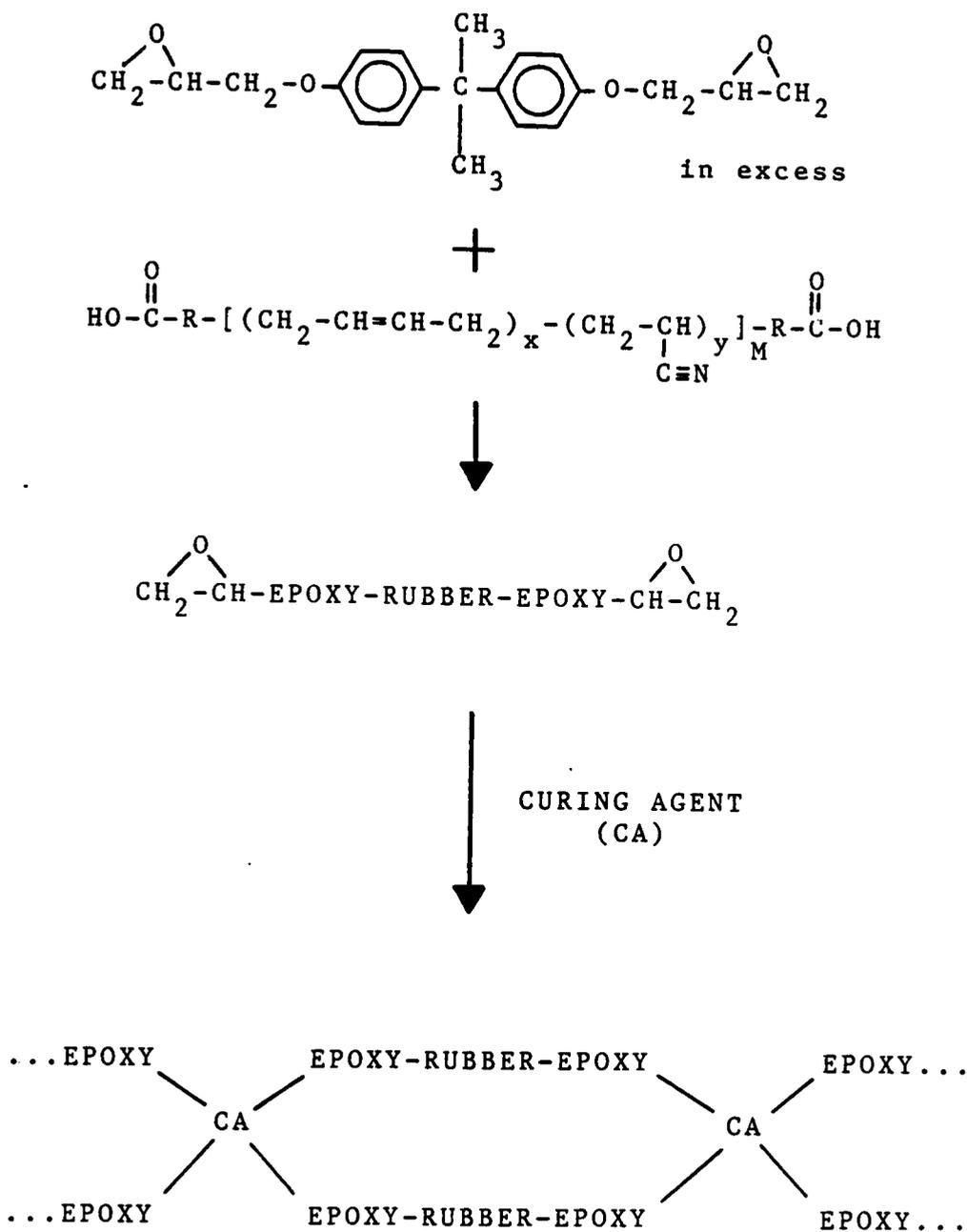
Figure 1.34. General reaction between epoxy resin (DGEBA type) and CTBN elastomer. Curing agent is usually a trifunctional or tetrafunctional amine.
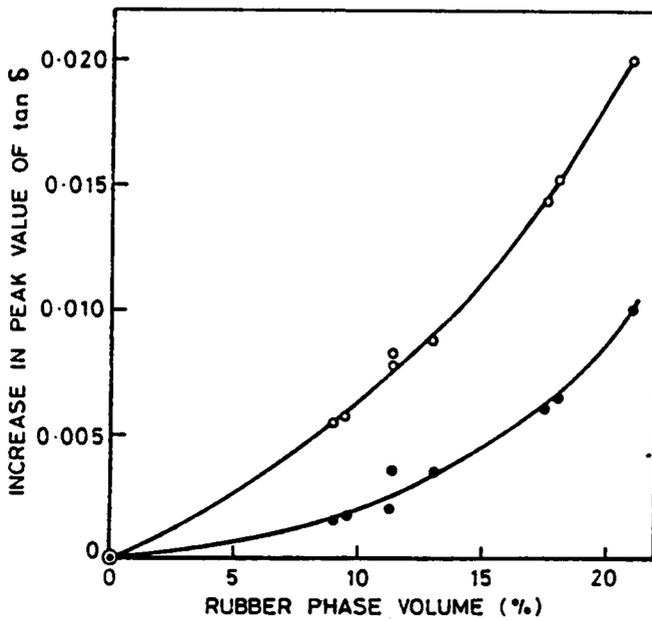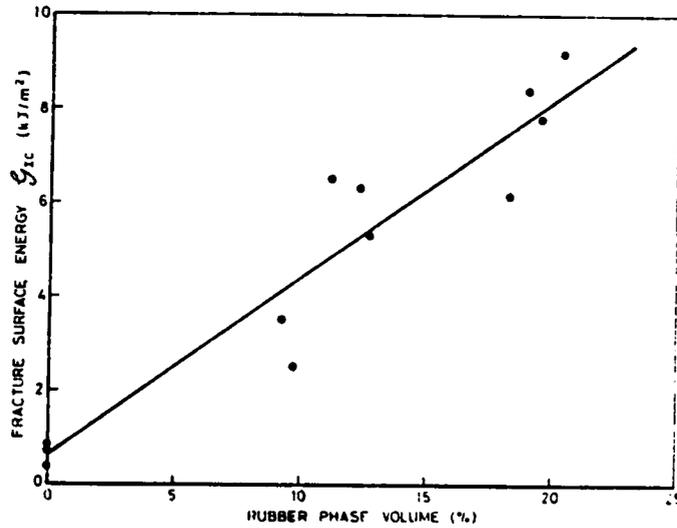
Figure 1.35. Effect of rubber phase volume on a) GIc and
b) increase in peak value of tan δ for fixed wt. % CTBN.
Figure (b) accounts for (•) simple difference in loss maximum for
modified and unmodified resins and (o) calculated height of rubber
damping peak allowing for diminished height of epoxy resin's
β-peak. See Table 1.4 for resin formulations. Ref. 130.
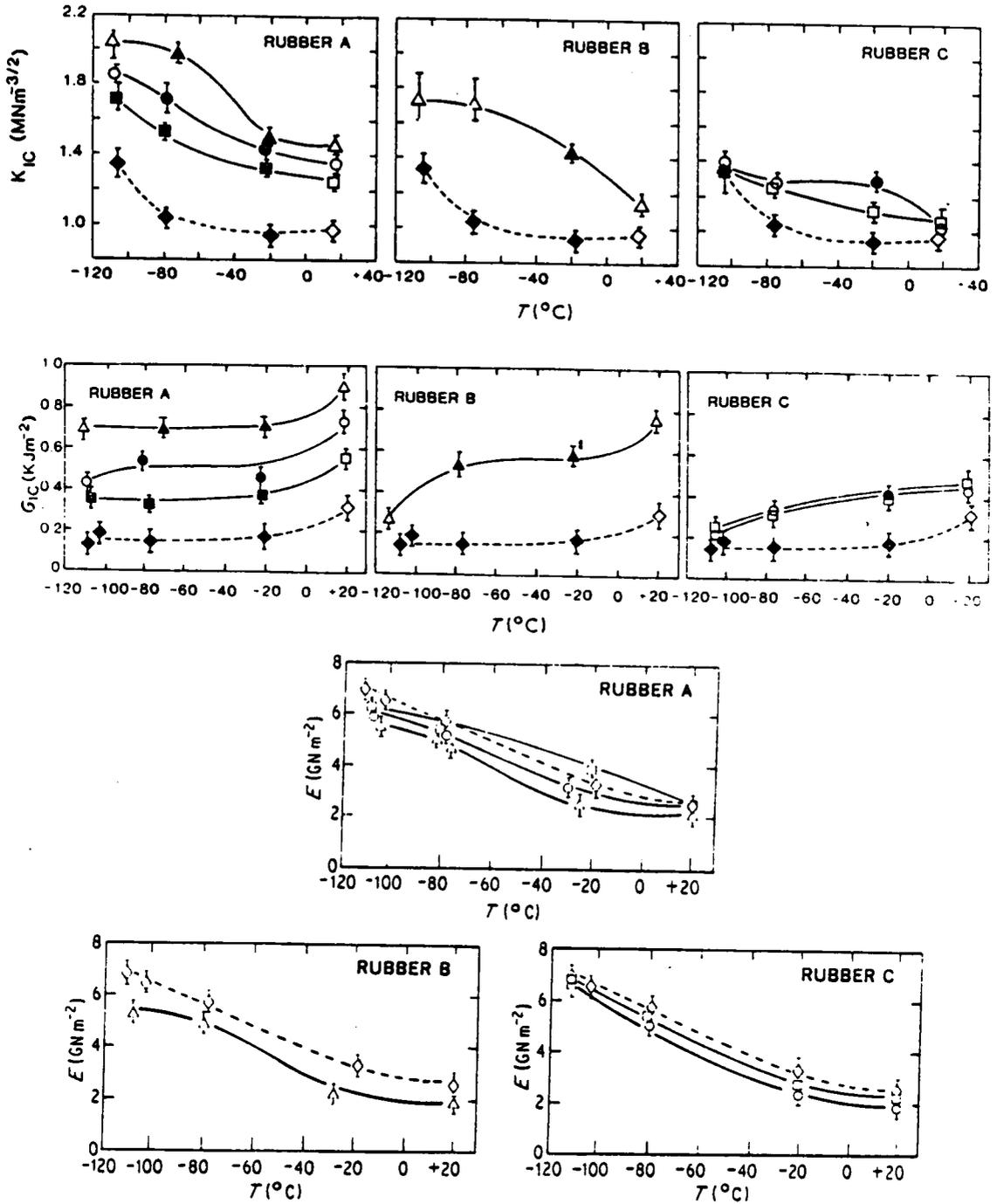
Figure 1.36. KIc, GIc, and Young's Modulus (E) as a function of temperature for DGEBA epoxy resin with varying volume fraction of rubber and % acrylonitrile (AN). Volume fraction is (i) changed by increasing initial rubber weight percent and (ii) determined by analysis of micrographs of polished sections. Rubber A: 27% AN, B: 18% AN, and C: 10% AN. Ref. 147.
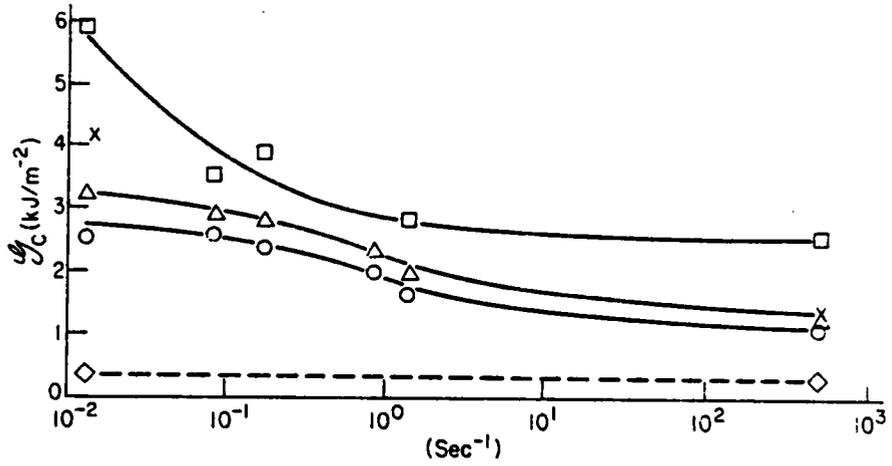
Figure 1.37. Fracture energy vs. strain rate for unmodified (------)
and several CTBN-modified epoxy resins. Ref. 152.
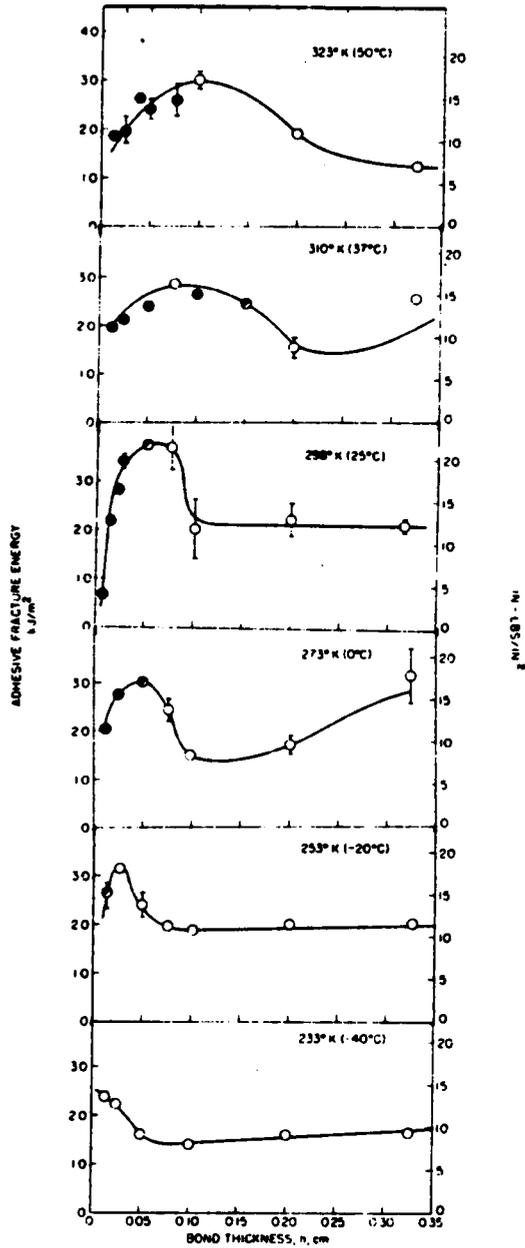
Figure 1.38. Adhesive fracture energy as a function of bond thickness at a series of temperatures at crosshead speed of 0.05 in/min: (o) unstable growth, (•) stable growth. Material contains 15% CTBN. Ref. 65.

CHAPTER TWO

SOLID-STATE PROPERTIES AND MORPHOLOGY

OF

SILOXANE-MODIFIED EPOXY RESINS

2.1. INTRODUCTION

Since the first epoxy resin patents were granted in the 1930's and 40's, properties of epoxy resins such as excellent chemical resistance, very good adhesion, and good electrical insulation have been utilized in many applications (1,2,3). These include surface coatings, adhesives, castings, and laminates. The versatility of these crosslinked systems stems in large part from the fact that one can choose from a wide variety of resins, curing agents, and preparatory conditions and often tailor a resin to suit a particular need.

Current demands for so-called high performance materials has heightened interest in epoxy resins as structural adhesives and as matrix resins for high-strength composites. Both of these applications take advantage of the resin's outstanding strength and modulus and generally good adhesion. However, such uses also require good fracture resistance and impact strength, properties which epoxy resins do not generally exhibit.

The most common route to toughening epoxy resins has involved the incorporation of elastomeric modifiers into the final glassy matrix. A reactive liquid elastomer is mixed with the resin and curing agent at relatively low temperatures to form a homogeneous mixture. As cure proceeds (generally at elevated temperatures), the increasing molecular weight of the epoxy matrix forces the elastomeric component to separate

within the crosslinked resin and form a second dispersed phase. Unlike thermoplastics modified with rubbers through blending, the ideal rubber-modified thermoset links the resin and the elastomer through covalent bonds such that, in the final state, the rubber, resin, and curing agent form a multi-phase three-dimensional glassy network. As will be discussed, the dispersed elastomeric domains act to alleviate crack propagation through various proposed mechanisms.

The principal objective of rubber modification is the improvement of fracture properties with the smallest possible decrease in modulus and strength. The CTBN and ATBN (carboxyl- and amine-terminated butadiene acrylonitrile) copolymers have done much towards reaching this end. The first publications by McGarry (4,5) as well as B. F. Goodrich co-workers Rowe, Siebert, and Drake (6,7) reported strong improvements in fracture surface work and fracture energy, respectively, with the addition of 5 to 15% CTBN. Particle sizes in the best of these systems range from 0.1 to 1.0 micron. Riew, Rowe, and Siebert (8) have reported 30- to 40-fold increases in fracture energy. Although they are successful as general purpose toughening agents for epoxies, CTBN and ATBN elastomers possess two drawbacks. First, their glass transition temperatures are high relative to most elastomers (9), which limits their application far below room temperature (10,11). Second, their highly unsaturated structure provides possible sites for reaction in oxidative and high temperature environments (12). *

This chapter describes the solid-state properties and morphology of a novel rubber-modified resin system, siloxane-modified epoxy resins.

Siloxane elastomers present a rather attractive alternative to the butadiene acrylonitrile elastomers most often used for epoxy modification. Polydimethylsiloxanes exhibit glass transition temperatures well below those of butadiene acrylonitrile modifiers (minimum -123°C vs. about -40°C) and also display very good thermal stability (13,14). Other favorable and potentially useful attributes include good weatherability, oxidative stability, and moisture resistance..

The non-polar nature and low surface energy of polydimethylsiloxanes constitute a thermodynamic driving force for them to migrate to the air-polymer interface, provided the chains are sufficiently mobile. This migration can occur with simple physical blends as well as in systems with chemically linked microphase-separated segments. During the early stages of cure of a siloxane-modified epoxy, before extensive crosslinking limits diffusion, such migration is considered possible and is believed to lead to the formation of a very hydrophobic and chemically bound surface coating (15). Knowledge of this non-fugitive "slippery" surface layer has led to investigation of the friction and wear properties of siloxane-modified epoxy resins (16,17).

The extensive body of literature on ATBN- and particularly CTBN-modified epoxies provides a wide base for future work in the general area of rubber modification of epoxies. Bascom, Hunston, and co-workers (18-22) have systematically studied the fracture behavior of materials containing up to 30 weight percent CTBN and elucidated the differences between their bulk and adhesive fracture properties. Sayre, Assink, Lagasse, and Kunz (23,24) have studied in detail the phase

structure and composition of CTBN-modified epoxy resins. Manzione, Gillham, and McPherson (25,26) have demonstrated how the nature of the cure, phase structure, and, ultimately, the mechanical properties can be controlled by acrylonitrile content of the elastomer and the curing conditions. Bucknall and Yoshii (27) pointed out the influence of several factors, including type and concentration of curing agent and solubility parameter and molecular weight of the modifier, on the final properties of a toughened epoxy resin.

It is not yet entirely clear how the addition of an elastomer to an epoxy network acts to increase fracture resistance. McGarry (4) and Bucknall (28) initially proposed that these modified glassy networks absorbed mechanical energy through crazing, much like high-impact polystyrene. This view was later found to be inadequate, particularly when applied to highly crosslinked thermosets such as those used for structural laminates. Further work towards an understanding of mechanisms is described by Yee (29) and Kunz et al (10,30).

Kinloch, Shaw, Tod, and Hunston (11) recently studied the fracture toughness behavior of CTBN-modified epoxy resins at temperatures from -93 to 60°C and at several displacement rates. Three basic types of crack growth were defined, and the corresponding fracture surface features were identified. The authors evaluated the principal mechanisms proposed for rubber toughening -- rubber tearing (10,30), crazing (4,28), and combination shear yielding and crazing (8,31) -- and described a collective rubber toughening mechanism. They concluded that the primary source of energy dissipation in unmodified

and CTBN-modified epoxies is yielding and plastic shear flow of the matrix. The formation of voids at the domain/matrix interface or within the domains themselves was regarded as a secondary but still important source of energy dissipation. Kinloch et al (11) point out that the interplay between these two mechanisms ultimately determines the contribution of each. A companion paper by Kinloch, Shaw, and Hunston (32) introduced the critical values of the applied stress and the crack tip radius as a unique fracture criterion for rubber-modified epoxies. Their relationship to the physical processes active during fracture is as yet unexplored.

The compatibility of the modifier with the resin system is considered an important factor in achieving toughening (28,33). The solubility parameter is a good indicator of the compatibility of one substance with another and, together with molecular weight and temperature, can adequately predict the nature of the phase separation of the elastomer from the resin during cure. Through copolymerization of dimethyl siloxane with partially aromatic diphenyl (DP) siloxane or polar methyl trifluoropropyl (TFP) siloxane, one can raise the solubility parameter of the siloxane elastomer from 7.5 $(cal/cc)^{1/2}$ close to that of the epoxy resin, approximately 9.2 (6). This is analogous to the manner in which the solubility parameters of ATBN and CTBN elastomers are controlled through acrylonitrile content (6)./

The control resin network used in this study was a diglycidyl ether-based epoxy resin crosslinked with a cycloaliphatic diamine. Co-oligomeric modifiers were prepared having varying percentages of TFP

and DP siloxane and aminoethylpiperazine end groups. Both siloxane and ATBN and CTBN elastomers were used as epoxy modifiers, the latter two having been included to facilitate direct comparisons between modifiers in similarly prepared networks.

Ideally, rubber toughening should be accomplished without substantial sacrifices in modulus. For each modified resin, flexural and Young's moduli and plane-strain fracture toughness (KIc) were determined. Examination of cold snap and KIc fracture surfaces by scanning electron microscopy showed the effects of modifier composition on the morphology of these multi-phase materials and enabled a morphological basis to be given to the mechanical properties.

The thermal stability of a select group of oligomers was assessed through a study of viscosity changes with high temperatures aging. Both siloxane and butadiene acrylonitrile liquid modifiers were included in this particular study.

Long-term stability of structural resin systems has in the last decade come to concern users of structural adhesives as well as fiber-reinforced resin composites. It has been shown (34) that the so-called physical aging process well known in amorphous thermoplastics can also occur in thermosetting resins, including rubber-modified resins. Prior to the major work described in this chapter, the author was involved in a study of physical aging in graphite fiber-reinforced composites. This study is described in an Appendix to this chapter.

2.2. EXPERIMENTAL

2.2.1. Materials

Epoxy resin Epon 828, a bisphenol A diglycidyl ether-based resin made by the Shell Chemical Co., was chosen as the control epoxy resin. Its average molecular weight is about 380 g/mol. Bis(4-aminocyclohexyl)methane (PACM-20) was the curing agent. Copolymers with varying weight percentages of dimethyl, methyl trifluoropropyl (TFP), and diphenyl (DP) siloxane with a controlled molecular weight of approximately 2200 g/mol were prepared from dimethyl siloxane tetramer, methyl trifluoropropyl cyclic trimer, and diphenyl tetramer via equilibration reactions with base catalysts, in particular tetramethylammonium siloxanolate and potassium siloxanolate. All siloxanes in this study had 2-aminoethylpiperazine (AEP) end groups. The oligomers were structurally characterized using FTIR and NMR spectroscopy. Number average molecular weights were determined by end group titration. Further details are given in Ref. 35.

The actual weight percentage of a specific type of siloxane unit in an oligomer can be calculated relative to the entire oligomer or the siloxane units alone. The number found by the first method, which includes the AEP end groups, will be smaller than that found by the second method. For example, this study utilized two oligomers of essentially 100% TFP siloxane. If the end groups are included in calculations of percent TFP siloxane, the number assigned to the

oligomer of the lower molecular weight is 70% while that for the higher molecular weight oligomer is 85%. Thus these end groups comprise an appreciable fraction of the oligomer molecular weight.

Siloxane-modified networks were prepared for testing via two steps. A linear precursor was generated by reacting the epoxy resin with the siloxane oligomer for one hour under vacuum at 65°C. PACM-20 was then added, and the mixture was stirred for five minutes under vacuum at 50°C. Previous studies indicated (15) that reaction between the AEP-terminated siloxane oligomers and the curing agent is not possible, as one would expect.

The epoxy/siloxane/PACM-20 mixture was poured into a hot (120°C) RTV-silicone mold of the precise shapes to be used for solid-state testing. The mixture was cured at 160°C for 2.5 hours. The curing time and temperature chosen were considered to provide enough mobility for network formation. This conclusion was partially based on earlier studies which found a glass transition temperature of 150°C for Epon 828/PACM-20 (36).

The B. F. Goodrich Company made available ATBN and CTBN rubbers of both low (10%) and high (17-18%) acrylonitrile (AN) content. Nominal molecular weights of these oligomers were about 3700. The ATBN oligomers are manufactured from CTBN oligomers of the same AN content via capping with AEP. The ATBN materials should have molecular weights just slightly higher than the corresponding CTBN oligomers, but, due to excess AEP remaining in the ATBN after capping,

the *titrated* molecular weights of the ATBN oligomers are considerably lower than their reported molecular weights. It is the titrated molecular weight that has been used to determine the appropriate amount of curing agent for complete network formation.

All networks, regardless of the modifier, were prepared identically. Hence, all modified resins were subjected to the same guidelines concerning the ratio of rubber to resin to curing agent and were cured according to the same schedule.

Glass transition temperatures were determined using a Perkin-Elmer DSC-II or DSC-IV at a heating rate of $10°C/min$. Several scans were run at $20°C/min$ on a DSC-IV to gain information on the breadth of the glass transition region.

2.2.2. *Sample Designation*

Each oligomer or modified resin can be described by two or three numbers, respectively. The box below illustrates the employed shorthand nomenclature. For example, a sample containing 10% by

```
----------------------------------------------------------------
:  NOMENCLATURE                                                :
:                                                              :
:    WT. PERCENT - MODIFIER MOL. WT. - WT. % COMONOMER        :
:       5,10,15              1500-4000         TFP, DP, AN      :
:                                                              :
:  EXAMPLES                                                    :
:                                                              :
:            Pure PDMS:  5-2190-0                              :
:          TFP Siloxane:  10-2070-40F                          :
:      Diphenyl Siloxane:  5-2250-20D                         :
:                 CTBN:  10C-3880-17AN                         :
:                 ATBN:  15A-2560-10AN                         :
:                                                              :
----------------------------------------------------------------
```

weight of a 40% TFP siloxane rubber of molecular weight 2070 g/mol would be designated 10-2070-40F. Differences between specific types of siloxane copolymers are given by changes in the third number of the sample code while differences between the end groups of the butadiene oligomers are given in the first number of the code as demonstrated by the examples given.

2.2.3. *Mechanical Properties*

Tensile moduli were measured from standard dog-bone samples (2.0 mm thickness, 4.7 mm width, and 22.0 mm gauge length) in a Model 1122

Instron. Flexural modulus was determined using a testing apparatus which consists of two aluminum/steel pieces attached to the Instron which is fitted with a tensile load cell. This device effectively performs an inverted three-point bend; the two side bars remain stationary above the sample as the central bar below the sample moves upward. Flexural samples measured ca. 52.0 x 1.7 x 13.1 mm and were tested using a 25.4 mm span (distance between the two side bars). Crosshead speed (CHS) for both flexural and tensile testing was 1.0 mm/min.

Fracture toughness was measured in a three-point bend (3PB) geometry for all materials and in a compact tension (CT) geometry for a select group of materials. Dimensions of each sample, the location of the crack and crack notch, and the orientation of the testing direction are given in Figure 2.1. Into the indicated notch was placed a sharp one-sided razor blade which was tapped lightly to make a short pre-crack. The CHS was 0.5 mm/min for both geometries. After fracture, the pre-cracks were enlarged with a magnifying glass, measured with vernier calipers, and calculated as the average of three values: side, center, side. The calculation of the fracture toughness will be described later in this chapter. All modulus and fracture toughness testing was done at ambient temperatures.

2.2.4. *Scanning Electron Microscopy*

Fracture surfaces were examined in an ISI, Inc. Super III-A SEM. Cold snap samples were fractured after being submerged in liquid nitrogen for ten minutes. Crack faces of the 3PB and CT specimens were also studied with SEM.

2.2.5 *High Temperature Aging*

The change in viscosity as a function of time at 125°C was monitored for the four butadiene acrylonitrile copolymers and two siloxane oligomers, AEP-1770-40F and HP-1370-30F. This last oligomer had hydroxypiperazine end groups. The oligomers were poured into 4-ounce glass jars which were covered with aluminum foil and capped with plastic lids. The jars were placed in a 125°C oven and removed periodically for viscosity measurements. A Brookfield RVT viscometer was used to determine viscosities of the aged oligomers at room temperature. The viscometer was calibrated using three standard viscosity oils also contained in 4-ounce glass jars. The viscometer's #5 and #6 spindles were used for the siloxane and acrylonitrile butadiene copolymers, respectively.

2.3. RESULTS AND DISCUSSION

2.3.1. Characteristics of the Siloxane-Modified Epoxy Networks

The synthesis of the siloxane-modified networks involved two steps as illustrated in Figure 2.2. In the first step, the piperazine-terminated polysiloxane oligomer (5-15 weight percent of the total network) was allowed to react with an excess of Epon 828. Reaction occurred between the secondary amine piperazine end groups of the polysiloxanes and the epoxide rings of Epon 828. After the completion of this first step, the reaction mixture contained excess unreacted Epon 828 and linear precursors resulting from the capping of the siloxane oligomer with Epon 828. In the second step, the final network was formed by reaction between the primary amine end groups of PACM-20 and the epoxide end groups on both Epon 828 and siloxane oligomers capped with Epon 828. It should be emphasized that the siloxane rubber modifier is chemically bonded to the epoxy matrix. The completeness of the crosslinking reaction has been shown by FTIR studies (35).

In addition to the PDMS elastomer depicted in Figure 2.2, this investigation also utilized two series of siloxane copolymers based on dimethylsiloxane: 1) copolymers of methyl trifluoropropyl (TFP) siloxane and dimethyl siloxane and 2) copolymers of diphenyl (DP) siloxane and dimethyl siloxane. Figure 2.3 provides structures for the oligomers, all of which had aminoethylpiperazine (AEP) end groups. Details on synthesis and chemical characterization of these modifiers are given in Ref. 35.

It is believed that inclusion of the more polar TFP unit and the more resonant DP unit can allow one to control the compatibility between epoxy and elastomer. In the case of TFP siloxane, one of the two methyl units of dimethyl siloxane is replaced with a TFP group whose strong electronegativity creates a dipole across an otherwise non-polar chain. The epoxy resin is more strongly attracted to this new polar elastomer, and the more TFP incorporated, the greater the affinity between resin and rubber. Therefore, as cure proceeds, a siloxane of higher TFP content will precipitate out later in the crosslinking process. It is possible that some siloxane of high TFP content could remain dissolved in the epoxy matrix after cure is complete. Since the mobility of the network system diminishes continuously with cure time, at the point where incompatibility is reached, the elastomer segments of each chain (see Figure 2.2) can coalesce with only so many other such segments. The net result is a particle size that is inversely proportional to TFP content. This concept of the effect of rubber-resin compatibility on phase separation during cure can be applied to the effects of increasing DP content relative to dimethyl content in a siloxane modifier. In this second case, the diphenyl unit interacts with the resin through its resonant phenyl rings. The preceding explanation also explains the consequences of raising acrylonitrile content in ATBN and CTBN oligomers. For any of these three cases, it is imperative that the resin, curing agent, and chosen elastomer be well-mixed before this sequence of events can take place.

Table 2.1 lists the glass transition temperatures for the pertinent siloxane oligomers as a function of TFP and DP contents. The percent of each comonomer is recorded with reference to the siloxane units as well as the entire oligomer. One notes the difference that this creates between the two nominally "100%" TFP siloxanes of different molecular weight. Note also the higher Tg values for the DP series at equal weight percents, a factor which limits their ease of synthesis and may affect their mobility during cure.

In Table 2.2 are tabulated the Tg values for resins modified with the siloxane copolymers described in Table 2.1. Transition temperatures for samples modified with oligomers containing primarily dimethyl siloxane units give little indication of intimate mixing between epoxy and rubber. Evidence for partial miscibility with increasing TFP or diphenyl content is suggested by the relatively lower Tg's for some of the modified resins, in particular 10-2070-40F, 10- and 15-1500-70F, 15-2290-40D, and 15-2730-60F.

The dynamic mechanical properties of the siloxane-modified epoxy networks have been investigated by Tran (35) using the Dynamic Mechanical Thermal Analyzer (DMTA). The cured control network was found to exhibit the two major relaxations observed in most epoxy polymers (37,38,39). A high temperature or α transition at 150°C corresponds to the major glass transition temperature of the network above which large chain motion takes place. The low temperature or β transition is a broad peak extending from -90° to 0°C with a center near -40°C. It has been attributed predominantly to the motion of the CH2-CH(OH)-CH2-O (hydroxyether) group of the epoxy (37,38,40).

The DMTA tan δ versus temperature curves of a series of siloxane-modified epoxy networks containing 10 wt% TFP siloxanes showed, in addition to the major glass transition and β peaks, a small damping peak corresponding to the glass transition temperature of the siloxane phase (35). This small peak substantiates the multiphase nature of the modified networks in which the epoxy resin and the elastomer are phase separated. The low temperature damping peak shifts to higher temperatures with increasing TFP content. The dependence of this transition peak on TFP content confirmed its assignment to the siloxane moiety.

The Tg values determined by DSC for the pure liquid siloxane oligomers were in good agreement with the values determined from DMTA of siloxane-modified epoxies. However, at 0 and 20% TFP content, the siloxane Tg from DMTA was about 16°C *higher* than the Tg found by DSC. This suggests that at TFP contents above 20%, the siloxane separates from the epoxy as a "purer" phase. This point will be discussed further in the next section. Also reserved for later discussion is the depression of the major epoxy transition with inclusion of the 2070-40F oligomer.

2.3.2. *Morphology and Solid-State Properties*

Morphological investigations clearly illustrate the enhancement of resin-rubber compatibility through siloxane copolymerization. SEM micrographs of cold snap surfaces for the control and four TFP siloxane-

modified resins are given in Figure 2.4. Increasing TFP content decreases particle size from about 50 to less than 5 microns. The make-up of the particles also changes. At low TFP content, the relatively large domains have a nodular character. Transmission electron microscopy of CTBN-modified epoxies (25-27) indicates that such particles are actually mixtures of resin and rubber although that same conclusion cannot necessarily be made in this case. It is suspected that these particles result from incomplete mixing caused by gross incompatibility between the liquid elastomer and liquid resin prior to cure. At the highest TFP contents, particles are smaller and homogeneous in texture. As will be seen, domains less than 1 μm result from modification with 2250-20D and especially 2290-40D. Domains are roughly textured for both diphenyl siloxane modifiers, becoming irregularly shaped in 15-2290-40D.

A primary effect of increasing siloxane molecular weight is illustrated in Figure 2.5. Small presumably homogeneous domains characterize the 15-1500-70F fracture surface (upper micrograph). When molecular weight for a pure TFP siloxane is doubled (refer to Table 2.1), the cold snap fracture surface shows a few large particles as well as small homogeneous uniformly textured domains.

Figure 2.6 shows the effect of snapping modified resin samples at room temperature rather than after immersion in liquid nitrogen. For the modified resin shown, the Tg of the oligomer is -91°C, well below room temperature. The size of the domains is approximately the same in either photo, but the domain character is better defined in the cold snap fracture surface.

Although it was demonstrated that the siloxane component of these materials migrates to the surface (top 50 A) during cure (15), there is no evidence that this creates a concentration gradient of siloxane throughout the entire sample thickness. However, in an effort to at least qualitatively determine the distribution of the elastomeric phase in these materials, SEM was used to examine the fast crack regions of 10-2330-20F and 10-2190-0 fracture toughness samples. These cleaved surfaces contain relatively few fracture artifacts and thus serve as reasonable cross-sections. They indicate that from one outside edge to the other, there exists an apparently even distribution of the elastomeric phase.

A toughened material, by definition, features improvements in fracture resistance without substantial loss of mechanical strength or modulus. Figures 2.7a and 2.7b illustrate that modification with the various siloxane oligomers only slightly influenced the flexural modulus of the base epoxy resin. As expected, the flexural modulus does decrease as rubber content increases. The decrease is less severe as either TFP or DP content increases. Although the Tg's of the TFP and DP oligomers increase dramatically with TFP or DP content, it is not likely that the difference in Tg between the various rubbers bears heavily on the modulus since modulus was obtained at room temperature.

Consideration of the nature of the phase separation in siloxane-modified epoxies permits a second explanation of these modulus trends. The morphologies observed contained elastomeric domains of a variety of

sizes and textures which changed with TFP content and molecular weight. Several examples of these are given in Figure 2.8a-d for siloxane modifiers containing 0, 40, 70, and 85 weight percent TFP siloxane. The figure captions provide descriptions and comments. The features of these fracture surfaces are referred to in the following discussion.

At low TFP content especially, the elastomeric particles are large and appear to be mixtures of epoxy and siloxane. If particularly large, about 50 μm in diameter, such domains were often observed on cold snap fracture surfaces to be weakly attached to the matrix such that gaps or voids existed between particle and matrix. Voids are well known to detract from modulus. Secondly, if the supposition that these large particles contain both elastomer and epoxy is correct, then the actual volume fraction of the elastomeric phase is larger than what would be calculated assuming the phase separation of the "pure" siloxane phase without any epoxy inclusions. It is the volume fraction of the phase separated elastomeric domains which is believed to proportionately lower modulus (25). In addition, if raising TFP content encourages miscibility between the modifier and the matrix, as has been suggested (35), the effective volume fraction of phase-separated elastomer may be lowered. Studies with CTBN-modified epoxies (25,26) have suggested that dissolved rubber is not as harmful to room temperature modulus as phase-separated rubber. A third situation is that where a small and more or less homogeneous domain adheres well to the matrix but where its size varies with TFP content. The strength of the interface may then partially control the modulus. For example, the siloxane-siloxane

contacts within a homogeneous rubber particle consist primarily of van der Waal's forces. In contrast, the forces across the siloxane-epoxy interface also include inherently stronger covalent bonds and possible dipole-dipole interactions. With increasing TFP, particles become smaller and surface-to-volume ratio goes up, and the resin-rubber interface may contribute to and help to improve the modulus.

In summary of these points, it is seen that isolation of particles from the epoxy matrix, the effective volume fraction of the elastomeric phase, and strength of the interface interact to control modulus. The morphology which a particular siloxane modifier promotes determines the contribution of any or all of these three factors to the modulus of the modified resin.

Two 60% TFP siloxane oligomers were prepared and used as modifiers for epoxy resins. For unknown reasons, these 60F modifiers did not fall in line with the regular progression of mechanical properties seen in the TFP siloxane series already described. They will therefore be discussed separately. The two oligomers had molecular weights of 2730 and 2320. Representative cold snap fracture surfaces shown in Figure 2.9 demonstrate that the 2730-60F modifier introduced large heterogeneous elastomeric domains which were only weakly attached to the epoxy matrix. The 15-2320-60F surface shown also shows heterogeneous particles, but they are considerably smaller and appear to be more firmly bound to the matrix. Both 15-2320-60F and 15-2730-60F contain a number of small particles. In keeping with the above explanation of how morphology affects modulus, the 2730-60F modifier

lowered flexural modulus more than did 2320-60F, as Figure 2.10 shows. These modulus values are, however, considerably lower than expected based on the performance of modifiers containing 40% TFP siloxane.

Figure 2.7c provides flexural modulus data for the CTBN- and ATBN-modified epoxies prepared for this study. Once again, modulus decreases with increasing rubber content, and increasing AN content seems to have an effect similar to increasing TFP or DP content in the siloxanes. If one compares the results of Figures 2.7a and 2.7b with Figure 2.7c, which are drawn on identical scales, one may observe that the TFP and DP siloxane-modified epoxies generally have higher moduli than the butadiene-modified resins. While subtle, this observation is in fact supported by Young's modulus data, a portion of which is given in Table 2.3.

These differences in modulus may be at least partially explained by DSC data such as that in Figure 2.11. It is seen that in general the glass transition regions of the ATBN- and CTBN-modified epoxies are broader and have a lower midpoint than those of the control and two siloxane-modified materials. This thermal data suggests that the butadiene oligomers are relatively more miscible with the epoxy and may act as plasticizers. As an additional point, it is likely that the higher molecular weight of the CTBN oligomers leads to a higher MW between network junction points and consequently, a lower crosslink density.

In the only such study known to the author, Sayre, Assink, and Lagasse (23) demonstrated (using energy dispersive X-ray analysis,

NMR, and DSC) that the interface between the CTBN (18% AN) and epoxy phases in a diethanol amine-cured Epon 828 resin was not diffuse and that only a small percentage of CTBN was actually dissolved in the matrix. They also found that about one half of the CTBN precipitated in particles measuring less than 0.1 μm (1000 Angstroms) across. Although the curing agent and curing schedule for the resins studied by Sayre and co-workers were not the same as those used in the present study, their characterization indicates that fine mixing can occur between CTBN and Epon 828.

Fracture toughness for siloxane-modified as well as ATBN- and CTBN-modified resins was monitored through KIc, plane-strain fracture toughness (41). The KIc values of at least five three-point bend (3PB) specimens of each material were calculated according to Equation (1)

$$KIc = \frac{6\ P}{B\ W^{1/2}}\ f(a/w) \qquad (1)$$

where P is the critical load, B is the sample's width, W is its thickness, and a is the length of the pre-crack. See Figure 2.1a. P is taken as the load at break. Letting R = a/w, the geometry factor Y = f(a/w) is as given in Equation (2).

$$Y = 1.93R^{1/2} - 3.07R^{3/2} + 14.53R^{5/2}$$
$$-25.11R^{7/2} + 25.80R^{9/2} \qquad (2)$$

A limited number of KIc values were obtained with a compact tension geometry for which KIc is calculated with Equation (3)

$$KIc = \frac{P}{B \, W^{1/2}} \quad f(a/w) \tag{3}$$

where symbol definitions are analogous to those for the 3PB test piece. See Figure 2.1b. The geometry factor for the CT specimen is given in Equation (4).

$$Y = 29.6R^{1/2} - 185.5R^{3/2} + 655.7R^{5/2} - 1017R^{7/2} + 638.9R^{9/2} \tag{4}$$

The criteria of ASTM E399 (41) were followed as closely as possible. The only criterion which could not be consistently satisfied was that for a straight pre-crack, +/- 5%.

In graphic presentation of KIc results, the error bars given for the control are typical of all those data points which do not have their own error bars. In cases where error exceeded 10%, individual error bars are provided and labelled with the corresponding symbol. Such large deviations are thought to result from the violation of the homogeneity criterion of linear elastic fracture mechanics at 15% of certain oligomers. (See, for example, Figure 2.4.)

Fracture toughness results for the TFP siloxane-modified epoxies are given in Figure 2.12a. With slight exception, modification with PDMS and 2330-20F gives virtually no improvement in KIc and in fact lowers KIc approximately linearly with weight percent of modifier! As TFP content climbs beyond 20%, KIc increases considerably, reaching a high in the 10-2070-40F material. Although one might question this particular piece of data, scrutiny of the numerical data reveals percent errors of only 4.2, 3.5, and 7.1 for the series of epoxy modified with 2070-40F. Furthermore, the 10% sample showed a depressed resin Tg (see Table 2.2) of 136°C followed by an increase to 150°C at 15% rubber content, suggesting that the borderline between miscibility and immiscibility is located between 10 and 15% of 2070-40F. The DMTA curve for 10-2070-40F (35) also showed considerable depression of the epoxy glass transition temperature. It was seen earlier that the ATBN and CTBN modifiers can also produce Tg depressions. Bucknall (28) has pointed out that a good toughening agent should be neither completely miscible nor immiscible with the material to be toughened.

Because the KIc value is quantitatively derived from processes occurring in the pre-crack front, these were examined by SEM. Figure 2.13 shows two of the outstanding morphological features observed. The pre-crack front of a 10-2330-20F sample, which gave a KIc value below that of the control (refer to Figure 2.12a), is shown in Figure 2.13a. One notes particularly the large heterogeneous particles of (presumably) both epoxy and elastomer. Rather than absorbing energy during loading, these particles rapidly tear, generally at an acute angle to the

direction of crack propagation. The tearing observed here is not entirely unexpected in light of the fact that many siloxane elastomers have relatively poor tear resistance at room temperature (13,42), which may be related to the large interval between room temperature and T_g (43). Kunz et al (10,30) have postulated a toughening mechanism involving particle stretching (energy absorption) and failure by tearing. However, the extent of tearing in this case and the associated KIc values suggest that the tearing is not a significant part of an energy dissipative process. Interestingly, each tear is located either near the interface of a large heterogeneous particle or within such a particle which may itself be a maze of resin-rubber interfaces. These tears might therefore be regarded as primarily interfacial failures.

The second noteworthy morphological feature is presented in Figure 2.13b. This micrograph depicts the KIc pre-crack front of 15-1500-70F, which had a KIc value significantly above that of the control, as shown in Figure 2.12a. The holes may be examples of the dilatation effect observed in CTBN-modified epoxies (19,22) in which rubber particles dilate in mutually perpendicular directions under the application of a triaxial stress and then collapse into spherical cavities following fracture. Dilatation requires a mismatch in coefficients of thermal expansion of resin and rubber (11). This effect will therefore be most striking when the elastomeric phase is homogeneous, as is apparently the case here.

KIc data for the DP siloxane-modified epoxies is provided in Figure 2.12b. Even at relatively low DP percentages, there is marked

improvement in KIc over the control. As the micrographs in Figure 2.14 show, the resins modified with these two oligomers exhibit smaller particle sizes than the TFP siloxane materials, however, the cavitation of the particles under fracture conditions is not as severe as in the TFP case. On the whole, the DP siloxane modifiers perform as well as or better than the TFP siloxane series.

Modification of epoxy resin with the 2730-60F and 2320-60F oligomers brought essentially no net change in fracture toughness. As Figure 2.15 shows, KIc is nearly constant within error over the range of rubber content for the 60F modified samples as a group. The 2320-60F modifier promoted higher fracture toughness than 2730-60F as one would expect from its smaller domain size.

One can now compare the KIc improvement obtained with siloxane modification with that obtained using ATBN and CTBN modifiers, shown in Figure 2.12c. (The specific results of Figure 2.12c will be discussed later.) Looking collectively at the data of Figure 2.12, it is seen that the 2070-40F oligomer is most competitive with the CTBN and ATBN oligomers at both 5 and 10% rubber content. The apparent partial miscibility of the 2070-40F oligomer is probably an important factor in this improvement.

The current interest in PDMS as an epoxy modifier lies partly in its low Tg relative to the ATBN and CTBN modifiers. Up to this time, however, improvements in KIc through copolymerization of dimethyl siloxane with TFP and DP siloxane require raising the Tg of the siloxane modifier above that of PDMS, as shown by Table 2.1. It is hoped that

increased understanding and control of the synthesis and morphologies of siloxane-modified epoxies will make it possible to retain the low Tg of the modifier while raising the fracture toughness of the resin. The true value of this objective could eventually be shown by measurement of KIc at temperatures below ambient.

The fracture toughness results presented thus far were derived from a fairly small 3PB specimen. In limited work with a proportionately larger 3PB sample (B ~ 6.4 mm), a similar KIc value was found for the control. A second geometry, compact tension (CT), was utilized for alternate determinations of KIc. The KIc values found with the CT specimens agreed within error with those obtained with the 3PB geometry, as shown in Table 2.4.

Study of the CT fracture surfaces by SEM reinforced earlier observations of the predominant features of fracture. The fracture surface of the unmodified epoxy was essentially featureless as before; a thin pre-crack front extended to a very smooth fast crack region. On the surface of the 10-2330-20F specimen observed there were found nodular 20-40μm particles. In the pre-crack front, such particles exhibited irregular tears when crossed with a microcrack but otherwise remained undisturbed and encircled by an extremely fine border. In the fast crack region, slightly larger particles appeared to be more severely torn. Those small particles which did exist appeared to be essentially uninvolved in the fracture processes. In the pre-crack front of a 10-2070-40F CT sample, the average domain sizes were approximately 10-20 μm and 1-3 μm, the larger ones generally being somewhat heterogeneous

in texture, the smaller ones presumably homogeneous. The larger domains in 10-2070-40F showed good adhesion to the epoxy matrix. The fast crack region showed similar features but finer microcracks. In general, the fracture surface of 10-2070-40F, which showed a KIc value above those of both the control and 10-2330-20F, was rougher than 10-2330-20F, suggesting that a larger fraction of 10-2070-40F participates in the fracture, thereby allowing greater energy dissipation.

Looking strictly at the butadiene-based oligomeric modifiers, one sees from Figure 2.12c that the CTBN-modified resins have higher KIc values than the ATBN-modified resins at high AN content. At low AN content, the situation is exactly the opposite. Close examination of the ATBN and CTBN domains in KIc fracture surfaces indicated that this reversal may have been caused by differences in particle morphology. Figure 2.16 points out these differences with four low magnification micrographs of resins modified with 10% of each of the four butadiene oligomers. Three of the samples show exclusively small-particle morphology while the 10C-3690-10AN surface contains large (25-50 μm) resin-rubber particles which coexist with small particles. The two lower micrographs in Figure 2.16 illustrate the distinct difference between the small ATBN and CTBN particles. For the CTBN's of either AN content, the small particles are homogeneously textured and have sharp edges. The ATBN particles, though small for both high and low AN content, are somewhat nodular and may simply be small resin-rubber particles. These variations in morphology probably follow from the excess AEP in the ATBN, the different reactivities of the carboxyl and amine end groups, or a combination of these two factors. It is interesting to note that the

small particles of either elastomer are roughly the same size. It is clear that when sizes are equivalent, more homogeneous domains promote greater fracture toughness.

2.3.3. *Effects of High-Temperature Aging on Oligomer Viscosity*

The current need for toughening agents with better thermo-oxidative stability than butadiene-based materials (44) is one of the principal reasons for the present research in siloxane-modified epoxies. Silicone polymers are generally suitable for application at temperatures ranging from -100° to near 300°C. Their overall resistance to degradation by oxygen, ozone, and sunlight is considered to be excellent (14). Oxidative cleavage of the siloxane chain is insignificant at temperatures below 200°C but becomes substantial beyond 250° (13). The presence of moisture appears to have an adverse effect between 120° and 275°C, particularly in situations where part design does not allow water to escape, as in a thick molding.

Butadiene acrylonitrile copolymers (45) find uses as precursors to solid crosslinked elastomers (nitrile rubber, NBR) and other materials as well as the liquid ATBN and CTBN oligomers. These low molecular weight liquids are also produced with hydroxyl, mercaptan, vinyl, or halogen end groups. Nitrile rubbers have only moderate ozone resistance. Natural rubber and styrene-butadiene rubber can be protected against ozone attack of the carbon-carbon double bond by the addition of anti-ozonates which bloom to the surface and form a barrier zone diffusion; NBR does not respond to such treatment. Hot air

resistance of nitrile rubber is better than that of natural rubber and polyisoprene, primarily through clever compounding. As such, nitrile rubbers are available which withstand continuous exposure to 90°-air for 12 months. Forty days is the limit at 120°C, while extensive degradation occurs after three days at 150°C.

Evaluation of the degradation of polymeric materials in various temperature ranges and environments often involves monitoring changes in certain mechanical and rheological properties. More detailed studies might enlist spectroscopy, differential scanning calorimetry, thermogravimetric analysis, and molecular weight determinations.

The liquid state of the oligomers at hand lends them easily to studies of viscosity changes with high-temperature aging. Okamoto (12) reported such a study of CTBN oligomers containing 0, 10, 18, and 26% AN. Aging was carried out at 50°, 75°, 100°, and 125°C for 350 hours (ca. two weeks) accompanied by periodic measurements of viscosity, carboxylic acid content, and volatile content. Samples aged at 125°C exhibited increases in viscosity regardless of AN content, as shown in Figure 2.17. The sharpness of the increase was dependent on AN content with 26% AN producing the fastest initial rise in viscosity. The viscosity tended to settle to a slow steady increase after about 100 hours of aging at 125°C.

Similar work was conducted here on the four ATBN/CTBN oligomers provided by B. F. Goodrich as well as two siloxane oligomers, AEP-1770-40F and HP-1370-30F. This second siloxane had hydroxypiperazine (HP)

end groups. The results of almost 400 hours of aging at 125°C are presented in Figure 2.18. The viscosities of the siloxane oligomers remained essentially constant over the course of the experiment. The CTBN oligomers initially increased in viscosity and seemed to reach a constant value after about 200 hours. The profile of the CTBN curves parallels that found by Okamoto (12) in both magnitude and nature. After a decrease in the first fifty hours, the ATBN oligomers showed a rapid and continuing rise in viscosity through the end of the aging period. The experiment was discontinued after 385 hours aging time.

The oligomers underwent several visual changes during the course of the experiment. Both siloxane elastomers darkened in color but remained transparent to translucent. After less than 50 hours of aging, A-2560-10AN had deposited a layer which increased in depth with further aging and turned from white to deep yellow. The rest of the liquid became darker and nearly opaque. This oligomer's viscosity could not be measured beyond 300 hours aging time due to its gummy consistency. The oligomers C-3690-10AN and A-1750-18AN gradually darkened with time. They became nearly opaque, developed dark "swirls," and gradually settled out a thin light-colored layer. Although it darkened with aging, C-3880-17AN lost little of its transparency.

Molecular weights of the elastomers before and after high-temperature aging are given in Table 2.5. The only notable change is the increase shown by the ATBN rubbers. It is believed that the yellow deposits found in the A-2560-10AN (and to some extent in the A-1750-18AN) consisted of phase separated unreacted AEP, the loss of which

would raise the titrated molecular weight of either ATBN closer to its literature value. FTIR spectra of the siloxane elastomers were no different after aging. The AEP and HP end groups showed no obvious differences in stability. The higher viscosity for HP-1370-30F is reasonable due to the stronger effects of the end groups at a lower molecular weight.

The basically constant viscosity for the siloxane copolymers illustrates their lack of appreciable thermal oxidation at 125°C. Nielsen (46) reported negligible changes in viscosity of a dimethyl silicone fluid up to and including 150°C. Indeed silicone fluids are widely used for oil baths at these temperatures because of their generally good thermo-oxidative stability. In chemo-rheological studies, Tobolsky and Shaw (47) found that dimethyl siloxane elastomers were more stable than methyltrifluoropropyl elastomers. This difference has been traced in part to interaction between fluorine and silicon which leads to the formation of $CF_2=CHCH_3$ (48). Polydimethyl siloxane's stability is generally improved through substitution of a phenyl group for one of the methyl groups (49). Thus in increasing order of thermal stability lie TFP, dimethyl, and diphenyl siloxane.

Tran (35) has evaluated the thermal stability of many of the oligomers investigated in this chapter using thermogravimetric analysis (TGA) under both air and nitrogen atmospheres. For experiments conducted under nitrogen, it was found that while the siloxanes generally began to lose weight at lower temperatures than the ATBN and CTBN oligomers (350-400°C), the loss was more gradual, extending over

an approximately 100-degree range. The ATBN's and CTBN's lost weight sharply and almost completely beginning at about 430° and continuing to near 470°C. Many of the siloxanes retained an appreciable percentage of their original weight. The same experiment run under an air atmosphere showed slightly lower stabilities than those found in nitrogen, as expected. Co-oligomers consisting primarily of TFP siloxane were judged less thermally stable than those based on diphenyl or dimethyl siloxane. No significant differences were seen between ATBN and CTBN which have amine and carboxyl end groups, respectively.

On the basis of the available results, it is difficult to make strong conclusions about the relative thermo-oxidative stabilities of the siloxane and ATBN or CTBN oligomers. The viscosity study presented here indicates that the long-term stability of the siloxanes is superior to that of ATBN and CTBN at a relatively low temperature (125°C). Recall that 150°C was the curing temperature chosen for network preparation. On the other hand, Tran's TGA study (35) shows that some of these siloxanes may begin to degrade at lower temperatures than some ATBN and CTBN oligomers when temperature is increased at a constant rate. However, the very sharp weight loss seen for the ATBN and CTBN oligomers suggests that, in practice, extreme temperatures could cause catastrophic failure of resins containing acrylonitrile-butadiene modifiers. Optimization of siloxanes as rubber tougheners must be achieved before study of the relative thermo-oxidative stabilities of these various oligomers is further pursued.

2.4. CONCLUSIONS

Epoxy resins modified with dimethylsiloxane, dimethyl-co-methyltrifluoropropyl siloxane, and dimethyl-co-diphenyl siloxane displayed mechanical properties and morphologies which depended strongly on the composition and molecular weight of the siloxane modifier. As apparent compatibility between the resin and rubber increased, the elastomeric domains in the modified epoxies became smaller in size and more homogeneous in texture. As rubber content was increased, modulus dropped at a rate dependent on the resin-rubber compatibility, allowing modulus effects to be given a morphological basis. Factors found to be particularly detrimental to modulus included weak bonding of rubber particles to the matrix, heterogeneous rubber particles, and large (> 10 μm) rubber domains in general. Fracture toughness performance could also be traced to the morphology of the siloxane-modified systems. It was found that siloxane modification improved fracture toughness relative to the unmodified epoxy if it fostered a significant population of small and homogeneously textured elastomeric domains and partial miscibility between the resin and rubber. The most promising benefits to fracture toughness came with use of dimethylsiloxane-based oligomers containing at least 40% methyltrifluoropropyl siloxane and 20 and 40% diphenyl siloxane. Comparison of siloxane-modified epoxies with CTBN- and ATBN-modified epoxies prepared under the same conditions proved instructive with regard to both property and morphology effects.

A brief study in which the viscosities of liquid modifiers were monitored as a function of aging at 125°C suggested that the siloxane oligomers may have slightly better thermal stability than the ATBN and CTBN modifiers. However, consideration of the results of timed heating rate/weight loss studies indicates that the siloxanes may in fact lose weight at a lower temperature than the acrylonitrile butadiene elastomers.

2.5. RECOMMENDATIONS FOR FUTURE STUDY

1. Observation of smaller particle sizes for diphenyl/dimethyl siloxanes but lower Tg values for TFP siloxanes indicates that the best balance of mechanical properties over a wide temperature range may be achieved with modification of epoxy resin with diphenyl/TFP siloxane oligomers, a first choice being a 30/70 diphenyl/TFP siloxane.

2. Use of siloxane modifiers of high dimethyl siloxane content is hampered by their apparent immiscibility with the epoxy resin. It is suggested that the end group of the siloxane modifers be chosen so as to bridge this miscibility gap in an effort to obtain smaller and more homogeneous rubber particles.

3. The relative thermo-oxidative stabilities of siloxane modifiers and butadiene acrylonitrile modifiers should be more firmly established as long as "good" thermal stability remains a primary reason for siloxane modification of epoxy resins.

4. The use of a small three-point bend fracture toughness specimen has been found to adequately measure the fracture toughness of a variety of materials *provided that sufficient care is taken in sample preparation, crack initiation, regulation of testing procedures, and data treatment.* These practices are crucial to any application of fracture mechanics methods. Of value to future studies of epoxies and other materials would be an automated crack initiation procedure, perhaps through use of the

Instron crosshead and clamps. Crack quality is one of the most important but least controllable aspects of these tests. An automated cracking system would increase KIc precision and promote more efficient use of research grade materials.

5. A resin modified with both CTBN and siloxane modifiers might be considered as a possible avenue to increased fracture toughness and improved surface hydrophobicity.

2.6. *APPENDIX: AGING STUDIES OF EPOXY RESIN/GRAPHITE FIBER COMPOSITES*

2.6.1. *Introduction*

Long-term stability and maintenance of original material properties can suffer from any number of outside factors. Epoxy resins are more chemically and thermally resistant than many other polymeric materials. However, like any material containing a significant amount of glassy or amorphous material, epoxy resins are susceptible to a process known as physical aging (50). This is true not only for cured epoxy resins containing no second major phase but also for rubber-modified resins (51) and fiber-reinforced epoxy resin composites (52). This latter type of material is the basis of this Appendix. In the brief review which follows, specific examples of physical aging will be restricted to epoxy resins although it is understood that physical aging can occur in any partially glassy material including linear amorphous polymers, semi-crystalline polymers, some low molecular weight organics, and inorganic glasses.

Physical aging results directly from the inability of a material to attain equilibrium immediately upon cooling through the glass temperature (Tg) at any practically possible cooling rate (53). As any potentially glassy material vitrifies, its rapidly climbing viscosity prevents its structural units from assuming the packing arrangements and conformational states of lowest energy. Consequently, after vitrification, a glass contains an excess amount of free volume beyond that normally needed for the van der Waal's radii and thermal vibrations. An excess enthalpy exists as well.

These parameters are often represented as in Figure 2.19. Both enthalpy and specific volume decrease linearly as they approach the glassy state. If a material can be cooled to a glass at an infinitely slow rate, the material passes from the liquid state to the equilibrium glassy state at a temperature usually called T2. In practice, the cooling occurs at some finite rate (accompanied by a dramatic increase in viscosity). The observed glass temperature will therefore occur at a temperature higher than T2, being lower for a slower cooling rate. If the glassy material is then annealed below Tg, its molecules will approach their equilibrium conformations and packing; specific volume and enthalpy will decrease, as indicated by the vertical arrows in Figure 2.19. The material will physically age.

Mechanical properties can be dramatically affected by physical aging. For example, modulus will generally increase with sub-Tg aging time as shown in Figure 2.20 where one may also note that elongation at break may decrease with aging time. Besides stress-strain tests, one may also monitor physical aging by tensile creep compliance tests, as used extensively by Struik (53). It has been common in this laboratory to follow physical aging using stress-relaxation experiments from which the stress value obtained after 10 minutes of relaxation is taken as a gauge of aging. When presented as a function of log aging time, it provides a convenient measure of the rate of aging. The "window" which a 10-minute stress value allows does limit the time period over which aging will be perceived, as demonstrated by Figure 2.21. However, it easily shows the relative rates of aging of a comparative series of materials.

This Appendix describes the author's part in a study of the physical aging of graphite fiber-epoxy resin composites. The specific goal of the work was to determine the relative rates of physical aging of the unreinforced epoxy resin as well as the composite both parallel and perpendicular to the fiber direction. This was achieved by monitoring stress-relaxation in the flexural mode to complement measurements made in the tensile mode. Pertinent results of the larger portion of the investigation are included for completeness.

2.6.2. *Experimental*

2.6.2.1 *Materials*

The graphite fiber-epoxy resin composite utilized in this study was prepared from impregnated plies of graphite fiber/NARMCO 5208. The chemical structures of NARMCO 5208 and the curing agent used, diaminodiphenylsulfone (DDS), are given in Figure 2.22. The uncured plies were received packed in dry ice and stored in a freezer until use. For sample preparation, the plies were allowed to come to room temperature, stacked in a uniaxial fiber orientation, placed between 5 mil thick Teflon film, cut in the desired dimensions for mechanical testing, and sandwiched between flat steel sheets. The force on the samples was then about 10^5 N/m^2. The samples were cured in an oven for 4.5 hours at 149°C followed by 1.5 hours at 177°C. This curing schedule was prescribed by NASA/Langley. When the curing schedule was completed, the samples were taken out of the oven and allowed to cool to room temperature in air.

Uncured bulk NARMCO 5208 resin samples were prepared by the following procedure. The frozen bulk resin was allowed to warm up to room temperature. A desired amount of resin was poured into a beaker and degassed in a 120°C vacuum oven for 10-20 minutes or until no gas bubbles could be observed. The resin was poured carefully into a Dow Corning RTV 3110 silicone rubber mold that had been preheated to 149°C. A piece of Teflon film was placed over the mold and the excess resin smoothed off by rolling a glass rod over the Teflon film. Samples were cured according to the same schedule used for the NARMCO composites. Once the cure time was ended, the entire mold was removed from the oven and "quenched" between two large metal plates at room temperature. Approximately 30 minutes later, the samples were removed from the mold.

Limited testing was carried out with an Epon 828/PACM-20 resin system. The liquid Epon 828 resin was first degassed for 10 minutes at 60°C. A molar equivalent of PACM-20 was added and mixed in well, and the mixture was degassed for about 15 minutes at 60°C. The mixture was then poured into a silicone rubber mold and excess resin was rolled off as described earlier. The mold was covered with a metal plate and the resin and hardener were cured for 1.5 hours at 150°C.

2.6.2.2. *Mechanical Testing*

Stress relaxation measurements were made on an Instron Model 1122 ambient temperatures. Stress relaxation was done in both tensile and

flexural modes for bulk cured resin and composites prepared such that testing could be conducted both parallel and perpendicular to the fiber direction. Tensile dog-bone samples were either 0.7 (4-ply) or 1.1 mm (6-ply) thick. These samples were clamped in the Instron such that the initial length was 4.0 cm. A fixed strain of 0.25 (bulk) or 0.50 (composite) was applied at a crosshead speed (CHS) of 10 mm/min, and the initial and 10-minute stress levels were recorded and used to calculate the percent stress relaxation as defined in Figure 2.23.

Flexural testing was performed using the Instron machine fitted with two aluminum/stainless steel pieces. The lower piece was fastened to the Instron base and held two stainless steel rods 0.6 cm in diameter and situated 6.35 cm apart, center to center. The upper piece was attached to the crosshead and tensile load cell of the Instron and held a third stainless steel rod which was centered between the two lower rods. A flexural composite sample measuring 7.5 x 2.5 x 0.08 cm (4-ply) or a cured bulk resin sample measuring 7.5 x 2.5 x 0.1 cm was placed above the single mobile rod of the test piece and below the two stationary rods. As the central bar moved up during testing, the test piece effectively performed an inverted three-point bend test. Composite samples were placed in the test piece such that the graphite fibers were either parallel or perpendicular to the rods of the test piece; the notation to be used here is provided in Figure 2.24. In order to keep deflections for the stress relaxation tests in the linear elastic region, 5 mm (NARMCO materials) and 4 mm (Epon 828/PACM-20) were chosen as the standard deflections. For each run, samples were deflected at a CHS of 100 mm/min and allowed to relax for 10 minutes after which the stress relaxation was calculated as in Figure 2.23.

2.6.3. *Results and Discussion*

Monitoring physical aging effects requires quenching a material from above its glass transition temperature to the temperature chosen for aging. Epon 828/PACM-20 resin samples were heated to 165°C for 10 minutes and quenched into cool tap water. Samples of NARMCO 5208 were heated to 200°C for 10 minutes and immediately quenched in cool tap water, at which time aging was considered to have begun.

Thermal analysis studies showed that NARMCO 5208 cured according to the schedule recommended by NASA/Langley was not fully cured as indicated by the development of an exotherm at temperatures slightly above the highest cure temperature (54). This exotherm indicated that further reaction had taken place, leading to a more extensive cure and raising the Tg of the resin. The short thermal treatment needed to start the sub-Tg aging experiment for NARMCO 5208 was found to raise the Tg of the resin from ~ 185°C to about 200°C. This treatment was not believed to introduce any *chemical* aging effects.

Figure 2.25 illustrates the differences in relative aging rates for NARMCO 5208 bulk resin and composites tested in the tensile mode. The topmost line shows that percent stress relaxation decreased most sharply for the bulk resin sample. Measurement of the stress relaxation in the direction perpendicular to the carbon fibers also showed a physical aging effect. The fact that the bulk resin exhibits greater magnitudes of stress relaxation than the composite was attributed to the larger volume fraction of resin in the bulk samples (1.0 vs. about 0.47). Morphological

differences between bulk and matrix resins were also considered to be a potential factor (54).

Tensile stress relaxation did not change with time for samples tested in the direction of fiber orientation, as shown by the lowest set of points in Figure 2.25. However, a finite amount of stress relaxation was observed. The flexural test was utilized to determine if this very small amount of stress relaxation in the test direction was caused by the difficulties of working with these high strength composites in their maximum strength direction; slippage in the Instron clamps was suspected.

The use of the flexural stress relaxation test was first applied to an Epon 828/PACM-20 resin system. Figure 2.26 illustrates that, as expected, the 10-minute flexural stress relaxation decreased linearly with log aging time at room temperature. As demonstrated by Figure 2.27, flexural testing of the NARMCO 5208 resin and resin composites verified that effectively no stress relaxation occurred in the direction dominated by the fiber. However, once more, in the direction, B, where the fiber and resin are acting in series, a physical aging effect was observed.

The larger study of which this work was a part showed a similar dependence of physical aging effects on fiber direction for the resin system Hercules 3501/DDS, which is chemically the same as the NARMCO 5208 system already discussed. However, the Hercules 3501 system studied had a Tg of 85°C immediately after curing vs. 185°C for

NARMCO 5208. The effect of the heating and quenching procedure on possible further curing and Tg changes was not reported for the Hercules resin.

The choice of sub-Tg annealing temperature (Ta) was found to affect the rate of physical aging as shown by stress relaxation measurements (54). Bulk NARMCO 5208 resins aged at 100°C showed a lower rate of aging (i. e., lower slope of a plot of stress relaxation vs. log aging time) than the same materials aged at room temperature. This was rationalized by assuming first that the free volume lost within ten minutes at Ta = 100°C was greater than that lost at Ta = room temperature due to the greater thermal energy available at 100°C. Since physical aging was monitored beyond ten minutes but not before, the initially faster rate at Ta = 100°C could not be observed experimentally. It was presumed that a sample aged for ten minutes at 100°C would have a lower free volume than a similar sample aged at room temperature. Therefore, the rate of physical aging measured beyond ten minutes is likely to be lower for the sample aged at the higher temperature since it effectively has a lower initial free volume.

2.6.4. *Conclusions*

This study showed that the effects of physical aging on the stress relaxation of a fiber-reinforced resin composite differed with the direction of measurement relative to the fiber orientation. Physical aging was easily observed in the bulk resin as well as in the direction transverse to the graphite fibers of the composites. Physical aging did

not manifest itself along the fiber direction, which was expected since this direction is dominated by the high strength, time independent carbon fibers.

REFERENCES

1. Potter, W. G., *Epoxide Resins,* Springer-Verlag: New York, 1970.

2. *Epoxy Resin Chemistry and Technology,* May, C. A., Tanaka, Y. eds., Marcel Dekker: New York, 1973.

3. *Epoxy Resin Chemistry,* Bauer, R. S., ed., Am. Chem. Soc. Adv. Chem. Ser., *114* (1979).

4. McGarry, F. J., Proc. Roy. Soc. Lond. A., *319,* 59 (1970).

5. McGarry, F. J., Sultan, J. N., 24th Ann. Tech Conf., Reinf. Plast./Compos. Div., SPI, Sect. 11-B (1969).

6. Rowe, E. H., Siebert, A. R., Drake, R. S., Mod. Plast., *47,* 110 (1970).

7. Rowe, E. H., 24th Ann. Tech Conf., Reinf. Plast./Compos. Div., SPI, Sect. 11-A (1969).

8. Riew, C. K., Rowe, E. H., Siebert, A. R., Am. Chem. Soc. Adv. Chem. Ser., *154,* 326 (1976).

9. Romanchik, W. A., Sohn, Geibel, J. F., Am. Chem. Soc. Symp. Ser., *221,* 85 (1982).

10. Kunz, S. C., Beaumont, P. W. R., J. Mater. Sci., *16,* 3141 (1981).

11. Kinloch, A. J., Shaw, S. J., Tod, D. A., Hunston, D. L., Polymer, *24,* 1341 (1983).

12. Okamoto, Y., Polym. Eng. Sci., *23,* 222 (1983).

13. Warrick, E. L., Pierce, O. R., Polmanteer, K. E., J. C. Saam, Rubber Chem. Tech., *52,* 437 (1979).

14. Cush, R. J., Winnan, H. W. in *Developments in Rubber Technology - 2*, Whelan, A., Lee, K. S., eds., Applied Science: London, 1981.

15. Riffle, J. S., Yilgor, I., Banthia, A. K., Tran, C., Wilkes, G. L., McGrath, J. E., Am. Chem. Soc. Symp. Ser., *221*, 21 (1982).

16. Yorkgitis, E. M., Tran, C., Eiss, N. S., Jr., Hu, T. Y., Yilgor, I., Wilkes, G. L., McGrath, J. E., Am. Chem. Soc. Adv. Chem. Ser., *208*, 137 (1984).

17. Eiss, N. S., Jr., Czichos, H., in Wear of Materials 1985, ASME: New York, in press.

18. Bascom, W. D., Cottington, R. L., J. Adhesion, *7*, 333 (1976).

19. Bascom, W. D., Cottington, R. L., Jones, R. L., Peyser, P., J. Appl. Polym. Sci., *19*, 2545 (1975).

20. Bascom, W. D., Hunston, D. L. in *Adhesion 6*, Allen, K. W., ed., Applied Science: London, 1982.

21. Bascom, W. D., Hunston, D. L., Timmons, C. O., Org. Coat. Plast. Chem., *38*, 179 (1978).

22. Bascom, W. D., Mostovoy, S., Org. Coat. Plast. Chem., *38*, 152 (1978).

23. Sayre, J. A., Assink, R. A., Lagasse, R. R., Polymer, *22*, 87 (1981).

24. Kunz, S. C., Sayre, J. A., Assink, R. A., Polymer, *23*, 1897 (1982).

25. Manzione, L.T., Gillham, J. K., McPherson, C. A., J. Appl. Polym. Sci., *26*, 907 (1981).

26. Manzione, L.T., Gillham, J. K., McPherson, C. A., J. Appl. Polym. Sci., *26*, 889 (1981).

27. Bucknall, C. B., Yoshii, T., Br. Polym. J., *10*, 53 (1978).

28. Bucknall, C. B., *Toughened Plastics*, London: Applied Science, 1977.

29. Yee, A. F., Pearson, R. A., General Electric Co., NASA Contractor Report 3718, 1983.

30. Kunz-Douglass, S.C., Beaumont, P. W. R., Ashby, M. F., J. Mater. Sci., *15*, 1109 (1980).

31. Sultan, J. N., McGarry, F. J., Polym. Eng. Sci., *13*, 29 (1973).

32. Kinloch, A. J., Shaw, S. J., Hunston, D. L., Polymer, *24*, 1355 (1983).

33. Meeks, S. C., Polymer, *15*, 675 (1974).

34. Ophir, Z. H., Emerson, J. A., Wilkes, G. L., J. Appl. Phys., *49*, 5032 (1978).

35. Tran, C., Ph. D. Thesis, VPI & SU (1984).

36. Yilgor, I., Yilgor, E., Banthia, A. K., Wilkes, G. L., McGrath, J. E., Polym. Bull., *4*, 323 (1981).

37. Ochi, M., Ozazaki, M., Shimbo, M., J. Polym. Sci.: Polym. Phys. Ed., *20*, 689 (1982).

38. Pogany, G. A., Polymer, *1*, 66 (1970).

39. Enns, J. B., Gillham, J. K., J. Appl. Polym. Sci., *28*, 2567 (1983).

40. Chang, T. D., S. H. Carr, Brittain, J. O., Polym. Eng. Sci., *22*, 1205 (1982).

41. Knott, J. F., *Fundamentals of Fracture Mechanics*, Wiley: New York, 1973.

42. Gent, A. N., Tobias, R. H., Am. Chem. Soc. Symp. Ser., *193*, 367 (1982).

43. Gent, A. N., Pulford, C. T. R. in *Developments in Polymer Fracture - 1*, Andrews, E. H., ed., Applied Science: London, 1979.

44. Bucknall, C. B., J. Elast. Plast., *14*, 204 (1982).

45. Bertram, H. H. in *Developments in Rubber Technology - 2*, Whelan, A., Lee, K. S., eds., Applied Science: London, 1981.

46. Nielsen, J. M., J. Polym. Sci.: Polym. Symp., *40*, 189 (1973).

47. Tobolsky, A. V., Shaw, M. T., Polym. Eng. Sci., *10*, 225 (1970).

48. Wright, W. W. in *Thermal Stability of Polymers*, Vol. 1, Conley, R. T., ed., Marcel Dekker: New York, 1970.

49. Economy, J., Mason, J. H. in *Thermal Stability of Polymers*, Vol. 1, Conley, R. T., ed., Marcel Dekker: New York, 1970.

50. Tant, M. R., Wilkes, G. L., Polym. Eng. Sci., *21*, 875 (1980).

51. Kong, E. S. W., Am. Chem. Soc. Symp. Ser., *221*, 171 (1982).

52. Kovacs, A. J., Fortschr. Hochpolym. Forsch., *3*, 394 (1963).

53. Struik, L. C. E., *Physical Aging in Amorphous Polymers and Other Materials*, Elsevier: Amsterdam, 1978.

54. Mohajer, Y., Yorkgitis, E., Wilkes, G., McGrath, J., Proceedings of the Critical Review; Techniques for the Characterization of Composite Materials, AMMRC, Watertown, MA, 1982, p. 339.

55. Petrie, S. E. B. in *Polymeric Materials: Relationship Between Structure and Mechanical Behavior*, Baer, E., Radcliffe, S. V., eds., Am. Soc. Met.: Metals Park, OH, 1975.

Table 2.1. Glass Transition Temperatures of Siloxane
            Oligomers

OLIGOMER#	WT. % COMONOMER*	Tg (°C)
2190-0	0	-126
2330-20F	25	-116
2070-40F	50	-91
2320-60F	75	na
2730-60F	75	-76
3130-85F	100	-58
1500-70F	100	-45
2250-20D	25	-88
2290-40D	50	-51

Tg values based on DSC scanning rate of 10°/min.
Wt. % comonomer based on total oligomeric weight.
* Wt. % comonomer without end groups.
na = not available

Table 2.2. Glass Transition Temperatures of Epoxy Networks
after Modification with Siloxane Oligomers

	WT. % RUBBER IN EPOXY*		
OLIGOMER	5	10	15
2190-0	158	153	152
2330-20F	157	147	151
2070-40F	150	136	150
2320-60F	159	153	149
2730-60F	156	156	140
3130-85F	150	150	150
1500-70F	151	145	140
2250-20D	149	150	148
2290-40D	159	154	140

* Tg of Epon828/PACM-20 is 150°C.

Table 2.3.   Selected Young's Moduli

SAMPLE	YOUNG'S MODULUS (10^3 MPa)
Control	1.11 +/- 0.17
15-2190-0	0.92 +/- 0.09
15-2070-40F	0.95 +/- 0.07
15C-3690-10AN	0.88 +/- 0.02
15C-3880-17AN	0.86 +/- 0.04
15A-2560-10AN	0.68 +/- 0.06
15A-1750-18AN	0.77 +/- 0.05

Crosshead speed = 1.0 mm/min.

Table 2.4. Comparison of KIc Results
from 3PB and CT Test Specimens

SAMPLE	KIc ($MNm^{-3/2}$)	
	3PB	CT
Epon 828/PACM-20	.83 +/- .04	.84 +/- .04
10-2330-20F	.76 +/- .06	.86 +/- .05
10-2070-40F	1.06 +/- .04	.95 +/- .06

Table 2.5.   Molecular Weights of Liquid Oligomers
Before and After Aging at 125°C

OLIGOMER WITH ORIGINAL MOL. WT.	MOL. WT. AFTER AGING
AEP-1770-40F	2050
HP-1370-30F	1960
C-3690-10AN	**
C-3880-17AN	**
A-2560-10AN	3580
A-1750-18AN	2170

Molecular weights determined by acid titration.
** These oligomers were not titrated soon after the
   aging experiment; some time later, they were too
   gummy for dissolution.
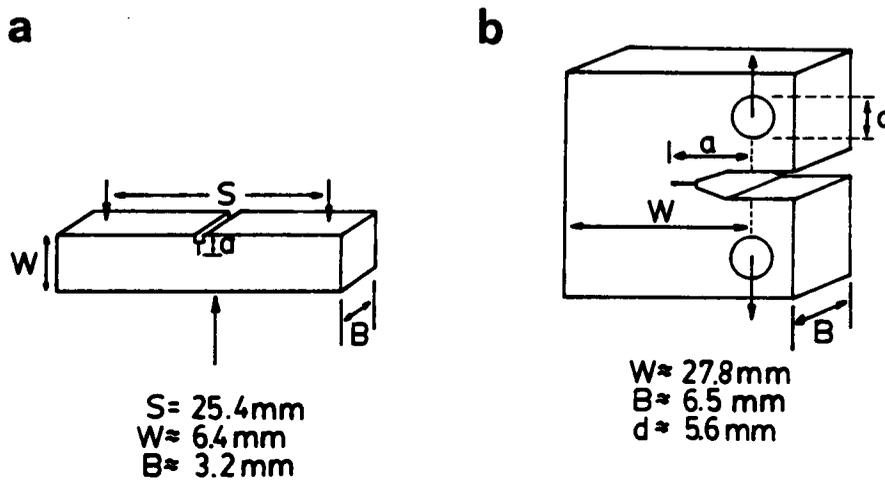
Figure 2.1. Fracture toughness test specimens: a) three-point bend and b) compact tension. Pre-crack length denoted by "a". Movement of crosshead is vertical for both.
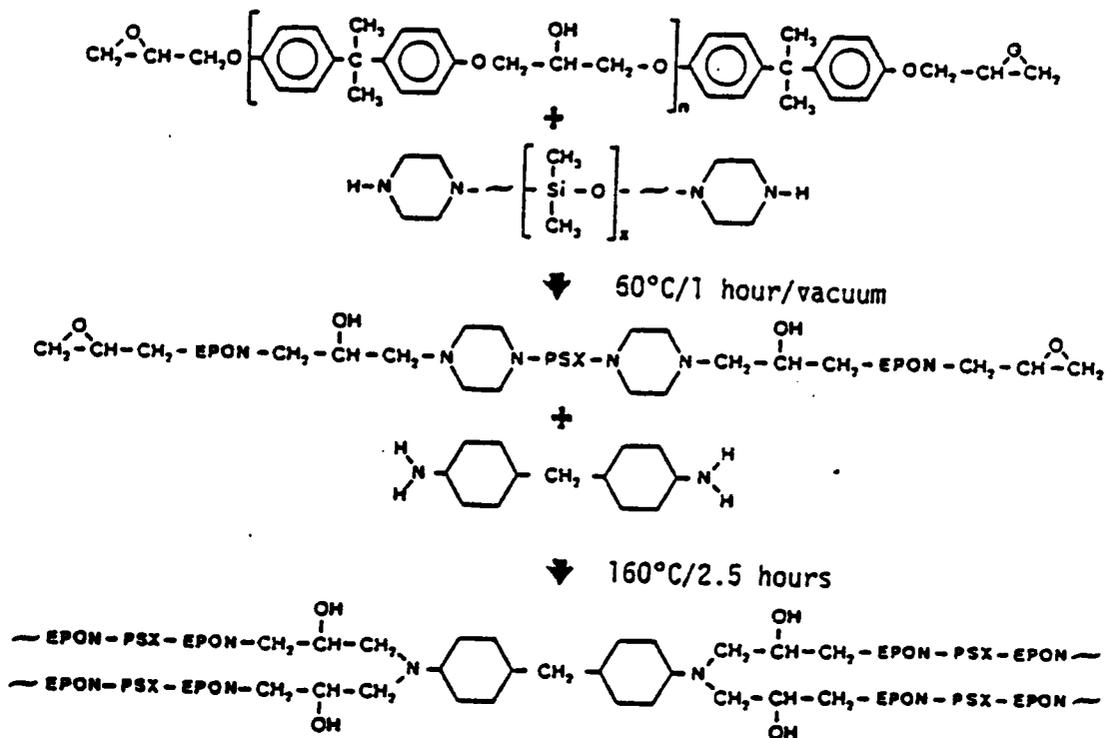
Figure 2.2. Two-step synthesis of siloxane-modified epoxy network. First step, capping of siloxane oligomer with Epon 828. Second step, crosslinking of Epon 828 and capped siloxane with PACM-20.
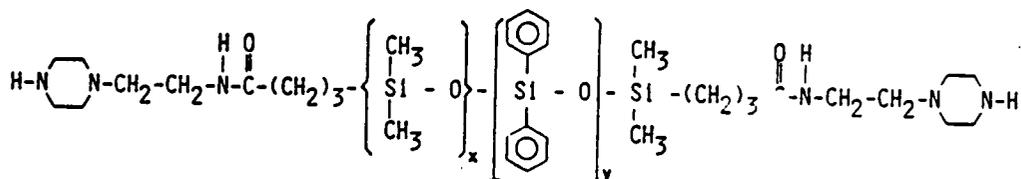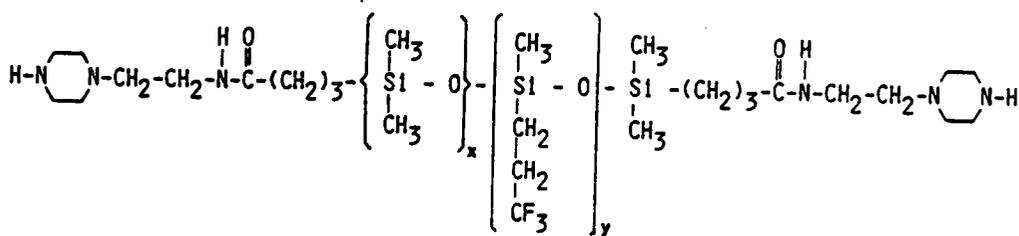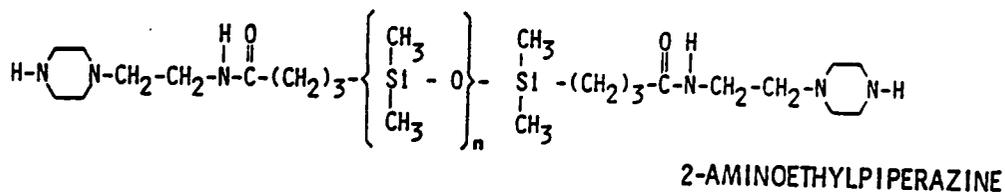
Figure 2.3. Siloxane oligomers used for epoxy modification.
From top, polydimethylsiloxane,
polydimethyl-co-methyltrifluoropropyl siloxane, and
polydimethyl-co-diphenyl siloxane. Aminoethylpiperazine is the
functional end group.
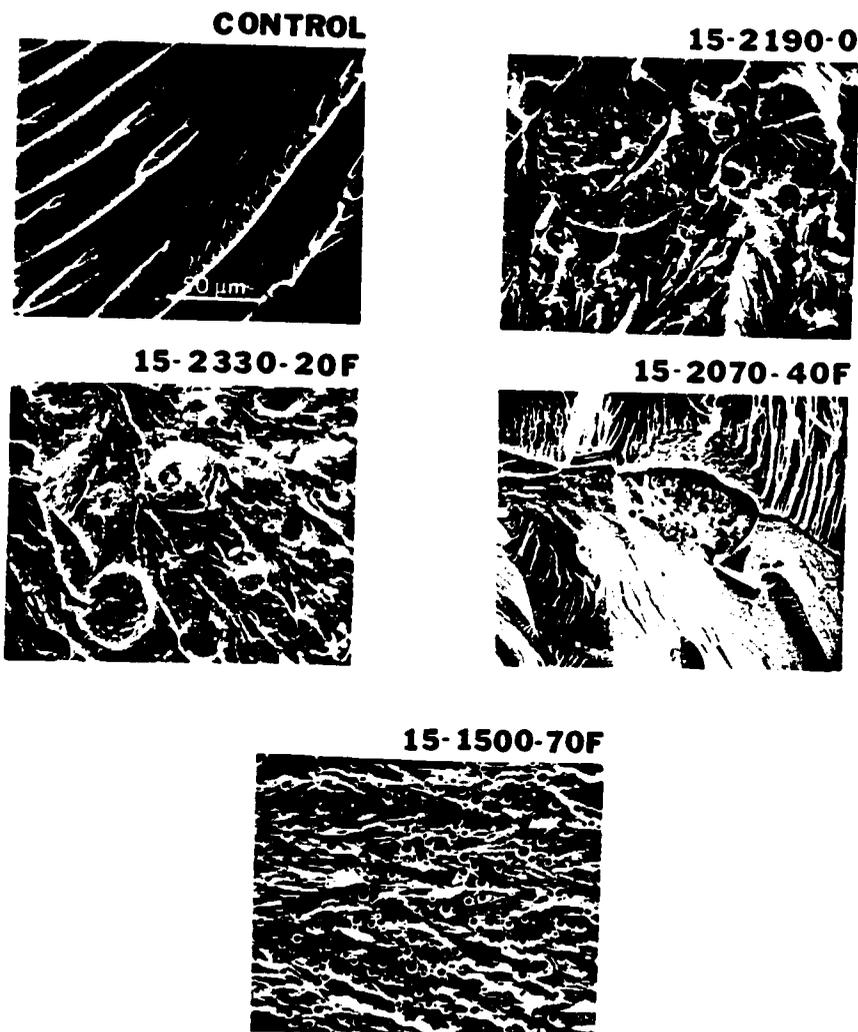
Figure 2.4. Cold snap fracture surfaces for unmodified resin and four siloxane-modified resins as a function of TFP siloxane content in modifier. Original SEM magnification, 300x.
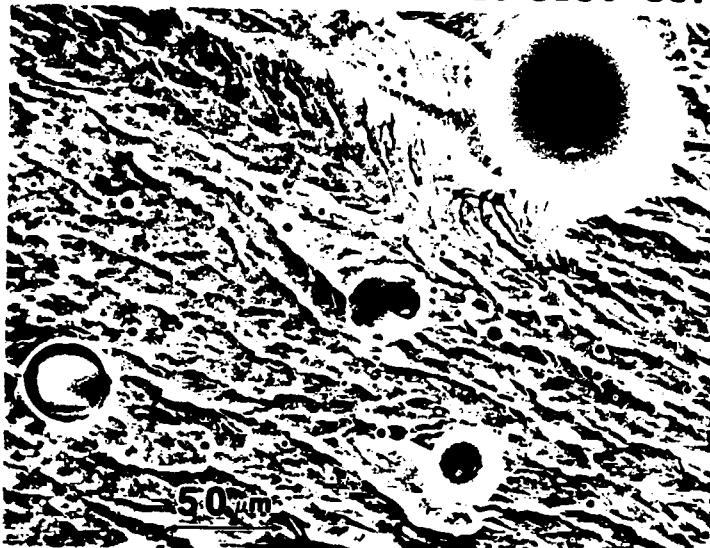
Figure 2.5.   Cold snap fracture surfaces showing effect of molecular weight of modifier on morphology.   Modifiers in top and bottom micrographs are nominally 100% methyltrifluoropropyl siloxane.   Original SEM magnification, 300x.

15-2070-40F

LIQUID N$_2$
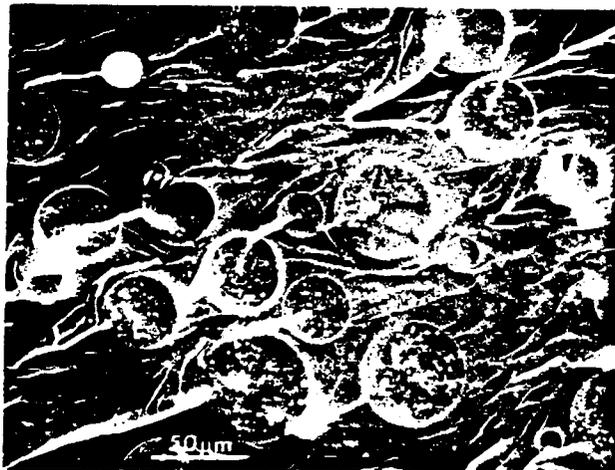
ROOM TEMP

Figure 2.6. Effect of snap temperature on fracture surface features for 15-2070-40F. Top, snapped after immersion in liquid nitrogen for ten minutes. Bottom, snapped at room temperature. Original SEM magnification, 300x.
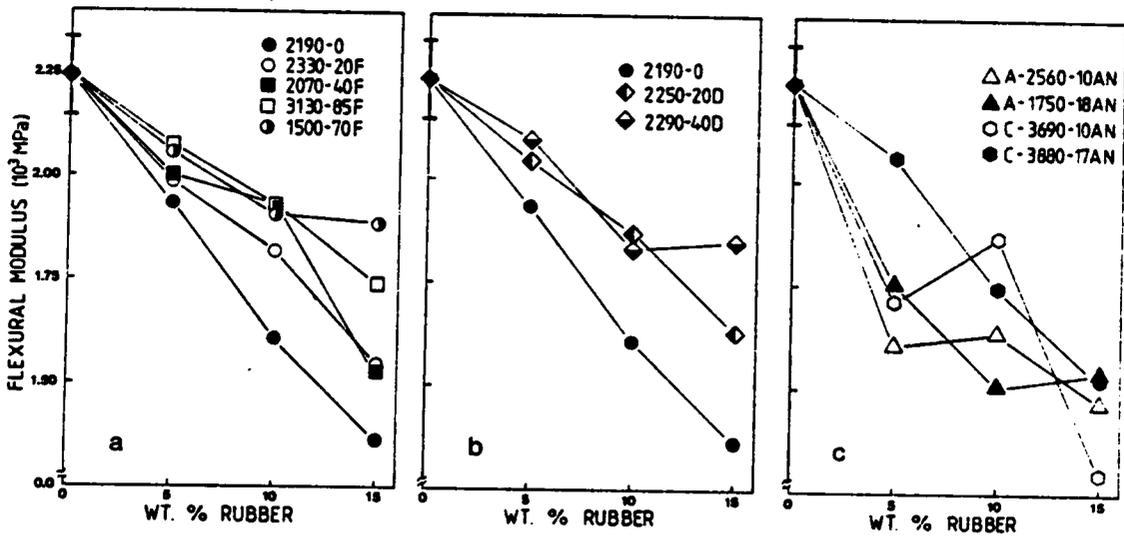
Figure 2.7. Flexural modulus as a function of rubber content and rubber composition: a) TFP siloxanes, b) DP siloxanes, c) ATBN and CTBN. Error bars on data point for control are typical for all other points.

15-2190-0

Figure 2.8. Cold snap fracture surfaces illustrating the
progression of elastomeric domain character moving from low
to high TFP content in siloxane-modified epoxy resins:

a) 15-2190-0 featuring large domains that may be a mixture of
resin and rubber,
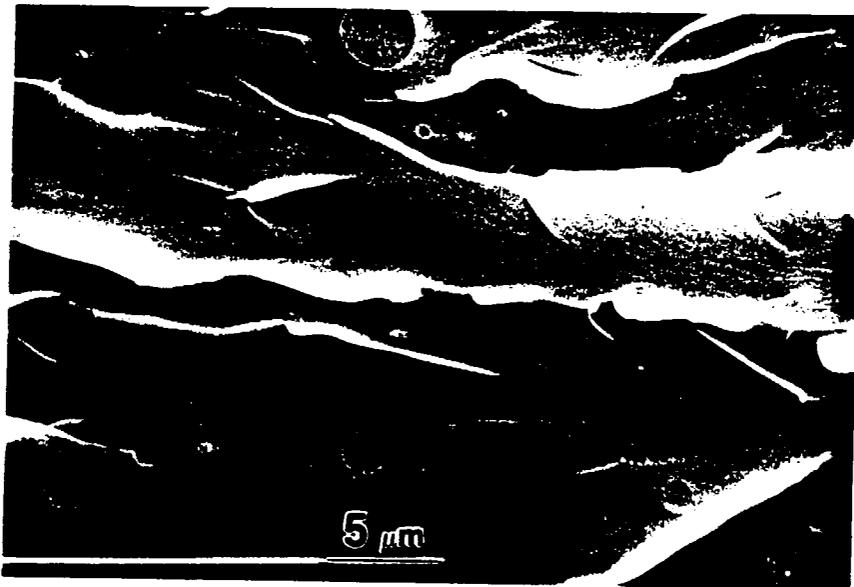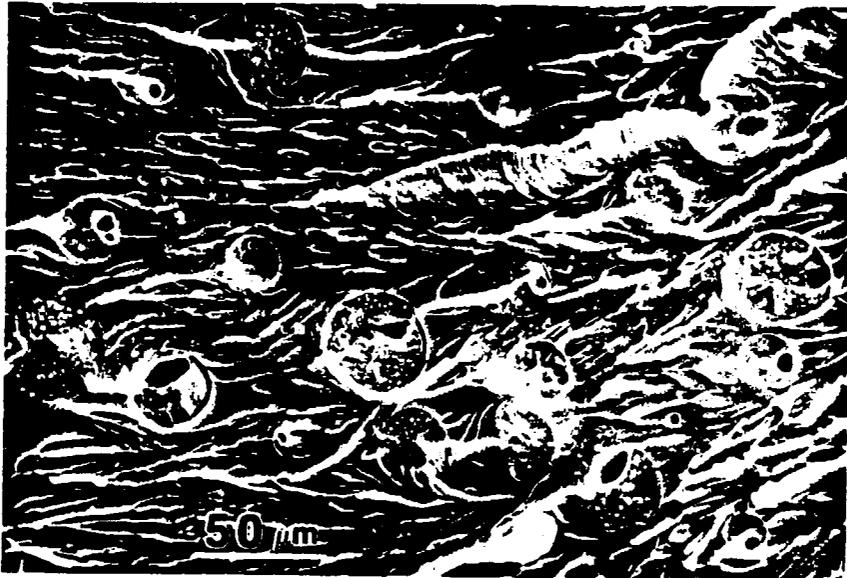
10-2070-40F

b) 10-2070-40F at low and high magnifications showing
coexistence of small and large heterogeneous structures,
some of which are weakly bonded to the matrix,
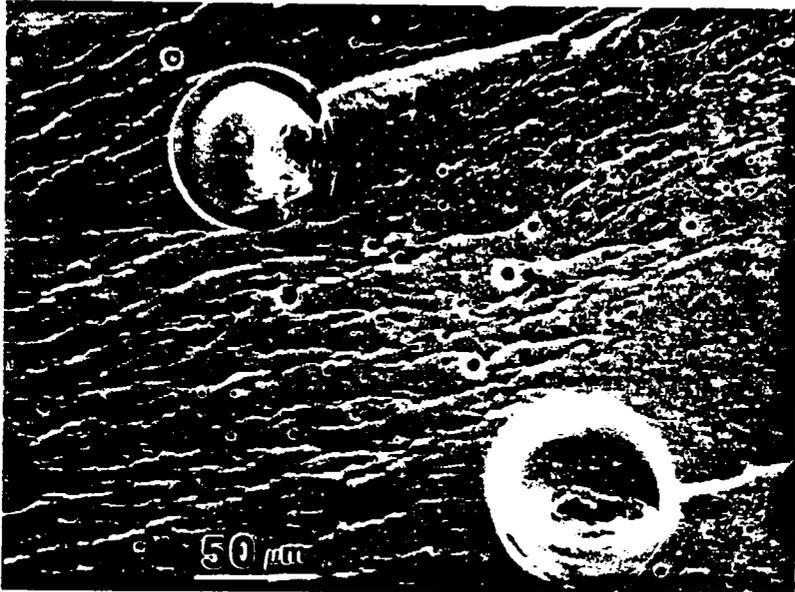
15 - 3130 - 85F

c) 15-3130-85F with range of
large heterogeneous particles showing weak bonding to matrix,
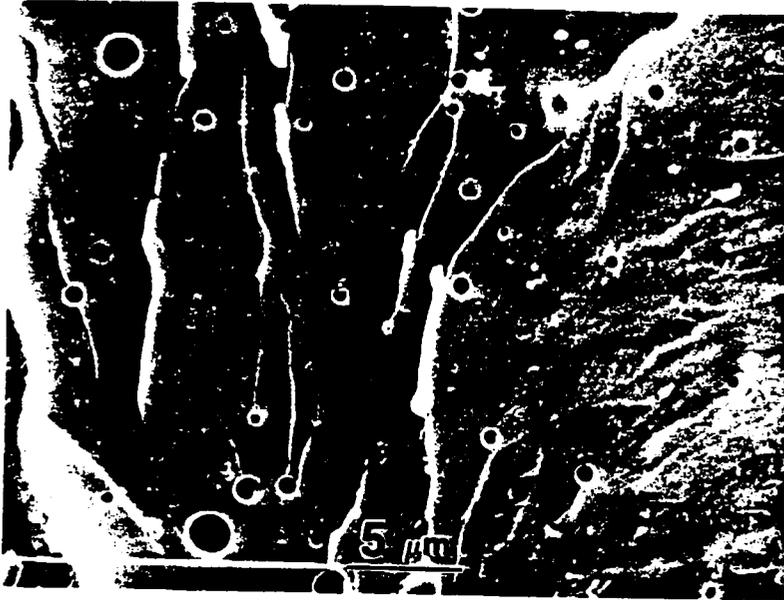
15-3130-85F
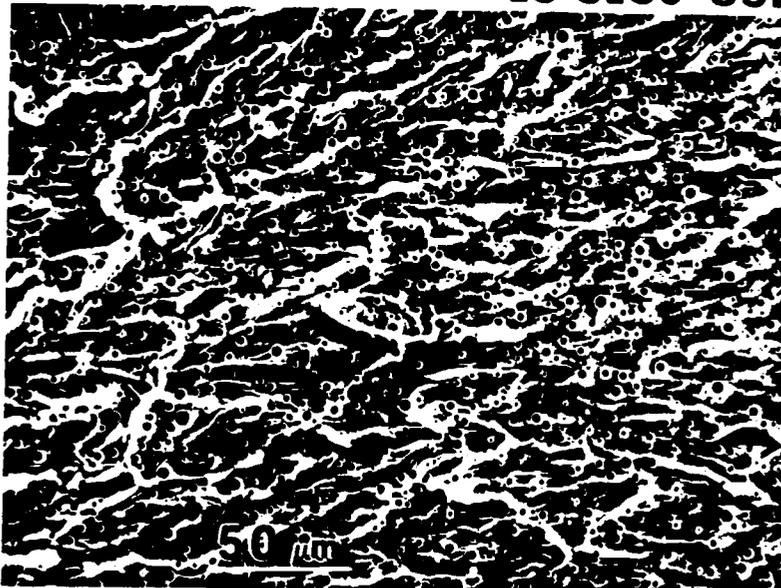
15-1500-70F

d) top, high magnification view of 15-3130-85F showing small particle size which occurs along with the large particle shown in (c), bottom, low magnification photo of 15-1500-70F showing exclusively small particle morphology encouraged by high TFP content and low molecular weight.

15-2320-60F   **15-2730-60F**

Figure 2.9. Cold snap fracture surfaces of 15-2730-60F and 15-2320-60F showing relative sizes of large particles and occurrence and size of smaller particles. Original SEM magnifications, 300x and 3000x.
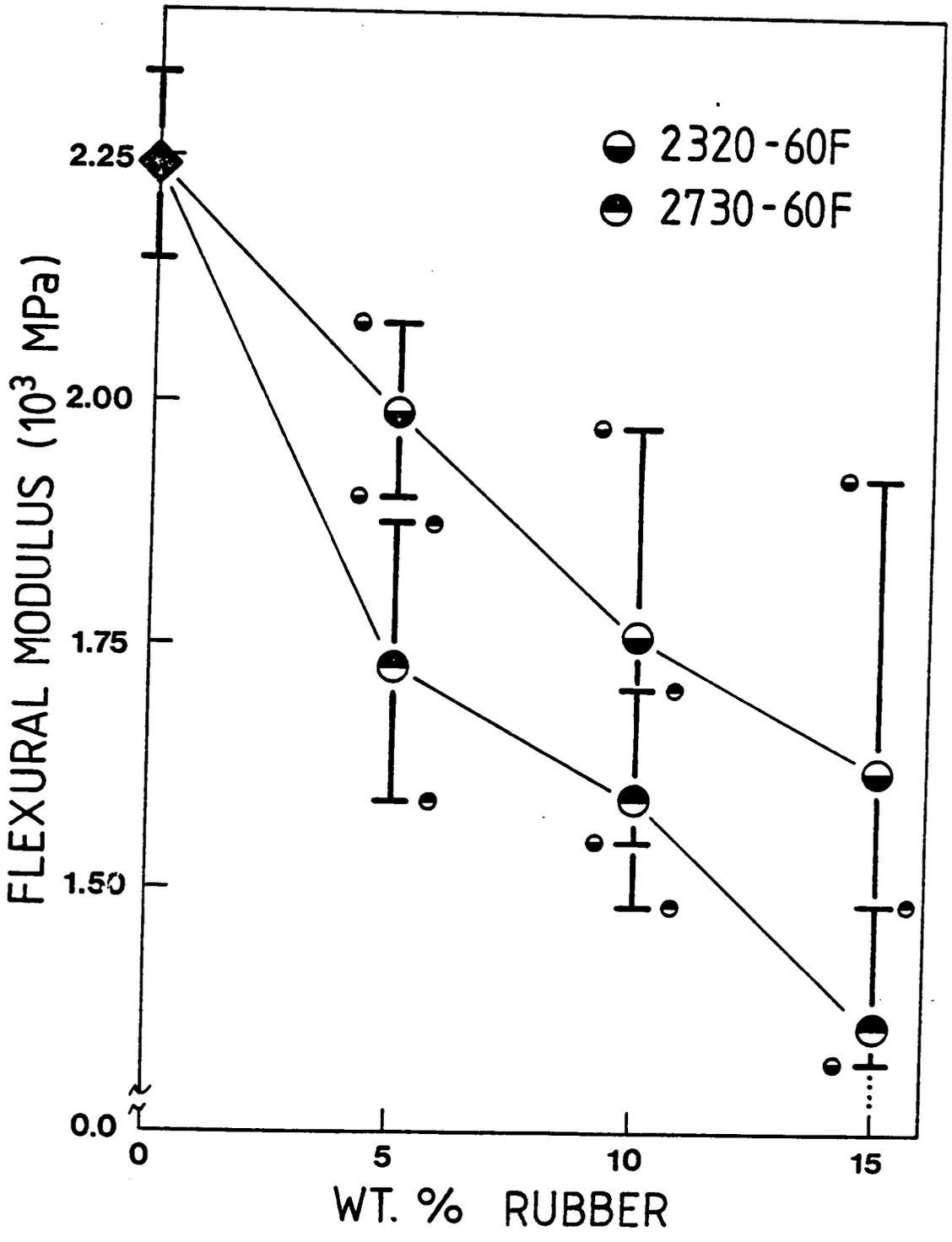
Figure 2.10.   Flexural modulus as a function of rubber content and rubber composition for resin modified with 2320-60F and 2730-60F. Error bars are provided for all data points and labelled with the appropriate symbol.
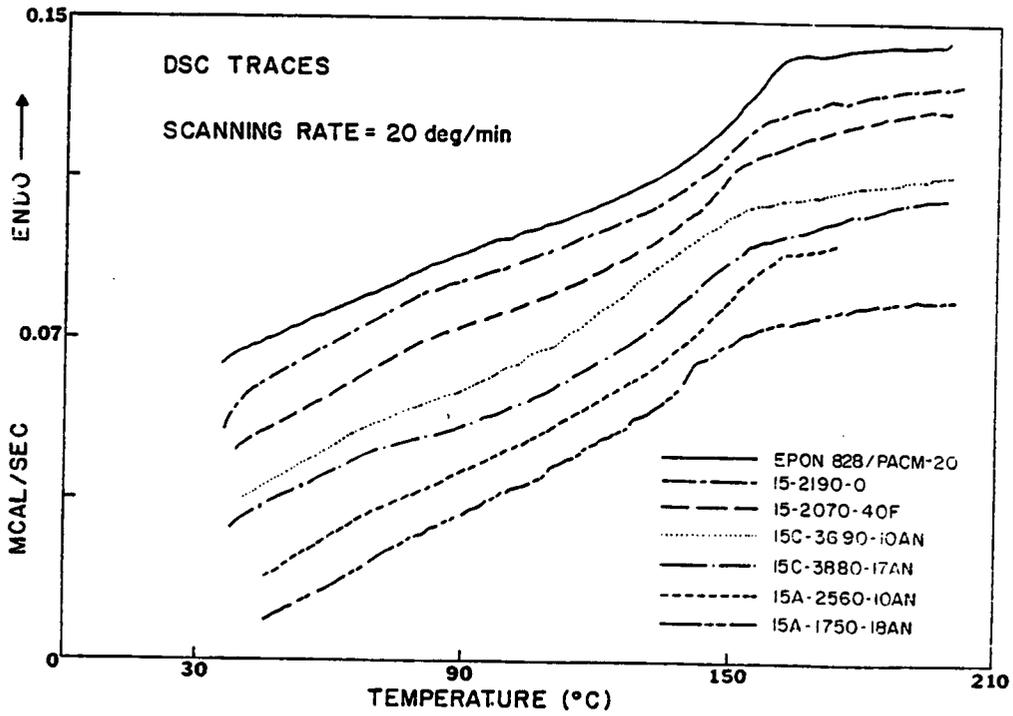
Figure 2.11. Normalized DSC scans of resin control and six modified resins. Curves have been shifted vertically.
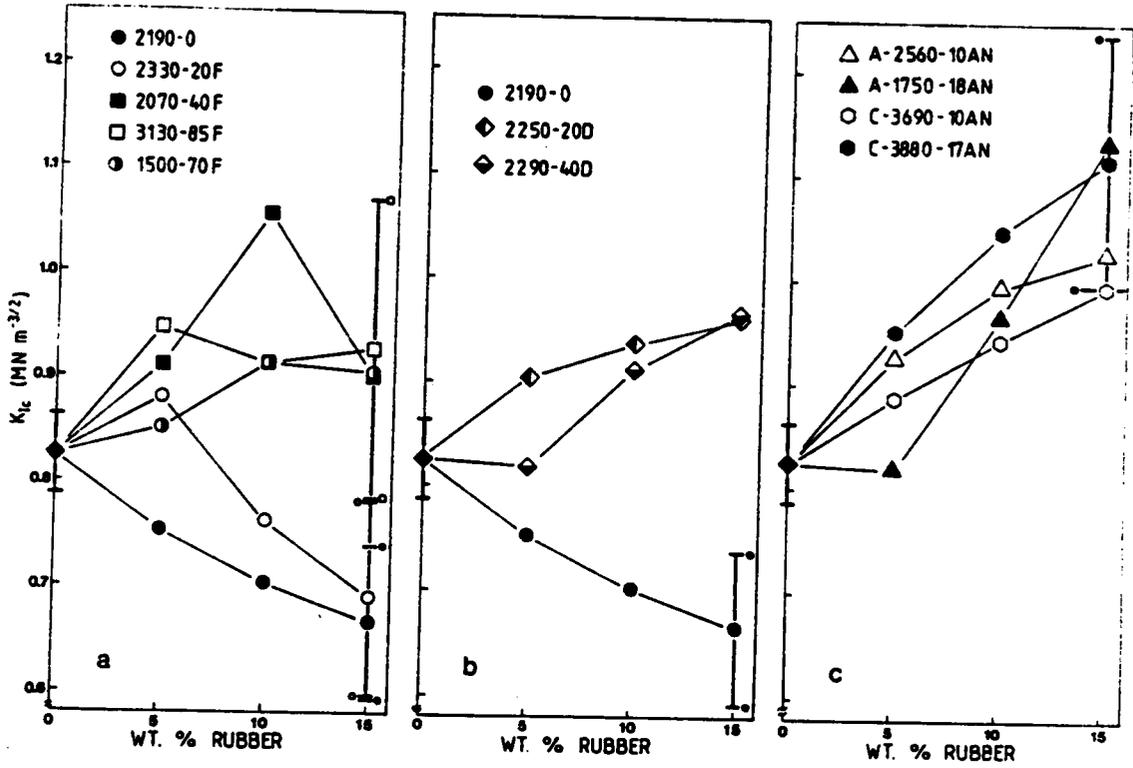
Figure 2.12. Fracture toughness as a function of rubber content and rubber composition: a) TFP siloxanes, b) DP siloxanes, c) ATBN and CTBN. See text for error bar usage.
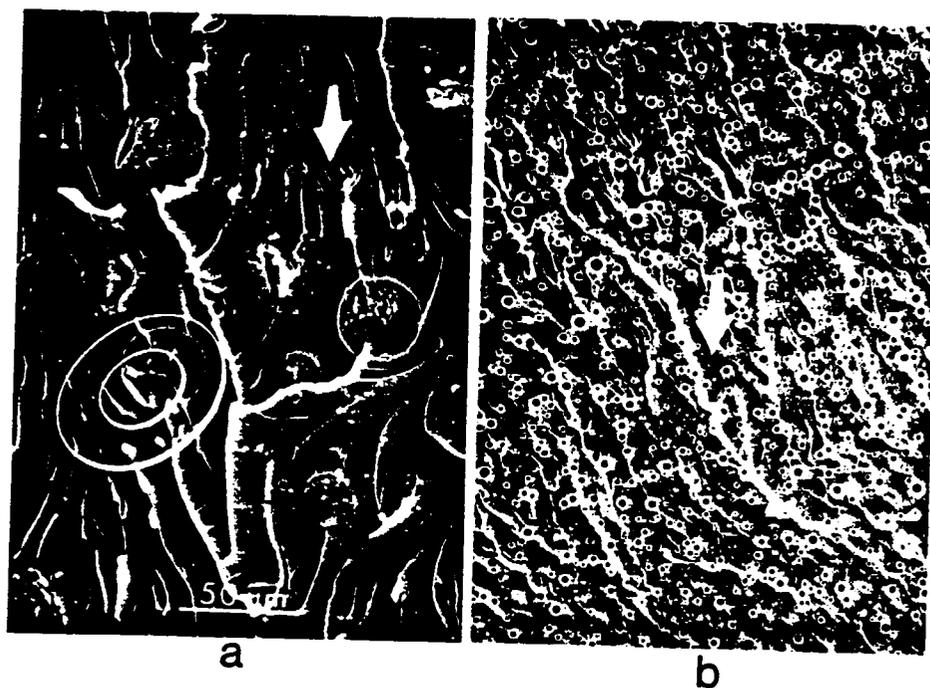
Figure 2.13. Pre-crack fronts of fracture toughness specimens:
a) 10-2330-20F and b) 15-1500-70F. Ellipses highlight torn
rubber domain. Arrows indicate direction of crack propagation.
Original SEM magnification, 300x.

10-2250-20D   **10-2290-40D**
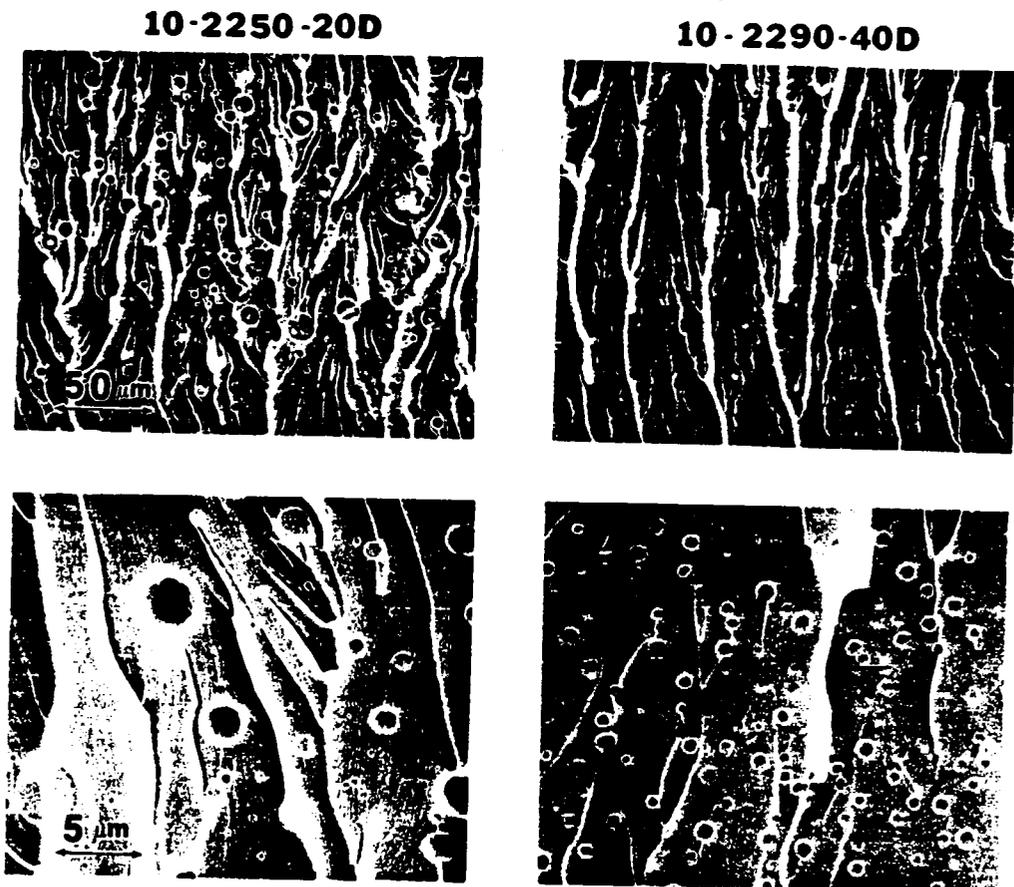
Figure 2.14. Pre-crack fronts of fracture toughness specimens for resin modified with dimethyl/diphenyl siloxane oligomers. Original SEM magnifications, 300x and 3000x.
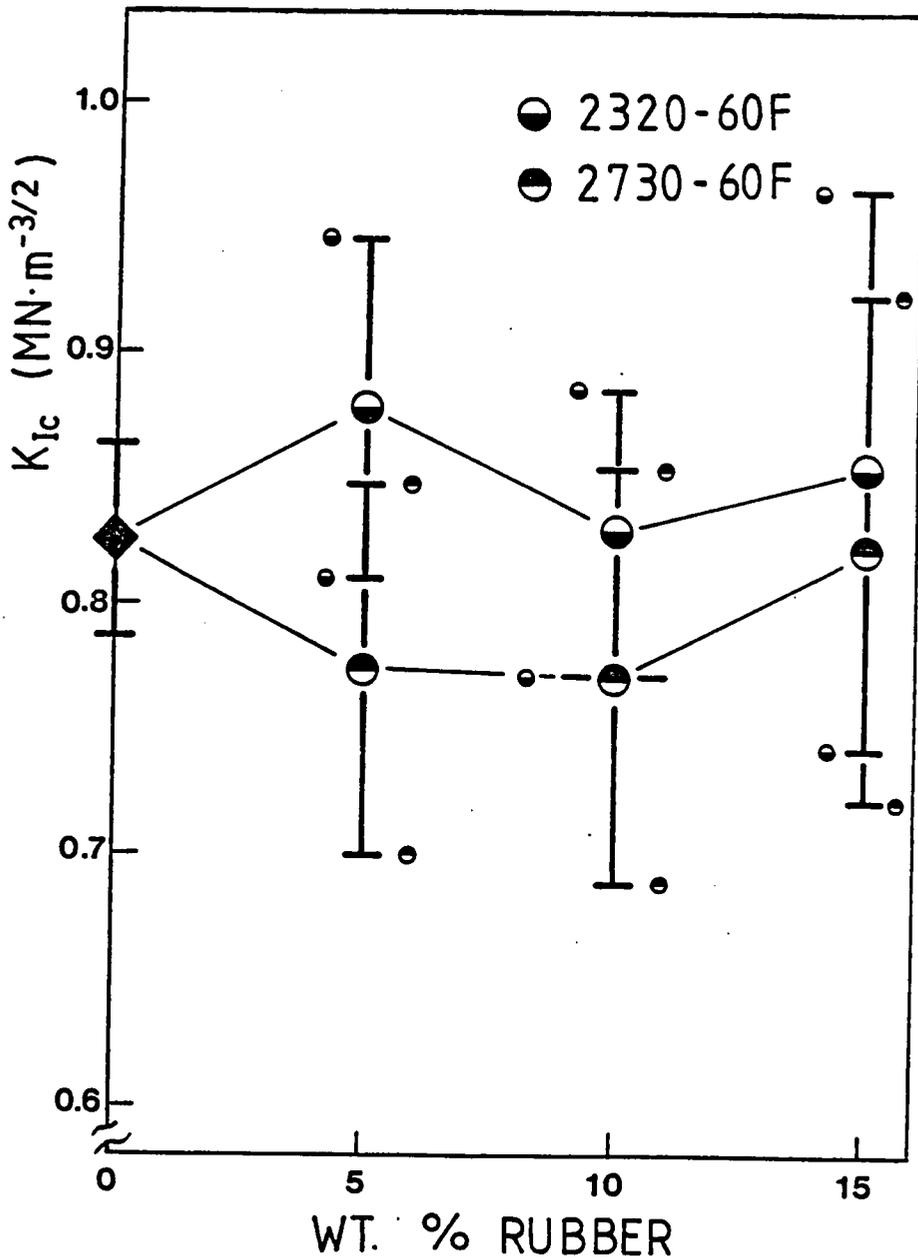
Figure 2.15. Fracture toughness as a function of rubber content and rubber composition for resin modified with 2320-60F and 2730-60F. Error bars are provided for all data points and labelled with the appropriate symbols.
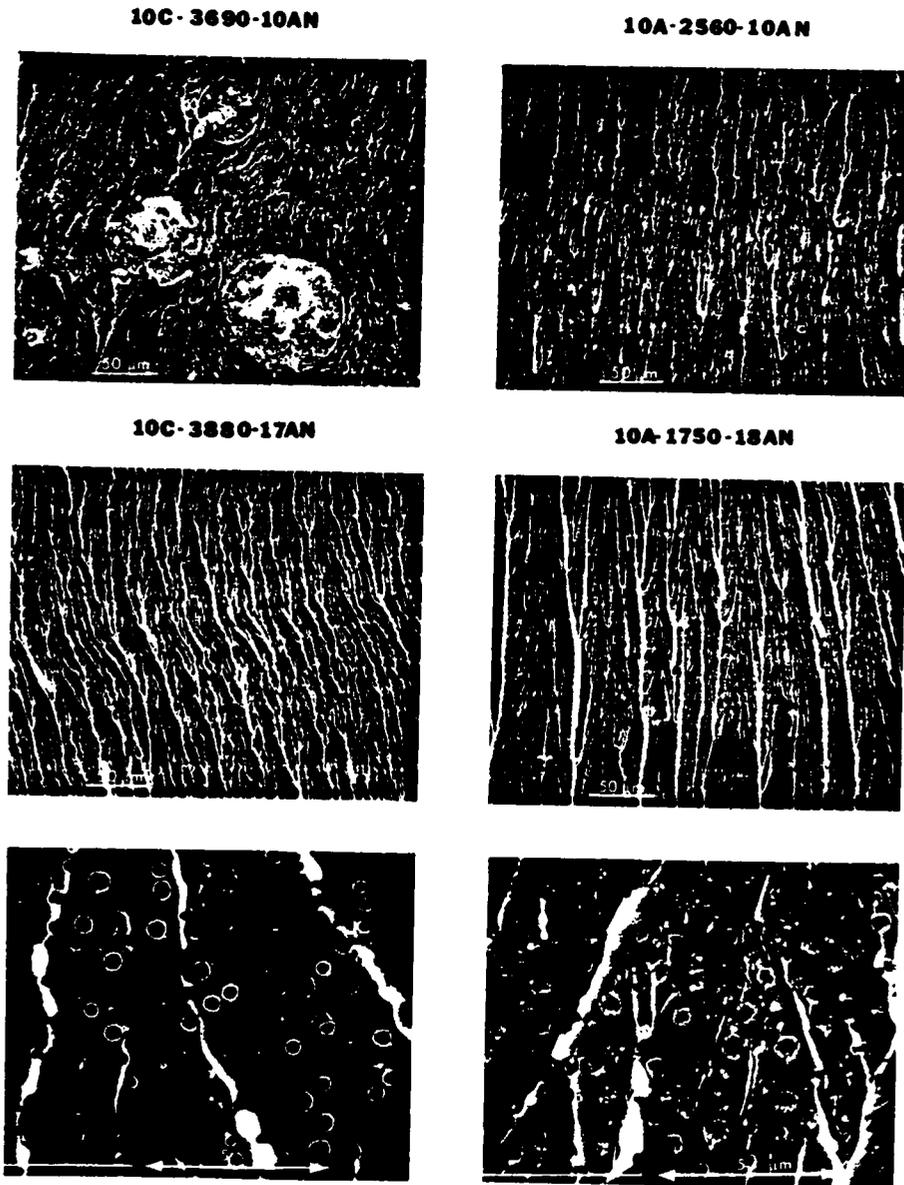
Figure 2.16. Pre-crack fronts of resin modified with 10% of ATBN and CTBN elastomers. At top, low magnification micrographs of the four indicated materials. At bottom, high magnification micrographs of small particles in 10C-3880-17AN and 10A-1750-18AN. Original SEM magnifications, 300x and 10000x.
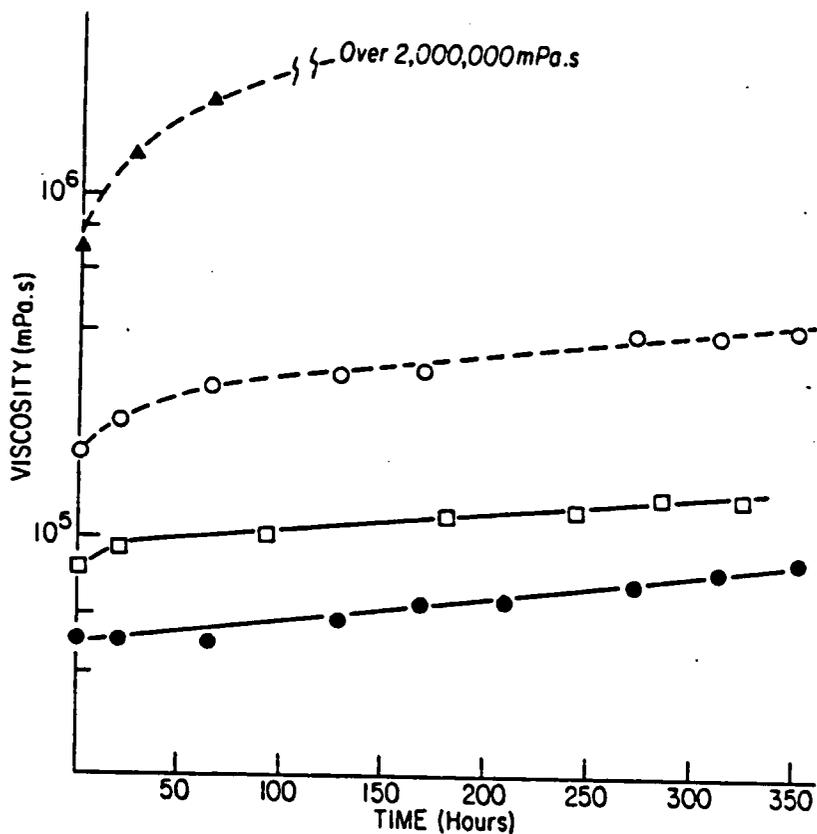
Figure 2.17. Changes in viscosity with aging at 125°C for various carboxyl-terminted butadiene acrylonitrile oligomers. Symbols: ●, 0% AN; □, 10% AN; O, 18% AN; ▲, 26% AN. From Ref. 12.
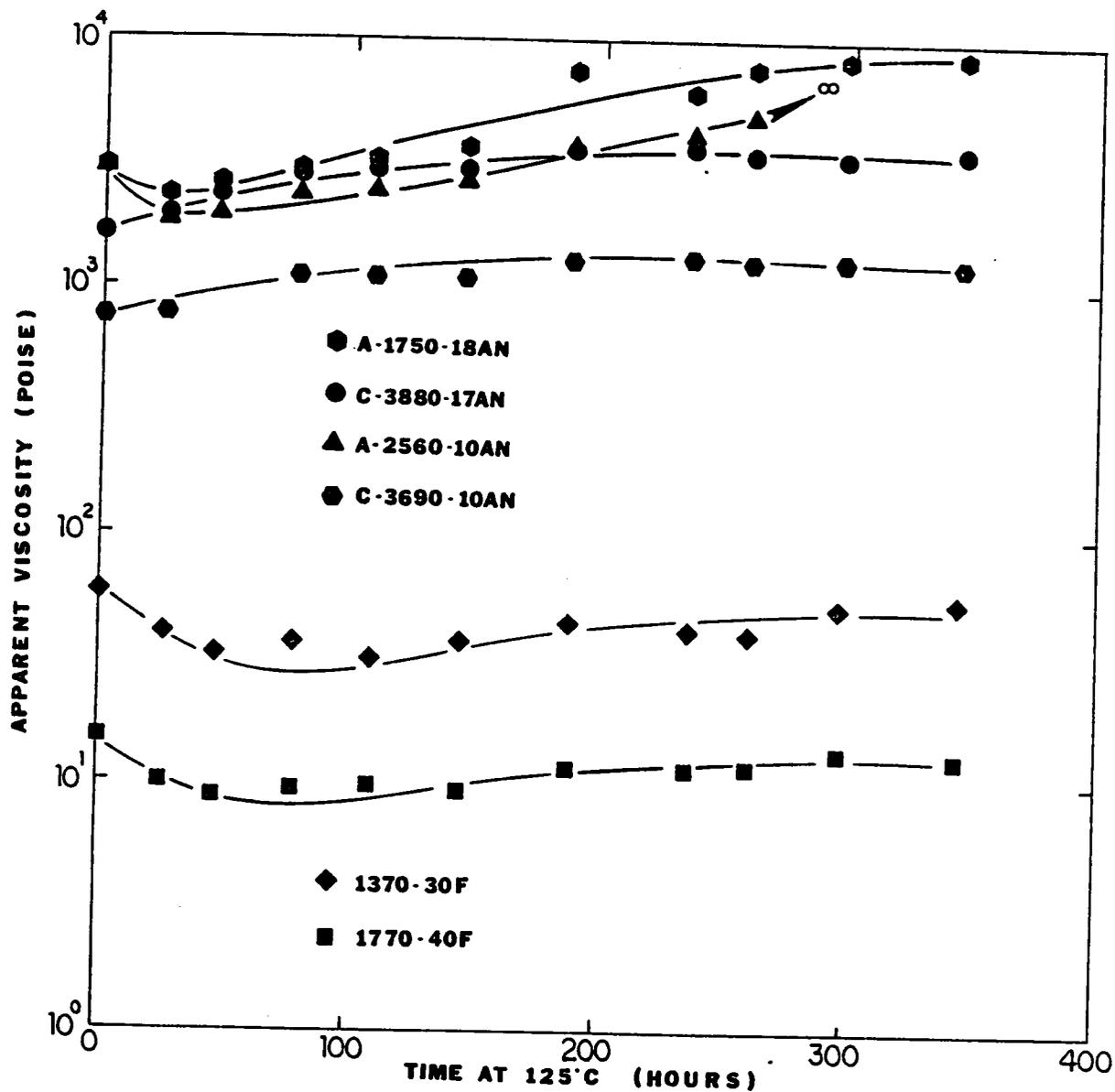
Figure 2.18. Changes in viscosity with aging at 125°C for two siloxane oligomers and ATBN and CTBN oligomers.
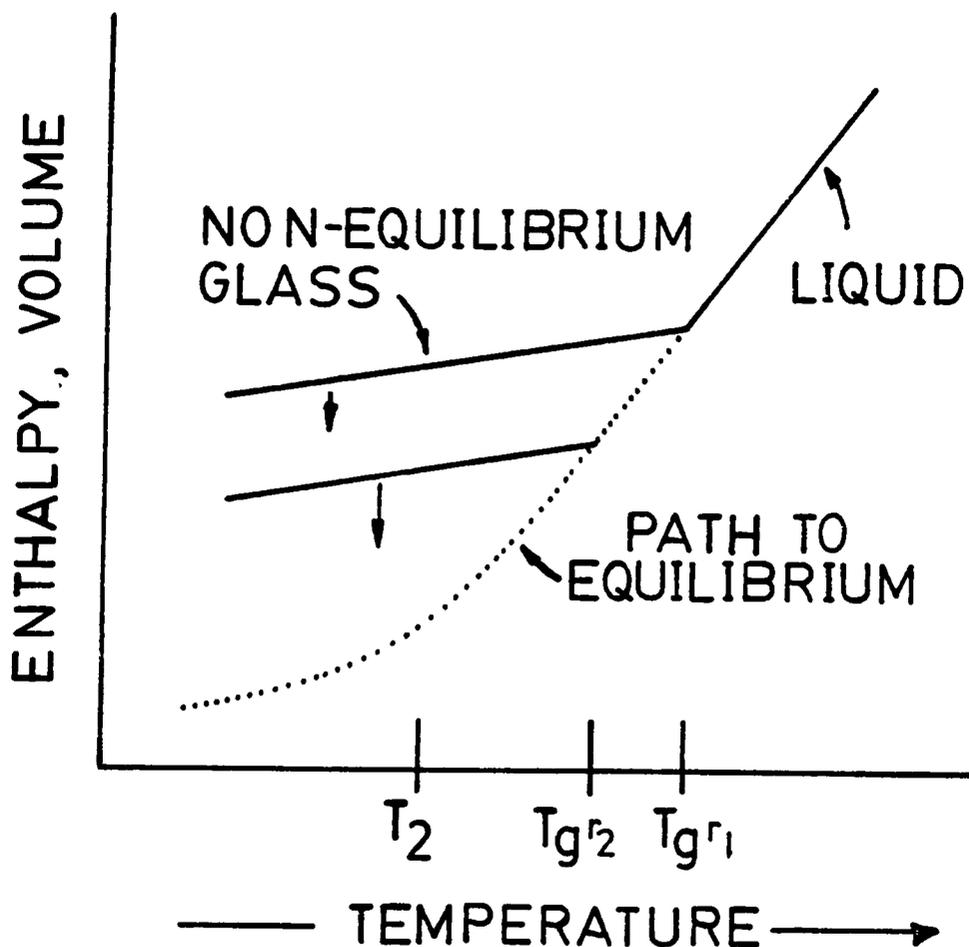
Figure 2.19. Schematic representation of changes in enthalpy and volume as a function of temperature. The dotted line indicates the equilibrium state which can be reached only by cooling at an infinitely slow rate. The arrows show the effect of physical aging in moving towards the equilibrium state. T2 is the glass transition temperature of an equilibrium glass while Tg is the glass transition temperature of a non-equilibrium glass cooled at some finite rate, r1 > r2. After Ref. 55.
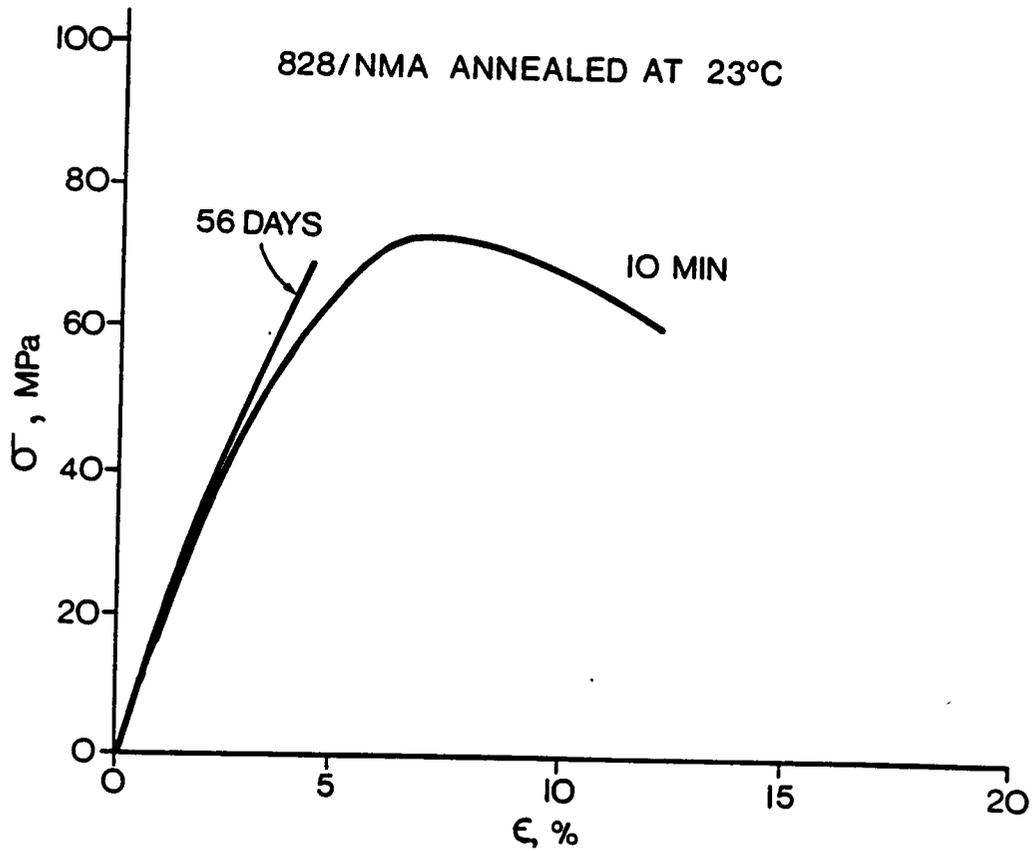
Figure 2.20.   Changes in stress-strain behavior for Epon 828 crosslinked with nadic methyl anhydride.   Times indicate periods of aging at room temperature prior to testing.   Ref. 34.
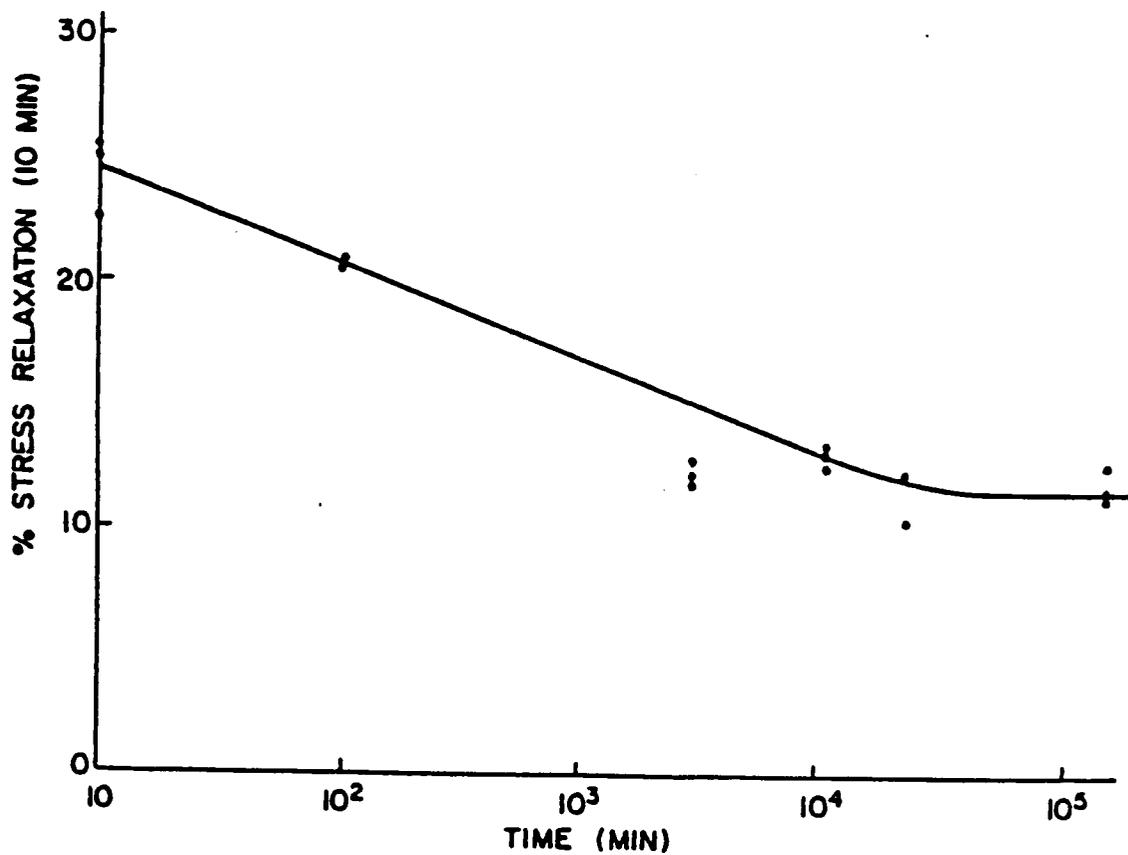
Figure 2.21. Percent 10-minute stress relaxation vs. log time for a crosslinked Epon 828 resin as a function of annealing time at 23°C. Ref. 34.

NARMCO 5208
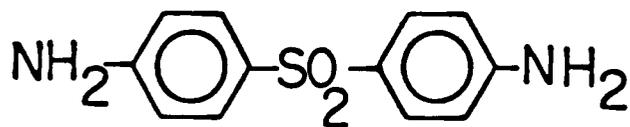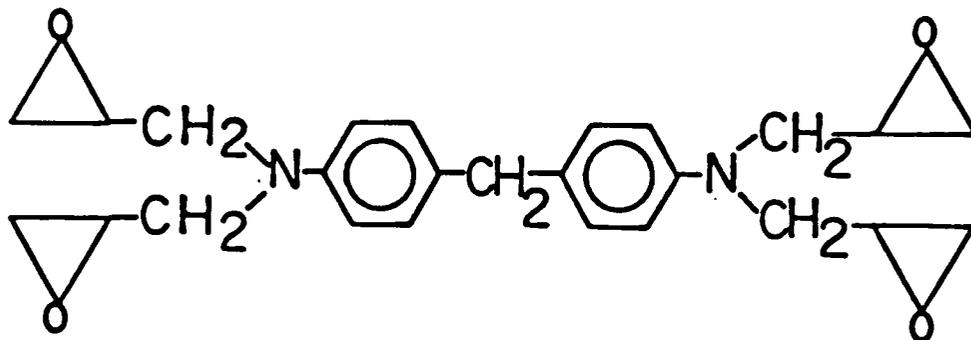
DDS

Figure 2.22. Structures of NARMCO 5208 resin and DDS curing agent.
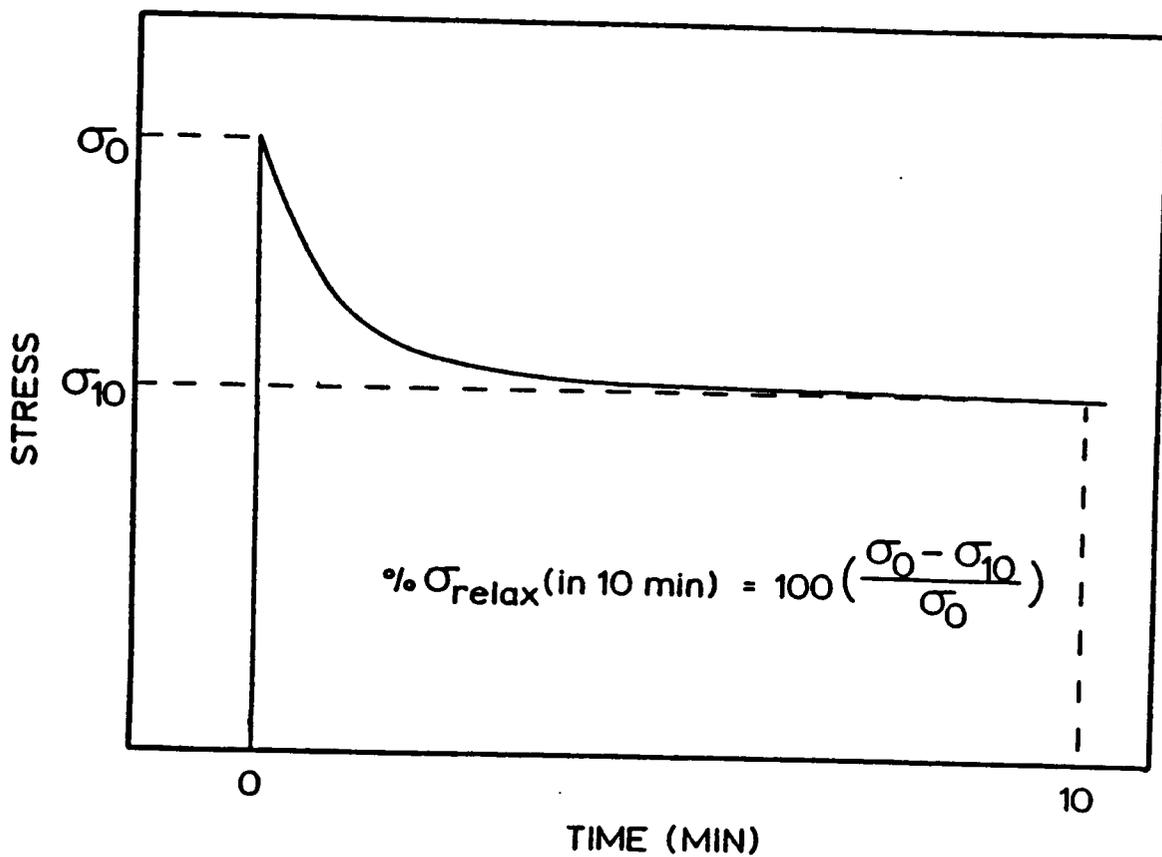
Figure 2.23. Schematic illustration of the stress relaxation curve and description of the calculation of percent stress relaxation. From Ref. 54.

FLEXURAL TEST
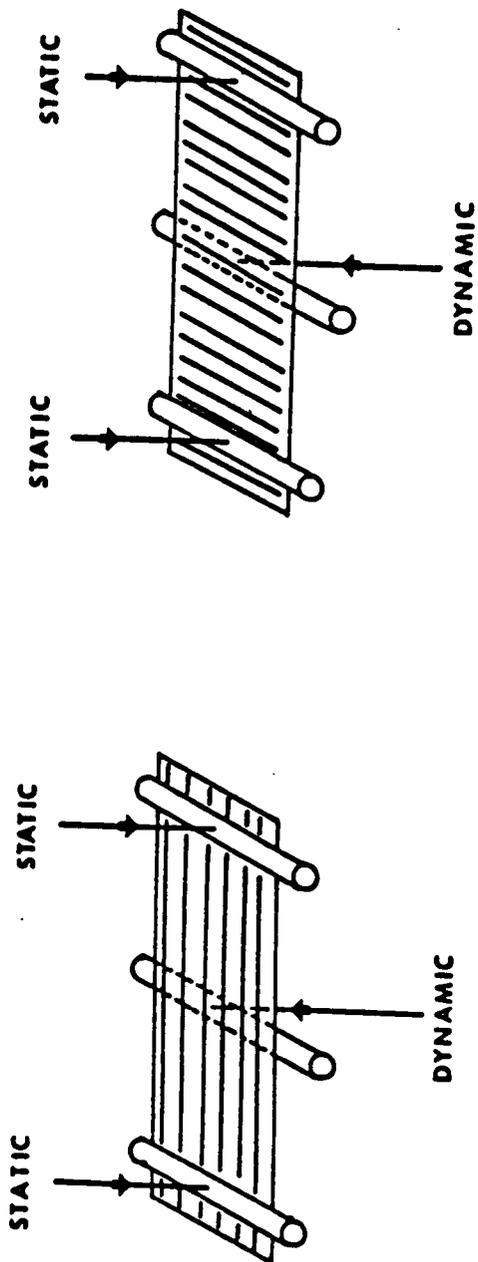
Across--A

Between--B

Figure 2.24. Notation for the orientation of the rods in the three-point bend test piece and the fibers in the resin composites.
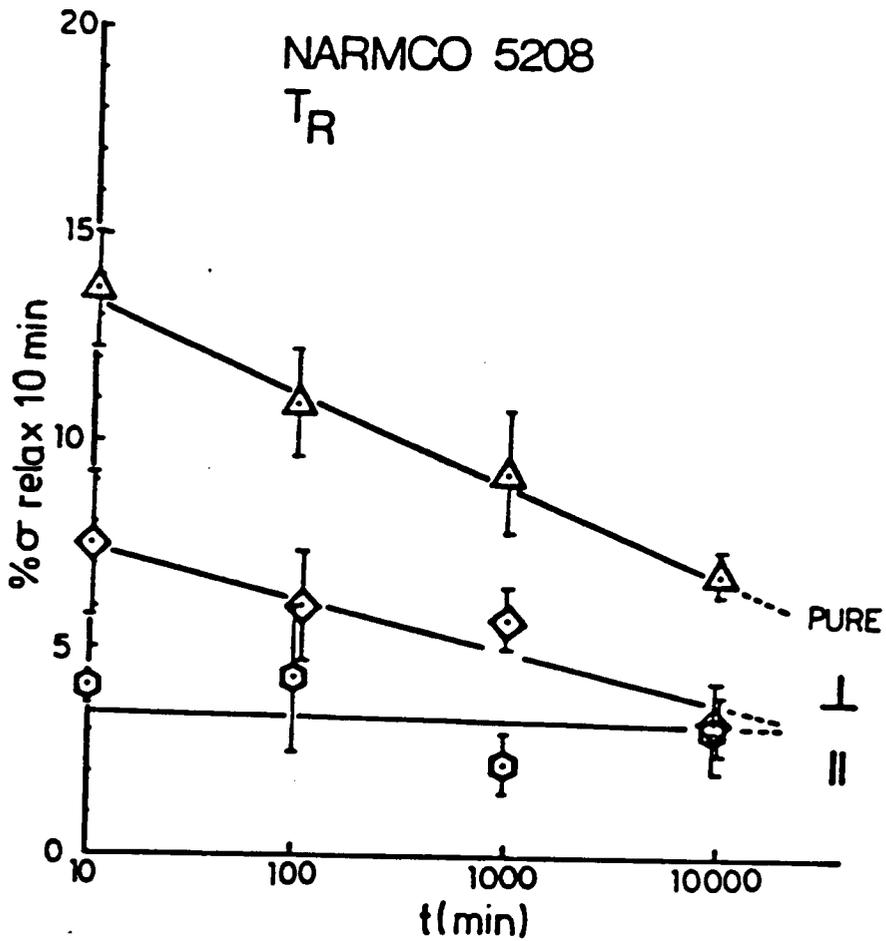
Figure 2.25. Stress relaxation as a function of log time aging at room temperature for NARMCO resin and composite systems. Tensile mode. Ref. 54.
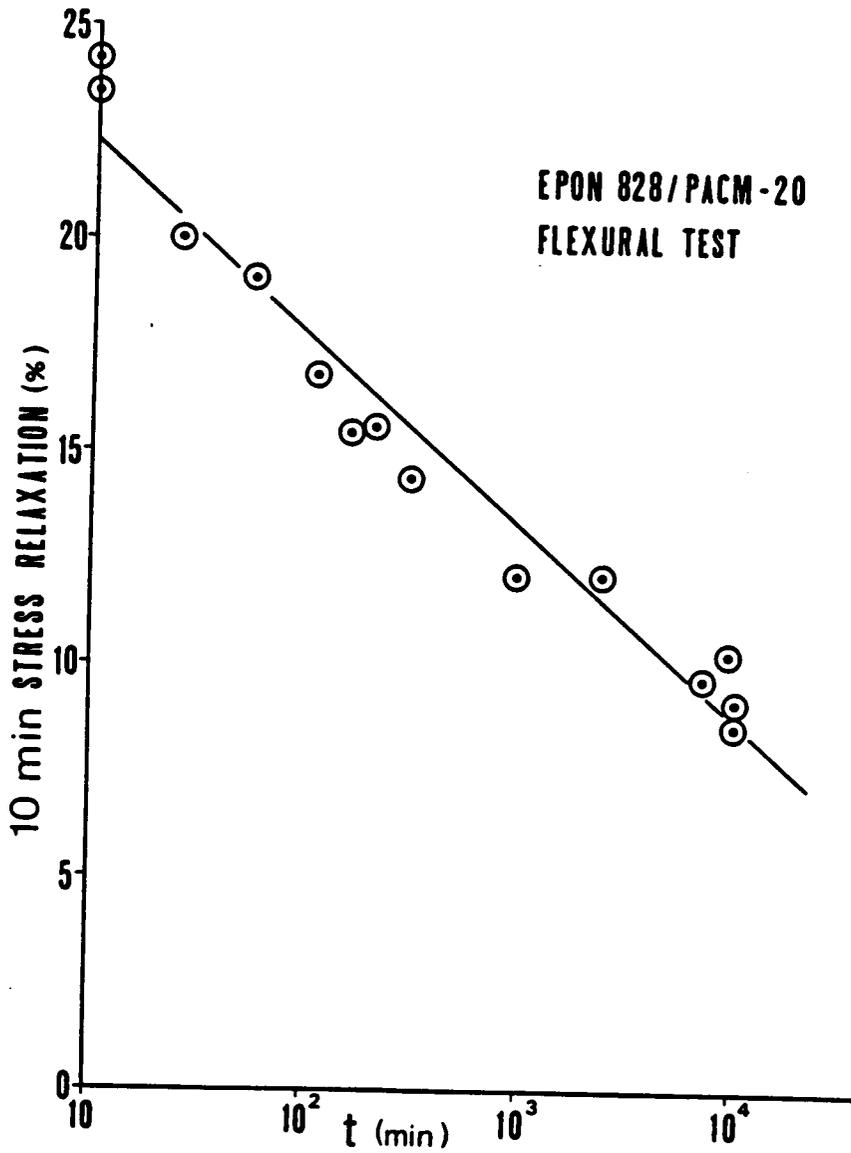
Figure 2.26.   Stress relaxation as a function of log time aging at room temperature for Epon 828/PACM-20 resin system.   Flexural mode.
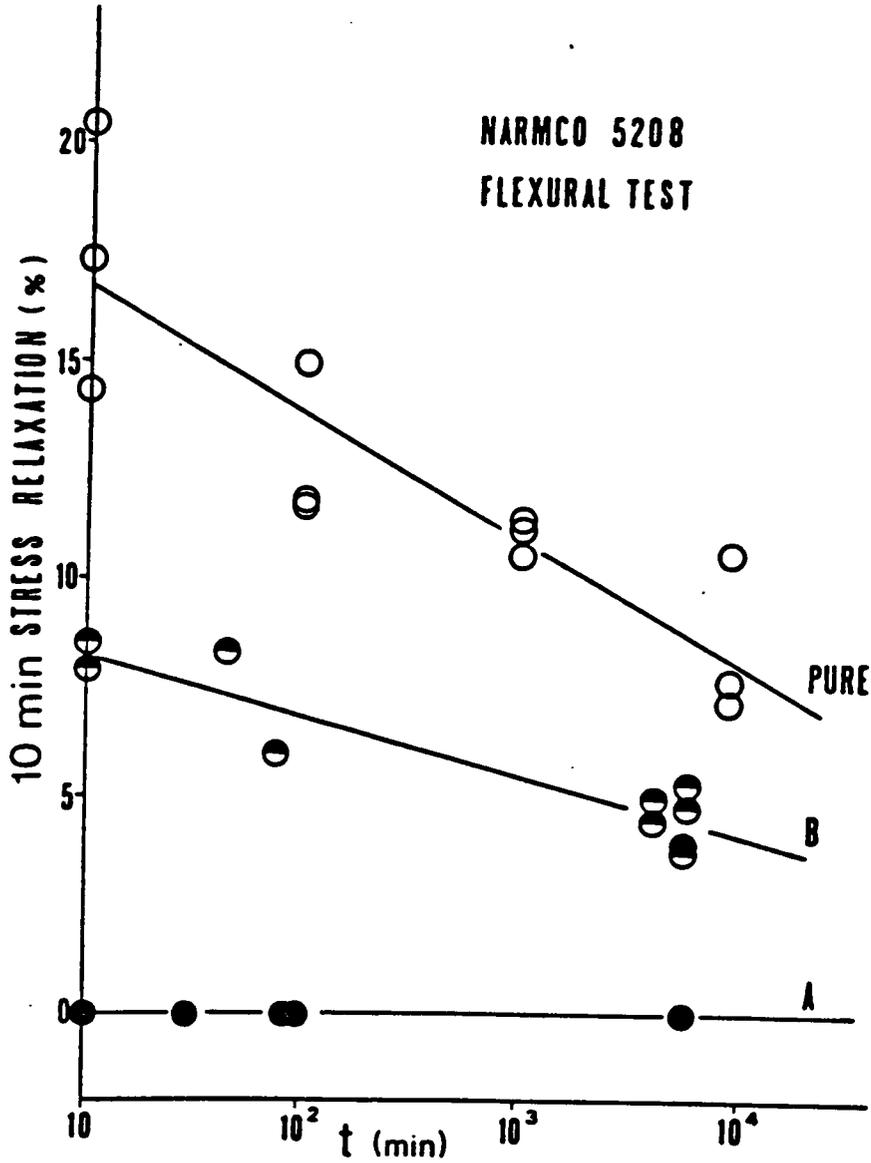
Figure 2.27. Stress relaxation as a function of log time aging at room temperature for NARMCO resin and composite systems. Flexural mode.

CHAPTER THREE

PLASTICIZATION OF POLYVINYL CHLORIDE

WITH DIBUTYL PHTHALATE, DIETHYLHEXYL SUCCINATE,

AND OTHER PLASTICIZERS

3.1. INTRODUCTION

3.1.1. Objectives of the Study

Polyvinyl chloride (PVC) in rigid, plasticized, and blended forms has been one of the world's top-selling thermoplastics for several decades. In spite of this fact, much is still not understood about its structure, morphology, and properties. Plasticized PVC in itself has spawned a huge body of literature as well as strongly supported the plasticizer market. It continues to be widely researched by polymer chemists, physicists, and rheologists.

Plasticized PVC is frequently referred to as a pseudo-network in which a small number of fringed micelle crystallites act as junction points. The plasticizer, often as much as 40 weight percent, is distributed in the amorphous matrix and does not completely destroy the crystalline network junctions even at high plasticizer concentrations. This unique cooperation between plasticizer and polymer allows PVC to remain a thermoplastic while taking on some of the characteristics of an elastomer. The final properties are a function of the amount and type of plasticizer as well as other additives and the processing conditions.

A 1952 paper by Schmieder and Wolf (1) showed the effects of two plasticizers, diethylhexyl succinate (DEHS) and dibutyl phthalate (DBP), on the dynamic mechanical behavior of PVC. Their torsion pendulum data, shown in Figure 3.1, illustrate the effects of DEHS and DBP on shear modulus and log decrement as a function of temperature

and plasticizer weight percent. As one would expect, the inflection points or peak temperatures of the curves shift down in temperature as the content of either plasticizer is increased, indicating a drop in the glass transition temperature, T_g. As DEHS content increases from 0 to 39.3 weight percent, the curves broaden considerably. Further increases to 59.2 weight percent DEHS cause the curves to narrow. In sharp contrast, increases in DBP content introduce neither substantial broadening nor narrowing.

To the author's knowledge, no one has studied these particular materials with regard to this curious dynamic mechanical behavior. In fact, these data are well known and commonly accepted although unexplained in more than a qualitative sense. They were presented in part as examples of dynamic mechanical behavior in polymers some time ago by Nielsen (2) and more recently by Ferry (3).

This chapter describes a systematic investigation of PVC plasticized with DEHS and DBP from a structure-property point of view. The study's ultimate goal is to understand why these two plasticizers affect the dynamic mechanical properties of PVC in such different ways, focusing especially on the broadening and subsequent narrowing shown in Figure 3.1.

3.1.2. *Concepts of Plasticization*

The choice of one plasticizer over another is generally a matter of weighing the major properties of both and making a decision based on a composite picture of each plasticizer. With respect to the particular resin being plasticized, one must consider primarily the permanence, resin compatibility, and efficiency of each plasticizer. Figure 3.2 from Boyer's review (4) presents the interrelationship of these three general properties. (Note that the term *solubility* will be used here rather than *compatibility*, except in cases where the latter term is considered to be more appropriate in view of prior use by an author or authors.) Early experience in the commercial use of plasticizers had shown that different plasticizers affected PVC quite differently (5). *Efficiency* became a generally used term describing everything from the extent of Tg depression to the ability to lower modulus to some arbitrary value.

The solubility of PVC with plasticizers and solvents has been approached both empirically and theoretically. In an early paper, Doty and Zable (6) obtained a large number of polymer-solvent interaction parameters (x) for PVC-solvent and PVC-plasticizer pairs via swelling experiments on thermally crosslinked PVC. While x was considered to be a function of temperature and concentration, it was generally concluded that a solvent for PVC would have a value less than 0.55. The choice of this particular number is confusing. Doty and Zable's documentation includes unpublished work from their own laboratory and two of Flory's early papers on solution thermodynamics (7,8). In Flory's papers as

well as his first book (9), it is quite clear that the critical value of x is 0.5 for a polymer of any appreciable molecular weight. Blanks and Prausnitz (10) specifically state that 0.5 is the critical value for solubility of a polymer and solvent.

In a study of the static mechanical behavior of gels of PVC and a score of plasticizers and solvents, Walter (11) proposed the slope of a log modulus-log concentration plot as a measure of the solvent power of liquids in PVC. The range 3.0-3.1 was suggested as the lower limit for "compatibility"; the greater the solvent power, the lower the modulus at equivalent plasticizer concentrations. Several other gauges of PVC-plasticizer interactions have appeared in the literature in the last 30 years. They will receive more attention later in this chapter.

PVC is believed to experience specific interactions with typical ester plasticizers. Based on the results of a Fourier transform IR (FTIR) spectroscopy study, Tabb and Koenig (12) suggested that solvation of amorphous PVC by ester plasticizers may occur through interactions between C=O and C-Cl bonds.

Several theories or mechanisms of plasticization (13) have been proposed. They are not specific to PVC but have been meant to be applied to any plasticized material. The gel theory considers that the plasticizer molecules form attachments with the polymer chain at regular intervals, thereby masking former points of attachment between chains. Doolittle (14,15) is credited (13) with the establishment of a thermodynamic basis of plasticization through his self-dubbed

mechanistic theory, which is a more formal version of the gel theory. The mechanistic theory proposes that the attractions between plasticizer molecules and plasticizer and polymer molecules constitute two equilibria which occur simultaneously; an aggregation-disaggregation equilibrium exists between plasticizer molecules while a solvation-desolvation equilibrium exists between plasticizer and polymer. The plasticizer molecules are thus considered to participate in a continuous exchange of attachment between themselves and the so-called "active centers" of the polymer chain.

The free volume theory revolves around measurement of T_g depression and in doing so ignores other factors very important to effective plasticization. It has, nonetheless, shown the importance of molar volume, plasticizer T_g, and polymer-plasticizer interactions.

Despite much research, many questions about plasticized PVC's morphology and localized structure have gone unanswered. What is the nature of the plasticizer as it exists within the PVC and the nature of the PVC/plasticizer "phase"? Can the plasticizer form a liquid-like phase within the PVC, and if it can, is this phase identical to that which it would form in bulk? To what extent does the plasticizer interact with the polymer chain? What are the contributions of steric effects, dipole-dipole interactions, dispersion forces, and other factors? Finally, how realistic is the classical concept that the pseudo-network of plasticized PVC is formed primarily by fringed micellar crystallites?

These are truly fundamental questions that require "getting inside" plasticized PVC. Unfortunately, much of what is known about polymeric materials requires "looking in" and formulating models which can then be tested through further experimental work. Because of its wide applicability to the end uses of plasticized PVC, dynamic mechanical analysis has been a principal experimental means of its examination.

3.1.3 *The Dynamic Mechanical Spectrum*

Like other polymeric materials, PVC and plasticized PVC are viscoelastic materials. When deformed, such materials dissipate some energy due to their viscous nature and store some energy due to their elastic nature. The dominance of the viscous or elastic nature in a polymeric material over a range of frequency or temperature is of interest to theoreticians as well as applied scientists and engineers.

The viscoelastic response of polymeric materials is frequently modelled by assembling combinations of springs and dashpots to represent their elastic and viscous components, respectively (16,17). Two widely used models or model elements are the Voigt and Maxwell elements. A Voigt element consists of a spring and dashpot joined in parallel. In the Maxwell model, a spring and dashpot are joined in series.

The Voigt model is particularly well suited for demonstrating creep resulting from application of a sustained fixed force. The Maxwell model is best suited for demonstrating stress relaxation in response to a

sustained fixed elongation (3,16). Polymers, however, usually exhibit both creep and stress relaxation. Consequently, practical models of polymer viscoelasticity are an ensemble of Maxwell, Voigt, and other elements. Each element has a characteristic relaxation time, denoted by τ = η/E, where η is the Newtonian viscosity, and E, the modulus. In the end, the material's viscoelastic response is represented by an infinite number of individual elemental relaxation times. One thus speaks of a distribution of relaxation times or a relaxation spectrum.

Murayama (18) represents the generalized Maxwell model's overall dynamic mechanical behavior with Equations (1) through (4). An infinite number of elements are subjected to a harmonic input, $\varepsilon = \varepsilon\ exp i\omega t$, at a constant frequency ω, resulting in the stress-strain relationship

$$\sigma = (E' + iE'')\ \varepsilon\ exp\ (i\omega t) \tag{1}$$

where

$$E' = \int_0^\infty \frac{\omega^2\ \tau^2}{1 + \omega^2\tau^2}\ \phi(\tau)\ d\tau \tag{2}$$

and

$$E'' = \int_0^\infty \frac{\omega\ \tau}{1 + \omega^2\tau^2}\ \phi(\tau)\ d\tau \tag{3}$$

and $\phi(\tau)$ represents the continuous distribution of relaxation times. A complex modulus can be defined as in Equation (4)

$$E^* = \frac{\partial\sigma}{\partial\varepsilon} = E' + iE'' \tag{4}$$

and is distinctly different from the real modulus, E. The real *part* of the complex modulus, E' (the dynamic or storage modulus), reflects the non-viscous elastic components while E" (the loss modulus) is related to the energy dissipative components. The ratio E"/E' is referred to as the loss tangent, tan δ. It represents the mechanical damping or internal friction of a material. Figure 3.3 depicts the behavior of both E' and E" as well as tan δ for natural rubber. For values of the log decrement Λ less than 1.0, the torsion pendulum damping measurement Λ is equal to πtan δ (2). The angle δ is the phase angle between the imposed strain and the delayed stress response implied by Equation (4).

The previous development of the Maxwell model, when applied to tan δ, gives a value of ωτ, implying a linear relationship between modulus and log ω. The Voigt model yields a similar result, and consequently neither model adequately portrays the behavior of tan δ (19).

One notes that the peak of the loss modulus curve (in Figure 3.3) is coincident with the inflection point of the dynamic modulus. This point of coincidence is labelled the glass transition temperature (Tg). The Tg of PVC generally lies between 80 and 90°C. Frequency can also be used as the major experimental variable in which case the peak of the loss modulus curve or the inflection point of E' is termed the resonant frequency of the system. The interrelationship of frequency and temperature is an important concept in viscoelasticity, leading to the application of time-temperature superposition, a subject reviewed very well by Ferry (3).

The breadth of the E', E", or damping (tan δ) curve as a function of temperature or frequency is closely related to the breadth of the relaxation spectrum. In general, a broad dynamic mechanical curve indicates a broad distribution of relaxation times, which in turn implies that a number of relaxations are active over a relatively wide temperature range. A material which exhibits such breadth is generally believed to be heterogeneous in some respect, at some level, either molecularly or sub-microscopically. If *macro*scopically or perhaps even *micro*scopically heterogeneous, it could be expected to exhibit two separate glass transition temperatures. A narrow dynamic mechanical curve, on the other hand, indicates a relatively narrow distribution of relaxation times, and one might infer that a material showing such behavior is relatively more homogeneous.

This study is therefore concerned with the possible sources of heterogeneity in plasticized PVC. One must begin by considering the structure and morphology of PVC in both rigid and plasticized forms.

3.1.4. *Structure and Morphology of Rigid and Plasticized PVC*

PVC (20,21) is generally produced by a suspension process which yields a particulate free-flowing product approximately 100-150 μm in diameter. The SEM photomicrograph in Figure 3.4 exemplifies the size and texture of these particles. Bulk polymerization, recently made viable by development of a two-stage process (21), produces a similar material.

The particulate nature of PVC extends from the reactor particles down to structures as small as 10 nm. Most researchers have termed the variety of structures grains, sub-grains, agglomerates, primary particles, domains, and microdomains (22-24) as shown in Figure 3.5. Another nomenclature is the Stage terminology (25,26) originally proposed by Faulkner (27) and illustrated in Figure 3.6. Both chemists and rheologists are interested in these structures, the chemist wanting to know how they are developed from the early stages of polymerization (25), the rheologist wanting to know how they are broken down or maintained during melt processing (28,29). Melt flow of PVC is now recognized to be of a particulate rather than molecular nature (26,30,31).

Of some interest to this study are the smallest particles, the microdomains, which are believed to be either nodules or crystalline moieties (23,24), and which supposedly contain approximately 50 chains (22). Microdomains have been found in PVC compounded with plasticizers at high temperatures (32), and it was observed through SEM studies of fracture surfaces that the plasticizer does not completely penetrate the microdomains. Increasing temperature generally shows greater homogeneity of a melt processed PVC, whether rigid (30,31) or plasticized (32). In no case is the processing temperature above the projected melting point of crystalline PVC, which is generally found to be well over 200°C. Some of the suggested values will be discussed later.

In addition to particulate species, suspension PVC can also display a second heterogeneity. A thin membrane consisting of the residue of suspension polymerization agents surrounds the final suspension particle. This skin is insoluble in PVC solvents but totals no more than 0.1 % by weight of the total polymer product. Filisko (33) has shown no specific effect of these membranes in low- and high-speed tensile testing. "Skinless" suspension PVC has been developed and marketed (34). Along with purity, which describes the residues of suspension, emulsion, and microemulsion polymers, virgin PVC is also characterized by its molecular weight and molecular weight distribution, particle size and distribution, density, porosity, and particle agglomeration. Molecular weight of PVC homopolymer is often given as a "K" value or an ISO viscosity number; Brydson (35) discusses both of these characterization parameters.

Unstabilized PVC degrades at temperatures as low as 90°C in only a few hours. At temperatures over 150°C, degradation will commence in only a few minutes. The progress of this degradation is characterized by a series of colors: yellow, orange, pink, scarlet, brown, and, finally, black. The polymer becomes highly unsaturated and conjugated (which produces the colors) and eventually crosslinks. Considerable amounts of HCl gas are liberated during this process. In the presence of water, the HCl gas is converted to hydrochloric acid. Various stabilizers have been developed which prevent significant thermal degradation in PVC (21,36). Even with the available stabilizers, PVC must be processsed below its melting point. This often prohibits complete fusion of the primary particles, particularly in the absence of plasticizers.

As commercially produced, PVC is not a simple homopolymer; one cannot lay down its repeat unit -CH2-CHCl- again and again and trace a path from one end of the chain to the other. Structural defects found by spectroscopic methods, particularly IR and NMR, include unsaturated carbon-carbon bonds, chain branching, initiator end groups, and oxygen moieties (37). The percentage of head-to-head units in PVC is thought to be very small and although not considered a strong factor in its ability to crystallize (38) may be related to its degradation (39). Berens (40) has estimated that if only 1 tertiary chlorine per 1000 C atoms existed in PVC, this would strongly affect the thermal stability of the polymer (41). Long sought evidence supporting the existence of tertiary chlorines was recently published in an article by Starnes et al (42) who conducted ^{13}C nmr analyses of PVC reduced with tri-n-butyltin hydride. The relationship between PVC's susceptibility to thermal degradation and its various structural defects was specifically addressed in a recent review by Naqvi (37). The interested reader may consult Tudos et al (43), Danforth et al (44), Nass (21), Titow (36), Starnes et al (42), and references therein for further details of PVC's thermal stability.

Conventional PVC, produced by free radical processes at about 50°C, is approximately 55% syndiotactic based on diad analyses, such a diad consisting of one pair of monomeric units with each of two Cl atoms on opposite sides of the chain, as shown below. PVC also contains an appreciable number of isotactic diads, also illustrated below.

```
Cl  H   H   H              Cl  H   Cl  H
- C - C - C - C -          - C - C - C - C -
H   H   Cl  H              H   H   H   H
```
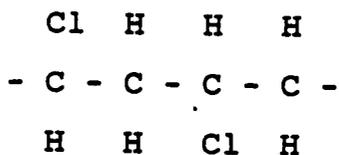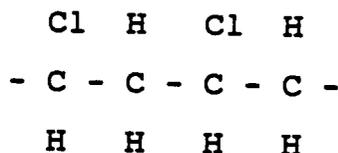
syndiotactic diad   *isotactic* diad

It has been estimated that up to 14 (45) but as few as 5 (46) PVC monomeric units may add in a syndiotactic fashion. These units are believed to crystallize by means of fringed micelle construction, such as that shown in Figure 3.7. It is generally agreed that the order perpendicular to the chain is much greater than that along the chain, as was first remarked upon by Natta and Corradini (47). The crystallinity of PVC is usually quoted as 0 to 15%. Even these very small figures are not in keeping with the known low syndiotacticity of the polymer. It has therefore been suggested that some atactic (48) or isotactic sequences (49) may be incorporated into PVC's crystallites.

A small amount of short chain branching is contained in PVC. It can be decreased by lowering the polymerization temperature (Tp). Branching is not, however, considered a primary determinant of the linearity of the polymer (38). As the Tp is lowered, the degree of syndiotacticity in PVC increases from 0.55 to at least 0.7. PVC prepared at low temperatures generally exhibits a higher softening point, higher tensile strength, greater resistance to creep, lower impact strength, and higher Young's modulus. Increases in syndiotacticity and the accompanying decrease in chain branching are surely partially responsible for the above mechanical property effects, but it is not

certain that they are entirely responsible (38). Smaller percentges of head-tail irregularities and other subtle structural defects may also contribute.

The values found for syndiotacticity differ somewhat according to the method of determination -- usually ^{13}C nmr or infrared spectroscopy -- as well as the peak or band separation in the spectra (50). King et al (51) have recently evaluated the use of ^{13}C nmr in tacticity determinations of PVC. They investigated possible sources of error, in particular, incomplete dissolution of the polymer, different T1 (spin-lattice relaxation) values, and unequal nuclear Overhauser enhancement (NOE) factors (52). King et al (51) attribute the only non-negligible effect to the NOE inequalities. Resolution of the proton decoupled ^{13}C nmr spectra is usually sufficient for estimation of tacticity in PVC, but it is possible to enhance peak separation with a second solvent, such as DMSO (50).

Degrees of tacticity measured by ^{13}C nmr and IR generally agree for conventional PVC (38), ^{13}C nmr being used more frequently, but the values found by IR are often higher than the proton nmr values for Tp less than about 50°C. See Figure 3.8. Wilkes (53) has indirectly suggested that this finding may result from the aggregation of PVC chains in solution, which would make the aggregated chains -- presumably of higher syndiotacticity -- less accessible to the nmr experiment. King et al (51) found that dissolution was not important to the ^{13}C nmr experiment but could foster irreproducibility in proton nmr.

Polymer association in solutions has become a subject of concern within polymer science where so many characterization techniques utilize solutions and where sample preparation frequently involves casting a film from solution. The formation of associations depends upon the polymer and solvent as well as the temperature and concentration. The "aggregates" which form consist of several molecules held together by secondary valence forces such as hydrogen bonding and dipole-dipole attractions. Their formation is frequently thermally reversible, being favored in certain solvents at certain temperatures and concentrations, depending on the polymer.

Hengstenberg (54) first observed association in PVC solutions in 1940 through sedimentation measurements. Doty, Wagner, and Singer (55) systematically studied PVC associations in dioxane via osmotic, ultracentrifuge, and light scattering experiments. The occurrence of PVC associations in THF has been shown by various investigators (56). Recently, DeVries, Bonnebat, and Carrega (57) considered the role of PVC aggregates in THF during light scattering, viscometry, and gel permeation chromatography experiments. Hengstenberg and Schuch (54) utilized the techniques of intrinsic viscosity, electron microscopy, sedimentation, and small-angle X-ray scattering to study PVC association in methyl ethyl ketone. They concluded that the aggregates incorporate between 11 and 25 chains and measure between 120 and 180 Angstroms in diameter. The extent to which these associations form in solutions with plasticizers, as opposed to solvents, is apparently not addressed in the literature.

No specific work of which the author is aware has extrapolated the presence of PVC aggregates in solution to PVC crystallinity in a solvent cast film. Filisko has contributed a short paper on this general topic (58). Carrega (49) notes that PVC aggregates appear non-crystalline by X-ray diffraction until they have been dried and annealed, however, the references given provide little support for such a statement. Lyngaae-Jorgensen (59) voices the opinion that the aggregates contain several chains held together by a crystalline nucleus.

Of interest in this regard is a recent paper in which Spevacek et al (60) showed through nmr and IR spectroscopy that syndiotactic (89.5%) polymethylmethacrylate could form aggregates in o-dichlorobenzene. Films cast from o-dichlorobenzene solutions under conditions very similar to those under which aggregates had been found showed crystallinity by wide-angle X-ray scattering (WAXS). For samples cast from solvents in which aggregation did not take place, WAXS showed no crystallinity.

Though small in proportion to its amorphous content, PVC's crystallinity has been fairly well characterized, but some questions remain concerning its crystalline structure and superstructure. Natta and Corradini (47), by analogy with 1,2-polybutadiene, assigned to PVC chains a planar zig-zag conformation and deduced from X-ray studies on oriented fibers that syndiotactic chain segments were the building blocks of its ordered crystallites. They assigned it the orthorhombic unit cell with dimensions of $a = 10.6 +/- 0.1$ A and $b = 5.4 +/- 0.1$ A. The a axis is perpendicular to the chain axis. Their later assignments (61) were

10.4, 5.3, and 5.1 A for the *a*, *b*, and *c* axes, respectively. The work of Wilkes, Folt, and Krimm (62) on single crystals of a low molecular weight PVC gave a somewhat more compact unit cell of dimensions 10.24, 5.24, and 5.08 A.

As stated earlier, the order along the chain axis (the *c* axis of the unit cell) is low, which Natta and Corradini attributed to the existence of short syndiotactic segments. They estimated that the crystalline fringed micelle structure had a 50 A lateral dimension, i. e., along the *a* axis. Wilkes et al (62) determined that about 12 repeat units spanned the thickness of their single crystals.

PVC of a rather high crystalline content has been produced in solution in the presence of butyraldehyde (63); at low temperatures under tungsten-iodine radiation (64), and at -78°C in a urea canal complex using radiation as the initiator (65). For the third material, White (65) provides X-ray spacings of 2.2, 2.5, 3.5, 4.5, and 5.2 A. Mammi and Nardi (66) report on the variability of the X-ray spacings found for PVC. Biais et al (67) do the same.

PVC generally shows no higher order arrangements of its crystallites. Several years ago, Utsuo and Stein (68) demonstrated the growth of spherulitic structures from PVC solutions in cyclohexanone after annealing for a few hours above 80°C. PVC spherulites in thin films cast from cyclohexanone had earlier been reported by Clark (69).

The presence of crystallinity in plasticized PVC was first shown in wide-angle X-ray patterns by Alfrey et al (70). The concept of a three-dimensional gel structure with crystallite crosslinks was introduced by Aiken, Alfrey, Janssen, and Mark in 1947 (71) as a means of explaining creep behavior in substantially plasticized PVC where flexibility was developed without the onset of flow. Later, Alfrey, Niederhorn, Stein, and Tobolsky (70,72) offered further support for this view through the techniques of X-ray diffraction, stress relaxation, dilatometry, and birefringence. It was believed that the total degree of crystallinity was quite small but that it took the form of small bundle-like crystallites made up of several polymer chains, creating a stable by thermally reversible three-dimensional network.

In the last few years, several articles have appeared as part of a joint study in two laboratories on a proposed two-crystal texture in oriented and dried PVC gels. Evidence for a crystal texture other than the accepted fringed micelle was taken from X-ray diffraction studies and supported by IR dichroism spectra. Lemstra, Keller, and Cudby (73) first presented the X-ray anomalies of a sharp meridional reflection at about 5.2 A. Guerrero, Keller, Soni, and Geil (45) later proposed that this reflection arose from crystals distinct from the fringed micelle and was marked by an *a* axis oriented parallel to the draw direction. A later paper presents a diagram of the proposed structure that is given in Figure 3.9. The thin platelets pictured in the figure have a lamellar character and according to the authors are either loosely connected or unconnected to the gel network (74). Keller, Geil, and co-authors rule against assigning the observed meridional reflection to the 200 plane of

the fringed micelle crystal for reasons including: 1) its spacing is significantly and reproducibly lower than the 5.25 to 5.35 A value that they note is usually given for the 200 plane, and 2) the 5.2 A reflection is very sharp relative to the other observed reflections, suggesting a considerably larger crystal than is usually expected for the fringed micelle.

Tasumi and Shimanouchi (75) had several years earlier used IR dichroism to address rigid PVC's orientation. They point out that reversals in dichroic ratios associated with certain bonds in PVC are first evident at a draw ratio of about 2.5 and often reverse themselves at draw ratios above 7.0. Their interpretation of these results was, however, several steps short of that of Keller, Geil, and co-authors (45,74).

Biais et al (67) released a paper at about the same time as Guerrero et al (45) which utilized the techniques of X-ray diffraction and FTIR to show evidence of lamellar or "ribbon-like" crystals characterized by chain-folding in unplasticized PVC powder. The ability or inability of different types of PVC's, i. e., mass, suspension, and emulsion, to develop fringed micellar and lamellar crystalline textures was discussed by Biais and co-workers. It was decided that the endothermic peaks formed in PVC by annealing arise from formation of the "ribbon-like" crystals. They reported that emulsion PVC contains fringed micelle structures which start to melt at about 140°C.

Reding, Walter, and Welch (76) pointed out the possibility of a polyhedral rather than "sheet-like" crystal texture after plasticization and annealing studies of PVC. However, their evidence indicated that the crystalline texture varied with syndiotactic content of the polymer. Because of its ordinarily low but appreciable degree of syndiotacticity, PVC has been likened to a copolymer in some respects (77,78). PVC's structural irregularities add to its copolymer nature. Based on studies with conventional copolymers, there is reason to believe that the composition of a copolymer may influence its ability to form either lamellar or fringed micelle crystallites.

For example, Berghmans, Govaerts, and Overbergh (79) studied the competitive gelation and crystallization of polyethylene terephthalate-co-isophthalate copolymers. They found that under certain conditions, polymers having certain comonomer ratios could form both micellar and lamellar crystallites. They also showed that fractionation of slightly different copolymers from the same batch could be accomplished by successive gelations, extractions, and centrifugations. Berghmans et al presented the schematic picture of Figure 3.10 showing the apparent *a* and *c* axis orientation of the gel forming micellar crystals. They did not postulate the position of a lamellar crystal in these gels' morphologies. The idea of fractionation via gelation was perhaps first put forward by Benson et al (80) in studies of copolymers of ethylene and 1-butene. Butene percentages below 1.5 mole % encouraged formation of lamellar crystals while larger butene contents (up to 6.0 mole %) easily allowed gel formation, presumably through formation of fringed micelle crystallites.

If these various postulations concerning the crystalline texture of PVC are in fact correct or partially correct, they raise serious questions about the internal structure of plasticized PVC. The possibility of a lamellar crystallite forming in conventional PVC has to be considered small, but only in comparison to more highly crystalline polymers such as polyethylene, polypropylene, and polyethylene terephthalate in which lamellar structures are well documented. However, it is not yet clear to what extent the different textures might occur in rigid PVC vs. conventionally plasticized PVC vs. PVC gelled in dilute solution. It may be added that Carrega has proposed that the spacings attributed to a different crystalline structure or texture may arise from crystalline isotactic sequences (49). Guerrero and Keller (78) consider this highly unlikely.

As a semi-crystalline material, PVC lacks one feature important to analysis by thermal methods; it degrades before its melting temperature can be reached. In spite of this obstacle, several researchers have used differential scanning calorimetry (DSC) to investigate not only the amorphous but the ordered states of PVC and plasticized PVC.

The crystalline melting point of PVC has been reported to be as low as 212°C (11) and as high as 310°C (81) with 273°C (82) being the most frequently quoted value. It may be beneficial to digress for a moment and consider the origin of these melting points. The value of 212°C was obtained by Walter (11) by plotting the temperature at which cylindrically shaped samples of PVC gels lost their shape under constant

heating and extrapolating to 100% polymer. The polymer contained 3.6% vinyl acetate. Kockott's value of 273°C (82) was calculated by considering PVC to be a copolymer of non-crystallizable isotactic and crystallizable syndiotactic units and represents the Tm^0 of completely crystallized syndiotactic PVC. Flory's theory of copolymer melting (83) was utilized in the analysis. Nakajima, Hamada, and Hayashi (81) applied Flory's (9) theory of melting point depression of a diluent (to be discussed later) to the melting of PVC films placed in diluents. This requires plotting the reciprocal of the observed melting temperature against the quantity $\{(v-\chi v^2)/V\}$ where v is the volume fraction diluent, V is the molar volume of the diluent, and χ is the Flory-Huggins interaction parameter (9). A value of Tm^0 is then obtained by extrapolation. Extrapolation was also used to determine the value of χ at the observed melting points; Doty and Zable's values (6) were employed for this task. The values of Tm^0 for PVC synthesized at -75° and -15°C were found by this method to be 310° and 285°C, respectively. The syndiotacticity of the first polymer was observed to be 0.77 while the polymer prepared at the higher temperature was 0.64. Therefore, Nakajima et al (81) determined a higher value for a partially syndiotactic PVC than Kockott (82) calculated for a perfectly syndiotactic polymer. It should be noted that it is theoretically incorrect to call these melting points Tm^0 since they do not represent the melting points of extended chain crystals.

Virgin PVC is believed to contain "primary crystallinity" (84) which is manifested by a very broad endothermic peak between about 110 to 220°C, as shown by DSC. Sharper endothermic peaks which result from

annealing PVC above its Tg are considered to be evidence of "secondary" crystallization by Juijn et al (84) in analogy with other semi-crystalline polymers (85). Juijn et al (84) maintained that the primary crystallinity of PVC, once destroyed, could be reformed only by precipitation of PVC from solution.

In Figure 3.11, taken from Illers (86), a DSC trace for unplasticized PVC that has been quenched from 220°C into ice water shows a distinct recrystallization exotherm followed by a broad endothermic peak. The same quench followed by annealing at 65°C (below Tg) for 96 hours does not erase this apparent recrystallization peak. However, if a sample is cooled slowly from 220° rather than quenched, Illers (87) finds no recrystallization peak. Grewer and Wilski (88) also apparently were able to observe a recrystallization exotherm in quenched PVC. However, Brown, Musindi, and Stachurski (89) failed to see a recrystallization exotherm for PVC quenched in ice water from 220°C.

Illers (87) and later Ohta et al (90) showed in detail the development of relatively sharp endotherms in neat PVC following annealing above Tg. Illers found that whether the PVC was annealed or not the measured heat of fusion did not differ appreciably from 11-12 J/g, as shown in Figure 3.12. The data of this figure support Illers' contention that these endotherms represent recrystallized fractions marked by larger crystal size and greater crystalline perfection but do not contain any "new" crystalline material.

The appearance of post-Tg annealing endotherms in DSC scans of plasticized PVC has been reported by Brown et al (89), Leharne, Park, and Norman (91), and Guerrero and Keller (78). One of the most complete annealing studies of plasticized PVC is likely that of Garrett and Goldfarb (92) who conducted annealings of PVC plasticized with 20 and 40 phr DOP at temperatures below and above Tg. Aging below Tg was found to produce the enthalpic relaxations which result from sub-Tg annealing of a glass (93). Garrett and Goldfarb found that annealing at temperatures up to 75°C introduced endotherms which move upwards in temperature with increasing annealing times. These endotherms were believed to occur by increases in either size or perfection of already existing crystalline structures. Garrett and Goldfarb theorize based on both kinetic and thermodynamic considerations that both the sub-Tg and post-Tg annealing processes are controlled by similar movements of the PVC backbone.

Considerable effort has been spent in attempts to quantify the magnitude of the Tg depression in polymers containing diluents. Simple equations such as Gordon and Taylor's (94) have been used routinely. Several more elaborate theoretical expressions have been developed by Boyer and Spencer (95), Couchman and Karasz (96), Kovacs (97), and Gibbs and DiMarzio (98). These and others are concisely reviewed by Pezzin (99).

It has been reported by Scandola et al (100), Roy, Brown, and St.-Pierre (101), Fried et al (102), Pezzin, Omacini, and Zilio-Grandi (103),

and Pizzoli et al (104) that the change in Tg with plasticizer content in PVC does not fall on a single smooth curve. Instead, behavior such as that shown in Figure 3.13 indicates that two curves, meeting in a "cusp," are needed to fit the data. Adachi and Ishida (105) have shown data for THF-PVC compositions which also suggest a cusp. Pizzoli et al (104), while verifying cusp formation for plasticized PVC, also demonstrated similar behavior in mixtures of dibutyl phthalate and phenolphthalein, showing that perhaps the presence of a polymer is not necessary for the cusp-like behavior of Tg-composition curves. As a matter of interest, the composition at which the cusp is located is often near 40 weight percent plasticizer.

Pezzin (99) concluded that existing statistical-thermodynamic treatments as well as free-volume treatments could not explain this behavior. Kovacs' treatment (97) comes close since it does predict a cusp-like behavior. Roy et al (101) achieved reasonable agreement by a thermodynamic modification of Kovacs' free-volume theory (97). Briefly, rather than assuming, as did Kovacs, that the excess volume fraction of mixing polymer and plasticizer is zero, Roy et al determined its value through measurements of the Flory-Huggins interaction parameter x over a wide range of concentrations using gas-liquid chromatography.

A different aspect of the Tg behavior of plasticized PVC has been studied by Bair and Warren (106), who interpreted the results of their DSC study of PVC plasticized with approximately 10 phr of three ester plasticizers as indicative of upper and lower glass transition temperatures. This conclusion rested partly on the authors' ability to

introduce endotherms below each of the Tg's (see Figure 3.14). Bair and Warren believed these endotherms to be enthalpic relaxations corresponding to each of the two transitions. In a more recent paper, Theodorou and Jasse (R49) reported upper and lower Tg's for PVC plasticized with up to 29 weight percent of several different plasticizers. The second Tg was generally higher than that of virgin PVC, as also reported by Bair and Warren (106). The latter authors attributed the upper Tg to non-crystalline syndiotactic segments. It is worth noting that Bair and Warren saw these effects in dry blended compression molded PVC/plasticizer mixtures, but Theodorou and Jasse (107) showed the same behavior in solution cast PVC. If the observations of two Tg's are valid, it is really rather surprising that there have been so few reports of two Tg's in plasticized PVC. It is suggested by the author that the cusp-like behavior of Tg exhibited with increasing plasticizer content may be related to the reported existence of upper and lower Tg values, requiring two curves to characterize the trends in Tg.

Soni, Geil, and Collins (32) have also noted two Tg values in samples prepared on a two-roll mill at various temperatures. However, the upper Tg in this case occurred at 82°C and corresponded to the Tg of the unplasticized PVC. The upper Tg was therefore assigned to regions of unplasticized PVC. Raising the milling temperature from 140° to 180°C reduced the magnitude of the transition, indicating that only a small fraction of unplasticized PVC remained after milling at 180°C. Plasticizer concentration in this study was 20, 40, and 60 phr.

Solid-state ^{13}C nmr studies of plasticized PVC carried out collaboratively by Douglass (108) and McBrierty (109) showed by free-induction decay experiments and T1 and T1ρ measurements that PVC containing 17 weight percent or less plasticizer (di-isodecyl phthalate) was heterogeneous. McBrierty (109) found that these heterogeneities were on the order of 100 A. Also using nmr techniques, Bashkirov and Maklakov (110) found somewhat larger size heterogeneities in PVC-glycerol systems formed under various conditions.

The singular support which further spectroscopic studies could lend to the study of plasticized PVC is, one would hope, forthcoming. Both FTIR and solid-state nmr (^{13}C and deuterium) are capable of addressing the complex interactions between and the mobility of the components of plasticized PVC within dimensions of several Angstroms. Equally important, both can in principal be carried out below room temperature and so provide direct comparison with the results of dynamic mechanical experiments.

The preceding section has identified several sources of heterogeneity in plasticized PVC. The polymer itself is much like a copolymer by virtue of a small amount of syndiotacticity and various structural defects. If melt processed it retains part of the particulate character of the virgin material. Even if solution cast, PVC's tendency to aggregate in a suitable solvent may influence the morphology of the resulting film. That morphology may be characterized by not one, but perhaps two crystalline textures. The panoramic view just presented will facilitate continued discussion of plasticized PVC with regard to the broadening or lack thereof in its dynamic mechanical spectrum.

3.1.5. *Broadening of the Dynamic Mechanical Spectrum*

Dielectric characterization of plasticized PVC predated dynamic mechanical analysis due to widespread use of PVC as an insulator. Dielectric work by Davies, Miller, and Busse (111), Fuoss (112), Fuoss and Kirkwood (113), and Fitzgerald and Miller (114) illustrated many trends later mirrored in dynamic mechanical (DM) data. These authors showed the characteristic lowering of Tg with increasing plasticizer content, the shifting of Tg to higher temperatures with increasing test frequency, and, to some extent, the broadening of the loss factor and/or dielectric constant curves with either plasticizer content or type. Of course, other effects are noted in both dielectric and dynamic mechanical data, particularly with regard to the influences of molecular weight and molecular weight distribution, branching, crystallinity, and thermal treatments on the α peak and β relaxation of rigid and plasticized PVC (115-23).

Joint dielectric and mechanical studies have shown some interesting effects. In Figure 3.15 are given Wolf's (124) dielectric and mechanical damping curves for PVC containing increasing amounts of diethylhexyl phthalate (DOP). Note that the compositions are shifted towards pure plasticizer for the dielectric data and towards pure PVC for the mechanical data. The mechanical damping curves show a strong broadening effect at 30% DOP while the dielectric data reveals a double peak at 40, 30, and 20% PVC. Wurstlin (125) attributed the appearance of a second peak to the motions of "bound" and "free" plasticizer at low and high plasticizer contents, respectively. The point at which the

dielectric damping peak separates was interpreted as a reflection of the freeing of the bound plasticizer molecules. However, Curtis (126) has pointed out that such curves can be constructed by superimposing PVC and plasticizer loss peaks. Hence, the presence or absence of two peaks at a given composition depends upon the molar ratios of the dipoles in the system (126).

Based on data such as that in Figure 3.16, Nielsen, Buchdahl, and Levreault (127) maintained that the value of x was not closely correlated with the half widths (a measure of breadth) of the damping curves at equal volume concentrations. They contended that increasing chain lengths of plasticizers in a homologous series most markedly influenced the broadening. This particular paper shows a good correlation between the half-widths of dielectric and DM damping functions although it is not a one-to-one correspondence.

In one of the few articles that even addresses DEHS, Hata, Tobolsky, and Bondi (128) drew attention to the broadening effect seen by Schmieder and Wolf (1). Figure 3.17 gives Hata et al's representation of Schmieder and Wolf's data through a plot of the shear modulus vs. T/Tg. A useful parameter, $s = - d \log E(10)/dT$, is taken from the inflection temperature, Ti, of a plot of log 10-sec modulus vs. temperature. Hata et al present data from several plasticizers in Figure 3.18 which along with Table 3.1 shows the effect of various plasticizers on the slope constant s. Most importantly, these data suggest that the solubility is not the overriding influence on the breadth of the glass transition, at least when comparing plasticizers of different structures.

Another interesting paper is that of Aklonis and Rele (129) which addressed the breadth question in plasticized polystyrene (PS) through measurement of a "steepness index." It is qualitatively the slope of a master curve obtained from stress-relaxation data in the glass transition region. Figure 3.19 provides a summary of their experimental conclusions. The authors' molecular interpretation of this phenomenon utilizes the term *dimensionality*. In the reference given, Tobolsky (130) does not expressly define *dimensionality*, however, one can easily grasp the meaning which Aklonis and Rele intended. As discussed earlier, the viscoelastic properties of polymers are often modelled by groupings of various elements. These elements represent chains within an environment formed by "identical" chains. Each element in a general model is characterized by a constant and is often placed on a one- or three-dimensional lattice in which only certain modes of motion (vibrations, rotation, etc.) are available at certain frequencies and temperatures. (Aklonis and Rele specifically deal with the three-dimensional damped Debye lattice.) The polymer's viscoelastic response must be considered to be dependent not only on the types of motion available to the isolated chain but on the intermolecular interactions between it and other chains.

Aklonis and Rele (129) postulate that the interactions between PS and a very soluble plasticizer are very similar to those between PS chains and so the polymer finds itself in an environment that is much the same as the environment in the unplasticized state. Dimensionality is thus preserved, and the viscoelastic response as monitored by the

steepness index is not substantially altered. If, however, polystyrene is not strongly soluble with the plasticizer, as, for example, DMP and DOP (see Figure 3.19), then the interactions between the PS and the plasticizer will be weaker than those between PS molecules alone and will lower the dimensionality of the system, thereby lowering the steepness index. This is an interesting interpretation in view of Busse's early and incisive observation that plasticization is characterized by the presence of "forces of two different orders of magnitude, strong forces along the fiber and weak forces around the fiber" (131).

Nakamura's study of plasticized PVC (132) specifically sought to explain the broadening effects of plasticizers. Compliance master curves were constructed for compositions of 32, 40, 49, and 59 weight percent plasticizer using DOP and tricresyl phosphate. Because the method of time-temperature superposition is not readily applied to semi-crystalline materials, Nakamura used the treatment of Ninomiya and Ferry (133). This includes various shift factors to compensate for finite amounts of crystallinity. The factor q, in particular, is a function of the volume fraction of crystallites in the entire system. Evidently, Nakamura (132) used the data reduction treatment of Ninomiya and Ferry to indirectly determine a "degree of crystallinity" for the systems investigated. An apparent melting temperature Tm' was defined as the temperature at which log q deviated from linearity. A plot of $(Tm'-Tg)$ vs. Tg was found to pass through a maximum at about 0.4 volume fraction. Nakamura thus attributed the broadening to the "degree of crystallinity," finding that it was a maximum near 32 weight percent plasticizer ($\sim$ 0.4 volume fraction). The interaction between the PVC and plasticizer is mentioned as a possible contributing factor.

Ward (19) stated simply that the breadth of the dynamic mechanical curve increases as the solubility between the plasticizer and the PVC decreases. This opinion was also voiced by Nielsen (2). Schmieder and Wolf (1), as far as is known by the author, gave no specific interpretation of the breadth differences seen in their data. However, Nielsen (2) references a later paper by Wolf (124) as showing such effects to be related to plasticizer solubility. It shall be shown here that solubility is certainly an important element, but one must also consider other aspects such as steric factors, molar volume, and the network structure of plasticized PVC.

A variety of experimental methods have been utilized in this study. Techniques employed included dynamic mechanical analysis, wide-angle X-ray scattering (WAXS), small-angle X-ray scattering (SAXS), differential scanning calorimetry (DSC), static mechanical testing, small-angle light scattering (SALS), and simple diffusion experiments. All of these were applied to DEHS- and DBP-plasticized PVC (henceforth referred to as DEHS-PVC and DBP-PVC). Because of the specific aim of the entire study, each of these techniques was not exhaustively applied. Rather, they were first evaluated as to their ability to point out differences in these two materials and used further when results showed promise.

Experimental results are presented and briefly discussed first for the DEHS-PVC and DBP-PVC systems. The second section extends some of the principal concepts gained through the study of DEHS-PVC and

DBP-PVC to PVC compounded with other plasticizers. Several common measures of solubility are presented and evaluated within the context of the observed dynamic mechanical behavior. Lastly, the total interaction of the plasticizer and the polymer network structure are considered collectively in a comprehensive interpretation of the broadening and renarrowing of the dynamic mechanical spectrum of these materials.

This chapter presents what is believed to be the only dedicated investigation of the effects of plasticization on the broadening of the dynamic mechanical spectrum of PVC. Its goal is not simply to verify the trends found by earlier researchers in this area but rather to understand what these trends imply about the internal structure of plasticized PVC and its direct effect on the dynamic mechanical response.

3.2. *EXPERIMENTAL*

3.2.1. *Materials*

Polyvinyl chloride (Diamond Shamrock 450) was kindly donated by Rohm and Haas Corp. It was in the form of a white powder and reportedly contained no heat stabilizer or other processing aid. Its viscosity average molecular weight was 107,000 g/mol as determined from intrinsic viscosity measurements in THF at 25°C (134). If one assumes a polydispersity of 2.0, which is reasonable for suspension PVC (49), it is possible to calculate a number average molecular weight (Mn) from intrinsic viscosity and the appropriate K and a constants (134). This was done using equations from Elias (135) and Schindler and Harper (136). The Mn of this PVC was calculated to be 56,000 g/mol. DEHS (Wickenol 159) was generously provided by Wickhen Products, Inc., Huguenot, NY. DBP was purchased from Fisher Scientific Co. Both of these esters are colorless, practically odorless, and slightly oily liquids at room temperature. The glass transition temperatures of PVC and the plasticizers are 86.4° for PVC, -99° for DEHS, and -88°C for DBP, as determined by DSC.

Several other plasticizers were included in this study. These included diethylhexyl phthalate (DOP), dipropyl phthalate (DPP), dibutyl sebacate (DBSe), and dibutyl succinate (DBSu). DOP (Union Carbide Flexol) was part of existing laboratory stock. DPP and DBSe were Eastman Kodak chemicals purchased from laboratory suppliers. DBSu was obtained from Pfaltz and Bauer, Inc.

The structures of the six plasticizers included in this study are given in Figure 3.20. The major physical properties of these plasticizers are listed in Table 3.2.

3.2.2. *Sample Preparation*

Most sample films were prepared by solvent casting from THF. To this end, appropriate weights of PVC and plasticizer were dissolved with stirring in about 50 mls of THF at room temperature. These solutions were poured into Teflon casting blocks which were covered with funnels to allow fairly slow evaporation of the casting solvent at room temperature. Early measurements indicated that about 48 hours after casting, films containing 40 and 60% plasticizer retained no more than 1.0% THF by weight. Films containing 10% plasticizer held less than 10% THF. A film of PVC alone retained nearly 20% THF after casting and drying at room temperature and pressure. The amount of THF trapped in the films is related to the location of Tg relative to room temperature. The 40 and 60% films are above their Tg's at room temperature, making THF escape relatively easy. With 10% or less plasticizer, Tg is above room temperature, and THF evaporation is hampered. This trapped THF effectively acts as a plasticizer, depressing Tg in both the 10% and neat PVC films. No routine effort was made to remove THF from films containing 40 and 60% plasticizer. In some cases, THF was removed from neat PVC film as well as those containing 10% plasticizer by vacuum drying at temperatures near 100°C for about 2 hours. This drying procedure caused a slight pinkish discoloration in the films. The *dried*

10% samples that were used for dynamic mechanical experiments were sealed in a double wrap of aluminum foil, heated to 180°C in an oven, and quenched quickly in ice water. This was done to erase the effects of the drying process. A series of DSC traces verified that this had been accomplished.

The preceding conditions define the standard plasticized films, which were approximately 15 mils thick. Such films were used for most testing excepting those cases outlined below. These standard films are designated simply by the plasticizer and its percentage in a standard film. As an example, a film prepared by the standard methods which contained 60% DEHS by weight would be called DEHS60. The usual weight percentages of plasticizer in these films were 10, 40, and 60%. Some films were prepared containing 75% plasticizer.

Compression molded films were made by pressing hand-mixed blends of polymer and plasticizer at temperatures between 150 and 180°C. These films are designated M. They were used for limited dynamic mechanical testing and for SALS studies.

The "reversibility" of plasticizer incorporation between 60 and 40% plasticizer contents was studied through a diffusion experiment as follows. Films containing 60 weight percent plasticizer (standard series) were sandwiched between two films of cast PVC (undried); the sandwiches were placed between Teflon sheets. They were laid in a 90°C oven and topped with a glass Petri dish lid on which was placed a slight weight. The films were periodically removed from the oven and weighed.

The experiment was conducted twice, first as a method of sample preparation in which the experiment was stopped when 40% plasticizer content was reached; samples so obtained are designated D since they are prepared by diffusion. Later this same experiment was repeated and extended to longer times as weight loss data was recorded. In addition, a rough measure was taken of the amount of plasticizer absorbed by a cast PVC film immersed in liquid plasticizer.

Films thicker than 15 mils were prepared for static mechanical testing by doubling the amounts normally cast for a 15 mil film. This was done to increase the accuracy of the load measurements during these experiments.

Several sample preparations involving specific thermal histories were conducted in conjunction with certain tests. These are described as needed to avoid repetition. Films containing any amount of plasticizer were transparent although surface texture sometimes concealed this fact.

3.2.3. *Solution NMR*

A ^{13}C nmr spectrum of the PVC was obtained through the courtesy of R. Subramanian at VPI&SU. A total of 3800 scans were taken on a 10% solution of the polymer in THF at room temperature using a pulse width of 3.0 Hz, sweep width of 22 kHz, and a relaxation delay of 1.5 sec. The peak resonances were assigned according to Carman (137) and tacticities calculated based on resonance peak intensities. Figure 3.21 gives the spectra obtained and Table 3.3 lists the results of the tacticity

calculation. The syndiotacticity found is in keeping with typical values for a commercial suspension-polymerized PVC (49).

3.2.4. *Dynamic Mechanical Studies*

Dynamic mechanical spectra were obtained on a Rheovibron Dynamic Viscoelastometer, Model DDV-II-C. Samples were generally cut from 15 mil films with a metal die measuring 4.6 X 0.48 cm. Unless noted otherwise, samples were loaded into the Rheovibron at room temperature and cooled to about -135°C in about 1 hour. Heating rate was 1 to 2°C/min, and the standard frequency was 11 Hz. Data was processed by computer.

3.2.5. *Wide-Angle and Small-Angle X-Ray Scattering*

It should be mentioned first that PVC strongly absorbs X rays, having a linear absorption coefficient of 87 cm^{-1} for CuKα radiation. Polymers with the elements C, O, H, and/or N generally have absorption coefficients between 5 and 8 (138). The optimum thicknesses for maximum scattering intensity range from 4.5 to about 15 mils for these materials, depending on plasticizer content. (See the Appendix for the appropriate calculations.) Most of the X-ray work reported here was conducted on samples which were thicker than the optimum thickness would recommend, but this did not substantially affect the results.

Materials were studied by photographic WAXS methods using a Philips PW1720 table-top X-ray generator equipped with Warhus cameras.

In general, sample films were mounted on a 20- or 25-mil pinhole stub and exposed to the X-ray beam for 20 hours. Sample-to-film distance was 7.6 cm. X-ray patterns were developed identically for each series of exposures.

The scattering behavior of neat PVC and liquid DEHS and DBP was also examined by WAXS. Sealed 1.5-mm quartz capillaries were fastened across a 15-mil pinhole stub and exposed as described above. An empty sealed capillary was run to provide a reference for any scattering or attenuation, of the incident beam by the quartz alone.

Two different SAXS systems were used to study the DEHS and DBP series of plasticized PVC. DEHS-PVC and DBP-PVC containing 40, 60, and 75 weight percent plasticizer were run on the 10m SAXS instrument at the Oak Ridge National Laboratory through the courtesy of R. C. Allen. The instrument (139) (and important experimental parameters) consisted of a rotating anode radiation source, a crystal monochromator, a pinhole collimator (1 mm x 1 mm), and a two-dimensional position-sensitive detector grid (placed 2126 mm from the sample). The data were treated as described in the Appendix and analyzed for structural information as will be described later.

Supportive SAXS measurements were made on an in-house slit collimating Kratky system. This instrument is equipped with a Siemens single-position detector from which data is collected via an interfaced PDP-8A Digital computer and a Teletype machine.

3.2.6. *Small-Angle Light Scattering*

SALS patterns were taken with an apparatus consisting of a He-Ne laser, analyzer, and Polaroid film holder mounted on a vertical optical bench. The films (designated M) were prepared as described earlier. This technique worked satisfactorily up to 60% plasticizer content.

3.2.7. *Differential Scanning Calorimetry*

A Perkin-Elmer DSC-4 with Scanning Autozero baseline correction was used for thermal analysis of materials. An indium standard ($Tm = 156.6°C$) was used for temperature calibration. Scanning rate was routinely 10 deg/min.

3.2.8. *Static Mechanical Properties*

Stress-relaxation and stress-strain tests were run on a Model 1122 Instron machine. All samples subjected to stress-relaxation were about 30 mils thick and were aged at ambient temperatures for four weeks post casting prior to testing. Samples were cut with a metal dog-bone die having a 22-mm gauge length. They were stretched to a fixed elongation at a crosshead speed of 100 mm/min and allowed to relax for at least 30 minutes. From the cumulative data of at least ten separate samples from the same film, the stresses measured after 30 minutes and the corresponding draw ratios were used in an approximate calculation of the "apparent molecular weight" between junction points. This approach assumes that plasticized PVC is a physically crosslinked material.

Limited stress-relaxation experiments on DEHS40 and DBP40 samples verified that the stresses measured at 30 minutes were analogous in relative magnitude to those found at nearly twenty-four hours. These results were obtained on a Tensilon UTM-II machine with 10-mm gauge length dog-bones. The Tensilon has better long-term stability than the available Instron machine.

Tensile stress-strain tests were run on the Instron using dog-bones with a 10-mm gauge length and a crosshead speed of 10 mm/min. Stress-relaxation and stress-strain experiments were conducted at ambient temperatures.

3.2.9. *Light Transmission*

The possibility that plasticizer might separate from PVC at temperatures below ambient was investigated using a low-temperature light transmission device assembled in the laboratory. The sample was clamped inside a copper block which was surrounded by a band heater, non-operative in this case. The flat surface of a copper cooling chamber was placed in contact with the copper block. The outer surface of the cooling chamber was insulated with a Teflon casing. Copper tubing (for liquid nitrogen flow) extended from this chamber through the Teflon casing. This assembly was placed inside a Warhus WAXS camera which was evacuated during testing. A thermocouple was located inside the copper block away from the cold contact surfaces. A light source was placed outside the camera at the end which would normally be attached to

a port of an X-ray tube. A photodiode used conventionally in an optical microscope was positioned inside the camera on the side of the sample opposite the light source. The diode registers a voltage in response to its reception of the transmitted light which is proportional to the percentage of the light transmitted through the sample. The question of low-temperature phase separation was raised only in the case of PVC containing 40% DEHS, so this particular material was the only one tested. The sample was a thin transparent film drawn on glass with a doctor's blade. Liquid nitrogen coolant lowered the temperature at an overall rate of about 1°C/min.

3.3. RESULTS AND DISCUSSION

3.3.1. Verification of the Reported Behavior

Three weight percents, 10, 40, and 60, were chosen as representative of the three extremes of the behavior noted in Figure 3.1. Table 3.4 lists the corresponding volume fractions and mole fractions for DEHS-PVC and DBP-PVC systems of 10, 40, 60, and 75 weight percents. (*DEHS-PVC* and *DBP-PVC* refer to materials containing these respective plasticizers as a class generally without regard to a specific plasticizer content.) At equivalent weight fractions, DEHS-PVC has a larger volume fraction plasticizer than DBP-PVC but a smaller mole fraction. The use of weight percents is most industrially relevant.

Dynamic mechanical spectra obtained in this laboratory at a frequency of 11 Hz are given in Figure 3.22 for DEHS-PVC and DBP-PVC. The trends noted by Schmieder and Wolf were easily reproduced, as seen by comparing Figures 3.1 and 3.22. Schmieder and Wolf's data consist of the dynamic shear modulus, G', and the log decrement, Λ, as a function of temperature at about 1 Hz. In general, $\Lambda = \pi \tan \delta$, although Nielsen (2) points out that this equality may not be accurate at Λ values greater than 1.0. If peak temperatures for the tan δ (T) curves are equated with those of the Λ curves, the transition temperatures indicated by the tan δ (T) curves are substantially higher than those of the Λ (T) curves. But if E" peak temperatures from the newer data (not shown) are compared with Schmieder and Wolf's data, reasonably good agreement

is reached. The frequency difference may also account for some of the discrepancy between transition temperatures.

Another factor separating the transition temperatures could be sample preparation. Schmieder and Wolf do not provide a description of sample preparation, but they indicate within their text that their materials were prepared at high temperatures. During the present investigation, compression molded films (DBP40-M AND DEHS40-M) were prepared by hand mixing PVC and neat plasticizer and pressing the mixtures at 170°C. The breadths and peak temperatures of the 40-M samples' damping curves were quite similar to those of the solution cast films. Schmieder and Wolf's formulation most likely contained a stabilizer. No additives have been used in the present study. There is evidence that a stabilizer can affect glass transition temperatures, relaxation properties, and effective plasticizer action (140-2). In summary then, the combined influences of frequency, sample preparation, and extra additives may account for the noted differences in transition temperatures.

3.3.2. *Wide-Angle X-Ray Scattering and Support Techniques*

PVC itself has been studied by WAXS in several different forms. Figure 3.23 shows WAXS patterns for PVC compression molded at 145°C, PVC cast from THF, and PVC grains placed in a sealed quartz capillary. Figure 3.23a shows little crystallinity for the compression molded film. A solution cast film of approximately equal thickness (see Figure 3.23b) shows weak but definite crystalline rings. The neat PVC contained in the quartz capillary exhibits only a low angle amorphous halo.

Figure 3.24a shows the scattering pattern of an empty quartz capillary for which a weak high-angle amorphous halo was observed. The neat plasticizers (Figures 3.24b and 3.24c) scatter in both low and high angle regions. DBP scatters with approximately equal intensity in both regions. Its low angle region extends to $2\theta = 13.0°$. DEHS scatters more strongly in the high angle region, and its low angle region extends to $2\theta = 7.5°$.

WAXS patterns for the DEHS-PVC and DBP-PVC systems are provided in Figure 3.25. It is seen that the crystalline rings for DEHS10 are considerably sharper than those for DBP10. The patterns for DEHS40 and DBP40 are very similar, both showing two broad but distinct crystalline rings and outer diffuse halos with an apparent maximum in intensity near the perimeter of the pattern. The two low-angle rings have become quite diffuse at 60 weight percent DBP content while remaining relatively sharp at 60 weight percent DEHS. The pattern for DBP75 is much like that for a completely amorphous material, showing inner and outer diffuse halos. The pattern for DEHS75 exhibits an intense halo which at least partially corresponds to the plasticizer's own amorphous scattering. It is difficult to say whether or not this intense halo hides any weak crystalline rings.

Comparison of the WAXS patterns for PVC (Figure 3.23) and 10% samples (Figure 3.25) gives every indication that the crystalline reflections observed are a consequence of solvent-induced crystallization (143). It is well known that crystallization can occur only if a polymer is

above its Tg and below its melting point (Tm); these two temperatures define what has been called the "crystallization window." Crystallization occurs at a maximum rate approximately midway between Tg and Tm.

Casting PVC from a liquid such as THF or THF/plasticizer lowers both the Tg and the Tm of the PVC, thereby enlarging the crystallization window. It is generally observed that Tg is depressed more than Tm by the presence of a diluent. Expressions which predict the influence of composition on the Tg of a polymer-diluent mixture do not involve any measure of the strength of polymer-diluent interactions (143). They depend primarily on combinations of the glass transition temperatures of the components, their specific heat changes at Tg, and various constants (99).

Depression of Tm, however, depends strongly on the interactions between the polymer and solvent as demonstrated by Flory's expression for Tm depression of a homopolymer by a diluent:

$$\frac{1}{Tm} = \frac{R}{\Delta Hu}\frac{Vu}{V}\left(v - \chi v^2\right) + \frac{1}{Tm'} \qquad (5)$$

where Tm is the calculated melting point, Tm' is the melting point of the same polymer in the absence of the diluent, Vu is the specific volume of PVC , R is the gas constant, v is the volume fraction of plasticizer, V is the specific volume of the plasticizer, ΔHu is the heat of fusion, and χ is the interaction parameter.

Applying Equation (5) to plasticized PVC required knowing ΔHu, Tm', and x. The x value of DBP was taken as 0.0 (6) while that for DEHS was estimated at 0.5. In general, x values near or below 0.0 indicate thermodynamic favorability for mixing. The x value chosen here for DEHS is conservatively high. Hata et al (128) give a x value of 0.39 for DEHS and reference Doty and Zable (6) and Darby, Touchette, and Sears (144), but neither of these papers lists a value for DEHS. Hata et al may have estimated a x value based on similar structures.

As discussed in the Introduction, the melting point of PVC is not measurable by standard techniques. Likewise, ΔHu has not been directly determined. Values of 273° (82) and higher (81) have been proposed as melting points of completely syndiotactic PVC, but the PVC used here is only 58% syndiotactic, based on nmr determination of its diad content. The value of 212°C proposed by Walter (11) may be considered the lower limit of Tm' although an even lower value of 174°C has been suggested by Anagnastopoulos, Coran, and Gamrath (145). Since it is very likely that the Tm' value for the PVC used in this study lies somewhere between 212° and 273°C, the effect of diluent concentration on melting point depression was determined using both temperatures. Values of the heat of fusion were taken to be 0.659 kcal/mol (145) and 2.7 kcal/mol (82) for the low and high values of Tm', respectively. Density of the PVC was taken to be 1.4 g/cc.

Figure 3.26 illustrates the magnitude of Tm - Tg for PVC containing 10, 40, 60, and 75 weight percent DEHS and DBP. Tg's were determined

from the peaks of E" vs. temperature curves. The range of Tm was calculated from Equation (5) using the parameters described above.

If one pays heed only to the lower Tm values (based on Tm' = 212°C), Figure 3.26 demonstrates how crystallinity may be equally encouraged in DEHS40 and DBP40 since room temperature lies near the middle of their crystallization windows. On the other hand, the Tm of DBP60 is very close to room temperature, thereby making crystallization less likely. The less soluble DEHS, however, depresses Tm less than DBP, thus making crystallization possible even at 60% content.

Using Tm' = 273°C to calculate the Tm of the plasticized materials indicates a minimal Tm depression, and suggests that the systems containing up to 75% plasticizer should remain semi-crystalline. Since WAXS has indicated that the 60% and certainly the 75% plasticized systems have negligible total crystallinity, it is very likely that 273°C is too high a value of Tm' for this application. The value of ΔHu chosen will, of course, also influence this result. The outcome of this analysis suggests that Equation (5) cannot be rigorously applied to plasticized PVC without more confident knowledge of the values of Tm' and ΔHu.

Equation (5) does not account for the excess of THF present when casting plasticized films which could further depress Tm as well as Tg until it has been removed from the film. However, the THF probably has an equivalent effect on both DEHS-PVC and DBP-PVC.

As further evidence for the greater solvent power of DBP over DEHS, it was found in static mechanical tests that 40 and 60% DBP lowered the modulus of PVC more than equivalent weight percents of DEHS. The shapes of the stress-strain curves are reminiscent of elastomeric materials. It is also significant that the stress following long-term relaxation of DBP40 is lower than that of DEHS40. These results will later be discussed in more detail.

A simple diffusion experiment showed that the incorporation of 60% plasticizer was reversible. The experiment consisted of sandwiching DEHS60 and DBP60 films between cast PVC films and placing these in a heated oven (90°C) under a light weight until weight loss measurements indicated that plasticizer content had reached approximately 40 weight percent. These films are denoted 40-D having been prepared via diffusion. As Figure 3.27 shows, these films demonstrate damping curves very much like those of 40% films, suggesting that the structures which lead to the broadening of these curves are formed reversibly.

It should be pointed out that the damping curve given in Figure 3.27 for DEHS40-D was taken 12 days after the sample was prepared. A sample tested 3 days after the diffusion preparation gave a damping curve with considerable scatter. After 12 days, a smoother curve was obtained; results from both the 3-day and 12-day old samples are shown in Figure 3.28. The smoother curve has a slightly lower peak temperature than typically seen for DEHS40 samples. This sort of behavior was not noted for DBP40-D. It is, of course, quite possible that the scattered data taken after 3 days was due only to experimental error.

Data taken during a longer run of the diffusion experiment (see Figure 3.29) shows the initial rate of weight loss to be greater for DBP60 than DEHS60. Absorption into the PVC was not a limiting factor since cast PVC absorbed DBP more quickly than it absorbed DEHS from the bulk liquid state. These weight loss trends suggest only that DBP is more mobile than DEHS within the plasticized material, i. e., the kinetics of plasticizer diffusion may well be the underlying driving force, and thus no inferences can be made here about the thermodynamics of PVC interaction with DEHS and DBP. No doubt DBP's greater mobility is assisted by its small molar volume relative to DEHS.

Diffusion studies by Ernes, Garg, and Williams (146) interestingly showed that diethylhexyl phthalate (DOP) diffused to the surface of a compression molded plaque of PVC much more slowly than did a mixture of predominantly linear dialkyl phthalates. Ernes et al attributed this to the steric "hook" of the 2-ethylhexyl group. DEHS possesses this same "hook."

It is appropriate at this time to directly compare the damping curves of DEHS40 and DBP40 materials of the standard, D, and M series. These are given in Figure 3.30. For DBP40, the breadth of the curves clearly decreases moving from the molded films (M) to the standard films to the films prepared via diffusion (D). For the DEHS40 samples, the trend progresses from M to D to the standards although the aging time needed for a smooth DEHS40-D curve may have influenced this result. Some irregularities also appear in the DEHS40-M tan δ curve. In spite of

these complications, it is reasonably clear that the 40-M curves are the broadest of the three. In addition, if it is assumed that DBP is not significantly influenced by kinetic/diffusion effects, the demonstration of a more narrow curve for the DBP40-D material suggests that a 40-D sample generally has the most narrow damping response of the three being considered here.

These results can be explained by considering the extent of plasticizer dispersion. A film originally containing 60% plasticizer is certainly swelled to a greater extent than a 40% film. When some of the plasticizer is drawn out of the 60% film by the diffusion experiment described earlier, the plasticizer will not be totally removed to regions of the material normally occupied by a sample originally containing only 40% plasticizer. It is very likely that some regions of the network inaccessible to the plasticizer of a 40% film are occupied by plasticizer in a 40-D material, the end result being that the plasticizer in 40-D is better dispersed. It is not possible to determine if DEHS40-D benefitted from this potential route of more efficient dispersion. The poorest dispersion would by this argument be expected in a 40-M film compression molded at 170°C. Molecular flow probably does not develop at this temperature (20,23,24,30,31).

Related to the work presented in this section is a short small-angle light scattering (SALS) study. Examination of solution cast PVC and plasticized PVC by SALS showed no defined scattering pattern. However, compression molding of PVC as well as hand-mixed DEHS-PVC and DBP-PVC compositions produced SALS patterns such as those shown

in Figure 3.31. Pressing neat PVC at progressively higher temperatures (Figure 3.31a) or pressing plasticizer-PVC mixtures of increasing plasticizer content (Figure 3.31b,3.31c) gradually diminished the intensity of the scattering. Subtle but not necessarily (in)significant differences are observed between DEHS-PVC and DBP-PVC.

The monotonic decrease in Hv light intensity with increasing scattering angle suggests that the scatterers are anisotropic rod-like regions. As discussed earlier, PVC shows no defined superstructure under normal conditions, therefore the elements which give rise to these SALS patterns must arise from some deformation of the original grains of the particulate PVC. During compression molding, the grains are flattened to some extent, but they do not completely melt. This is visually obvious in the case of the neat PVC and may be assumed to occur to some extent in the plasticized materials due to the relatively mild conditions employed for film preparation.

Molding neat PVC at higher temperatures or with increasing amounts of plasticizer will allow a more uniform (spherical) flattening of the grains and better fusion. This could account for the observed decrease in scattering intensity under these conditions.

A 1978 paper by Wenig (147) included what may be the only published SALS pattern for PVC; it is similar to these patterns in that it indicates the presence of rod-like scatterers. Wenig interpreted the patterns based on WAXS and SAXS data, neither of which is sensitive to the dimensions which SALS can probe; his explanations are therefore somewhat unsatisfactory.

3.3.3. *Differential Scanning Calorimetry and Support Techniques*

The DSC studies of plasticized and unplasticized PVC reviewed in the Introduction indicate that DSC might be used, at least qualitatively, to monitor changes in crystallinity in DEHS-PVC and DBP-PVC. One could regard crystallinity as a heterogeneity in plasticized PVC and, therefore, a potential source of broadening of its dynamic mechanical spectra.

No one has to the author's knowledge investigated the influences of more than one plasticizer on the endothermic peak associated with crystallinity. Nor has the effect of isothermal crystallization on the dynamic mechanical properties of plasticized PVC been investigated. The following study considers these points using the variables of time, composition, and plasticizer. In conjunction with changes in thermal history, DSC was coupled with dynamic mechanical spectra and WAXS studies for a more complete materials characterization.

To begin this study, the DSC behavior of unplasticized PVC will be considered. Shown in Figure 3.32 is a series of DSC scans on neat PVC powder as received. A very broad endotherm is seen in the first scan which is not completely restored in the second scan, indicating, in line with Illers' (87) interpretations, that complete recrystallization did not occur as the sample was being quenched (at 320°C/min) following the first scan. Curves 3 through 6 in Figure 3.32 show the ease of formation of an endotherm when the sample is heated to a temperature above its Tg. Simply heating the sample to a specific temperature and quenching

produces an endotherm above the final temperature of the previous scan (see Curves 4, 5, and 6 in Figure 3.32.)

Figures 3.33a-d show four series of DSC scans demonstrating the effect of room temperature annealing and plasticizer content on the crystallization endotherm. Scans were taken of the four different materials 11 months following casting and 4 and 25 days following quenching from 120°C. The endotherm distinctly shifts upward along the temperature axis and sharpens somewhat with annealing time. The peak temperature of the endotherm lies at slightly higher temperatures for the DEHS-PVC material, and it appears that the peaks for the DEHS-PVC materials are slightly sharper, particularly for the well-aged DEHS40 material.

Damping curves for plasticized materials with a very similar thermal history are shown in Figure 3.34. DBP40 and DEHS40 were subjected to three separate treatments: aging at room temperature for 10 months following casting (aged), aging at room temperature for about one month following casting (short aging), and quenched from 90°C to liquid nitrogen temperatures followed by a rapid loading into the Rheovibron which was immediately cooled. A quench of DEHS40 from 180°C into liquid nitrogen followed by loading into the pre-cooled Rheovibron (-30°C) gave a curve virtually identical to that obtained via the quench from 90°C. From Figure 3.34, it is clearly seen for DEHS40 that the "quenched" peak is the most narrow, the "aged" peak, the broadest.

A rather abrupt change in slope was observed in many of the DSC scans just above 105°C (see, for example, Figure 3.33). It was reproducible from one scan to another for both neat and plasticized PVC. In many instances, it is simply superimposed on the DSC trace as if it were part of the baseline, however, the baselines from the DSC showed no such irregularity. When the temperature scanning rate of the DSC was changed in an attempt to shift this "blip," it could not be relocated with certainty. Because it cannot be dismissed as an instrumental artifact, it has been left in the traces. Other irregularities occasionally appeared in the DSC traces of the plasticized samples. Unlike the previous effect, these were not reproducible from sample to sample and rarely occurred near the same temperature and never with a similar magnitude. They have been left in the scans although it is likely that they arose from contamination.

It was observed during the earliest DSC experiments that the plasticized materials could form more than one endotherm under certain conditions. Other semi-crystalline materials, such as polyethylene, can do this as well (85). There has been one report of this phenomenon in unplasticized PVC (49). Several annealing and cooling experiments were designed to find the temperature range of endotherm formation and the time necessary for endotherm formation at various temperatures. Some of these were done wholly in the DSC, but others were done with larger samples so that the effects of thermal history could be monitored with dynamic mechanical and WAXS analysis as well as DSC.

When contained in the crimped DSC sample pans, plasticized PVC lost less than 0.1% of its original weight as seen by weighing before and after high temperature treatments. However, if open to air or vacuum, plasticized PVC was found to rapidly lose a significant amount of plasticizer when exposed to temperatures of 150° or 180°C. Therefore, the thermal treatment of "bulk" samples involved a special containment method. Sample films of an appropriate size were placed between Teflon films, wrapped in aluminum foil, and placed on a platform inside an 8 oz. jar laid on its side. This method was varied somewhat according to the annealing time and temperature. Samples were weighed before and after annealing to verify that the weight loss did not exceed 1.0% of the original sample weight.

Figure 3.35 shows two series of DSC traces for samples subjected to step coolings. In these experiments, the samples were heated to 180°C from room temperature at 10 deg/min and quenched sequentially to 150, 120, 90, 60 and 30°C at 320 deg/min. They were held at each of the five temperatures for 5, 15, or 120 minutes before being cooled to the next lower temperature. Following annealing at the lowest temperature for the prescribed period of time, they were scanned to 180°C at 10 deg/min. The programming capabilities of the DSC-IV were used for this treatment.

The DSC curves in each set of Figure 3.35 show that while limited, ordering does occur in DEHS40 and DBP40 within short times. Step coolings of DBP40 showed negligible endotherm formation at short times (5 minutes) although endotherms developed easily at longer times. The

endotherms observed for DEHS40 following the 120-min step cooling are sharper than those found for DBP40, but their peak temperatures are not substantially different. Slight differences are apparent for the peaks resulting from annealings at 120 and 150°C. For either plasticizer, annealing at 120°C appears to produce the sharpest endotherm.

These data complement earlier results suggesting that DBP is a better solvent for PVC than is DEHS. The DSC endotherms of DEHS-PVC show a sharper and larger crystallization endotherm than identically treated DBP-PVC, indicating that DEHS allows more crystallinity to develop at a given temperature. In accordance with the concept of solvent- or liquid-induced crystallization (143), both of the plasticizers allow crystallization to develop at lower temperatures than is observed for neat PVC, but the greater solvent power of DBP allows less crystallinity to develop. The use of the words "more" or less" in describing the crystallinity are qualitative and only meant to describe the apparent extent of recrystallization of disordered PVC. It is instructive to note that crystallization has apparently occurred here well above the T_m values calculated for 40 and 60% plasticizer compositions based on a T_m' value of 212°C. (Refer to Figure 3.26.) This suggests that 212°C and/or 0.659 kcal/mol are unrealistically low values of T_m' and ΔH_u, respectively.

Larger sample sizes were subjected to a step cooling that was as close as possible to the DSC treatment described earlier insofar as temperatures and times were concerned. The films were prepared for these high temperature exposures using the jar containment system

described earlier. The jars with films were transferred from one equilibrated oven to another as the step cooling schedule dictated. Time at each of the steps was 120 minutes.

A *slow* cooling was also carried out. This consisted of heating films wrapped in Teflon and aluminum in a 120°C oven for fifteen minutes and turning off the oven to allow cooling at a rate of about 1 deg/min. Weight losses from slow coolings were less than 1.0%. From each treated film, a sample was removed for DSC, Rheovibron, and WAXS studies.

Figure 3.36 provides DSC traces for bulk step cooled and slow cooled DEHS40 and DBP40. As was found for the samples step cooled in the DSC, the traces for the bulk step cooled samples show multiple endotherms for both DEHS40 and DBP40. The DSC traces of the slow cooled samples show a gradual endothermic rise extending from above 120° to near room temperature. The respective damping curves are given in Figure 3.37 and compared with samples aged for about one month. They show the slow cooled samples having the narrowest curve and the one month-old samples having the broadest. WAXS patterns for the treated samples were very similar to those for untreated samples.

Based on the relatively constant heat of fusion values found for PVC, Illers (87) stated that isothermal annealing of rigid PVC does not create new amounts of crystallized material. The discrete DSC peaks produced through annealings were believed to represent a recrystallized fraction characterized by increased crystal size and crystal perfection. If this is true, then the "quenched" samples in this study would be

expected to have a minimal degree of crystalline perfection; although most of the primary crystallites have been melted, they have been given a very small amount of time for formation into what Juijn et al (84) termed "secondary" crystallinity. In the slow cooled samples, there would be an intermediate amount of crystallinity since the films were exposed to a range of temperatures between 120°C and room temperature. Finally, the highest crystalline order is then expected in the step cooled materials due to their exposure to discrete temperatures from 180°C down to room temperature.

In summary, it has been found that the broadest damping peak in all cases is that of a sample aged for 10 months at room temperature. This sample was annealed for the longest time at the lowest annealing temperature. Samples subjected to higher temperatures as part of quenching, step cooling, and slow cooling procedures, which might be expected to have greater or lesser amounts of crystalline order, in all cases showed a more narrow damping curve. However, the magnitudes of the changes observed in the damping curves are not large, and *one might conclude at this point that crystallinity or differences in crystallinity are not in themselves responsible for the contrasting breadths of the mechanical damping curves of DEHS-PVC and DBP-PVC.* This statement stands in conflict with Nakamura's (132) study of the viscoelastic properties of plasticized PVC containing up to 60 weight percent plasticizer. (This study was discussed in the Introduction.) However, as Nakamura did not investigate any other properties of the materials, the conclusion that maximimum crystallinity leads to maximum broadening was legitimate based on the available data.

The preceding work can be examined in a manner found useful in the previous section by considering the dispersion of the plasticizer. The argument there was that the plasticizer was dispersed more uniformly at higher temperatures. On this basis, the step cooled samples might be expected to show a more narrow damping curve than the slow cooled samples. This has not been observed, but may be rationalized as follows. The slow cooled samples, though they have not been taken to the high temperatures seen by the step cooled samples, most likely contain very small crystallites which do not substantially change the morphology of the PVC. Step cooled samples might be expected to have a higher number of fairly large crystallites and a more highly developed network structure which inhibits plasticizer dispersion, thus leading to a broader damping curve. Although not shown in Figure 3.37, the quenched films (see Figure 3.34) produced the most narrow damping peaks, thus behaving in accordance with this explanation since they have seen high temperatures but been given virtually no time for crystallization. Exposure to higher temperatures apparently "loosens" the PVC network to allow better dispersion of the plasticizer.

Although the author now believes that crystallinity is not *in itself* responsible for the large differences noted in the dynamic mechanical behavior of DEHS-PVC and DBP-PVC, it is still possible that the nature of the crystallinity in the two materials is not exactly the same. Recent work referred to in the Introduction which suggests that both fringed micelle and lamellar crystallites can exist in PVC prohibits one from sweeping aside the relevance of crystallinity on the basis of these

results. If the DBP-PVC network is formed differently than is DEHS-PVC's network due to contrasts in crystalline texture, then the dynamic mechanical properties of both materials may be influenced. However, the fact remains that these various thermal treatments did not induce any major changes in the observed dynamic mechanical behavior.

3.3.4. *Small-Angle X-Ray Scattering*

It has been emphasized throughout this chapter that the broadening of their respective dynamic mechanical curves suggests a greater level of heterogeneity for DEHS-PVC than for DBP-PVC. The simple light transmission experiment described in the Experimental section established that no heterogeneities on the order of a thousand Angstroms developed in DEHS40 as it was cooled down to temperatures near -95°C. Another technique was needed to look at smaller dimensions. Small-angle X-ray scattering (SAXS) has become a powerful analytical tool for studying phases with sizes of 20 to a few hundred Angstroms. These phases must be delineated from each other by differences in electron density since it is this difference that creates the contrast "seen" by a probing X-ray beam. Considering, in the simplest case, that PVC, DEHS, and DBP are the three possible phases contained in these materials, the knowledge that their respective electron densities are 0.4317, 0.3100, and 0.3395 electrons/A^3 indicates that an X-ray beam will be able to distinguish each of the two plasticizers from PVC. (These values are calculated in the Appendix.) Let us examine the information available from SAXS analysis likely to assist this investigation.

Experimental SAXS data must be corrected for instrumental and material effects before quantitative information can be extracted. The extent of these corrections depends upon the specific information desired, but generally involves four factors. *Monochromatization*, or elimination of all but the desired wavelength of radiation, can usually be accomplished with a metal foil filter or a "tunable" crystal monochromator. *Parasitic scattering*, due to the finite edges of the slit or pinhole and any other surfaces through which or along which the incident beam passes before being scattered, can be subtracted using a SAXS scan with no sample in place. In the irradiated sample, heterogeneity within an observed phase or thermal density fluctuations can give rise to *background scattering*. This can be eliminated using mathematical analyses such as those of Vonk, Ruland, and Bonart (148). If a slit geometry is used, the registered intensity of a single angle is actually "smeared" over several angles. Such data must be desmeared before certain quantitative information can be derived.

The peak in a curve of scattering intensity as a function of scattering angle 2θ is frequently referred to as the Bragg spacing of a system. As its label suggests, the Bragg spacing corresponds, through Bragg's law (138), to a "periodic characteristic distance" within a particular material. In plasticized PVC, the spacing implied by the Bragg peak is generally taken as the center-to-center distance between crystallites (149).

The invariant, Q, is an integral expression of the scattering curve (138):

$$Q = \int_0^\infty s^2 \, I(s) \, ds \qquad (6)$$

where $s = (2 \sin\theta)/\lambda$; λ is the wavelength of $K\alpha$ radiation, 1.54 A. From Equation (6) one can derive $<\rho^2>$, the mean electron density fluctuation. For a two-phase material where the two phases are themselves homogeneous and are separated by sharp boundaries, the value of $<\rho^2>$ can be written as in Equation (7)

$$<\rho^2> = \phi_1 \, \phi_2 \, (\rho_1 - \rho_2)^2 \qquad (7)$$

where ϕ_1 and ϕ_2 are the volume fractions of the two phases and ρ and ρ are their respective electron densities. Equation (7) may be extended to the case of three phases, themselves homogeneous and separated by sharp interfaces:

$$<\rho^2> = (\rho_1 - \rho_2)^2 \, \phi_1 \, \phi_2 \; + \; (\rho_1 - \rho_3)^2 \, \phi_1 \, \phi_3$$
$$\qquad (8)$$
$$+ \; (\rho_2 - \rho_3)^2 \, \phi_2 \, \phi_3$$

where ϕ_3 and ρ_3 are the volume fraction and electron density of the third phase. In real materials, interfaces are rarely "sharp" but usually have some finite dimension. To account for this situation, Khambatta et al (150) have modified Equation (7) for the case where a diffuse boundary separates two homogeneous phases:

$$\langle \rho^2 \rangle = (\rho_1 - \rho_2)^2 (\phi_1 \phi_2 - \phi_3/6) \tag{9}$$

where ϕ_3 is the volume fraction of the interphase. No explicit morphological assumptions are made through these relationships. In practice, they reflect only the extent of phase mixing based on comparison between measured and calculated values of $\langle \rho^2 \rangle$. That is, one can experimentally determine a measure of $\langle \rho^2 \rangle$ from Equation (6) and compare it in some way with values calculated from equations such as (7), (8), and (9) given above.

The correlation function provides information about the periodicity of phases within a system and therefore the extent of inhomogeneity (151). The one-dimensional correlation function is given in Equation (10)

$$\gamma(x) = \frac{\int_0^\infty I(s) \, s^2 \cos(2\pi sx) \, ds}{\int_0^\infty I(s) \, s^2 \, ds} \tag{10}$$

This function often shows a periodicity with the distance x. The value of x corresponding to the first peak in $\gamma(x)$ is called the correlation distance. It represents a characteristic distance in any nonhomogeneous material. Further information about the system can be gained from the three-dimensional correlation function given in Equation (11).

$$\gamma(r) = \frac{\int_0^\infty I(s) \, s^2 \sin(2\pi sr)/2 \; sr \, ds}{\int_0^\infty I(s) \, s^2 \, ds} \tag{11}$$

If $\gamma(r)$ is equal to 1.0, the scattering is said to be perfectly correlated and the material completely homogeneous. It is also possible for $\gamma(r)$ to show some periodicity. From $\gamma(r)$, one can learn the average size of all inhomogeneities having a size comparable to the wavelength of X rays, the randomness of domain placement, and other structural details. For further details, the reader may consult the previous references as well as Higgins and Stein (152) and Glatter and Kratky (153).

Published SAXS analyses of plasticized PVC have been limited primarily to milled and compression molded materials. As part of a series of studies of such materials, Gezovich and Geil (154) have shown SAXS curves for PVC plasticized with dioctyl phthalate (n-DOP). The plasticized samples were prepared by milling at 170° for five minutes. Unplasticized PVC was pressed at 190°C for five minutes. Experimental scattering curves from a slit X-ray scattering system were corrected for parasitic scattering and subjected to the Lorentz correction, which strictly speaking, should be applied only to a lamellar system. The data so obtained are provided in Figure 3.38. The angle of the Bragg peak is observed to decrease with increasing plasticizer content, indicating a larger interdomain spacing. The unplasticized PVC shows only a monotonic decrease in scattering intensity. Geil and co-workers (32,154) have observed by SEM that domains believed to be unfused primary particles of PVC swell with increasing plasticizer content and also move further apart. The suggestion has been made that the plasticizer is located primarily in the matrix surrounding these particles and swells the matrix, thus increasing the interdomain spacing. Swelling calculations by Summers (155) indicate that this interpretation may be valid.

Nielsen and Jabarin (156) studied unplasticized PVC using SAXS and found a strong influence of thermal treatment as well as orientation. To analyze their data, which did not contain a discrete SAXS peak, Nielsen and Jabarin used a Guinier approach from which one can determine the radius (or radii) of gyration of a system of particles of arbitrary shape. They detected two sizes of ordered regions, 500 A and 120 A (or less). The larger domains respond to orientation by elongating in the draw direction and decreasing in size transverse to the draw direction. Nielsen and Jabarin make no inferences about the nature of these two domains. The orientation exhibited by the larger domains is of interest in view of the SALS results discussed earlier. As was pointed out there, the rod-shaped SALS scatterers could have resulted from the non-spherical compression of ordered regions of the polymer particles.

Blundell (157) has shown that annealing PVC above its Tg apparently enhances its order such that a SAXS peak can be resolved, corresponding to a spacing of about 100 A. The data was interpreted by Blundell as indicative of a dispersion of "spherical crystalline nodules" in an amorphous matrix, as suggested by electron microscopy studies (158).

The SAXS study of solution cast PVC or highly plasticized PVC has been sparse. One of the few such papers is concerned with concepts that are quite relevant to the present study. Dorrestjin et al (149) conducted studies of gels containing 10% PVC in diethylhexyl phthalate

(DOP) and monitored changes in dynamic modulus and SAXS behavior as a result of annealing. Dynamic modulus values were found to increase with aging time at temperatures between -20° and 110°C. As aging progressed, the materials passed from a liquid-like to a rubber-like state. Scattering intensity as well as the invariant (see Equation (6)) of the gels increased with time. However, the intercrystallite spacing, as denoted by the Bragg peak position, did not change with aging time. Dorrestjin and co-authors attributed these changes to an increase in the number of "elastically effective chains" through the growth of existing crystallites rather than the development of new ones. On the basis of an unchanging intercrystallite spacing with aging time, Dorrestjin et al concluded that the location and number of crystallites are essentially constant. This last point was encountered earlier in this chapter with regard to the DSC results of Garrett and Goldfarb (92).

The SAXS portion of this study was limited to 40, 60, and 75 weight percents. All of these samples were prepared by the standard method and therefore not subjected to any treatment for the removal of residual solvent. All were aged at room temperature for the same length of time. Their scattering curves were obtained at ORNL as described earlier. Data from a Kratky slit SAXS system were obtained for comparative purposes only.

Data obtained at ORNL was treated for background scattering according to the method of Bonart (148). Bonart's correction consists of plotting $s^4 I(s)$ vs. s^4, and the obtained slope (see Figure 3.39) is subtracted uniformly from each intensity value. This treatment assumes

that the data is desmeared; pinhole collimation produces a finite but very small amount of smearing. Exact determination of $<\rho^2>$ requires conversion of the experimental intensity to absolute intensity through some known standard such as Lupolen polyethylene (148,159). While this conversion was not possible because of insufficient data, a value could be obtained that was proportional to $<\rho^2>$. Experimental measurements based on Q (Equation (6)) were ratioed to the Q values from the corresponding 40% plasticizer samples. Values calculated from the ideal two-phase model of Equation (7) were also ratioed to the respective 40% plasticizer values. The Appendix gives details on the manipulation of all of the SAXS data presented in this chapter.

The angular dependence of the scattered intensity is shown in Figure 3.40 as a function of plasticizer type and content. A maximum in intensity is seen for all the samples examined. The spacings as calculated from Bragg's law are listed in Table 3.5 and are seen to change very little with increasing plasticizer content, with the exception of DEHS75. Experimental scattering curves from the Kratky SAXS system (not shown) generally showed a decrease in the angle of the Bragg peak with increasing plasticizer content, however, without the proper corrections (as discussed earlier), it is difficult to draw any definite conclusions from the Kratky data. Several attempts were made to discern a SAXS peak from a sample containing no plasticizer. Samples examined by the Kratky included a thin (6 mil) solution cast film dried for several hours near 100°C under vacuum. Another sample consisted of a stack of several films (total ~ 3 mil thick) prepared by drawing a THF solution of PVC with a doctor's blade. Neither showed a reproducible maximum in the SAXS curve.

The correlation distances obtained from the peaks of the first maxima of the one-dimensional correlation functions are given in Table 3.5 for the six plasticized materials studied at ORNL. As with the Bragg spacings, there is little change in the correlation distance with increasing plasticizer content. The only sizable increase is again found between DEHS60 and DEHS75. The three-dimensional correlation functions, $\gamma(r)$, are given in Figure 3.41. These are very similar for all six materials. Their form indicates that the materials examined possess a small amount of order.

The initial slope of $\gamma(r)$ may often be related by Equation (12)

$$\gamma(r) = \exp(-r/l_p) \tag{12}$$

to the inhomogeneity length, l_p, which represents the average size of any system inhomogeneity in a two-phase system. Application of Equation (12) to the three-dimensional correlation functions shown in Figure 40 gives l_p values of 2.8, 2.7, and 3.5 nm for DEHS40, 60, and 75 and values of 2.6, 2.5, and 2.4 nm for DBP40, 60, and 75. As in the case of the Bragg spacing and the correlation distance, the l_p value for DEHS75 is larger than that for all other samples. Unlike the Bragg spacing and the correlation distance, the inhomogeneity length measures the average dimension across (or through) all inhomogeneities. It therefore reflects the size of both correlated and non-correlated structures in the material.

The calculated and experimental $<\rho^2>$ ratios are plotted in Figure 3.42 as a function of plasticizer content for DBP-PVC and DEHS-PVC. The DBP60, DBP75, and DEHS60 ratios hold fairly closely to the ratios for the calculated values, indicating that whatever the extent of phase mixing, it is similar for these three compositions. Once more substantial deviation is seen for DEHS75, its undeniably larger ratio suggesting that it probably possesses a higher degree of phase separation than the other three materials.

Taken as a whole, these semi-quantitative SAXS data suggest no significant difference between the 40 and 60% systems; one can assume that they are mixed equally well and possess similar order to their structures. It is noted, however, that Bragg spacings, correlation distances, and inhomogeneity lengths of DEHS-PVC are consistently larger than those of DBP-PVC. Although DEHS75 shows relatively large increases in these dimensions, of more interest here would be differences between the 40 and 60% materials. One must remember that these data may not necessarily reflect the extent of plasticizer/polymer mixing that may exist or develop upon cooling to lower temperatures. In other words, any of the quantities estimated here may be temperature dependent.

It is somewhat surprising that these data indicate a larger distance between crystallites in DEHS-PVC. Having shown that DBP is a better solvent for PVC than DEHS, one would expect that fewer crystallites would develop in DBP-PVC and thus yield a larger intercrystallite

distance than similar DEHS-PVC materials for the same amount of polymer. However, DBP's greater solvent power may act to inhibit growth of crystalline material rather than its nucleation.

3.3.5. *Comparative Study of Six Plasticizers*

Midway through the work described in the preceding pages, it became clear that any conclusions that might be drawn regarding the effects of DEHS and DBP on PVC could certainly be studied with other plasticizers. Several plasticizers were chosen for this second study. Criteria consisted almost entirely of structure and solubility parameter. Figure 3.20 illustrates the plasticizers chosen for this work. Diethylhexyl phthalate (DOP) and dibutyl succinate (DBSu) were chosen from a structural point of view. DBSu, DOP, DEHS, and DBP comprise a complete permutation of the phthalic and succinic acid "roots" as well as 2-ethylhexyl and butyl side chains. A range of solubility parameters between DEHS and DBP is also realized with these choices. Two additional choices, dipropyl phthalate (DPP) and dibutyl sebacate (DBSe) round out the set in terms of solubility parameters.

Considerable effort has been given towards measurement, calculation, and compilation of solubility parameters and similar measures of the relative solubility between low molecular weight and polymeric components. These concepts are particularly important to the coatings industry as well as the fabricators of plasticized vinyl chloride polymers and copolymers. One can often directly measure some of these quantities, but it has become common to calculate solubility parameters from chemical

structure and various easily obtained physical properties. (An example will be given shortly.) The values obtained can serve as at least a first approximation in many cases. In fact, for polymer-polymer blends, they are often the only convenient method of estimating relative miscibilities prior to synthesis and blending.

The first widely used method of estimating solubility parameters was that of Small (160). It consists of adding together the molar attraction constants for each group in the low molecular weight substance (or the polymer monomeric unit) and dividing by the molar volume. An example of the calculation for DBP is given below.
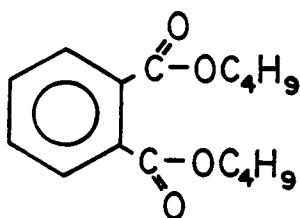
DBP

1 Phenylene (658) = 658
2 COO (310)   = 620
6 methylene (133) = 798
2 methyl (214)   = 428

ΣF = 2504

$$\delta = \frac{\Sigma F}{MW/density} = \frac{2504}{278.35/1.0462} = 9.41 \ (cal/cc)^{1/2}$$

Sears and Darby (13) give appropriate examples of the application of the method along with a listing of the group molar attraction constants. Small's molar attraction constants were later revised by Hoy (161) through extensive measurements of vapor pressures. Van Krevelen (162) lists comparative tables for application of Small's and Hoy's methods along with a third method devised by himself (162).

One of the drawbacks of the *single* solubility parameter is its inapplicability to polar and hydrogen-bonding substances. Using a single solubility parameter, for example, one would not predict the solubility of PVC in THF or cyclohexanone. The work of Hansen (163) and Crowley, Teague, and Lowe (164) introduced the use of three-dimensional solubility parameters whereby separate parameters are applied to dispersion forces, polar attractions, and hydrogen bonding. While they may be helpful in many applications, such elaborate schemes are usually not needed for PVC and diester plasticizers.

Dielectric constants were proposed as a measurement of solubility by Darby, Touchette, and Sears (144) with emphasis on PVC and plasticizers. They have tabulated many values, and additional values are easily obtained with a dielectric spectrometer.

Refractive index has been utilized in calculations of solubility parameters (165). Like the dielectric constant, this measure of solubility relates the polarizability of a liquid to its ability to interact with a polymer. The calculation is derived from the Lorenz-Lorentz equation, but in final form is partly empirical due to the absence of a universal constant. Lawson and Ingham (165) suggest the use of either of two equations. The first (Equation (13)) utilizes a fixed constant, 30.3, and may be applied to any compound:

$$\delta \sim 30.3 \left(\frac{n^2 - 1}{n^2 + 2} \right) \qquad (13)$$

where n is the refractive index. A second equation, given below, uses a constant that is chosen on the basis of the structural class into which the plasticizer falls. For aliphatic esters, the constant C is 353.3 +/- 30.9.

$$\delta \sim C\left(\frac{n^2 - 1}{n^2 + 2}\right)^{1/2} \tag{14}$$

Solubility parameters calculated with refractive indices tend to be lower than those calculated by other means, as will be seen later. Sears and Darby (13) comment on the use of refractive index itself as an index of solubility; a minimum value of 1.5 generally indicates borderline solubility while a value of 1.6 usually indicates "actual" solubility.

Experimental determinations of solubility include those of Doty and Zable (6) and Walter (11) discussed in the Introduction. More recently, Anagnostopoulos, Coran, and Gamrath (145,166-7) have introduced the "microtest for compatibility" which involves placing on the hot stage of an optical microscope a few grains of PVC in a small pool of the liquid of interest and recording the temperature at which the interface between the particles and the plasticizer becomes visually diffuse. Crude application of Flory's equation for melting point depression (9) (Equation (5)) allows one to calculate x, the interaction parameter. Several other means of experimentally determining solvent or plasticizer solubility have been proposed. These include interaction parameters derived from viscosity data (168), viscosity itself (14), and solubility parameters derived from surface tension values (169).

Table 3.6 lists pertinent physical properties of the six chosen plasticizers. Table 3.7 gives various measures of solubility following from the preceding discussion. Attention to this tabulation points up the strong solubility of DBP with PVC as compared to four of the remaining plasticizers, DPP abstaining. DBP has a higher solubility parameter regardless of the method of calculation, a lower x value from the microtest for compatibility, a higher dielectric constant, and a higher slope in a log modulus-log concentration curve. DEHS, on the other hand, shows the lowest solubility parameter using molar attraction constants (but not using refractive indices), the lowest dielectric constant, and the lowest slope using Walter's method. No trend is seen for either molar volume or molecular weight although density seems to increase with solubility parameter. While data for DPP is more limited, the information in Table 3.7 indicates that it would be equally if not more soluble with PVC than DBP.

The influence of solubility on the broadening of the dynamic mechanical spectrum has been alluded to by several authors (2,3,19,124,127,128,129,132), but only one paper that might be described as a systematic study (127) has actually been published. Figure 3.43 shows how the degree of solubility -- as denoted by solubility parameter -- translates to dynamic mechanical behavior for PVC plasticized with each of the 6 chosen plasticizers. Weight percents for each of the 6 series are 10, 40, and 60. It is immediately clear that decreasing the solubility parameter of the plasticizer promotes greater broadening in the curves at 40 weight percent plasticizer. The curves

for materials containing 60% plasticizer are generally narrower than those corresponding to 40% plasticizer content.

Some unusual features appear in the DBSu-PVC and DBSe-PVC curves. At 40% plasticizer content, their damping curves exhibit a low shoulder both above and below the main transition. DBSu60 exhibits a narrow damping peak at approximately the same temperature as the lower temperature shoulder of the 40% curve. However, the damping curve for DBSe60 consists of a rather weak peak about 15°C below that of the 40% material. The irregularities seen in these damping peaks result from the fact that both DBSe and DBSu can crystallize. In neat form, each exhibits a melting point, as shown by DSC scans given in Figure 3.44. DBSe demonstrates no apparent Tg and no recrystallization endotherm. One must presume that it crystallizes completely and spontaneously upon cooling. DSC traces for neat DBSu show incomplete crystallization as indicated by a weak Tg at -111°C.

In Figure 3.45 are provided DSC scans (second runs) for the DBSe and DBSu 40 and 60% materials. There was no substantial difference between the first and second scans of these materials except that the first scans showed a small crystallization endotherm above room temperature which does not appear in the second scans. The DSC trace of DBSe60 given in Figure 3.45 indicates a gross phase separation, exhibiting what may be a Tg of about -77°C and a fairly sharp crystalline melting point at about -30°C, lower than the -12°C found for the neat plasticizer. What might be a recrystallization exotherm for the neat plasticizer is observed near -50°C. The DSC scan for DBSu60 indicates relatively "normal" DSC behavior.

It is common practice to compound flexible PVC using more than one plasticizer, usually for economic reasons but often to obtain special properties, such as low-temperature flexibility, in addition to the more general effects of plasticization. For a two-component plasticizer, the solubility parameter can be calculated (170) as in Equation (15)

$$\delta(\text{mixture}) = \phi_1 \delta_1 + \phi_2 \delta_2 \tag{15}$$

where ϕ_1 and ϕ_2 are the respective volume fractions of the two plasticizers. According to Equation (15), an equimolar mixture of DBP and DEHS (to be called DEHS/DBP) has a solubility parameter of 8.87. Damping curves for PVC plasticized with such a mixture at 40 and 60 weight percent are shown in Figure 3.46 and compared with the corresponding DEHS-PVC and DBP-PVC compositions. As expected, the damping curves for the DEHS/DBP compositions are broader than those of DBP-PVC but more narrow than those of the DEHS-PVC compositions. The Tg of DEHS/DBP60 lies clearly between those of DBP60 and DEHS60, as indicated by the peak temperatures of the respective damping peaks.

This comparative study of several plasticizers has demonstrated the effects of plasticizer solubility on the dynamic mechanical behavior of plasticized PVC in a much more straightforward form than is presently available (127). The data presented in this section illustrate that the breadths of the damping curves for PVC undeniably broaden at 40% plasticizer content to an extent that is directly correlated with the difference in the solubility parameters between PVC and the plasticizer.

Increasing plasticizer content to 60% induces a narrowing of the curves. This effect has also been demonstrated with a plasticized PVC containing an equimolar mixture of an aromatic and aliphatic ester for which a "composite" solubility parameter can be calculated (see Equation (15)). This result is particularly important as most commercial plasticized PVC contains a mixture of plasticizers. Furthermore, the behavior shown follows not only the trends predicted on the basis of solubility parameter but agrees quite well with several other measures of solubility (see Table 3.7). In the next section, the concept of solubility will be extended to the static mechanical properties of plasticized PVC.

3.3.6. *Effects on Static Mechanical Properties*

Plasticized PVC owes its unusual mechanical properties to its ability to form a cohesive network while imbibed with substantial amounts of plasticizers. This network is believed to be held together by small crystallites, which resist solvation such that the elastomeric qualities of the network are retained at high plasticizer contents. The remainder of this section empirically treats plasticized PVC as a network in which the greater solubility of one plasticizer over another may manifest itself.

Although it is theoretically incorrect to apply the theories of rubber elasticity to these materials, such application is useful in a rough estimate of the "apparent molecular weight" between network junction points. From the work of Flory, Rabjohn, and Schaffer (171) comes Equation (16)

$$\frac{\sigma}{\lambda - 1/\lambda^2} = \frac{RT}{V_u M_j} \left(1 - \frac{2 M_j}{M_n} \right) \nu^{1/3} \qquad (16)$$

where σ is the equilibrium engineering stress, λ is the draw ratio (L/L_0), R is the natural gas constant, T is the temperature, V_u is the specific volume of the polymer, M_n is the number average molecular weight, and ν is the volume fraction of polymer. A plot of equilibrium stress versus ($\lambda - 1/\lambda^2$) should yield a straight line from whose slope one can derive M_j, the molecular weight between junction points.

Films containing 40 or 60% of each sample were prepared by standard casting methods and aged for four weeks at room temperature. A fresh dog-bone specimen of each sample film was used to obtain the stress following 30 minutes of relaxation at a fixed draw ratio. The use of a 30-minute stress to approximate the equilibrium stress has been suggested by Patterson, Padgett, and Peppas (173). Limited stress relaxation experiments carried out to longer times (see, for example, Figure 3.47) illustrate that DBP40 reaches a lower stress than DEHS40 following relaxation for nearly 24 hours, but the stress after 30 minutes shows the same relative difference.

As per Equation (16), the "equilibrium" stress was plotted versus ($\lambda - 1/\lambda^2$) for each sample. Examples for DEHS40 and DBP40 are given in Figure 3.48. The scatter of the data is typical for the 40% samples, but the low load deflection for the 60% materials introduced somewhat more error into the measurements. Two lines were drawn through each set of

points, as shown in the figure. The longer solid lines, which pass through zero, were drawn in by hand as the best visual fits including (0,0). The shorter dotted lines were calculated using linear regression without including (0,0) as a data point. For application of Equation (16), Mn and density of the PVC have been taken to be equal to $5.6(10^4)$ g/mol and 1.4 g/cc, respectively.

The Mj values obtained from the slopes of the "calculated" lines are plotted in Figure 3.49 as a function of solubility parameter. Similar results were found for the lines obtained by visual analysis. Although the six points of each graph do not show any particular trend, other than the fact that Mj generally increases with solubility parameter, it is seen that separating the phthalate and aliphatic diester plasticizers into two groups allows a linear relationship to be established for each group. The higher slope of the line drawn for the succinate and sebacate plasticizers indicates a sharper drop of Mj with decreasing solubility parameter.

These results therefore suggest that increasing the solubility of the plasticizer with PVC dissuades more chains from becoming part of the PVC network. The more soluble plasticizers very likely inhibit the crystallization which leads to the formation of network junction points. These results say nothing about the distribution of Mj.

It was noted during this investigation that DBP40 could display a stress-strain response such as that illustrated in Figure 3.50. After the completion of the annealing and stress-relaxation studies that have

already been described, a short study of the stress-strain behavior of DEHS-PVC and DBP-PVC at 40 and 60% plasticizer levels was conducted to join these earlier pieces of work. One set of samples was examined after seven months of aging at room temperature. Sections of these same films were annealed at 120°C for 3 hours. Recall that the sharpest endotherm induced in the DSC-annealing studies resulted from annealing at 120°C. The jar containment system used with earlier bulk annealing studies was again employed to minimize plasticizer loss. The samples were slowly cooled to room temperature after the annealing and subjected to stress-strain tests 24 hours later.

The results of those tests are shown in Figures 3.51a and 3.51b. Each of the two sets of stress-strain curves refers to annealed and unannealed samples of PVC containing either 40% (3.51a) or 60% (3.51b) of DEHS or DBP. The first item to be noted is the weak upturn in stress near 250% strain exhibited by DBP40 after room temperature aging. Upon annealing at 120°C, this feature no longer appears as the curve shows a very gradual change in slope before entering a linear region from which no upturn in stress occurs. In general, annealing either 40% or 60% materials at 120°C lowered the modulus and imparted greater linearity to the stress-strain curves. This linearization is particularly marked for DEHS-PVC.

The reduction in modulus with the 120° annealing suggests that the number of "crosslinks" has been reduced, most likely through melting and recrystallization, so that the crystalline crosslinks incorporate fewer network chains. The molecular weight between crosslinks would be

expected to increase, however, no data supporting this speculation is presently available. Modulus of PVC gels has been found to increase with annealing time at a constant temperature (91,149,173). Without the factor of time, it is difficult to further assess this particular aspect of the data of Figure 3.51.

The change in shape of the stress-strain curves with the 120° annealing is the most striking feature of Figure 3.51. One will recall from earlier discussions of the proposed two-crystal texture of oriented PVC films that Tasumi and Shimanouchi (75) found that the dichroic ratios of certain bonds in PVC reversed themselves near a 2.5 draw ratio (150% strain). Interestingly, this is the region of the stress-strain curve of unannealed DBP40 in which a weak change in slope occurs to be followed by an upturn in stress near 300% strain. This latter feature is usually indicative of strain-induced crystallization in crosslinked elastomers.

The fact that DBP40 showed this upturn in stress while DEHS40 did not suggests that the network structures of the two materials are indeed different in some respect. Furthermore, it has been noted in stress-strain tests of plasticized PVC films aged for random times at room temperature that the trend toward the type of behavior shown by unannealed DBP40 is greater with increasing solubility of the plasticizer in PVC. To address this latter point, WAXS patterns were taken of oriented DPP40, DBP40, DOP40, and DEHS40 extended to draw ratios of 4.0 and 5.0. It is at these draw ratios where changes first became evident in the WAXS patterns of DEHS40 and DBP40. The WAXS

patterns obtained are given in Figures 3.52a and 3.52b for $\lambda = 4.0$ and $\lambda = 5.0$, respectively. Although the amorphous scattering is strong in these patterns, one can still discern a fairly fine meridional reflection in the patterns. Close inspection suggests that the reflection in question -- the same one which Guerrero et al (74) claim as evidence of a lamellar crystal -- is strongest in DPP and weakens as one moves down in solvent power to DBP, DOP, and finally DEHS. As the intensity and sharpness of the meridional reflection is lost, a greater intensity is seen in the equatorial regions of the WAXS patterns. These observations in themselves are interesting as WAXS studies of oriented PVC containing intermediate amounts of plasticizer have not yet been reported in the literature.

Annealing at 120°C was shown in Figure 3.51a to radically alter the stress-strain properties of DEHS40 and, in particular, DBP40. Significant changes are also shown in the WAXS patterns of oriented and annealed DBP40 and DEHS40, as shown in Figure 3.53. After the 120°C annealing, the sharp meridional reflection is no longer evident in DBP40 at a draw ratio of 5.0 and is weak and diffuse in DEHS40. Further, the equatorial reflections have become stronger, especially for DBP40. The WAXS patterns of the unoriented 120°C annealed films presented no definite changes from those of the untreated films.

It was not the objective of this research to delve into the precise identification of the crystalline textures of plasticized PVC. However, the results presented in Figures 3.51-3.53 expose several unexplored areas, a few of which will be mentioned here. First, the results

(unsurprisingly) suggest that the network structure of plasticized PVC is greatly affected by both thermal history and plasticizer, type. Developments presented here indicated that while plasticizer type *is* an important factor in the dynamic mechanical properties of these materials, thermal history *is not*. One is thus led to the belief that it may be the plasticizer alone which most seriously affects PVC's dynamic mechanical properties. Second, the data indicate that the observed meridional reflection (located here at about 5.25 A) arises from a structure which is integrally involved with the deformation of the plasticized PVC network; hence, the suggestion (74) that the proposed lamellar crystals are not connected to the PVC network is in doubt. And third, it is indeed curious that in the case of DBP40, the disappearance of the meridional reflection is coincident with the loss of the stress upturn in the stress-strain curve. This point suggests that the meridional reflection may result from strain-induced crystallizaton.

3.3.7. *Network Structures of Plasticized PVC*

At this point, three separate observations need to be reconciled. It was shown earlier by SAXS that the intercrystallite spacing did not change substantially between 40 and 60% plasticizer content. It was shown by WAXS and supported by DSC that the crystallinity present in DBP60 and DEHS60 is far less than that in DBP40 and DEHS40. Finally, the analysis just presented suggested that the molecular weight between effective crosslinks is found to increase about three times when plasticizer content is raised from 40 to 60%.

The observed decrease in apparent crystallinity and the increase in Mj with increasing plasticizer content are quite consistent with each other. The essentially unchanging intercrystallite spacing which is implied by the SAXS results is not, at first glance, in agreement with either of the other two experimental results. Nor does it agree with the findings of, for example, Geil and associates (154,158) and Shtarkman et al (174) who found that the Bragg peak of plasticized PVC moved to lower angle (larger spacings) as plasticizer content was lowered. However, their samples were melt processed, and in such materials, the increase in the Bragg spacing is believed to reflect the swelling of the connective matrix in which unfused PVC grains are embedded. If a solution cast PVC is swollen with additional plasticizer, one would also expect the crystalline crosslinks to spread apart.

The samples studied here were not prepared in that way. They are not preformed networks swollen with greater and greater amounts of plasticizer. Instead, they are networks formed from solubilized PVC chains which have formed networks in the presence of greater and greater amounts of plasticizer. In other words, the network is newly formed every time, the only constant factors being the polymer itself and the approximate volume of the casting solution. This distinction is drawn in order to bring out the fact that it may not be entirely correct to assume that the structure of a plasticized PVC sample originally containing 60% plasticizer is identical to that of a 40% sample swollen with sufficient plasticizer to bring it to 60% plasticizer content. At the very least, this concept may be an oversimplification.

The three observations concerning Mj, crystallinity, and the intercrystallite spacing will for the moment be considered apart from dynamic mechanical results. The three principal observations will be evaluated in terms of the possible network structures of plasticized PVC. Much of this discussion will by necessity be hypothetical, but this is unavoidable.

As a first possibility, consider the suggestion by Yang and Geil (175) that PVC/solvent gels containing 10% or less PVC by weight consist of a network stabilized by entanglements with intermolecular hydrogen bonding. It is doubtful that this type of network realistically describes a moderately plasticized PVC, but it is introduced here for the sake of completeness. In deriving their model, Yang and Geil (175) utilized the Ferry-Eldridge equation, which initially *assumes* two chains per crosslink point (176), to *deduce* that their gels contained two chains per crosslink point. Harrison, Morgan, and Park (176) have pointed out a few of the pitfalls of the Ferry-Eldridge approach. Although Yang and Geil (175) acknowledge the formation of crystals in their gels, they postulate that the growth of crystals occurs *after* the gel has formed.

On the basis of this morphology, assume for this first case that plasticized PVC actually contains very few *network forming* fringed micelle crystallites and is stabilized primarily by molecular entanglements, as suggested by Yang and Geil. The molecular weight between crosslinks will go up with increasing plasticizer content as it becomes easier for chain *dis*entanglement. The small degree of micellar

crystallinity will fall dramatically simply by virtue of a dilution effect. However, the experimental observation of an unchanging intercrystallite spacing is at odds with this model because, if present in only small amounts (175), the dissolution of only a few micellar crystallites would in fact be expected to shift the Bragg peak to lower angles to be interpreted as a larger intercrystallite spacing. The Bragg peak, however, requires only that some *structure* be packed regularly so that the Bragg condition is met. These structures do not necessarily have to be crystalline, but even if chain entanglements give rise to the SAXS peak, the destruction of these by greater amounts of plasticizer will also be expected to result in a shift of the Bragg peak. However, the electron density of a chain entanglement involving only two chains cannot be expected to be different from the surrounding environment, so it is highly doubtful that entanglements can give rise to the discrete scattering peak observed in SAXS. It must be remembered that the relatively intense reflections seen in the WAXS patterns of 40% samples indicate that the degree of crystallinity of their polymer component is not insignificant. One could thus vary this first model to include a higher percent crystallinity at 40% plasticizer content. However, in adherence to the model, the crystalline moieties would be structurally removed from the network and the crosslinks would arise almost exclusively from molecular entanglements.

The aforementioned view can be rejected or accepted for a number of reasons. Any entanglement which is comprised of only two polymer chains must link very stiff chains or the network will collapse. However, PVC gels are soft and mobile and so the PVC network chains might be

assumed to deform along with the solvent or plasticizer. If the network is held together tightly enough to prohibit chain disentanglement, then the network must be rather hard, and this is not observed. However, if the entanglements are like sliding knots, deforming the network could cause the "knots" to slide to various positions along the chain. There are, unfortunately, frictional forces to be overcome in "sliding" chains over each other, making this deformation mechanism somewhat difficult to accept. The deformability of a PVC gel is certainly better understood if the crosslinks are considered to be crystallites which link still flexible PVC chains, therefore, this author is inclined to put aside the notion of molecular entanglements as the principal crosslinks of plasticized PVC as a model of the materials considered here. The author will not argue whether it adequately describes the mechanical properties of a PVC gel containing less than 10% PVC.

Next consider the popular concept of the network crosslinked by fringed micelle crystallites as illustrated in Figure 3.54. Based on the available WAXS data, one might assume that at 40% plasticizer content, there are numerous fringed micelle crystallites which incorporate crystallizable segments from a number of different PVC chains. For the sake of agreement with the observed SAXS results, assume for the time being that when the plasticizer content is increased to 60%, the location of the crosslinks remains the same as before, but the number of chains included in each one is much lower. It is reasonable to assume that any given chain will still remain attached to the network, but now at fewer points, having been "disconnected" from other points. Thus in moving from 40 to 60% plasticizer content, the number of elastically effective

chains is lower as is the crystallinity while the distance between crystallites has changed very little. If, in fact, the view of a 60% sample as a swollen 40% sample is valid, the intercrystallite spacing must change, unless those chains which are removed from the larger crystallites somehow reform smaller crystallites spaced between the sites of the originally larger crystallites.

The third possible model requires the postulation of two co-existing crystalline textures, one being a fringed micelle and the other being lamellar. Figure 3.55 illustrates this third case; it is quite similar to that given by Keller, Geil, and co-workers (74). The plasticized network structure is established by fringed micelle crystallites which gather in several chains to establish a crosslink. Interspersed in the amorphous regions of the system are lamellar crystallites characterized by chain folds, leading to Biais and co-workers' use of the term "ribbon-like" crystals (67). The intercrystallite spacing seen by SAXS in this case may be an average of the distances between both types of crystallites but only if they are approximately equidistant. Otherwise, two separate Bragg peaks might be observed. If, however, the crystallites are very randomly dispersed, no distinct Bragg peak will be observed. Of course, it is possible that one crystal form could be regularly spaced while the other is randomly placed.

SAXS studies of neat PVC carried out by Nielsen and Jabarin (156), which were discussed earlier, provided evidence that two distinct ranges of domain sizes exist in neat PVC, one about 500 A and another about 120 A or less. If these two types of domains were also found in plasticized

PVC, their SAXS behavior might conform in part to the model described above.

Upon addition of more plasticizer to the network described above, the fringed micellar crystallite crosslinks will be spread further apart; this will result in an increase in the molecular weight between network junction points. However, the incongruity of an unchanging intercrystallite spacing is not resolved by this model unless, as with the second model, the network is assumed to contain a number of "reformed" crystallites.

A fourth alternative is available unless one adheres scrupulously to the adjacent re-entry chain folding model of a lamellar crystallite. Specifically, any chain entering a folded lamellar structure can just as easily enter a micellar structure and vice versa. Likewise, either type of crystal will contain crystallized segments of a number of different chains. Thus both lamellar and micellar crystals may act as crosslinks for the pseudo-network. However, it has been suggested (45,74) that the lamellar crystallites are either loosely connected or entirely unconnected to the network and therefore would not expected to be a dominant source of crystallite crosslinks. If this is true, this fourth model is reduced to the third. Keller et al (45,74) give no solid evidence for this lack of connectivity. Their statement appears to be an intrinsic result of their postulation that the a-axes of the proposed lamellar crystallites orient with the draw direction. Their ability to orient in this way evidently suggested that the lamellar crystallites are not "held" to the network (177).

If, however, it is assumed that lamellar crystallites can act as network junction points, then the observed increase in Mj and decrease in crystallinity as well as the observed lack of change in the intercrystallite spacing will be explained as in the first and third models. But where in this *fourth* model do the lamellar crystals fit? Within the scope of the study at hand, it must be assumed that they would act much like the fringed micelle crystallites in holding the network together. Indeed the results of the preliminary studies of oriented plasticized films discussed earlier suggest that the lamellar crystallites are intimately involved with the PVC network. That data implied that the proposed lamellar crystallites substantially influence the static mechanical properties of plasticized PVC.

None of these four models can be confidently accepted, primarily because they do not easily explain the unchanging SAXS spacing. The suggestion of a "reformed" network joined by crystallite crosslinks gives the second, third, and fourth models some corroboration with all three of the critical experimental observations. This reformation rests on the supposition that a 60% plasticized PVC is equivalent to a *swollen* 40% plasticized PVC. Without acceptance of this idea, the present idea of a "reformed" network lacks solid agreement with the observed increase in Mj. This concept may, however, be modified to include a network reformed *during the stress relaxation experiments*. The modification, while purely hypothetical, accounts for the fact that the number of elastically effective network chains must be reduced upon adding 60% plasticizer rather than 40% while the intercrystallite spacing is maintained.

Let it be assumed that the size of the crystallites in the 60% network is very small, as is suggested by the diffuse WAXS reflections obtained from 60% samples. It is very likely that these crystallites are comprised of only a few chains. If a plasticized PVC containing equidistantly spaced crystallites is placed under a fixed elongation, those crystallites which are only weakly connected to the network may well fail under the stress. They are consequently disconnected from the network, effectively increasing the molecular weight between junction points. Even if many of the crystallites lost only one chain, this could still increase the molecular weight between crystallite crosslinks. For example, consider a PVC chain which is joined to the network at three points, that is, it contains three segments which are part of network crystallites and two uncrystallized segments which comprise two *network* chains. If the middle segment is disconnected from its crystallite, the molecular weight between the two remaining crystallized segments will now be equal to the sum of the molecular weights of the two original network chains.

By the fifth model, the equal distance between network bonding crystallites in the undeformed state is not maintained upon deformation. But the SAXS results were taken from undeformed networks, which would still show an unchanging crystallite spacing. One might then suggest that SAXS be used to find if the intercrystallite spacing has changed upon deformation, but this assumes that the "disconnected" crystallizable segments will not recrystallize. This may be expected to happen to some extent, however, it is not likely that these crystallites will support any stress since they have been formed from "relaxed" chains.

A final and sixth model may also be considered; its basic features are generally illustrated in Figure 3.56. The crystallites occur in small pockets and are surrounded by an amorphous matrix which is rich in plasticizer at high plasticizer content. At both 40% and 60% plasticizer content, the crystallites are spaced equally, but the pockets in which they are located are not spaced equally. The pockets are located *randomly* in the matrix and form what are in actuality the physical crosslinks of the system. A stress relaxation experiment will measure the molecular weight of the chains *between* but not within the pockets, and SAXS will measure the regular spacing between the crystallites within the pockets but not measure a discrete spacing for the crystallite pockets. It would be necessary for these pockets to contain only a few crystallites in order to establish a regular spacing.

This sixth model does not require acceptance of the swelling concept elaborated upon previously. It does ask that the crystallites be regularly spaced within small regions, and so one must identify a driving force for the spacing beteen crystallites to be independent of plasticizer content. It is thus perhaps useful to consider that when crystallization occurs, it will very likely occur randomly, nucleated by dust, surface irregularities of the casting block, minute PVC aggregates, and various impurities, such as the suspension "skin." Once one stable crystallite is formed, it may provide a site for further crystallization because of decreased chain mobility in its immediate vicinity. As it develops, this process enriches the matrix with plasticizer and lessens the chances of nucleation of crystallites within it.

This model possesses one advantage over the second, third, fourth, and perhaps fifth models. It very clearly explains how a plasticized PVC network of very low crystallinity can remain intact. Instead of crystallites occurring at random within the PVC, they occur in clusters and each reinforces those nearby so that the strength of each crosslink is not that of a single fringed micelle crystallite but is equivalent to the collective strength of two or more.

The model can accommodate a lamellar crystallite. If located in the region immediately surrounding the fringed micelle crystallite pockets, lamellar crystallites would further reinforce the system's crosslinks. For the simplest case, it must be assumed that these lamellae would be dispersed randomly in the plasticized PVC.

Let us review the salient features of each of the six models. The first model described is that in which crystallinity may exist but is not responsible for network formation; physical crosslinks are formed by chain entanglements. The second, third, and fourth models propose that plasticized PVC is a network in which individual crystallites form physical crosslinks. The second model views fringed micelle crystallites as the sole crystalline moiety and thus the sole source of crosslinks. The third model considers that lamellar crystallites may exist with fringed micelle crystallites but that only the latter type of crystallites comprise the crosslinks. Finally, in the fourth model, both fringed micelle and lamellar crystallites act as network crosslinks. In order for any of these three particular models to achieve complete agreement with

the observations of decreased crystallinity, increasing Mj, and an unchanging Bragg spacing, it has been necessary to postulate that plasticized PVC containing 60% plasticizer is equivalent to a 40% plasticized PVC which is swollen with an additional 20% plasticizer. One must further accept that such a network has an unchanging intercrystallite spacing because the greater mobility of the amorphous chains in a 60% plasticized PVC *disconnects* some of the crystallized chains from the larger crystallites of the 40% plasticized PVC. These freed chains now recrystallize in between the main crystallites so that the intercrystallite spacing is constant. If this condition cannot be met, then a fifth model has been proposed. Namely, a plasticized PVC with a fixed intercrystallite spacing (40 or 60% plasticizer) is placed under a fixed elongation, and those dispersed crystallites which cannot sustain the imposed stress will either disintegrate or, at the least, lose a few chains. This will result in an increased Mj for the 60% plasticized PVC *under the conditions of the experiment*. The sixth and final model portrays plasticized PVC as a matrix composed of amorphous polymer chains and plasticizer in which are randomly dispersed pockets or domains containing PVC crystallites which are spaced uniformly *within the pocket*. These "pockets" act as the physical crosslinks of the system.

These proposed models are strictly representations of the possible arrangements of the components of plasticized PVC into a network structure having a reasonable mechanical integrity. They are based on what is currently known or strongly believed concerning PVC.

Ultimately, one would like to gain a physical picture of plasticized PVC which joins the most likely network structure with the structural interpretation of the dynamic mechanical analysis which forms the core of the present investigations. This will be pursued in the final section of this chapter.

3.3.8. Plasticization Mechanisms

The influences of the solubility between PVC and particular plasticizers on several aspects of plasticized PVC's behavior have been clearly demonstrated in this work. However, a structural understanding of this observed trend is lacking. For example, how does a more soluble plasticizer function within the PVC network, including its crystallites, entanglements, and amorphous regions? In short, when speaking of a plasticizer in PVC, what does it mean to be more soluble?

Aubin and Prud'homme (178) proposed that local fluctuations in concentration of two immiscible components cause the broadening in DSC traces of blends of PVC and poly-α,α'-dimethyl-β-propiolactone. However, their conclusion warrants a second look in light of recent work by Prest and Roberts (179) who studied miscible and immiscible blends of poly(2,6-dimethyl 1,4-phenylene oxide) (PXE) with polystyrene and poly (vinyl methyl ether) (PVME) with polystyrene. The first blend is miscible through its entire composition range, but the authors noted that the region of its glass transition temperature was broadened even though miscibility was indicated by a single glass transition temperature. The

second blend may be phase separated via selective annealing near its lower critical solution temperature (LCST) (179). Prest and Roberts evaluated the relaxation mechanisms during sub-Tg aging studies of these two blends. The miscible blends of PS/PXE and slowly cooled PVME/PS produced results which suggested that the breadths in the Tgs of the miscible blends, rather than indicating localized fluctuations of the concentration of the individual components of the blends, appeared to result from compositionally dependent changes in the average relaxation times as well as the structures of the blended systems. However, the behavior of *immiscible* blends prepared by annealing PVME/PS mixtures in the vicinity of the LCST suggested to Prest and Roberts that the broadening of their glass transition regions did arise from fluctuations in the concentration of the two polymers and led to a distribution of relaxation times.

PVC plasticized with low molecular weight liquids ordinarily shows a single glass transition temperature which is observed to be broadened by the presence of plasticizer. A greater broadening occurs in the presence of a plasticizer of lower solvent power. If a PVC/plasticizer blend can be considered to be similar to a polymer/polymer blend, then the study of Prest and Roberts (179) implies that the PVC and plasticizer may be considered soluble in the absence of a narrow glass transition.

Nielsen et al (127) and Boyer and Spencer (95) showed in the late 1940's that x could not account for all observed physical property effects in plasticized PVC. Wales (180) maintained that solubility depends on molar volume and solubility or interaction parameter. Fedors (181) has

also indicated that molar volume and solubility parameter are interrelated. As will unfold here, molar volume surely is a second important parameter; it incorporates differences in not only molecular size, but plasticizer conformation, flexibility, mobility, and packing ability, i. e., steric effects. These interrelated factors complement each other and together with x, or the relative magnitude of δ, determine the phase state of the plasticizer in PVC.

It is known, but often ignored, that x is both temperature and concentration dependent (6,9). Elevating the temperature theoretically lowers x while changing solvent concentration causes x to change in a manner dependent on the solvent-polymer pair (9). Su, Patterson, and Schreiber (182) have used gas-liquid chromatography (GLC) to examine the thermodynamic interaction of n-DOP with PVC over a wide concentration range. Experimentally, their study employed a GLC support column coated with plasticized PVC through which volatile solvent "probes" were eluted. From the measured retention times, it was possible to determine x values between solvent {1}, polymer {2}, and plasticizer {3}, x23, for example, representing the interaction parameter between PVC and n-DOP. Figure 3.57 shows the observed change in x23 with volume fraction of PVC. While initially negative, x23 becomes positive as the volume fraction of plasticizer approaches 0.5. This indicates that mixing has become thermodynamically unfavorable between 0.4 and 0.5 volume fraction plasticizer. These results suggested to Su et al (182) that PVC and n-DOP were not mixed randomly at the higher plasticizer contents. If mixing is no longer favorable, it is reasonable to speculate that some local phase separation may occur near 0.5 volume fraction.

The Russian literature reportedly demonstrates (183) that below 50 to 55% plasticizer content, "there are observed closed cells filled with the free plasticizer." At concentrations beyond 50 to 55%, "the plasticizer forms a continuous phase into which there is submerged a swelled fibrillar network probably having some individual molecular 'bridges'"(183). These opinions are echoed by other Soviet writers (184-6). Diffusion experiments show that energies of activation beyond 50 to 55% plasticizer are similar to those of the pure plasticizer (183). Mechanical properties such as elastic modulus as well as dye diffusion rate, gas permeability, and apparent activation energy of dye diffusion have been reported to dramatically depart from linear or near linear behavior near 50% plasticizer concentration, as Figure 3.58 illustrates. Although these data point out the strong influence of plasticizer concentration on various properties of plasticized PVC, they do not conclusively demonstrate the presence of phase separated plasticizer in PVC. It is unfortunate that much of the work done by Soviet scientists in this regard is physically and/or linguistically inaccessible as it might allow a more critical evaluation of the description of plasticized PVC outlined above.

The Western literature provides some support for the proposition that plasticizers may phase separate within plasticized PVC. For example, in a birefringence study of uniaxially drawn plasticized and unplasticized PVC, Hibi et al (187) supposed that the plasticizer (20, 30, and 50 parts) was not molecularly dispersed in the plasticized materials but retained its "massive" or bulk state. However, Hibi et al made this

interpretation based on the initial assumption that the plasticized films could be considered "aggregates" of a structural unit made up of PVC surrounded by plasticizer molecules. Exactly what spatial arrangement was intended is not known.

During studies of gas diffusion in plasticized PVC, Sefcik, Schaefer, and others (188) encountered a diminished nmr signal intensity for the plasticizer between 30 and 40% tricresyl phosphate (TCP) content. This they attributed to either enhanced mobility of still homogeneously distributed TCP or its phase separation into liquid-like regions. Sefcik et al (188) did not study TCP-PVC at weight percents beyond 40.

For completeness, the SEM study of Franck (189) should be mentioned. He examined replicas of several PVC-plasticizer mixtures in the SEM and found what might be interpreted as plasticizer-rich regions in materials containing 65% by weight of the generally soluble plasticizers dibutyl phthalate and tricresyl phosphate. At 35 weight percent plasticizer, the structures of the plasticized materials appeared to be fairly homogeneous although not the same for each plasticizers' compositions. In contrast, a plasticizer with low PVC solubility, dioctyl sebacate, gave evidence of poor phase mixing even at 35 weight percent in PVC. However, Franck points out that the interpretations of micrographs are often ambiguous.

From the study at hand, it has been seen that a fully crystallizable plasticizer (DBSe) can indeed crystallize at 60% content in PVC, but not

at 40%. At 60% content, DBSe ceases to effect a further decrease in Tg. It is indeed interesting and useful to note that the damping peak for DBSe60 is indeed low and broad, as would be anticipated for a phase separated system. DBSu, on the other hand, perhaps because its driving force for crystallization may not be as great as DBSe's, does not exhibit crystallization at 60% plasticizer content and continues to lower Tg. It must be pointed out though that DBSe has a solubility parameter of only 8.63 while DBSu's is 8.94, therefore, DBSu's lack of crystallinity, and therefore, of distinct phase separation, may result from its greater solubility with PVC.

Several investigators have studied mixtures of PVC and other polymers with crystallizable liquids. Golovin et al (190-1) have studied mixtures of 2,4-dinitrotoluene (DNT) with butadiene acrylonitrile rubber (Mn = 40,000) and cellulose nitrate. Phase diagrams were constructed from measurements of Tm of the DNT using optical methods (light transmission), DSC, and/or DTA (differential thermal analysis). The Tm values of the DNT/cellulose nitrate systems were also determined by a vapor pressure method; an equilibrium Tm was taken to be that temperature at which the vapor pressures of the additive above solution and pure plasticizer were equivalent. The kinetics of DNT crystallization for the same system were investigated in a later paper (192).

Ceccorulli et al (193-5) have studied mixtures of PVC with the homologous series of aliphatic stearates, $CH_3-(CH_2)16-COO(CH_2)n-CH_3$, where n = 1-16. These crystallizable compounds are used (at the higher

molecular weights) as processing aids in PVC, that is, they promote fusion of the PVC grains. Their solubility in PVC was found to decrease as the value of n increased and to increase with increasing temperature. Experimental evaluations of these not unexpected finds included calorimetric investigations of the melting of excess stearates, Tg depression, and viscosity studies. The x parameter was estimated using the Flory-Rehner equation (196) as well as the approximate relationship

$$x = \frac{V}{RT} (\delta_1 - \delta_2)^2 \qquad (17)$$

where V is the molar volume of the plasticizer. The stearates investigated by Ceccorulli and co-workers showed crystallinity at weight percents in PVC as low as about 10%.

From Mj measurements collected in this work, it was found that Mj increased nearly threefold upon increase of plasticizer content from 40 to 60%, whereupon the plasticizer volume fraction increases from 0.5 to about 0.7. Guzeyev et al's data over a wide range of concentration shows an exponential increase in Mj for PVC plasticized with up to 70 volume percent didecyl phthalate (197). In spite of these dramatic expansions, the network remains mechanically strong, held together by small crystallites which resist dissolution. WAXS studies from the present investigation show negligible crystallinity at 60 and 75 weight percents, particularly for DBP-PVC, but the effective polymer concentration at these compositions is very small, and minuscule amounts of crystallinity could easily escape detection. Though study of 75% samples has been

limited in this work to WAXS and SAXS analysis, it might be noted that these materials, while flaccid, do not flow at ambient temperatures. In fact, the gels studied by Park et al (91,173,176), Geil et al (45,74,175), and Dorrestjin et al (149), to mention a few principal investigators, still exhibit characteristics of solids at 90 and 95 weight percent plasticizer.

It may thus be considered that the addition of PVC to pure plasticizer sets in motion a struggle for phase continuity by the minority PVC. It must be presumed based on the mechanical integrity of a highly plasticized PVC that the PVC achieves and retains some continuity even at very low polymer concentrations. On the opposite side, PVC diluted with plasticizer constitutes a similar struggle as now the plasticizer strives for continuity. It can be assumed in this case, however, that, at least at low concentrations, the plasticizer is molecularly dispersed. As composition nears 50/50 from either side, the continuity of both plasticizer and PVC is compromised. At this point, both plasticizer and polymer may be considered to be highly displaced from their "normal" arrangements. The structure of this plasticized system is far removed from either pure PVC or pure plasticizer. It is no doubt also important that the PVC has apparently attained a maximum crystallinity at these compositions.

With these points in hand, the remainder of this section will look at the structures of the plasticizers studied here in order to determine how their differences in solubility affect their interactions with PVC. All six of the plasticizers studied will be included in this discussion although, by necessity, DEHS and DBP will sometimes be compared alone.

On the basis of the Mj trends with solubility parameter (refer to Figure 3.49), it appears reasonable to once more separate the phthalate plasticizers from the succinate and sebacate plasticizers. When this is done, the molar volumes of each of the two series (see Figure 3.59) decrease moving from low to high solubility parameter and also from broad to narrow damping responses. It is very important to make this separation, particularly since consideration of the molecular conformations available to DBP, DPP, and DOP sets them apart from DEHS, DBSe, and DBSu. Structurally, DBSe, DBSu, and DEHS are much like the conventional linear polyesters in that they can "stretch out." Assuming that DBSe and DBSu both crystallize in a chain extended fashion, it is very likely that DEHS also prefers an extended chain conformation. Its ethylhexyl side chains likely prevent it from crystallizing.

The phthalate plasticizers are bulky molecules which must move primarily by translation and rotation of the entire molecule. Lengthening the side chain increases the molar volume, and as Linhardt (198) (as reported by Nakamura (132)) pointed out, opens up a wider range of comformations, therely encouraging a wider range of relaxation modes. The modes of motion for the "linear" plasticizers are therefore most likely greater in number than those of the phthalates, strictly from a qualitative standpoint. The most important point to be made here is that those modes are *different* than those of the phthalates.

It cannot be overstated that the environment seen by the PVC surrounded by the linear plasticizers is distinctly unlike that created by the phthalate plasticizers. The situation is schematically illustrated in Figure 3.60 by representing DEHS and DBP, the principal players, as a cylinder and a sphere, respectively. PVC is depicted as a box. This drawing was made approximately to scale as not to distort any important dimensions. Each DEHS molecule spans about four PVC repeat units while each DBP unit spans just about two vinyl chloride units. However, because DBP-PVC has a higher mole fraction plasticizer than DEHS-PVC at any given weight fraction, the dipole density of the DBP-PVC will be higher than that of an equivalent composition of DEHS-PVC.

If one considers the placement of the C=O groups in DEHS and DBP, possibilities being given in Figure 3.61, the chance of DBP forming strong bonds with two PVC chain segments is fairly good since its C=O groups are usually facing out from each other. DEHS, depending on its conformation, may bond with segments of two PVC chains, or only one. It is interesting in this regard to consider the melting points of the homologous series of aliphatic dicarboxylic acids. Those acids which have an even number of methylene groups between the carboxylic acid groups, such as succinic, adipic, and sebacic acid, have considerably higher melting points than those acids with an odd number of methylene units, such as malonic and glutaric acid. See Table 3.8. These strongly suggest that the "even" acids pack into crystals in a conformation which is energetically more stable than its alternatives. If the diesters of these acids retain the preference for a planar zigzag arrangement, then DEHS may be considered to exist primarily in a conformation which

results in its C=O groups being on opposite sides of the chain and allows it to bond with two separate PVC chain segments. (See Figure 3.61a.) Several years ago, Leuch (199) proposed the model given in Figure 3.62 for the associations between PVC and plasticizer molecules. This model shows the C=O groups of a linear plasticizer facing the chain *without regard* for the number of methylene groups between the carbonyl groups. Since this cannot always be expected, it is thus reasonable to expect that the linear plasticizers might actually form attractions between two different PVC chains. Of course, the convenience of picturing intermolecular interactions in two dimensions often leads one to forget that real molecules interact in three dimensions. Representing PVC and plasticizer molecules lying side by side in two dimensions ignores the ability of real molecules to arrange themselves in a more disordered fashion.

These considerations lead the author to believe that one of the major differences between the linear and the phthalate plasticizers lies in the manner in which they separate the PVC chains from each other. The compact phthalate molecules form a rigid link between two PVC chains. The amount of the polymer chain which is accessible to these associations is lessened as the side groups of the ester lengthen. The linear plasticizers, in contrast, form a mobile link between PVC chains. The amount of the polymer chain accessible to their carbonyl groups is also lessened as their alkyl side chains lengthen.

Under small-scale deformations, as in the Rheovibron experiment, the associations between plasticizer and PVC will be either maintained or

disrupted. If they are maintained, the PVC chains, held in place by the *rigid* phthalate molecules will comprise a relatively homogeneous system and so very likely exhibit a more narrow damping peak. The more accessible the chain is to the plasticizer, the more rigidly the chain will be held and the narrower will be its damping response. The associations between the plasticizer and PVC may, of course, be destroyed under small-scale deformations. The ease of movement of a dislodged plasticizer molecule will be partly governed by the size of the alkyl side groups, smaller ones most likely giving the least resistance.

The linear plasticizer will form a flexible link between the PVC chains. Under small deformations, that flexible link will allow both plasticizer and polymer to move, utilizing a variety of energy dissipative mechanisms. For this relatively heterogeneous system, the damping peak will then be less narrow than for a PVC plasticized with a rigid phthalate. If its secondary bond with the chain is broken, the dislodged linear plasticizer will move more slowly than the small and compact phthalate molecule. Resistance to this movement will be greater as the alkyl chain length is increased and, if that side group is a bulky ethyl hexyl group, resistance will be even greater.

The plasticizing mechanisms of these diesters are active only in the amorphous phase of the PVC. A greater solubility and lower molar volume will encourage penetration of the plasticizer into more regions of the PVC network, resulting in a more homogeneous dispersion of the plasticizer. In this case, *homogeneity* may be thought of as the probability of finding a molecule of the plasticizer incorporated at any

point in the bulk plasticized material. Finally, the better dispersed the plasticizer is, and the greater its solvent power with PVC, the more difficult it will be for crystallinity to be developed or maintained.

3.3.9. *A Comprehensive Model*

Gathering all of the available observations and postulations of the previous sections into one comprehensive model must include the earlier attempts to reconcile the compositionally dependent changes in the molecular weight between crosslinks, crystallinity, and SAXS Bragg spacing. In addition, in order to be truly comprehensive, the model must incorporate the ideas about plasticizer mechanisms laid out in the previous section.

A model has been constructed from the available evidence and is schematically depicted in Figure 3.63 for plasticizer contents of 10, 40, and 60%. The extremes in plasticizer compatibility between DBP and DEHS are represented by Figures 3.63a and 3.63b, respectively. At 10% content, either plasticizer exists as a dispersed phase. As the plasticizer volume fraction approaches 50% (about 0.4 weight fraction, 0.10 mole fraction), a given plasticizer molecule will begin to find fewer sites for bonding with PVC. Keep in mind that the plasticizers are capable of bonding with two chains, therefore a calculated mole fraction of 0.1 plasticizer actually represents 2 moles of carbonyl groups for every 9 moles of VC repeating units. Because many of the units are excluded from plasticizer contact because of shielding alkyl groups, the ratio of carbonyl groups to available "active centers" is greater than

2:9. If unable to bond with the PVC, the plasticizer molecules will begin to congregate with each other. Simultaneously, the plasticizer will slowly progress from the dispersed phase to the continuous phase. The continuous phase may be more precisely described as an amorphous phase which contains plasticizer as well as PVC chains which bridge the continuous phase. As the continuous phase is shifted from a PVC matrix to a plasticizer-rich amorphous matrix, the observed damping behavior will reflect a more homogeneous distribution of relaxation times, but the rules determining the breadth of the damping curve will still follow those given earlier for the linear and phthalate plasticizers. Consequently, DBP60 will show a more narrow damping peak than DEHS60.

The model does not ignore the semi-crystalline nature of PVC. In keeping with the observed unchanging intercrystallite spacing of the crystallites, the crystallites are positioned equidistantly in a PVC rich phase. This phase is continuous at lower plasticizer contents, however, it does contain plasticizer. This polymer rich phase becomes the dispersed phase as the plasticizer content is increased beyond 40 weight percent. Pockets of PVC crystallites form the crosslinks of the PVC network at all plasticizer contents and are the last remaining PVC-rich regions at high plasticizer contents.

3.4. *SUMMARY OF IMPORTANT CONCLUSIONS*

The research presented in this chapter contributes in many ways to current understanding of the structure and properties of plasticized PVC. Perhaps most significantly, it shows in one unified work the effects of plasticizer solubility on crystallization phenomena, static mechanical behavior, and dynamic mechanical behavior. Together with the results of structural analysis by X-ray scattering techniques and careful consideration of the molecular cooperation between plasticizer and polymer, this has allowed a comprehensive picture of plasticized PVC's structure to be assembled.

It has been shown that plasticizer solubility with PVC manifests itself in several aspects of the behavior of the plasticized polymer. WAXS studies indicated that the crystalline order of the system is noticeably enhanced by plasticization. They further showed how a more soluble plasticizer will allow less crystallinity than a less soluble plasticizer as its concentration exceeds 40 weight percent. Thermal analysis was used to investigate the formation of the crystallization endotherm of plasticized PVC, and the effects of composition, plasticizer solubility, and isothermal annealings were found to be interrelated. A principal conclusion was that the less soluble plasticizer promoted a more rapid development of the crystallization endotherm, regardless of plasticizer content. In addition, the less soluble plasticizer apparently allowed a gher degree of crystallization, as suggested by the higher relative nitudes of the associated crystallization endotherms.

The primary thrust of this investigation was to learn how a plasticizer directly influences the breadth of the dynamic mechanical spectrum of plasticized PVC. Data that has been in the literature more than 30 years (1) showed that diethylhexyl succinate (DEHS), a less solbule plasticizer, broadened the spectrum considerably at 40% weight content. At 60% content, the spectrum narrows. A more soluble plasticizer, dibutyl phthalate (DBP), was shown in the same study (1) to introduce a negligible amount of broadening. Investigation of PVC plasticized with DEHS and DBP as well as four other plasticizers has in the present investigation indicated that the extent of broadening is directly related to the solubility between the polymer and plasticizer. Decreasing plasticizer solubility leads to an increasing breadth in the dynamic mechanical spectrum. In cases where the plasticizer remained amorphous, the damping curve for a material containing 60% plasticizer was generally more narrow than that found for a 40% plasticized PVC.

Somewhat surprisingly, no correlation was found between crystallinity *per se* and the breadth of the dynamic mechanical spectrum. Various thermal histories which were believed to comprise a wide range of crystalline make-up resulted in insignificant changes in damping peak breadth. No trends could be established between extent and/or perfection of crystallinity. For the most part, the associated results could be explained simply on the basis of the level of plasticizer dispersion. A better dispersed plasticizer resulted in a narrower mechanical damping curve.

On the other hand, the *static* mechanical properties of plasticized PVC were found to reflect not only plasticizer solubility but thermal history as well. This was revealed by measurements of an apparent molecular weight between network junction points (Mj) and stress-strain behavior. The value of Mj was found to increase with plasticizer solubility. Stress-strain behavior pointed out the lowered modulus and tensile strength of PVC containing a more soluble plasticizer. But more significantly, it was shown that the more soluble the plasticizer, the greater the tendency of the stress-strain behavior to emulate that of a crosslinked rubber capable of strain-induced crystallization.

WAXS studies of oriented films showed that a meridional reflection reported to be associated with a lamellar structure in PVC/solvent gels (45,74,177) was somewhat sharper in PVC containing 40% of a more soluble plasticizer. However, films which had been annealed at 120°C and then oriented showed a very weak if any meridional reflection in WAXS patterns. These findings and those described above suggested that the crystalline texture associated with the meridional reflection is intimately involved with the crystallite-crosslinked pseudo-network structure of plasticized PVC.

The breadth of the dynamic mechanical spectrum and the glass transition region in general are often considered to reflect the homogeneity of a material, a more homogeneous material displaying a more narrow transition. With this in mind, SAXS investigations of DEHS-PVC and DBP-PVC were conducted in an effort to gain general information

about the small-scale heterogeneities possibly present in plasticized PVC. These studies showed that the systems were fairly well mixed and that the heterogeneities giving rise to the scattering were somewhat larger in DEHS40 and DEHS60 than in the corresponding DBP-PVC materials. The most surprising result of this SAXS study was that the intercrystallite spacing of the 40 and 60% plasticized materials did not change significantly with increasing plasticizer content.

Between 40 and 60% plasticizer content, it was observed that i) the total crystallinity of the plasticized systems decreased significantly, ii) M_j increased approximately threefold, and iii) the intercrystallite spacing remained essentially constant. Attempts to reconcile these crucial experimental results led to consideration of several possible network structures for plasticized PVC. These will not be detailed here as they are discussed exhaustively within the chapter. Although more than one of these network "models" could have been adopted to explain the observed behavior, the model chosen is believed to provide the most straightforward explanation of the observations presented here and found in plasticized PVC in general.

Briefly, that model depicts (solution cast) plasticized PVC as being made up of an amorphous matrix in which are randomly dispersed "pockets" of PVC crystallites. These crystallites are regularly spaced within these pockets, thus giving rise to the observed lack of change in the intercrystallite spacing with plasticizer content. Because the pockets, which serve as the network junction points, contain two or more crystallites, they serve to anchor the network much more firmly than

would an isolated crystallite. This clustering of crystallites is believed to foster good mechanical integrity in plasticized PVC, particularly in cases of high plasticizer content where the total amount of crystallinity is infinitesimally low.

The amorphous matrix described by this model is made up of uncrystallized PVC chains amongst which are dispersed plasticizer. The level of dispersion of that plasticizer is highest when the plasticizer has a small molar volume and is very soluble with the PVC. As the two characteristics deviate from the ideal case, that is, molar volume increases and solubility decreases, the matrix becomes more heterogeneous, leading to a broader damping curve. At plasticizer contents beyond 40 weight percent, the amorphous matrix becomes rich in plasticizer and the system becomes more homogeneous, thereupon narrowing the damping curve.

3.5. RECOMMENDATIONS FOR FUTURE STUDY

1. The results presented indicate that static mechanical properties are highly sensitive to the network morphology of plasticized PVC. Study of the static mechanical properties of plasticized PVC could be developed further (in conjunction with WAXS orientation studies) as a means of refining the conclusions already reached. A greater range of thermal histories, plasticizer types, and plasticizer contents are considered to be essential elements of the proposed work.

2. It is suggested that the apparent lack of any significant change in the SAXS Bragg spacing with increasing plasticizer content be verified. It is this experimental result which proved to be most difficult to account for in formulating a model of the network structure of plasticized PVC that was consistent with all of the experimental results. Regardless of the outcome of the proposed SAXS verification, the pocket model of plasticized PVC is considered to be a viable alternative to the classical concept of isolated network-forming crystallites.

3. The use of small-angle neutron scattering (SANS) has potential as a probe for these systems. For example, chemistry permitting, one could preferentially deuterate the alkyl chain segments of a diester plasticizer and study the segregation/isolation of a plasticizer species in PVC as a function of plasticizer content. If the plasticizer is large enough, one might be able to learn something about its conformation; this approach might be restricted to the linear plasticizers, a good example being dibutyl sebacate.

4. Several years ago, Kinjo and Nakagawa (Polymer J., 4, 143 (1973)) investigated the dynamic mechanical properties of PVC containing small amounts of plasticizer. They observed a low temperature (~ -155°C) damping peak in PVC plasticized with up to 12.5 weight percent of several plasticizers. The lowest temperature for which data has been obtained in this study is about -140°C. Because the peak was detected only in cases where the plasticizer contained alkyl side chains, it was attributed to the motions of these side chains. An investigation of the behavior of this low temperature peak may be helpful in determining the nature of the "phase inversion" believed to occur at intermediate levels of plasticizer in PVC. One might consider the influence of alkyl chain length, plasticizer solubility, thermal history, and composition on the size and temperature location of this low temperature relaxation.

3.6. *APPENDIX: SMALL-ANGLE X-RAY SCATTERING*

3.6.1. *Manipulation of SAXS Data*

The quantitative information derived from the SAXS data obtained at ORNL varied somewhat with the method of data treatment. Two factors figured in these differences. One was the method of background correction. Bonart's background correction method was the only one of the three standard such corrections applicable since the Vonk and Ruland methods require high angle data. However, it was possible to determine an empirical constant background correction by averaging the approximately linear and near zero tail of the SAXS curve beyond $s = 0.02$, which was made up of 37 data points. This value will be referred to as the alternate background correction.

A second factor influencing results was the choice of integration limits (over s) for the IMSL computer routines used to determine the invariant, Equation (6) in the text. The lower limit was set at 0.0. The upper limit was set at either $s = 0.02$ or 0.03. An example of the affected area is given in Figure 3.64. As a matter of interest, the integration value found by the IMSL routines was verified using a simple trapezoidal construction.

The data was not thoroughly rotated through the two backgrounds and the two maximum integration limits. As Table 3.9 indicates, the alternate background corrections were similar in magnitude for all

samples as were the Bonart background corrections. The background for DBP75 was generally smaller than that for the other samples. Tables 3.10-3.12 indicate the variability of the data within the maximum integration limits. Where applicable, sample plots are referred to and included. Also included here is the Fortran computer program written to perform the data treatment.

```
C
C.................................................
C
C   PREPARED BY ELAINE YORKGITIS, MAY 1984, CONTINUALLY REVISED
C
C   INPUT CONSISTS OF
C      1.  SAMPLE DESCRITION
C      2.  VARIABLES DESCRIBING THE:
C          - NUMBER OF DATA SETS TO BE PROCESSED
C          - RANGE OF THE CORRELATION DISTANCE IN ANGSTROMS
C          - NUMBER OF INTENSITY/ANGLE DATA PAIRS TO BE READ
C          - A CONSTANT BACKGROUND CORRECTION FACTOR
C      3.  ANGLE (K) AND INTENSITY
C
C   INTENSITY VALUES ARE ASSUMED TO BE EITHER EQUAL TO
C   OR PROPORTIONAL TO ABSOLUTE INTENSITY
C
C   CAN OUTPUT DATA TO THE PLOTALL PLOTTING ROUTINE FOR
C   EITHER INTENSITY OR INVARIANT PLOTS
C
C.................................................
C
C
      INTEGER NK, IC, IER, NOSETS, F, G, H, I, J, NOX,
     *        X
      REAL K(90), BPAR1(4), BPAR2(4), C(85,3),
     *     A, B, Q, Y1(90), Y2(90), INVAR, TOP(500),
     *     CORR(500), BKG, CORR3D(500), TOP3D(500),
     *     Y3D(90), S(90) INTK(90)
C
      CHARACTER*50  SAMPLE(10)
      DATA BPAR1, BPAR2/8*0.0/
C
      READ (5,*) NOSETS, NOX, NK, BKG
      IC = NK - 1
C
      DO 10 F = 1,NOSETS
C
```

```
      READ (5,99) SAMPLE(F)
   99 FORMAT (A50)
C
      DO 20 G = 1,NK
        READ (5,*) K(G), INTK(G)
        S(G) = K(G)/(2.0*3.14159)
        INTK(G) = (INTK(G)-BKG)
   20 CONTINUE
C
      DO 25 I = 1,NK
        Y2(I) = (S(I)**2)*INTK(I)
   25 CONTINUE
C
C
C  THE FOLLOWING STATEMENTS CALL UPON THE IMSL AREA
C  CALCULATION ROUTINES ICSICU AND DCSQDU
C
C  "A" AND "B" ARE THE INTEGRATION LIMITS CORRESPONDING TO
C  THE ANGULAR FUNCTION "S";  FOR EXAMPLE, IN THE PRESENT
C  SETUP, THE AREA OF INTEGRATION WOULD BE FROM
C  S = 0.0 TO 0.03
C
      CALL ICSICU (S,Y2,NK,BPAR2,C,IC,IER)
      A = 0.0
      B = 0.03
      CALL DCSQDU (S,Y2,NK,C,IC,A,B,Q,IER)
      INVAR = Q
C     WRITE (6,102) IER
C 102 FORMAT(/' ERROR MESSAGE FOR DENOMINATOR IS ',I5//)
      IER = 0
C
      DO 30 X = 1,NOX
C
C
      DO 40 I = 1,NK
        Y1(I) = (S(I)**2)*INTK(I)*
     *          COS(S(I)*X*2.0*3.14159)
        Y3D(I) = (S(I))*INTK(I)*
     *           (SIN(S(I)*X*2.0*3.14159))/
     *           (2.0*3.14159*X)
   40    CONTINUE
C
      CALL ICSICU (S,Y1,NK,BPAR1,C,IC,IER)
      CALL DCSQDU (S,Y1,NK,C,IC,A,B,Q,IER)
C     WRITE (6,103) X,IER
C 103 FORMAT(/' ERROR MESSAGE FOR NUMERATOR FOR X1D= ',
C    *         I5,' IS ',I5/)
C
      TOP(X) = Q
      CORR(X) = TOP(X)/INVAR
C
      CALL ICSICU (S,Y3D,NK,BPAR1,C,IC,IER)
      CALL DCSQDU (S,Y3D,NK,C,IC,A,B,Q,IER)
C     WRITE (6,107) X,IER
C 107 FORMAT(/' ERROR MESSAGE FOR NUMERATOR FOR R= ',
C    *         I5,' IS ',I5/)
C
```

```
       TOP3D(X) = Q
       CORR3D(X) = TOP3D(X)/INVAR
C
   30 CONTINUE
C
       WRITE (6,104) SAMPLE(F)
  104 FORMAT ('1','  SAXS RESULTS FOR  ',A50//)
C
C   PROGRAM CAN EXECUTE ONE OF THE TWO FOLLOWING OUTPUT
C   STATEMENTS TO "4"
C
C   IF THE FIRST SET OF DATA CONSISTING OF INTK, Y2, AND S
C   IS SENT TO "4," PLOTALL WILL PLOT THE ANGULAR
C   INTENSITY PLOT AND THE INVARIANT PLOT
C
C   IF THE SECOND SET OF DATA CONSISTING OF CORR AND
C   CORR3D IS SENT TO "4," PLOTALL WILL PLOT THE
C   ONE- AND THREE-DIMENSIONAL CORRELATION FUNCTIONS
C
       DO 50 J = 1,NK
          WRITE (4,105) INTK(J), Y2(J), S(J)
  105     FORMAT (3E20.6)
   50 CONTINUE
C
       DO 50 J = 1,NOX
          WRITE (4,105) CORR(J), CORR3D(J)
  105     FORMAT (2F20.6)
   50 CONTINUE
C
       WRITE (6,110) INVAR
  110 FORMAT (//'  INVARIANT IS',E20.6)
C
C
   10 CONTINUE
       STOP
       END
```

The plotall program will not be described. Samples of its output have been included in the preceding descriptions.

The choice of the maximum integration limits most strongly affects the calculation of the invariant integral. This is quite reasonable since the neglected or included area will be for the most part divided out in the calculation of the one- and three-dimensional correlation functions. The value of the invariant integral, however, must stand alone. The

$<\rho^2>$ ratio values of the DBP-PVC series are affected little by the choice of integration limits. However, although the ratio values determined for DEHS-PVC may vary somewhat, the trends noted in what has to be regarded as only a representation of $<\rho^2>$ are the same. The use of the larger alternate background correction might bring closer agreement.

Overall, the general conclusion that little deviation is seen between 40 and 60% samples is not violated. DEHS75 once more generally shows larger phase dimensions than its counterpart 40 and 60% samples while DBP75 remains fairly close to its corresponding 40 and 60% values.

3.6.2. *Calculation of Mass Absorption Coefficient*

The mass absorption coefficient (μ/ρ) is a useful parameter as it enables one to determine the optimum thickness for X-ray scattering for a particular material. As Figure 4.65 illustrates, intensity of scattering passes through a maximum for thickness $1/\mu$. The parameter μ is referred to as the linear absorption coefficient. Unlike μ/ρ, μ requires knowledge of density and therefore depends to some extent on the state of the material.

Alexander (138) has presented a clear outline for the μ/ρ calculation of Nylon 66. A similar calculation for polyvinyl chloride is given in Table 3.13. The μ/ρ values for each element may be obtained from appropriate tables, such as the one included in Alexander's book. Alternatively, one may calculate a μ/ρ value (200) from the equation

$$\mu/\rho = CNZ^4\lambda^n /A$$

where
- N is Avogadro's number,
- Z is the atomic number,
- A is the atomic weight of the element,
- λ is the wavelength of impinging X radiation,
- n is an exponent -- between 2.5 and 3.0, and
- C is a constant which is approximately the same for all elements.

Using the method given in Table 3.13, the values of μ/ρ calculated for DEHS and DBP are 5.03 and 6.12 inverse cm, respectively. The optimum thicknesses of the 10, 40, 60, and 75 weight percent compositions of DEHS-PVC and DBP-PVC are given in Table 3.14. These are based on a density of 1.4 for PVC.

3.6.3. *Calculation of Electron Density*

The calculation of electron density requires totalling the number of electrons in a material. Using molecular weight and mass density, one can then calculate an electron density ED. The general formula is:

$$E.\,D. = \frac{\text{\# electrons}}{\text{Mol. Wt. (g/mol)}} \bullet N \bullet \text{Mass density (g/cc)}$$

where N = Avogadro's number.

Multiplication by the factor 10^{-24} will give the ED in units of electrons per cubic Angstrom. One may also see ED expressed in moles of electrons per cc. Obviously, many other combinations are possible. The following examples calculate the ED for PVC, DEHS, and DBP.

Example 1. Polyvinyl Chloride

-CH2-CHCl-   # electrons = 2C(6) + 3H(1) + 1Cl(17) = 32
                density = 1.4 g/cc
                MW repeat unit = 62.5 g/mol

$$ED = 32 \times 6.022(10^{23}) \times (10^{-24}) \times 1.4/62.5$$

$$= 0.4317 \ e/A^3$$

Example 2. DEHS

$$\begin{matrix} & & C_2H_5 \\ O{=}C{-}O{-}CH_2CH{-}(CH_2)_3{-}CH_3 \\ CH_2 \\ CH_2 \\ O{=}C{-}O{-}CH_2CH{-}(CH_2)_3{-}CH_3 \\ & & C_2H_5 \end{matrix}$$ # electrons = 20C(6) + 38H(1) + 4O(8) = 190
density = 0.928 g/cc
MW = 342.54 g/mol
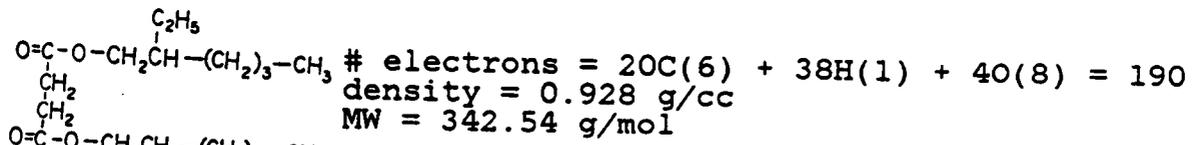
DEHS $$ED = 190 \times 6.022(10^{23}) \times (10^{-24}) \times 0.928/342.54$$

$$= 0.3100 \ e/A^3$$

Example 3. DBP
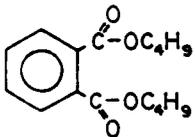
# electrons = 16C(6) + 22H(1) + 4O(8) = 590
density = 0.928 g/cc
MW = 342.54 g/mol

DBP

$$ED = 150 \times 6.022(10^{23}) \times (10^{-24}) \times 1.0462/278.35$$

$$= 0.3395 \ e/A^3$$

REFERENCES

1. Schmieder, K., Wolf, K., Kolloid-Z. Z., *127*, 65 (1952).

2. Nielsen, L. E., *Mechanical Properties of Polymers and Composites*, Vol. 1, Marcel Dekker: New York, 1974.

3. Ferry, J. D., *Viscoelastic Properties of Polymers*, Third Edition, Wiley: New York, 1980.

4. Boyer, R. F., J. Appl. Phys., *20*, 540 (1949).

5. Lawrence, R. R., McIntyre, E. B., Ind. Eng. Chem., *41*, 689 (1949).

6. Doty, P., Zable, H. S., J. Polym. Sci., *1*, 90 (1946).

7. Flory, P. J., J. Chem. Phys., *9*, 660 (1941).

8. Flory, P. J., J. Chem. Phys., *10*, 51 (1942).

9. Flory, P. J., *Principles of Polymer Chemistry*, Cornell Univ. Press: Ithaca, NY, 1953.

10. Blanks, R. F., Prausnitz, J. M., I&EC Fund., *3*, 1 (1964).

11. Walter, A. T., J. Polym. Sci., *13*, 207 (1954).

12. Tabb, D. L., Koenig, J. L., Macromolecules, *8*, 929 (1975).

13. Sears, J. K., Darby, J. R., *The Technology of Plasticizers*, Wiley: New York, 1982.

14. Doolittle, A. K., J. Polym. Sci., *2*, 121 (1949).

15. Doolittle, A. K., Chap. 1 in *Plasticizer Technology*, Vol. 1, Bruins, P., ed., Reinhold: New York, 1965.

16. Alfrey, T., Jr., *Mechanical Behavior of High Polymers*, Wiley: New York, 1948.

17. Aklonis, J. J., MacKnight, W. J., Shen, M., *Introduction to Polymer Viscoelasticity*, Wiley: New York, 1972.

18. Murayama, T., *Dynamic Mechanical Analysis of Polymeric Material*, Elsevier: Amsterdam, 1978.

19. Ward, I. M., *Mechanical Properties of Solid Polymers*, Wiley: London, 1971.

20. *Particulate Nature of PVC*, Butters, G., ed., Applied Science: London, 1982.

21. *Encyclopedia of PVC*, Nass, L. I., ed., Marcel Dekker: New York, 1976.

22. Allsopp, M. W., Pure Appl. Chem., *53*, 449 (1981).

23. Geil, P. H., J. Macromol. Sci. -- Chem., *A11*, 1271 (1977).

24. Geil, P. H., J, Macromol. Sci. -- Chem., *A11*, 1461 (1977).

25. Clark, M., Chap. 1 in *Particulate Nature of PVC*, Butters, G., ed., Applied Science: London, 1982.

26. Portingell, G. C., Chap. 4 in *Particulate Nature of PVC*, Butters, G., ed., Applied Science: London, 1982.

27. Faulkner, P. G., J. Macromol. Sci., *B11*, 251 (1979).

28. Cogswell, F. N., Pure Appl. Chem., *52*, 2033 (1980).

29. Sieglaff, C. L., Pure Appl. Chem., *53*, 509 (1981).

30. Berens, A. R., Folt, V. L., Trans. Soc. Rheol., *11*, 95 (1967).

31. Berens, A. R., Folt, V. L., Polym. Eng. Sci., *9*, 27 (1969).

32. Soni, P. L., Geil, P. H., Collins, E. A., J. Macromol. Sci. -- Phys., *B20*, 479 (1981).

33. Filisko, F. E., Polym. Eng. Sci., *14*, 352 (1974).

34. Bystedt, J., Lundquist, J., J. Vinyl Technol., *2*, 209 (1980).

35. Brydon, J. A., *Plastics Materials*, Fourth Edition, Butterworth Scientific: London, 1982.

36. Titow, W. V., Chap. 9 in *PVC Technology*, Fourth Edition, Titow, W. V., ed., Elsevier: London, 1984.

37. Naqvi, M. K., J. Macromol. Sci. -- Rev. Macromol. Chem. Phys., *C25*, 119 (1985).

38. Pezzin, G., Plast. Polym., *37*, 295 (1969).

39. Caraculacu, A. A., Pure Appl. Chem., *53*, 385 (1981).

40. Berens, A. R., Polym. Eng. Sci., *14*, 318 (1974).

41. Abbas, K. B., Pure Appl. Chem., *53*, 411 (1981).

42. Starnes, W. H., Schilling, F. C., Plitz, I. M., Cais, R. E., Freed, D. J., Hartless, R. L., Bovey, F. A., Macromolecules, *16*, 790 (1983).

43. Tudos, F., Kelen, T., Nagy, T. T., Chap. 7 in *Developments in Polymer Degradation - 2*, Grassie, N., ed., Applied Science: London, 1979.

44. Danforth, J. D., Spiegel, J., Bloom, J., J. Macromol. Sci. -- Chem., *A17*, 1107 (1982).

45. Guerrero, S. J., Keller, A., Soni, P. L., Geil, P. H., J. Polym. Sci.: Polym. Phys. Ed., *18*, 1533 (1980).

46. Wilski, H., Kolloid-Z. Z., *238*, 426 (1970).

47. Natta, G., Corradini, P., J. Polym. Sci., *20*, 25 (1956).

48. Bockman, O., Brit. Plast., 364 (June 1956).

49. Carrega, M. E., Pure Appl. Chem., *49*, 569 (1977).

50. Liu, N., Tong, S. N., Koenig, J. L., J. Appl. Polym. Sci., *25*, 2205 (1980).

51. King, J., Bower, D. I., Maddams, W. F., Pyszora, H., Makromol. Chem., *184*, 879 (1983).

52. Mochel, V. D., J. Macromol. Sci. -- Revs. Macromol. Chem., *C8*, 289 (1972).

53. Wilkes, C. E., Macromolecules, *4*, 443 (1971).

54. Hengstenberg, H. A., Schuch, E., Die Makromol. Chem., *74*, 55 (1964).

55. Doty, P., Wagner, H., Singer, S., J. Phys. Coll. Chem., *51*, 33 (1947).

56. Crugnola, A., Danusso, F., J. Polym. Sci.: Polym. Lett., *6*, 535 (1967); Lyngaae-Jorgensen, J. H., Die Makromol. Chem., *167*, 31 (1967); and references therein.

57. De Vries, A. J., Bonnebat, C., Carrega, M., Pure Appl. Chem., *26*, 209 (1971).

58. Filisko, F. E., Polym. Prepr., *14*, 744 (1973).

59. Lyngaae-Jorgenssn, J., Polym. Eng. Sci., *14*, 342 (1974).

60. Spevacek, J., Schneider, B., Baldrian, J., Dybal, J., Stokr, J., Polym. Bull., *9*, 495 (1983).

61. Natta, G., Bassi, I. W., Corradini, P., Attai. Accad. Naz. Lincie, Cl. Sci. Fis., Mat. Natur. Rend., *31*, 17 (1961). Referenced in Ref. 62.

62. Wilkes, C. E., Folt, V. E., Krimm, S., Macromolecules, *6*, 235 (1973).

63. Rosen, I., Burleigh, P. H., Gillespie, J. F., J. Polym. Sci., *54*, 31 (1961).

64. Manson, J. A., Iobst, S. A., Acosta, R., J. Polym. Sci.: Part A-1, *10*, 179 (1972).

65. White, D. M., J. Am. Chem. Soc., *82*, 5678 (1960).

66. Mammi, M., Nardi, V., Nature, *199*, 247 (1963).

67. Biais, R., Geny, C., Mordini, C., Carrega, M., Brit. Polym. J., 179 (Dec 1980).

68. Utsuo, A., Stein, R. S., J. Polym. Sci.: Polym. Lett., *3*, 49 (1965).

69. Clark, R. J., J. Polym. Sci., *51*, S71 (1961).

70. Alfrey, T., Jr., Wiederhorn, N., Stein, R., Tobolsky, A., Ind. Eng. Chem., *41*, 701 (1949).

71. Aiken, W., Alfrey, T., Jr., Janssen, A., Mark, H., J. Polym. Sci., *2*, 178 (1947).

72. Alfrey, T., Jr., Wiederhorn, N., Stein, R., Tobolsky, A., J. Coll. Sci., *4*, 211 (1949).

73. Lemstra, P. J., Keller, A., Cudby, M., J. Polym. Sci.: Polym. Phys. Ed., *16*, 1507 (1978).

74. Guerrero, S. J., Keller, A., Soni, P. L., Geil, P. H., J. Macromol. Sci. -- Phys., *B20*, 161 (1981).

75. Tasumi, M., Shimanouchi, T., Spectrochim. Acta., *17*, 731 (1961).

76. Reding, F.P., Walter, E. R., Welch, F. J., J. Polym. Sci., *56*, 225 (1962).

77. Mandelkern, L., *Crystallization of Polymers*, McGraw-Hill: New York, 1964.

78. Guerrero, S. J., Keller, A., J. Macromol. Sci. -- Phys., *B20*, 167 (1981).

79. Berghmans, H., Govaerts, F., Overbergh, N., J. Polym. Sci.: Polym. Phys. Ed., *17*, 1251 (1979).

80. Benson, R., Maxfield, J., Axelson, D. E., Mandelkern, L., J. Polym. Sci.: Polym. Phys. Ed., *16*, 1583 (1978).

81. Nakajima, A., Hamada, H., Hayashi, S., Die Makromol. Chem., *95*, 40 (1966).

82. Kockott, D., Kolloid-Z. Z., *198*, 17 (1964).

83. Flory, P. J., Trans. Farad. Soc., *51*, 848 (1955).

84. Juijn, J. A., Gisolf, J. H., de Jong, W. A., Kolloid-Z. Z., *235*, 75 (1969).

85. Wunderlich, B. A., *Macromolecular Physics*, Volume 3, Academic Press: New York, 1980.

86. Illers, K. H., Die Makromol. Chem., *127*, 1 (1969).

87. Illers, K. H., J. Macromol. Sci. -- Phys., *B14*, 471 (1977).

88. Grewer, Th., Wilski, H., Kolloid-Z. Z., *226*, 46 (1968).

89. Brown, H. R., Musindi, G. M., Stachurski, Z. H., Polymer, *23*, 1508 (1982).

90. Ohta, S., Kajiyama, T., Takayanagi, M., Polym. Eng. Sci., *16*, 465 (1976).

91. Leharne, S. A., Park, G. S., Norman, R. H., Brit. Polym. J., *11*, 7 (1979).

92. Garrett, T. B., Goldfarb, L., J. Appl. Polym. Sci., *21*, 1395 (1977).

93. Tant, M. R., Wilkes, G. L., Polym. Eng. Sci., *21*, 1875 (1980).

94. Gordon, M., Taylor, J. S., J. Appl. Chem., *2*, 1, (1952).

95. Boyer, R. F., Spencer, R. S., J. Polym. Sci., *2*, 157 (1947).

96. Couchman, P. R., Karasz, F. E., Macromolecules, *11*, 117 (1978).

97. Kovacs, A. J., Adv. Polym Sci., *3*, 394 (1963).

98. DiMarzio, E. A., Gibbs, J. H., J. Polym. Sci., *A1*, 1417 (1963).

99. Pezzin, G., Ital. Conv. Macromol. Sci., 1983, p. 27.

100. Scandola, M., Ceccorulli, G., Pizzoli, M., Pezzin, G., Polym. Bull., *6*, 653 (1982).

101. Roy, S. K., Brown, G. R., St.-Pierre, L. E., Polymer (Korea), *7*, 23 (1983); Roy, S. K., Brown, G. R., St.-Pierre, L. E., Int. J. Polymeric Mater., *10*, 13 (1983).

102. Fried, J. R., Lai, S.-Y., Kleiner, L. W., Wheeler, M. E., J. Appl. Polym. Sci., *27*, 2869 (1982).

103. Pezzin, G., Omacini, A., Zilio-Grandi, F., Chim. Ind. (Milan), *50*, 309 (1968).

104. Pizzoli, M., Scandola, M., Ceccorulli, G., Pezzin, G., Polym. Bull., *9*, 429 (1983).

105. Adachi, K., Ishida, Y., J. Polym. Sci.: Polym. Phys. Ed., *14*, 2219 (1976).

106. Bair, H. E., Warren, P. C., J. Macromol. Sci. -- Phys., *B20*, 381 (1981).

107. Theodorou, M., Jasse, B., J. Polym. Sci.: Polym. Phys. Ed., *21*, 2263 (1983).

108. Douglass, D. C., Am. Chem. Soc. Symp. Ser., *142*, 147 (1980).

109. McBrierty, V. J., Far. Disc. Chem. Soc., *68*, 78 (1979).

110. Bashkirov, B. Sh., Maklakov, A. I., Vysokomol. Soyed., *A24*, 762 (1982).

111. Davies, J. M., Miller, R. F., Busse, W. F., J. Am. Chem. Soc., *63*, 361 (1941).

112. Fuoss, R. M., J. Am. Chem. Soc., *63*, 369, 378 (1941).

113. Fuoss, R. M., Kirkwood, J. G., J. Am. Chem. Soc., *63*, 385 (1941).

114. Fitzgerald, E. R., Miller, R. F., J. Coll. Sci., *8*, 148 (1953).

115. Utracki, L. A., Jukes, J. A., J. Vinyl Technol., *6*, 85 (1984).

116. Kisbenyi, M., J. Polym. Sci: Part C, *33*, 113 (1971).

117. Petersen, J., Ranby, B., Die Makromol. Chem., *133*, 251 (1970).

118. Diaz Calleja, R., Polym. Eng. Sci., *19*, 596 (1979).

119. Roche, E. J., Polym. Eng. Sci., *23*, 390 (1983).

120. Pezzin, G., Ajroldi, G., Casiraghi, T., Garbuglio, C., Vittadini, G., J. Appl. Polym. Sci., *16*, 1839 (1972).

121. Deshpande, D. D., Tiwari, V. K., Polym. J., *15*, 377 (1983).

122. Pezzin, G., Ajroldi, G., Garbuglio, C., J. Appl. Polym. Sci., *11*, 2553 (1967).

123. Harrell, E. R., Chartoff, R. P., Polym. Eng. Sci., *14*, 362 (1974).

124. Wolf, K., Kuntstoffe, *41*, 89 (1951).

125. Wurstlin, F., Kolloid-Z. Z., *113*, 18 (1949).

126. Curtis, A. J., in *Progress in Dielectrics*, Vol. 2,
     Birks, J. B., ed., Wiley: New York, 1960.

127. Nielsen, L. E., Buchdahl, R., Levreault, R., J. Appl. Phys.,
     21, 607 (1950).

128. Hata, N., Tobolsky, A. V., Bondi, A., J. Appl. Polym. Sci.,
     12, 2597 (1968).

129. Aklonis, J. J., Rele, V. B., J. Polym. Sci.: Polym. Symp.,
     46, 127 (1974).

130. Tobolsky, A. V., J. Polym. Sci.: Part C, *9*, 157 (1965).

131. Busse, W. F., J. Phys. Chem., *36*, 2862 (1932). Referenced
     in Ref. 13.

132. Nakamura, K., J. Polym. Sci.: Polym. Phys. Ed., *13*,
     137 (1975).

133. Ninomiya, K., Ferry, J. D., J. Polym. Sci.: A-2, *5*,
     195 (1967).

134. *Polymer Handbook*, Second Edition, Brandrup, J.,
     Immergut, E. H., eds., Wiley: New York, 1975.

135. Elias, H.-G., *Macromolecules-1: Structure and Properties*,
     Plenum Press: New York, 1977.

136. Schindler, A., Harper, D., J. Polym. Sci.: Polym. Chem. Ed.,
     17, 2593 (1979).

137. Carman, C. J., Macromolecules, *4*, 445 (1971); *6*,
     725 (1973).

138. Alexander, L. E., *X-Ray Diffraction Methods in Polymer Science*,
     Wiley: New York, 1969.

139. Hendricks, R. W., J. Appl. Cryst., *11*, 15 (1978).

140. Gancheva, T. S., Dinev, P. D., Eur. Polym. J., *18*, 159 (1982).

141. Natov, M. A., Gancheva, T. S., Vysokomol. Soyed., *A14*, 2354 (1972).

142. Duiser, J. A., Keijzers, A. E. M., Polymer, *19*, 889 (1978).

143. Rebenfeld, L., Makarewicz, P. J., Weigmann, H.-D., Wilkes, G. L., J. Macromol. Sci. -- Rev. Macromol. Chem., *C15*, 279 (1976).

144. Darby, J. R., Touchette, N. W., Sears, J. K., Polym. Eng. Sci., *7*, 295 (1967).

145. Anagnastopoulos, C. E., Coran, A. Y., Gamrath, H. R., J. Appl. Polym. Sci., *9*, 181 (1960).

146. Ernes, D. A., Garg, B. K., Williams, R. L., J. Appl. Polym. Sci., *29*, 383 (1984).

147. Wenig, W., J. Polym. Sci.: Polym. Phys. Ed., *16*, 1635 (1978).

148. Tyagi, D., Ph. D. Thesis, VPI&SU, 1985.

149. Dorrestjin, A., Keijzers, A. E. M., te Nijenhuis, K., Polymer, *22*, 305 (1981).

150. Khambatta, F. B., Warner, F., Russell, T., Stein, R. S., J. Polym. Sci., *14*, 1391 (1976).

151. Van Bogart, J. W. C., Ph. D. Thesis, Univ. of Wisconsin-Madison, 1981.

152. Higgins, J. S., Stein, R. S., J. Appl. Cryst., *11*, 346 (1978).

153. *Small Angle X-Ray Scattering*, Glatter, O., Kratky, O., eds., Academic Press: London, 1982.

154. Gezovich, D. M., Geil, P. H., Int. J. Polym. Mater., *1*, 3 (1971).

155. Summers, J. W., J. Vinyl Technol., *3(2)*, 107 (1981).

156. Nielsen, G. F., Jabarin, S. A., J. Appl. Phys., *46*, 1175 (1975).

157. Blundell, D. J., Polymer, *20*, 934 (1979).

158. Singleton, C. J., Stephenson, T., Isner, J., Geil, P. H., Collins, E. A., J. Macromol. Sci. -- Phys., *B14*, 29 (1977).

159. Pilz, I./Kratky, O./Schmitz, P. J., J. Coll. Inter. Sci., *21*, 24 (1966); *24*, 211 (1967); *30*, 140 (1969).

160. Small, P. A., J. Appl. Chem., *3*, 71 (1953).

161. Hoy, K. L., J. Paint Technol., *42*, 76 (1970).

162. Van Krevelen, D. W., *Properties of Polymers, Their Estimation and Correlation with Chemical Structure*, Second Edition, Elsevier: Amsterdam, 1976.

163. Hansen, C. M., J. Paint Technol., *39*, 104 (1967).

164. Crowley, J. D., Teague, G. S., Jr., Lowe, J. W., Jr., J. Paint Technol., *38*, 269 (1966).

165. Lawson, D. D., Ingham, Nature, *223*, 614 (1969).

166. Anagnostopoulos, C. E., Coran, A. Y., J. Polym. Sci., *57*, 1 (1962).

167. Anagnostopoulos, C. E., Coran, A. Y., Gamrath, H. R., Modern Plastics, 141 (Oct 1965).

168. Bohdanecky, M., Coll. Czech. Chem. Commun., *34*, 2065 (1969).

169. Koehnen, D. M., Smolders, C. A., J. Appl. Polym. Sci., *19*, 1163 (1975).

170. Gardon, J. L., J. Paint Technol., *38*, 43 (1966), and references therein.

171. Flory, P. J., Rehner, N., Shaffer, M. C., J. Polym. Sci., *4*, 225 (1949), referenced in Ref. 172.

172. Patterson, K. G., Padgett, S. J., Peppas, N. A., Coll. Polym. Sci., *260*, 851 (1982).

173. Leharne, S. A., Park, G. S., Eur. Polym. J., *19*, 1147 (1983).

174. Shtarkman, B. P., Lebedev, V. P., Yatsynina, T. L., Kosmynin, B. P., Gerasimov, V. I., Genin, Ya. A., Tsvankin, D. Ya., Vysokomol. Soyed., *A14*, 1629 (1972).

175. Yang, Y. C., Geil, P. H., J. Macromol. Sci. -- Phys., *B22*, 463 (1983).

176. Harrison, M., Morgan, P. H., Park, G. S., Brit. Polym. J., *3*, 154 (1971).

177. Keller, A., in *Structure-Property Relationships of Polymeric Solids*, Hiltner, A., ed., Plenum Press: London, 1983, p. 26.

178. Aubin, M., Prud'homme, R. E., Macromolecules, *13*, 365 (1980).

179. Prest, W. M., Roberts, F. J., Jr., 28th IUPAC Macromolecular Symposium, (1982).

180. Wales, M., J. Appl. Polym. Sci., *15*, 293 (1971).

181. Fedors, R. F., Polym. Eng. Sci., *14*, 147 (1974).

182. Su, C. S., Patterson, D., Schreiber, H. P., J. Appl. Polym. Sci., *20*, 1025 (1976).

183. Shtarkman, B. P., Razinskaya, I. N., Acta Polym., *34*, 514 (1983).

184. Gancheva, T., Marinova, A., Vysokomol. Soedin., *B24*, 264 (1982), from Chemical Abstracts.

185. Rabinovich, I. B., Mochalov, A. N., Tsvetkova, L. Ya., Khlyustova, T. B., Moseyeva, Ye. M., Maslova, V. A., Acta Polym., *34*, 482 (1983).

186. Frenkel, S., Acta Polym., *34*, 499 (1983).

187. Hibi, S., Maeda, M., Kubota, H., Minra, T., Polymer, *18*, 137 (1977).

188. Sefcik, M. D., Schaefer, J., May, F. L., Raucher, D., Dub, S. M., J. Polym. Sci., *21*, 1041 (1983).

189. Franck, A., Die Angew. Makromol. Chem., *29/30*, 179 (1973).

190. Golovin, V. A., Lotmentsev, Yu. M., Andreyev, V. A., Vysokomol. Soedin., *A18*, 1073 (1976).

191. Golovin, V. A., Lotmentsev, Yu. M., Yershov, S. M., Demchenko, M. D., Vysokomol. Soedin., *A25*, 443 (1983).

192. Golovin, V. A., Lotmentsev, Yu. M., Il'in, A. B., Kondokova, N. N., Vysokomol. Soedin., *A25*, 2300 (1983).

193. Ceccorulli, G., Pizzoli, M., Scandola, M., Pezzin, G., Crose, G., J. Macromol. Sci. -- Phys., *B20*, 519 (1981).

194. Ceccorulli, G., Pizzoli, M., Scandola, M., Pezzin, G., Polym. Commun., *24*, 107 (1983).

195. Pizzoli, M., Pezzin, G., Ceccorulli, G., Scandola, M., Crose, G., in *Macromolecular Solutions*, Seymour, R. B., Stahl, G. A., eds., Pergamon Press: New York, 1982, pp. 70-83.

196. Flory, P. J., Rehner, J., J. Chem. Phys., *11*, 521 (1943).

197. Guzeyev, V. V., Malinskii, Yu. M., Shkalenko, Zh. I., Vysokomol. Soedin., *A17*, 1843 (1975).

198. Linhardt, F., Kuntstoffe, *53*, 18 (1963).

199. Leuchs, D., Kuntstoffe, *46*, 547 (1956), referenced by Buszard, D. L., Chap. 5 in Ref. 36.

200. Rabek, J. F., *Experimental Methods in Polymer Chemistry*, Wiley: London, 1980, Chap. 28.

Table 3.1

Solubility Measures of Various PVC Plasticizers
from Hata, Tobolsky, and Bondi (128)+

Plasticizer	$\Delta E \left(\text{kcal}/\text{mol}\right)$	x	$(\delta_1 - \delta_2)^2$
Tricresyl phosphate	13.1	0.38	1.0
DOP	11.3	0 +/- 0.02	1.0
DBP	7.7	-0.05	0.1
Poly (propylene adipate)	---	0.22	0.5
Ethoxylated soybean oil	---	--	---
DEHS	7.0	0.39	1.1
Di-2-ethylhexyl adipate	6.0	0.28	1.2
Tri-2-ethylhexyl phosphate	6.5	-0.30	2.0

+   References are given in Ref. 128.

Table 3.2

Major Physical Properties of Plasticizers Studied+

Plasticizer	Mol. wt. (g/mol)	Density (g/cc)	Molar Volume (cc/mol)	δ*
DBP	278.4	1.0462	266.1	9.41
DEHS	342.5	0.928	361.1	8.48
. . . .	. . . .	. . . .	. . . .	. . . .
DOP	390.0	0.982	397.2	8.86
DPP	250.3	1.071	233.7	9.60
DBSu	230.0	0.974	236.1	8.94
DBSe	314.5	0.9329	337.1	8.63

* Calculated from Small's constants (13)

Table 3.3

Degrees of Syndiotacticity from ^{13}C nmr

Triad	Resonance position (ppm)	Intensity	Fractional Intensity
rr	59.2274	12.257	0.342
mr	58.2251	17.200	0.479
mm	57.3477	6.428	0.179

% syndiotactic diads = (r) = (rr) + 1/2(mr)

$$= 0.342 + 1/2(0.479) = 0.582$$

% isotactic diads = (m) = (mm) + 1/2(mr)

$$= 0.179 + 1/2(0.479) = 0.418$$

Table 3.4

Weight Percents and Corresponding Mole and Volume Fractions

| | DBP | | DEHS | |
Wt. Percent	Volume Fraction	Mole Fraction	Volume Fraction	Mole Fraction
10	.129	.024	.144	.020
40	.471	.130	.501	.108
60	.667	.252	.694	.215
75	.801	.402	.819	.354

Table 3.5

Bragg Spacings and Correlation Distances from SAXS

Sample	Bragg Spacing (nm)	Correlation Distance (nm)+
DEHS40	15.2	10.9
DEHS60	14.9	11.1
DEHS75	19.0	12.2
DBP40	12.9	10.4
DBP60	14.2	10.0
DBP75	13.9	11.1

+ Analysis methods and variability of the given values
  are discussed in the Appendix.

Table 3.6 Physical Properties of Six Plasticizers

Plasticizer	Mol. Wt. (g/mol)	Density (g/cc)	Molar Volume (cc/mol)	Boiling Point (°C)	Tm(°C)	Tg(°C)	Refractive Index (25°C)
DBP	278.4	1.046	266.06	340_{760mm}	---	-88	1.493
DEHS	342.5	0.928	361.12	184 (flash point)	---	-99	1.443
DOP	390.0	0.982	397.15	384_{760mm}	---	-80	1.4852
DPP	250.3	1.071	233.71	131_{1mm}	---	-88	1.494
DBSu	230.0	0.974	236.14	275_{760mm}	-29	-111	1.4299 (20°C)
DBSe	314.5	0.933	337.12	349_{760mm}	-12	none	1.4390

Table 3.7 Measures of Solubility Between PVC and Plasticizers

Plasticizer	δ_{Small}	$\dfrac{\log \text{modulus}}{\log \text{conc'n}}$	microtest for compatibility^x	Dielectric Constant†	δ(Eq.13)	δ(Eq.14)*
DPB	9.41	3.90	-0.05	6.42$^{25°C}$/6.65$^{18°C}$	8.81	10.13
DEHS	8.48	3.40	NL	4.12$^{18°C}$	8.03	9.68
DOP	8.86	3.47	-0.03	5.18$^{25°C}$	8.69	10.06
DPP	9.60	NL	NL	NA	8.82	10.14
DBSu	8.94	NL	NL	5.02$^{25°C}$	7.83	9.55
DBSe	8.63	NL	NL	4.92$^{26°C}$	7.97	9.64

NL = not listed
NA = not available

†18° values obtained in T.C. Ward's Lab.
* C = 353.3

Table 3.8

Melting Points of Aliphatic Dicarboxylic Acids

HOOC -- $(CH_2)_n$ -- COOH

Acid	n	Melting point (^{0}C)
Oxalic	0	189.0
Malonic	1	136.0
Succinic	2	185.0
Glutaric	3	98.0
Adipic	4	151.0
Sebacic	8	134.5

Table 3.9. Background Corrections

Sample	Bonart Bkg Correction	Alternate Bkg Correction
DEHS40	0.7307	1.164 +/- 0.305
DEHS60	0.8765	1.046 +/- 0.241
DEHS75	0.8156	1.031 +/- 0.217
DBP40	0.8124	1.168 +/- 0.310
DBP60	0.8093	1.150 +/- 0.206
DBP75	0.4134	0.555 +/- 0.146

Table 3.10. Correlation Distances (nm)
(Bonart Bkg Correction)

Sample	Maximum Integration Limit	
	$s = 0.02$	$s = 0.03$
DEHS40	11.2	10.9
DEHS60	11.2	11.1
DEHS75	14.1	12.2
DBP40	10.7	10.4
DBP60	11.1	10.0
DBP75	11.1	11.1

Table 3.11. Inhomogeneity Lengths (nm)
(Bonart Bkg Correction)

Sample	Maximum Integration Limit	
	$s = 0.02$	$s = 0.03$
DEHS40	2.8	2.8
DEHS60	2.8	2.7
DEHS75	3.7	3.5
DBP40	2.1	2.6
DBP60	2.5	2.5
DBP75	2.4	2.4

Table 3.12.   Invariant Ratios+
              (Bonart Bkg Correction)

| | Maximum Integration Limit | |
Sample	s = 0.02	s = 0.03
.DEHS40	1.0	1.0
DEHS60	0.783	0.759
DEHS75	0.999	0.974
DBP40	1.0	1.0
DBP60	1.049	1.045
DBP75	0.577	0.571

Table 3.13.   Calculation of μ/ρ
for Polyvinyl Chloride

Chemical composition: C2H3Cl

Molecular weight per repeat unit: 62.5 g/mol

Amorphous density: 1.385 g/cc
Maximum crystalline density: 1.53 g/cc

ATOM	N	At.wt. (A)	μ/ρ	$n_i A_i$	ω_i	$\omega_i \left(\frac{\mu}{\rho}\right)_i$
C	2	12.01	4.60	24.02	0.384	1.766
H	3	1.01	0.435	3.03	0.048	0.021
Cl	1	35.45	106.0	35.45	0.567	60.102
			SUMS →	62.5	~ 1.000	61.889

$\mu/\rho = 61.889$

$61.889 \cdot 1.4 = 86.64$ inv. cm = μ

$1/\mu = t(opt) = .0115$ cm = 4.5 mils

Table 3.14. Optimum Thicknesses (in mils)
for DEHS-PVC and DBP-PVC Films

Wt. % Plasticizer	DEHS-PVC	DBP-PVC
10	5.3	5.2
40	8.6	8.1
60	13.1	12.0
75	19.9	17.8

Values based on volume fractions.

Figure 3.1. Temperature dependence of shear modulus (G) and log decrement (Λ) for PVC containing increasing amounts of a) diethylhexyl succinate and b) dibutyl phthalate. Samples prepared by compression molding. Data obtained on a torsion pendulum at about 1 Hz. Ref. 1.
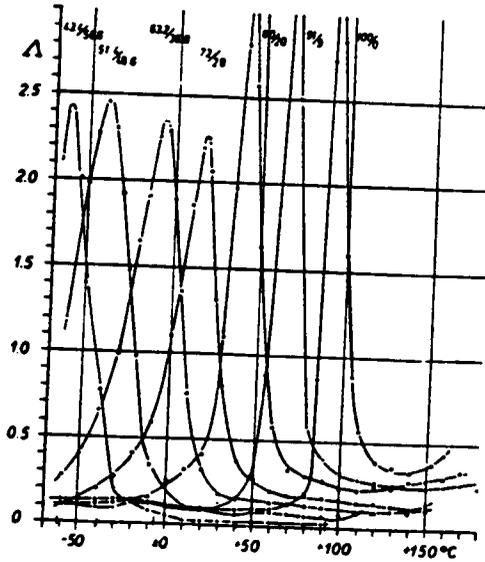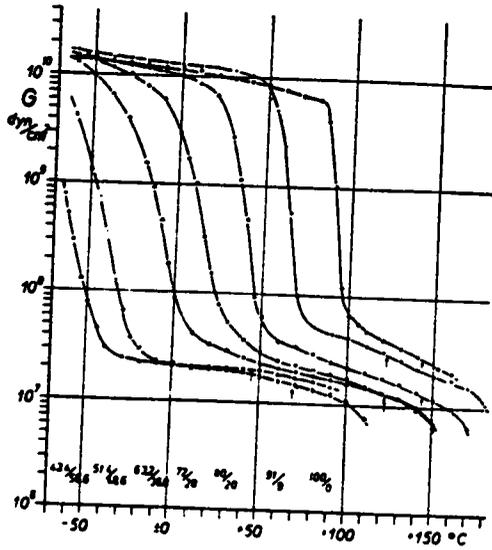
b
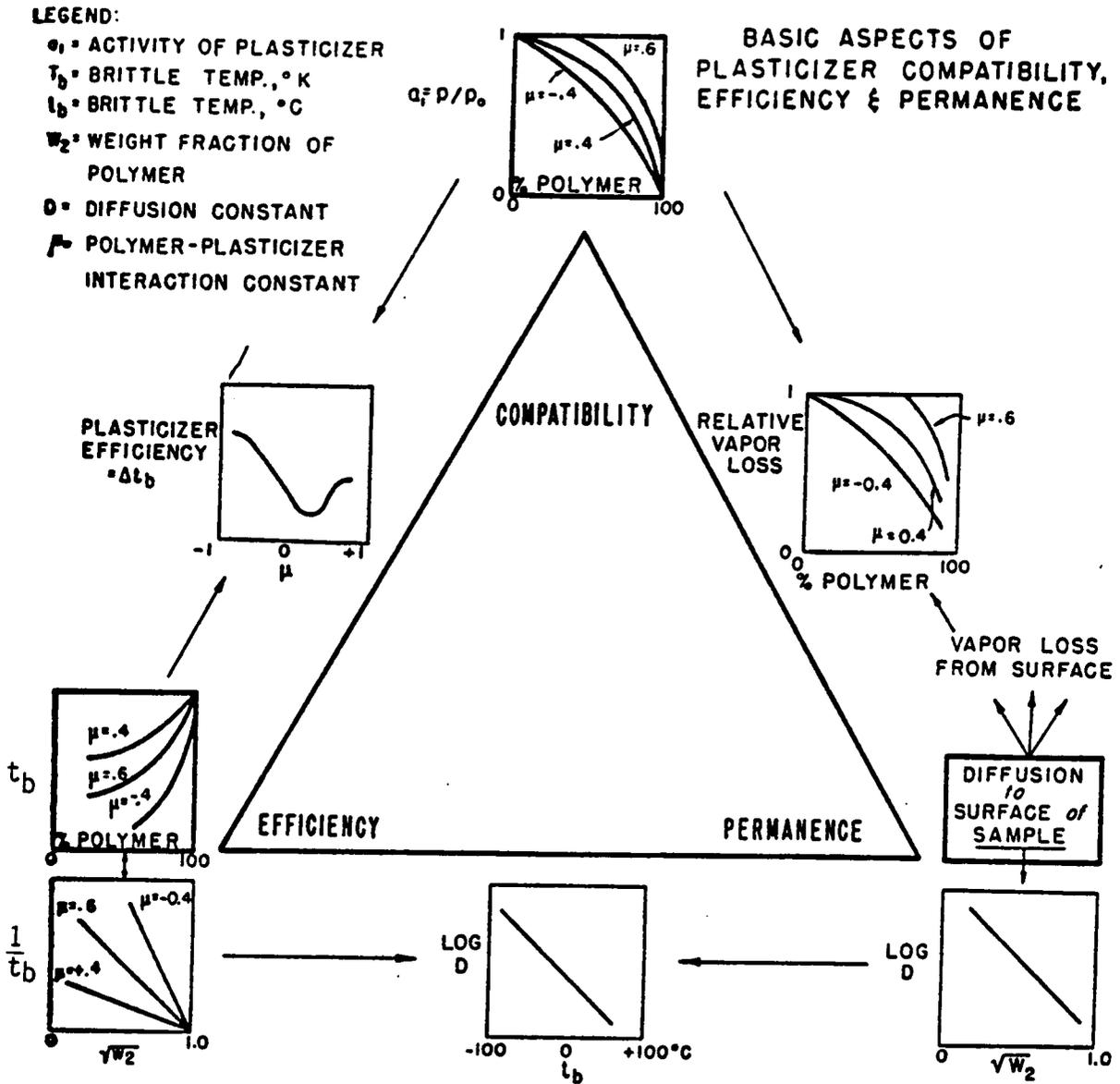
Figure 3.2. Interrelationship of compatibility, efficiency, and permanence for PVC and plasticizers. Ref. 4.
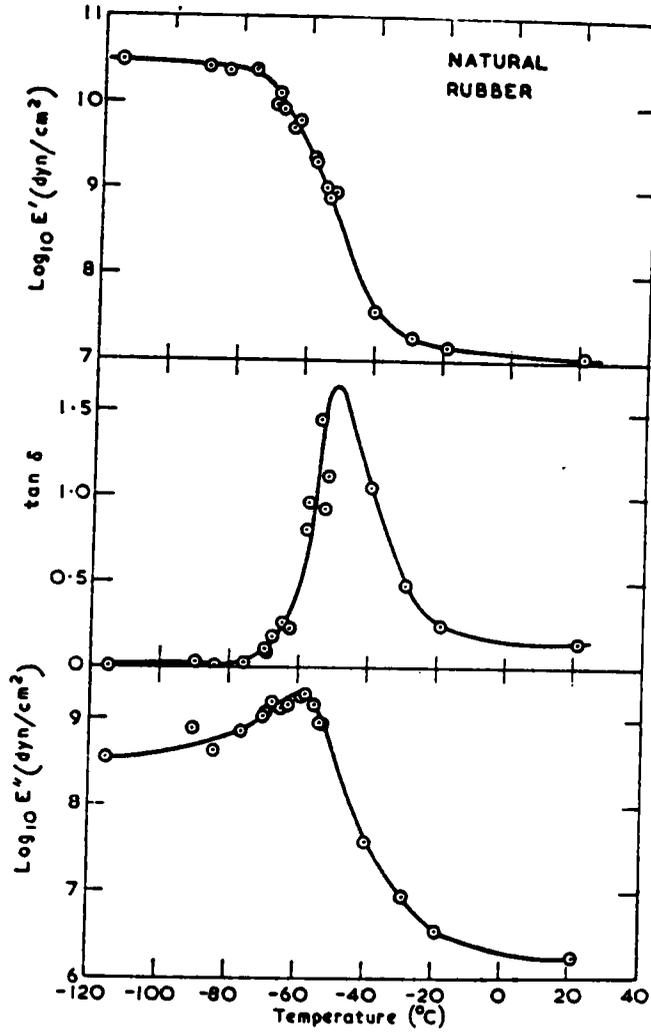
Figure 3.3.   Behavior of E', E", and tan δ for natural rubber.
After Read, Proc. 5th Int. Cong. Rheol., 4, 71 (1970).
From Ref. 2.
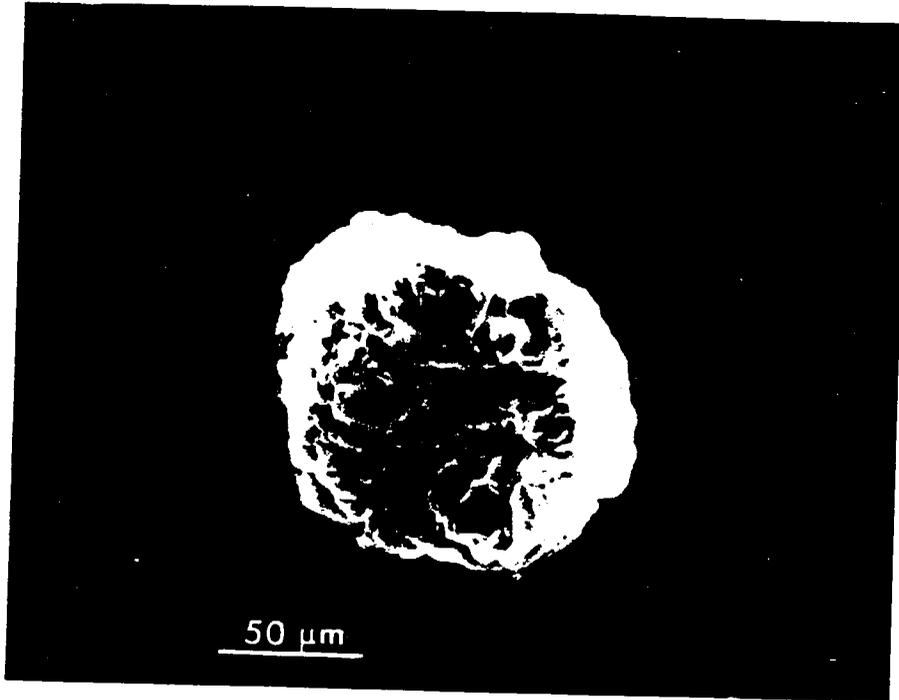
Figure 3.4.   SEM micrographs of PVC resin grain.   By author.
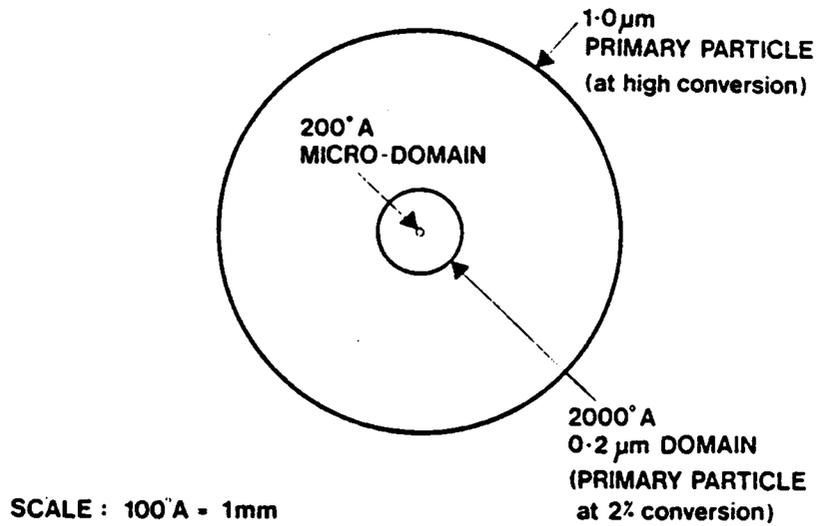
Scale Model of PVC

Submicroscopic Structure
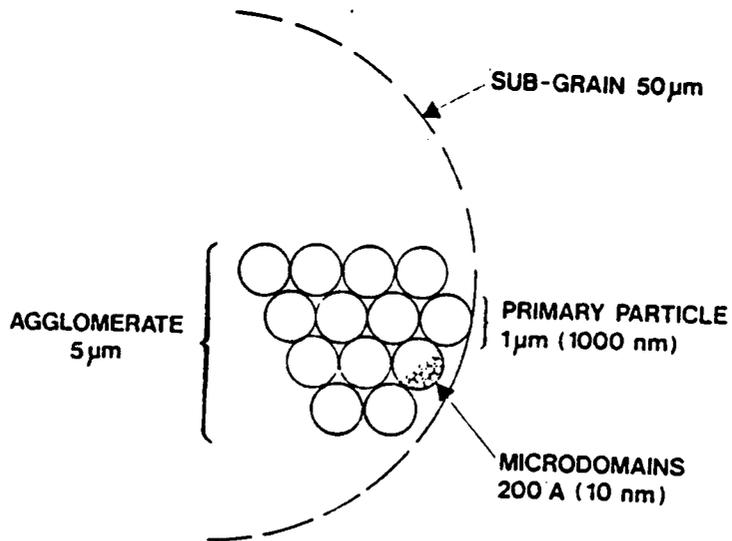
Model of PVC Grain Morphology

Figure 3.5. Structure and terminology of PVC grain substructures.
Ref. 22.
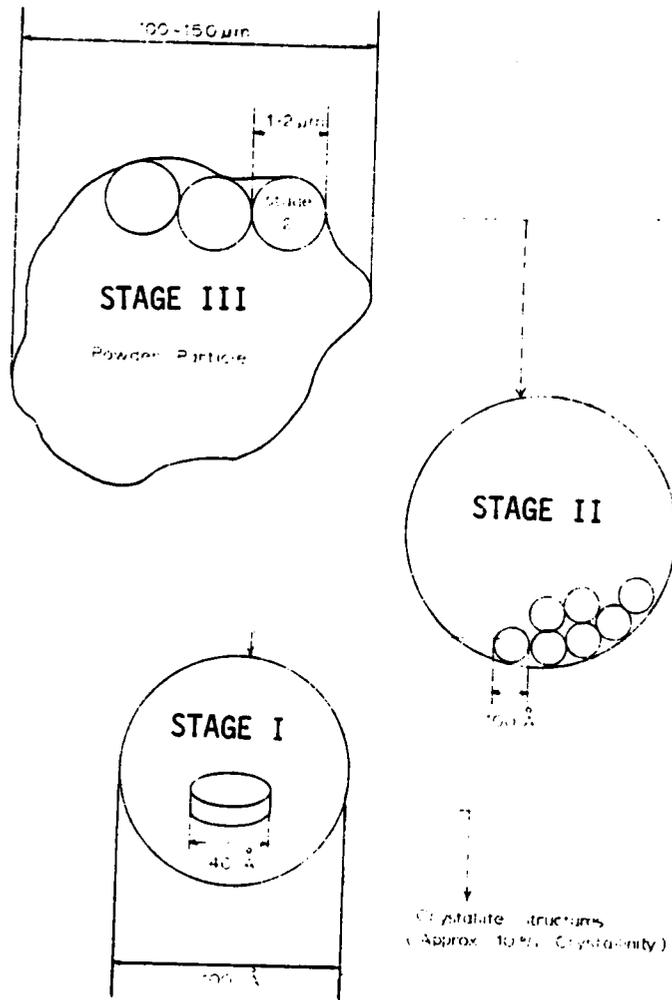
Figure 3.6. Stage terminology used to describe PVC grain structure. Ref. 26.

Figure 3.7. Schematic concept of the fringed micelle.
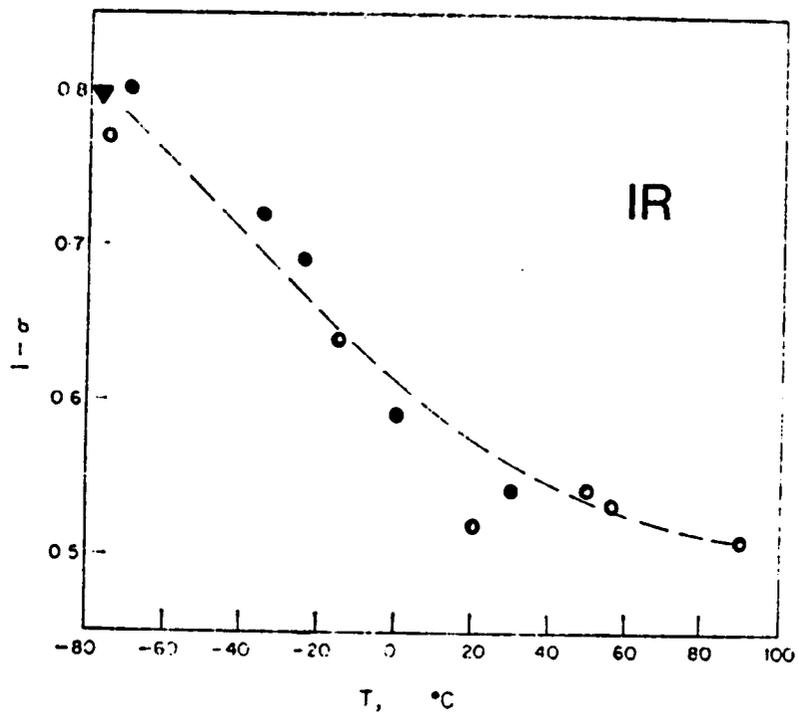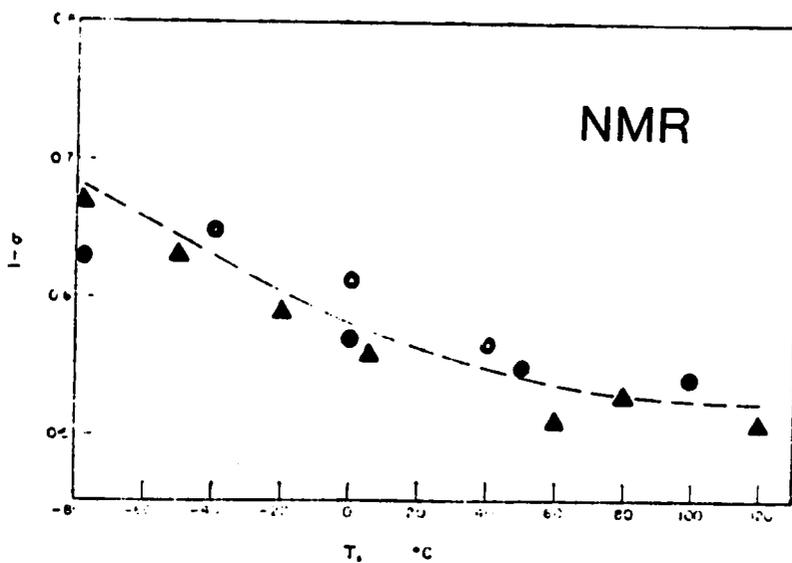
Figure 3.8. Syndiotacticity (1-σ) as a function of polymerization temperature. Data obtained from a) IR and b) nmr. Ref. 38. Data taken from various sources; see Ref. 38.

DRAW DIRECTION ⟶
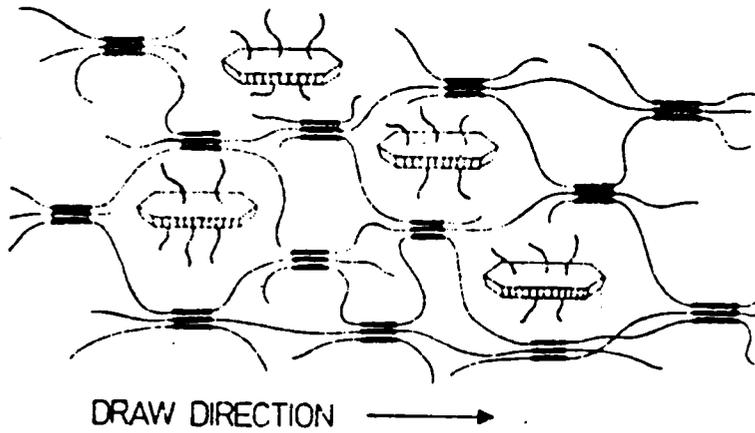
Figure 3.9. Schematic model of the two-crystal texture of PVC gels. Ref. 74.
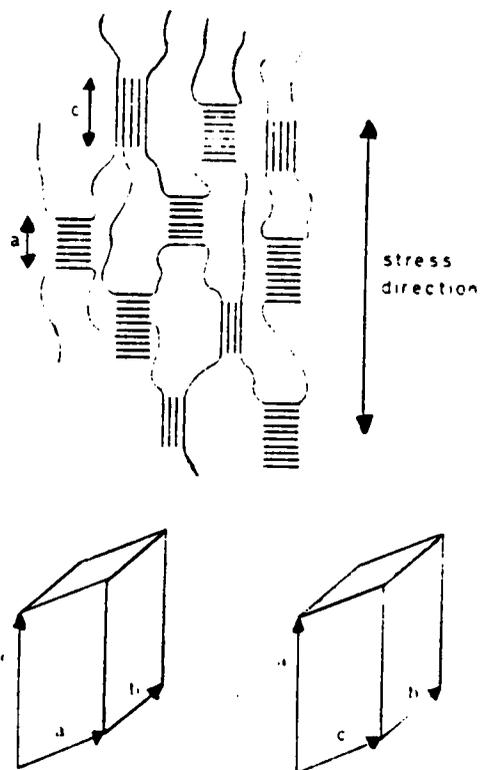
Figure 3.10.   Orientation of fringed micelle structures in gels of polyethylene terephthalate-co-isophthalate.   Ref. 79.
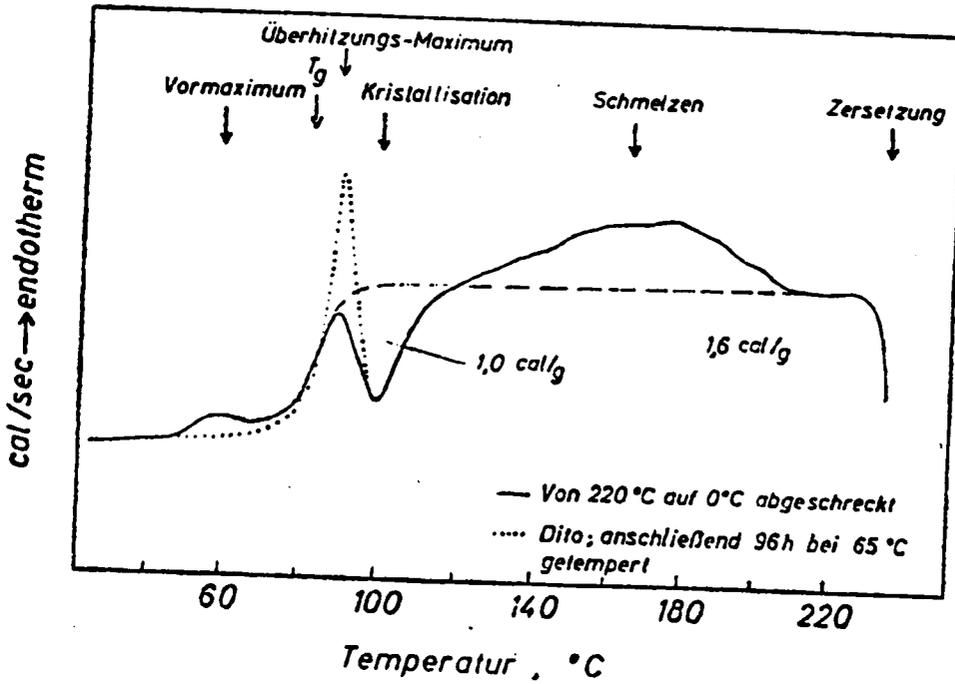
Figure 3.11. DSC traces showing the use of quenching from 220°C to obtain a crystallization exotherm upon reheating unplasticized PVC. Ref. 86.
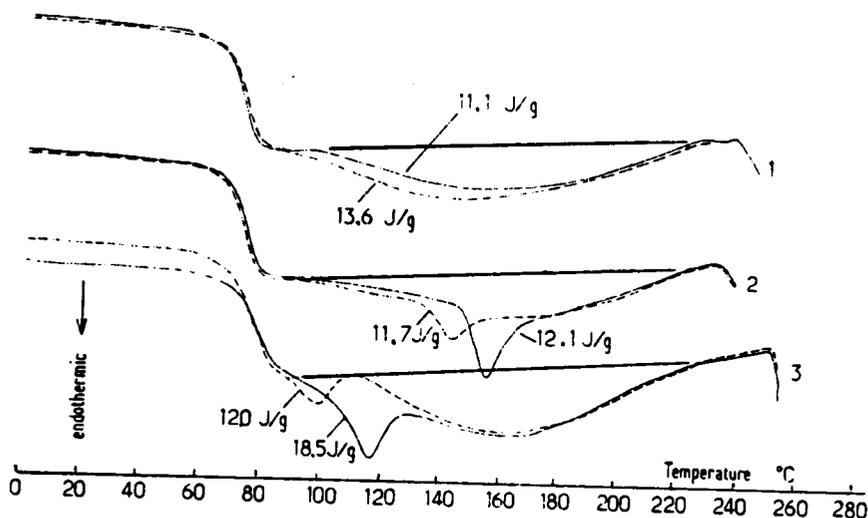
Figure 3.12. Effects of isothermal annealing on PVC. Heat of fusion values measured from endotherms remains essentially constant. Sample 1 cooled from 240°C at a rate of (___) 20°C/min or (---) 1°C/min; sample 2 cooled from 240°C at rate of 20°C/min and annealed at 130°C for (---) 5 min or (___) 16 hrs; sample 3 quenched from 25°C (should be 250°C? -author-) (5 sec) into ice water and annealed at 90°C for (---) 5 min or (___) 16 hrs. Ref. 87.
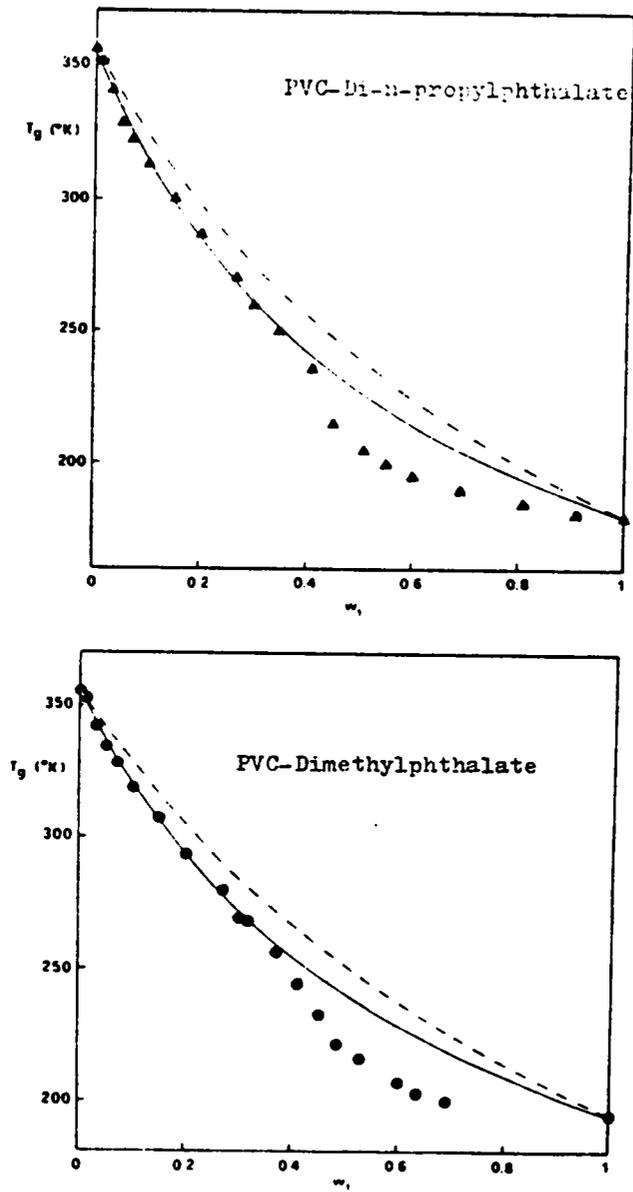
Figure 3.13. Examples of the "cusp-like" behavior of Tg with increasing plasticizer content in PVC. Ref. 99.
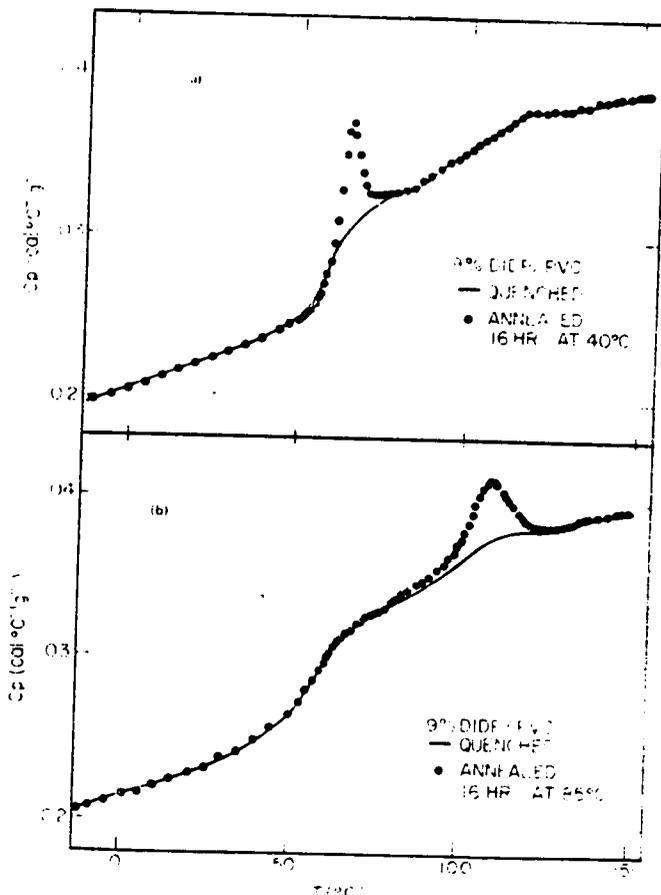
Figure 3.14. Introduction of enthalpy relaxation peaks by selective annealing of lightly plasticized PVC which reportedly displays upper and lower Tg values. DIDP = diisodecyl phthalate. Ref. 106.
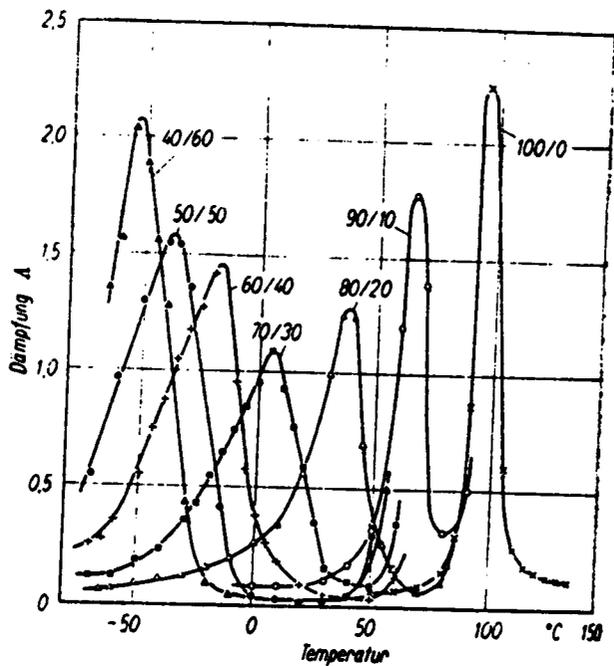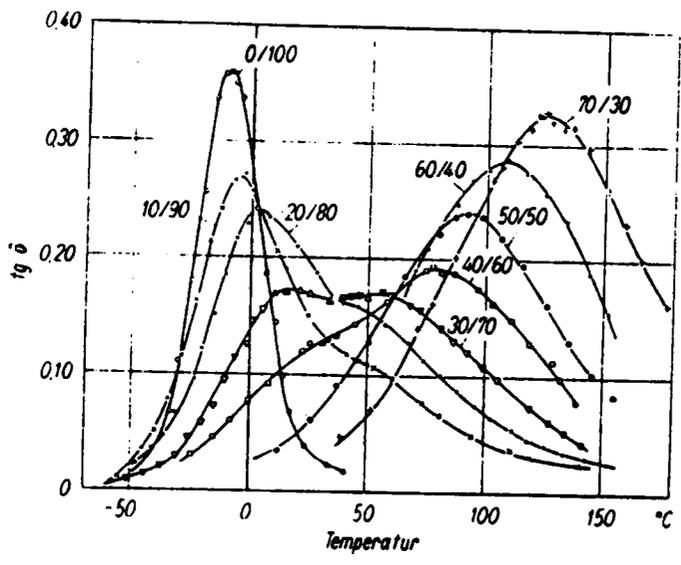
Figure 3.15. Temperature dependence of a) mechanical damping (frequency ~ 1 Hz) and b) dielectric damping (frequency 10^7 Hz) for PVC containing increasing amounts of diethylhexyl phthalate. Ref. 124.
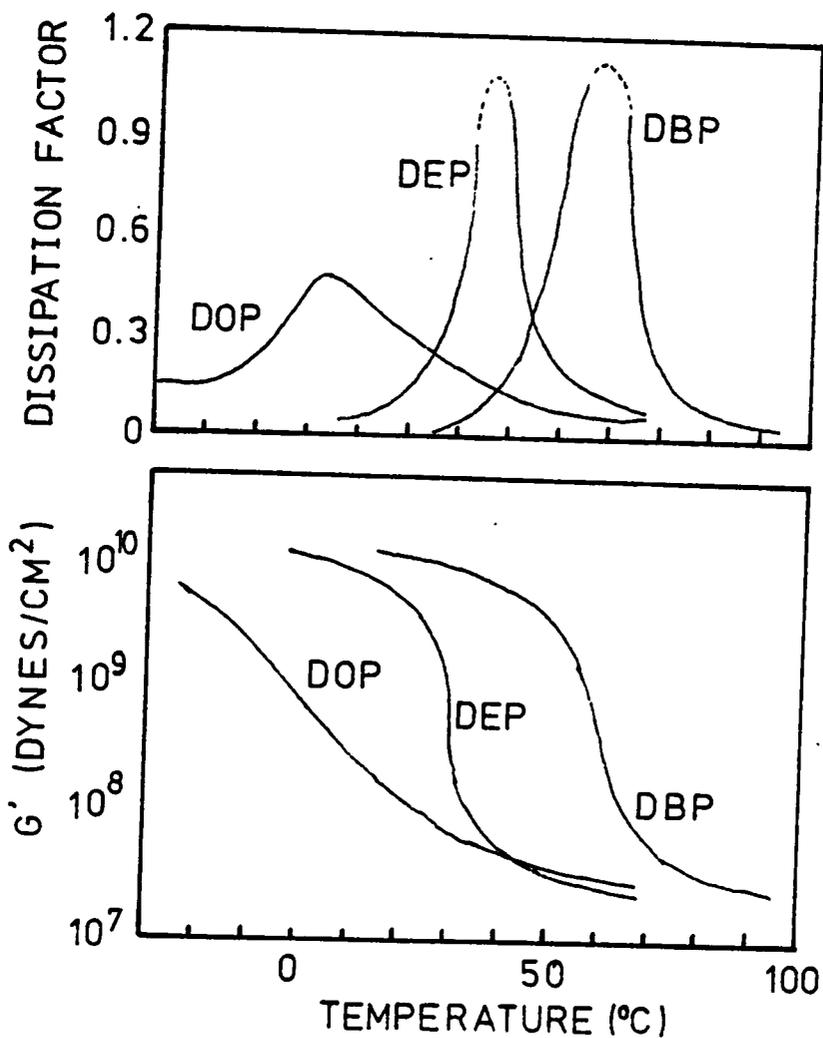
Figure 3.16.   Dynamic shear modulus and dissipation (damping)
factor as a function of temperature for plasticized PVC containing
volume fractions 0.158 DBP,, 0.254 diethyl phthalate (DEP), and 0.402
DOP. The respective x values of these plasticizers are
-0.04/-0.01, 0.42/0.49, and 0.01/0.03 at temperatures of
53°/76°C (6). Adapted from Ref. 127.
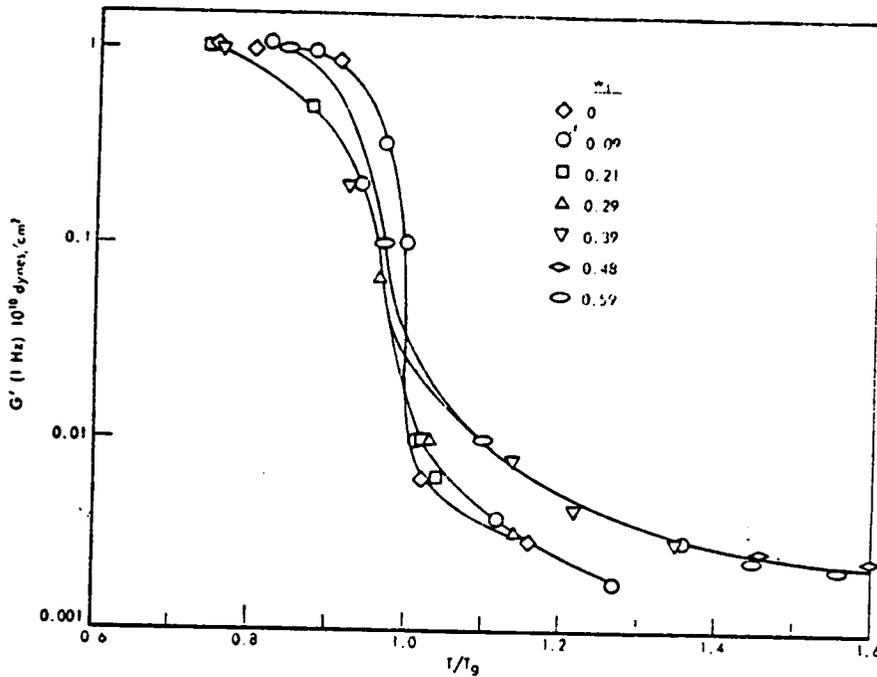
Figure 3.17. Dynamic shear modulus of DEHS-PVC of various weight fractions plasticizer as a function of T/Tg. With data from Ref. 1. Ref. 128.
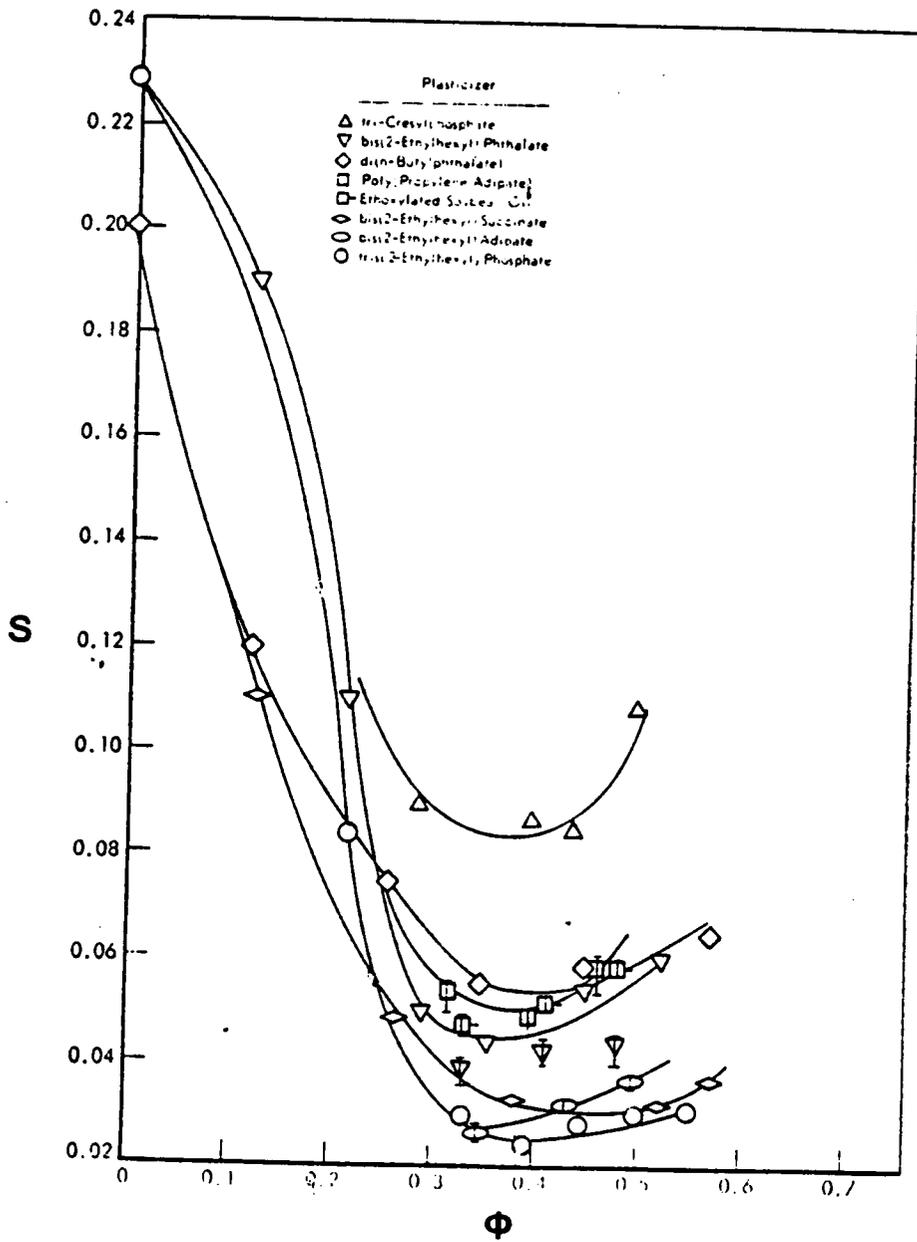
Figure 3.18. Slope constant *s* vs. volume fraction of a variety
of plasticizers. Ref. 128. See also Table 3.1.
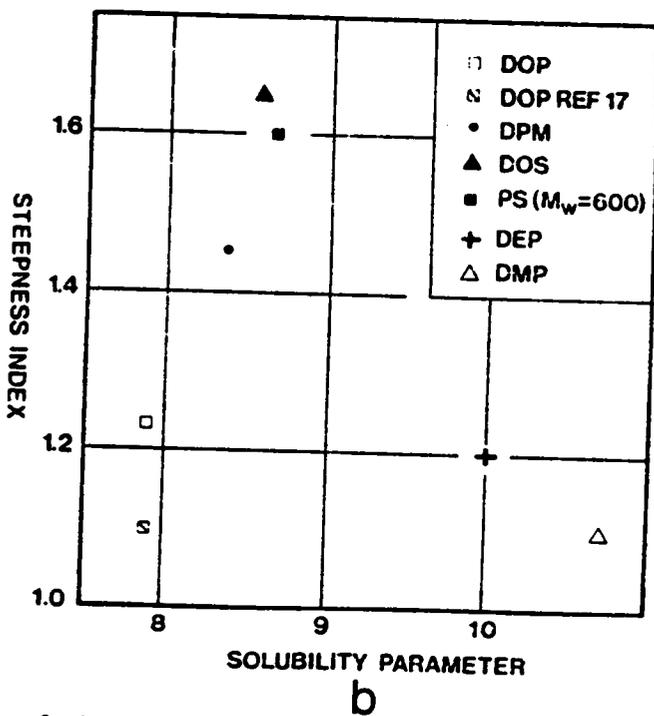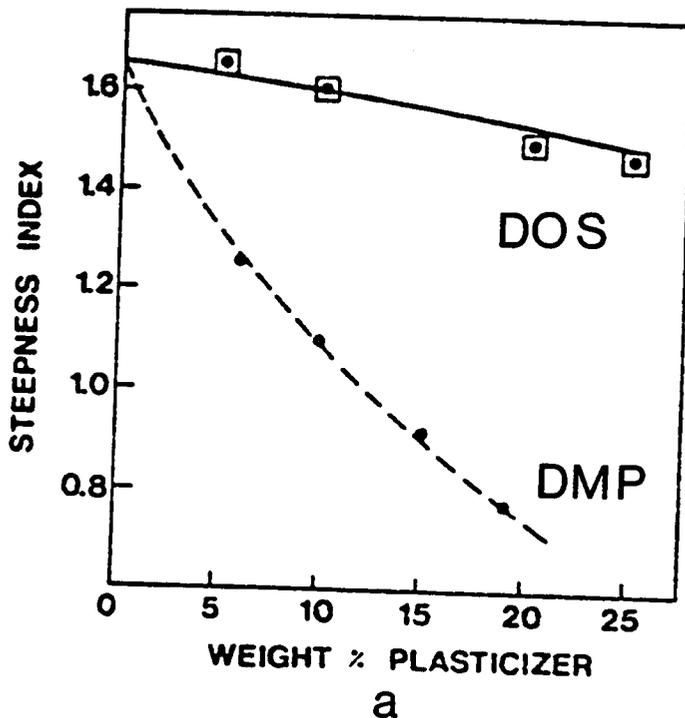
Figure 3.19. Steepness index a) as a function of weight percent plasticizer for dimethyl phthalate and dioctyl sebacate in polystyrene and b) as function of solubility parameter for polystyrene containing 10% of various plasticizers. Ref. 129. PS-DMP data in (a) from L. L. Chapoy, A. V. Tobolsky, Chem. Scrip., 2, 44 (1972). DOP data in (b) from R. E. Kelchner, Ph. D. Thesis, Univ. S. Cal., 1970, p. 70.
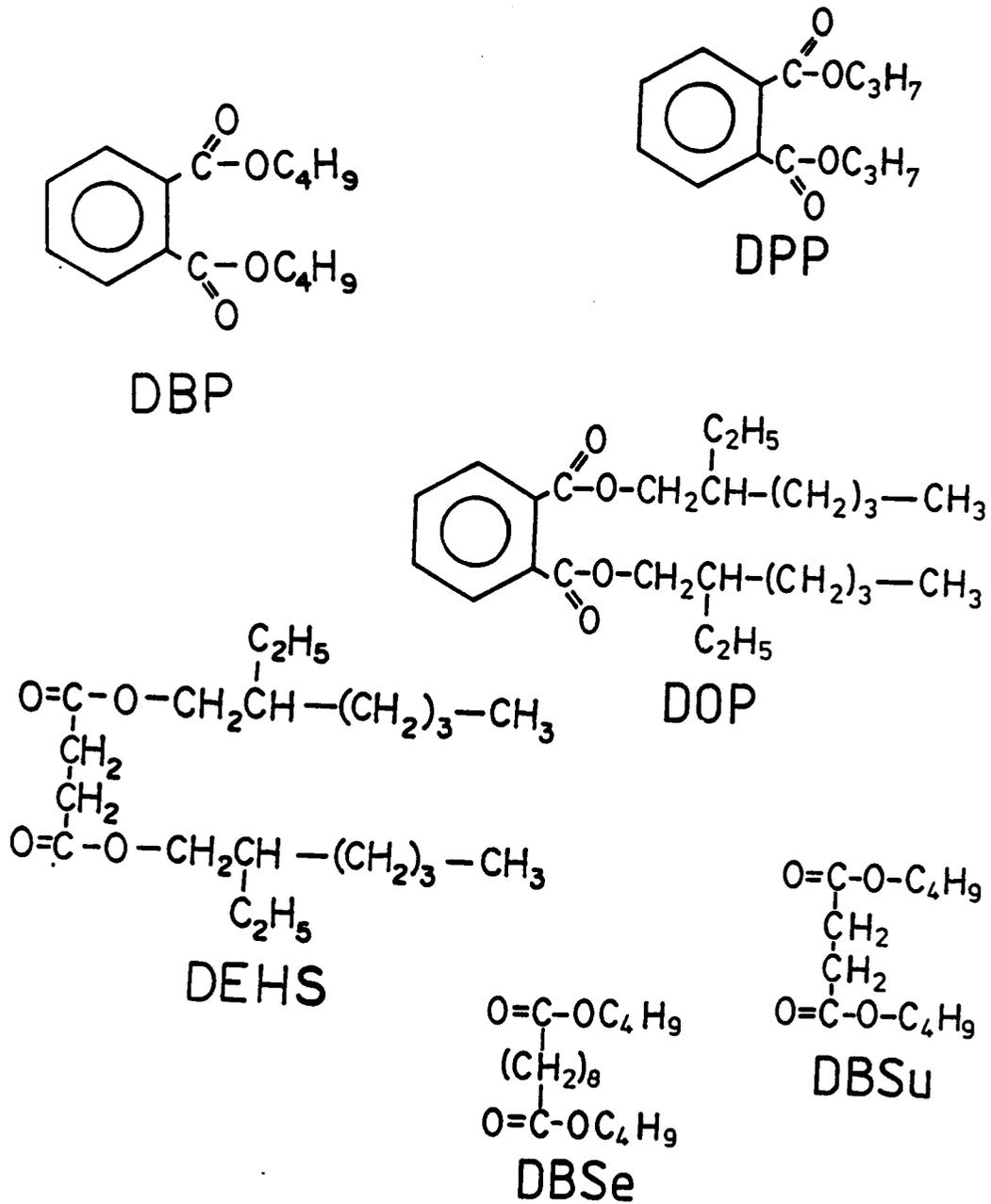
Figure 3.20. Chemical structures of the six plasticizers used in this study. See text for abbreviations.
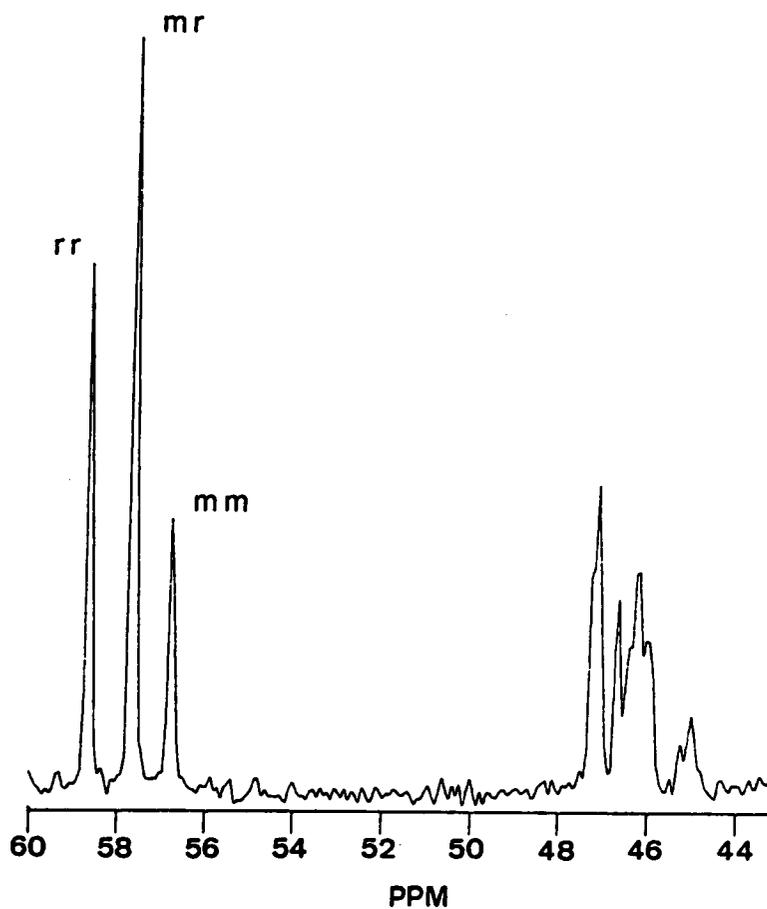
Figure 3.21. ^{13}C nmr spectrum of Diamond Shamrock 450 taken in THF at room temperature. See text for experimental parameters.
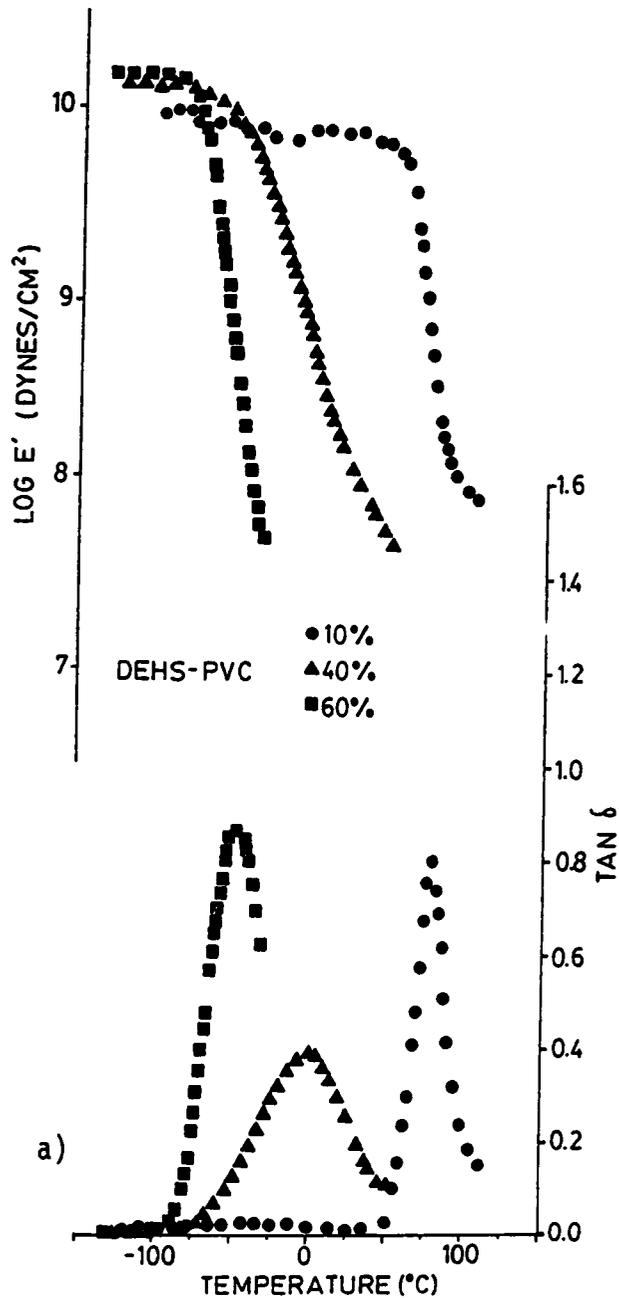
Figure 3.22. Dependence of E' and tan δ on temperature for PVC containing increasing amounts of a) diethylhexyl succinate and b) dibutyl phthalate. Samples prepared by solution casting. Samples containing 10% plasticizer was dried as described in Experimental Section. Data obtained on the Rheovibron at 11 Hz.

b)
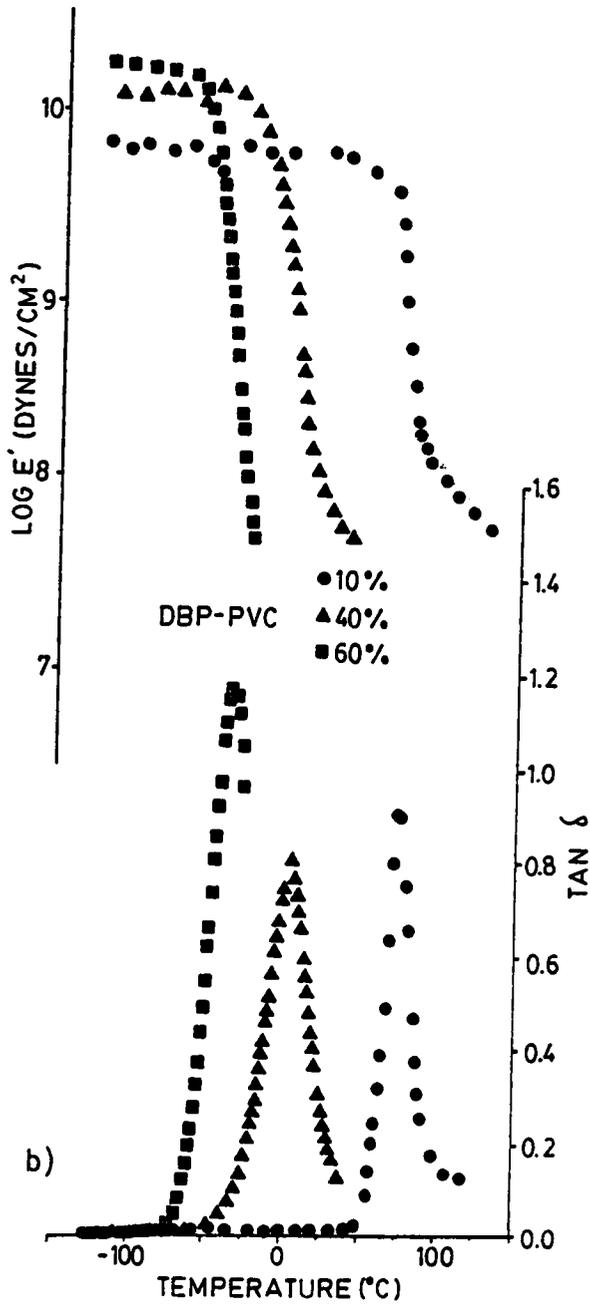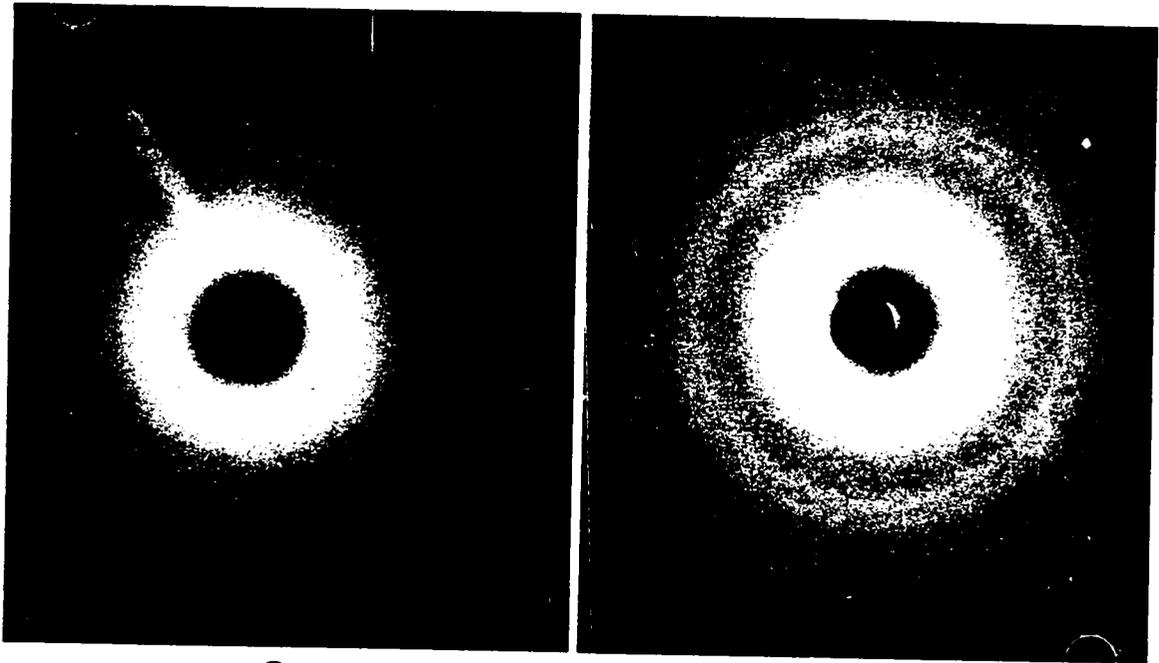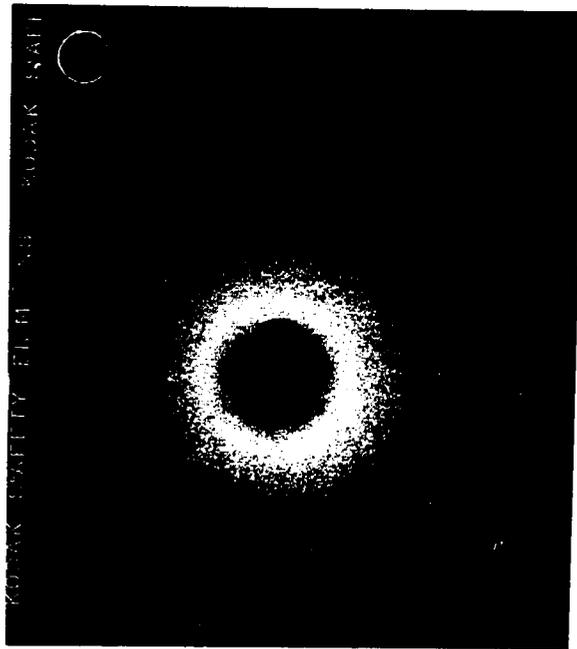
Figure 3.23. WAXS patterns of PVC: a) compression molded at 145°C; b) cast from THF, undried, and c) neat, loaded into 1.5 mm quartz capillary.
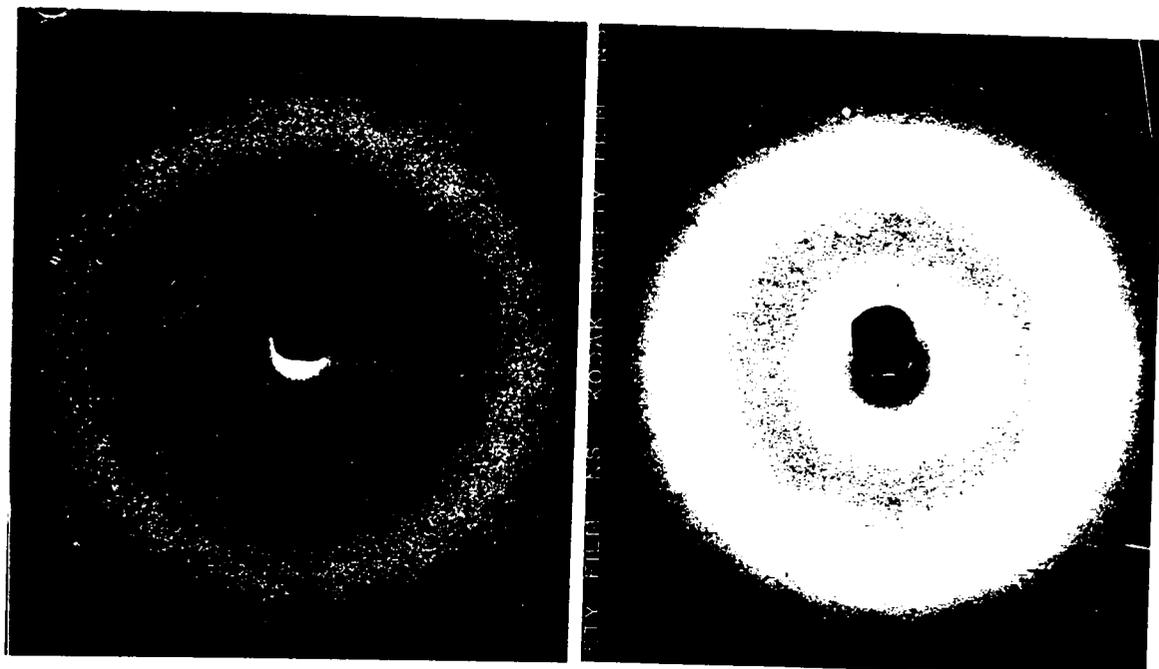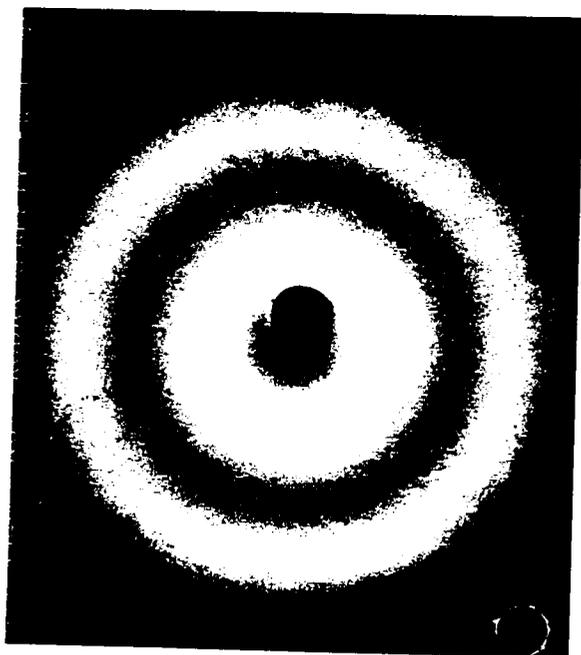
Figure 3.24. WAXS patterns of a) empty quartz capillary, b) neat DEHS in capillary, and c) neat DBP in capillary.
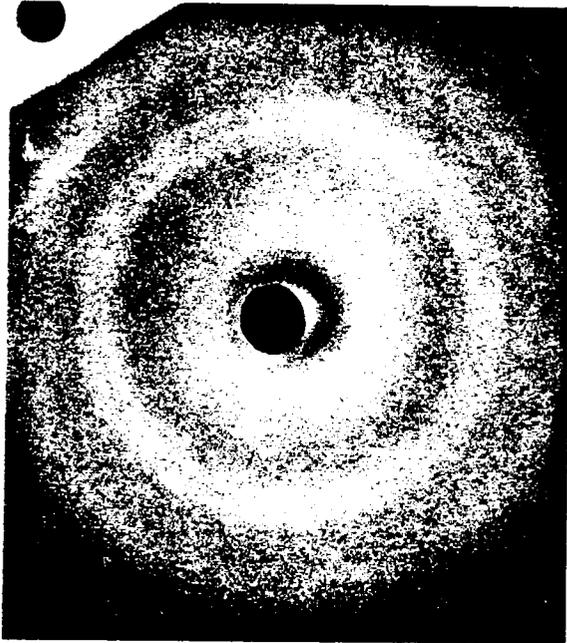
DEHS10
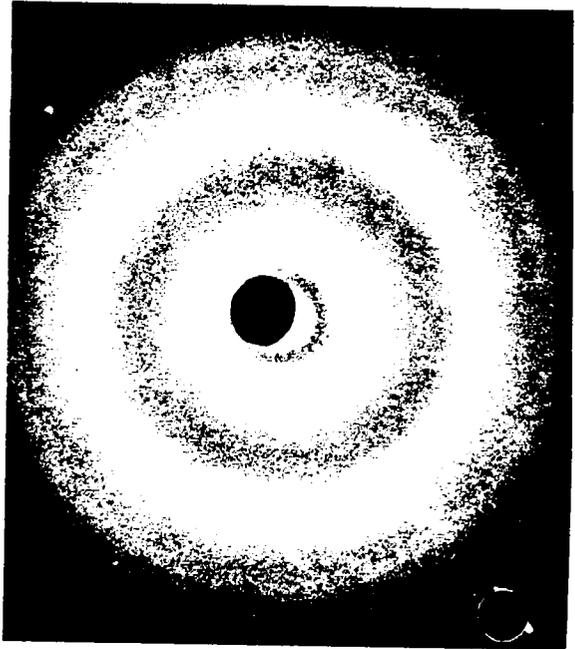
DEHS40
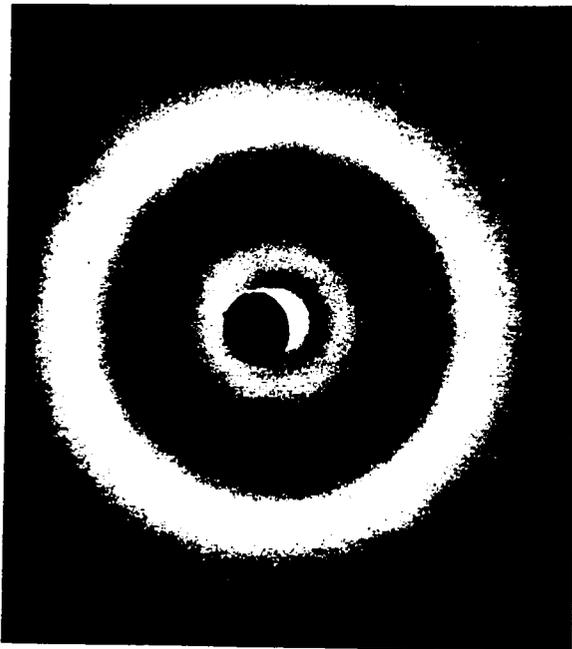
DEHS60 **a** DEHS75
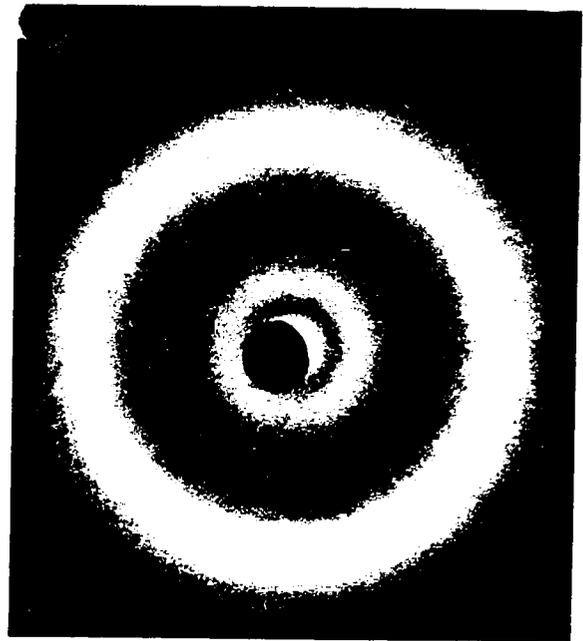
Figure 3.25. WAXS patterns of a) DEHS-PVC and b) DBP-PVC containing 10, 40, 60, and 75 weight percent plasticizer.

DBP10

DBP40

DBP60

b
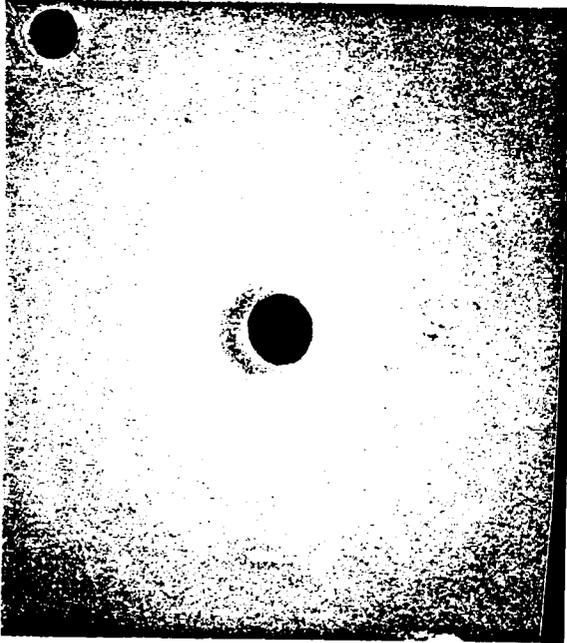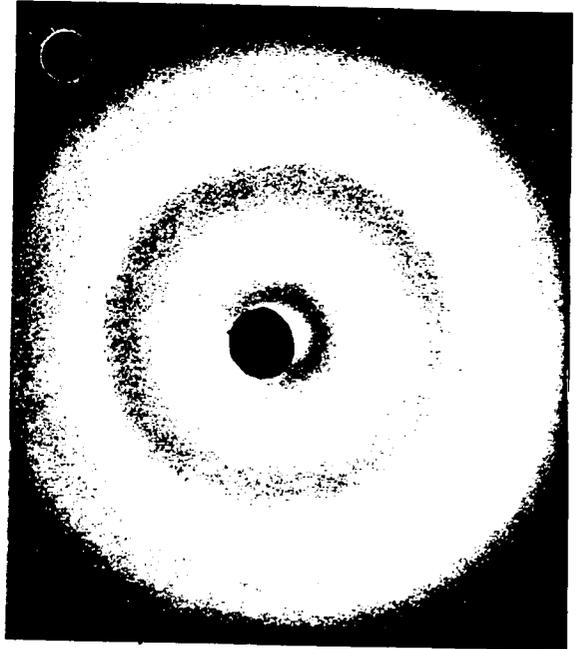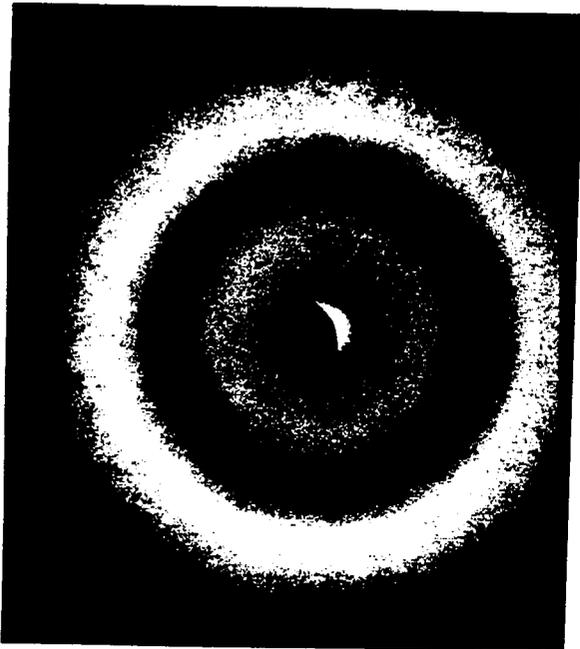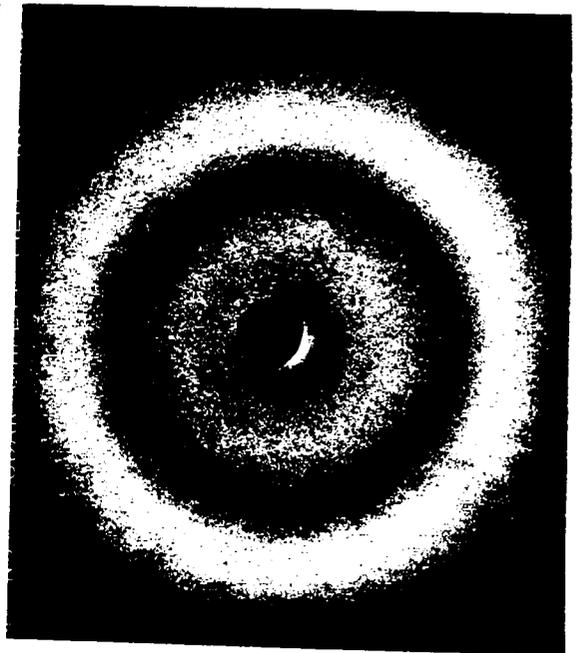
DBP75
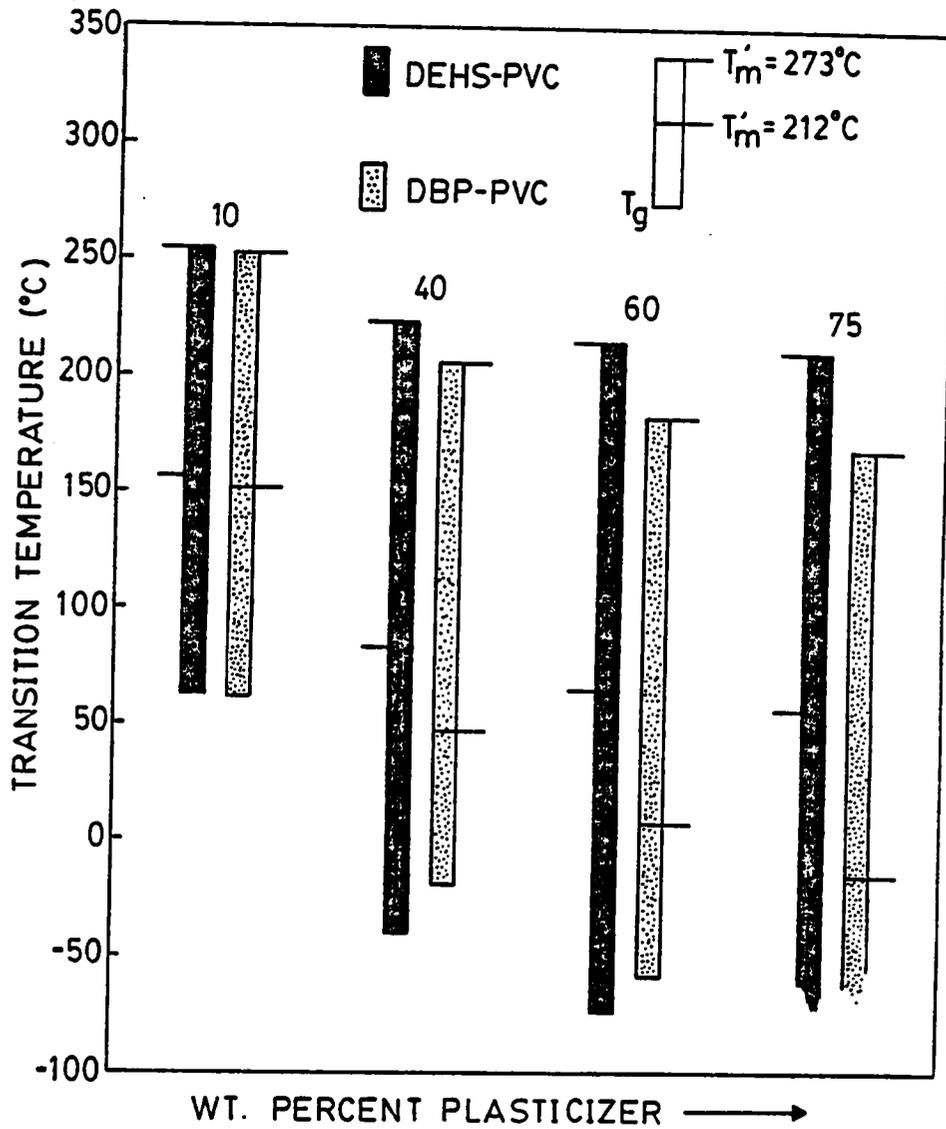
Figure 3.26. Crystallization window of plasticized PVC. Tm calculated from two different Tm' and ΔHu values, as described in text. Tg taken from peak of E".
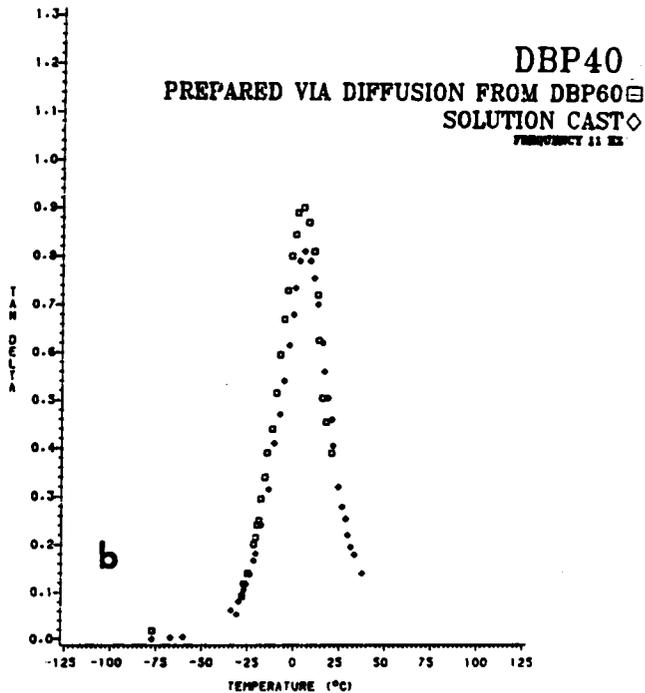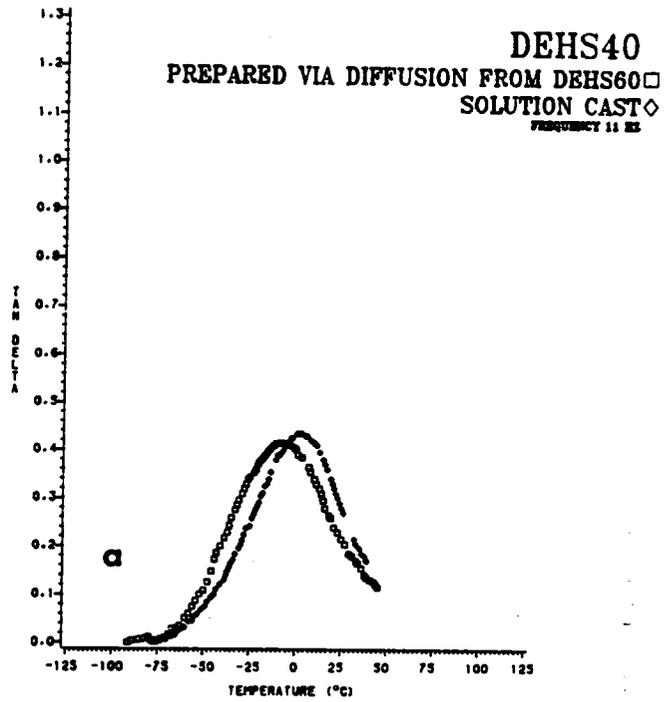
Figure 3.27. Dependence of tan δ on temperature for PVC containing 40% of a) diethylhexyl succinate and b) dibutyl phthalate. Samples prepared by diffusion from films containing 60% plasticizer. Data is compared with a sample originally containing 40% plasticizer.
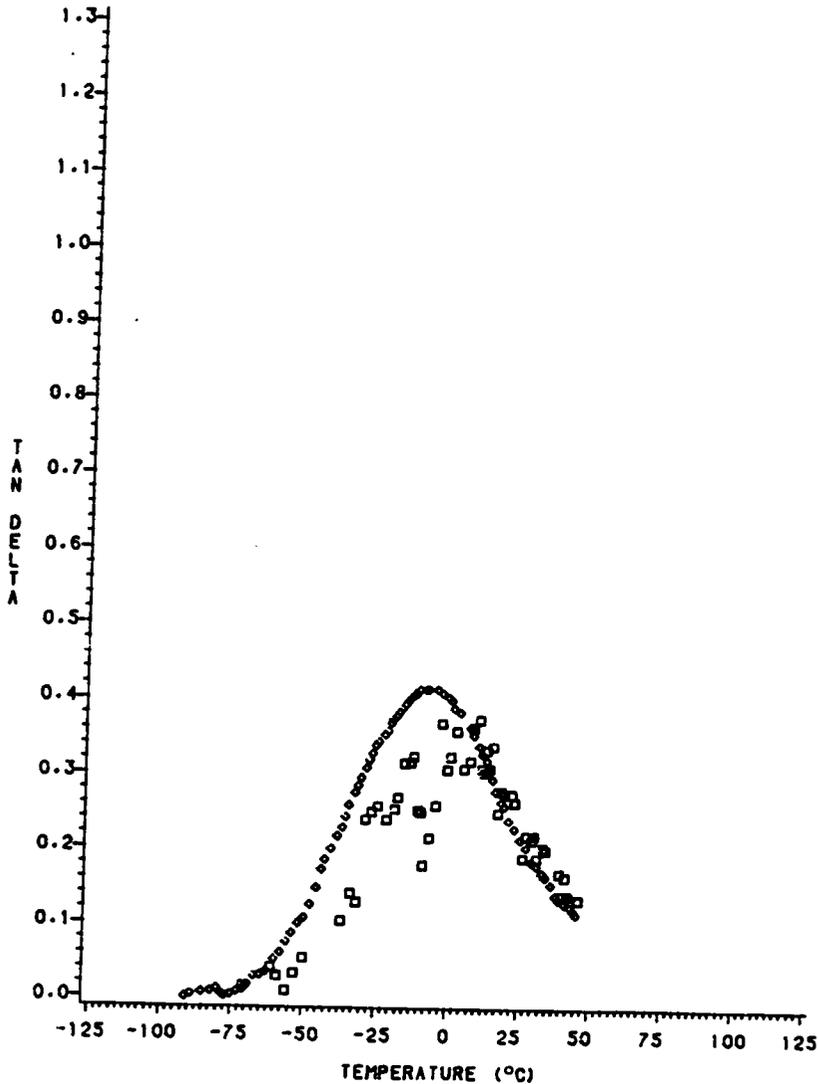
Figure 3.28. Dependence of tan δ on temperature
for PVC containing 40% of diethylhexyl succinate. Data obtained
either 3 or 12 days after sample preparation by diffusion from film
containing 60% plasticizer.
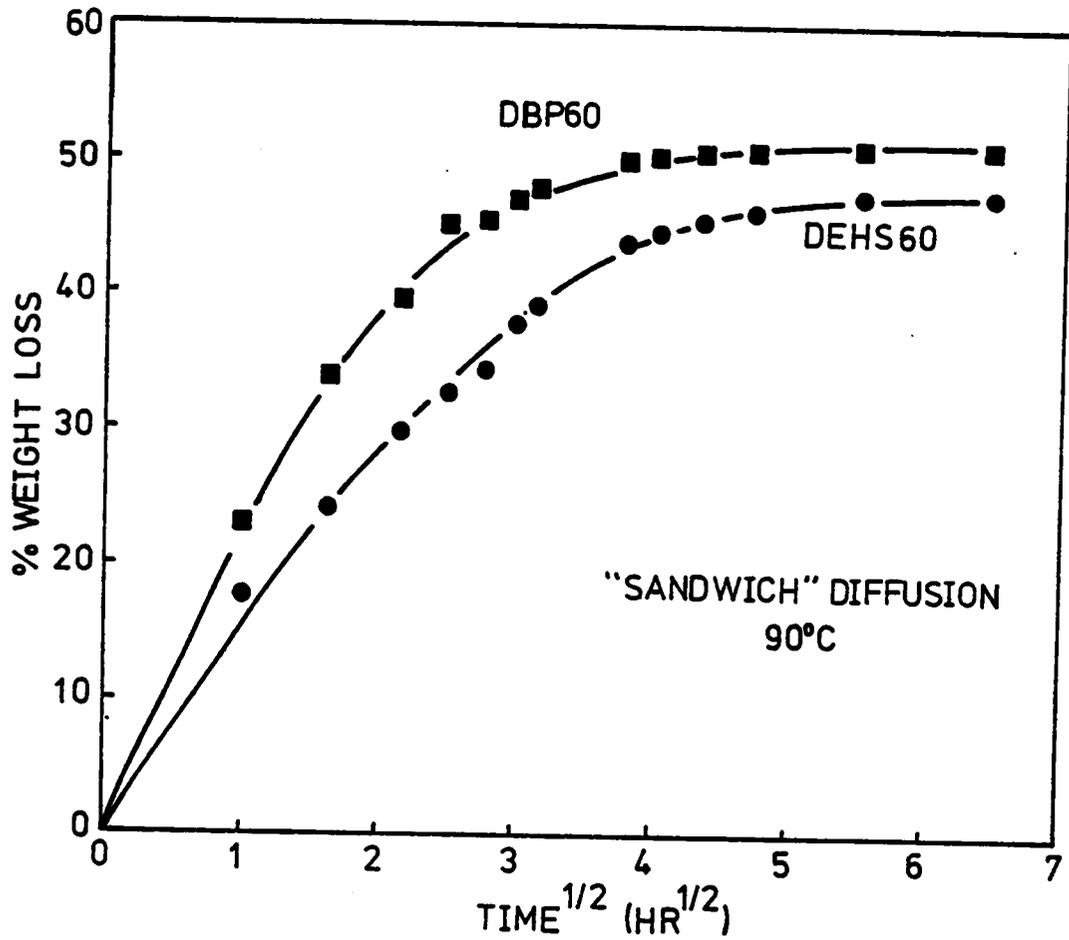
Figure 3.29. Weight loss as a function of square root of time for DEHS60 and DBP60 sandwiched between cast PVC films. Temperature 90°C.
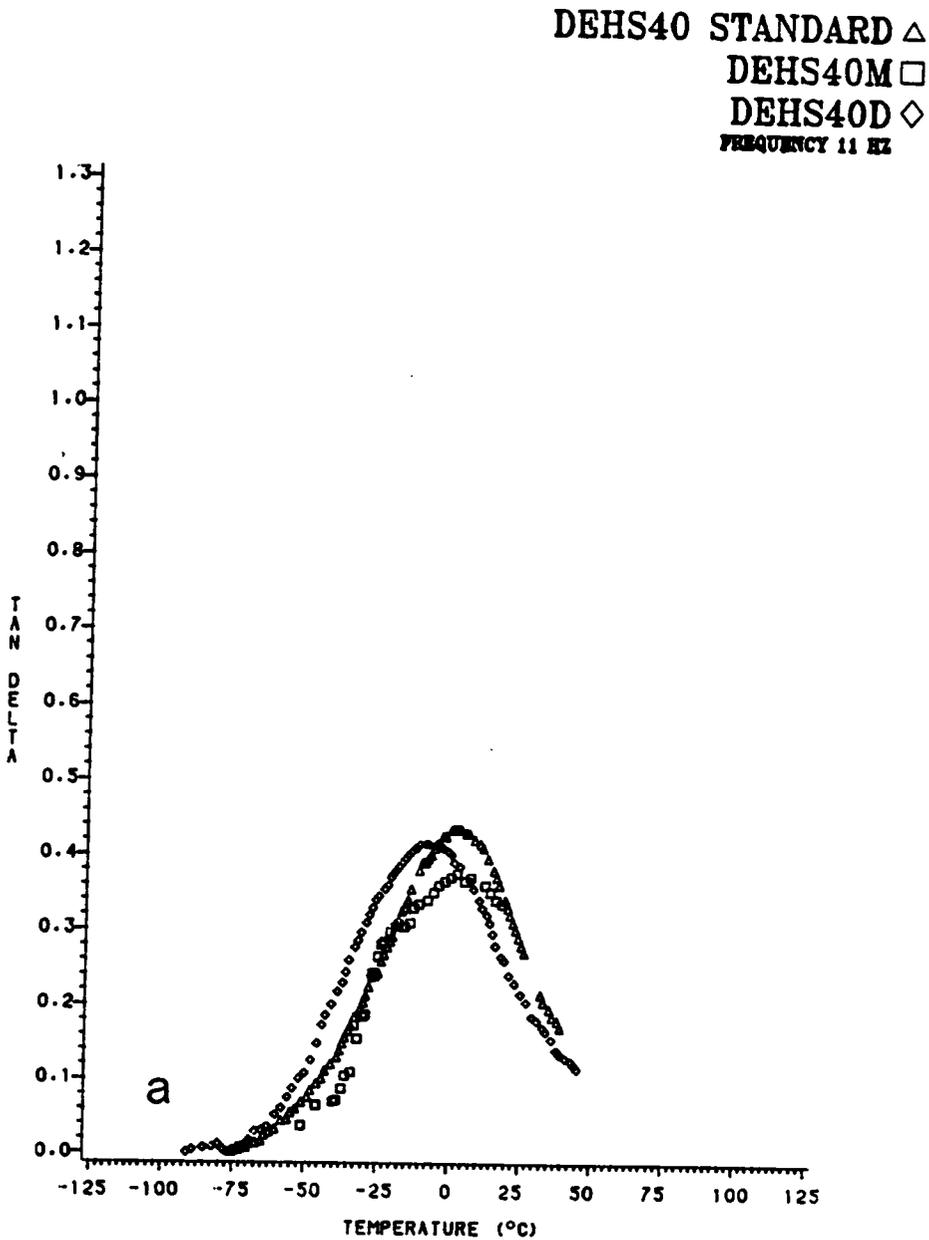
Figure 3.30. Dependence of tan δ on temperature for PVC
containing 40% of a) diethylhexyl succinate and b) dibutyl
phthalate. Samples prepared by standard method, by diffusion from
films containing 60% plasticizer (40D), and by compression molding
(40M), as noted in legend.

DBP40 STANDARD △
DEHS40M □
DEHS40D ◇

FREQUENCY 11 HZ

150°

180°

a
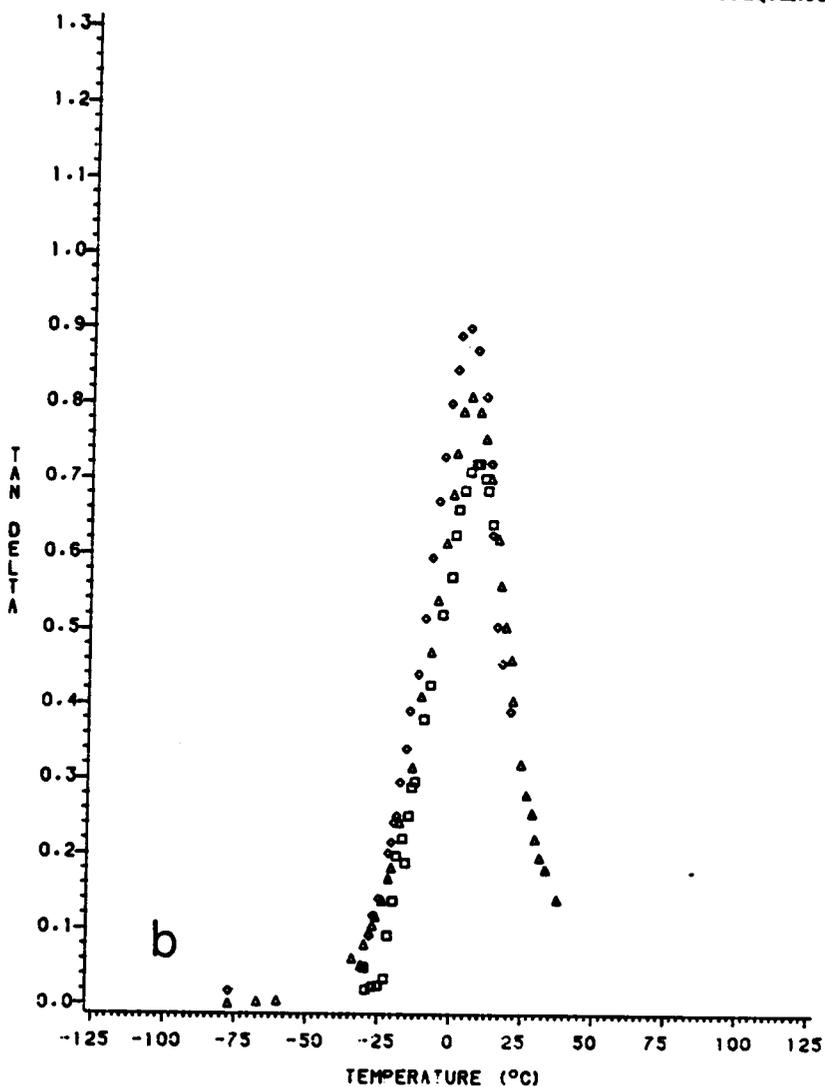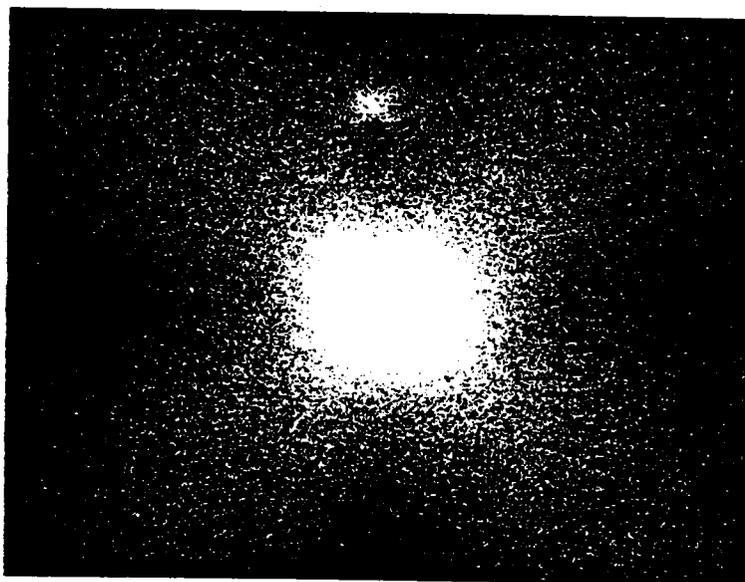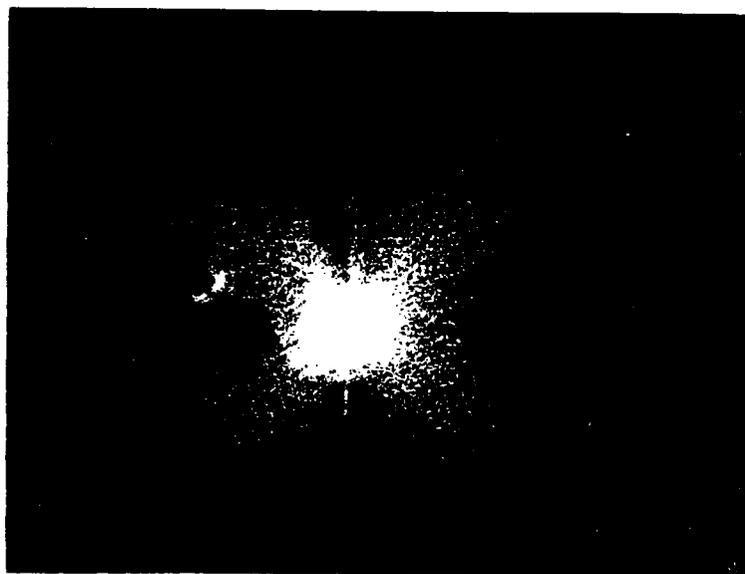
Figure 3.31. Small-angle Hv light scattering patterns of a) neat PVC compression molded at 150° and 180°C, b) DEHS-PVC compression molded at 170° with increasing amounts of plasticizer, and c) DBP-PVC compression molded at 170° with increasing amounts of plasticizer.
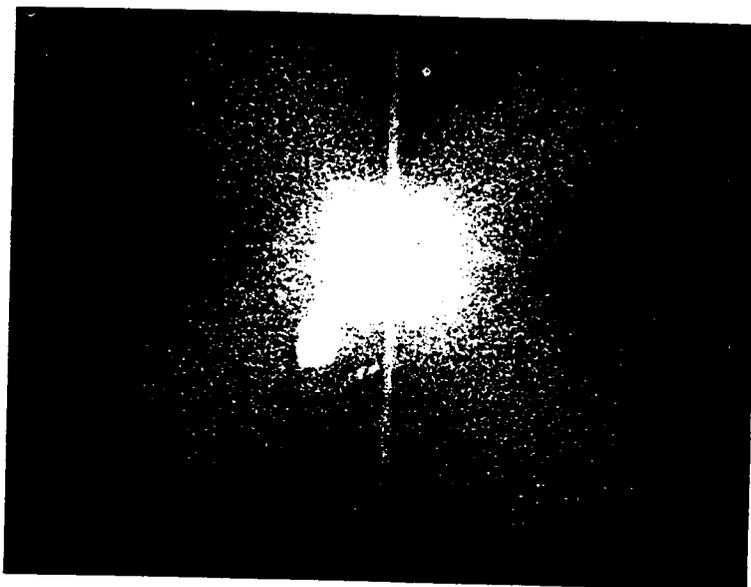
DEHS10
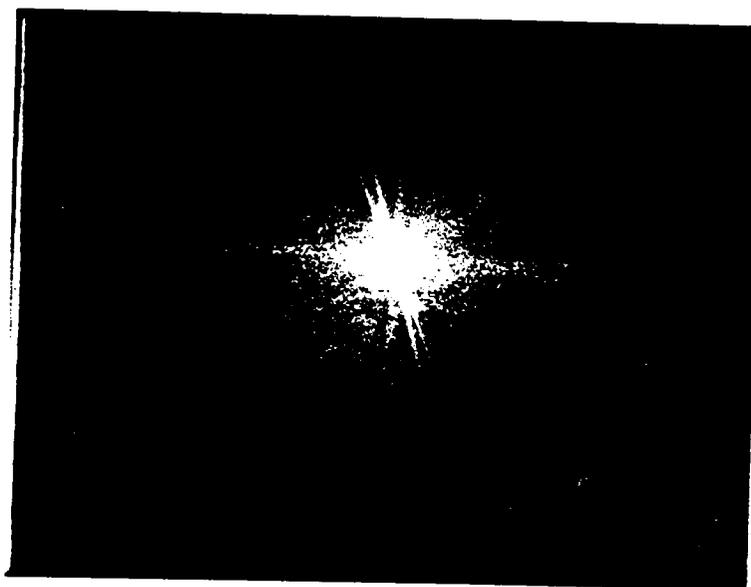
b DEHS40

DEHS60

DBP10

C   DBP40

DBP60

NEAT PVC
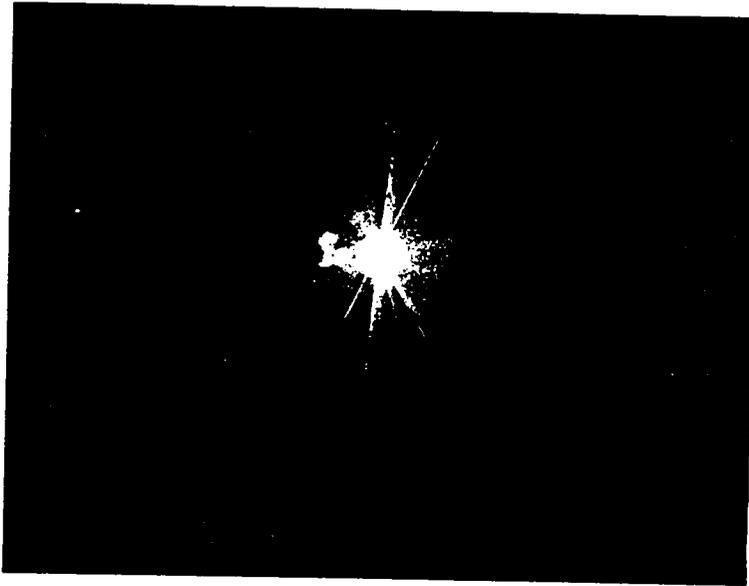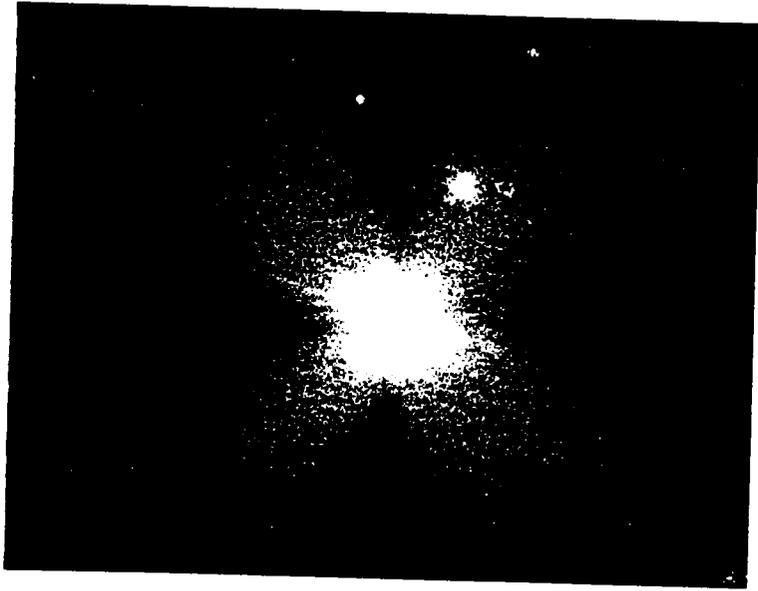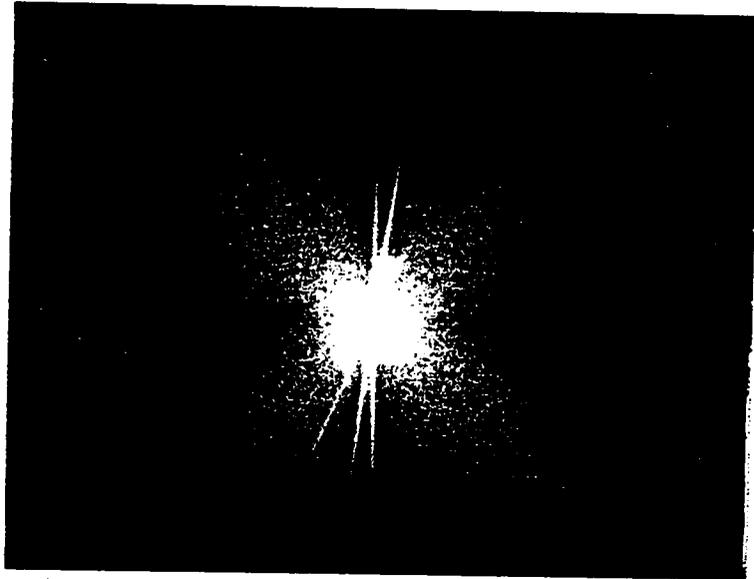
1 To 180°C, Quench to 30°C
2 To 180°C, Quench to 30°C

   sample heated to 100°C,
   held for 30 minutes,
   quenched to 30°C

3 To 100°C, Quench to 30°C
4 To 130°C, Quench to 30°C
5 To 150°C, Quench to 30°C
6,7 To 180°C, Quench to 30°C

Figure 3.32.   Normalized DSC traces of neat PVC after various
thermal treatments as described in legend.   Scanning rate
10°C/min.
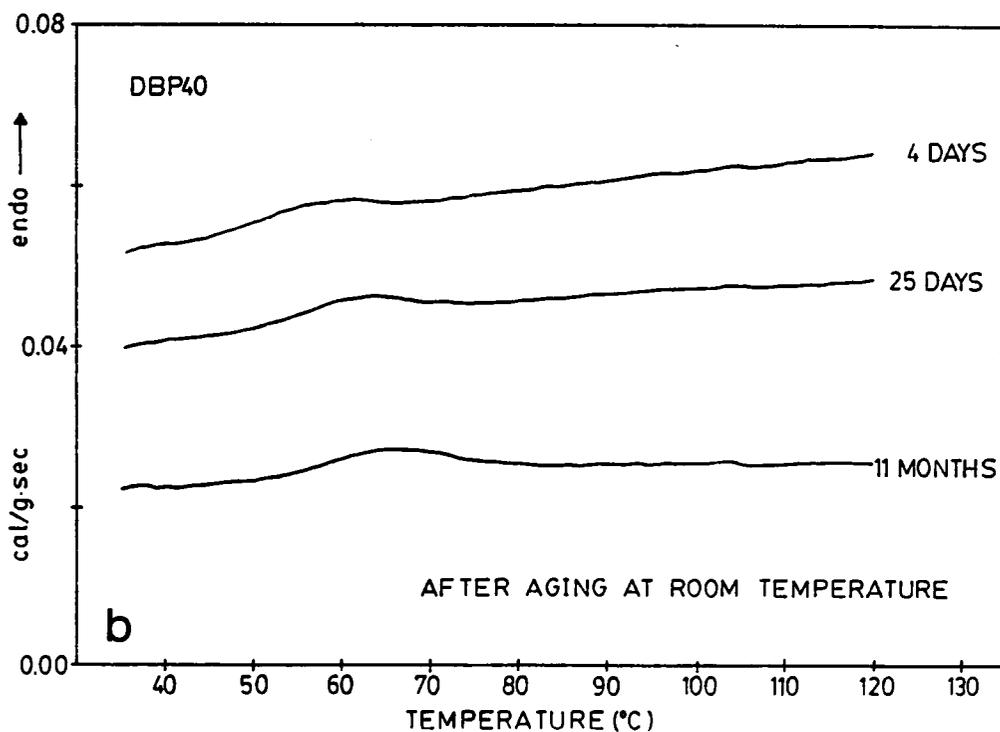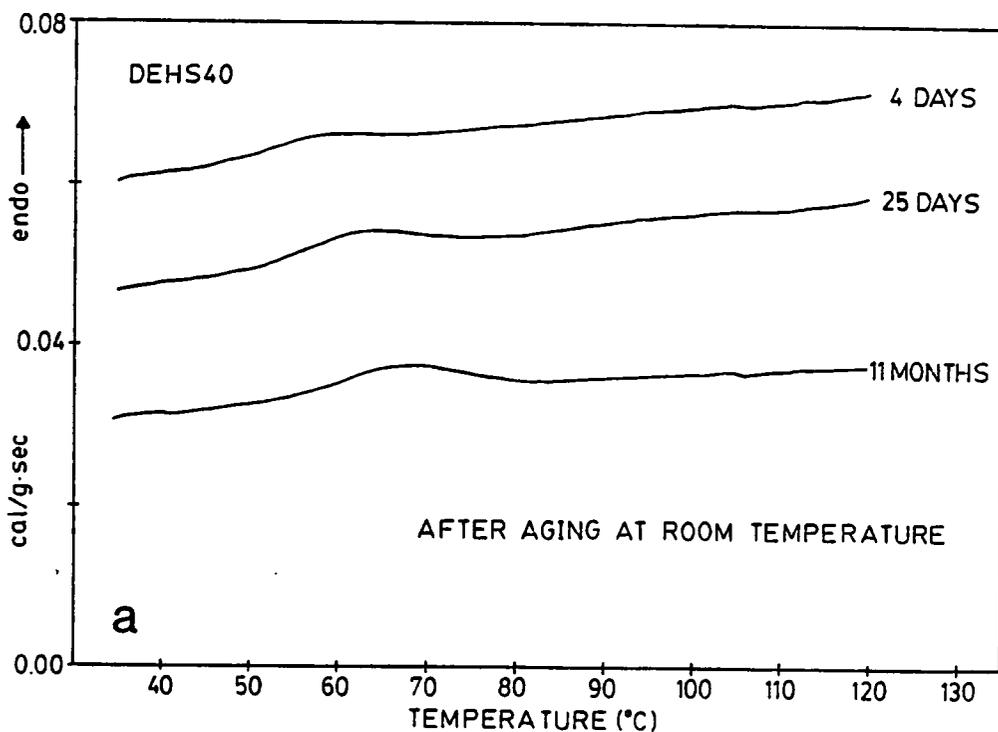
Figure 3.33. Normalized DSC traces showing the effects of room temperature aging on the magnitude and temperature position of the crystalline endotherm in plasticized PVC. Samples and aging times as noted. Scanning rate 10°C/min.
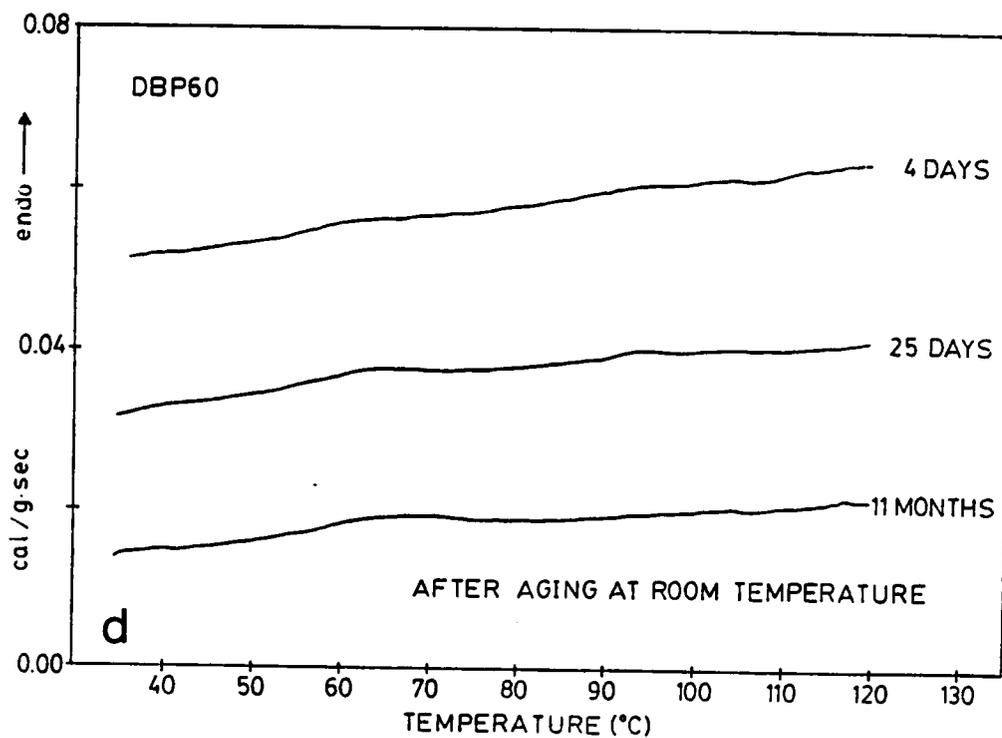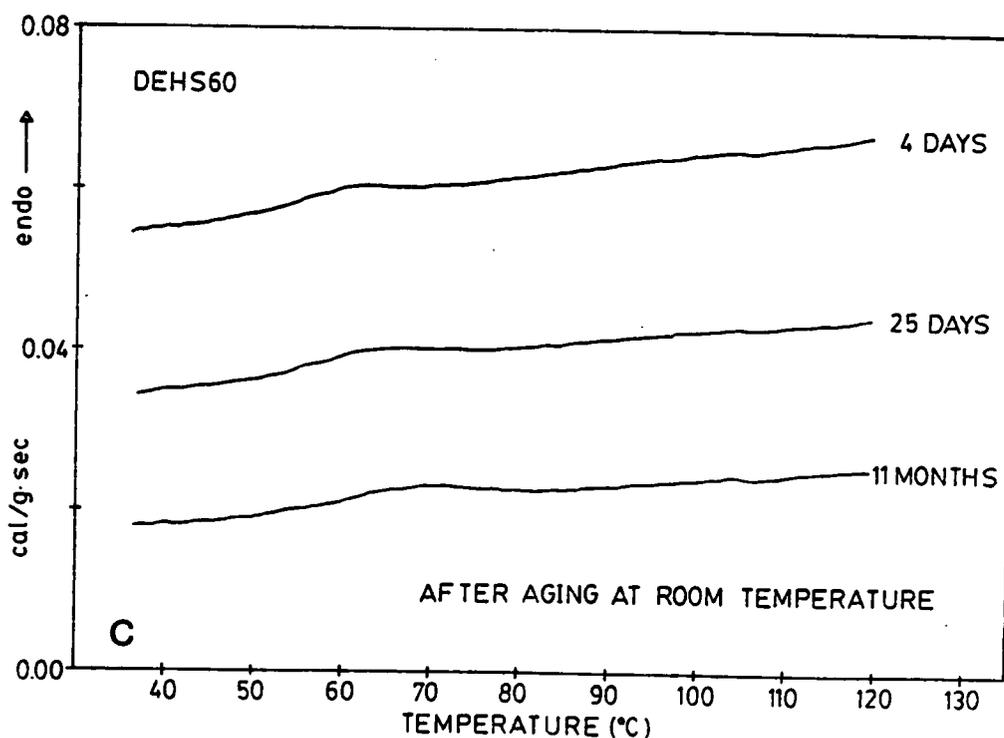
DEHS40.
QUENCHED/SHORT AGING/AGED
FREQUENCY 11 HZ
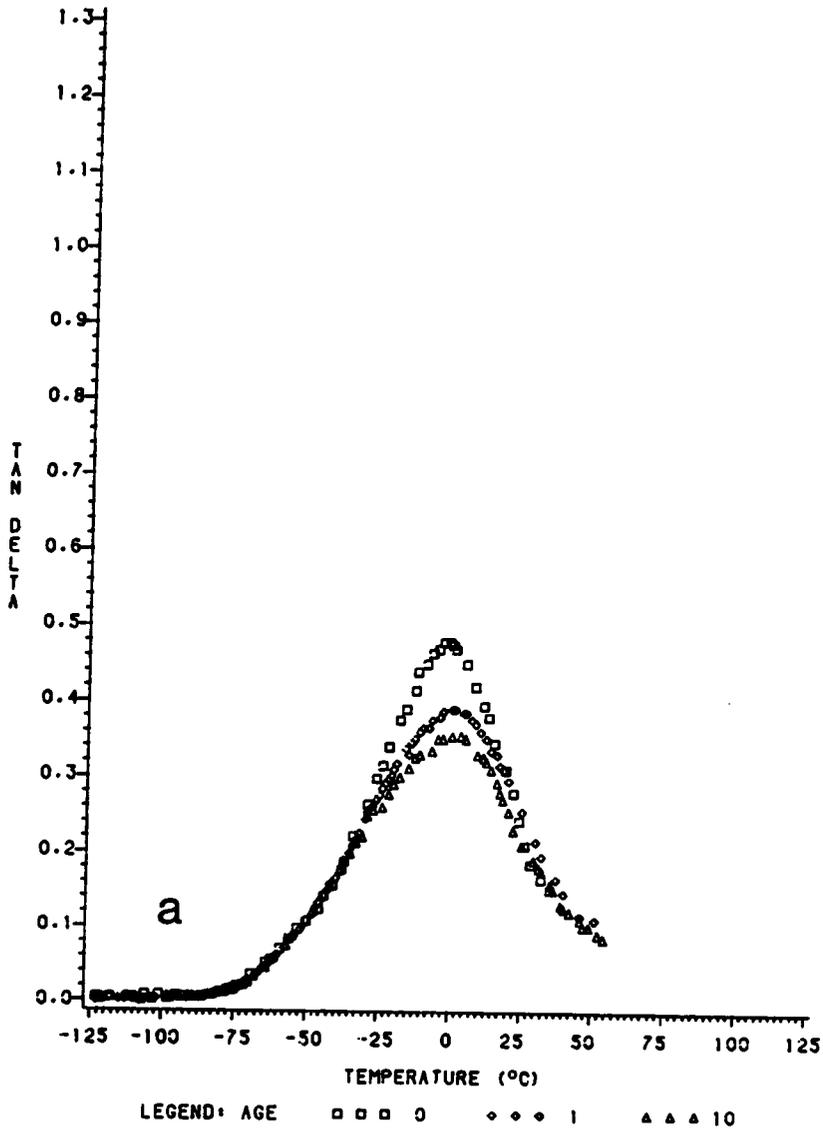
Figure 3.34. Dependence of tan δ on temperature for PVC containing 40% of a) diethylhexyl succinate and b) dibutyl phthalate. Samples quenched or aged at room temperature for one or ten months as indicated by aging time (0, 1, or 10) in legend.

DBP40
QUENCHED/SHORT AGING/AGED
FREQUENCY 11 HZ

LEGEND: AGE ▫ ▫ ▫ 0   ◆ ◆ ◆ 1   ▲ ▲ ▲ 10
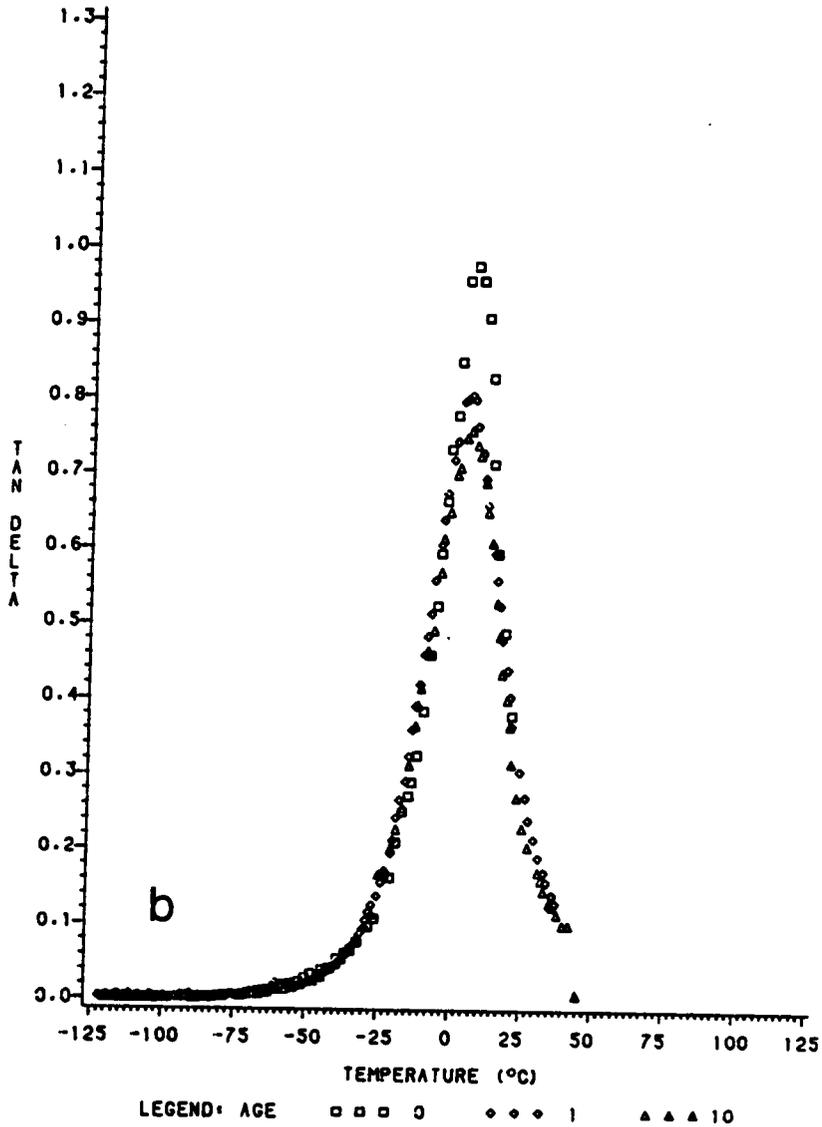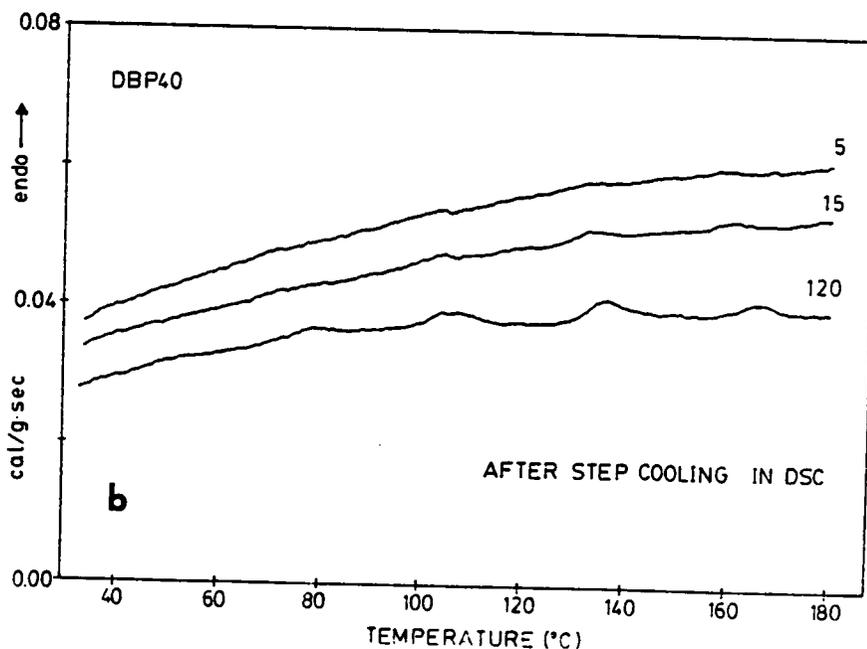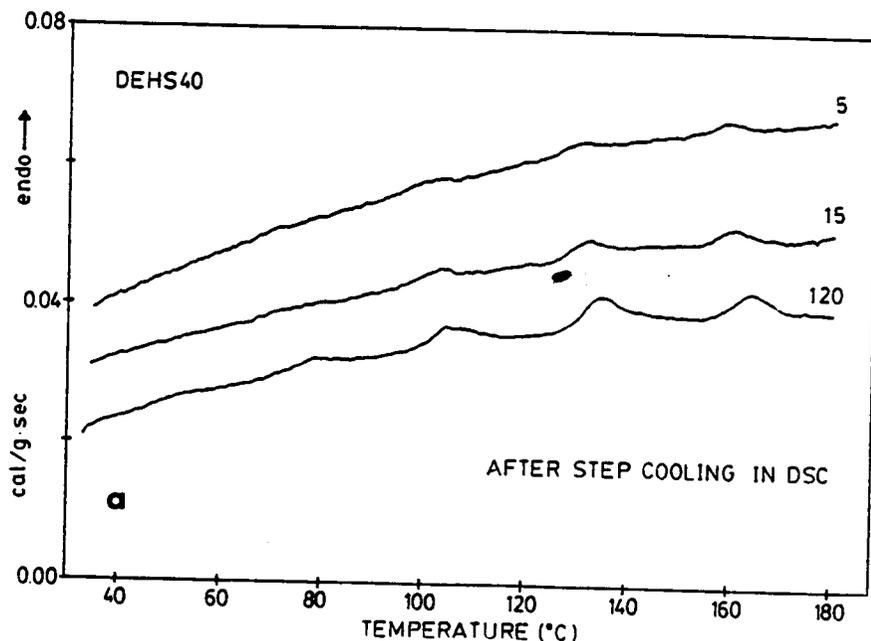
Figure 3.35. Normalized DSC traces showing the effects of step cooling on the magnitudes and temperature positions of crystalline endotherms in a) DEHS40 and b) DBP40. Samples heated to 180°C at 10°/min and quenched sequentially to 150°, 120°, 90°, 60°, and 30°. Samples held at each of the latter five temperatures for 5, 15, or 120 minutes. Scanning rate of traces shown was 10°C/min.
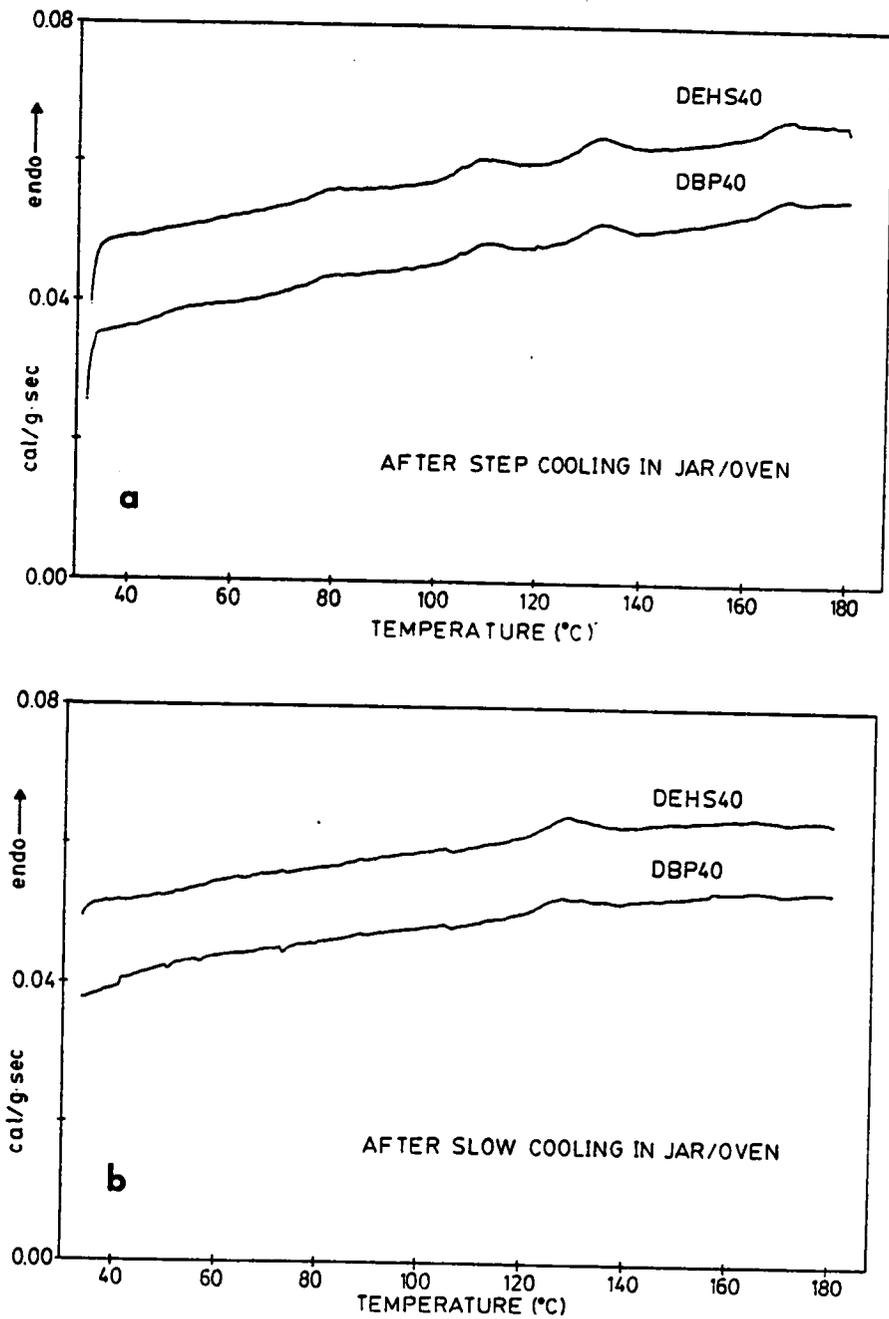
Figure 3.36. Normalized DSC traces showing the effects of a) step cooling and b) slow cooling on the magnitudes and temperature positions of crystalline endotherms in DEHS40 and DBP40. Samples prepared as described in text. Aging time at step positions was 120 minutes. Slow cooling commenced at 120°C. Scanning rate of traces shown was 10°C/min.
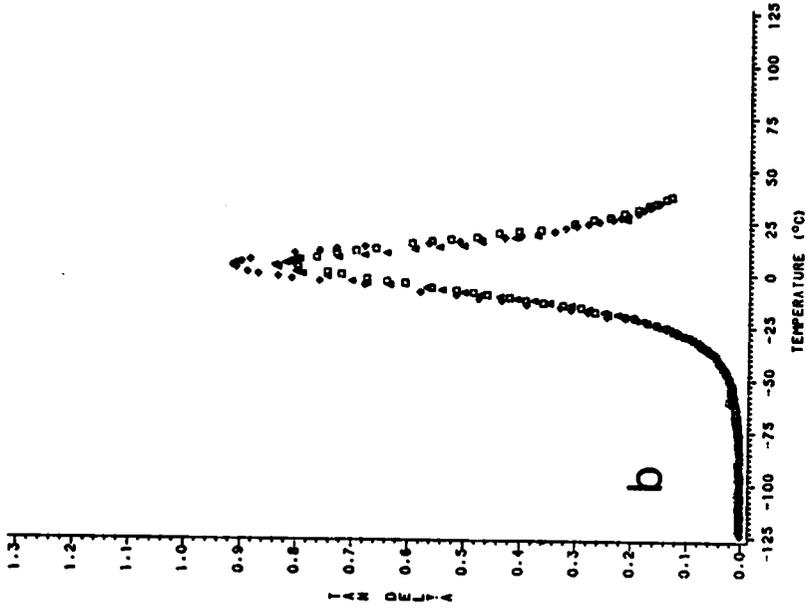
Figure 3.37. Dependence of tan δ on temperature for PVC containing 40% of a) diethylhexyl succinate and b) dibutyl phthalate. Samples step cooled, slow cooled, or aged at room temperature for 1 month as indicated.
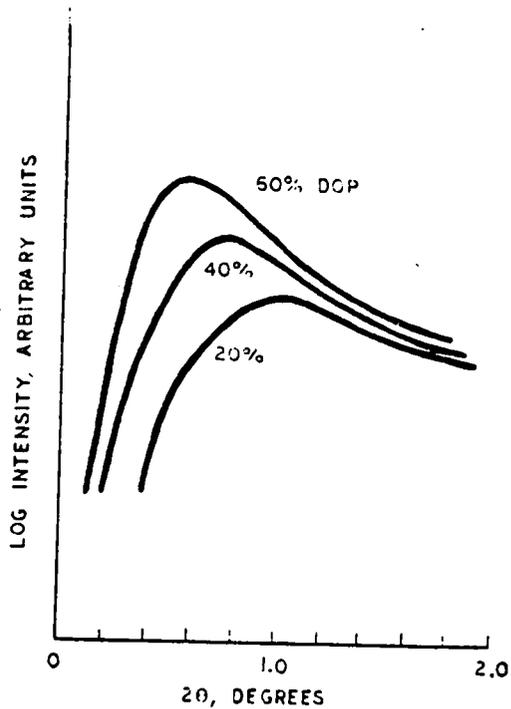
Figure 3.38. Change in SAXS peak position for PVC containing various amounts of DOP. Films prepared by milling. SAXS curves corrected for parasitic scattering and subjected to the Lorentz correction. Ref. 154.
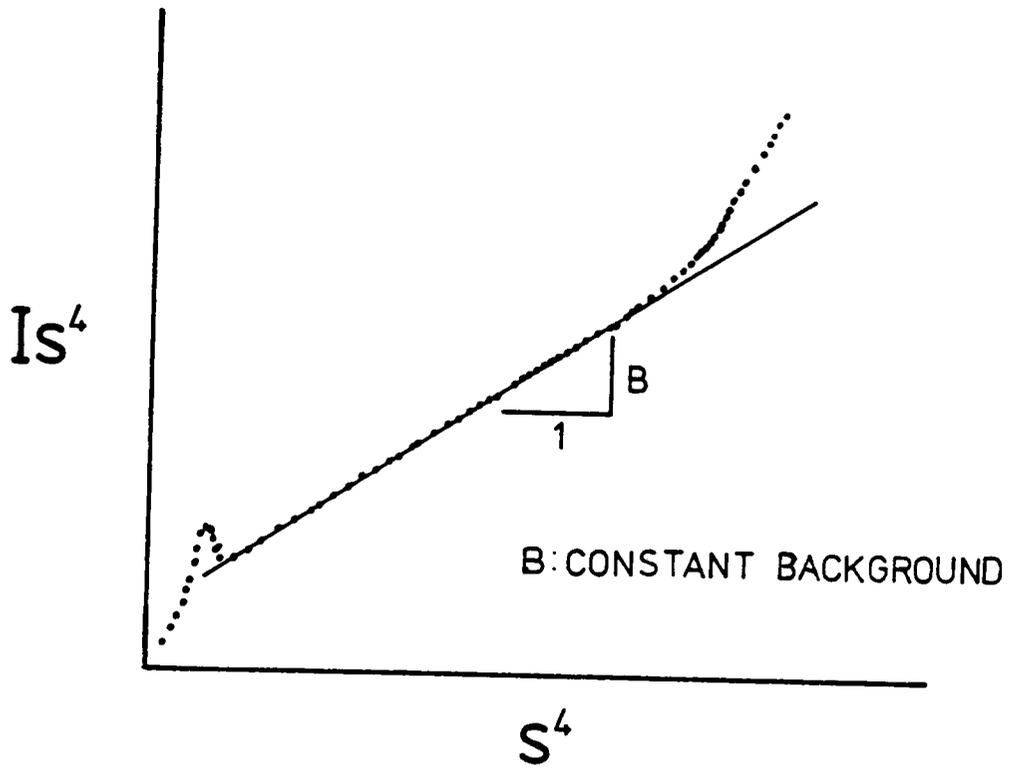
Figure 3.39. Schematic description of the Bonart background correction.
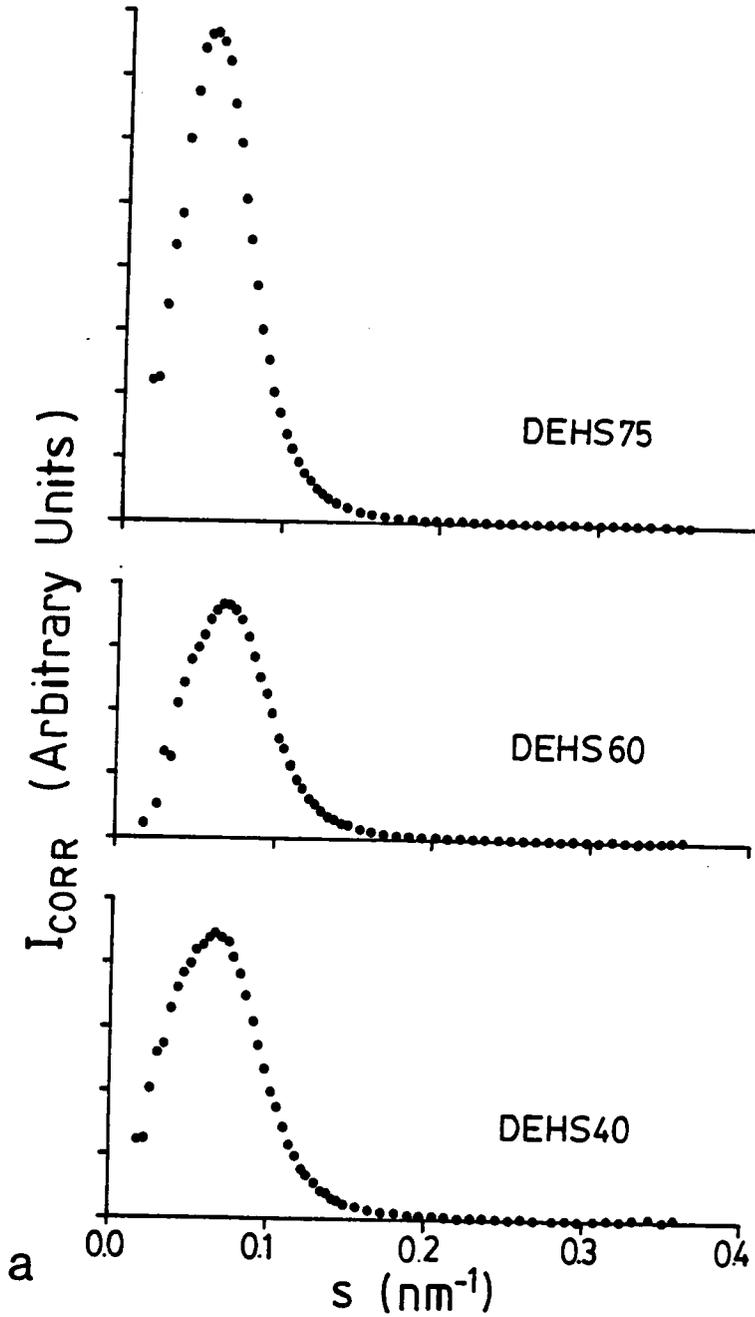
Figure 3.40. SAXS scattering curves (ORNL) for a) DEHS-PVC and b) DBP-PVC containing increasing amounts of plasticizer. Data subjected to Bonart background correction. Intensities are proportional to absolute intensity by the same constant factor.
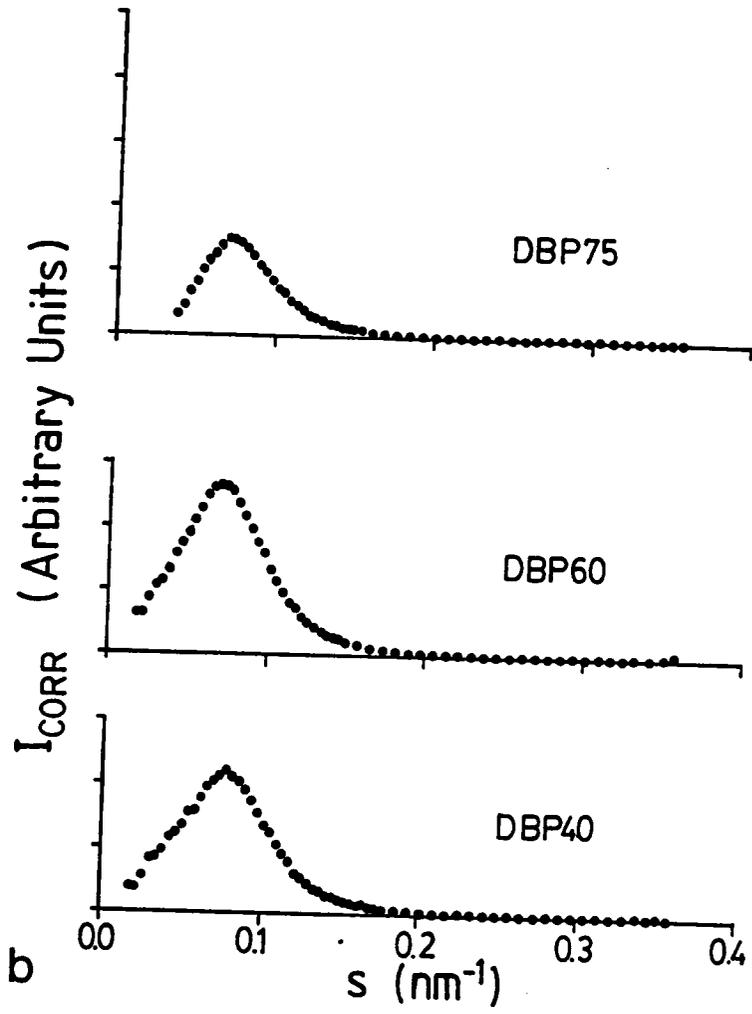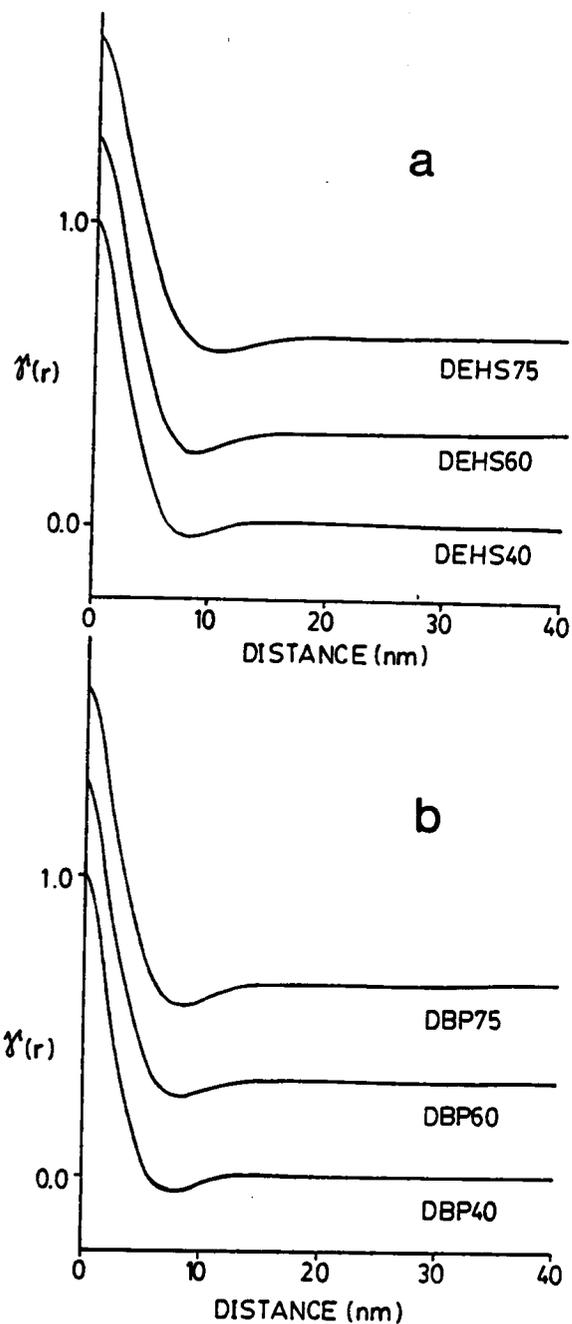
Figure 3.41. Three-dimensional correlation functions for
a) DEHS-PVC and b) DBP-PVC. The for 60 and 75% curves have
been shifted vertically; for each curve, $\gamma(r=0) = 1.0$.
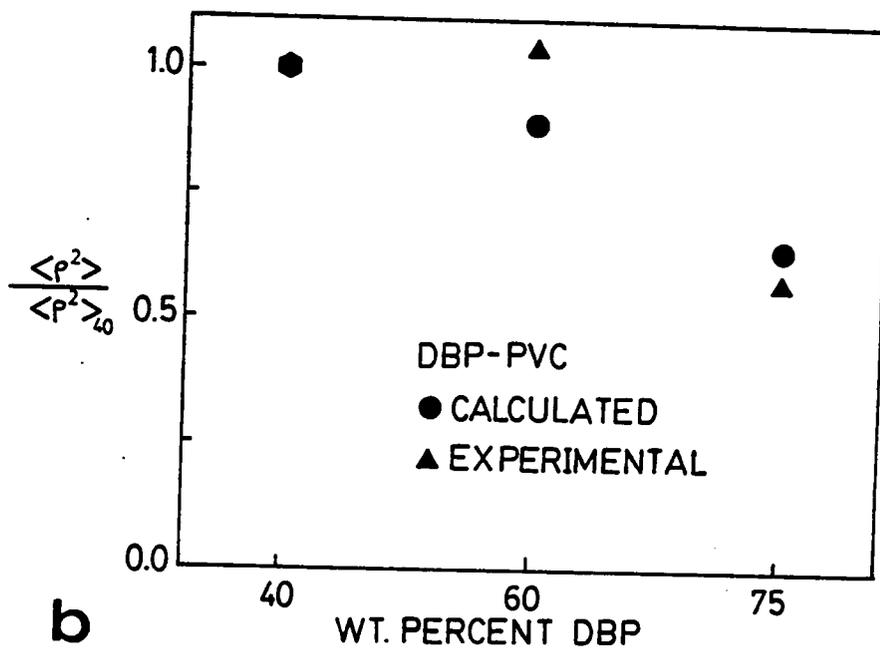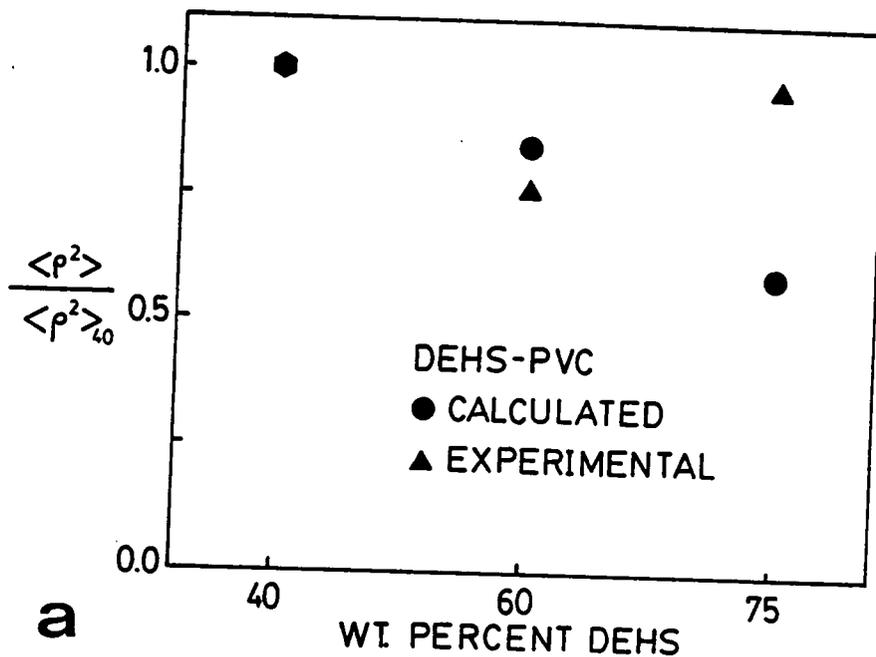
Figure 3.42. Calculated and experimentally measured ratios of mean electron density fluctuations for a) DEHS-PVC and b) DBP-PVC; values normalized with value obtained for DEHS40 or DBP40.
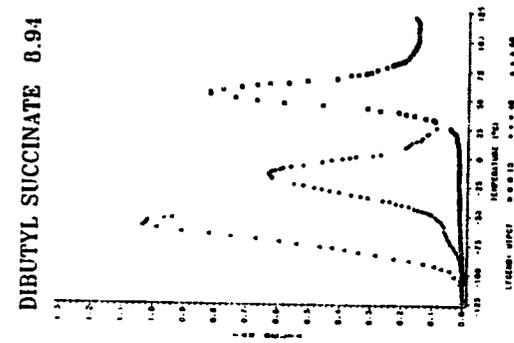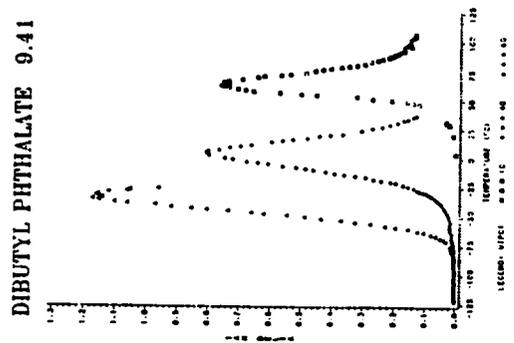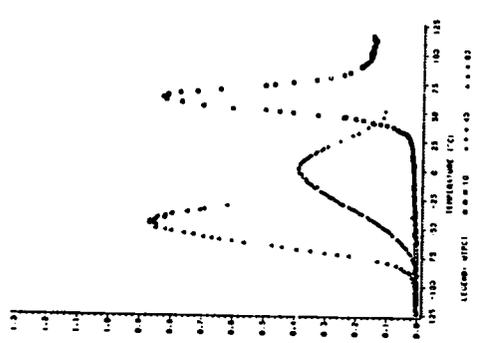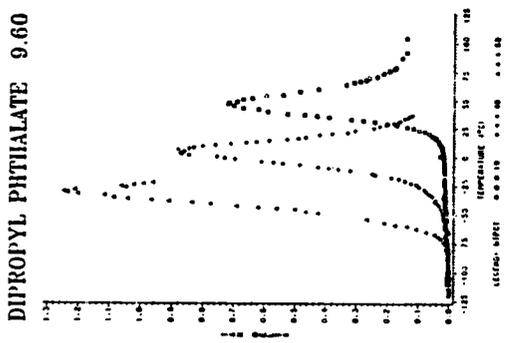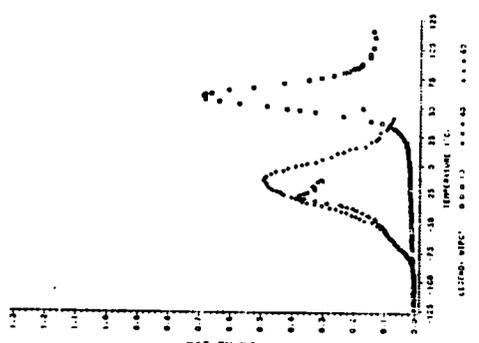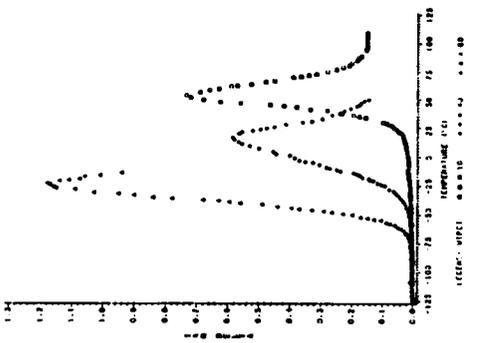
Figure 3.43. Dependence of tan δ on temperature for PVC containing 10, 40, and 60 weight percent of six different plasticizers with solubility parameters as noted. Samples prepared by standard method and aged approximately one month at room temperature.
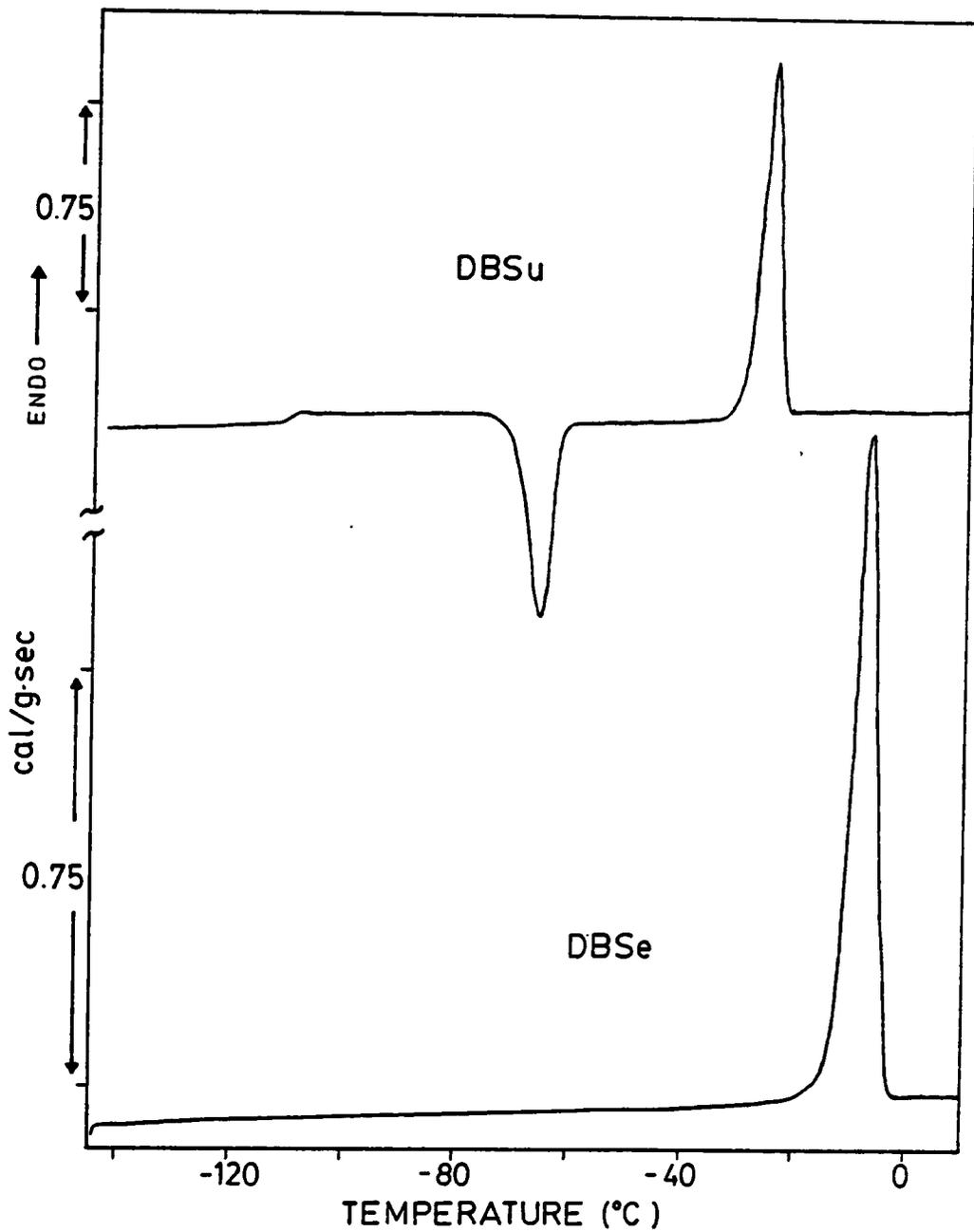
Figure 3.44.   Normalized DSC traces of neat DBSe and neat DBSu.
Scanning rate 10°C/min.
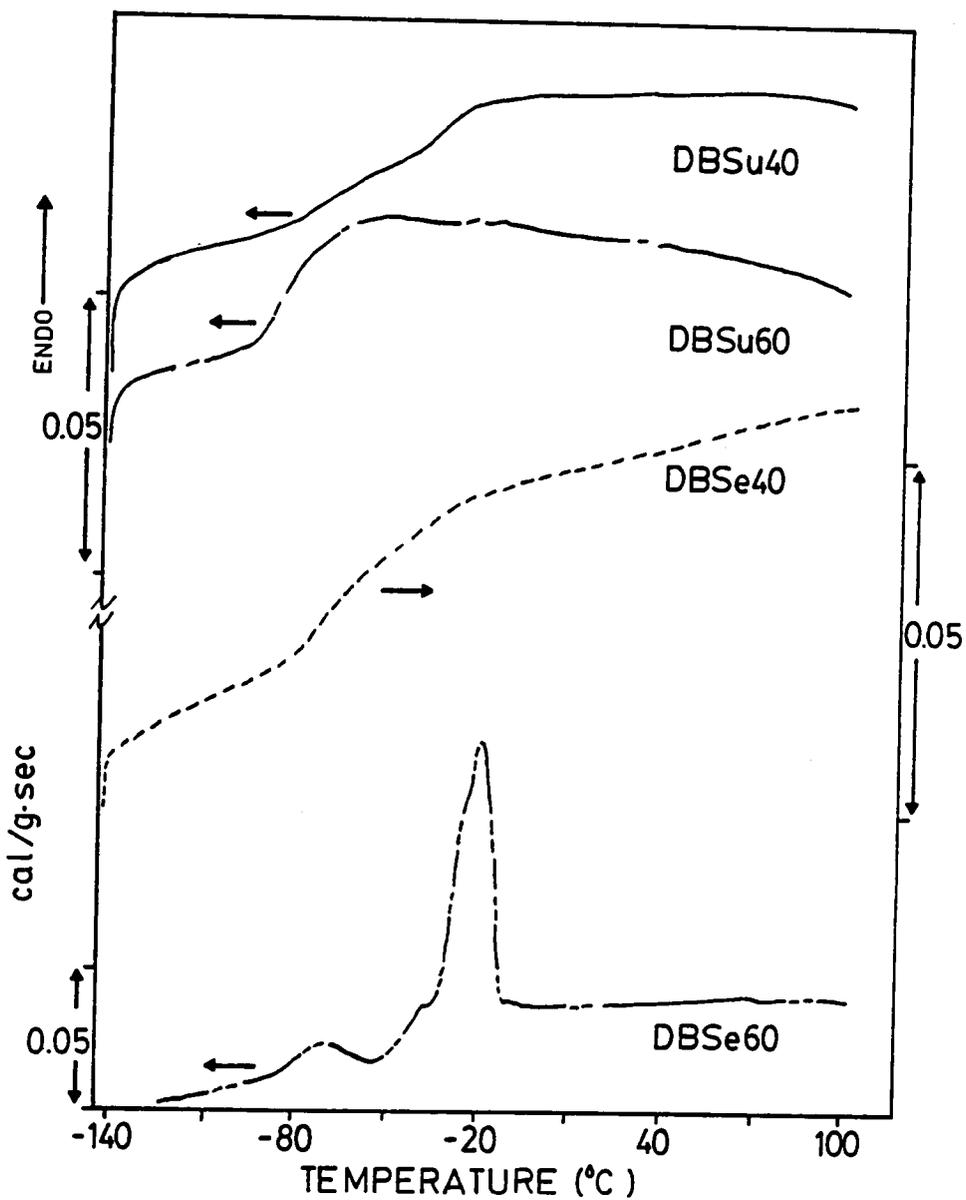
Figure 3.45.   Normalized DSC traces of DBSe40 and 60 and DBSu40 and 60. Scanning rate 10°C/min.

DEHS
DBP
DEHS/DBP
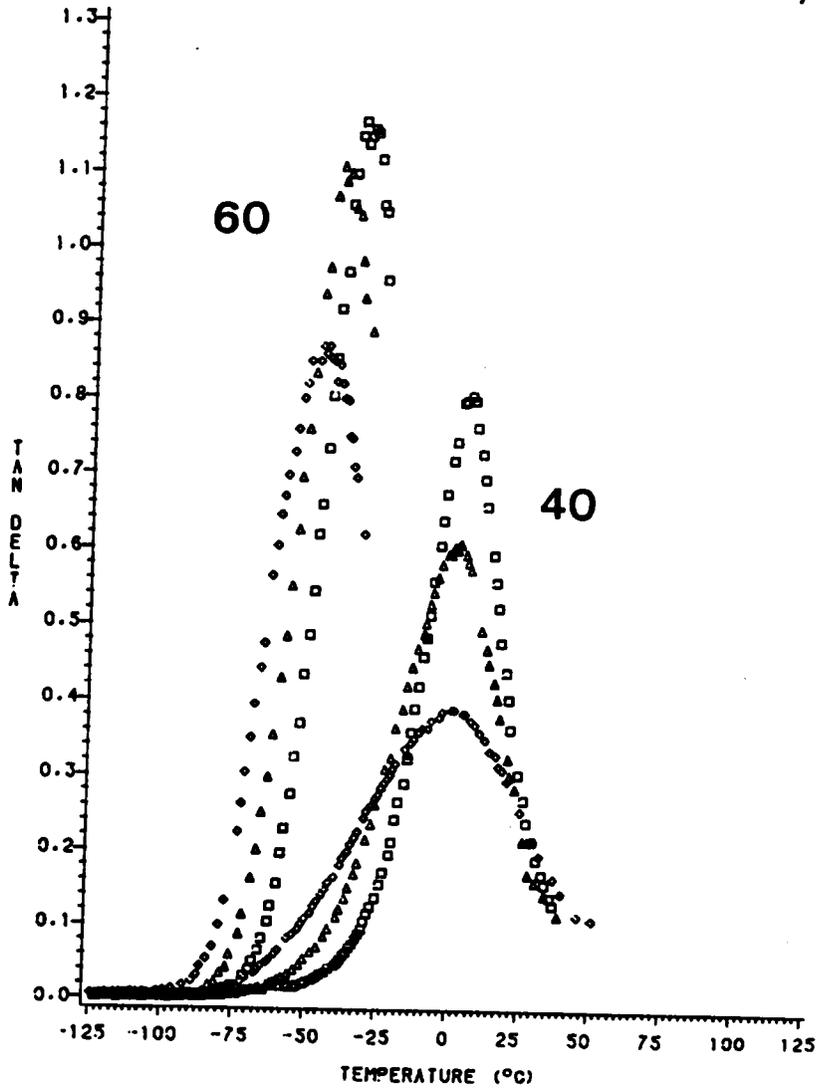
Figure 3.46.   Dependence of tan δ on temperature
for PVC containing 40 and 60 weight percent of DEHS, DBP, and
equimolar mixture of DEHS and DBP (DEHS/DBP).   See legend
for symbol definitions.
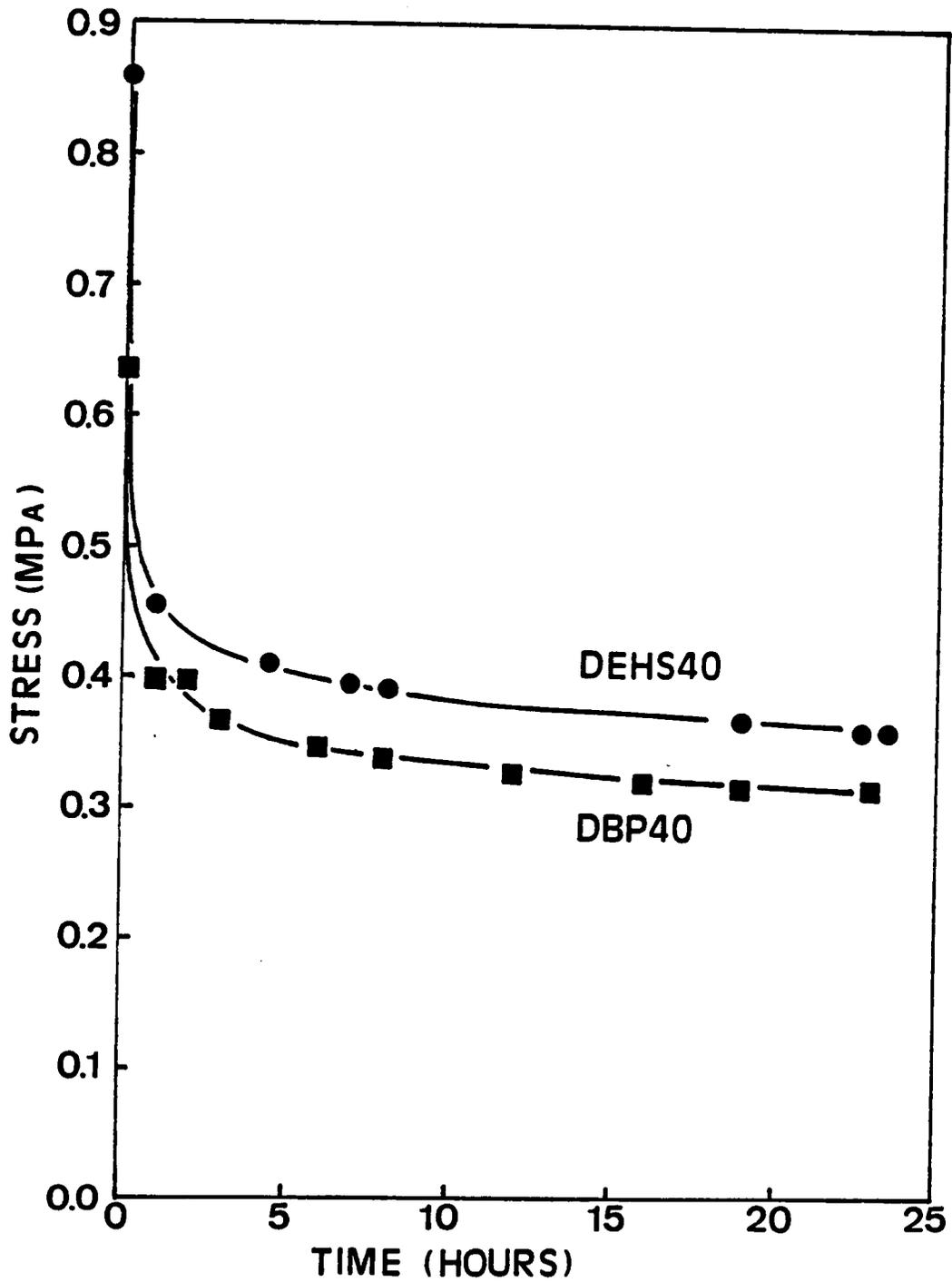
Figure 3.47. Long-term stress relaxation of DEHS40 and DBP40. Draw ratio = 1.5.
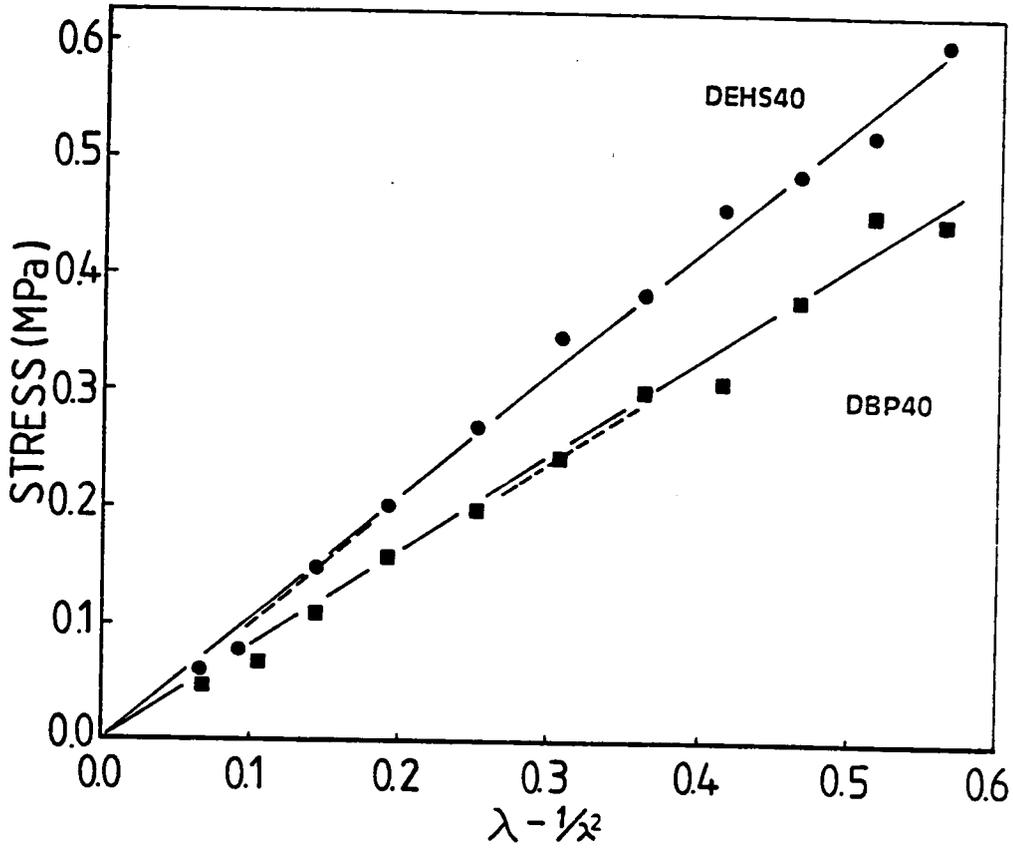
Figure 3.48.   Plot of 30-minute engineering stress vs. $\lambda - 1/\lambda^2$ for DBP40 and DEHS40.   See text for determination of slope.
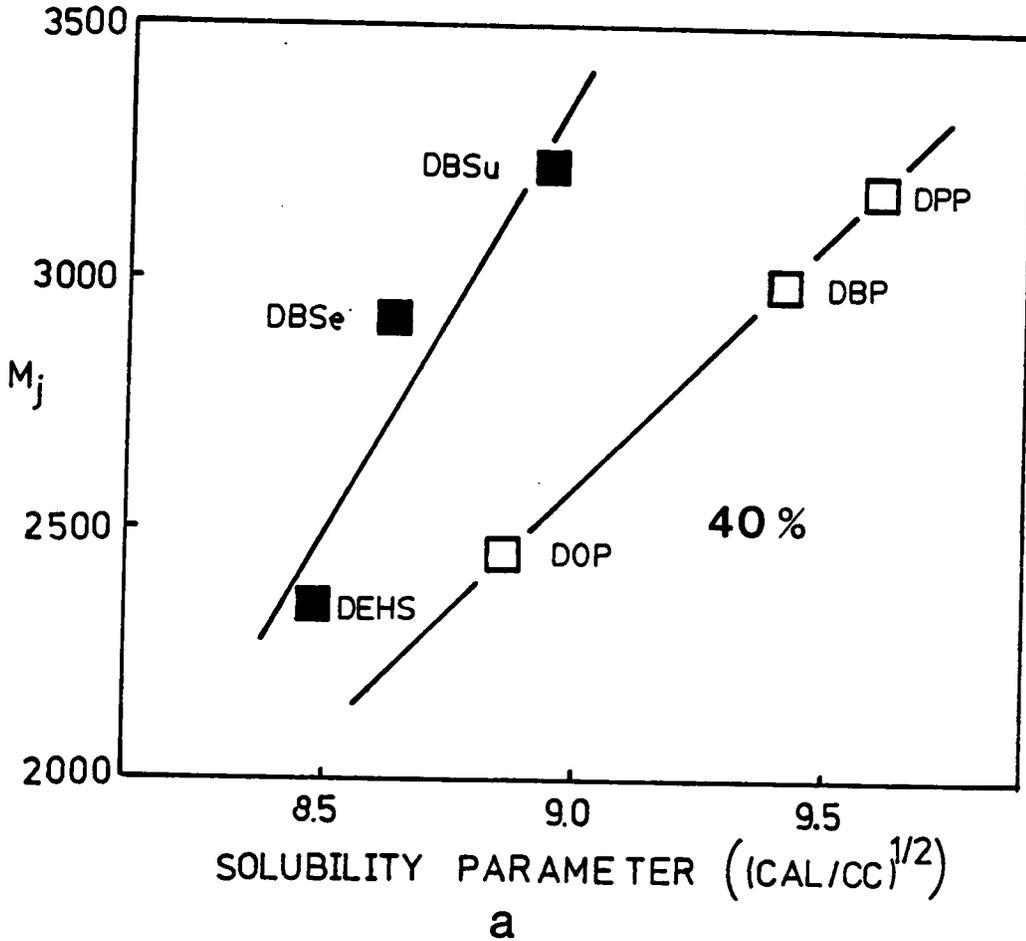
Figure 3.49. Molecular weight between junction points (Mj) as a function of solubility parameter for a) 40% and b) 60% compositions. Mj obtained from "calculated" line as described in text.

SOLUBILITY PARAMETER $((CAL/CC)^{1/2})$

b
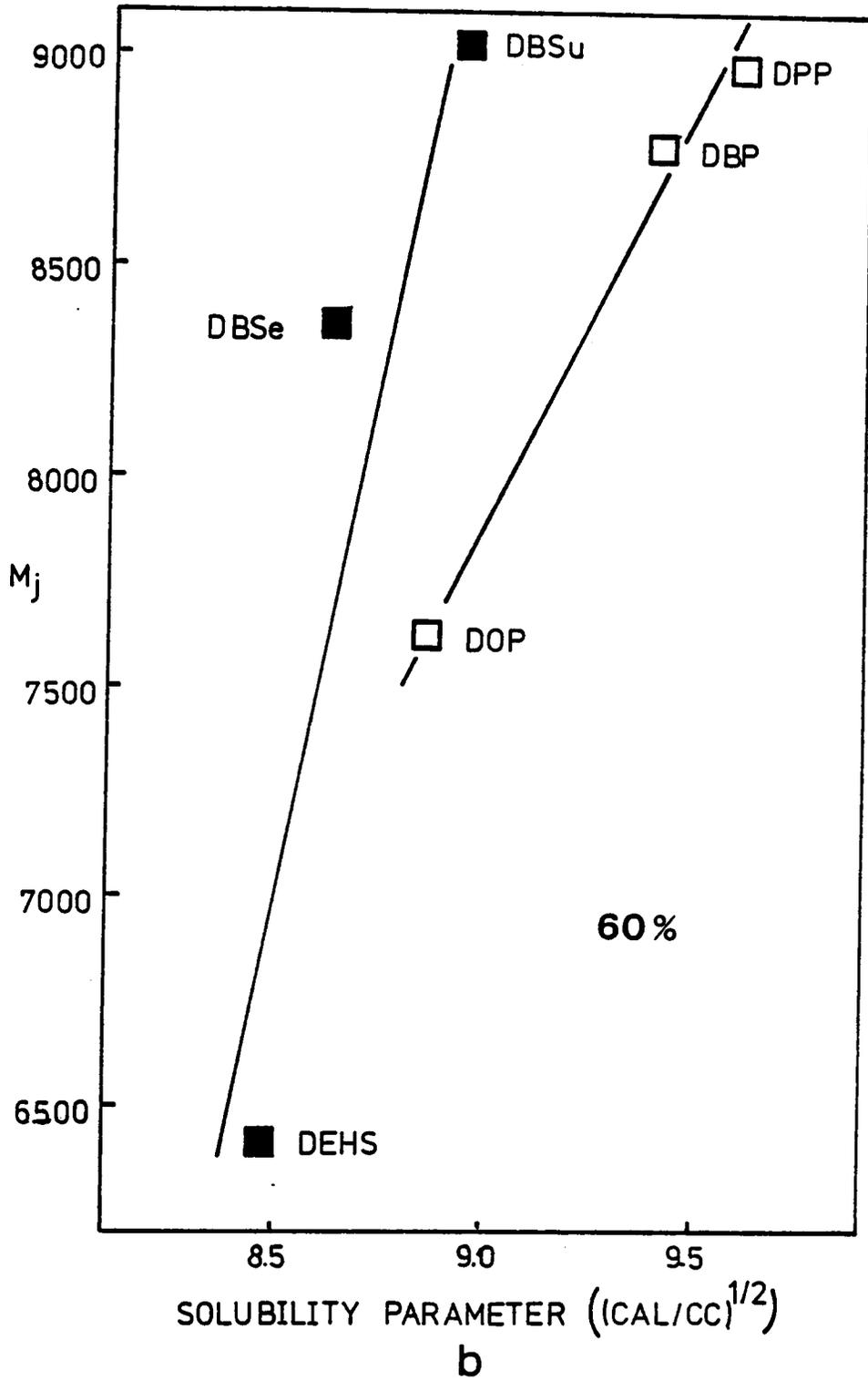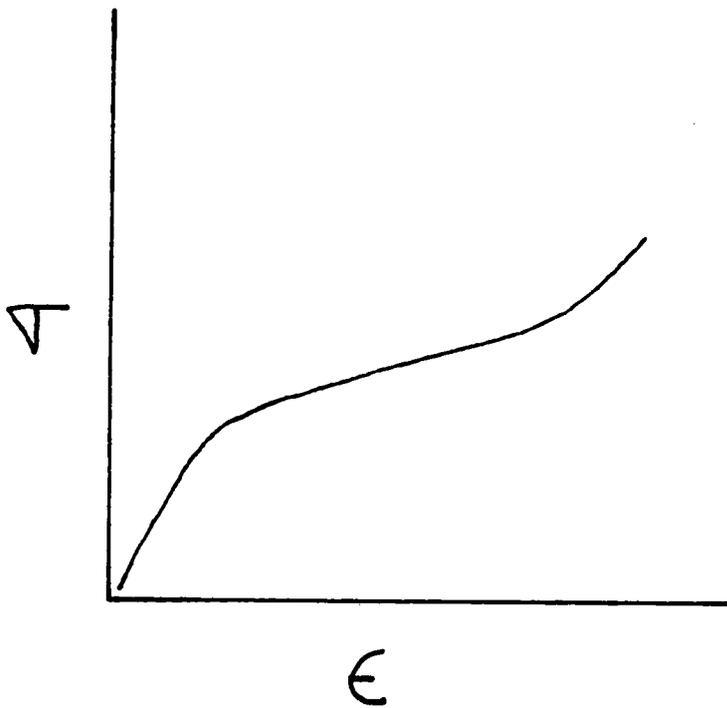
Figure 3.50. Generalized stress-strain behavior of a crosslinked elastomer showing stress upturn indicative of strain-induced crystallization.
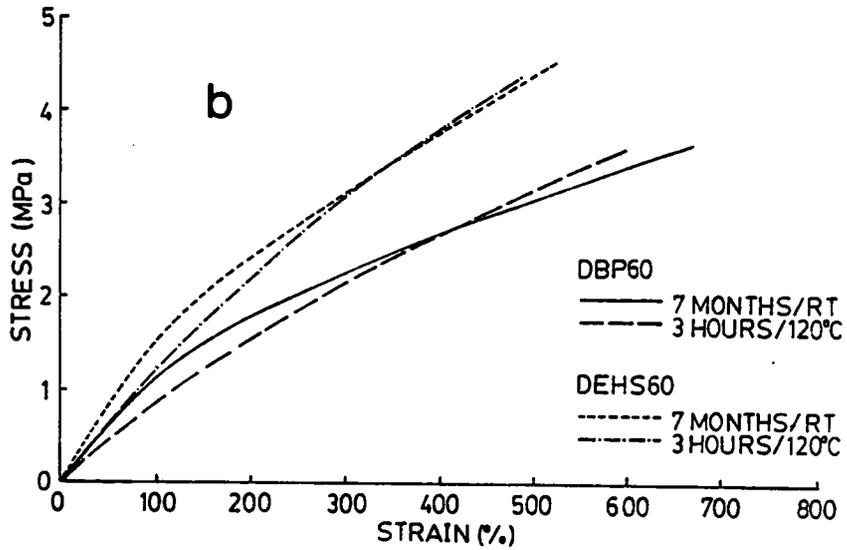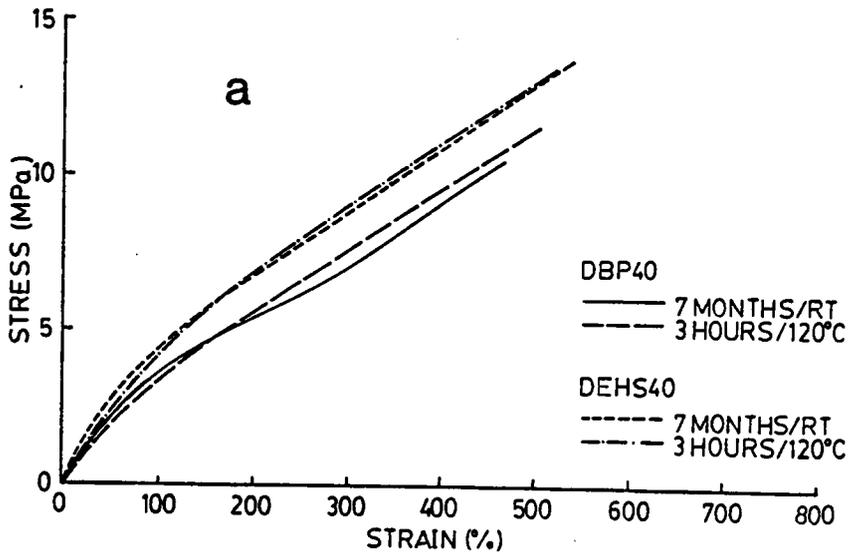
Figure 3.51. Stress-strain behavior of unannealed and 120°C annealed DEHS-PVC and DBP-PVC at a) 40 and b) 60% plasticizer levels.

DPP40

DBP40

DOP40

DEHS40

a

Figure 3.52.   WAXS patterns for DPP40, DBP40, DOP40, and DEHS40 (in order of decreasing solubility parameter) at draw ratios of a) 4.0 and b) 5.0.   Draw direction is vertical.   See Table 3.7 for respective solubility parameters of plasticizers.

DPP40
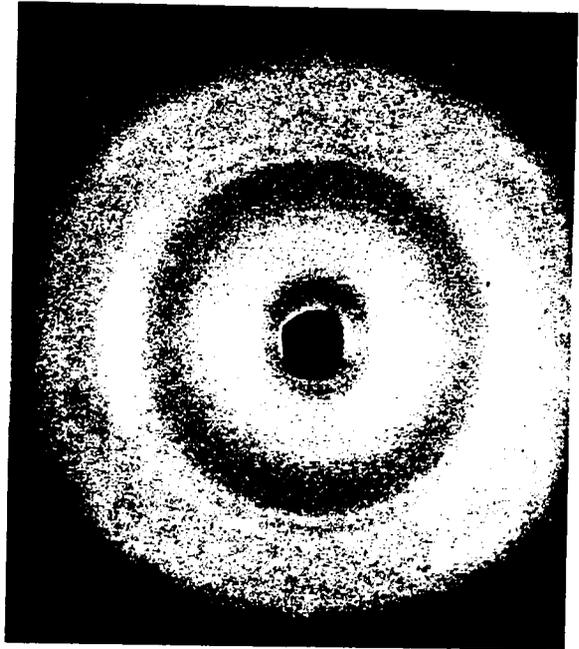
DBP40
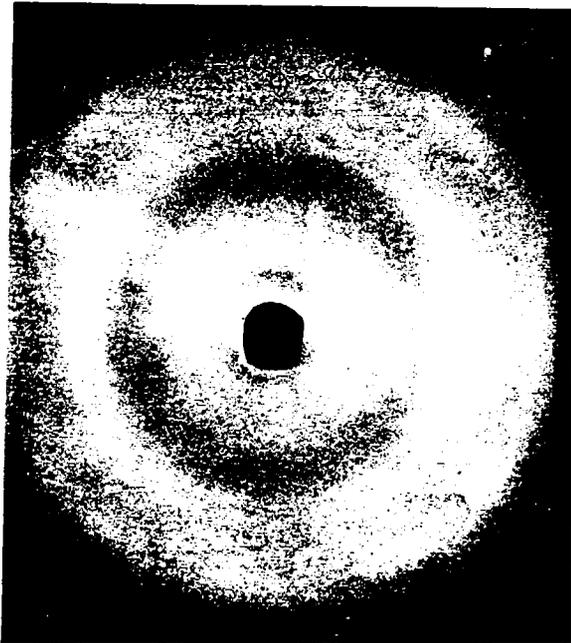
DOP40   b   DEHS40
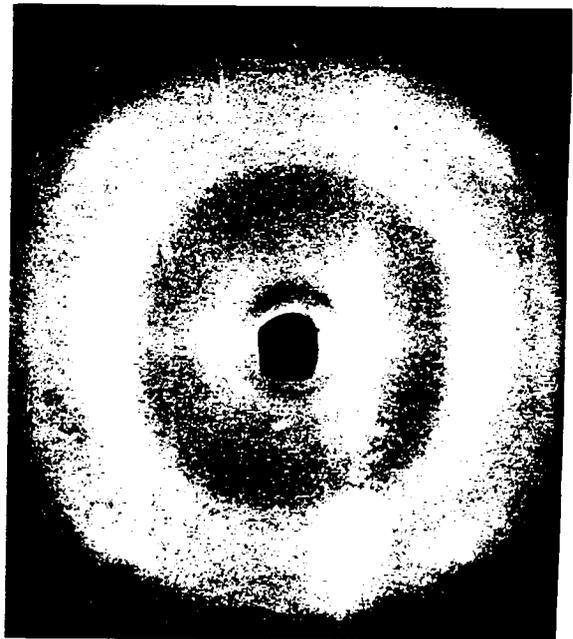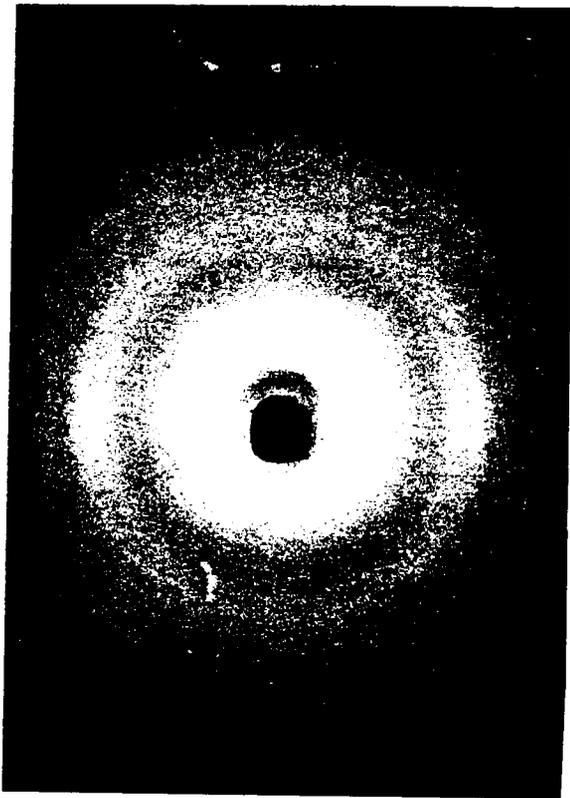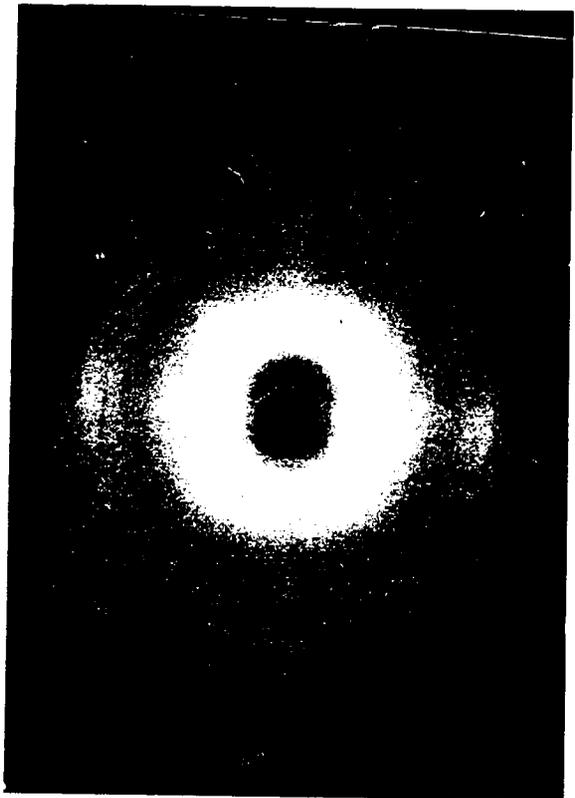
DEHS40   DBP40

Figure 3.53. WAXS patterns of oriented DEHS40 and DBP40 after three-hour annealing at 120°C. Draw direction is vertical. Draw ratio is 5.0.
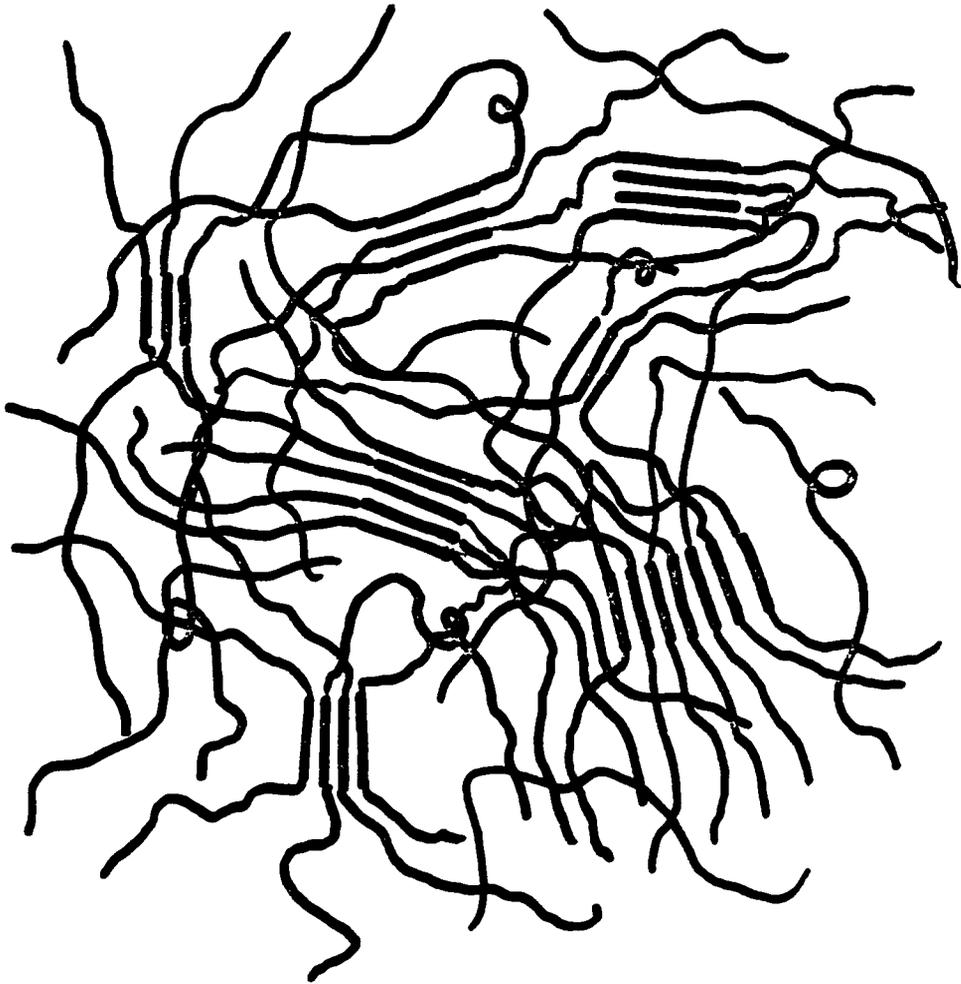
Figure 3.54. Fringed micelle model of plasticized PVC with micelle crystallites providing physical crosslinks.
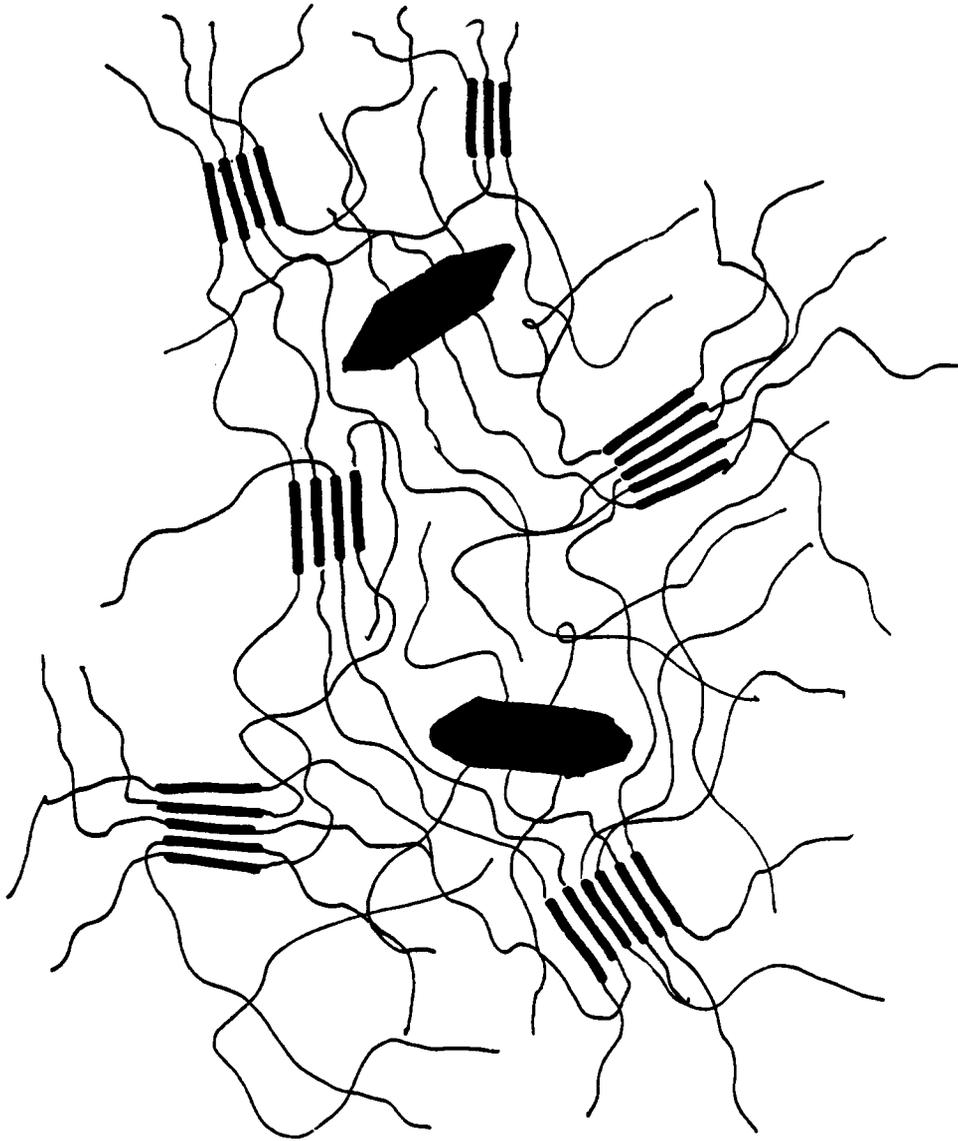
Figure 3.55. Two-crystal texture model of plasticized PVC with
fringed micelle crystallites providing physical crosslinks.
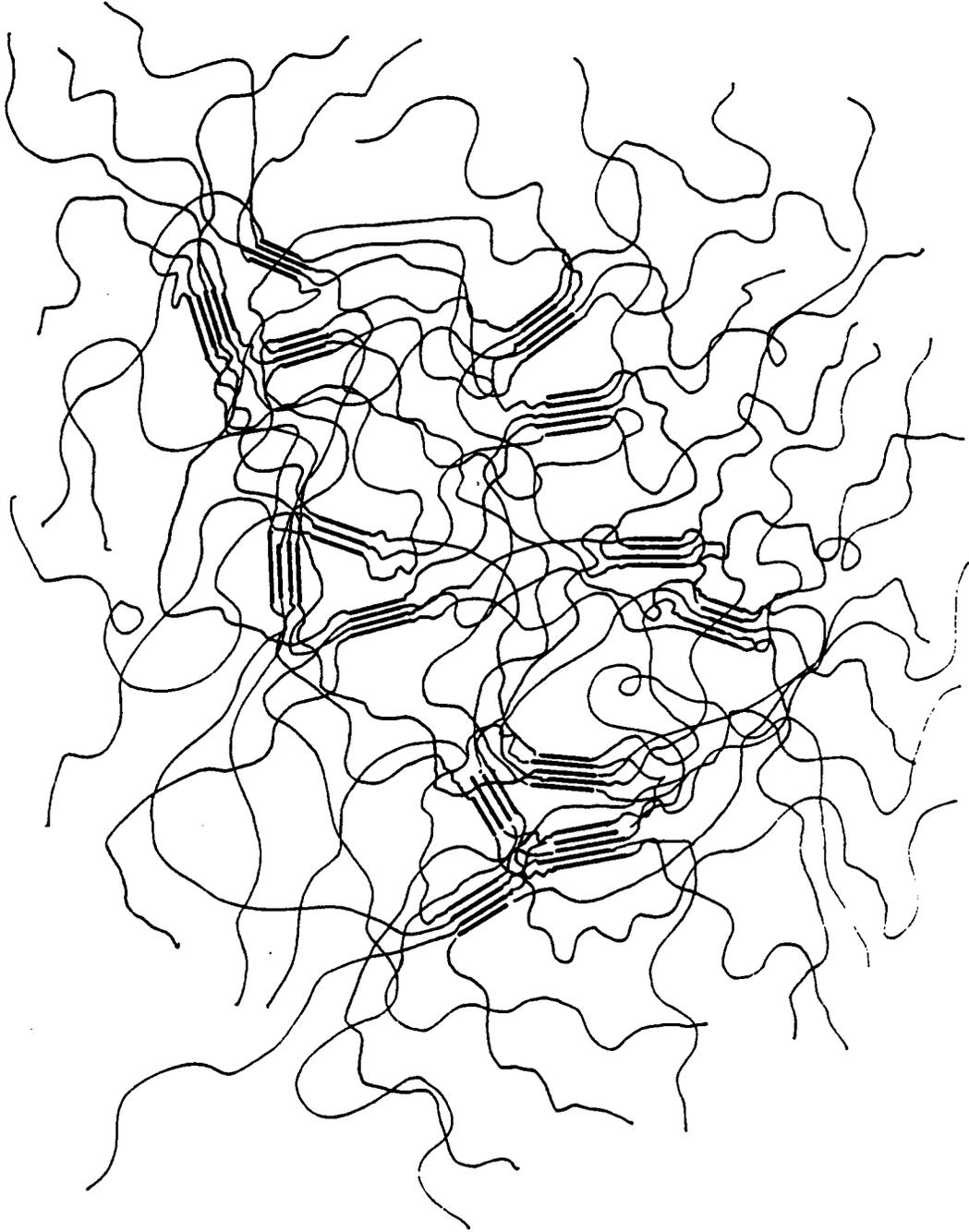
Figure 3.56. Generalized concept of the pocket model of plasticized PVC.
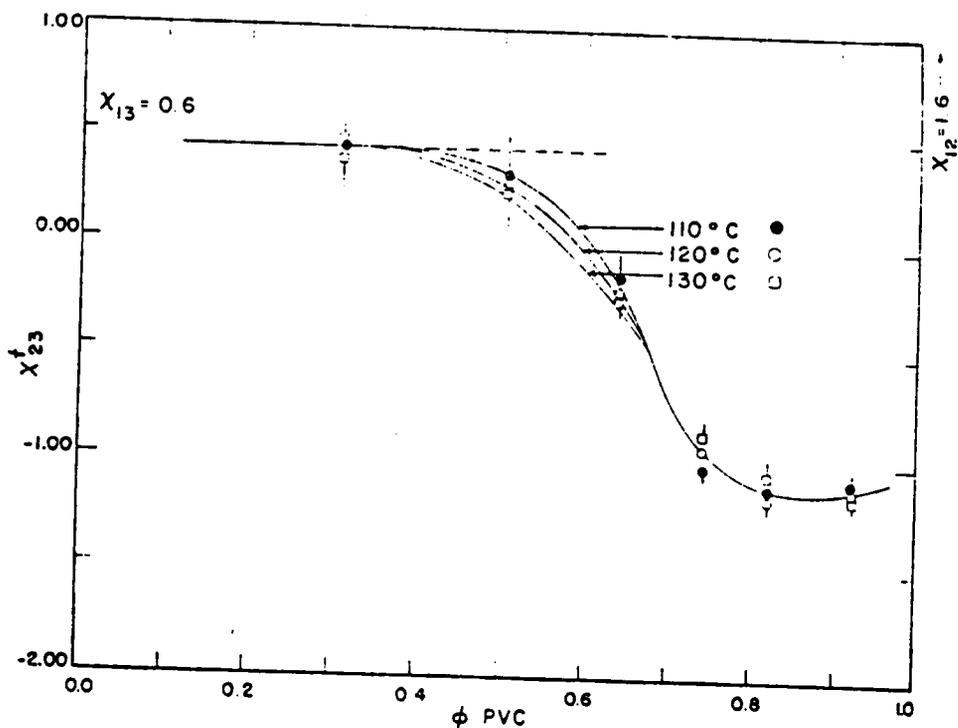
Figure 3.57. The PVC-plasticizer interaction parameter as a function of concentration for n-DOP. Temperature dependence also illustrated. Ref. 188.
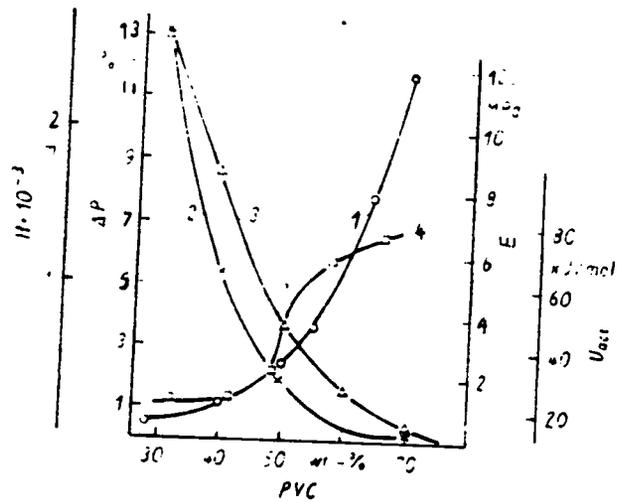
Figure 3.58. Dependence of elastic modulus E (1), dye diffusion rate H (2), gas permeability ΔP (3), and apparent activation energy (Uact) of dye diffusion (4) as a function of DBP concentration in PVC. Ref. 183.
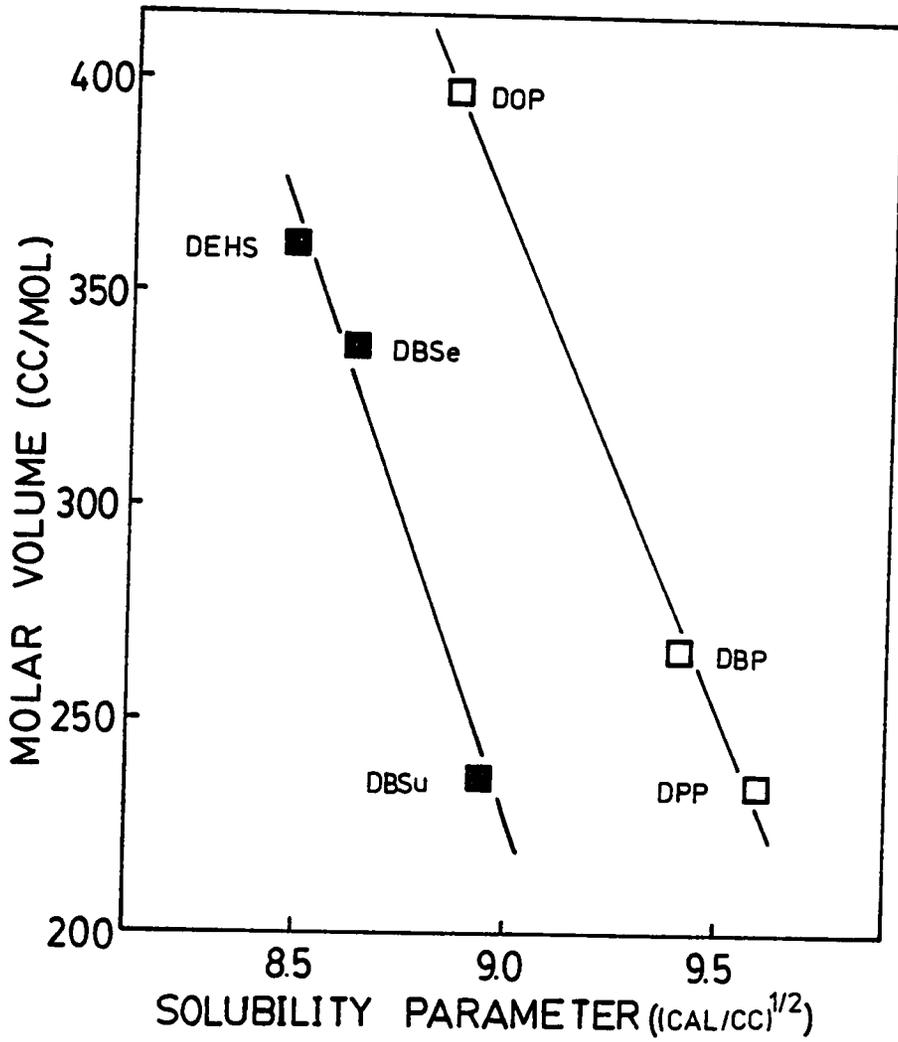
Figure 3.59. Molar volume of six plasticizers as a function of solubility parameter.
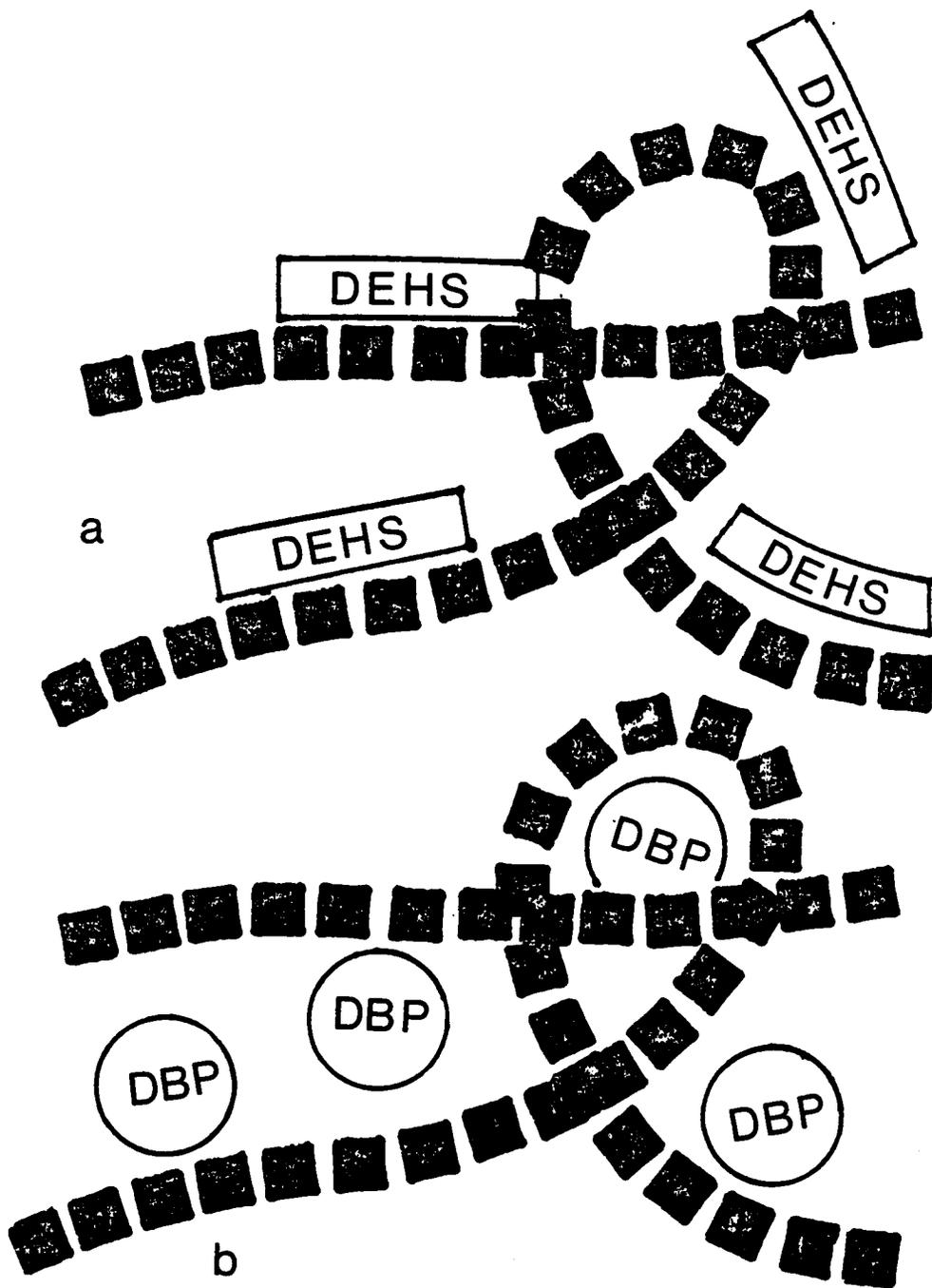
Figure 3.60. Shape and volume representations of a) DEHS and b) DBP as compared to PVC. DBP is represented by a sphere. DEHS is represented by a cylinder with L/D ratio of about 3.5. Vinyl chloride repeat unit is represented by a cube. Dimensions for scaling calculated on the basis of molar volumes.
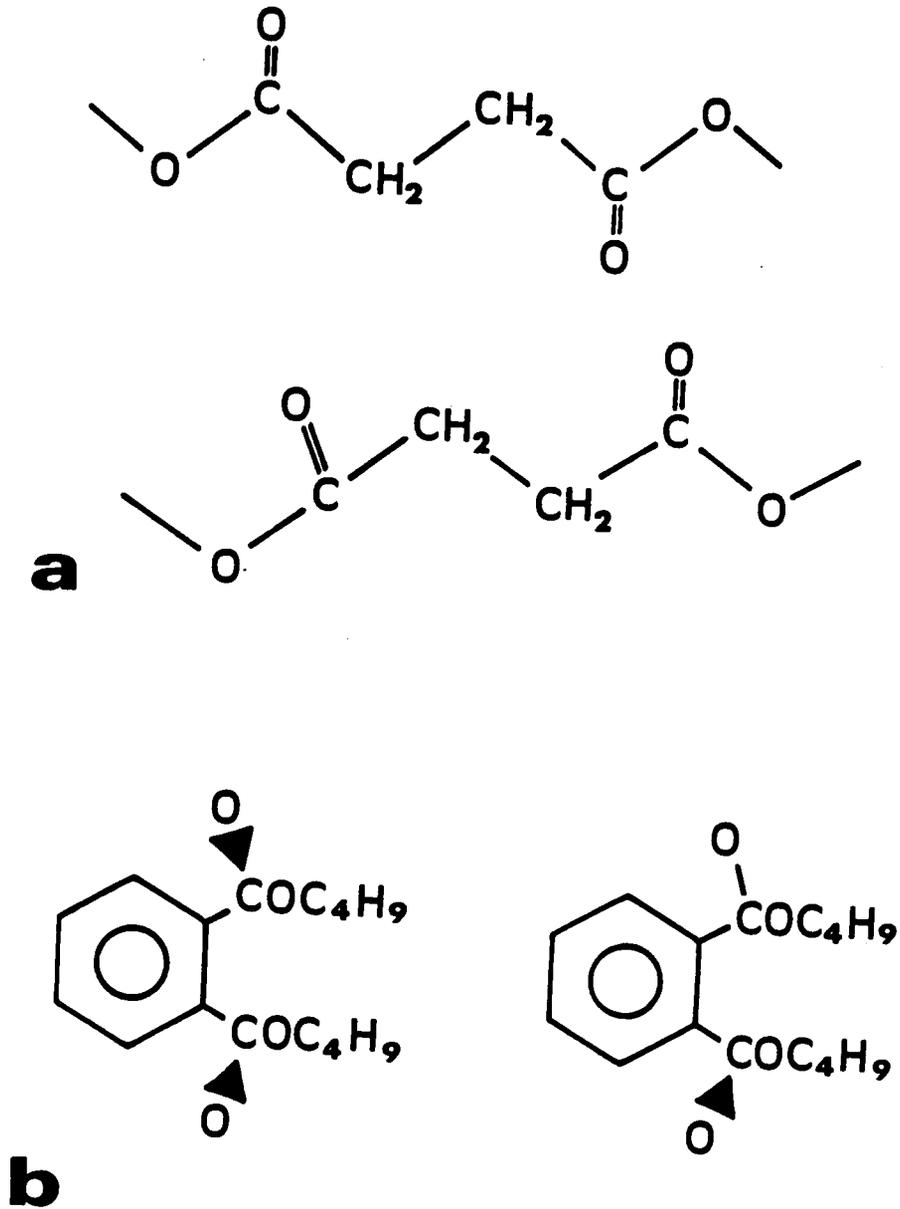
Figure 3.61. Suggestions of possible orientations of carbonyl groups of a) DEHS and b) DBP.
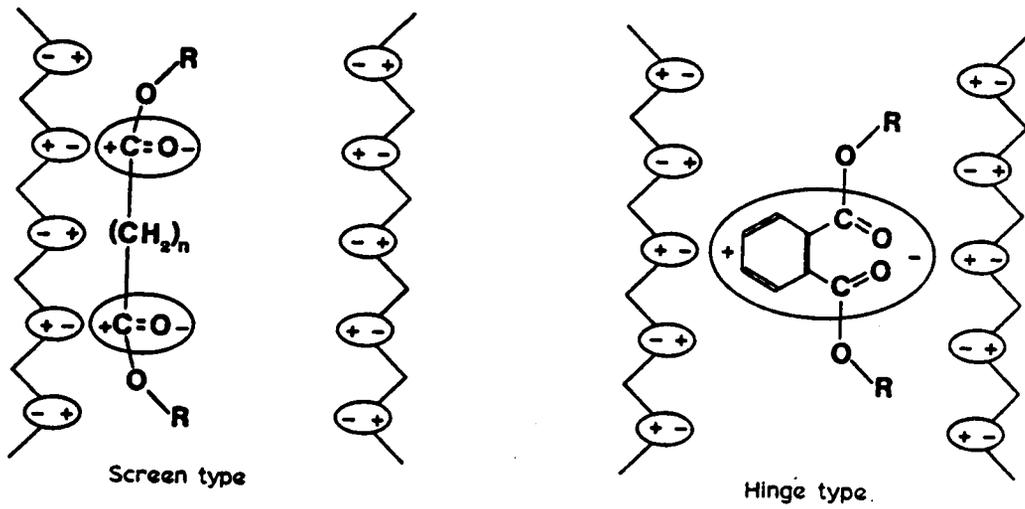
Figure 3.62. Leuch's model of the interaction of aliphatic and phthalate ester plasticizers with PVC. Ref. 13, after Ref. 199.
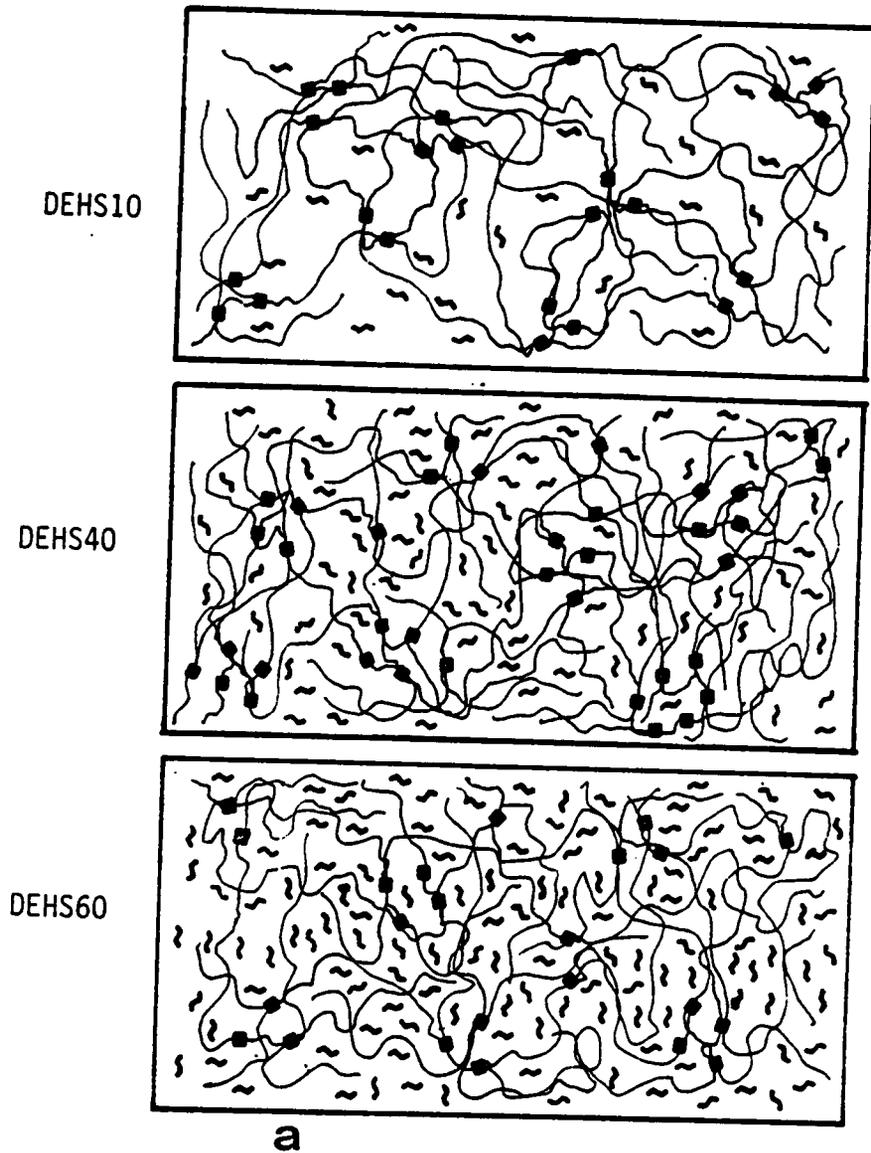
Figure 3.63. Model of plasticized PVC containing increasing amounts of a) DEHS and b) DBP. DBP is represented by a circle, DEHS by a short wavy line. Evolution described fully in text.

DBP10
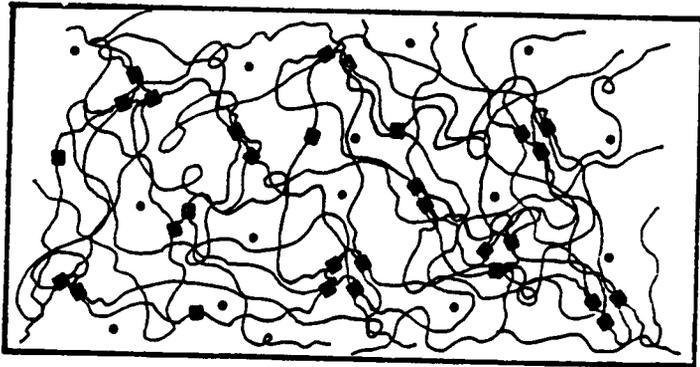
DBP40
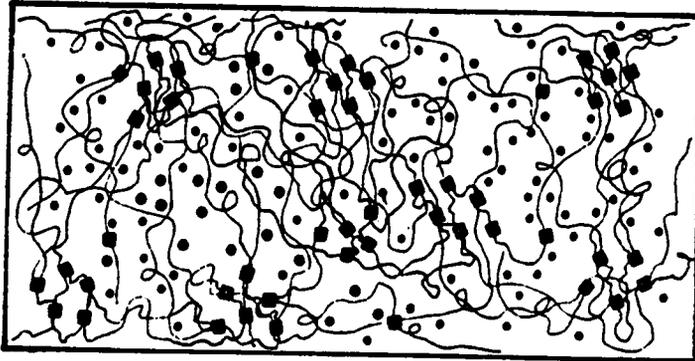
DBP60
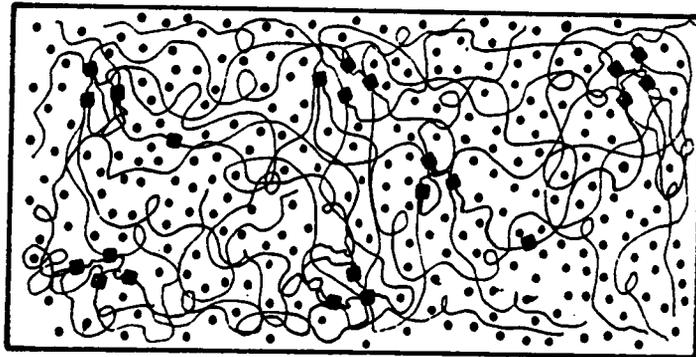
b
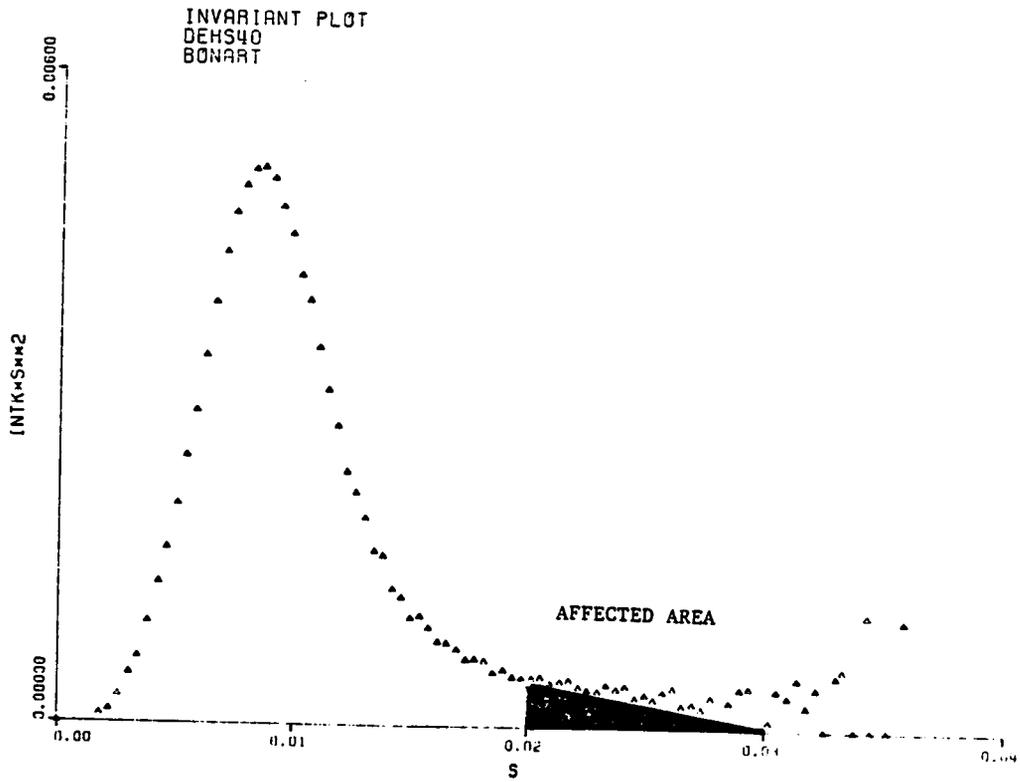
Figure 3.64. Example showing the area affected by the choice of the upper integration limit for determination of the invariant. See Equation (6).
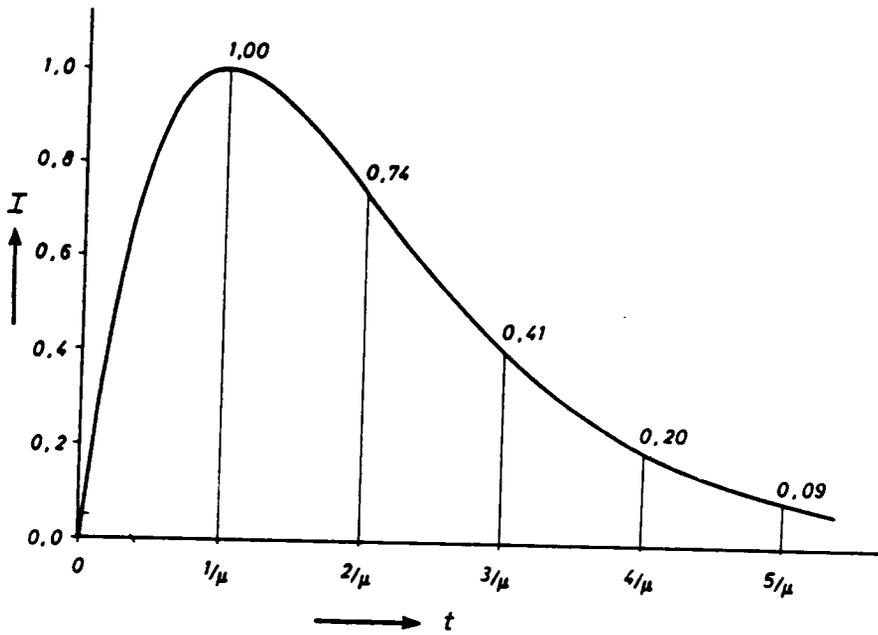
Figure 3.65. Dependence of scattered intensity I on sample thickness t. Ref. 153.

CHAPTER FOUR

CHEMICAL MODIFICATION OF POLYBUTADIENE

WITH ISOPROPYL AZODICARBOXYLATE

FOR USE AS A POTENTIAL IMPACT MODIFIER

4.1. INTRODUCTION

Impact modification of an amorphous or semi-crystalline polymer with elastomers requires a dispersed elastomeric phase and good adhesion between the elastomer and the matrix. Because most polymers are generally immiscible with each other, the first requirement is easily met. However, achieving *phase separation with good adhesion* mandates that the elastomer and the matrix be compatible with each other. The degree of compatibility between the modifier and the "host" polymer strongly influences the morphology of the final material and hence its impact strength or toughness.

Many elastomers are based on hydrocarbons and are not capable of specific interactions which might make them miscible or at least compatible with polar polymers. They are therefore prohibited from being used as impact modifiers in many polymers. However, by altering the chemistry of such an elastomer it may be possible to control its compatibility with another polymer.

This chapter describes the use of *chemical modification* as a means of enhancing the affinity of a hydrocarbon elastomer, polybutadiene, for polymers capable of specific interactions. The modification procedure involves the "ene" reaction between isopropyl azodicarboxylate (IAD) and high 1,4 polybutadiene, as depicted in Figure 4.1. For each unit of IAD that reacts, the hydrocarbon backbone is endowed with two pendant ester groups, which lend it a degree of polarity dependent upon the extent of IAD modification. It is expected that an IAD-modified

polybutadiene (PB) may be capable of specific interactions with suitable polymers through polar attractions or hydrogen bonding. If so, this could expand the number of polymers which might be successfully impact modified with polydiene rubbers.

The research to be discussed here consists of two parts. The first is the chemical modification of PB with IAD and characterization of the modified polymers. The second part focuses on the characterization of blends of polyvinyl chloride (PVC) and IAD-modified PBs. PVC was chosen as the matrix for this preliminary investigation primarily because of its demonstrated miscibility with polymers containing in-chain and pendant ester groups. Polyesters fill the first category (1-4) while polyacrylates and polymethylmethacrylates typify the second (5-7). However, in principle, modification of PB with IAD might be expected to enhance its miscibility with other "polar" polymers such as polyesters, polyacrylates, styrene-acrylonitrile copolymers, and polyamides.

The potential of IAD modification of polybutadienes as a means of controlling their polarity was first demonstrated by Schulz et al (8) in an investigation of IAD modification of various PBs with regard to reactivity, distribution of modified units, and basic structure-property information. The microstructure of the unmodified PB was shown to have a profound effect on the final product. Schulz and co-workers found that the 1,4 backbone reacted more easily with IAD than did the 1,2 backbone. Reaction with 1,4 PB was believed to be predominantly an add-on process resulting in a blocky distribution of modified units leading to a multiphase morphology. IAD adds to 1,2 PB in a random

fashion, and, in contrast to the modified 1,4 polymers, IAD-modified 1,2 PB is thought to have a single-phase morphology (8). The tan δ vs. temperature curves given in Figure 4.2 were provided as support for this conclusion. They show a broadening of the damping peak for 15 mol% IAD on a 1,4 PB followed by the development of two peaks at 37 mol % IAD. The tan δ curve of a modified 1,2 PB (Figure 4.2b) reveals little broadening after IAD modification to 30 mol%.

Spiewak, Bryant, and Schulz (9) conducted further studies of the structure-property relationships in IAD-modified PB. They showed that IAD modification of 1,4(*cis,trans*) PBs enhanced their green (uncured cohesive) strength and tack (autoadhesive strength). The first term refers (9) to the stress-strain properties of an uncured filled rubber while the second term refers to the response of the material in a peel test. The most recent paper in the area of IAD-modified PBs (10) gave evidence of a unique strain-induced phase separation in modified 1,4(*cis,trans*) PBs. Figure 4.3 demonstrates the stress-strain behavior produced by this reported phase separation at high (> 41.4%) IAD content.

The ene reaction may be either cyclic or acyclic (11), IAD modification of PB falling into the latter category. Butler and co-workers (12-14) have performed several cyclic ene-based modifications of unsaturated hydrocarbon polymers using triazolinediones in reactions

like the one shown below:
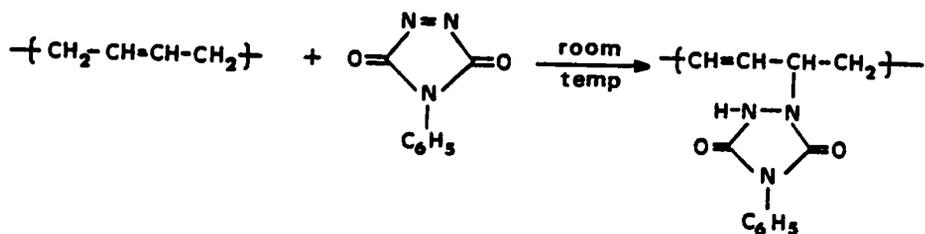
Elastomeric surfaces may even be selectively modified with triazolinediones (11).

Campbell, Loeber, and Tinker (15,16) have demonstrated the versatility of the ene reaction by grafting a monofunctional azodicarboxylate-terminated polystyrene onto polyisoprene. The first reactions were carried out in cyclohexane at 60°C (15). Later studies (16) showed that the reaction could occur solely by mechanical dry mixing of the monofunctional polystyrene with polyisoprene at temperatures above the glass transition of polystyrene, ~ 100°C.

General aspects of the ene reaction have been reviewed by Hoffman (17). Chemical modification of polydienes and other unsaturated polymers via the ene reaction and many other means was reviewed by Brydon and Cameron (18) in 1975 and updated in 1982 by Schulz, Turner, and Golub (11).

Most impact modifiers are based on polybutadiene, but nearly all such applications require the rubber and the matrix to be "compatibilized" by a suitable method. For example, high-impact polystyrene utilizes a grafting reaction between PB and styrene to

improve the adhesion of the rubber to the styrene matrix. ABS, a toughened styrene acrylonitrile copolymer, contains a dispersed phase composed primarily of styrene and acrylonitrile grafted to PB particles. Epoxy resins are toughened with a copolymer of butadiene and acrylonitrile. Optimal toughness is usually obtained at an acrylonitrile content of 18 or 27% (19). PVC is toughened with several copolymers based on PB, principal examples being methacrylate-butadiene-styrene and ABS. These applications demonstrate that toughness can indeed be increased through control of the PB's compatibility with the matrix.

The present investigation was begun with several small-scale IAD modifications of PVC. The modified polymers were characterized using ^{13}C nmr and Fourier transform infrared (FTIR) spectroscopy. They were used in conjunction with UV spectroscopy to construct a routine method of determining the extent of IAD modification in polybutadienes of a similar microstructure and molecular weight. Larger quantities of IAD-modified PB were produced by scaling up the reaction. These modified polymers were blended with PVC homopolymer in solution. Miscibility was evaluated using differential scanning calorimetry (DSC). Stress-strain and more limited impact testing comprised the mechanical property analysis. Morphological study was accomplished by SEM inspection of various fracture surfaces.

4.2. EXPERIMENTAL

4.2.1. Materials

All initial small-scale IAD modifications were carried out on a high 1,4 polybutadiene (PB) prepared by R. D. Allen in the Chemistry Department at VPI&SU. He polymerized butadiene anionically in cyclohexane using sec-butyl lithium as initiator. The reaction was conducted under high vacuum at ambient temperature. Using the infrared method of Haslam et al (20) as described by I.-C. Wang (21), the microstructure of this PB was found to be 53.7% trans-1,4, 39.4% cis-1,4, and 6.9% 1,2 (vinyl). Its number average molecular weight was believed to be about 60,000.

I. W. Wang of Phillips Petroleum provided several polybutadienes of various microstructures. Two high-1,4 PBs were reserved for large-scale modification reactions. They had number average molecular weights very near 60,000 and were determined by IR methods (at Phillips) to be 51.2 or 51.1% trans-1,4, 38.5 or 38.6% cis-1,4, and 10.3% 1,2. A third PB with a molecular weight of 80,000 and very similar microstructure was used for blending studies. These three PBs were prepared by anionic polymerization procedures in cyclohexane using n-butyl lithium as initiator along with a very small amount of THF. The reaction temperature was 70°C.

Isopropyl azodicarboxylate (IAD) was purchased from Muskegon Chemical Co., Muskegon, MI. At room temperature, it is a deep yellow liquid. It has a boiling point of 110-114°C at 10-12 mm Hg. It was used as received. Toluene was purchased from Fisher Scientific Co. It was distilled and dried over 3 A molecular seives.

Rohm and Haas Co. provided generous amounts of Geon 86, a suspension polymerized polyvinyl chloride (PVC) manufactured by B. F. Goodrich. It was stabilized with 0.5 weight percent of a tin mercaptide. The PVC was reported to have number average and weight average molecular weights of about 40,000 and 80,000, respectively. Intrinsic viscosity measurements in THF at 25°C gave a viscosity average molecular weight of about 70,000, but this result has to be considered approximate due to the presence of the stabilizer. The polymer's glass transition temperature was 88°C as measured by DSC at 10°C/min.

4.2.2. Modification Procedures

For the small-scale IAD modifications, a 100 ml two-necked round-bottom flask with a ground glass stopper and serum cap was used as the reaction vessel. To this flask was added approximately 1.0 g of PB and 20 ml of toluene to make a 5% w/v solution. Agitation was maintained using a magnetic stir bar. Prior to closure, the flask was flushed with dry nitrogen. The flask was placed in a temperature-controlled 50°C bath overnight to dissolve the PB. After dissolution, the temperature of the bath was raised to 80°C. A particular amount of IAD was injected into the flask through the serum cap using a 2 cc syringe. The reaction

mixture was kept in the 80°C bath for 24 hours and then removed and cooled to room temperature. It was observed that the color of the solution progressed from a deep yellow to a pale yellow as the reaction proceeded. The reaction product was precipitated in methanol or, at high (> 25%) conversions, in hexane. It was redissolved, precipitated once more, and washed with methanol. The anti-oxidant Irganox 1010 was added during the precipitations and washings. The final product was dried for a few hours in a room temperature vacuum oven and stored in a freezer.

Scale-up of the modification was carried out in a 500 ml three-necked round-bottom flask equipped with a magnetic stir bar. PB and toluene were loaded into the flask through the center neck which then served first as a nitrogen outlet and later as a thermometer holder. The two side necks were fitted with serum caps. A hypodermic needle plunged through one of the serum caps was used to flush the vessel with dry nitrogen. As the needle was removed, a thermometer was inserted into the center neck; a stainless steel thermocouple probe was then inserted through the pierced serum cap. The flask was placed in a temperature-controlled heating mantle supported by a magnetic stir plate. About 25 g of polymer and 200 ml of toluene were used in the large-scale reactions, giving a concentration of about 12.5 % w/v. The dissolution and reaction schedule and product recovery procedure were the same as those used for the small-scale preparations.

4.2.3. *Characterization of IAD-Modified PBs*

Three polymers modified in the small-scale reactions were analyzed by ^{13}C nmr, FTIR, and UV spectroscopy. ^{13}C nmr spectra were obtained in d-chloroform at ambient temperatures by R. Boyer of the Analytical Services Group of VPI&SU's Chemistry Department. Delay between scans was greater than the 4.7 sec T1 reported by Schulz et al (8) for the carbonyl carbon of an IAD-modified PB. The next highest T1 was said to be 0.87 sec. The assignments made by Schulz et al for IAD-modified 1,4 PB were used by the author to calculate the percent IAD added. This will be discussed in detail later.

FTIR spectra were taken on a Nicolet MX-1 spectrometer using films cast directly on KBr windows. The spectra of IAD was obtained by squeezing the liquid between two KBr disks.

UV spectra were obtained on a Perkin-Elmer UV/Vis spectrometer. Solutions were made in chloroform at a concentration of 0.08% (w/v) and diluted to 0.04%. Spectra were obtained between wavelengths of 300 and 200 nm, and the peak absorbance scanned twice manually.

4.2.4. *Blend Preparation*

PVC was blended with 10, 25, and 50% by weight of modified and unmodified PBs by THF dissolution followed by precipitation in methanol. Samples were administered Irganox 1010 during this operation. The collected precipitate was dried under vacuum for 3 hours at 105°C.

Several attempts were made to blend PVC with chlorinated polyethylenes to obtain a "standard" impact-modified PVC. No convenient solvent could be found to prepare blends in quantities large enough for mechanical testing. Use of the CSI-Max Laboratory Mixer/Extruder led to rapid degradation of the polymers and necessitated immediate dismantling and cleaning of the Extruder. Preparation of PVC/CPE blends was consequently suspended.

4.2.5. *Thermal Analysis*

A Perkin-Elmer DSC-4 with Scanning Autozero baseline correction was used to determine transition temperatures of blends and blend components. An indium standard (Tm = 156.6°C) was used for temperature calibrations. Scanning rate was 10 deg/min.

Thermogravimetric analysis (TGA) was conducted on one of the PVC/PB blends and one modified PB by E. Yilgor at VPI&SU. The modified PB (scanned at 10°C/min) did not show significant weight loss until the temperature was close to 300°C. When the blend and the modified elastomer were heated to 175°C and held there for 10 minutes, weight loss was not observed in either case. All TGA runs were conducted in air.

4.2.6. *Mechanical Testing*

Samples of PVC and PVC/PB blends were prepared for mechanical testing by compression molding at 170°C. Materials were aged several days before impact testing and 24 hours before stress-strain testing.

Falling weight impact tests were conducted on several samples through the courtesy of Alex Lou at Phillips Petroleum. The rate was 50 in/sec (1.27 m/sec). Samples were molded disks approximately 5 cm in diameter and about 0.17 cm thick.

Stress-strain tests were run on a Model 1122 Instron at crosshead speeds of 1 and 100 mm/min. Dog-bone samples with a 10-mm gauge length were cut from compression molded films. All mechanical testing was done at ambient temperatures.

4.2.7. *Scanning Electron Microscopy*

Fracture surfaces were examined in an ISI, Inc. Super III-A SEM. Cold fractures·were effected by "soaking" films in liquid nitrogen for 10 minutes and breaking the films while they were still immersed in the coolant. Fracture surfaces of impact and stress-strain specimens were also examined with SEM.

4.3. RESULTS AND DISCUSSION

4.3.1. Characterization of IAD-Modified Polybutadienes

The work of Schulz et al (8) indicated that ^{13}C nmr could be used for quantitative measure of the percentage of IAD-modified butadiene units. Figure 4.4a provides their spectra for PB of high 1,4 content modified with 0.0, 7.9, and 23.3 mol% IAD. The signals are labelled with letters corresponding to specific carbons on the converted 1,4 units as shown on the structure provided. Figure 4.4b repeats this structure and outlines the method by which mol% IAD conversion may be calculated using each carbon. An example calculation is given. In particular, note that the appearance of the "e" peak at 59.5 ppm gives clear evidence of a successful reaction.

Spectra for three IAD-modified PBs were obtained under conditions where the nuclear Overhauser effect (NOE) was active as well as inactive (NNE). The NOE (22-3) utilizes the energy exchange between carbons and attached hydrogens to enhance the ^{13}C resonance signal which is weak due to the naturally low ^{13}C population. Because attached hydrogens are essential to a full NOE, the NOE optimization will not be available to carbonyl carbons (such as "g" in Figure 4.4). Hence, NOE ^{13}C nmr spectra gave disproportionately low signal intensities for the "g" carbon. Even the "h" and "e" carbons did not show a full NOE enhancement since they hold only one H. The NNE spectra were consequently used for quantitative analysis of several small-scale modified PBs.

Three polymers modified in the small-scale reactions were selected for use in establishing a routine analysis of the extent of IAD modification. Based on preliminary ^{13}C nmr analysis, these three polymers were believed to span the range of IAD-modification expected to increase the polarity of PB while allowing it to remain an elastomer at room temperature. The ^{13}C spectra of these three modified elastomers are shown in Figure 4.5. Again, the signal at 59.5 ppm indicates attachment of IAD to the PB chain. Using the method described by Figure 4.4 and discussed previously, their IAD contents were determined to be 3.3, 10.5, and 27.0 +/- 0.5 mol%.

The UV absorbances measured at 249 nm for these same three modified PBs are plotted against mol% IAD in Figure 4.6. The use of UV as a gauge of the extent of reaction assumes that, first, the IAD reacts in a blocky fashion as shown in several ways by Schulz and co-workers (8-10) for high 1,4 PB and, second, the successive addition of two IAD units to two adjacent butadiene units occurs as shown below:

$$- CH2 - CH = CH - CH2 - CH2 - CH = CH - CH2 -$$

$$
\begin{array}{c}
- CH2 - \underset{\underset{IAD}{|}}{CH} - \underset{\underset{IAD}{|}}{CH} - CH = CH - CH = CH - CH2 - \qquad I
\end{array}
$$

$$
\begin{array}{c}
- CH2 - \underset{\underset{IAD}{|}}{CH} - CH = CH - CH = CH - \underset{\underset{IAD}{|}}{CH} - CH2 - \qquad II
\end{array}
$$
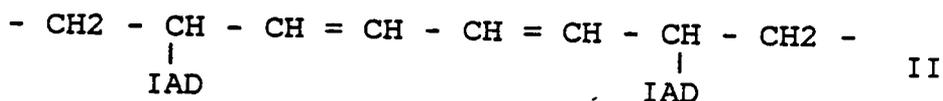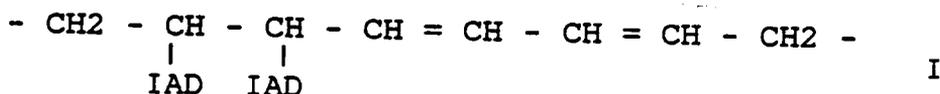
Structure II would be preferred due to the steric difficulties presented by Structure I. The result in either case is a conjugated double bond

(-C=C-C=C-) which is capable of UV absorption (24). Neither every nor every other IAD addition to the PB chain will necessarily lead to a conjugated double bond, however, on the average the number of such bonds may increase approximately proportionately to the extent of IAD modification.

Further information about these modified polymers can be gained through FTIR spectroscopy. Figure 4.7 provides FTIR spectra of a high 1,4 PB, IAD, and an IAD-modified PB (10.5 mol% IAD). The absence of any strong absorbance in the 1750 wavenumber region of the PB spectrum is noted. IAD absorbs strongly at 1770 wavenumbers, characteristic of the C=O group. Two low absorbances are seen for IAD near 3500 wavenumber, perhaps related to its N=N moiety. Reaction between IAD and PB shifts the C=O absorbance to about 1710 wavenumbers. Campbell, Loeber, and Tinker (15,16), whose work with an azoester-terminated polystyrene was referred to earlier, found a shift from 1785 to 1740 wavenumbers upon conversion of an azodicarboxylate to a hydrazodicarboxylate.

The FTIR spectrum of the IAD-modified PB in Figure 4.7 shows a distinct band near 3300 wavenumbers which indicates the presence of an N-H absorption. An N-H group is formed by the abstraction of a hydrogen from the azoester compound during the ene reaction. Although there is some overlap with IAD in this region of the spectrum, the apparent N-H absorption is much stronger and is situated at a lower wavenumber than the very weak bands of IAD in the 3500 wavenumber region of the spectrum. A rigorous quantitative analysis of these

spectra regarding the extent of IAD modification is prevented by overlaps, however, the FTIR spectra complement the ^{13}C nmr spectra by also indicating that the IAD had reacted with the PB.

It was found that the mol% IAD added was linearly related to the ratio of ml IAD/g PB used in the small-scale reactions, as shown in Figure 4.8. For subsequent reactions, Figure 4.8 could be used as an approximation of the proportion of reactants necessary to reach a desired modification level. It must be emphasized that the UV calibration curve (Figure 4.6) and the reactant ratio curve (Figure 4.8) may only be applied with confidence to another PB of similar microstructure and molecular weight. This is particularly important in the case of the 1,4 PB due to its tendency to add on IAD in a blocky manner (8).

With the successful completion of the small-scale reactions, the reaction was scaled up to 25 grams as described earlier using a PB of similar microstructure. IAD modification was to be limited to only a few mol% so as not to destroy the elastomeric nature of the PB relative to room temperature. The IAD contents of the four modified PBs prepared in large batches are given in Table 4.1 along with their glass transition temperatures and the nomenclature to be used. A PB modified with, for example, 11 mol% IAD will be referred to as PB11.

The DSC traces in Figure 4.9 show the change in breadth of the glass transition region for increasing IAD content. The curve for PB9 exhibits a fairly broad lower Tg but its glass transition actually extends to near -20°C. The Tg for PB9 in Table 4.1 was taken from the low

temperature part of the trace, hence it is somewhat below what might be expected for a 9% conversion.

4.3.2. *Properties and Morphology of PB/PVC Blends*

In the following discussion, all blends will be referred to by a label such as 10PB5, which indicates that 10% (by weight) PB5 has been blended with PVC. The label "PB" will be used to refer to polybutadienes in general whether modified or not. Unmodified PB will be called "PB0."

DSC indicated no change in the Tg of the PVC at 10 or 25 weight percents of the various modifiers. Tg remained essentially constant at 87 +/- 1°C. It was noted in the DSC traces of the 50/50 blends that modification with PB5, PB9, and PB11 tended to broaden the glass transition region of the PVC, however, no change in the PVC Tg was observed. Another effect was noted for the 50PB11 blend whose first and second scans are shown in Figure 4.10. In this case, the PVC glass transition in the second DSC heating showed a smaller specific heat (Cp) difference than the first scan. This might indicate better phase mixing between PVC and PB11 following a quench from 140°C. However, the measured Tg did not change. On the whole, DSC analysis thus suggested complete phase separation of the PVC and IAD-modified PBs. Construction of three-dimensional models of an IAD-modified PB indicated that its carbonyl carbons are accessible for intermolecular interactions, so steric obstacles to PVC interacting with IAD-modified PB via this route may be assumed to be small. It is possible that the blocky nature

of IAD-modification of 1,4 PB promotes more interaction between IAD-modified PB chains both intermolecularly and intramolecularly than it does between PVC and the modified PBs.

Phase separation was also suggested by the translucence and mild yellow color of some of the blends in film form. These features were not always uniform, particularly at 10% rubber, but occurred as swirls. Sahajpal (25) has pointed out that if the refractive index of a dispersed phase in a PVC blend is lower than that of PVC, the composition will be somewhat yellow and hazy to an extent dependent on the difference between the refractive indices of the matrix and dispersed phase. The refractive indices of polybutadiene and PVC are about 1.52 and 1.54, respectively (26).

The fracture surface morphologies of the blends proved to be rather puzzling. As shown in Figure 4.11 for the 10% blends, the surfaces of the materials were covered with crater-like structures of various sizes. Although no strong trend was observed, these "holes" were found to be smallest for 10PB11. Drying the precipitated blends at higher temperatures before compression molding (105°C vs. ambient temperatures) resulted in the same structure as did repressing a once-molded film. Compression molding followed by quenching under pressure had little effect. Evidently, the craters did not result from residual solvent. The temperature of pressing (170°C) was far below the reported "retroene" reaction temperature (8). TGA measurements described in the Experimental Section showed that substantial weight loss did not occur at or near the molding temperatures. Degradation did not then appear to be the source of the craters.

It is difficult to accept that the craters contain, or once contained, rubber because they cover a very large percentage of the surface, even at 10% rubber content. At 25% rubber level, there appears to be some increase in the size of the craters, as Figure 4.12 shows. Finding the rubber itself was not a simple task. Micrographs of 10PB0 and 25PB0 gave vague evidence of rubber in sub-surface lumpiness and stretched surface structures (see, for example, Figure 4.13), but SEM examination of fracture surfaces provided no conclusive information about the quality of the adhesion of the rubber to the matrix. However, at room temperature, all the elastomers but PB11 flow easily given enough time. Poor adhesion, usually marked by gaps or voids, might therefore be hard to detect in these materials.

Falling weight impact tests on PVC and 10PB11 showed a drop in impact strength upon rubber modification. PVC fractured in a ductile manner and exhibited a breaking energy of about 65 in-lb. However, 10PB11 fractured in a brittle fashion with a breaking energy of only 2 in-lb. The load vs. displacement curves in Figure 4.14a illustrate the sharp differences in energy absorption. SEM examination showed that the impact fracture surface of the latter material was literally covered with the enigmatic craters. See Figure 4.14b. These results suggest that the porous structure was detrimental to impact strength.

Further studies of mechanical properties and morphology were conducted using low and high speed tensile testing in conjunction with SEM. Samples included were 10PB0, 25PB0, 10PB11, 25PB11, and PVC.

Experimental crosshead speeds were chosen such that initial strain rates were 0.00167 and 0.167 inverse sec. The strain rate of a falling weight impact test is 0.1 to 10 inverse sec (27).

The stress-strain behavior observed for PVC at low and high elongation rates is shown in Figure 4.15. At low rates, a neck formed at about 5% elongation and spread from the middle of the tensile dogbone to both its ends accompanied by a slight but reproducible increase in stress. High speed testing induced a sharper necking. Samples broke after the neck had propagated only a short distance. A small amount of stress whitening was seen at the very tips of the fractured high speed samples, but otherwise PVC showed no whitening.

Fracture surfaces of the PVC broken at high and low rates were distinctly different. As Figure 4.16 illustrates, the lower speed crack began at one end of the sample and fanned out to the other end. The fracture mode was ductile rather than brittle (28) and involved more than one plane of crack propagation. Ductility was observed on a fine scale in the final stages of fracture, as Figure 4.16c shows.

PVC demonstrated dramatic ductility under high speed tensile testing. Figure 4.17 shows the extensive plastic deformation of both the surface and the sample as a whole. At the initiation end of the sample, there were found a few local parabolic markings suggestive of brittle fracture (28,29). These are believed to be initiated by impurities and other heterogeneities. However, even in the early stages of crack propagation, the ductility was remarkable. The most striking features of

the fracture surfaces were the tuft-like elongated strands. The effect of aging on the stress-strain response of PVC homopolymer was not explicitly investigated, but it was noted that the response of a sample aged two months was qualitatively the same as these materials, which were aged 24 hours after molding.

The possibility that dissolution and precipitation might alter the deformation processes of PVC was briefly investigated. The graphic results of low and high speed tensile testing were essentially the same as those given in Figure 4.15 for samples molded from neat powder. Comparing the SEM micrographs in Figure 4.18 with those in Figures 4.16 and 4.17 indicates one point of difference: the tufts or strands formed at high speeds appear to be spread further apart and to be much finer for solution treated PVC. See especially Figures 4.18b and Figure 4.17.

Blends of PVC with 10 weight PB0 or PB11 displayed stress-strain behavior at both high and low deformation rates which ranged between ductile and brittle. Brittle responses such as those shown in Figure 4.19 were invariably traced to a lack of plastic deformation and the occurrence of the familiar craters on the tensile fracture surface. Examples of the features observed for brittle behavior in the 10% blends are shown in Figure 4.20.

In most cases, the 10% blends demonstrated a ductile response. However, as one might see by comparing Figure 4.21 with Figure 4.15, the 10% blends yielded less sharply and at lower stresses than unmodified

PVC. At the lower rate of deformation, PVC showed higher ultimate elongation, but the reverse was true at the higher deformation rate. Corresponding tensile fracture surfaces such as those in Figure 4.22 showed limited plastic deformation and drawing in the ductile 10PB0 and 10PB11 specimens.

The tensile behavior of 25PB0 was uniform from sample to sample at low and high speeds. Examples of stress-strain responses and fracture surfaces are given in Figures 4.23 and 4.24, respectively. A slight amount of yielding is observed on the fracture surface of the low speed specimen. This corroborates with its stress-strain response which showed behavior intermediate between ductile and brittle (30). Irregularly shaped structures abounded on both low and high speed fracture surfaces, perhaps due to rubber inclusions.

PVC modified with 25 weight percent PB11 (see Figure 4.25) demonstrated ductility where 25PB0 had shown only brittleness. Tensile surfaces of both low and high speed fractures of 25PB11 showed fairly uniform yielding as Figure 4.26 demonstrates.

Table 4.2 lists average modulus values for specimens whose stress-strain curves are given in Figures 4.15, 4.19, 4.21, 4.23, and 4.24. As expected, modulus dropped with rubber modification. Blends containing PB0 suffered somewhat sharper losses than those containing equal weight percents of PB11. This suggested that PB11 may have promoted better phase adhesion and perhaps was somewhat compatible with PVC. It may be noted that during tensile testing of the PB/PVC blends, slight

amounts of stress whitening were often observed along the gauge length of the dogbone samples and generally remained at the fracture tip after fracture.

The method of blend preparation, dissolution in a common solvent followed by precipitation in a common non-solvent, deserves further discussion. Consider that the crater-like fracture surfaces look much like a fibrous network with a defined pore size, particularly for the PB11/PVC blends. See, for example, Figure 4.12. The "lines" of the network may well be PVC since it is the dominant component. Precipitating a polymer in a solvent below its Tg is effectively a spinning process since the material comes out of solution in strands. In the presence of an immiscible second component, individual strands may remain more separate from each other. The observation of considerably finer tufts in the tensile fracture surface of solution processed PVC (Figure 4.18) suggested that this strand character may persist in a compression molded film even in the absence of an immiscible second polymer. Of course, these comments are purely speculative, but it is believed that they are a reasonable assessment of some of the possible ramifications of the solution blending process.

The properties of impact-modified PVC have been found to depend strongly on its morphology (31-33). The morphology which promotes good impact strength varies from one modifier to another. In some cases, such as the methacrylate-butadiene-styrene modifiers, the modifier functions best as a uniformly dispersed phase (31,32). Other modifiers, chlorinated polyethylene being a good example, reportedly

impart the highest impact strength when present as a "network" around partially fused PVC particles (33). Although the open literature on impact-modified PVC is scarce, no study of which the author is aware has utilized solution blending for blend preparation. It was, however, unavoidable in this study due to the rapid degradation encountered in using the available laboratory extruder. Compounding with a two-roll mill might produce better results since it does not require extensive fusion of the PVC and could in principle allow processing at relatively low temperatures. Whether the impact properties of blends of PVC with IAD-modified PB would be improved by a dispersed or continuous morphology could not be determined since the morphologies of the blends were not fully characterized.

4.4. CONCLUSIONS

Polybutadienes of high 1,4 microstructure have been successfully modified with isopropyl azodicarboxylate (IAD). A fast and inexpensive method of determining the extent of IAD modification has been developed which utilizes UV spectroscopy in conjunction with absolute measurements by ^{13}C nmr. This method may be generally applied to any PB of high 1,4 content.

Based on Tg criteria, PVC was found to be immiscible with 10 and 25 weight percent PB modified with up to 11 mol% of IAD. DSC study indicated that limited miscibility between the elastomer and PVC may have occurred in a 50/50 blend containing an 11 mol% IAD-modified PB. It was found from high speed tensile testing that blends containing 25 weight percent of the 11 mol% IAD-modified PB were significantly more ductile than a similar blend of PVC with unmodified PB. Thus far, however, no improvements have been made upon the impact properties of the rigid PVC.

The morphologies observed for the PB/PVC blends were puzzling, particularly with regard to the unexplained occurrence of "craters" on various fracture surfaces. Mechanical property testing and SEM studies of the corresponding fracture surfaces indicated that these craters are not conducive to good toughness.

4.5. RECOMMENDATIONS FOR FUTURE STUDY

1. The use of roll milling or another method of melt mixing should be investigated for blending of PB and PVC. It is believed that this method of processing may provide better control of the blend morphology and perhaps indicate the mode (dispersal or network) in which the IAD-modified PBs might best function as PVC impact modifiers. Based on a speculative explanation given in the main text, melt mixing may eliminate the "craters" found to be synonymous with brittle fracture behavior.

2. The somewhat surprising result that 11 mol% IAD-modification of PVC did not depress the Tg of PVC might be looked at further using higher percentages of IAD modification. The addition of more IAD may substantially increase the reported block lengths of azoester-modified butadiene units at the levels where PVC miscibility is achieved. However, if Spiewak, Bryant, and Schulz (9) are correct in their assessment of "strain-induced phase separation" at higher levels of IAD modification, such materials might act as interesting modifiers for PVC or polymers with which they are compatible. While IAD levels higher than 11 mol percent will no doubt raise the Tg of the modified PBs, it is to be remembered that the IAD-modified high 1,4 PBs have a very broad glass transition which if located over a suitable temperature range could perhaps still be exploited to give good general purpose toughening.

3. PVC blends containing 10% of either unmodified PB or 11 mol% IAD-modified PB were essentially identical in stress-strain response. However, the same IAD-modified PB incorporated at 25 weight percent performed significantly better than the 25% blend containing the unmodified PB. The effect of modifier concentration on mechanical properties is therefore worthy of continued study.

4. Useful information about the phase separation in the investigated PVC blends might be gained from dynamic mechanical analysis. This technique is often more sensitive than DSC in assessing the nature of phase separation.

5. Because PVC is known to be notch sensitive, it would be beneficial to evaluate future impact-modified PVC materials using a notched impact test such as the Izod or Charpy test (ASTM-D256).

REFERENCES

1. Prud'homme, R. E., Polym. Eng. Sci., *22*, 90 (1982).

2. Ziska, J. J., Barlow, J. W., Paul, D. R., Polymer, *22*, 918 (1981).

3. Woo, E. M., Barlow, J. W., Paul, D. R., J. Appl. Polym. Sci., *28*, 1347 (1983).

4. Coleman, M. M., Varnell, D. F., Runt, J. P., in *Polymer Alloys, III*, Klempner, D., Frisch, K. C., Plenum Press: New York, 1983.

5. Walsh, D. J., Higgins, J. S., Doube, C. P., McKeown, J. G., Polymer, *22*, 168 (1981).

6. Walsh, D.J., Cheng, G. L., Polymer, *25*, 495 (1984).

7. Walsh, D.J., Cheng, G. L., Polymer, *25*, 499 (1984).

8. Schulz, D. N., Spiewak, J. W., Valaitis, J. K., Mochel, V. D., Barzan, M. L., Macromolecules, *13*, 1367 (1980).

9. Spiewak, J. W., Bryant, L. A., Schulz, D. N., J. Appl. Polym. Sci., *26*, 4331 (1981).

10. Hamed, G. R., Shieh, C.-H., Schulz, D. N., Polym. Bull., *9*, 525 (1983).

11. Schulz, D. N., Turner, S. R., Golub, M. A., Rubber Chem. Tech., *55*, 809 (1982).

12. Butler, G. B., Williams, A. G., J. Polym. Sci.: Polym. Chem. Ed., *17*, 1117 (1979).

13. Leong, K.-W., Butler, G. B., J. Macromol. Sci. -- Chem., *A14*, 287 (1980).

14. Butler, G. B., Ind. Eng. Chem. Prod. Res. Dev., *19*, 512 (1980).

15. Campbell, D. S., Loeber, D. E., Tinker, A. J., Polymer, *19*, 1106 (1978).

16. Campbell, D. S., Loeber, D. E., Tinker, A. J., Polymer, *20*, 393 (1979).

17. Hoffman, H. M. R., Angew. Chem. Int. Ed. Eng., *8*, 556 (1969).

18. Brydon, A., Cameron, G. G., Chap. 4 in *Progress in Polymer Science*, Vol. 4, Jenkins, A. D., ed., Pergamon Press: Oxford, 1975.

19. Drake, R., Siebert, A., SAMPE Quarterly, *6*, 11 (1975).

20. Haslam, J., Willis, H. A., Squirrel, D. C. M., *Identification and Analysis of Plastics*, Second Edition, Iliffe Books: London, 1972.

21. Wang, I.-C., Ph. D. Thesis, VPI&SU, 1981.

22. Levy, G. C., Lichter, R. L., Nelson, G. L., *Carbon-13 Nuclear Magnetic Resonance Spectroscopy*, Second Edition, Wiley: New York, 1980.

23. Mandelkern, L., Pure Appl. Chem., *54*, 611 (1982).

24. Rabek, J. F., *Experimental Methods in Polymer Chemistry*, Wiley: New York, 1980.

25. Sahajpal, V., Chap. 4 in *Developments in PVC Technology*, Henson, J. H. L., Whelan, A., eds., Applied Science: London, 1973.

26. *Polymer Handbook*, Second Edition, Brandrup, J., Immergut, E. H., eds., Wiley: New York, 1975.

27. Reed, P. E., Chap. 4 in *Developments in Polymer Fracture - 1*, Andrews, E. H., ed., Applied Science: London, 1979.

28. Andrews, E. H., *Fracture in Polymers*, American Elsevier: New York, 1968.

29. Kanninen, M. F., Rosenfield, A. R., Hoagland, R. G., in *Deformation and Fracture of High Polymers*, Kausch, H. H., Hassell, J. A., Jaffee, R. I., eds., Plenum Press: New York, 1973.

30. Titow, W. V., Chap. 11 in *PVC Technology*, Fourth Edition, Titow, W. V., ed., Elsevier: London, 1984.

31. Lutz, J. T., Polym.-Plast. Technol. Eng., *21*, 99 (1983).

32. Breuer, H., Haaf, F., Stabenow, J., J. Macromol. Sci. -- Phys., *B14*, 387 (1977).

33. Siegmann, A., Hiltner, A., Polym. Eng. Sci., *24*, 869 (1984).

Table 4.1.   Glass Transition Temperatures
             for IAD-modified Polybutadienes

Sample	Mol% IAD	Tg ($^\circ$C)*
PB0	0	-87
PB3	3	-75
PB5	5	-68
PB9	9	-69
PB11	11	-33

----

*   DSC scanning rate 10°C/min.

Table 4.2. Young's Modulus*

Sample	Modulus (10^3 MPa)
PVC	1.87
10PB0	1.24
10PB11	1.41
25PB0	0.48
25 PB11	0.70

----

* Average of moduli found at 1 and 100 mm/min.

$$\left(CH_2-CH=CH-CH_2\right) \ + \ \overset{\displaystyle N-\overset{\displaystyle O}{\overset{\|}{C}}-OR}{\underset{\displaystyle N-\underset{\displaystyle O}{\overset{\|}{C}}-OR}{\|}}$$

toluene
80°C

$$\left(CH=CH-\underset{\displaystyle \underset{H-N-COOR}{\overset{|}{N}-COOR}}{\overset{|}{CH}}-CH_2\right)$$

$$R = -\overset{\displaystyle CH_3}{\underset{\displaystyle CH_3}{\overset{|}{CH}}}$$
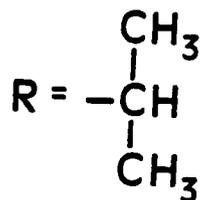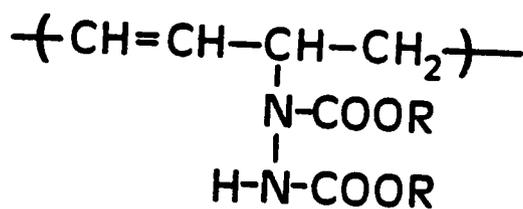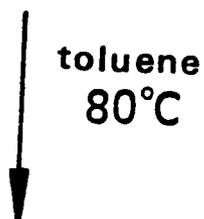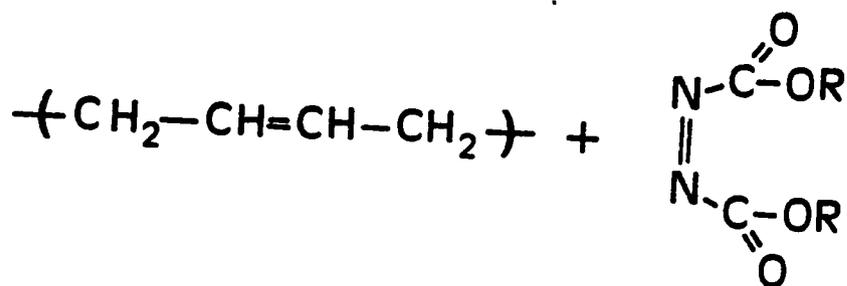
Figure 4.1. Reaction between 1,4 polybutadiene and IAD to make an isopropyl azodicarboxylate-modified polybutadiene.
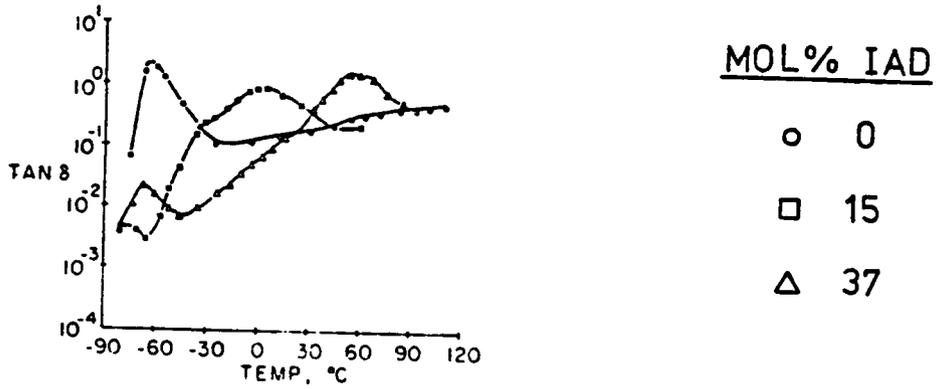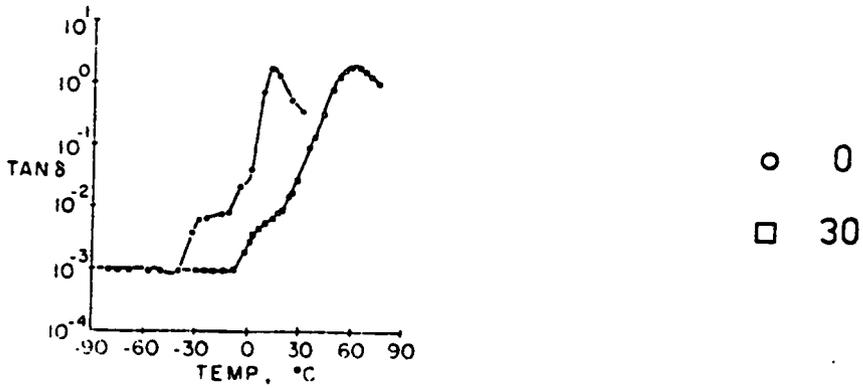
Figure 4.2.   Mechanical damping curves for a) 1,4 and b) 1,2 polybutadienes modified with varying amounts of IAD as noted. Frequency 110 Hz.   Ref. 8.
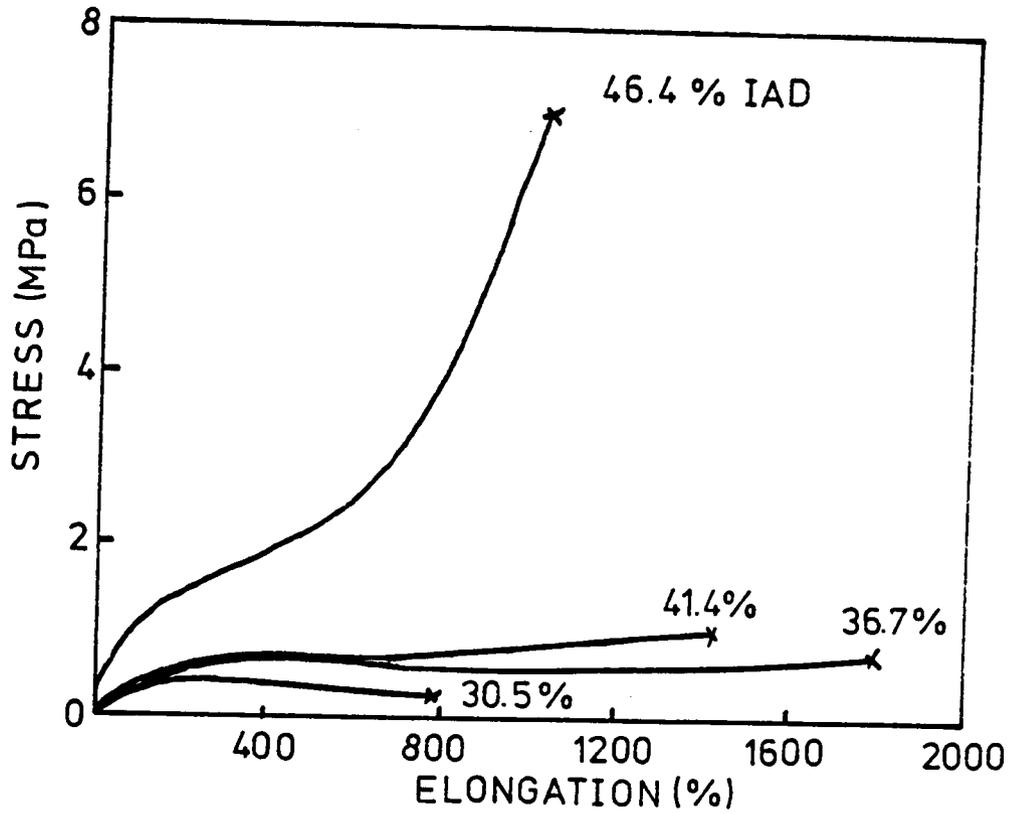
Figure 4.3.   Stress-strain behavior of an uncured 1,4(*cis,trans*) PB
modified with increasing amounts of IAD.   Adapted from Ref. 10.
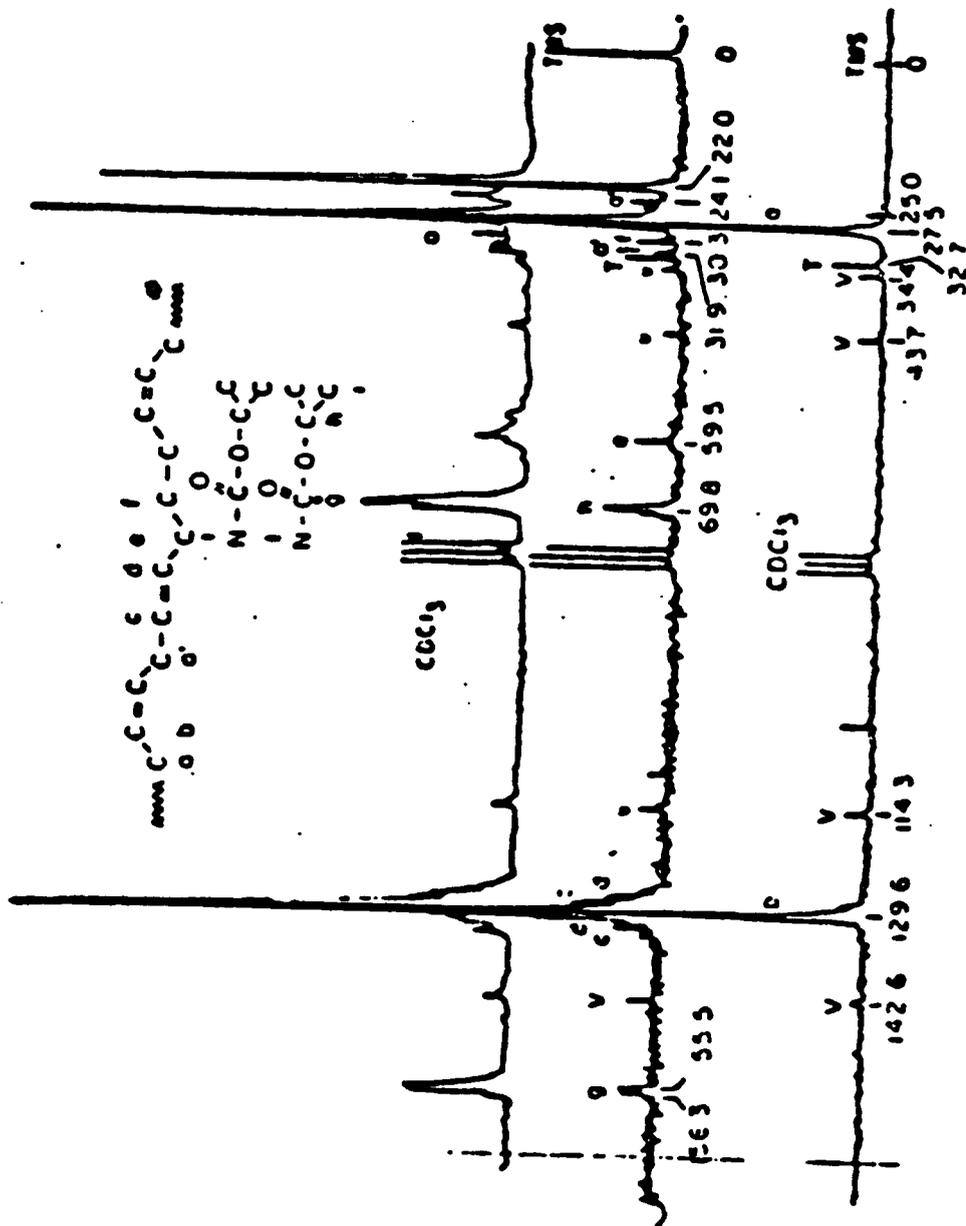
Figure 4.4a. ^{13}C nmr spectra for 1,4 polybutadiene modified with 0.0, 7.9, and 23.3 mol% IAD. Structure of modified butadiene unit labelled with resonance signal from spectra. Ref. 8.

^{13}C CALCULATION OF PERCENT IAD MODIFICATION
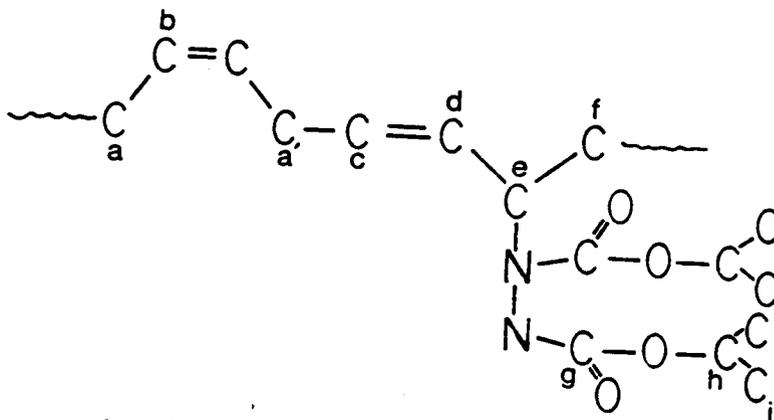
a → unconverted unit
  (one for *cis*, one for *trans*)

b → unconverted unit

e → converted unit (1 carbon)

g → converted unit (2 carbons)

h → converted unit (2 carbons)

i → converted unit (4 carbons)

c/d → converted unit (2 carbons)

Example: %IAD (g) = $\dfrac{g/2}{g/2 + a}$

Figure 4.4b. Structure of IAD-modified PB with nmr peak assignments for each carbon. Explanations of calculation of mol% IAD for modified 1,4 PB.
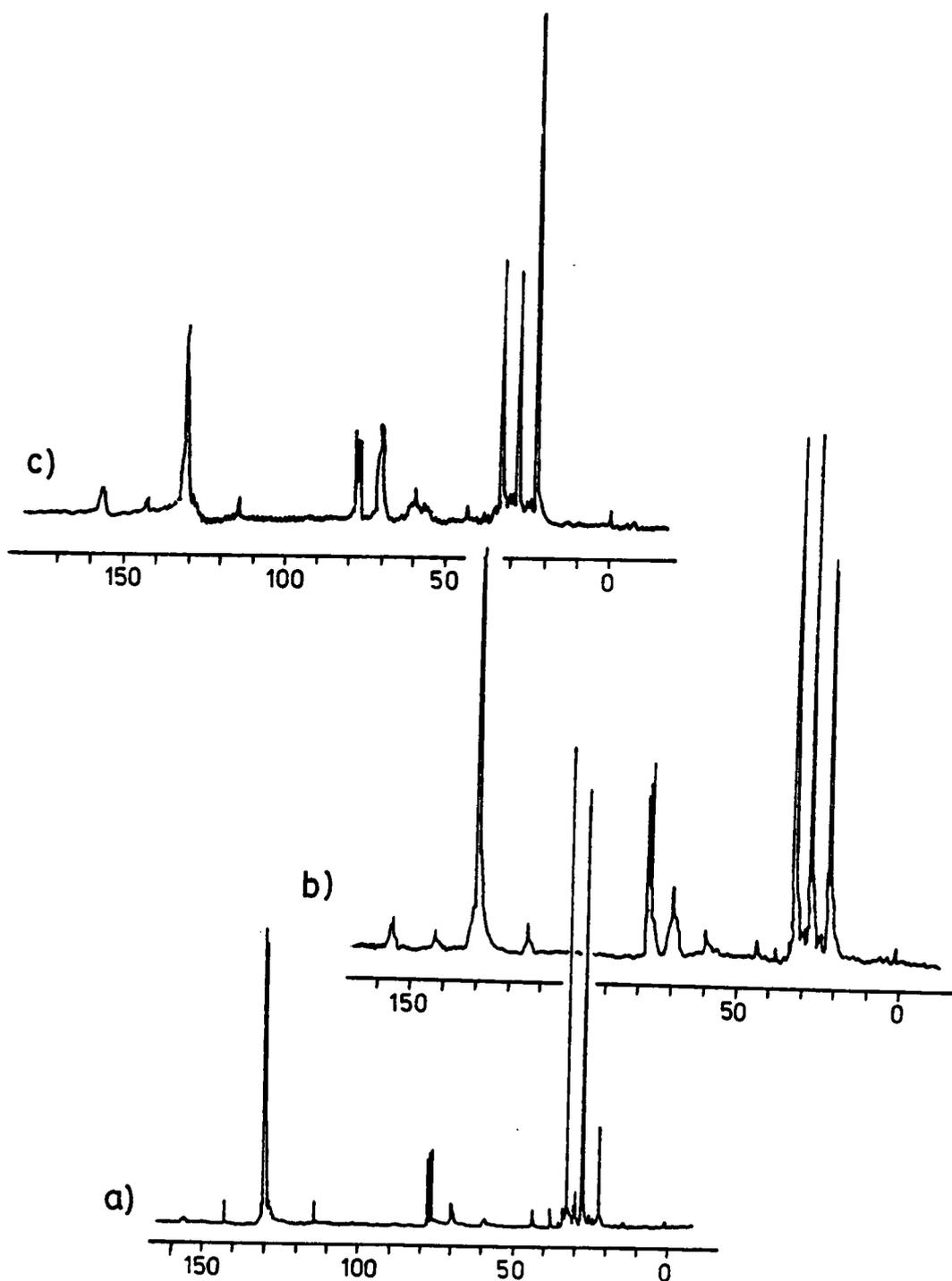
Figure 4.5. ^{13}C nmr spectra for three IAD-modified 1,4 PBs prepared in small-scale reactions: extent of IAD modification a) 3.3 mol%, b) 10.5 mol%, and c) 27.0 mol%.
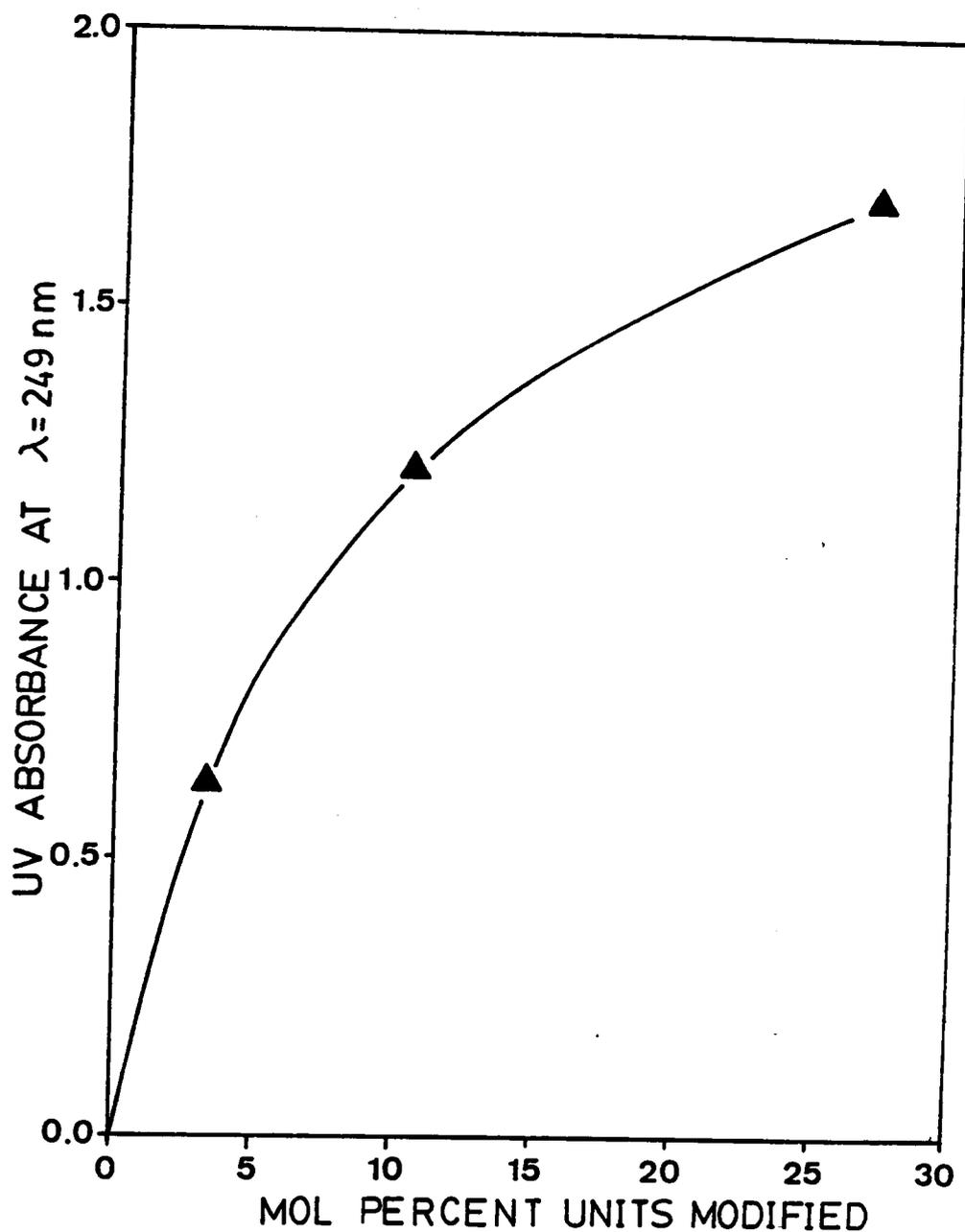
Figure 4.6. UV absorbance at 249 nm for IAD-modified PBs. This comprises a calibration curve suitable for determining the extent of IAD modification from similar PBs.
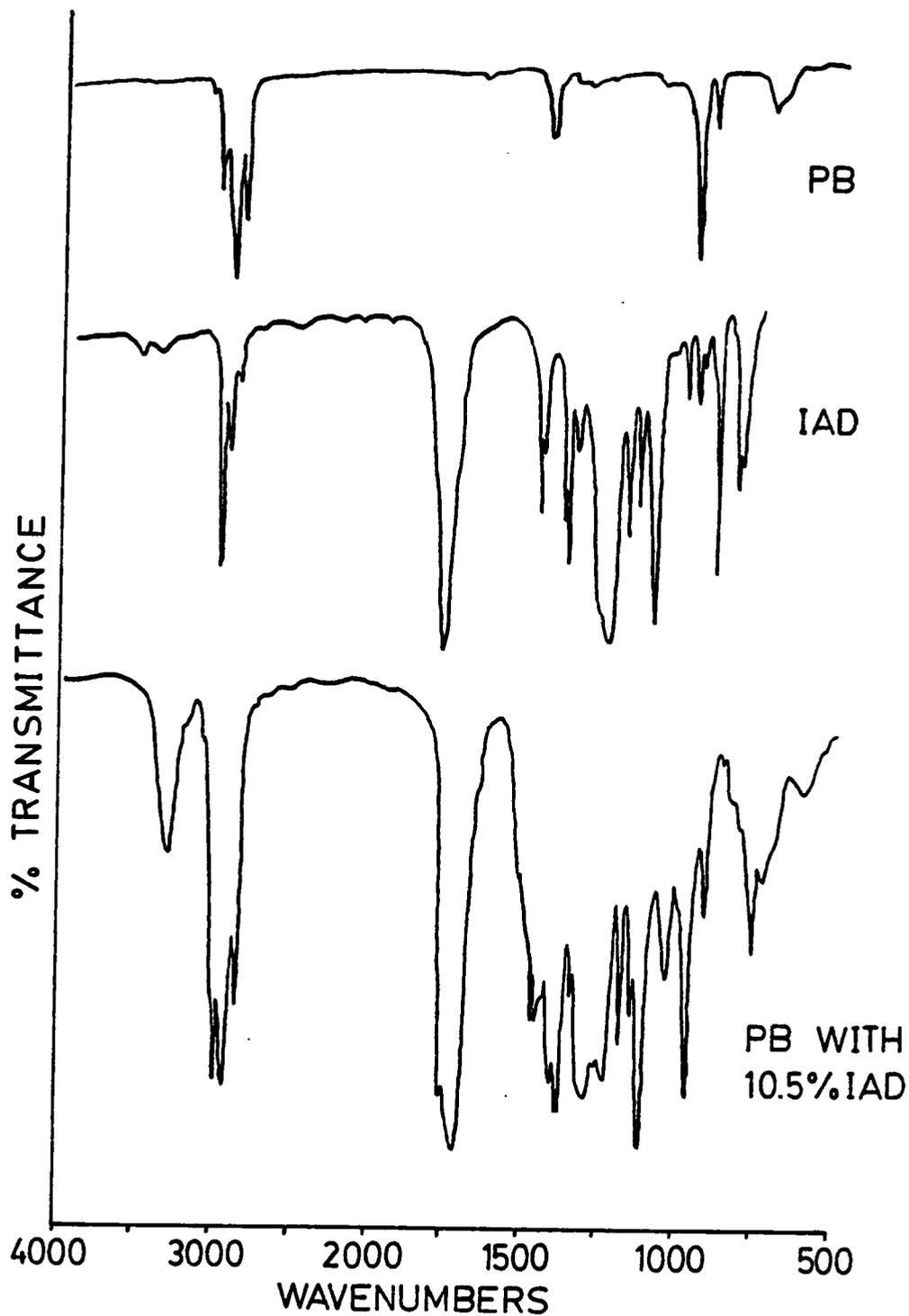
Figure 4.7. FTIR spectra of unmodified 1,4 PB, IAD, and IAD-modified (10.5% mol) PB.
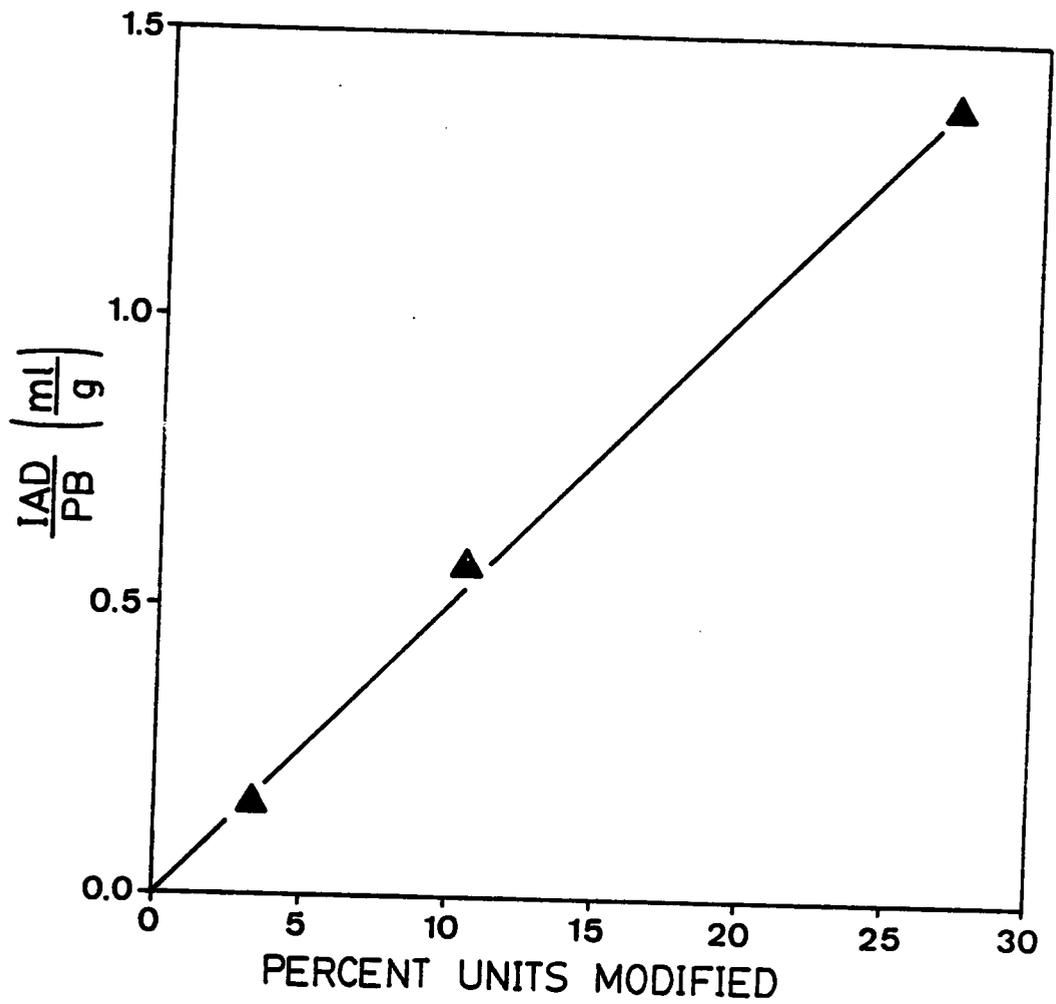
Figure 4.8. Extent of IAD modification for ratios of reactants used in small-scale reactions.
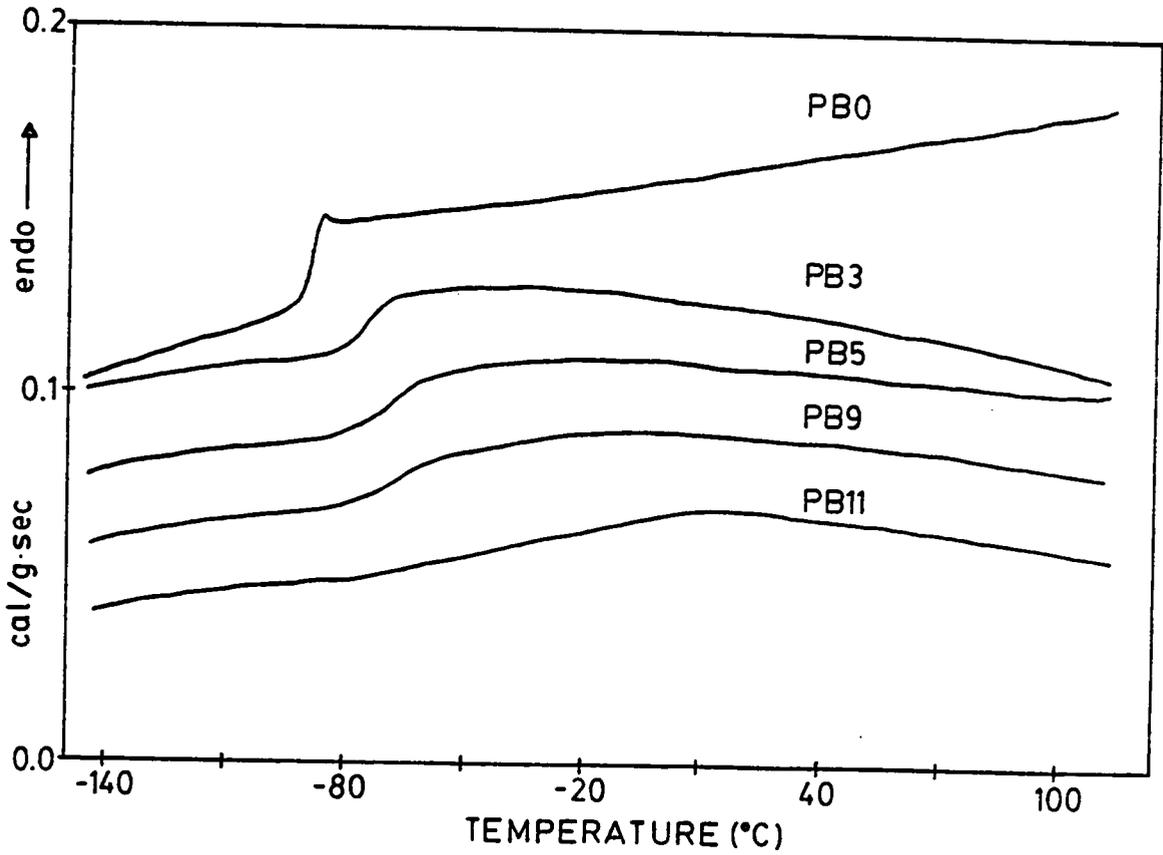
Figure 4.9.   Normalized DSC traces for 1,4 PB modified with 0, 3, 5, 9, and 11 mol% IAD.   Scanning rate = $10°C/min$.
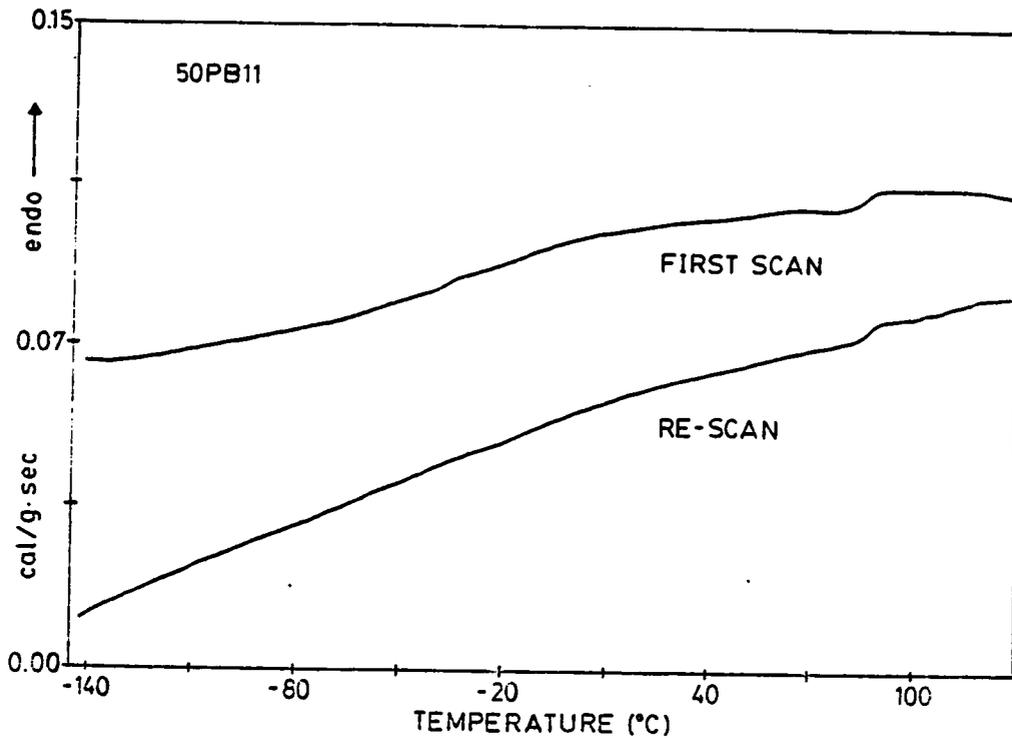
Figure 4.10. Normalized DSC traces of 50PB11. Second scan follows quench from 140 to -140°C at 320°C/min. Scanning rate = 10°C/min.
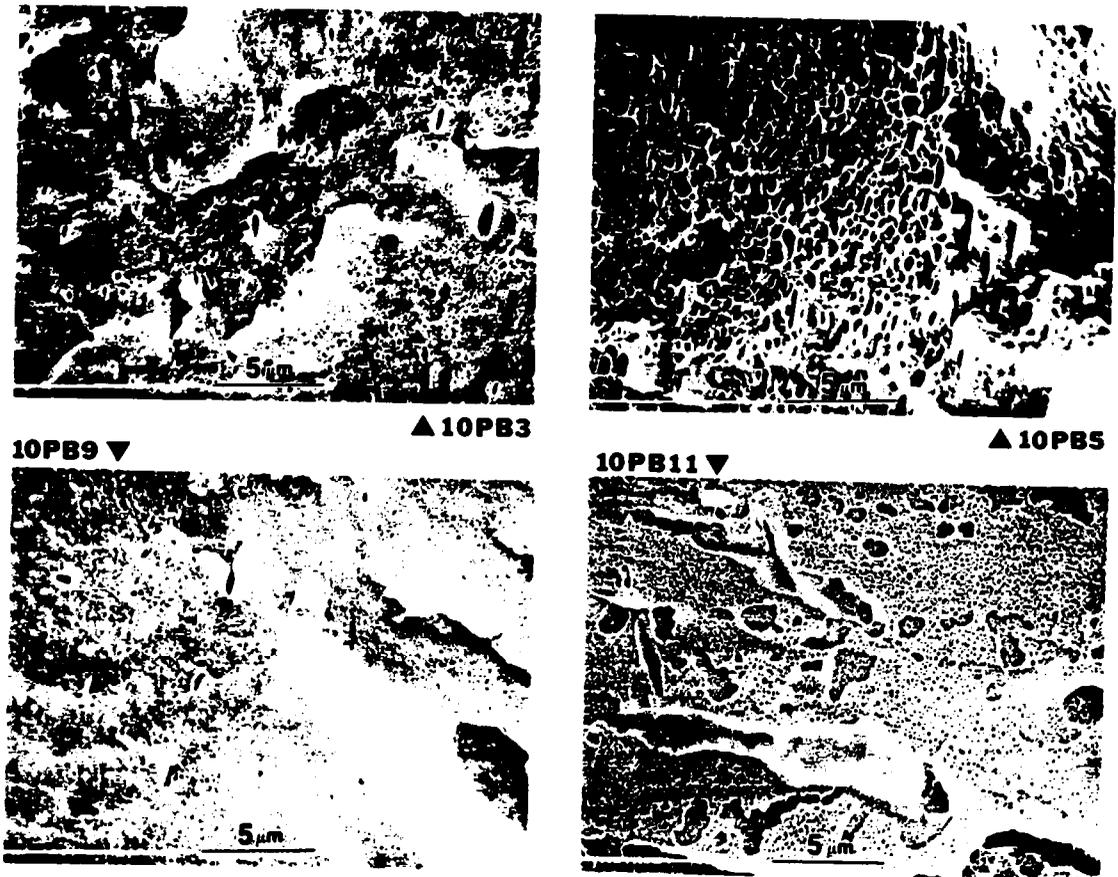
Figure 4.11. Cold fracture surfaces of PVC blends containing 10% of various IAD-modified 1,4 PBs. Original SEM magnification 5,000x.
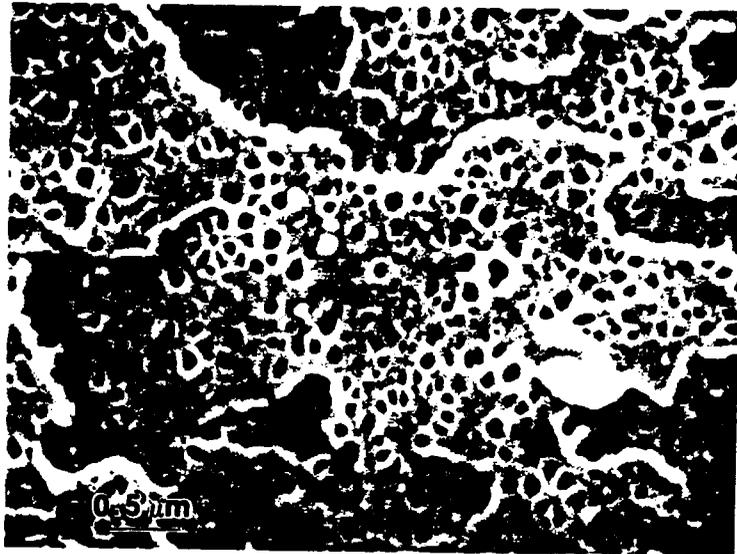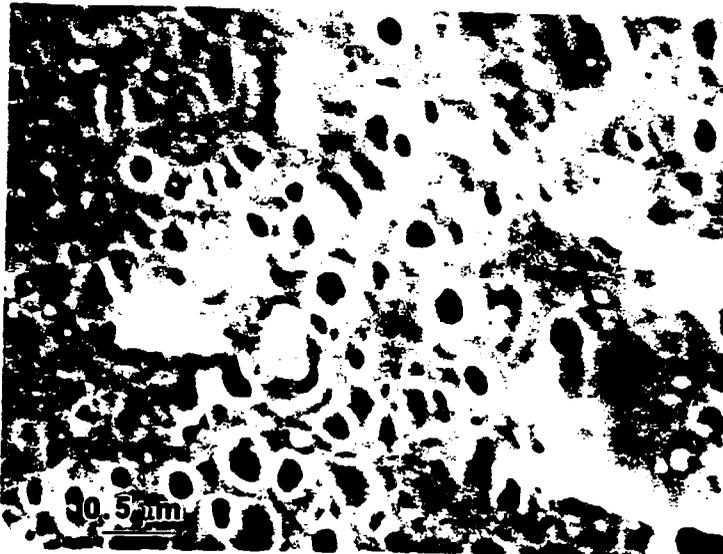
Figure 4.12. Cold fracture surfaces of PVC blends with 10 and 25% PB11. Original SEM magnification 20,000x.
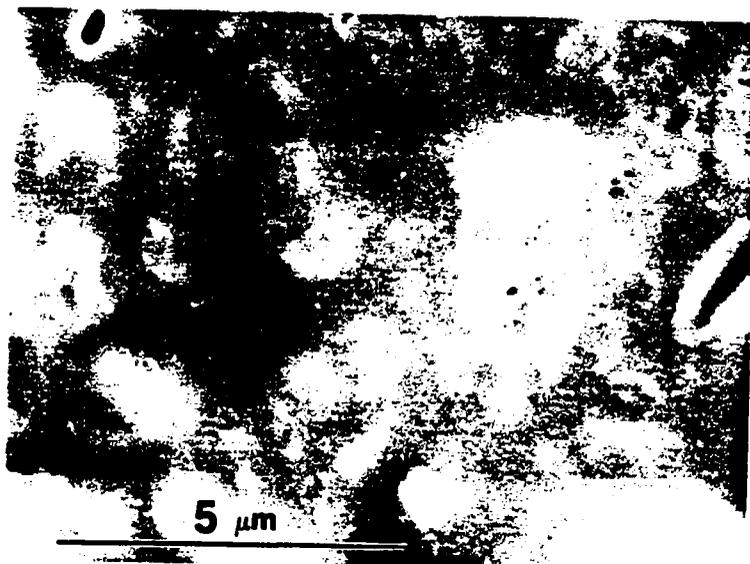
Figure 4.13. Cold fracture surfaces of 10PB0 and 25 PB0. Original SEM magnifications 10,000x and 5,000x.

LOAD COMPARISON

.... 10PB11

_____ and ---------- PVC
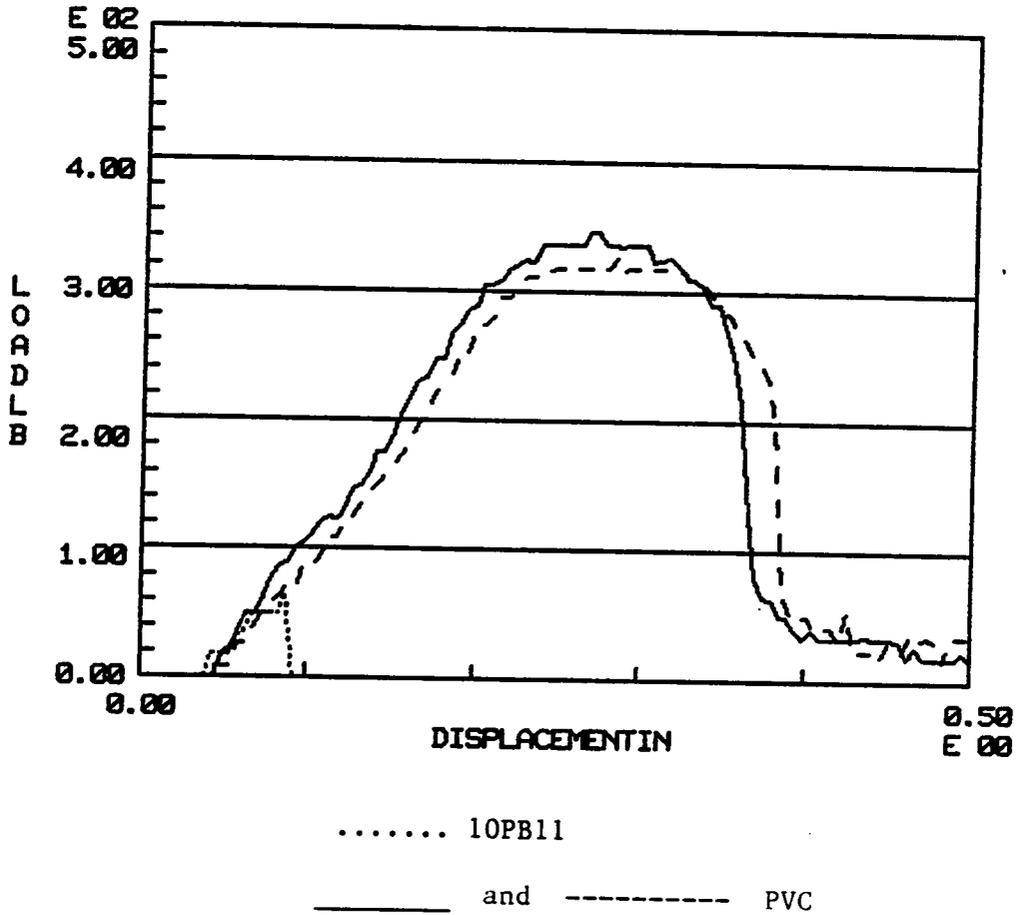
Figure 4.14a. Load vs. displacement in a falling weight impact test for Geon 86 PVC unmodified and containing 10 weight percent PB11, as noted in legend. Impact rate 1.27 m/sec.
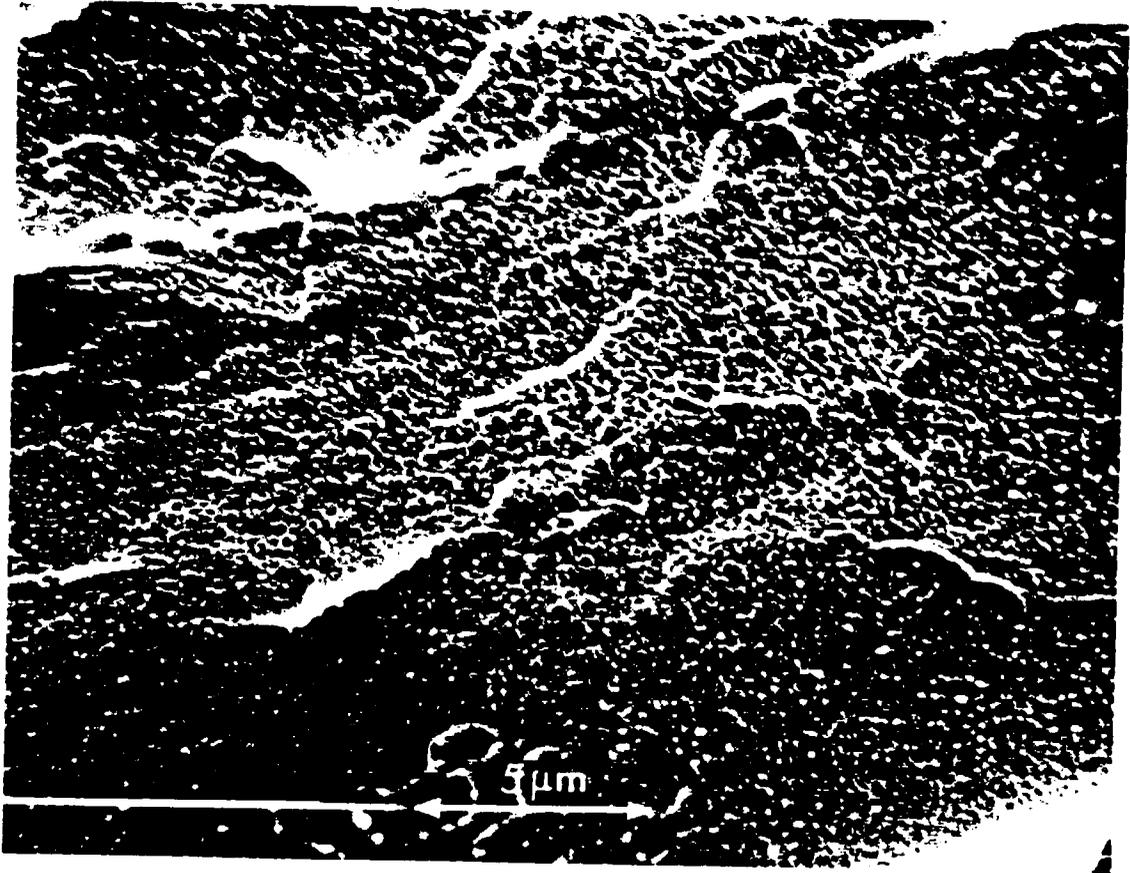
Figure 4.14b. Impact fracture surface for 10PB11 broken in test shown in (a). Original SEM magnification 5,000x.
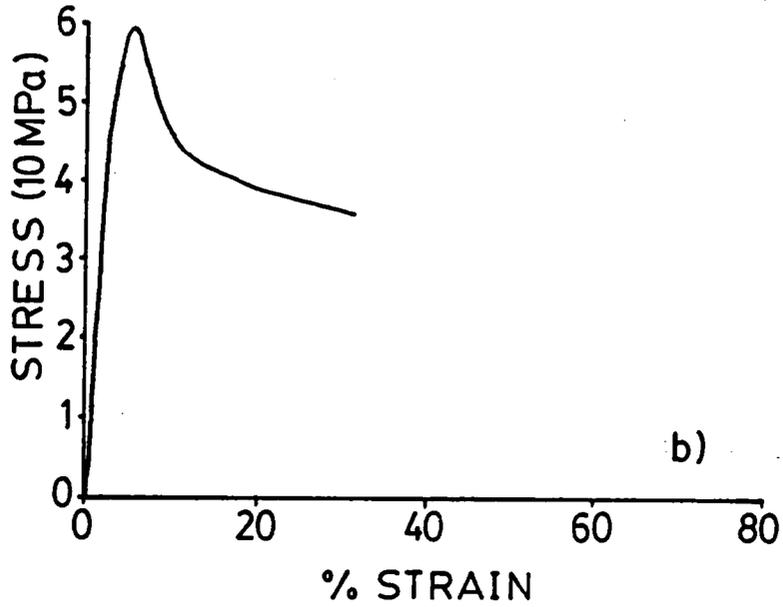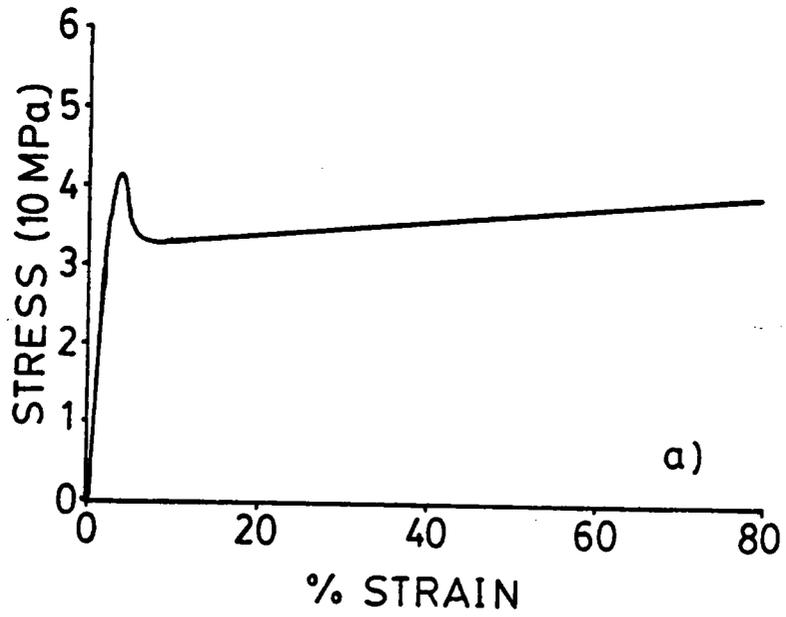
Figure 4.15. Stress-strain curves of unmodified PVC taken at crosshead speeds of a) 1 mm/min and b) 100 mm/min.
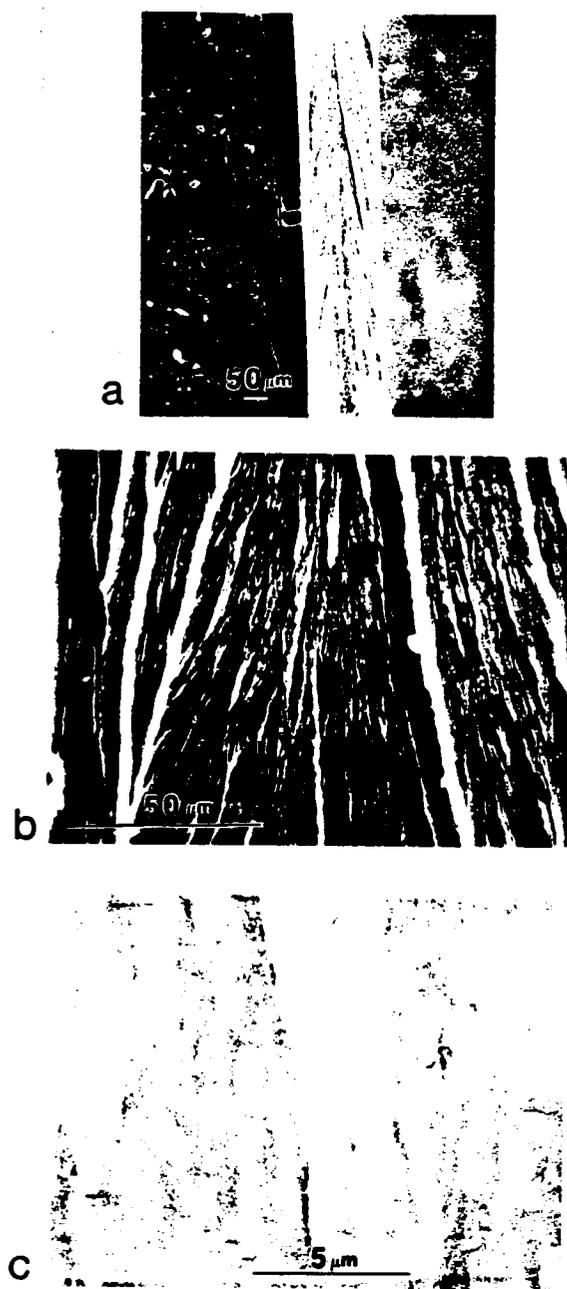
Figure 4.16. Fracture surfaces for unmodified PVC fractured in tensile test at 1 mm/min: a) full view of sample, b) near middle of sample, and c) near ultimate fracture end. Original SEM magnifications 70x, 700x, and 7000x, respectively.
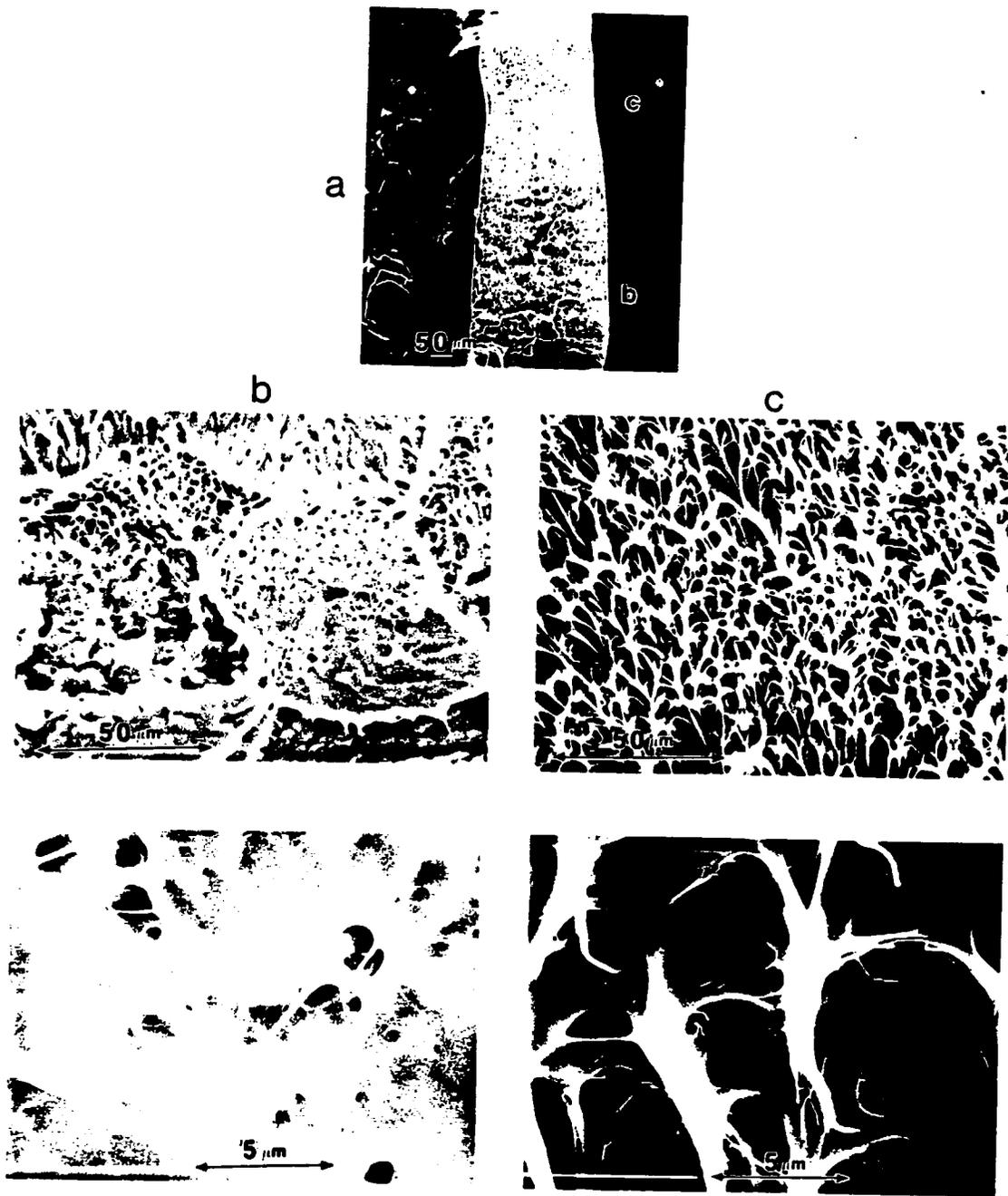
Figure 4.17. Fracture surfaces for unmodified PVC fractured in tensile test at 100 mm/min: a) full view of sample, b) low and high magnifications of initiation end of sample, and c) low and high magnifications of ultimate fracture end of sample. Original SEM magnifications 70x, 700x, and 7000x.
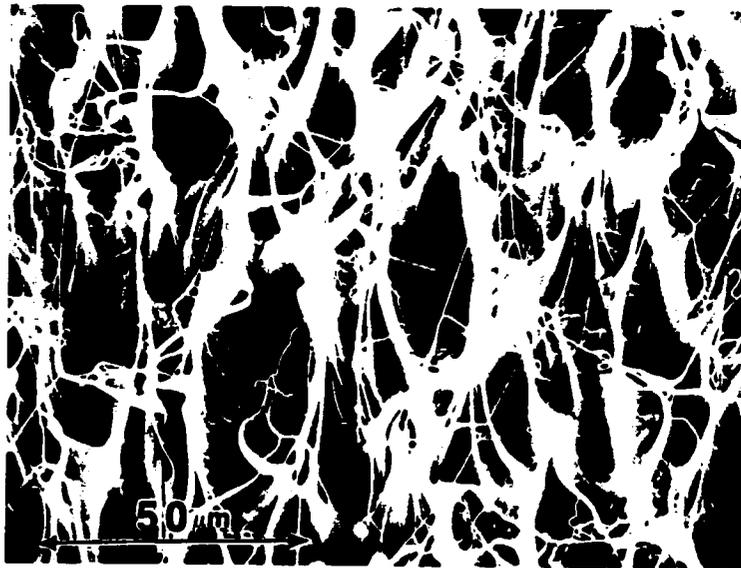
Figure 4.18. Tensile fracture surfaces for unmodified PVC prepared by dissolution, precipitation, and vacuum drying: a) fractured at 1 mm/min and b) fractured at 100 mm/min. Original SEM magnification 700x.
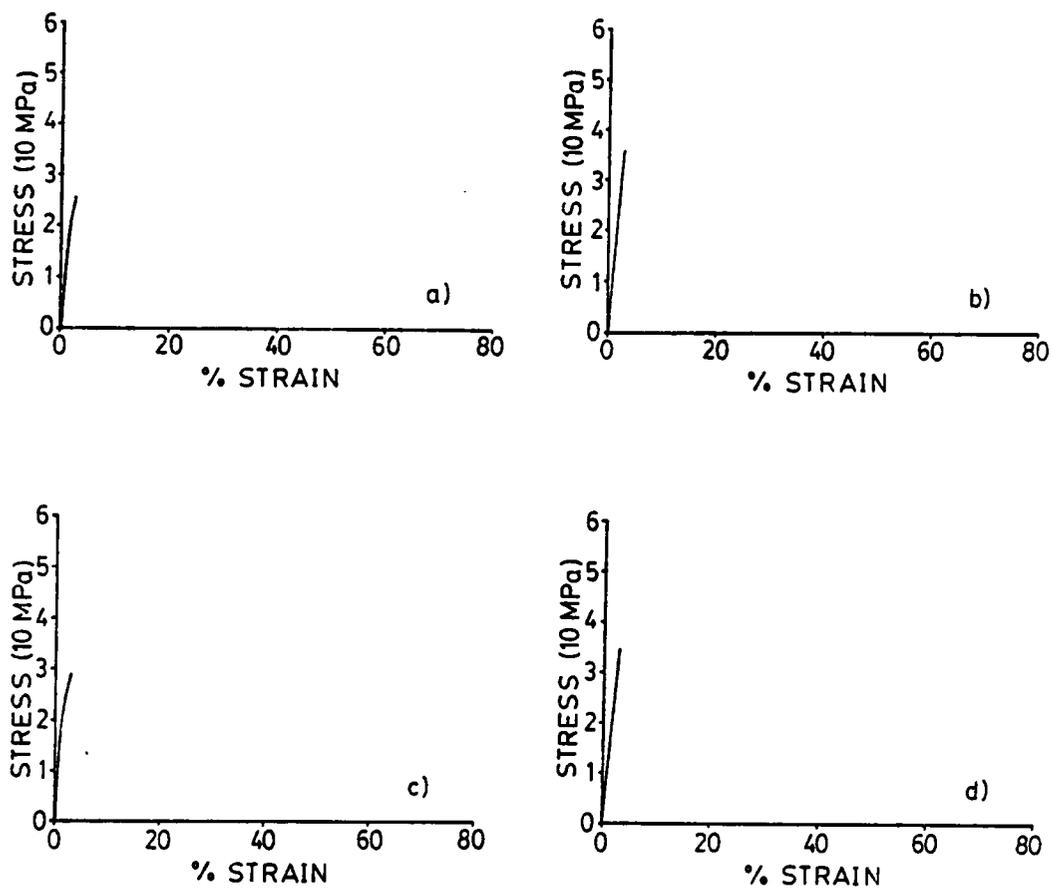
Figure 4.19. Examples of brittle stress-strain behavior for 10PB0 at a) 1 and b) 100 mm/min, and 10PB11 at c) 1 and d) 100 mm/min.
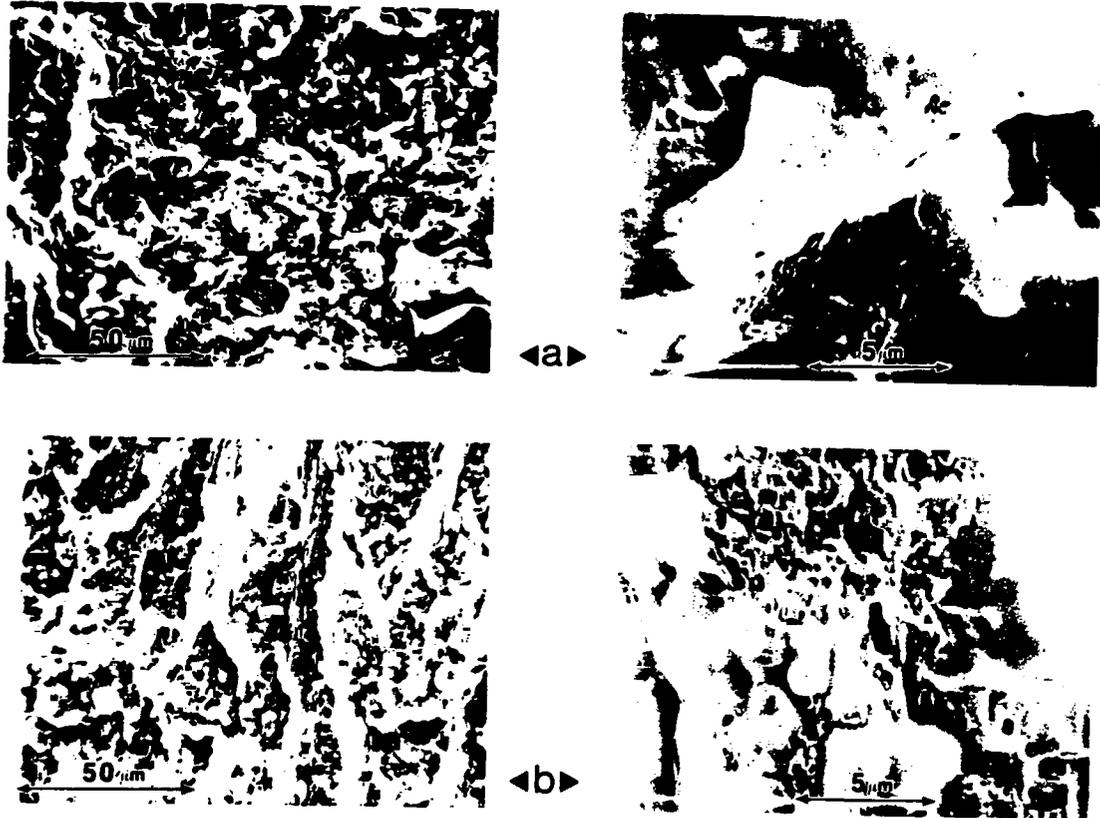
Figure 4.20.   Brittle tensile fracture surfaces for 10PB0 at
a) 1 and b) 100 mm/min, and 10PB11 at c) 1 and d) 100 mm/min.
Original SEM magnifications 700x and 7000x.
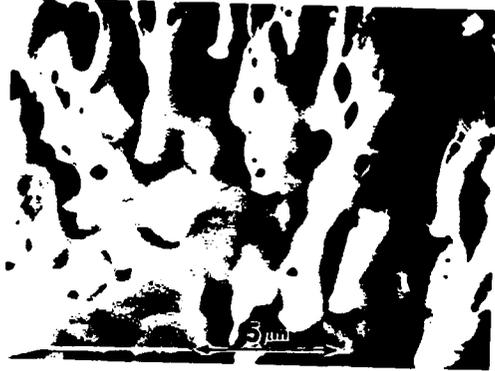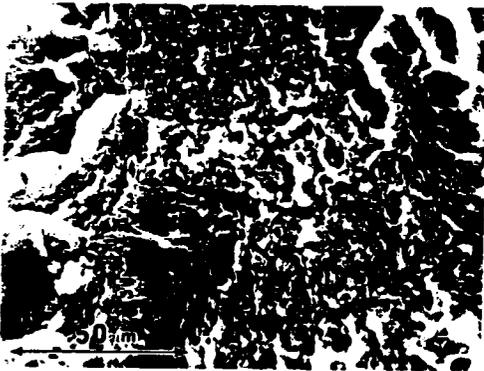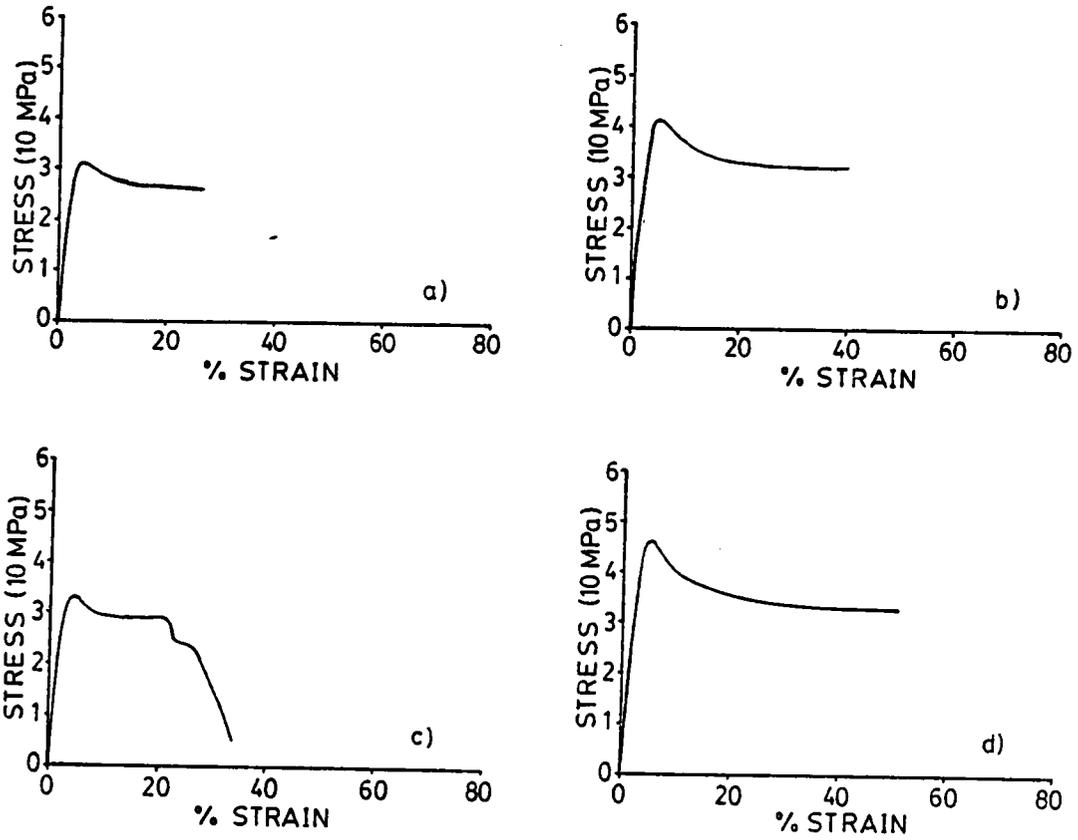
Figure 4.21. Examples of ductile stress-strain behavior for 10PB0 at a) 1 and b) 100 mm/min, and 10PB11 at c) 1 and d) 100 mm/min.
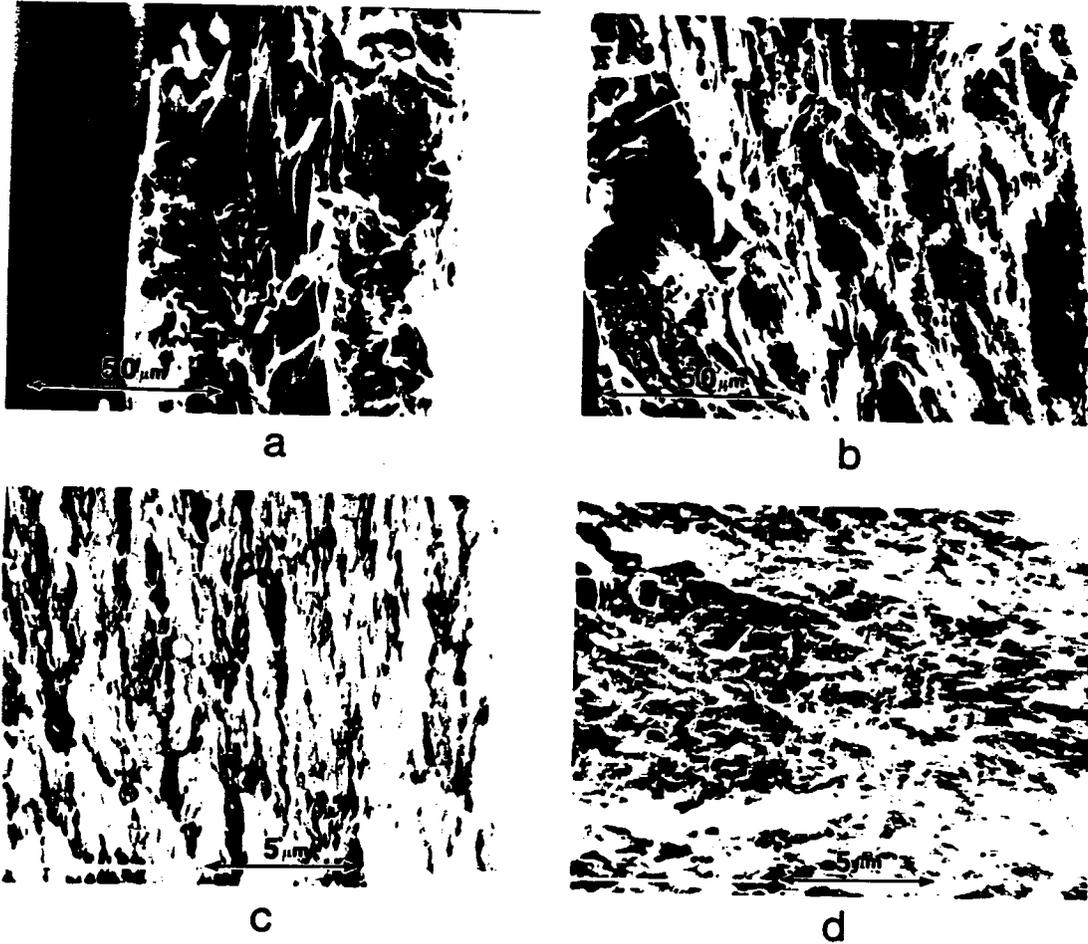
Figure 4.22.   Ductile tensile fracture surfaces for 10PB0 at
a) 1 and b) 100 mm/min, and 10PB11 at c) 1 and d) 100 mm/min.
Original SEM magnifications 700x or 7000x.
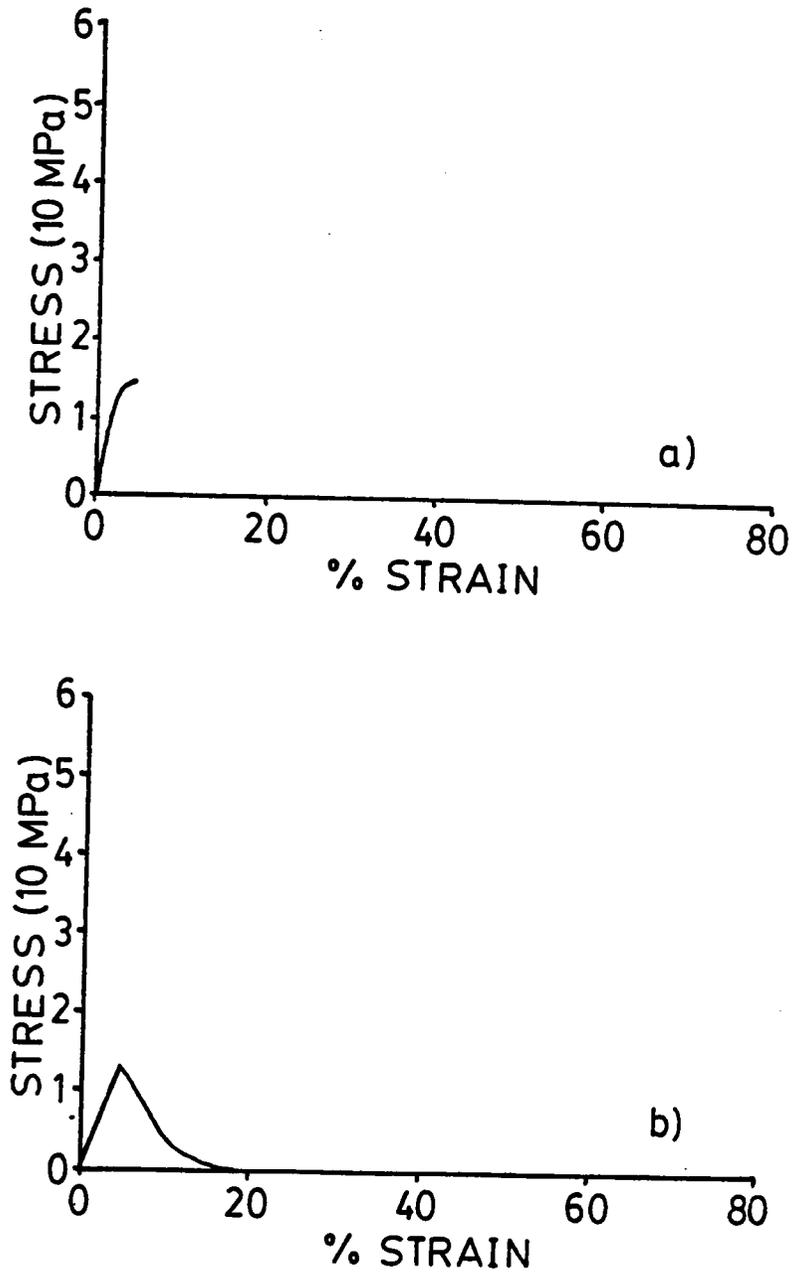
Figure 4.23. Tensile stress-strain response for 25PB0 at a) 1 and b) 100 mm/min crosshead speed.
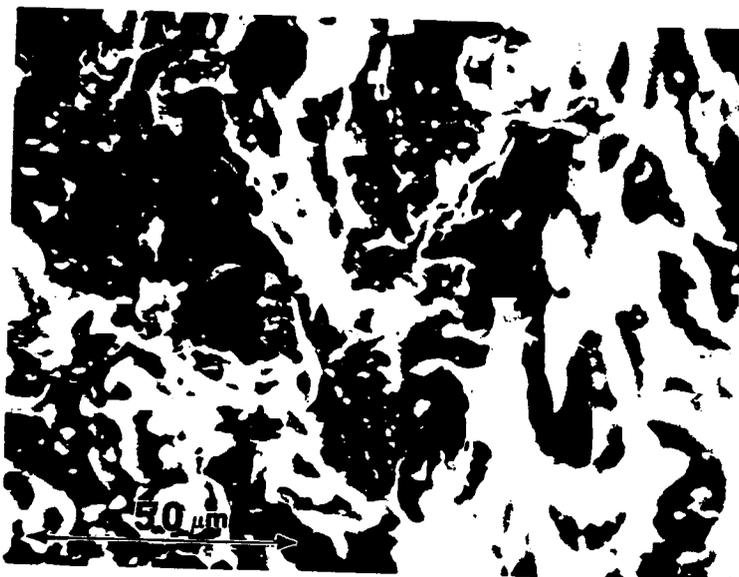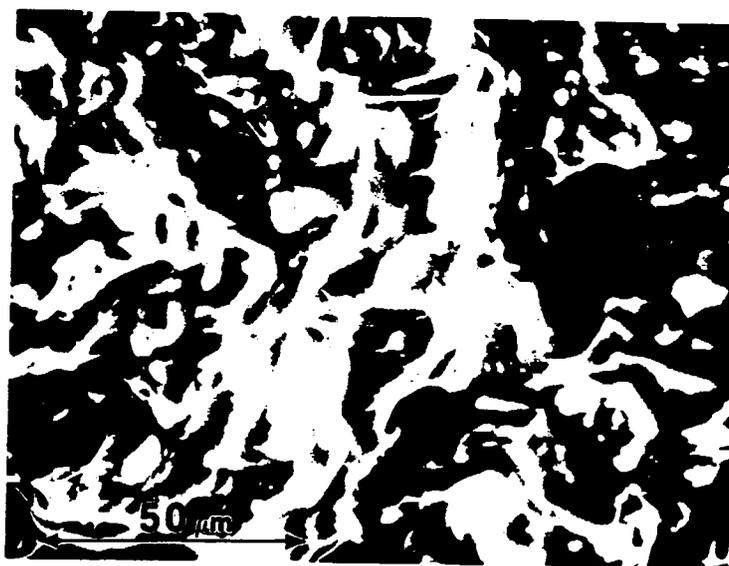
Figure 4.24. Tensile fracture surfaces for 25PB0 at a) 1 and b) 100 mm/min crosshead speed. Original SEM magnification 700x.
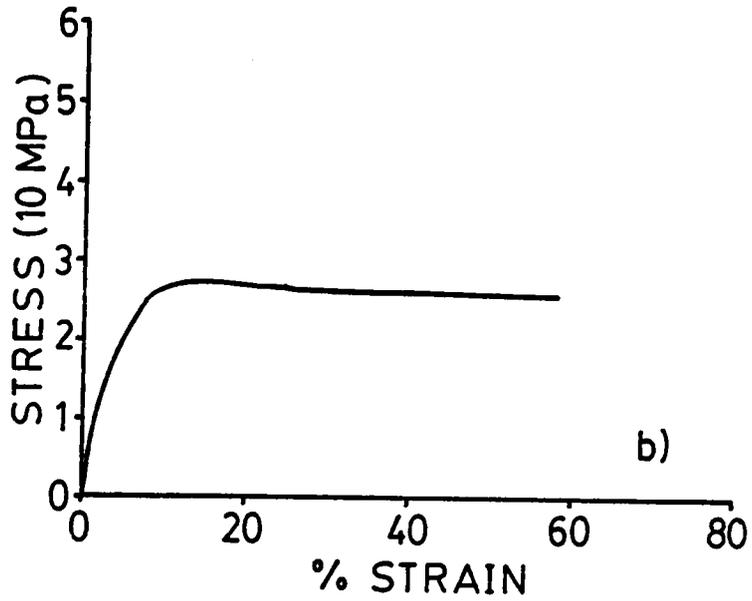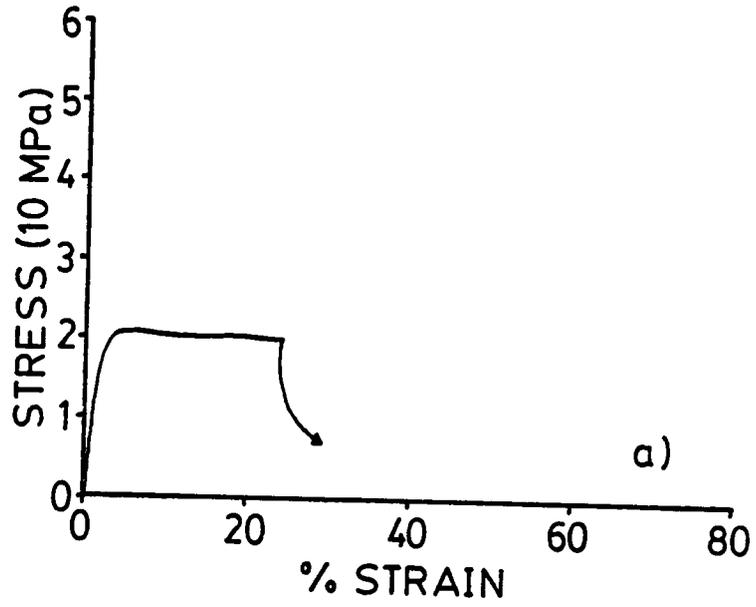
Figure 4.25. Tensile stress-strain response for 25PB11 at a) 1 and b) 100 mm/min crosshead speed.
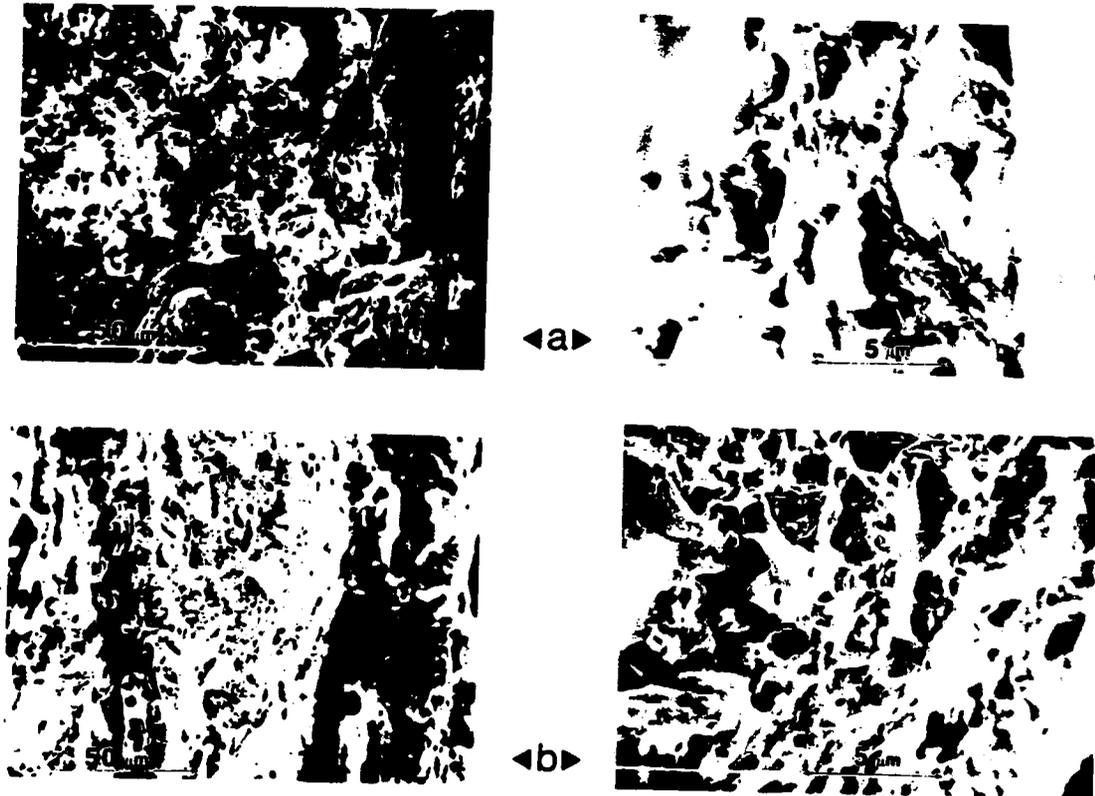
Figure 4.26. Tensile fracture surfaces for 25PB11 at a) 1 and
b) 100 mm/min crosshead speed. Original SEM magnifications 700x and
7000x.